

# Analysis of Internal Strains and Mechanics During Simulated Repetitive Lifting Motions in Human Lumbar Spinal Segments

**Dhara Amin**

BEng (Mechanical) (Honours)



A thesis submitted to the College of Science and Engineering  
in total fulfilment of the requirements of the degree of  
Doctor of Philosophy

Principal Supervisor: Associate Professor John J. Costi

Associate Supervisor: Professor Mark Taylor

March 5, 2019



# Table of Contents

Table of Contents .....	iii
List of Figures .....	ix
List of Tables .....	xvii
Abbreviations .....	xx
Abstract .....	xxi
Declaration .....	xxiii
Acknowledgements .....	xxiv
List of Publications .....	xxvi
Conference Abstracts .....	xxvii
Awards & Prizes .....	xxviii
Chapter 1 Introduction.....	1
1.1 Motivation .....	1
1.2 Aims.....	2
1.3 Significance .....	3
1.4 Thesis Outline .....	3
Chapter 2 Literature review .....	6
2.1 Anatomy .....	6
2.1.1 Lumbar vertebral column .....	6
2.1.2 Intervertebral disc.....	6
2.1.2.1 Nucleus Pulposus .....	6
2.1.2.2 Annulus Fibrosus .....	7
2.1.2.3 Cartilaginous Endplates .....	7
2.1.3 Lumbar Vertebra .....	8
2.1.4 Ligaments.....	8
2.1.5 Functional Spinal Unit .....	9
2.2 Disc Degeneration .....	9
2.3 Biomechanical testing of the intervertebral disc.....	10
2.3.1 Compression .....	11
2.3.2 Flexion and Extension .....	11
2.3.3 Lateral Bending .....	12
2.3.4 Axial Rotation .....	12
2.3.5 Shears.....	13
2.4 Lumbar Disc Herniation .....	13
2.4.1 Symptoms/Effects.....	15
2.4.2 Clinical Causes.....	15

2.4.3	Treatment.....	15
2.4.3.1	Nonsurgical Treatments .....	16
2.4.3.2	Surgical Treatments.....	16
2.5	LDH due to lifting .....	16
2.6	Biomechanics of Repetitive Lifting.....	17
2.7	LDH and Disc Degeneration .....	20
2.8	Mechanism of failure.....	21
2.8.1	Sudden Failure.....	28
2.8.2	Repetitive Failure .....	31
2.9	Conclusion .....	35
2.10	Internal Disc Strains.....	36
2.10.1	Methods .....	36
2.10.2	Strain Measurements.....	40
2.10.3	Conclusion .....	40
Chapter 3	New findings confirm regional internal disc strain changes during simulation of repetitive lifting motions.....	41
3.1	Abstract .....	42
3.2	Introduction.....	42
3.3	Materials and Methods .....	44
3.3.1	Specimens and Preparation .....	44
3.3.2	Mechanical Testing .....	45
3.3.2.1	6DOF .....	45
3.3.2.2	Simulated repetitive lifting.....	49
3.3.3	Data and Statistical Analysis .....	49
3.3.3.1	Validation of Wire Grid Technique.....	50
3.4	Results .....	51
3.5	Discussion.....	58
3.6	Conclusion .....	61
Chapter 4	Lumbar Intervertebral Disc Multiaxial Mechanics are Altered after Simulated Repetitive Lifting Movements.....	63
4.1	Abstract .....	64
4.2	Introduction.....	64
4.3	Methods .....	65
4.3.1	Specimens.....	65
4.3.2	Specimen Preparation.....	65
4.3.3	Mechanical Testing .....	66
4.3.4	Data and Statistical Analysis .....	67
4.4	Results .....	68

4.4.1	Stiffness.....	71
4.4.2	Phase Angle.....	73
4.5	Discussion.....	75
4.6	Conclusion .....	78
Chapter 5	Effect of unsafe repetitive lifting on disc mechanics: an internal disc threshold and multiaxial mechanical properties.....	79
5.1	Abstract .....	80
5.2	Introduction.....	80
5.3	Methods .....	81
5.3.1	Specimens and Preparation .....	81
5.3.2	Mechanical Testing .....	82
5.3.2.1	6DOF Testing.....	82
5.3.2.2	Simulated Repetitive Lifting .....	83
5.3.3	Data and Statistical Analysis .....	83
5.4	Results.....	85
5.4.1	Maximum shear strain at cycle 1 and last loading cycle (failure).....	85
5.4.2	Failure Mode .....	86
5.4.3	Failure strain by failure mode.....	88
5.4.4	6DOF before and after simulated repetitive lifting.....	88
5.4.4.1	Control vs Experimental Groups.....	88
5.4.4.2	Symmetry .....	88
5.4.4.3	Stiffness.....	89
5.4.4.4	Phase angle .....	89
5.5	Discussion.....	91
5.6	Conclusion .....	94
Chapter 6	Understanding the Impact of Repetitive Lifting Towards Lumbar Disc Herniation: A Clinically Relevant Biomechanical Cadaveric Study.....	95
6.1	Abstract .....	96
6.2	Introduction.....	96
6.3	Materials and Methods .....	97
6.3.1	Specimens and preparation .....	97
6.3.2	Simulated repetitive lifting and internal disc strain .....	98
6.3.3	Damage assessment.....	100
6.3.4	Data and statistical analysis .....	100
6.4	Results.....	101
6.4.1	Safe versus unsafe lifting.....	101
6.4.2	MRI and macroscopic damage score.....	103
6.4.3	MRI damage score and MSS.....	105

6.4.4	Macroscopic damage score and MSS.....	105
6.4.5	Failure mode and MSS.....	106
6.4.6	Failure mode and MRI damage score .....	107
6.4.7	Failure mode and macroscopic damage score.....	108
6.4.8	Failure mode, Pfirrmann grade and disc level .....	110
6.5	Discussion.....	110
6.6	Conclusion .....	114
Chapter 7	Conclusions and Future Recommendations .....	115
7.1	Principle Findings .....	115
7.1.1	Internal disc strains are the largest in the anterior and posterolateral regions under both safe and unsafe simulated repetitive lifting .....	115
7.1.2	6DOF mechanics are altered after simulated repetitive lifting.....	115
7.1.3	Large shear strains correlated with tissue damage .....	116
7.1.4	Mechanistic understanding of disc herniation .....	116
7.2	Significance .....	117
7.3	Future Recommendations .....	118
7.4	Concluding Statement.....	119
Chapter 8	References.....	121
Appendices.....		135
Appendix A .....		135
A.1	Error between detector positions .....	135
A.1.1	Methods .....	135
A.1.2	Results .....	140
A.1.2.1	Wire Grid Intersections.....	140
A.1.2.2	Disc Periphery Markers .....	144
A.1.2.3	Endplate Markers .....	146
Appendix B .....		149
B.1	Validation of the strain measurement technique.....	149
B.2	Simulated Safe Lifting .....	151
B.2.1	Stiffness .....	151
B.2.1.1	Shears and Compression.....	151
B.2.1.2	Bending and Rotation .....	152
B.2.2	Phase Angle.....	153
B.2.2.1	Shears and Compression.....	153
B.2.2.2	Bending and Rotation .....	154
B.3	Simulated Unsafe Lifting.....	155
B.3.1	Stiffness .....	155

B.3.1.1	Shears and Compression.....	155
B.3.1.2	Bending and Rotation .....	156
B.3.2	Phase Angle.....	157
B.3.2.1	Shears and Compression.....	157
B.3.2.2	Bending and Rotation .....	158
Appendix C	.....	159
C.1	Principal Strains .....	159
C.1.1	Simulated safe repetitive lifting .....	160
C.1.1.1	Cycle 1 .....	160
C.1.1.2	Cycle 500 .....	166
C.1.1.3	Cycle 1000 .....	171
C.1.1.4	Cycle 5000 .....	176
C.1.1.5	Cycle 10000 .....	181
C.1.1.6	Cycle 15000 .....	186
C.1.1.7	Cycle 20000 .....	191
C.1.2	Simulated unsafe repetitive lifting.....	196
C.1.2.1	Cycle 1 .....	196
C.1.2.2	Failure.....	202
Appendix D	.....	207
D.1	Maximum shear strain plots for individual specimens for both simulated repetitive lifting groups.....	207
D.1.1	Simulated safe repetitive lifting.....	207
D.1.1.1	Specimen 1 .....	207
D.1.1.2	Specimen 2 .....	208
D.1.1.3	Specimen 3 .....	209
D.1.1.4	Specimen 4 .....	210
D.1.1.5	Specimen 5 .....	211
D.1.1.6	Specimen 6 .....	212
D.1.1.7	Specimen 7 .....	213
D.1.1.8	Specimen 8 .....	214
D.1.2	Simulated unsafe repetitive lifting.....	215
D.1.2.1	Specimen 1 .....	215
D.1.2.2	Specimen 2 .....	216
D.1.2.3	Specimen 3 .....	217
D.1.2.4	Specimen 4 .....	217
D.1.2.5	Specimen 5 .....	218

D.1.2.6	Specimen 6 .....	218
D.1.2.7	Specimen 7 .....	219
Appendix E	.....	221
E.1	Multiaxial mechanics under simulated repetitive lifting.....	221
E.1.1	Simulated safe repetitive lifting .....	222
E.1.2	Simulated unsafe repetitive lifting.....	223
Appendix F	.....	225
F.1	6DOF load-unload curves before and after simulated unsafe repetitive lifting.....	225
F.1.1	Shears and Compression.....	225
F.1.2	Bending and Rotation .....	226
Appendix G	.....	227
G.1	Comparison of safe and unsafe repetitive lifting.....	227
G.1.1	Methods: Statistical Analysis .....	227
G.1.2	Results .....	227
G.1.2.1	Failure strain .....	227
G.1.2.2	6DOF mechanics .....	229
Appendix H	.....	233
H.1	Damage score.....	233
H.1.1	MR images.....	235
H.1.2	Macroscopic Images.....	265
Appendix I	.....	295
I.1	Corresponding MR images, macroscopic images, and strain maps .....	295
I.1.1	Simulated safe repetitive lifting .....	295
I.1.2	Simulated unsafe repetitive lifting.....	299

## List of Figures

<b>Figure 2-1</b> Transverse and coronal sections of the disc (Newell et al., 2017). .....	6
<b>Figure 2-2</b> The components of the lumbar vertebral body (Adams, 2002) .....	8
<b>Figure 2-3</b> Posterior view of the zygapophysial (facet) joint,.....	8
<b>Figure 2-4</b> Functional spinal unit including the locations of the ligaments (Newell et al., 2017) .....	9
<b>Figure 2-5</b> Twelve loading directions applied to the FSU (Chang et al., 2011) .....	11
<b>Figure 2-6</b> Images of the three clinical classifications of LDH: disc protrusion, nuclear extrusion, and sequestration.....	14
<b>Figure 2-7</b> MRI images of LDH (Rajasekaran et al., 2013) .....	14
<b>Figure 2-8</b> During lifting the back muscles generate an extensor moment (EM) to overcome the flexion moment due to body weight (w) and weight being lifted (W). .....	18
<b>Figure 2-9</b> Free Body Diagram of lifting a weight with bent knees and straight back, where EM is the extension moment (Adams, 2002; Dolan and Adams, 1998). .....	19
<b>Figure 2-10</b> Herniation (hyperflexion) model developed by Adams et al. (Adams and Hutton, 1982), where FSU was flexed at a fixed angle and loaded in compression .....	28
<b>Figure 2-11</b> Mechanisms of LDH (mid-annulus (top panel) and endplate junction (bottom panel)) under a sudden overload (flexion + compression, (Wade et al., 2014) .....	29
<b>Figure 2-12</b> Images showing the lateral tracking of the nucleus and then migration down to the posterior/posterolateral regions (van Heeswijk et al., 2017). The * and arrows are representing locations of nucleus material found in the transverse slice .....	30
<b>Figure 2-13</b> Mechanics of LDH under complex sudden overload (Wade et al., 2017). Top panel: sagittal view and bottom panel: transverse view .....	31
<b>Figure 2-14</b> Mechanism of LDH under repetitive loading based on human FSUs (Adams and Hutton, 1985) .....	33
<b>Figure 2-15</b> Mechanism of LDH under repetitive loading based on ovine FSUs (Berger-Roscher et al., 2017) .....	33
<b>Figure 3-1</b> a. An overview of the testing sequence. b. Left and right stereoradiographs showing the wire grid, calibration beads, disc periphery and endplate markers. c. Prespective line drawing of the wire gird, endplate and dis periphery markers taken from Costi et al., 2008.....	46
<b>Figure 3-2</b> This photo shows the testing setup used in this research. The specimen is inside the calibration cage which is coupled to the hexapod robot .....	47
<b>Figure 3-3</b> Left Image: Nodal coordinates of the disc grid used to interpolate displacements and calculated strains (173 nodes). .....	50

<b>Figure 3-4</b> T1 MRI images of FSUs pre- and post-repetitive lifting. a. Pre-test sagittal (TR: 750 ms TE: 13 ms thickness: 4 mm) b. Post-test sagittal (TR: 750 ms TE: 13 ms thickness: 4 mm) c. Pre-test axial (TR: 2900 TE: 14 ms thickness: 2 mm) d. Post-test axial (TR: 2900 TE: 14 ms thickness: 2 mm). Images (ab) and (cd) are two different specimens. Herniation is evident in (b) and nucleus disruption and posterior annular tears are evident in (d).....	52
<b>Figure 3-5</b> Internal disc average displacements in the axial and lateral view at each cycle interval (averaged across all seven specimens, lateral view: positive x is anterior). Magnification: 2x.....	54
<b>Figure 3-6</b> Mean (95% CI) MSS as a function of cycle number (averaged across seven specimens and all regions combined). * indicates a significant difference in respect to the cycle on the left of the bar (i.e. for the top horizontal bar, a significant difference in respect to cycle 1) .....	55
<b>Figure 3-7</b> Contour plots showing MSS (%) at each of the different cycle time points ...	56
<b>Figure 3-8</b> Mean (95% CI) MSS as a function of disc region (average across seven specimens and all cycles combined). .....	57
<b>Figure 3-9</b> Mean (95% CI) MSS as a function of disc region and cycle number (averaged across all seven specimens). Bars represent significant interactions within each region and cycle number ( $p < 0.05$ ) .....	58
<b>Figure 4-1</b> Average load vs. displacement curves for shear and compression DOF, before and after simulated repetitive lifting (averaged over 14 specimens). Dotted lines represent 95% CI.....	69
<b>Figure 4-2</b> Average load vs. displacement curves for all bending 6DOF directions before and after simulated repetitive lifting (averaged over 14 specimens). Dotted lines represent 95 % CI.....	70
<b>Figure 4-3</b> Mean (95% CI) stiffness and phase angle before and after repetitive loading (averaged over 14 specimens) in compression (C). * denotes significance ( $p < 0.05$ ).....	71
<b>Figure 4-4</b> Mean (95% CI) stiffness and phase angle before and after repetitive loading (averaged over 14 specimens) in bending directions: extension (EXT), flexion (FLEX), left and right axial rotation (LAR, RAR, respectively) and lateral bending (LB). * denotes significance ( $p < 0.05$ ).....	72
<b>Figure 4-5</b> Mean (95% CI) stiffness and phase angle before and after repetitive loading (averaged over 14 specimens) in shear directions: right and left lateral shear (RLS, LLS, respectively), anterior shear (AS), and posterior shear (PS). * denotes significance ( $p < 0.05$ ) .....	73

<b>Figure 4-6</b> Effect of failure mode on stiffness (Mean, 95%CI, $p > 0.104$ , averaged over 14 specimens) for extension (a.) and flexion (b.).....	74
<b>Figure 4-7</b> Effect of failure mode on phase angle (Mean, 95%CI, $p > 0.054$ , averaged over 14 specimens) for extension (a.) and compression (b.).....	74
<b>Figure 5-1</b> An overview of the testing sequence (adapted from (Amin et al., 2018 Manuscript Under Review-b). .....	83
<b>Figure 5-2</b> Contour plots showing MSS (%) at cycle 1 and failure averaged over all specimens ( $n = 8$ ) .....	85
<b>Figure 5-3</b> Mean (95% CI) MSS as a function of disc region for cycle 1 and at failure. The image of the disc identifies the nine regions (shaded). * denotes regions having significant differences in MSS between cycle 1 and failure .....	86
<b>Figure 5-4</b> Internal average tissue displacement vectors (top row: lateral view, middle row: axial view) and average MSS (bottom row: axial view) for the three different failure modes (no injury, disc protrusion, and endplate failure). .....	87
<b>Figure 5-5</b> Mean (95% CI) MSS as a function of disc region broken down by failure mode: no injury, disc protrusion, and endplate failure. * denotes significant difference compared to no injury. + denotes significant difference compared to a disc protrusion .....	88
<b>Figure 5-6</b> Mean (95% CI) stiffness and phase angle before and after simulated repetitive lifting in shear and bending directions:.....	90
<b>Figure 5-7</b> Mean (95% CI) stiffness and phase angle before and after simulated repetitive lifting in compression (Comp). * denotes significance between before and after simulated repetitive lifting ( $p < 0.05$ ) .....	90
<b>Figure 6-1</b> Schematic of the testing procedure .....	100
<b>Figure 6-2</b> Pre-test MRI (a) mid-sagittal T1 (c) mid-axial T2. Post-test MRI (b) mid-sagittal T1 (d) mid-axial T2, demonstrating an LDH in the same specimen .....	101
<b>Figure 6-3</b> MSS for the safe and unsafe lifting groups. Right image identifies each of the nine regions. * denotes significant differences between each group ( $p < 0.05$ ).....	102
<b>Figure 6-4</b> Correlation between MRI damage score and macroscopic damage score for all regions combined ( $r_s = 0.651$ , $p < 0.001$ ), where the scores were averaged over all three raters (inter-observer). .....	103
<b>Figure 6-5.</b> Left to right images: MRI axial slice, macroscopic axial slice, and the MSS map after repetitive loading for example specimens with (1) No injury, (2) Nucleus migration (left and right posterolateral) and (3) A posterior central LDH (see <b>Appendix I</b> ).....	104
<b>Figure 6-6</b> Correlation between MRI damage score and MSS for all regions combined ( $p > 0.120$ ), where the scores were averaged over all three raters (inter-observer). Scores from	

16 specimens and 9 disc regions are represented here (144 data points, some data points are over lapping). The scoring scale was 0 = no damage; 1 = annular tears/delamination; 2 = migrating nucleus; 3 = disc protrusion; 4 = disc herniation.....	105
<b>Figure 6-7</b> Macroscopic damage score vs MSS for the left lateral region ( $r_s = 0.486$ , $p < 0.037$ , $n=16$ , only experimental group). The macroscopic damage score was averaged between the three observers .....	106
<b>Figure 6-8</b> Failure mode vs MSS for left lateral ( $r_s = 0.724$ , $p = 0.018$ , $n=16$ , experimental group, some data points are overlapping).....	107
<b>Figure 6-9</b> Failure mode (herniation pathway) vs MRI damage score for the posterior and left posterolateral regions ( $p < 0.037$ , $n=30$ , both control and experimental groups, some data points are overlapping) .....	108
<b>Figure 6-10</b> Failure mode vs macroscopic grading for left and right posterolateral, and posterior regions ( $p < 0.031$ , $n = 30$ , both control and experimental groups, some data points are overlapping).....	109
<b>Figure 6-11</b> Failure mode vs Pfirrmann grade .....	110
<b>Figure 6-12.</b> Failure mode vs. total MRI damage score (left) and failure mode vs macroscopic damage score (right). .....	112
<b>Figure 7-1</b> Drawing of mechanistic theory of LDH developed from this research.....	117
<b>Figure A-1</b> Image of the setup for determining the error between positioning the detector at $56^\circ$ and upright. In this figure, the detector is placed at $56^\circ$ . After taking the images, the detector was positioned upright (vertical against the calibration cage).....	136
<b>Figure A-2</b> Axial image of the mock-up specimen with wire grid (5 by 6). The wires are represented by numbers, which were used to identify the intersections (i.e. 1 x 7 is the intersection of wires 1 and 7). The mock-up specimen is positioned inside the calibration cage in this photo.....	137
<b>Figure A-3</b> Left (left image) and right (right image) x-ray images when detector was positioned at 56 degrees. The calibration beads, wire grid, disc periphery, and endplate markers are annotated on the figure .....	138
<b>Figure A-4</b> Left (left image) and right (right image) x-ray images when detector was positioned upright. A visual understanding of the different markers is outlined in <b>Figure A-3</b> .....	139
<b>Figure A-5</b> Digitised coordinates (x and y) of the wire grid intersections calculated from the detector positioned at $56^\circ$ and upright .....	143
<b>Figure A-6</b> Digitised coordinates (x and y) of the disc periphery markers calculated from the detector positioned at $56^\circ$ and upright .....	145

<b>Figure A-7</b> Digitised coordinates (x and y) of the endplate markers calculated from the detector positioned at 56° and upright .....	147
<b>Figure B-1</b> Mean (95% CI) stiffness before and after wire grid insertion of specimens in the simulated safe repetitive lifting group for shear and compression directions. ....	151
<b>Figure B-2</b> Mean (95% CI) stiffness before and after wire grid insertion of the specimen in the simulated safe repetitive lifting group for bending and rotation directions. ....	152
<b>Figure B-3</b> Mean (95% CI) phase angle before and after wire grid insertion of the specimen in the simulated safe repetitive lifting group for shear and compression directions. ....	153
<b>Figure B-4</b> Mean (95% CI) phase angle before and after wire grid insertion of the specimen in the simulated safe repetitive lifting group for bending and rotation directions. ....	154
<b>Figure B-5</b> Mean (95% CI) stiffness before and after wire grid insertion of the specimen in the simulated unsafe repetitive lifting group for shear and compression directions. ....	155
<b>Figure B-6</b> Mean (95% CI) stiffness before and after wire grid insertion of the specimen in the simulated unsafe repetitive lifting group for bending and rotation directions. ....	156
<b>Figure B-7</b> Mean (95% CI) phase angle before and after wire grid insertion of the specimen in the simulated unsafe repetitive lifting group for shear and compression directions. ....	157
<b>Figure B-8</b> Mean (95% CI) phase angle before and after wire grid insertion of the specimen in the simulated unsafe repetitive lifting group for bending and rotation directions. ....	158
<b>Figure C-1</b> Average 3D Principal strains for cycle 1 of the simulated safe repetitive lifting group. ....	165
<b>Figure C-2</b> Average 3D Principal strains for cycle 500 of the simulated safe repetitive lifting group. ....	170
<b>Figure C-3</b> Average 3D Principal strains for cycle 1000 of the simulated safe repetitive lifting group. ....	175
<b>Figure C-4</b> Average 3D Principal strains for cycle 5000 of the simulated safe repetitive lifting group. ....	180
<b>Figure C-5</b> Average 3D Principal strains for cycle 10000 of the simulated safe repetitive lifting group. ....	185
<b>Figure C-6</b> Average 3D Principal strains for cycle 15000 of the simulated safe repetitive lifting group. ....	190
<b>Figure C-7</b> Average 3D Principal strains for cycle 20000 of the simulated safe repetitive lifting group. The blue vectors represent compressive strain and red vectors represent	

tensile strain. Four views are presented in this figure. Top Left: Axial View, Top Right: Lateral View, Bottom Left: Posterior View, Bottom Right: Oblique View.....	195
<b>Figure C-8</b> Average 3D Principal strains for cycle 1 of the simulated unsafe repetitive lifting group. ....	201
<b>Figure C-9</b> Average 3D Principal strains for failure of the simulated unsafe repetitive lifting group. ....	206
<b>Figure D-1</b> Contour plots showing MSS (%) at each of the cycle time points until failure for specimen 1.....	207
<b>Figure D-2</b> Contour plots showing MSS (%) at each of the cycle time points until failure for specimen 2.....	208
<b>Figure D-3</b> Contour plots showing MSS (%) at each of the cycle time points until failure for specimen 3.....	209
<b>Figure D-4</b> Contour plots showing MSS (%) at each of the cycle time points until failure for specimen 4.....	210
<b>Figure D-5</b> Contour plots showing MSS (%) at each of the cycle time points until failure for specimen 5.....	211
<b>Figure D-6</b> Contour plots showing MSS (%) at each of the cycle time points until failure for specimen 6.....	212
<b>Figure D-7</b> Contour plots showing MSS (%) at each of the cycle time points until failure for specimen 7.....	213
<b>Figure D-8</b> Contour plots showing MSS (%) at each of the cycle time points until failure for specimen 8.....	214
<b>Figure D-9</b> Contour plots showing MSS (%) at cycle 1 and failure for specimen 1.....	215
<b>Figure D-10</b> Contour plots showing MSS (%) at cycle 1 and failure for specimen 2.....	216
<b>Figure D-11</b> Contour plots showing MSS (%) at cycle 1 and failure for specimen 3.....	217
<b>Figure D-12</b> Contour plots showing MSS (%) at cycle 1 and failure for specimen 4.....	217
<b>Figure D-13</b> Contour plots showing MSS (%) at cycle 1 and failure for specimen 5.....	218
<b>Figure D-14</b> Contour plots showing MSS (%) at cycle 1 and failure for specimen 6.....	218
<b>Figure D-15</b> Contour plots showing MSS (%) at cycle 1 and failure for specimen 7.....	219
<b>Figure F-1</b> Average load vs. displacement curves for shear and compression DOFs, before and after simulated unsafe repetitive lifting. Dotted lines represent 95% CI.....	225
<b>Figure F-2</b> Average load vs. displacement curves for all bending 6DOF directions before and after simulated unsafe repetitive lifting. Dotted lines represent 95 % CI.....	226
<b>Figure G-1</b> Mean (95% CI) failure MSS as a function of disc region for safe and unsafe repetitive lifting. * denotes significance with respect to safe lifting.....	228

<b>Figure G-2</b> Mean (95% CI) failure MSS as a function of failure mode for safe and unsafe repetitive lifting. * denotes significance with respect to safe lifting.....	228
<b>Figure G-3</b> Mean (95% CI) stiffness for shear and compression directions comparing simulated safe versus unsafe repetitive lifting. * denotes significance ( $p<0.05$ ).....	229
<b>Figure G-4</b> Mean (95% CI) stiffness for bending and rotation directions comparing simulated safe versus unsafe repetitive lifting. * denotes significance ( $p<0.05$ ).....	230
<b>Figure G-5</b> Mean (95% CI) phase angle for shear and compression directions comparing simulated safe versus unsafe repetitive lifting. * denotes significance ( $p<0.05$ ).....	231
<b>Figure G-6</b> Mean (95% CI) phase angle for shear and compression directions comparing simulated safe versus unsafe repetitive lifting. * denotes significance ( $p<0.05$ ).....	232
<b>Figure I-1</b> Left to right images: MRI axial slice, macroscopic axial slice, and the MSS map after simulated safe repetitive lifting for specimen 1 .....	296
<b>Figure I-2</b> Left to right images: MRI axial slice, macroscopic axial slice, and the MSS map after simulated safe repetitive lifting for specimen 2 .....	296
<b>Figure I-3</b> Left to right images: MRI axial slice, macroscopic axial slice, and the MSS map after simulated safe repetitive lifting for specimen 3 .....	296
<b>Figure I-4</b> Left to right images: MRI axial slice, macroscopic axial slice, and the MSS map after simulated safe repetitive lifting for specimen 4 .....	297
<b>Figure I-5</b> Left to right images: MRI axial slice, macroscopic axial slice, and the MSS map after simulated safe repetitive lifting for specimen 5 .....	297
<b>Figure I-6</b> Left to right images: MRI axial slice, macroscopic axial slice, and the MSS map after simulated safe repetitive lifting for specimen 6 .....	297
<b>Figure I-7</b> Left to right images: MRI axial slice, macroscopic axial slice, and the MSS map after simulated safe repetitive lifting for specimen 7 .....	298
<b>Figure I-8</b> Left to right images: MRI axial slice, macroscopic axial slice, and the MSS map after simulated safe repetitive lifting for specimen 8 .....	298
<b>Figure I-9</b> Left to right images: MRI axial slice, macroscopic axial slice, and the MSS map after simulated unsafe repetitive lifting for specimen 1 .....	299
<b>Figure I-10</b> Left to right images: MRI axial slice, macroscopic axial slice, and the MSS map after simulated safe repetitive lifting for specimen 2 .....	299
<b>Figure I-11</b> Left to right images: MRI axial slice, macroscopic axial slice, and the MSS map after simulated safe repetitive lifting for specimen 3 .....	300
<b>Figure I-12</b> Left to right images: MRI axial slice, macroscopic axial slice, and the MSS map after simulated safe repetitive lifting for specimen 4 .....	300
<b>Figure I-13</b> Left to right images: MRI axial slice, macroscopic axial slice, and the MSS map after simulated safe repetitive lifting for specimen 5 .....	300

**Figure I-14** Left to right images: MRI axial slice, macroscopic axial slice, and the MSS map after simulated safe repetitive lifting for specimen 6..... 301

**Figure I-15** Left to right images: MRI axial slice, macroscopic axial slice, and the MSS map after simulated safe repetitive lifting for specimen 7..... 301

## List of Tables

<b>Table 2-1</b> Review of <i>in vitro</i> biomechanical studies investigating LDH by sudden overload and repetitive loading. Studies are organised by type of loading and then chronologically by year .....	22
<b>Table 2-2</b> Review of <i>in vitro</i> studies reporting internal disc strains .....	38
<b>Table 3-1</b> Specimen characteristics, including degenerative (Pfirrmann) grade, initial disc height, applied cycles, disc height loss, and failure mode. Initial disc height was calculated from the unloaded FSU using lateral x-ray image .....	53
<b>Table 4-1</b> Characteristics for those specimens that were successfully tested to 20,000 loading cycles, which include Pfirrmann grade, lumbar level, change in FSU height, and failure mode.....	68
<b>Table 4-2</b> Required sample size for each failure mode to detect significance for stiffness and phase angle in all loading directions .....	76
<b>Table 5-1</b> Mean cycles to failure, disc height loss, and breakdown of the failure mode of specimens for control and experimental groups .....	87
<b>Table 6-1</b> Specimen demographics, Pfirrmann grade, applied cycles and failure mode. Data is sorted by lifting regime, failure mode and cycles. The specimens that underwent strain measurement are identified in the MSS column .....	99
<b>Table 6-2</b> Specimen-specific results for specimens that failed by LDH or disc protrusion and their relationships to the injury site, regions of highest MRI and macroscopic damage, and regions of largest and smallest MSS. Specimens 1-3 failed by LDH, and specimens 4-11 failed by disc protrusion .....	113
<b>Table A-1</b> Mean (95% CI) x-, y- and z-coordinate values of the intersections calculated from the five repeats of the digitised x-rays where the detector was positioned at 56° and upright. Wire grid intersections are based on <b>Figure A-2</b> , where 1 x 7 represents the intersection of wires 1 and 7 .....	140
<b>Table A-2</b> The mean (95% CI) x-, y- and z-coordinate values for the disc periphery makers calculated from five repeats of the digitised x-rays where the detector was positioned at 56° and upright.....	144
<b>Table A-3</b> Mean (95% CI) x-, y- and z-coordinate values for the endplate makers calculated from five repeats of the digitised x-rays where the detector was positioned at 56° and upright.....	146
<b>Table B-1</b> The p-values showing the interactions between group (control and experimental) and intervention (before and after wire grid insertion) for each loading	

direction. There were no significant differences before and after wire gird insertion in any direction for both stiffness and phase angle .....	150
<b>Table C-1</b> Mean (95% CI) of 3D principal strains at each node (1 – 173) for simulated safe repetitive lifting at cycle 1.....	160
<b>Table C-2</b> Mean (95% CI) of 3D principal strains at each node (1 – 173) for simulated safe repetitive lifting at cycle 500.....	166
<b>Table C-3</b> Mean (95% CI) of 3D principal strains at each node (1 – 173) for simulated safe repetitive lifting at cycle 1000.....	171
<b>Table C-4</b> Mean (95% CI) of 3D principal strains at each node (1 – 173) for simulated safe repetitive lifting at cycle 5000.....	176
<b>Table C-5</b> Mean (95% CI) of 3D principal strains at each node (1 – 173) for simulated safe repetitive lifting at cycle 10000.....	181
<b>Table C-6</b> Mean (95% CI) of 3D principal strains at each node (1 – 173) for simulated safe repetitive lifting at cycle 15000.....	186
<b>Table C-7</b> Mean (95% CI) of 3D principal strains at each node (1 – 173) for simulated safe repetitive lifting at cycle 20000.....	191
<b>Table C-8</b> Mean (95% CI) of 3D principal strains at each node (1 – 173) for simulated unsafe repetitive lifting at cycle 1.....	196
<b>Table C-9</b> Mean (95% CI) of 3D principal strains at each node (1 – 173) for simulated unsafe repetitive lifting at failure.....	202
<b>Table D-1</b> Specimen characteristics (failure mode, level, grade, and applied cycles) for the simulated safe repetitive lifting cohort that underwent strain measurement. This table provides a cross-reference for the images presented in this section (D.1.1) .....	207
<b>Table D-2</b> Specimen characteristics (failure mode, level, grade, and applied cycles) for the simulated unsafe repetitive lifting cohort that underwent strain measurement. This table provides a cross-reference for the images presented in this section (D.1.2) .....	215
<b>Table E-1</b> Mean (95% CI) flexion moment (-M <sub>x</sub> ), right axial rotation moment (-M <sub>z</sub> ), and compressive force (-F <sub>z</sub> ) at cycle 1 and the final applied cycle under simulated safe repetitive lifting for the control group, experimental group, and both groups combined. The mean (95% CI) disc height loss over the applied cycles is also presented. ....	222
<b>Table E-2</b> Mean (95% CI) initial disc height (mm) calculated from a lateral x-ray of FSU for the specimens in the safe repetitive lifting group. The initial disc height is presented for the control group, experimental group, and both groups combined. ....	222
<b>Table E-3</b> Mean (95% CI) flexion moment (-M <sub>x</sub> ), right axial rotation moment (-M <sub>z</sub> ), and compressive force (-F <sub>z</sub> ) at cycle 1 and the final applied cycle under simulated unsafe	

repetitive lifting for the control group, experimental group, and both groups combined. The mean (95% CI) disc height loss over the applied cycles is also presented. ....	223
<b>Table E-4</b> Mean (95% CI) initial disc height (mm) calculated from a lateral x-ray of FSU for the specimens in the unsafe repetitive lifting group. The initial disc height is presented for the control group, experimental group, and both groups combined. ....	223
Table H-1 Specimen characteristics, which include lifting regime, failure mode, MSS measurement, level, Pfirrmann grade, and applied cycles. This table provides a cross-reference for the images presented in this appendix .....	234
<b>Table I-1</b> Specimen characteristics (failure mode, level, grade, and applied cycles) for the simulated safe repetitive lifting cohort that underwent strain measurement. This table provides a cross-reference for the images presented in this section (I.1.1) .....	295
<b>Table I-2</b> Specimen characteristics (failure mode, level, grade, and applied cycles) for the simulated unsafe repetitive lifting cohort that underwent strain measurement. This table provides a cross-reference for the images presented in this section (I.1.2) .....	299

## Abbreviations

Disc	Intervertebral disc
LDH	Lumbar disc herniation
6DOF	Six degrees of freedom
FSU	Functional spinal unit
3D	Three-dimensional
2D	Two-dimensional
MRI	Magnetic Resonance Imaging
Nucl	Nucleus
Ant	Anterior
Post	Posterior
LPostLat	Left posterolateral
RPostLat	Right posterolateral
LLat	Left lateral
RLat	Right lateral
LAntLat	Left anterolateral
RAntLat	Right anterolateral
Comp	Compression
Flex	Flexion
Ext	Extension
LAR	Left axial rotation
RAR	Right axial rotation
LB	Lateral bending
RLS	Right lateral shear
LLS	Left lateral shear
AS	Anterior shear
PS	Posterior shear

## Abstract

Repetitive manual handling is a common cause of work-related back disorders, which include disc injuries, such as herniation, and low back pain. Disc herniation commonly occurs in younger individuals aged 25-55 years old as a result of repetitive stressing of the low back, which is associated with lifting. Despite its high resilience, intervertebral discs can be damaged during repetitive loading, causing cumulative damage and leading to injuries. Few *in vitro* studies have developed a mechanistic understanding of disc herniation using macro and microstructural analysis of disc tissue via imaging after repetitive loading. However, the initiation and propagation of disc herniation are still poorly understood since prior studies used non-physiological loading regimes that may impact the mechanism. In addition, no internal disc mechanics were measured during the applied repetitive loading to give an insight into disc tissue deformations and its association to disc injury. Therefore, the overall aim of this thesis was to determine the effects of simulated repetitive lifting and the resulting tissue failure on internal disc strains, and six degrees of freedom (6DOF) disc mechanics.

To achieve this aim, thirty cadaver lumbar functional spinal units (FSUs) were subjected to a sequence of 6DOF testing followed by simulated repetitive lifting (*safe* or *unsafe*) and repeated 6DOF testing. To measure mechanical properties before and after repetitive lifting, the FSUs underwent  $\pm$ 6DOF tests at 0.1 Hz for 5 cycles. Each specimen underwent an equivalent of one year of simulated repetitive lifting under safe (15 FSUs) and unsafe (15 FSUs) levels of compression, in combination with flexion, and right axial rotation for 20,000 cycles or until failure. Safe or unsafe lifting was applied as a compressive load to mimic holding a 20 kg weight either close to, or at arm's length, from the body, respectively. Internal disc strains were measured using a wire-grid and radiosterometric analysis. After testing, failure and disc damage were assessed from comparing pre- and post-test magnetic resonance imaging (MRI) and macroscopically.

For the first time internal disc strains, specifically maximum shear strains (MSS), were measured during simulated repetitive safe lifting. Largest magnitude of percent shear strains was found in the anterior (76%), posterolateral (64%), and left lateral (60%) regions. In addition, MSS only increased by 8% from cycle 1 to cycle 20000, demonstrating the resilience of the disc. After simulated safe repetitive lifting, 73% of specimens were injured, having failure modes of an annular protrusion, endplate failure, or disc herniation. Largest magnitude of percent shear strains, annular protrusion and herniation were found in the posterolateral regions, which is consistent with clinical

observations. The disc mechanics were also altered after simulated safe repetitive lifting. Decreases in stiffness were found in compression, flexion, and lateral shear with an increase in extension. For phase angle, increases were found in compression, left axial rotation, and posterior shear with a decrease in extension. However, there was no association between failure mode and mechanical properties. The changes in mechanical properties could be caused by a combination of deformation in anterior annulus due to the applied flexion, tissue damage, reduced disc height, and a migrating centre of rotation.

Internal disc strains and mechanics were then measured under simulated unsafe repetitive lifting. This loading regime led to 60% of the specimens failing via endplate failure with no disc herniation observed. The largest magnitude of percent MSS was found in the posterolateral (72%) and anterior (70%) regions, which was similar under safe lifting. The MSS of disc protrusion and endplate failure specimens was larger than the no injury specimens, suggesting the existence of a damage threshold of 50% strain. Above this threshold, the risk of tissue damage associated with disc injuries such as disc protrusion and endplate failure increased. Changes in disc mechanics were observed after simulated unsafe repetitive lifting in all 6DOF directions, however, they were no different than those found during safe lifting. The lack of differences between the two groups suggests that measuring the 6DOF mechanics alone was not sufficient to detect tissue level and regional disc damage.

Finally, the associations between internal disc strains, failure mode, and disc damage assessed via MRI and macroscopically for both lifting groups were examined. It was found that MSS increased with progression of disc injury towards herniation in the left lateral region under a combination of repetitive compression, flexion and right axial rotation. This finding provides evidence that the lateral region is more vulnerable than previously understood. Correlations between MSS and tissue damage further verified current clinical knowledge, where damage associated with disc protrusion and disc herniation was predominantly located in the posterior and posterolateral regions. This research further demonstrated that unsafe lifting places the disc at greatest risk of injury.

The disc mechanics measured within this thesis are vital in providing guidelines for finite element models to conduct studies in disc injury and repair, as well as optimising future disc replacement designs. Clinically, this research provides unique insights into the structure-function-injury relationships of disc tissue during repetitive lifting, and in future, may contribute to recommending important preventative lifting strategies in workplace guidelines to minimise the risk of herniation.

## Declaration

I certify that this thesis does not incorporate without acknowledgement any material previously submitted for a degree or diploma in any university; and that to the best of my knowledge and belief it does not contain any material previously published or written by another person except where due reference is made in the text.

Dhara Amin

December 17, 2018

## Acknowledgements

When I moved to Australia in 2014 for my Whitaker International Fellowship, I didn't think I would still be here four years later writing my PhD thesis. Throughout my candidature, I've been able to build amazing relationships and call many of my colleagues, friends and mentors. This note is dedicated to them as I reflect on all of their support and guidance throughout my time here at Flinders University.

I don't think I could have finished this journey without the help and support of my supervisor, John Costi. He has embraced every goal I've set out, supported every competition or grant I've applied to, and dealt with all the ups and downs during my thesis. John has taught me everything about being a scientist and an academic through my years. He has been patient when I've been excited, upset and angry. He's brought clarity to all situations. I, also, am beyond grateful for his support (private scholarship) during my last six months of my candidature, which allowed me to focus on writing. I can't express in words how thankful I am for this, I don't think I would have been able to finish this thesis without the financial support. John has become a friend, a mentor, and someone I look up to! Thank you from the bottom of my heart, John, couldn't have done it without you!

I would also like to sincerely thank Kenneth Pope, Egon Perilli, Mark Taylor, and David Hobbs for all of their guidance in research, teaching, and my career. The chats I've had with each of you have been inspiring, thought-provoking, and very helpful. Thank you for always listening to me in my ups and downs but also allowing me to process and supporting me. You all have become mentors to me and I know I can reach out to each one of you in the future!

To my lab mates and co-authors, you have been the best! It was a pleasure to go through this experience with Javad; thank you for your endless heart to hearts and support in pursuing my goals. To Brian Freeman, you've given me so much advice, that I greatly appreciate. But also, thank you for making conference dinners hilarious, and for your contribution to my research. You always brought a new perspective! To Christina Moawad and Michael Russo, thanks for keeping me sane during my data collection. I had so much fun having a fellow American by my side, Christina! You made coming into the lab at 6 am fun and I definitely miss our chats but also our dance parties in the lab! Michael, I don't know what to say but you're my 'work wife' and I appreciate you so much!

To the Medical Device Research Institute, thank you for all of the support you've provided. More specifically, Kelly Knight, thank you for listening and embracing my ideas but also

helping me out in everything media related. Thank you to Aisha, Aaron, and Karen for all of your support and allowing me to be a part of the Medical Device Partnering Program. To my fellow PhD candidates, these four years would not have been as amazing without you. Dermot, Rowan, Mark, Albert, Laura, Sophie, and Robbie, thank you for lending an ear when I needed it, celebrating with me, engaging in my crazy social ideas, and being my friends. This journey would have been really difficult without you guys and gals.

To engineering services, thank you for all of the technical help. More specifically, Richard, thank you for your jokes and memes but also your support with the hexapod and anything lab related. Thank you to Boyin for the immense amount of help with coding the LabVIEW GUI and your support in regards to the hexapod. Also, sincere thanks to Pawel Skuza for the statistical guidance in my publications. I always learned a lot during our meetings. To Dr Orso Osti, thank you for allowing me to support myself during my PhD. You've pushed me in my writing and my research. It's been a pleasure working with you!

My family and friends. You have been the biggest support system during my time here in Australia. Even with the time difference, you have taken every call and listened to every complaint. I can't thank you enough. To my mom, brother, dad, and grandmother, thank you for the endless love and faith. To my aunts, uncles, and cousins, thank you for your support. To my friends both here and far, you are amazing! Jess, Sarah, Steph, Tyson, Brad, Beau, Jade, Matt, and Emma, thank you so much for the laughs and your faith in me. You guys have always supported me in everything I set out to do but most importantly you've made Australia home! To Mimi, Varisha, Vini, and Princi, you girls rock! Thank you for being my people and acknowledging my hard work. Finally to my friends in the USA, you have stuck with me through these four years and continue to amaze me with your support. Thank you, Chelsea, Ravi, Olivia, Erin, Jenna, and Erica!

Finally, thank you to my guru, Mahant Swami Maharaj, and Bhagwan Swaminarayan, for watching over me and giving me the strength to take on this journey.

## List of Publications

Amin, D.B., Moawad, C.M., Costi, J.J., 2018. New findings confirm regional internal disc strain changes during simulation of repetitive lifting motions. *Annals of Biomedical Engineering*. Manuscript under Review.

Amin, D.B., Moawad, C.M., Costi, J.J., 2018. Lumbar intervertebral disc multiaxial mechanics are altered after simulated repetitive lifting movements. *Journal of Biomechanics*. Manuscript under Review.

Amin, D.B., Moawad, C.M., Costi, J.J., 2018. Effect of unsafe repetitive lifting on disc mechanics: an internal disc threshold and multiaxial mechanical properties. *European Spine Journal*. Manuscript Submitted.

Amin, D.B., Tavakoli, J., Freeman, B.J.C., Costi, J.J., 2018. Understanding the impact of repetitive lifting towards lumbar disc herniation: a clinically relevant biomechanics cadaveric study. *Spine*. Manuscript under Review.

## Conference Abstracts

Amin D.B., Moawad C.M., Costi J.J., Analysis of Internal Disc Strains during simulation of repetitive lifting motions. Australian and New Zealand Orthopaedic Research Society Annual Scientific Meeting, October 2018, Perth, Australia. Oral presentation.

Amin D.B., Moawad C.M., Costi J.J., Multiaxial lumbar intervertebral disc mechanics are altered after simulated repetitive lifting movements. Australian and New Zealand Orthopaedic Research Society Annual Scientific Meeting, October 2018, Perth, Australia. Oral presentation.

Amin D.B., Moawad C.M., Costi J.J., Multiaxial lumbar intervertebral disc mechanics are altered after simulated repetitive lifting movements. Adelaide Centre for Spinal Research, September 2018, Adelaide, Australia. Oral Presentation

Amin D.B., Moawad C.M., Costi J.J., Analysis of internal disc strains and injury during simulation of repetitive lifting motions. International Society of the Study of Lumbar Spine, May 2018, Banff, Canada. Oral Presentation

Amin D.B., Moawad C.M., Costi J.J., Analysis of internal disc strains and injury during simulation of repetitive lifting motions. Spine Society of Australia, April 2018, Adelaide, Australia. Poster Presentation.

Amin D.B., Moawad C.M., Stanley R., Ding B., Costi J.J., Radiostereometric analysis of internal disc strains during more physiological simulation of repetitive lifting motions. Australian and New Zealand Orthopaedic Research Society Annual Scientific Meeting, Sept 2017, Adelaide, Australia. Oral presentation.

Amin D.B., Moawad C.M., Stanley R., Ding B., Costi J.J., Three-Dimensional lumbar intervertebral disc internal strains during combined repetitive loading. Spine Society of Australia, April 2017, Hobart, Australia. Oral Presentation.

## Awards & Prizes

- **Flinders University Student Association (FUSA) Development Grant** to attend the Australian and New Zealand Orthopaedic Research Society (Perth Australia), October 2018
- **Travel Grant** to attend Australian and New Zealand Orthopaedic Research Society Conference, Perth, Australia, October 2018
- **Institute of Engineering and Technology Present around the World Competition Asia Pacific Finalist**, Singapore, Singapore, August 2018
  - Presented on 'Myth busting slipped discs' based on my research
- **South Australian winner of Fresh Science**, Adelaide, Australia, June 2018
  - Resulted in widespread media coverage:
  - Channel 10 Australia:  
[https://m.facebook.com/story.php?story\\_fbid=713340309043604&id=233842463347174](https://m.facebook.com/story.php?story_fbid=713340309043604&id=233842463347174)
  - Channel 9 Australia:  
<https://twitter.com/9NewsAdel/status/1047048108910235649>
  - Channel 7 Australia:  
<https://www.facebook.com/7NewsAdelaide/videos/307390756421147/>
- **Elaine Martin Travel Grant** to attend Internal Society of Study of Lumbar Spine Annual Meeting (Banff, Canada), Awarded \$2000, May 2018
- **Institute of Engineering and Technology Present around the World Competition Australian Winner**, Coogee Beach, Australia, April 2018
- **Best Poster Award**, Spine Society of Australia Annual Meeting April 2018
- **Institute of Engineering and Technology Present around the World Competition South Australian Winner**, Adelaide, Australia, October 2017
- **Semi-Finalist – 3 Minute Thesis Competition** at Flinders University June 2017
- **Best Presentation Award** at Adelaide Centre for Spinal Research Conference August 2015

# Chapter 1 Introduction

## 1.1 Motivation

In Australia, approximately 13.6 percent of the population reported having back problems that include low back pain, disc disorders, and sciatica (AIHW, 2015). Of those, 44 percent have difficulty in completing daily tasks of mobility and self-care (AIHW, 2015). Currently, back disorders impose a financial burden on society, exceeding \$50 billion in the US (Davis et al., 2012) and \$605 million in Australia annually (AIHW, 2009: Cat. no. PHE 115). Furthermore, the second most common back problem for hospitalisation in 2015-2016 was lumbar disc disorders with radiculopathy (10.1 %, (Development, 2014). A common disc disorder with radiculopathy is disc herniation, which is usually associated with work-related injuries that involve repetitive lifting tasks. Disc herniation is common in those aged between 25-64 years (Jordan et al., 2011), with almost a quarter of all work-related injury claims arising from manual labour workers with back problems (AIHW, 2015). Due to the clinical, economical and societal burden of back problems, it is important to study the failure mechanisms that cause disc herniation to help prevent disc injury and develop better treatments.

The disc is a complex resilient structure, composed of a highly hydrated nucleus pulposus, a fibrocartilaginous annulus fibrosus, and vertebral endplates. The hydrated nucleus acts as a shock absorber that is pressurized when subjected to axial compressive loads, which create radial compressive and circumferential tensile stresses in the annulus. This mechanism allows the disc to resist and distribute compressive, bending, shear and twisting movements. However, during herniation, damage to the annulus leads to tears through which nuclear material extrudes, causing a loss of hydration and pressure. The extruded nucleus impinges on the spinal nerves causing radicular pain down the legs called sciatica.

Manual handling guidelines recommend safe lifting limits of 25 kg for men and 16 kg for women when loads are held close to the body (Administration; Cooper, 2018). The recommended maximum weight is *reduced* to 5 kg for loads being held at arm's length (Administration; Cooper, 2018). Unsafe lifting practice occurs when these limits have been exceeded. Herniation is commonly caused by repetitive lifting during bending and twisting (Kelsey et al., 1984b), however, these motions are difficult to apply in-vitro without using a six degree of freedom (6DOF) mechanical testing device. In-vitro studies have attempted to reproduce disc herniation by applying a sudden or repetitive (fatigue) load of compression + flexion, + axial rotation or + lateral bending (Adams and Hutton, 1982,

1985; Berger-Roscher et al., 2017; Callaghan and McGill, 2001; Gordon et al., 1991; Wade et al., 2014, 2015). Repetitive loading is representative of a manual handlers' loading history on the spine, which can lead to gradual failure of the disc. In contrast, applying a sudden overload mimics disc injury by a car accident or awkward falls.

These in-vitro studies have contributed to the current understanding of disc herniation initiation/propagation and the site of failure. Disc herniation occurs by either annulus rupture or annulus - endplate junction failure (Wade et al., 2014), with the latter occurring more often (Rajasekaran et al., 2013). However, the two loading regimes (sudden overload vs. repetitive loading) have led to different mechanistic theories regarding the initiation and propagation of herniation based on structural (macro and micro) analysis. Nucleus extrusion via endplate junction failure was found more so under sudden overload versus annulus failure under repetitive loading.

To further understand the propagation of disc herniation under repetitive loading and how this affects the mechanical function of the disc, it is important to measure internal disc mechanics. Disc pressure measurements can provide information on internal tissue 'stress profiles', in particular for the nucleus (McMillan et al., 1996), and internal disc strains have been measured using various techniques (Costi et al., 2007; O'Connell et al., 2007; O'Connell et al., 2011b; Showalter et al., 2016; Tsantrizos et al., 2005; Yoder et al., 2014). The measurement of internal disc deformation and 6DOF disc mechanics can provide an understanding of the effects of repetitive lifting on the disc tissue and identify the strain/stiffness thresholds that indicate damage progression to lumbar disc herniation. However, strains have only been measured in cadaveric specimens during isolated 6DOF directions using radiostereometric analysis with markers (Costi et al., 2007; O'Connell et al., 2007) and under physiological loads of compression using MRI (O'Connell et al., 2007). Furthermore, no studies have measured three-dimensional (3D) internal disc strains in lumbar spine segments during simulated repetitive lifting (physiological loading) to understand disc injury/herniation propagation.

## 1.2 Aims

Therefore, the overall aims of this research were to understand the effects of simulated repetitive lifting on disc tissue by measuring internal disc strains, 6DOF mechanical properties, and using imaging for structural analysis. More specifically, the aims were:

**Aim 1:** Develop and validate a method for measuring internal 3D disc strain during repetitive loading.

**Aim 2:** Measure the change in internal 3D disc strains during simulated safe and unsafe repetitive lifting in lumbar spinal segments from donors aged between 25 and 64 years old.

**Aim 3:** Measure the effect of simulated repetitive lifting (safe and unsafe) on 6DOF mechanical properties (stiffness and phase angle) and the resulting failure mode.

**Aim 4:** Compare simulated safe and unsafe repetitive lifting to examine whether unsafe lifting leads to a greater risk of disc injury.

**Aim 5:** Examine the correlations between tissue damage assessed via imaging, internal disc strains, and failure mode after simulated repetitive lifting.

Safe repetitive lifting was defined as low compression repetitive lifting where a combination of 1.0 MPa compression + bending + axial rotation was applied to the specimens. Unsafe repetitive lifting was defined as high compression repetitive lifting where a combination of 1.7 MPa compression + bending + axial rotation was applied to the specimens.

### 1.3 Significance

This research will determine, for the first time, the mechanical failure criteria of lumbar disc tissue after repetitive combined lifting motion by measuring how lumbar disc tissue deformation (strain) changes, and how they relate to changes in macroscopic assessment of tissue damage. Scientifically, the magnitudes of internal disc strains will provide physiological guidelines for conducting studies on disc injury and repair using finite element models, as well as optimising future disc replacement designs. Clinically, this research will provide unique insights into the structure-function-injury relationships of disc tissue during daily activities and may contribute to recommending important preventative lifting strategies in workplace guidelines to minimise the risk of herniation.

### 1.4 Thesis Outline

To achieve the aims outlined above, the thesis is organised into the following chapters:

**Chapter 1** presents the introduction to the thesis, highlighting the motivation, aims, and significance of this body of work

**Chapter 2** provides a review of the literature contributing to current knowledge of the mechanisms involved in lumbar disc herniation

**Chapter 3** validated the strain measurement technique and measured internal disc strains during simulated safe lifting (*Aim 1 and Aim 2*)

**Chapter 4** measured 6DOF disc mechanics before and after simulated safe repetitive lifting (*Aim 3*)

**Chapter 5** explored the effect of simulated unsafe repetitive lifting on internal disc strains and 6DOF mechanics. A comparison between the two loading modalities was also determined. (*Aim 2, Aim 3, and Aim 4*)

**Chapter 6** examined the correlations between internal disc strains and tissue damage assessed via imaging (*Aim 4 and Aim 5*)

**Chapter 7** presents the conclusions and future recommendations

**Appendix A:** Error between x-ray detector positions in relation to the strain measurement technique

**Appendix B:** Validation of strain measurement technique

**Appendix C:** Principal strains

**Appendix D:** Specimen-specific maximum shear strain contour plots under simulated unsafe lifting

**Appendix E:** Bending and rotational moments, compressive force, and disc height at the start and end of the simulated repetitive lifting

**Appendix F:** 6DOF load – unload curves before and after simulated unsafe repetitive lifting

**Appendix G:** Comparison of the mechanics associated with safe and unsafe repetitive lifting

**Appendix H:** Disc damage score

**Appendix I:** Axial MR images, macroscopic images and shear strain contour plots for the association of disc damage and internal disc strains after simulated repetitive lifting



## Chapter 2 Literature review

### 2.1 Anatomy

The primary function of the human spine is to provide support for the body's weight, protect the spinal cord, and allow for mobility. The spine consists of stacked vertebrae with intervertebral discs (disc) in between for distribution of the load as well as ligaments and muscles for support.

#### 2.1.1 Lumbar vertebral column

The lumbar vertebral column is located at the bottom of the spine, above the sacrum, connecting the thoracic spine to the pelvis. It consists of five vertebrae, sequentially named (from superior to inferior) L1 to L5 with their respective disc, where the disc is named according to the adjoining vertebra (e.g. L1-L2 disc). The vertebrae and discs within the lumbar region are the largest of the entire spine since they support most of the body's weight. Lordosis is found within this section of the spine due to the erect stance of humans (Adams, 2002).

#### 2.1.2 Intervertebral disc

The lumbar disc is a highly complex structure that absorbs and transmits significant loads along the spinal column while allowing deformation for flexibility. The disc is also the largest avascular organ the human body and composed of three components: the nucleus pulposus (nucleus), annulus fibrosus (annulus), and cartilaginous endplates (CEP, **Figure 2-1**).

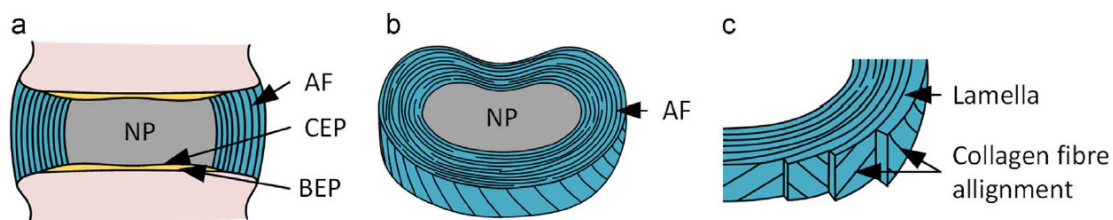


**Figure 2-1** Transverse and coronal sections of the disc (Newell et al., 2017). AF – Annulus Fibrosus, NP – Nucleus Pulposus, BEP – Boney Endplate, CEP – Cartilaginous Endplate

##### 2.1.2.1 Nucleus Pulposus

The nucleus pulposus is the inner gelatinous centre of the disc that behaves like a pressurised fluid, which is constrained by the concentric lamellae of the annulus fibrosus. It is composed of water (70-85%, (Keyes and Compere, 1932; McNally and Adams, 1992),

proteoglycans (~50% dry weight, (Adams, 2002; Dickson et al., 1967; Iatridis et al., 1996), and collagen (<20% dry weight, (Adams, 2002; Eyre, 1988; Inoue and Takeda, 1975). Proteoglycans are molecules that can retain large amounts of water, allowing the nucleus to bulge radially when compressed, helping to brace the annulus and resist compressive loads (Keyes and Compere, 1932; McNally and Adams, 1992). If the nucleus loses its capability to retain water, the annulus is more likely to buckle, and the tissue is then continuously compressed. The majority of the collagen is type II, which is commonly found in compressive load-bearing structures such as articular cartilage (Adams, 2002; Eyre, 1988; Iatridis et al., 1996).

#### 2.1.2.2 Annulus Fibrosus

The annulus fibrosus is made up of fifteen to twenty 0.05 to 0.5 mm thick concentric lamellae (sheets of collagen) packed together circumferentially around the nucleus (Cassidy et al., 1989; Inoue and Takeda, 1975; Marchand and Ahmed, 1990). The fibres in each lamella are arranged obliquely from the vertebrae at an angle of approximately 65° to the longitudinal axis, with their orientation alternating in successive lamellae (Adams, 2002). This orientation the structure and helps resist tension. Furthermore, the strong and stiff nature of the annulus in addition to a pressurised nucleus allows the disc to sustain high compressive loads, however, it is still pliable to allow for bending motions (Adams, 2002).

The majority of the annulus consists of water (60-75%), proteoglycans (~20% dry weight), collagen (50-70% dry weight), and elastin (2%), (Adams, 2002; Adams et al., 1977; Buckwalter, 1995; Mikawa et al., 1986; Yu et al., 2005). Type I collagen is the most abundant and is found predominately in the outer annulus. Other tensile structure like ligaments and skin also contain type I collagen. The concentration of type II collagen increases in the inner annulus due to its proximity to the nucleus (Adams, 2002).

#### 2.1.2.3 Cartilaginous Endplates

The cartilaginous endplates are located at the superior and inferior ends of the disc, binding the disc to the vertebral bodies. These endplates cover the nucleus and part of the annulus, not extending to the periphery of the annulus since the ring apophysis encircles the endplate (Adams, 2002). The fibres of the annulus are anchored superiorly and inferiorly into the endplates (Hashizume, 1980; Inoue, 1981; Rodrigues et al., 2012). It is primarily made up of hyaline cartilage. The endplate is known to play a role in the nutrition of the disc and if the endplate is damaged, the swelling of the disc and nutrient transfer are disrupted (Adams, 2002).

### 2.1.3 Lumbar Vertebra

The lumbar vertebra is one unit that consists of the lumbar vertebral body and posterior elements. The body is a short bone that is comprised of trabeculae bone surrounded by cortical bone (Adams, 2002). Each vertebral body is separated by the disc and zygapophysial joints (posterior elements).

Posterior elements of the vertebra include the pedicles, transverse processes, spinous process and articular processes (**Figure 2-2**). Each pedicle is a pillar of bone located on the posterolateral side of the vertebral body. They are known to transmit forces from the posterior elements to the vertebral body. From the pedicles, a plate of bone called lamina projects to the midline fusing together to form the spinous process (**Figure 2-2**). The vertebral foramen is the space or channel where the spinal cord passes through. A rectangular, flattened bar of bone, called the transverse process, projects laterally from the junction of the pedicle and lamina. These processes are sites of muscle attachments (Adams, 2002).

This image was removed for copyright purposes

**Figure 2-2** The components of the lumbar vertebral body (Adams, 2002)

The superior articular facet of one vertebra joins with the inferior articular facet of another vertebra to make the zygapophysial joint (facet joint, **Figure 2-3**). This joint provides a locking mechanism between two consecutive vertebrae, limiting their rotational and sliding (shear) movements (Adams, 2002).

This image was removed for copyright purposes

**Figure 2-3** Posterior view of the zygapophysial (facet) joint, showing the connection between the superior articular processes and inferior articular processes (Adams, 2002)

### 2.1.4 Ligaments

There are five important ligaments within the vertebral column: ligamentum flavum (LF), supraspinous ligament (SSL), interspinous ligament (ISL), anterior longitudinal ligament (ALL), and posterior longitudinal ligament (PLL). The PLL and ALL are ligaments that run along the posterior and anterior surfaces of the disc respectively, connecting the discs and vertebral bodies. In particular, the PLL is an important ligament for protecting against posterior disc injuries that may impact the spinal cord. Additionally, it has been

shown that ligament damage can increase the risk of LDH (Adams and Hutton, 1982; Siddiq et al., 2019).

### 2.1.5 Functional Spinal Unit

The functional spinal unit (FSU) consists of a vertebra – disc –vertebra segment (**Figure 2-4**) and is primarily used in biomechanical testing of the disc. FSUs include the posterior elements and all five previously mentioned ligaments.

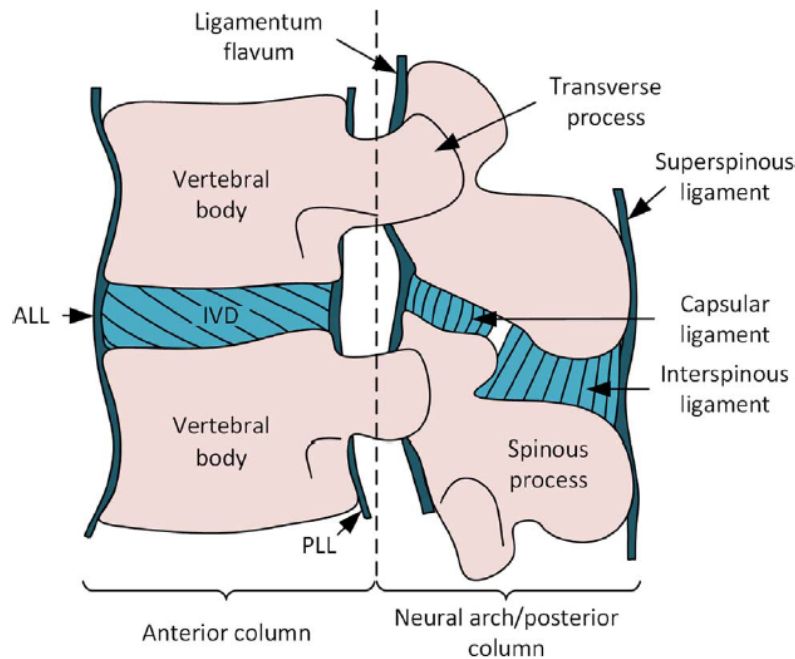


**Figure 2-4** Functional spinal unit including the locations of the ligaments (Newell et al., 2017)

## 2.2 Disc Degeneration<sup>1</sup>

Disc degeneration is associated with biochemical and mechanical changes resulting from structural alterations in the nucleus pulposus, annulus fibrosus and vertebral endplate (Adams et al., 2000; Galbusera et al., 2014). The loss of water in the nucleus and corresponding decrease in disc height places higher stresses on the annulus (Adams et al., 1996), theoretically contributing to greater viscous damping of the solid phase than seen in normal disc tissue. These increased annular stresses may lead to the formation of annular tears and clefts (Osti et al., 1992; Przybyla et al., 2006; Vernon-Roberts et al., 2007), calcification of the endplates (Benneker et al., 2005; Rajasekaran et al., 2010; Wang

<sup>1</sup> The description of disc degeneration is taken from the following paper: Amin, D.B., Sommerfeld, D., Lawless, I.M., Stanley, R.M., Ding, B., Costi, J.J., 2016. Effect of degeneration on the six degree of freedom mechanical properties of human lumbar spine segments. *Journal of orthopaedic research* : official publication of the Orthopaedic Research Society.

et al., 2012) and an increase in osteophyte formation (Al-Rawahi et al., 2011; Lipson and Muir, 1980). In addition to structural changes, disc degeneration can lead to clinical and mechanical instability (Kirkaldy-Willis and Farfan, 1982; Morgan and King, 1957).

Clinically, the definition of joint instability is when a patient with back problems transitions from mildly to severely symptomatic with the least provocation (Kirkaldy-Willis and Farfan, 1982). Kirkaldy-Willis and Farfan further characterised the relationship between degeneration and instability by defining three clinical and biomechanical stages: temporary dysfunction, instability, restabilisation (Kirkaldy-Willis and Farfan, 1982). Furthermore, mechanical instability is defined as increased abnormal motion relative to the load applied in comparison to normal, which does not necessarily always evoke a clinical response (Kirkaldy-Willis and Farfan, 1982).

### 2.3 Biomechanical testing of the intervertebral disc

The human spine is a complex structure that allows for multi-directional, 6DOF movements under dynamic loads during daily activities. Understanding how the spine responds to those movements and loads is critical for the development of new spinal implants and surgical treatments for disc injuries. To experimentally measure this response *in vitro*, excised human FSUs are mechanically tested to obtain viscoelastic and poroelastic properties of the disc by measuring stiffness, phase angle, and range of motion. These properties have been extensively studied under uniaxial compression (Beckstein et al., 2008; Koeller et al., 1984; O'Connell et al., 2011a; Virgin, 1951). However, the natural loading conditions of the spine during daily life are not limited to compression, therefore it is important to understand its behaviour in all 6DOF loading directions (anteroposterior/lateral shear, axial rotation, lateral bending, flexion, extension, and compression, **Figure 2-5**).

Panjabi et al. first proposed applying six forces and six moments on thoracic spinal segments to obtain three-dimensional loading curves of the disc (Panjabi et al., 1976). Later, Patwardhan et al. demonstrated the need for a compressive axial follower load on lumbar spinal columns (L1-S1) during 6DOF testing, in order to better mimic physiological conditions (Patwardhan et al., 1999). A variety of 6DOF loading devices and corresponding testing protocols have been developed to apply those forces and moments. For example, a system of pulleys and weights (Panjabi et al., 1981), cables and linear actuators (Lysack et al., 2000; Patwardhan et al., 1999), or stepper motors and linear bearings (Goertzen et al., 2004; Wilke et al., 1994) have been used. More recent technologies have allowed the use of a robotic arm (Thompson et al., 2003) or a Stewart platform (Ding et al., 2014;

Stokes et al., 2002) for application of more accurate 6DOF loading on biological specimens and measurement of mechanical properties.

However, most daily activities and motions that lead to disc injury involve a combination of motions rather than just one. This introduces a new complexity to the testing and requires the use of enhanced testing devices like the robotic arm or Stewart platform, which can simultaneously apply multiple loading directions on the FSU.

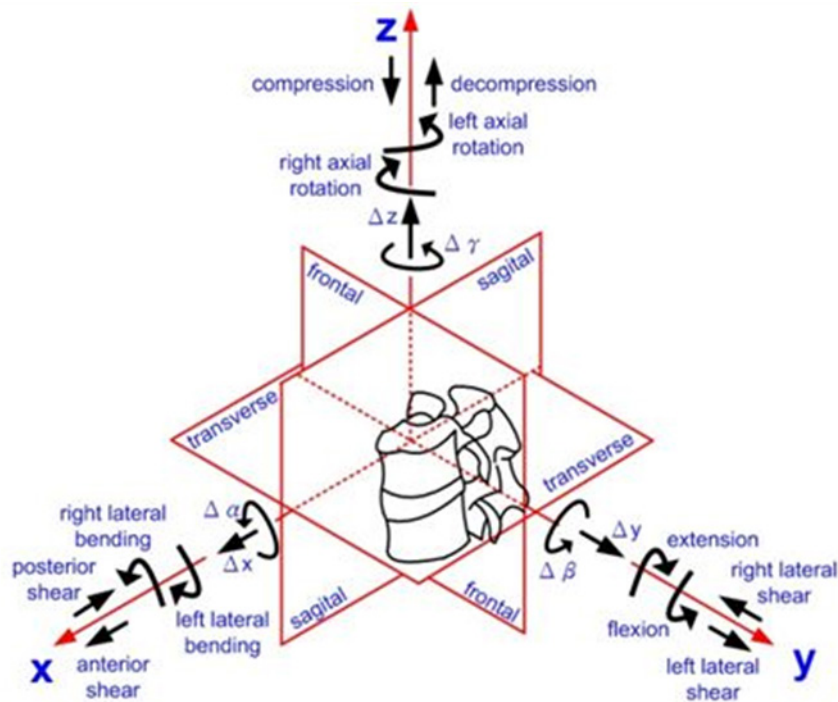


**Figure 2-5** Twelve loading directions applied to the FSU (Chang et al., 2011)

### 2.3.1 Compression

Under compression, the nucleus is pressurised and the annulus bulges radially as the force is transferred down the spine. The engagement of the facet joints during compression is dependent on disc degeneration, posture, and time of day, and the ligaments are not engaged during compression (Adams, 2002). High compressive loads can lead to endplate fracture or crushing of the vertebra (Adams and Dolan, 2012; Brinckmann et al., 1988; Hamanishi et al., 1994). The axial compressive properties of the disc have been measured most often. Compressive modulus of the FSU ranges from 4 – 25 MPa (Amin et al., 2016a; O'Connell et al., 2015) and stiffness from 1000 – 5000 N/mm (Alkalay et al., 2015; Amin et al., 2016a; Beckstein et al., 2008; Costi et al., 2008; Kasra et al., 1992).

### 2.3.2 Flexion and Extension

Flexion and extension are the forward or backward bending of the spine, respectively. Under flexion, the anterior annulus is compressed, while the posterior annulus is

stretched. Flexion also stretches the posterior ligaments (PLL, ISL, and SSL) and decompresses the facet joints (Adams, 2002). The *in vivo* range of motion for flexion increases from 8° at L1-2 to 13° at L4-5 and decreases to approximately 8° at the L5-S1 disc (Pearcy et al., 1984; Pearcy and Tibrewal, 1984). These ranges of motion are important in understanding the physiological limit of the spine. Costi et al. measured 6DOF mechanical properties (stiffness and phase angle) of normal disc tissue without facets, while Amin et al., measured 6DOF properties of degenerative disc tissue with facets (Amin et al., 2016b; Costi et al., 2008). These studies found that flexion stiffness ranged from 1 – 4 Nm/°. However, most studies that measure bending properties of the disc have reported ROM as they have loaded the disc under a pure bending moment without a compressive preload (Fujiwara et al., 2001; Krismer et al., 2000; Tanaka et al., 2001; Zirbel et al., 2013). It is important to note that bending stiffness is non-linear, where stiffness increases with compressive preload (Amin et al., 2016b; Costi et al., 2008).

Under extension, the posterior annulus is compressed, and the anterior annulus is stretched. The ALL is stretched while the other ligaments are not engaged (Adams, 2002). The facet joints are engaged during extension and limit the range of motion in this direction. The *in vivo* range of motion for extension decreases from 5° at L1-2 to 1° at L3-4. It then increases to 2° at L4-5 and 5° at L5-S1 (Pearcy et al., 1984; Pearcy and Tibrewal, 1984). Extension stiffness of the disc ranges from 4.7 to 15 Nm/° (Amin et al., 2016b; Costi et al., 2008).

### 2.3.3 Lateral Bending

Lateral bending is bending to the side, where either the left or right lateral annulus is compressed, while the contralateral side is stretched. During lateral bending, the facet joint is engaged. The *in vivo* range of motion for lateral bending is similar from L1-2 to L3-4 at about 5° and then decreases to 2° at L4-5 and 1° at L5-S1 (Pearcy and Tibrewal, 1984). The lateral bending stiffness of the disc ranges from 3.5 to 5 Nm/° (Amin et al., 2016b; Costi et al., 2008; Zirbel et al., 2013).

### 2.3.4 Axial Rotation

Axial rotation is the twisting of the spine, where the fibres of the annulus in the direction of twisting will undergo tension. Furthermore, the facet joints restrict the *in vivo* rotational movement of the spine to about 1° (Pearcy and Tibrewal, 1984). Axial rotation stiffness of the disc ranges from 1.5 to 8 Nm/° (Amin et al., 2016b; Costi et al., 2008; Zirbel et al., 2013).

### 2.3.5 Shears

Anterior, posterior and lateral shear are forward, backward and sideways (respectively) translation of the spine. Shear forces play an important role in injuries and engage the facet joint (Kim et al., 2012; Marras et al., 2001). Clinical research has shown that people with lower back pain experience a 75% greater lateral shear force than those without (Marras et al., 2001), indicating the importance of shear loading and its mechanical response (Kim et al., 2012; Lu et al., 2005). However, the shear mechanics of the disc/FSU have not been extensively studied. Stiffness in anterior shear ranges from 100 – 800 N/mm and in posterior shear, it ranges from 200 – 480 N/mm (Amin et al., 2016b; Costi et al., 2008; Lu et al., 2005). Lateral shear stiffness ranges from 150 – 300 N/mm (Amin et al., 2016b; Costi et al., 2008).

The previously reported stiffness magnitudes in all the 6DOF directions are for discs that range from normal to severely degenerated. Stiffness decreases with an increase in degeneration until it stabilises at Pfirrmann grade 5 (Pfirrmann et al., 2001) by increasing in the shear and bending directions (Amin et al., 2016b). However, in compression, stiffness continues to increase as degeneration progresses. These changes help our understanding of how disc degeneration affects the disc. It's important to note that there is no current information on 6DOF stiffness or energy absorption of normal discs with facet joints.

Other studies have also measured mechanical properties of the disc under bending and compression to understand the effects of nucleotomy (removal of the nucleus, (Showalter et al., 2014) or disc lesions (injury to disc annulus,(Thompson et al., 2000). Nucleotomy leads to a decrease in compressive modulus and stiffness. Disc lesions such as annular tears (radial and concentric) and rim lesions lead to an increase in stiffness in flexion and extension, however, a decrease in stiffness for axial rotation. Understanding the changes in 6DOF mechanics after disc injury can give insights into preventive measures and considerations for developing new implants or therapies.

## 2.4 Lumbar Disc Herniation

Direct health expenditures for back disorders, including disc injuries, in 2008-2009 amounted to \$320 million in Australia, which was 12% of total musculoskeletal expenditure. Disc disorders are both a social and economic burden on society ((AIHW), 2009). Lumbar disc herniation (LDH) is a disc injury found amongst younger individuals in comparison to other musculoskeletal diseases, with a majority (two thirds) lying within the 25-64 year age group (Jordan et al., 2011). Males are three times more likely to

experience an LDH than females (Awad and Moskovich, 2006). The most common cause for LDH was body stressing through repetitive movement or handling objects in a work environment (AIHW, 2015).

LDH is defined as the migration of nucleus pulposus material away from its natural position within the disc, disrupting the annulus and impinging on the spinal nerves (**Figure 2-7**). There are three clinical classifications of herniation: protrusion, extrusion, and sequestration (**Figure 2-6**, (Adams and Hutton, 1982; Awad and Moskovich, 2006; Jordan et al., 2011). A disc protrusion occurs when the annulus bulges, however, all nuclear material is still contained within the disc. This is the mildest form of herniation. A disc extrusion occurs when the annulus is ruptured, and nuclear material is extruded but still attached to the disc, impinging on the spinal nerves. Finally, the most severe form of LDH is classified as a disc sequestration. This is when the extruded nuclear material is no longer attached to the disc. The composition of the herniated tissue is mostly nuclear material but it can consist of annular or endplate material (Moore et al., 1996).

**This figure was removed due to copyright purposes**

**Figure 2-6** Images of the three clinical classifications of LDH: disc protrusion, nuclear extrusion, and sequestration (**Source:** [https://www.shutterstock.com/image-illustration/types-stages-lumbar-disc-herniation-herniated-289987997?src=LlwzvqU2zuBWUFb8\\_JDjiA-1-1](https://www.shutterstock.com/image-illustration/types-stages-lumbar-disc-herniation-herniated-289987997?src=LlwzvqU2zuBWUFb8_JDjiA-1-1))

Herniated discs are commonly found in the lower back (lumbar region) but can also occur in the neck (cervical region) and rarely in the mid-back (thoracic region). Clinically, the diagnosis of LDH can be confirmed via a physical examination and magnetic resonance imaging (MRI, **Figure 2-7**).

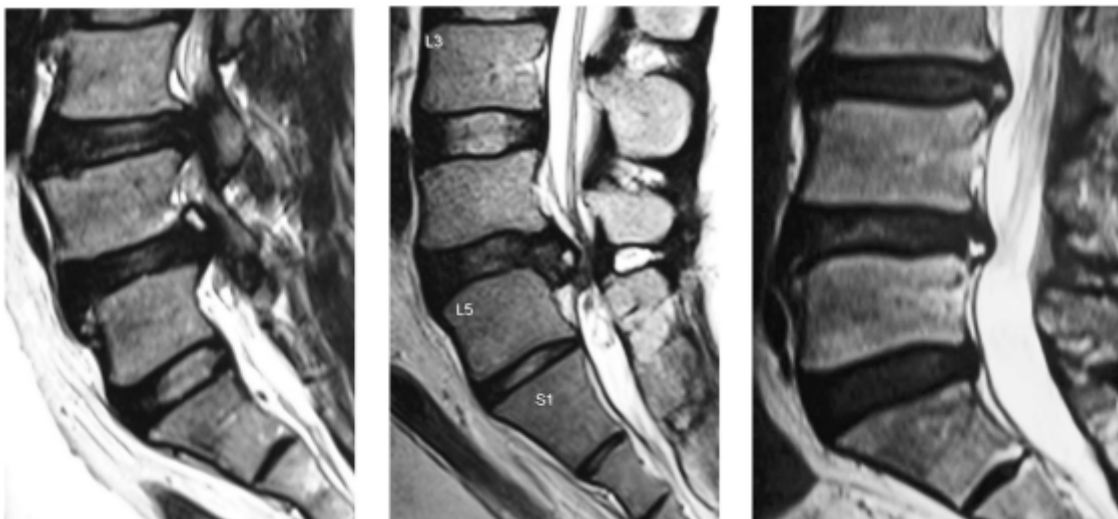


**Figure 2-7** MRI images of LDH (Rajasekaran et al., 2013)

### 2.4.1 Symptoms/Effects

Symptoms include radiating pain from the buttock, down the leg, to the feet. Often there is numbness or tingling in the feet or muscle weakness. These symptoms are known as sciatica and occur because the extruded spinal tissue is impinging ON the nerves in the spine, causing pain in the extremities. Approximately 1-2% of the population between the ages of 30-50 are affected by sciatica (Jordan et al., 2011). Long terms effects can include disc degeneration and low back pain (Adams et al., 2000; Vernon-Roberts et al., 1997; Videman et al., 1990).

### 2.4.2 Clinical Causes

Seeing as LDH is diagnosed retrospectively, after patients present with pain, it is difficult to predict how the herniation occurred. Factors that can increase the risk of herniation include:

- a. **Repetitive lifting:** Mechanical fatigue from repetitive heavy lifting can lead to disc failure (Kelsey et al., 1984b).
- b. **Sudden impact:** Impacts on the spine found in car accidents or injury can cause high compressive forces and hyperflexion in the disc (Adams and Hutton, 1982).
- c. **Long durations of sitting:** Desk jobs call for long durations of sitting, which causes higher disc pressure (Andersson, 1981), and flattens the lumbar lordosis (Wilder et al., 1988).
- d. **Excessive vibration:** Source of vibration (i.e. truck driving) that loads the spine cyclically at its natural frequency. This is where people experience the largest internal mechanical stresses and strains (Wilder et al., 1988).
- e. **Disc degeneration:** As the disc degenerates, there are more annular tears and clefts (Lama et al., 2013; Moore et al., 1996).
- f. **Obesity:** Excessive body weight can put more mechanical stress on the spine and disrupt disc nutrition (Shiri et al., 2014).
- g. **Consequences of Smoking:** Coughing due to smoking can put more pressure on the lumbar discs (Kelsey et al., 1984a).
- h. **Pregnancy:** More mechanical stress on lumbar discs from carrying the fetus and ligamentous laxity at the end of pregnancy (Kelsey et al., 1975).

### 2.4.3 Treatment

The type of treatment is a controversial topic amongst clinicians. Some believe that surgical intervention is the best treatment for herniation and others believe that medicine and therapy are more appropriate. However, treatment depends on the severity of the herniation, length of time, and the nature of the symptoms.

### 2.4.3.1 Nonsurgical Treatments

Nonsurgical treatments such as rest, anti-inflammatories, epidural injections and physical therapy are the first form of treatment. Most herniated discs resolve on their own within 6-12 weeks and approximately 80% achieve a good recovery with nonsurgical treatments (Weber, 1994). Anti-inflammatories and epidural injections can help with reducing pain and inflammation while increasing mobility. Physical therapy increases core strength and flexibility, allowing the patient to return to normal activities. Nonsurgical treatments are successful because the volume of herniated tissue decreases and the nucleus pulposus is reabsorbed (Cribb et al., 2007). Once the disc ruptures, the immune system can then absorb the material in the spinal canal by sending macrophages, allowing the herniation to subside naturally (Cribb et al., 2007).

### 2.4.3.2 Surgical Treatments

If excruciating pain is still persistent after 6-8 weeks, or if the patient has a massive extrusion or sequestration, the surgeon will most likely operate (Awad and Moskovich, 2006). Surgical treatment addresses the leg symptoms rather than the back pain. The surgical treatment for an LDH is a discectomy, where the surgeon removes up to 2 grams of NP (Awad and Moskovich, 2006; Moore et al., 1996). In the US alone, approximately 300,000 discectomies are performed each year, which makes it the most common surgical procedure performed by a spine or neurosurgeon (Koebbe et al., 2002). The removal of herniated tissue from the discectomy could change the disc mechanics and potentially lead to disc degeneration, however, this is still unknown.

## 2.5 LDH due to lifting

Industries with the highest number of compensation claims include manufacturing, health, community services, and construction. About 43% of those claims can be attributed to body stressing through repetitive movement or handling objects and 23% of those claims indicated that the location of injury was the back ((AIHW), 2009). Furthermore, epidemiological studies have concluded that repetitive heavy lifting is associated with an increased risk of LDH (Andersson, 1981; Kelsey, 1975; Kelsey et al., 1984b; Mundt et al., 1993). Seidler et al., found that repetitive weight lifting or carrying is significantly associated with LDH, which is accompanied by natural osteochondrosis or spondylosis (Seidler et al., 2003).

Andersson et al. found that frequent lifting with twisting or lateral bending can lead to increased back pain (Andersson, 1981). Kelsey et al. concluded that there is a high risk for LDH when lifting more than 11.3 kg with twisting and knees not bent (Kelsey et al.,

1984b). Those whose job required lifting more than 11.3 kg more than 25 times per day on average had a three times greater risk of LDH than those who did not (Kelsey et al., 1984b). Bending the knees while lifting heavy objects, allows the legs to take most of the load, reducing the stresses within the back (Kelsey et al., 1984b). In addition, *in vivo* disc nucleus pressure measured when lifting a 20 kg box with straight knees was 2.3 MPa in comparison to 1.7 MPa with flexed knees (Wilke et al., 1999). Similar increases in nucleus pressure were observed when holding a 20kg box close to the body (1.0 MPa) versus at arm's length (1.8 MPa, (Wilke et al., 1999). Adding a twist while bending to lift increased the risk of LDH even if the lifting was less frequent. However, twisting or torsion on its own does not increase the risk of LDH (Kelsey et al., 1984b).

Biomechanical studies using cadaver tissue have made similar conclusions where torsion did not lead to herniation (Adams and Hutton, 1981), however, combined compression, flexion and axial rotation (Drake et al., 2005; Farfan et al., 1970; Veres et al., 2010) or lateral bending did (Adams and Hutton, 1982; Shirazi-Adl, 1989). Finite element studies have shown that axial rotation and lateral bending during lifting can put the disc at great risk of injury as the fibre and shear strain and stress are the largest in the posterolateral region (Natarajan et al., 2008; Schmidt et al., 2007b; Shirazi-Adl, 1989). Taken together, unsafe lifting can be classified as lifting by bending and twisting, while not flexing the knees, or by holding an object at arm's length.

## 2.6 Biomechanics of Repetitive Lifting

During lifting, the back muscles generate an extensor moment (EM) to counteract the forward bending moment created from your body weight and the weight being lifted (**Figure 2-8** and **Figure 2-9**, (Adams, 2002). Lifting without bent knees increases the lever arm (D) and increases the compressive and shear force applied to the spine (**Figure 2-8**). However, lifting with bent knees decreases the lever arm (D) and decreases the force (**Figure 2-9**). In addition, bent knees help keep the back straight, while bending down with straight legs can lead to a rounded back, which then increases the disc pressure and intra-abdominal pressures applying further strain on the back muscles and leading to back pain (Adams, 2002). Further considerations include the distance between the body and the weight being lifted. If the object is closer to the body, it is more beneficial than further away from where arms are extended as that increases the lever arm and thus the moment (Andersson et al., 1976; Wilke et al., 1999).

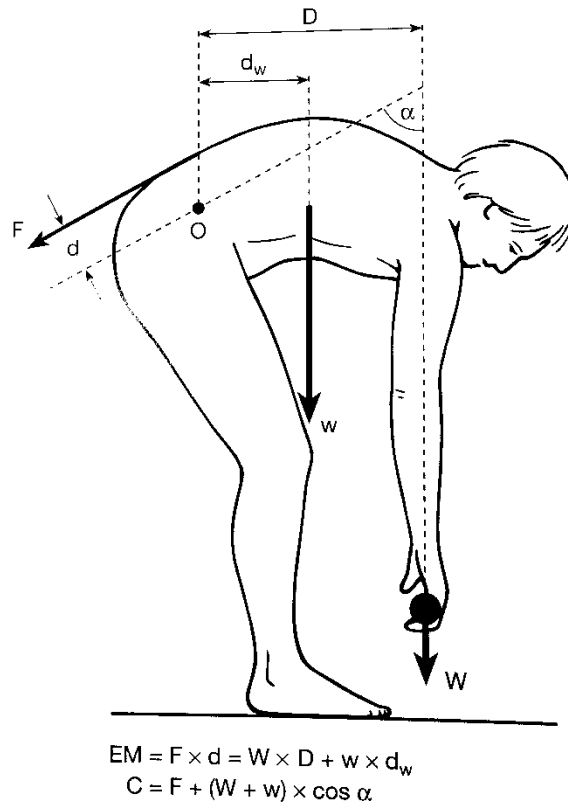


**Figure 2-8** During lifting the back muscles generate an extensor moment (EM) to overcome the flexion moment due to body weight ( $w$ ) and weight being lifted ( $W$ ). The average lever arm ( $d$ ) of the extensor muscles is much smaller than lever arms  $D$  and  $d_w$  of  $W$  and  $w$ , respectively. Therefore, the force in the back muscles ( $F$ ) is much greater than  $W$  or  $w$  and the spine is subjected to a high compressive load.  $O$  is defined as the location lumbar disc and  $\alpha$  is the forward bending angle (Adams, 2002)

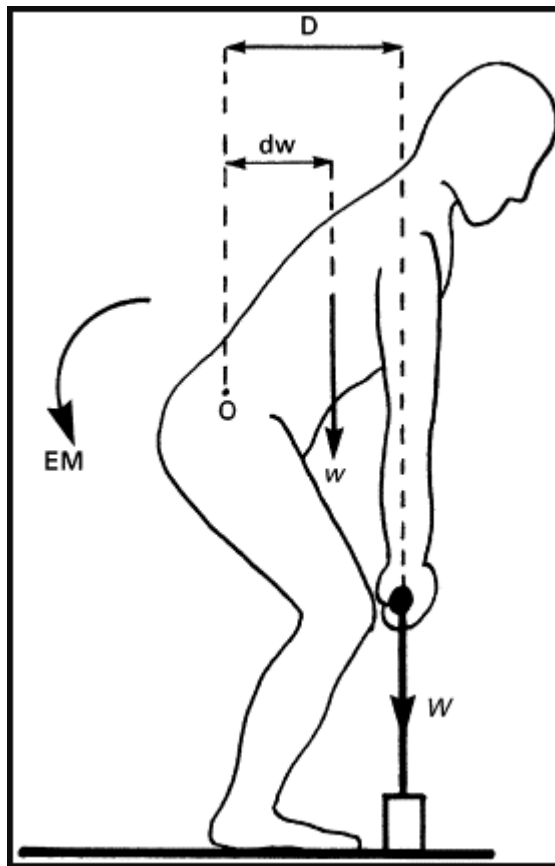


**Figure 2-9** Free Body Diagram of lifting a weight with bent knees and straight back, where EM is the extension moment (Adams, 2002; Dolan and Adams, 1998). Refer to **Figure 2-8** for definitions of each symbol

Kinematics studies have found that repetitive lifting (symmetric and asymmetric) leads to fatigue of the erector spinae muscles (Bonato et al., 2003; Dolan and Adams, 1998; Mehta et al., 2014). Fatigue leads to a significant increase in lumbar flexion angle (4.7°, (Dolan and Adams, 1998; Mehta et al., 2014), and a 36% increase in bending moment acting on the lumbar spine (Dolan and Adams, 1998). In contrast, there is a decrease in extensor moment with an increase in a number of lifts, which is likely due to the transition from lifting with the legs to bent back lifting (Dolan and Adams, 1998). Increases in the bending moment acting on the lumbar spine were also found with heavier weights and increased lift frequency (Lavender et al., 1999; Marras et al., 2006). When lifting with a twist, the rotation moment is the greatest when lifting an object in front and then placing it to the side and is dependent on lift frequency (Lavender et al., 1999). With lateral bending, the moment is greatest when moving the object from one side to another with greater moments produced with larger reach distance (Lavender et al., 1999).

However, the effect of repetitive lifting on the disc, which is a site of injury, is poorly understood. Natarajan et al. used finite element modelling to apply kinematic data (force patterns) collected from 8 lifting tasks on an L4-L5 FSU (Natarajan et al., 2008). The lateral shear forces (750 N) were the greatest under lateral bending. In addition, the facet contact force, fibre and shear stresses were the greatest under lateral bending, implying that lifting that incorporates lateral bending puts the disc at greatest risk of injury (Natarajan et al., 2008). Currently, there is no experimental data on the effects of repetitive lifting on disc mechanics.

## 2.7 LDH and Disc Degeneration

Adams et al. first proposed a link between LDH and disc degeneration, where the largest percentages of discs failing via herniation under sudden overload were grade 2 discs on the Galante scale (Adams and Hutton, 1982; Galante, 1967). These discs tend to have a weakened annulus with tears forming, however, the nucleus still exhibits hydrostatic properties, allowing it to rupture through the annulus under large flexion and compressive loads. As discs degenerate further, the nucleus becomes more fibrous, making it difficult to extrude. In addition, mildly degenerated discs are more likely to be found in individuals between the ages of 25-55 years old, which is the population most susceptible to LDH. Furthermore, a previous study has found that disc degeneration doesn't precede LDH, however, it may occur after a disc has herniated (Lama et al., 2013). Schmidt et al., also predicted that mildly degenerated discs were more likely to herniate based on fibre and shear strain within the disc under simulated lifting motions for different degrees of degeneration (Schmidt et al., 2007b).

## 2.8 Mechanism of failure

It can be concluded that certain types of combined loading lead to LDH, and more recent research has been conducted to understand the initiation, propagation, and failure site of LDH. Rajasekaran et al. believes that the site and pattern of failure can be attributed to mechanical forces (Rajasekaran et al., 2013), finding that the majority of *in vivo* LDH occurred at the endplate junction (65%) instead of the failure of the annulus. *In vitro* studies have studied the effects of mechanical forces on LDH by applying either sudden or repetitive combined loading to FSUs to understand the mechanisms of LDH. However, there is a lack of consistency in mechanistic theories since it is influenced by load application (**Table 2-1**). Furthermore, most of the studies have developed an understanding of LDH using healthy ovine specimens, which is a valid model for the lumbar disc but may lead to different failure patterns.

In general, the posterior longitudinal ligament is found to be stretched or ruptured in those with LDH (Newman, 1952; Rissanen, 1960). For this to occur, there needs to be enough flexion to stretch the ligament and strain the posterior annulus. A high compressive force is produced during lifting, which leads to tension in the annulus due to a compressed nucleus. With a torsional load superimposed, the tension in the annulus fibres increases, potentially exceeding their tensile failure point and rupturing (Drake et al., 2005; Veres et al., 2010). When a lateral bending load is induced after flexion, the lateral posterior annulus is further stretched, coupled rotation moments can occur and the pelvic rotation about the frontal plane is limited, causing injury (Adams and Hutton, 1982).

**Table 2-1** Review of *in vitro* biomechanical studies investigating LDH by sudden overload and repetitive loading. Studies are organised by type of loading and then chronologically by year

Study	Type of Loading	Subjects (FSU)	Axial Compression (AC)	Flexion (flex)/Extension (ext)	Axial Rotation (AR)	Lateral Bending (LB)	Image Analysis	Results	Failure Site	Mechanism
Adams et al. 1985	Repetitive Loading (cycles until failure, f = 0.67 Hz)	Human (n = 29)	Cyclic compression applied until failure. Magnitude increased by 500N every 30 min.	Fixed flexion angle that was increased throughout testing to a maximum of 12-19°	-	Specimens rotated 15° about the sagittal plane	Dye tracking nucleus migration and macroscopic assessment (axial)	<ul style="list-style-type: none"> <li>· Six of 29 FSUs failed by disc prolapse and others due to endplate fracture (14) or vertebra/sacrum crumbled (4).</li> <li>· Peak loads ranged from 2.5 to 4 kN, and testing duration between 1 and 8 hours.</li> </ul>	Annulus	<ol style="list-style-type: none"> <li>1. Distortion of the lamellae</li> <li>2. Nucleus penetrates through the packed lamellae of the posterolateral corners</li> <li>3. Extrusion of the nucleus via radial tear</li> <li>4. Ruptured but stable</li> </ol>
Gordon et al. 1991	Repetitive Loading (cycles: 37,260, f = 1.5 Hz)	Human (n = 14)	Fixed load of 1,334N (applied using position control)	Cyclic flexion from 0° to 7°. (1.5 Hz half triangular waveform)	Determined by axial displacement and rotational stiffness. Remained < 3°	-	MRI and macroscopic assessment (axial)	<ul style="list-style-type: none"> <li>· 10 of 14 FSUs failed by the annular protrusion and 4 with nuclear extrusion.</li> <li>· All FSUs showed annular tears in the posterolateral region.</li> </ul>	Annulus	The result of annular disruption and loading combination

Study	Type of Loading	Subjects (FSU)	Axial Compression (AC)	Flexion (flex)/Extension (ext)	Axial Rotation (AR)	Lateral Bending (LB)	Image Analysis	Results	Failure Site	Mechanism
Callaghan et al. 2001	Repetitive Loading (cycles: 86,400, f = 1 Hz)	Porcine (n = 26)	One of three fixed loads (260, 867, or 1,472N)	1. Cyclic flex-ext position control (45°/s) 2. Cyclic flexion-extension in load control (10-44 Nm/s)  Angles and moments were specific to each specimen according to ROM test	-	-	Dye tracking nucleus migration and X-rays	<ul style="list-style-type: none"> <li>· 15 of 26 FSUs failed by disc prolapse, 8 under load control and 6 under position control with moderate to high compressive loads (867 or 1,472 N).</li> <li>· All herniation occurred in the posterior or posterolateral region</li> <li>· Failure occurred between 75,000 and 85,000 cycles for load control and between 34,500 and 71,000 cycles in position control.</li> </ul>	Annulus	Annular delamination with nucleus travelling circumferentially to the posterior and posterolateral regions.
Drake et al. 2005	Repetitive Loading (cycles: 6000, f = 1 Hz)	Porcine (n = 18)	Fixed preload of 1472 N	Cyclic flex - ext (based on ROM test)	5 Nm	-	Dye tracking nucleus migration and X-rays	<ul style="list-style-type: none"> <li>· All specimens herniated</li> <li>· Flex - Ext stiffness increased, and hysteresis decreased with an axial torque</li> </ul>	Annulus	Initiation in the annulus followed by failure of the facet joints leading to the increased rotation and increased tensile strain on the annulus
Wilke et al. 2016	Repetitive Loading (cycles: 1200, f = 0.5 Hz)	Ovine (n = 8)	Fixed preload of 800N	Cyclic flex (0° - 12°)	Cyclic axial rotation (0° - 4°)	Cyclic lateral bending (0° - 9°)	MRI and Micro CT	<ul style="list-style-type: none"> <li>· Four of eight failed by disc prolapse and 2 by protrusion. Other two failed by delamination.</li> <li>· Majority failed at the endplate (4), while other failed at the annulus (2).</li> <li>· Failure occurred within 500 cycles.</li> </ul>	annulus - endplate junction and annulus	The bone may be the initiation site for herniation

Study	Type of Loading	Subjects (FSU)	Axial Compression (AC)	Flexion (flex)/Extension (ext)	Axial Rotation (AR)	Lateral Bending (LB)	Image Analysis	Results	Failure Site	Mechanism
Berger-Roscher et al. 2017	Repetitive Loading (cycles: 1000, f= 2Hz)	Ovine (n = 30)	Cyclic (0-800N)	Cyclic flex (0 – 13°)	Cyclic AR (0 - 4°)	Cyclic LB (0 - 10°)	MRI and Micro CT	<ul style="list-style-type: none"> <li>· Different combinations of loading were applied (AC + Flex + AR + LB and one direction was removed for each other combination)</li> <li>· 13 specimens failed via endplate junction failure and 4 via annulus failure solely, however, no herniation</li> <li>· Most endplate junction failure occurred under all combinations of loading</li> <li>· Annular failure was commonly observed in Flex + AC + AR</li> </ul>	annulus-endplate failure	Healthy disc traumatically loaded, initiating an endplate defect that does not affect the CEP, with more compression, CEP ruptures and nuclear material is pressed out
Adams et al. 1982	Sudden Overload	Human (n = 61)	Ramp until failure (unknown velocity)	Fixed flexion angle: L5-S1 (10.1°), L4-5 (14.5°), L3-4 (11.7°), L2-3 (10.9°), L1-L2 (8.3°)	-	-	Macroscopic assessment (axial)	<ul style="list-style-type: none"> <li>· 26 of 61 FSUs failed by disc prolapse.</li> <li>· Others failed by either endplate fracture (32) or hyperflexion vertebral fracture (3)</li> <li>· Prolapse occurred central or posterolateral (contralateral side to applied LB)</li> </ul>	annulus-endplate junction	Slightly degenerated discs of lower lumbar levels are more susceptible to herniation.

Study	Type of Loading	Subjects (FSU)	Axial Compression (AC)	Flexion (flex)/Extension (ext)	Axial Rotation (AR)	Lateral Bending (LB)	Image Analysis	Results	Failure Site	Mechanism
Wade et al. 2014	Sudden Overload	Ovine (n = 24)	Ramp until failure (40 mm/min)	Fixed flexion angle of 10° (physiological extreme in the ovine spine)	-	-	Microstructural (Sagittal)	<ul style="list-style-type: none"> <li>· 13 of 24 FSUs failed by disc prolapse in the posterior or posterolateral region and others failed by endplate fracture (11)</li> <li>· 5/24 failed via annulus-endplate junction failure and 5/24 failed via mid-span annular rupture</li> </ul>	Failure of disc wall (annulus and junction failure)	Disc wall failure due to high fibre strains from endplate geometry. Failure commences in the mid then outer annulus, the inner annulus and nucleus bulge into the defect. Loading then increases the effects.
Wade et al. 2015	Sudden Overload	Ovine (n = 24)	Ramp until failure (400 mm/min)	Fixed flexion angle of 10° (physiological extreme in ovine spine)	-	-	Microstructural (Sagittal)	<ul style="list-style-type: none"> <li>· 14/24 failed via annular - endplate junction, 6/24 via mid-span annular failure, 4/24 via endplate fracture</li> <li>· Faster loading rate resulted in more annulus-endplate failures</li> </ul>	Failure of disc wall (Predominately annulus-endplate junction failure)	High loading rate leads to a defect in the annulus-endplate junction before the mid-span annulus, this defect then allows the inner annulus and nucleus to bulge progressing towards herniation

Study	Type of Loading	Subjects (FSU)	Axial Compression (AC)	Flexion (flex)/Extension (ext)	Axial Rotation (AR)	Lateral Bending (LB)	Image Analysis	Results	Failure Site	Mechanism
Wade et al. 2017	Sudden Overload	Ovine (n = 30)	Ramp until failure (40 mm/min) (20° offset compression)	Fixed flexion angle of 7°	Fixed 5° anti-clockwise direction	offset flexion adds an element of right lateral bend'	Microstructural (Sagittal)	<ul style="list-style-type: none"> <li>· Smaller load required to herniate than flexion + AC</li> <li>· 23 specimens failed via herniation in the posterior or posterolateral regions</li> <li>· Presence of non-continuous tearing and circumferential tracking</li> <li>· Complex loading introductions shear on disc tissue</li> </ul>	Failure of the disc wall (Predominately annulus failure)	<ol style="list-style-type: none"> <li>1. Mid annular damage in alternating lamellae</li> <li>2. Inner disc material extrudes into those defects via rupture and delamination.</li> <li>3. If compressed further, remaining lamellae (relaxed ones) continue to fail at vulnerable locations, then leading to extrusion to nuclear material</li> </ol>
Shan et al. 2017	Sudden Overload	Ovine (n = 30)	Ramp until failure (400 mm/min) (20° offset compression)	Fixed flexion angle of 7°	Fixed 5° anti-clockwise direction	offset flexion adds an element of right lateral bend'	Microstructural (Sagittal)	<ul style="list-style-type: none"> <li>· Smaller load required to herniate than complex loading at a low rate (40 mm/min)</li> <li>· Less endplate junction failures and majority failed via mid-span annular tear in the posterior or posterolateral region</li> <li>· Damage to anterior and lateral annulus was found</li> <li>· More damage was found on the left side (contralateral to applied loading)</li> </ul>	Failure of disc wall (Predominately annulus failure)	High loading rate plus complex loading lead to the initiation of herniation in the mid-span annulus and not a defect at the annulus-endplate junction. This was followed by a circumferential and radial tear (more common)

Study	Type of Loading	Subjects (FSU)	Axial Compression (AC)	Flexion (flex)/Extension (ext)	Axial Rotation (AR)	Lateral Bending (LB)	Image Analysis	Results	Failure Site	Mechanism
van Heeswijk et al. 2017	Sudden Overload	Ovine (n = 14)	Ramp until failure (40 mm/min)	Fixed flexion angle of 10° (physiological extreme in the ovine spine)	-	-	Microstructural (Transverse)	<ul style="list-style-type: none"> <li>High prevalence of disruption in the lateral annulus with nuclear material tracking circumferentially towards the posterior and posterolateral regions</li> </ul>	Failure of disc wall (annulus)	Failure of lateral annulus first with nuclear material migrating from lateral down to the posterolateral and posterior regions via circumferential delamination
Schollum et al. 2018	Sudden Overload	Ovine (n = 41)	Ramp until failure (40 mm/min and 400 mm/min) (20° offset compression)	Fixed flexion angle of 7°	Fixed 5° clockwise direction	offset flexion adds an element of left lateral bend	Microstructural (Sagittal)	<ul style="list-style-type: none"> <li>Smaller load required to herniate in the low rate (40 mm/min) than the high rate (400 mm/min)</li> <li>More facet and vertebral fractures were observed in the high rate loading</li> <li>Facet engagement plays a role in the failure</li> </ul>	Failure of disc wall (annulus and endplate-junction failure)	Initiation in the annulus with alternate lamellae damage. Failure propagation further determined by facet engagement

### 2.8.1 Sudden Failure

Adams et al. first studied disc prolapse due to sudden high loading in 1981 on human FSUs and developed a herniation model (**Figure 2-10**) for *in vitro* studies (Adams and Hutton, 1982). Each FSU was subjected to flexion just beyond the physiological limit and then compressed until failure. Of the 61 FSUs tested, 26 produced prolapse and the other FSUs resulted in an endplate fracture. This study determined that sudden prolapses can occur in mature discs in less than a second and are caused by a single high compressive load on a flexed disc.

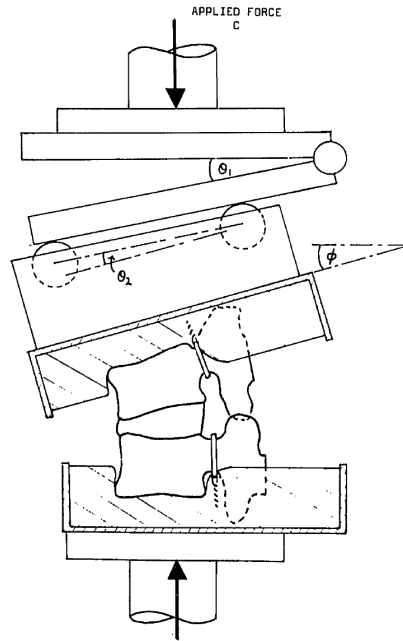


**Figure 2-10** Herniation (hyperflexion) model developed by Adams et al. (Adams and Hutton, 1982), where FSU was flexed at a fixed angle and loaded in compression

Since then, extensive systematic work has been undertaken by a research group from New Zealand to understand the initiation and propagation of LDH using healthy ovine specimens. Utilising the herniation model developed by Adams et al., this group tested the effect of loading rate (40 and 400 mm/min) and two combinations of motions (compression + flexion, and compression + complex loading (non-concordant and concordant), (Schollum et al., 2018; Shan et al., 2017; van Heeswijk et al., 2017; Wade et al., 2014, 2015; Wade et al., 2017). This led to the finding that ovine discs fail at lower loads under complex postures (3.58 – 11.6 kN) in comparison to just flexion (5.92 – 15 kN) under both loading rates. This implies that asymmetric lifting could lead to a greater risk of LDH.

Adams et al. found compressive failure loads to be approximately 2.7 to 13 kN, in comparison to Wade et al. who found loads to be between 6.1 to 11.78 kN (Adams and Hutton, 1982; Wade et al., 2015). These variations in magnitudes may be due to the difference in flexion angles, hydration, and the use of human versus ovine specimens. Both

studies determined that flexion angles representing the physiological extreme, resulted in herniation and herniation occurred in the posterior or posterolateral region of the annulus

The microstructural analysis in the sagittal plane from the New Zealand group showed that different failure patterns were found under the various combinations of loads and loading rates (**Table 2-1**). Under flexion and low loading rates (Wade et al., 2014), LDH initiated with a mid-span annular tear, which then progressed into LDH with increasing compression (**Figure 2-11**). The nucleus and the inner annulus bulged into the defect which created a pathway for extrusion of the nucleus. Under flexion and high loading rates (Wade et al., 2015), the initiation was a defect to the annulus-endplate junction (**Figure 2-11**). With increasing compression, the inner annulus and nucleus bulged into the defect leading to LDH at the endplate junction.

Additionally, from the microstructural analysis in the transverse plane, it was found that there was lateral tracking of the nucleus under flexion + compression (sudden overload). The images showed that the nucleus would migrate laterally (initial failure in the lateral annulus, **Figure 2-12**) and then track down to the posterolateral/posterior regions via delamination. This tracking has not been observed previously in human FSUs and may be a result of the loading modality or ovine specimens.

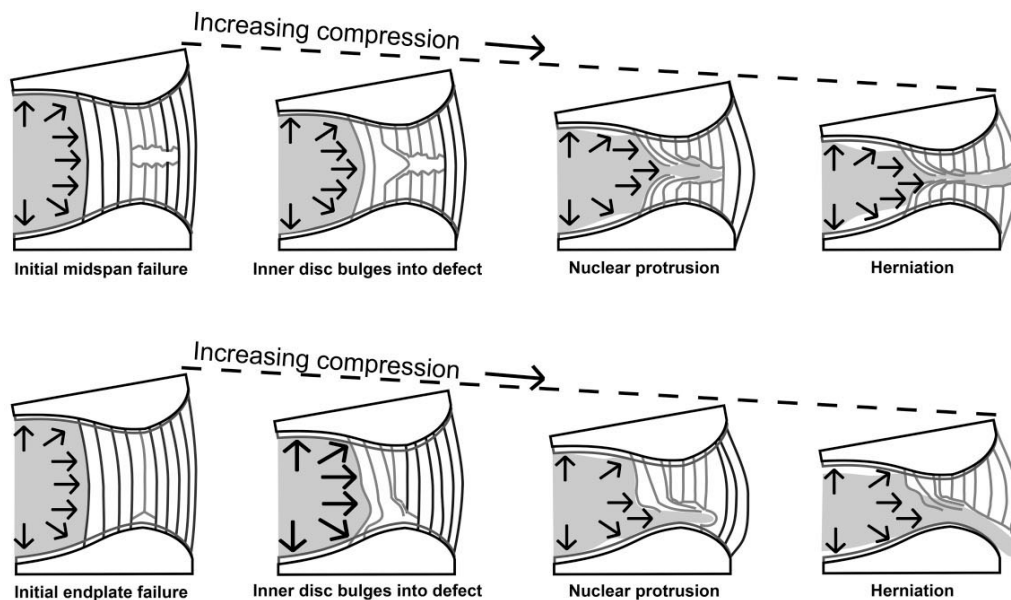


**Figure 2-11** Mechanisms of LDH (mid-annulus (top panel) and endplate junction (bottom panel)) under a sudden overload (flexion + compression, (Wade et al., 2014))

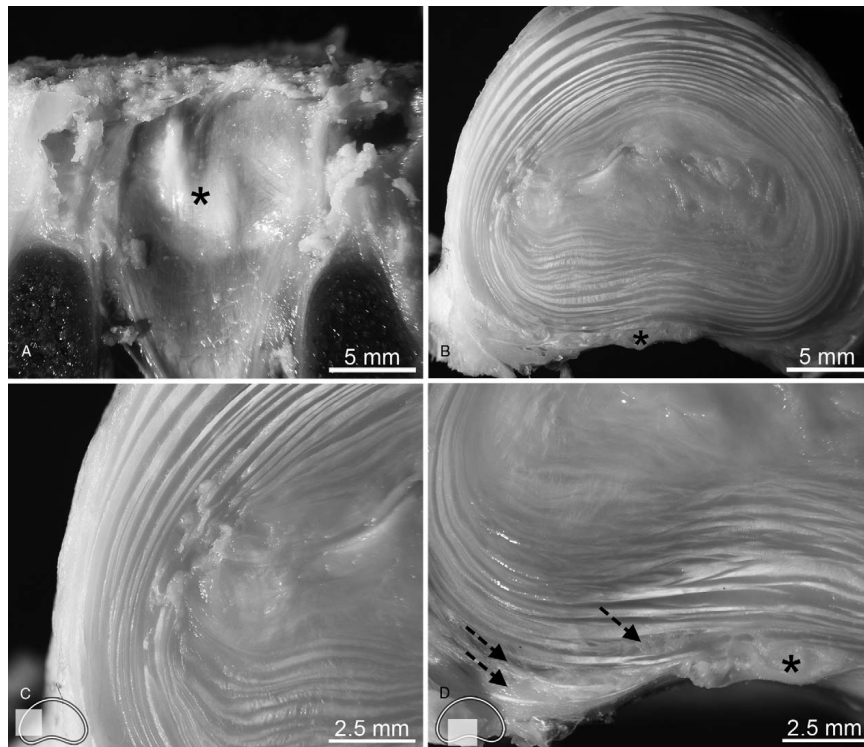


**Figure 2-12** Images showing the lateral tracking of the nucleus and then migration down to the posterior/posterolateral regions (van Heeswijk et al., 2017). The \* and arrows are representing locations of nucleus material found in the transverse slice

Under complex sudden overload where the ovine FSU was under fixed flexion, axial rotation, and lateral bend, the initiation of LDH occurred at the mid-span annulus where failure was found in alternating lamellae (**Figure 2-13**, Schollum et al., 2018; Shan et al., 2017; Wade et al., 2017). The nucleus then migrated into those defects. With increasing compression, the remaining lamellae (relaxed) continued to fail, leading to a pathway of nuclear extrusion. Essentially, there was circumferential tracking of the nucleus via delamination in the annulus as a result of the shear force (AP and lateral shear) induced via the complex posture. Sudden overload via high loading rate under complex postures resulted in a larger number of facet fractures, which indicated that there is load sharing within the facet joints and can influence the mechanism of LDH (Schollum et al., 2018; Shan et al., 2017).

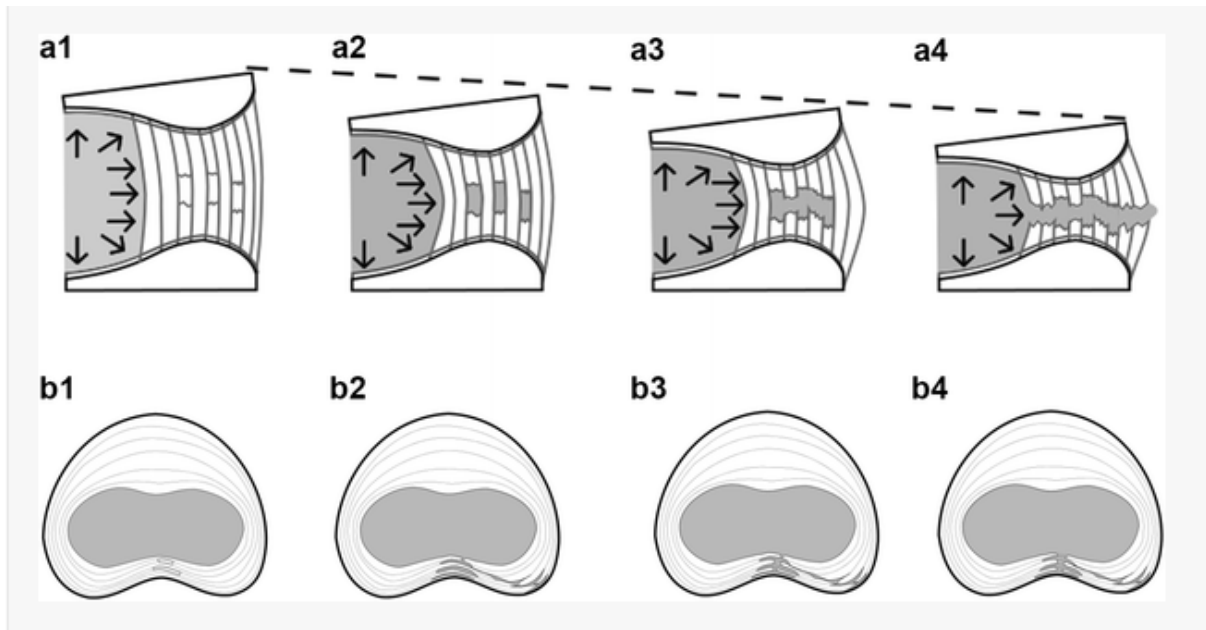


**Figure 2-13** Mechanics of LDH under complex sudden overload (Wade et al., 2017). Top panel: sagittal view and bottom panel: transverse view

### 2.8.2 Repetitive Failure

Repetitive motions can cause damage accumulation that occurs faster than adaptive remodelling (Maroudas et al., 1975), leading to injury. Adams et al. also studied LDH via repetitive loading using the same herniation model from the sudden overload study, however, this study applied cyclic compression to replicate fatigue (Adams and Hutton, 1985). Although the model was not physiological since lifting would be mimicked by cyclic flexion, six of the 29 specimens failed due to gradual prolapse and others due to endplate fracture. In addition, LDH occurred after 2,400 to 19,300 cycles in healthy discs. Bending moments acting on the spine during herniation were only measured by Callaghan et al. and Drake et al. and they found bending moments as large as 20.1 Nm and 29.2 Nm, respectively (Callaghan and McGill, 2001; Drake et al., 2005). However, both of those studies used porcine specimens, which may not be indicative of the potentially larger moments found in human specimens.

Other studies also found herniation due to repetitive loading, however, different testing regimes were used (**Table 2-1**). Gordon et al. applied combined compression, flexion and axial rotation on human lumbar FSUs (Gordon et al., 1991). Callaghan et al. applied cyclic flexion-extension in load and position control with one of three constant compressive loads on porcine FSUs (Callaghan and McGill, 2001). Drake et al. applied combined compression and flexion with an axial torque on porcine FSUs as well (Drake et al., 2005). Finally, Wilke et al. and Berger-Roscher et al. applied a combination of cyclic flexion, lateral bending, and axial rotation with a constant compressive load on ovine FSUs (Berger-

Roscher et al., 2017; Wilke et al., 2016). These differences in applied loading raise the question, what is physiological loading regime?

Interestingly, all studies resulted in LDH even though the loading regimes were different. A low percentage of LDH was observed in the Adams and Gordon studies, which used human FSUs, indicating it is difficult to reproduce LDH via repetitive loading. The more recent studies have been able to apply more physiological loading with the application of cyclic flexion, axial rotation, and lateral bending with a constant compressive preload. However, it is still unclear whether the more physiological loading regime will lead to closer replication of LDH in FSUs.

Adams hypothesised that gradual prolapse had five stages of failure (**Figure 2-14**, (Adams and Hutton, 1985). Stage one is self-selection of the disc, where L4-5 and L5-S1 discs with pulpy nucleus positioned posteriorly and thinner posterior annulus are more prone to herniation (Adams and Hutton, 1985). Distortion of lamellae due to repetitive loading occurs with lamellae packing closely together in the posterolateral region, leading to radial fissures and migration of the nucleus (Adams and Hutton, 1985). The nucleus eventually breaks through the lamellae via a radial tear and then beyond the posterior longitudinal ligament causing extrusion (Adams and Hutton, 1985). Extrusion, however, is not observed in all discs. Adams also predicted that once the disc herniated, it stabilises and does not leak indefinitely (Adams and Hutton, 1985). The results from the Gordon et al. study also supported the theory of distorted lamellae and disruption of the annulus causing nuclear extrusion/protrusion (Gordon et al., 1991). In contrast, Drake et al. applied axial torque instead of axial rotation, which resulted in a mechanistic theory regarding the failure of the facet joints and its impact on annular disruption leading to extrusion (Drake et al., 2005).

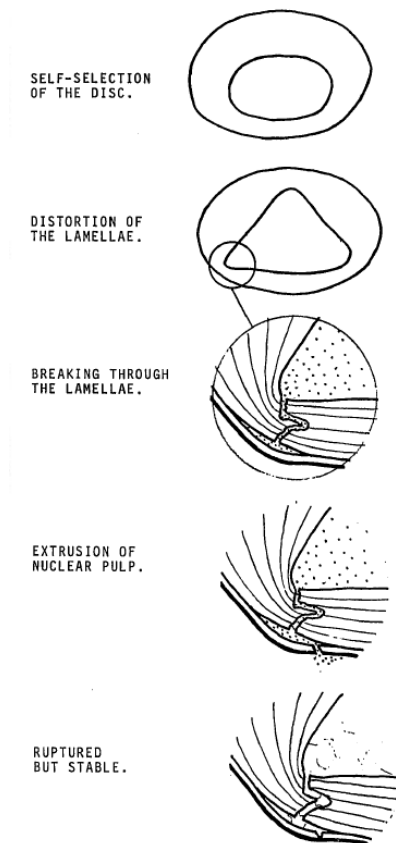


**Figure 2-14** Mechanism of LDH under repetitive loading based on human FSUs (Adams and Hutton, 1985)

Wilke et al. and Berger-Roscher et al. found that their combination of loading led to frequent endplate junction failures that did not necessarily result in LDH (Berger-Roscher et al., 2017; Wilke et al., 2016). Therefore, they theorised that herniation initiates with an endplate defect that does not affect the cartilaginous endplate, however, with additional compression the cartilaginous endplate ruptures and the nuclear material is eventually pushed out (Berger-Roscher et al., 2017; Wilke et al., 2016). This theory is similar to the one proposed by Wade et al, in relation to high rate loading under sudden overload in flexion, however, the failure occurs via the bone (**Figure 2-15**).

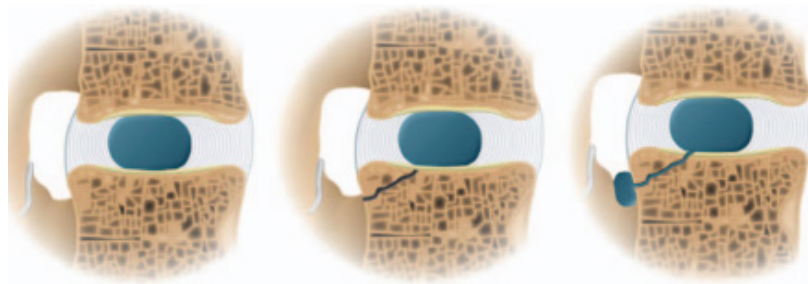


**Figure 2-15** Mechanism of LDH under repetitive loading based on ovine FSUs (Berger-Roscher et al., 2017)

With the differences in mechanistic understanding of LDH, it is still unclear how repetitive loading affects LDH. Clinically, *in vivo* LDH due to endplate junction failure is more common than annulus rupture (Rajasekaran et al., 2013). Based on the mechanistic theories presented in **Table 2-1**, endplate junction failure is commonly found in sudden overload at high loading rate (400 mm/min) under a simple forward bend (flexion) or repetitive loading at extreme levels of lumbar flexion, axial rotation, and lateral bending. Endplate junction failure was also found under complex sudden overload, however, not as frequently.

Clearly, the mechanisms for LDH are influenced by load application, which encompasses sudden or repetitive loading, a combination of loading direction, and loading rate. Currently, an understanding of the initiation and propagation of LDH is only present for sudden overload due to systematic studies completed by the New Zealand group. However, under repetitive loading, there is no systematic mechanistic theory of LDH, and since LDH commonly occurs with repetitive lifting, it is important to understand the mechanisms. In addition, no studies have been conducted on human FSUs under sudden overload with a complex posture. Therefore, the theories proposed by the New Zealand group have not been further justified with human tissue.

Furthermore, the studies represented in **Table 2-1** have hypothesised that combined loading leads to increased shear and tensile strain within the annulus causing delamination or tearing, which allows extrusion of the nucleus. Finite element (FE) studies have confirmed this by measuring fibre and shear stress and strain under different combinations of lifting motions (Natarajan et al., 2008; Schmidt et al., 2007b; Shirazi-Adl, 1989). Shirazi-Adl first measured fibre strain under combined loading using a non-linear FE model of the disc (Shirazi-Adl, 1989). He found that fibre strain was greater than 20% when axial rotation and lateral bending was applied with flexion and compression. In addition, the maximum fibre strain occurs in the innermost layer of the posterolateral region, which causes rupture of the annulus radially. Similarly, Schmidt et al. found the largest fibre strain to be 19.6% under lateral bending and axial rotation in the posterolateral annulus. The fibre strains increased with degeneration (Schmidt et al., 2007b). He also measured shear strain, finding that under flexion and axial rotation the maximum shear strain is 47% in the innermost layers of the posterolateral region in mildly degenerated discs.

However, no studies have measured the internal disc strain during repetitive or sudden combined loading experimentally to quantify the thresholds that lead to annulus/disc injury.

## 2.9 Conclusion

In summary, LDH occurs more frequently in those who are engaged in repetitive lifting. The injury is thought to occur over time, as high repetitive (sub-failure) stresses are created within the disc leading to a gradual LDH. These stresses are further increased by improper lifting technique which includes straight knees, holding an object at arm's length, twisting or laterally bending. However, the mechanism for herniation under repetitive loading is still unclear as only a few studies have studied the effect of repetitive loading on LDH. In addition, as LDH is influenced by the direction of loading, it is important to apply the most physiological combined loading regimes and take a systematic approach in developing a mechanistic understanding of LDH. Furthermore, using MRI, X-rays, and macroscopic assessment to understand LDH *after* repetitive loading is important. However, measuring internal disc strains *during* repetitive loading can provide an understanding of the initiation and propagation of LDH as well as the cumulative damage occurring within the disc. Measuring internal disc strains can also help validate finite element models and help build more robust models that can predict the failure patterns under thousands of different loading conditions.

## 2.10 Internal Disc Strains

Improvements in mechanical testing machines for biological tissue has allowed for extensive research on external disc mechanics (i.e. material properties, surface strains, failure loads and range of motion). For example, a majority of the previously mentioned studies determined the magnitude of forces and moments that caused LDH. However, those studies did not consider internal disc mechanics (i.e. disc deformation) to provide a quantitative analysis of injury initiation and propagation.

Several challenges are present when measuring *in vitro* internal disc mechanics. For example, it is difficult to observe internal disc tissue movement under mechanical loading without an imaging device. To quantify that movement, it necessitates the insertion of transducers or markers (Krag et al., 1987; Seroussi et al., 1989) in addition to stereoradiography. This interrupts the disc tissue and may affect disc mechanics. However, this method can be used with most materials testing devices, allowing for strain measurement under large or combined loads associated with disc injury (Costi et al., 2007). In contrast, medical imaging such as MRI during loading has been used to non-invasively measure internal disc strains, however, the loading devices are limited in the applied physiological loads and directions such as only compression, flexion, or extension (O'Connell et al., 2007; O'Connell et al., 2011b; Showalter et al., 2016; Yoder et al., 2014). For example, metallic mechanical testing devices required for applying high loads or combined loading directions cannot be used with an MRI, limiting the ability to measure strains during injury.

### 2.10.1 Methods

Few studies have attempted to measure internal disc deformation under isolated loading directions despite the experimental challenges (**Table 2-2**). Prior to 1987, studies only measured surface strains or qualitatively measured nucleus movement (Shah et al., 1978). Different methods were used to measure internal disc deformation experimentally, including marker or wire insertion and medical imaging, which are currently used. Krag et al. and Seroussi et al. inserted a line of six markers (metallic beads) into the mid-sagittal plane of the disc (Krag et al., 1987; Seroussi et al., 1989). These markers were then tracked before and after loading using radiography to determine two dimensional (2D) internal disc strains. Using a similar method, Tsantrizos et al. inserted a grid of wires into the mid-sagittal plane to measure 2D strains within the entire area of the disc (Tsantrizos et al., 2005) and Costi et al. further developed the method to quantify strains in 3D using stereoradiography (Costi et al., 2007). Marker and wire insertion methods can give an accurate indication of internal disc deformation under any type of loading as the wires and

markers can deform with the tissue, however, these methods are invasive, which can affect disc tissue quality and its mechanics.

In 2007, O'Connell et al. used digital image correlation to quantify internal disc strains non-invasively from MRI images in 2D (O'Connell et al., 2007). From the same group, Yoder et al. developed a mechanical testing machine from nonmagnetic materials to quantify strains in 3D using magnetic resonance imaging (Yoder et al., 2014). Chan et al., measured internal disc strains during cyclic compressive loading using a non-magnetic testing device and MRI (Chan and Neu, 2014). However, the testing machines used with MRI limit the type and magnitude of loads that can be applied to the disc. Currently, internal disc strains using non-invasive techniques have been measured in only compression, flexion, and extension. However, various daily activities and disc injuries are a result of complex loading, it is important to be able to measure internal disc strains under those loading conditions. Another non-invasive method includes using finite element modelling to calculate internal disc mechanics (Schmidt et al., 2007b; Shirazi-Adl, 1989). However, it is difficult to directly validate strains from FE models without experimental data under all directions of loading. In 2015, Showalter et al. developed a disc strain template for Pfirrmann grade III L4-5 discs under compression and compared it to an FE model, which produced similar results (Showalter et al., 2016). This strain template could be used in the future to measure internal disc strains under complex loading conditions and various disc pathologies.

**Table 2-2** Review of *in vitro* studies reporting internal disc strains

Author	n <sup>1</sup>	Method	Type of Loading	Loading Direction	Magnitude of load	Location	Measurement Parameters	Radial Strains (%)	Axial Strains (%)	Circumferential Strains (%)	Shear Strains <sup>2</sup>
Tsantrizos et al., 2005	5	Wire Insertion	Static	Compression	1000N	A, L, PL	Mean (SD) Strain (%)	A: -1.7 (1.3) PL: -4.1 (1.5)	-	A: 3.0 (0.6) PL: 2.2 (1.6)	-
				Flexion	All bending directions: 10Nm + 500N			A: 6.8 (3.0) PL: -5.7 (2.0)		A: 2.5 (2.1) PL: 0.8 (0.7)	
				Extension	10Nm + 500N			A: -3.9 (1.3) PL: 4.7 (1.9)		A: 0.6 (0.6) PL: 3.0 (1.2)	
				Lateral Bending	compression			A: -2.0 (0.7) PL: 6.5 (1.8)		A: 1.0 (0.5) PL: 3.9 (2.5)	
Costi et al., 2007	9	Wire Insertion	Static	Anterior Shear	0.9 mm	A, AL, L, PL, P, NP	Mean (95% CI) 3D Maximum Shear Strains (%/mm or %/°)	-	-	-	A: 7 (0.05) P: 5.5 (0.75)
				Posterior Shear	-0.9 mm						A: 6.75 (0.1) P: 7.5 (0.5)
				Lateral Shear	±0.7 mm						A: 6.75 (1) P: 8.5 (0.5)
				Compression	1.1 mm						A: 7.8 (1) P: 10.4 (0.6)
				Lateral Bending	±4.8°						A: 1.25 (0.25) P: 1.75 (0.25)
				Flexion	-5.3°						A: 3.25 (0.5) P: 2.5 (0.5)
				Extension	5.3°						A: 2.5 (0.25) P: 2 (0.5)
Axial Rotation	±2.5	A: 1.5 (0.25) P: 2 (0.5)									
O'Connell et al., 2007	7	MRI	Static	Compression	1000N	A, NP, P	Mean (SD) Strain (%)	A: 2.6 (3.9) P: 1.6 (2.5)	A: -5.9 (4.0) P: -3.4 (1.9)	-	A: 5.0 (4.0) P: 2.6 (0.2)

Author	n <sup>1</sup>	Method	Type of Loading	Loading Direction	Magnitude of load	Location	Measurement Parameters	Radial Strains (%)	Axial Strains (%)	Circumferential Strains (%)	Shear Strains <sup>2</sup>
O'Connell et al., 2011	14	MRI	Static	Compression + Flexion	-5° and 1000 N compression	A, NP, P	Interquartile range of strain (%)	A: 3 to 6 P: 1 to -4	A: -6 to -10 P: 0 to -6	-	A: 2.5 to 4 P: 3 to 3.5
				Compression	1000 N			A: -6 to 8 P: -4 to 12	A: -10 to 3 P: -13 to -1		A: 4 to 4.7 P: 4 to 4.5
				Compression + Extension	5° and 1000 N compression			A: -4 to 0 P: 3 to 10	A: -4 to 1 P: -7 to -10		A: 2.5 to 3.5 P: 2 to 3
Yoder et al., 2014	9	MRI	Static	Compression	15% grip to grip applied compressive strain <sup>3</sup>	A, AL, L, PL, P	Mean (SD) strain (%)	A: 1.75 (1.5) P: 3.5 (3.5)	A: -9 (4) P: -15 (5)	A: 2 (1.5) P: 2.5 (1.5)	-
Showalter et al., 2015	7	MRI	Static	Compression	-10.3% ± 3.5% applied compressive strain	A, AL, L, PL, P	Interquartile range of strain (%)	A: 1.8 to 3.8 P: 1.5 to 4.2	A: -6.5 to -14.5 P: -12.5 to -17.5	A: 1.5 to 3.25 P: 1 to 3	-

<sup>1</sup>n signifies sample size and all studies used human FSUs.

<sup>2</sup>units of shear strain are indicated in the measurement parameters column

<sup>3</sup>strain was based on midsagittal disc height and applied at 0.1 mm/s.

A – Anterior, AL – Anterior Lateral, L – Lateral, PL – Posterior Lateral, P – Posterior, NP – Nucleus Pulposus.

Multiple regions are reported within each study, however, this table focuses on the anterior and posterior regions as these were reported in all studies.

### 2.10.2 Strain Measurements

Based on **Table 2-2**, similar magnitudes of radial and circumferential strain under compression in the anterior and posterior regions were found with both the invasive (O'Connell et al., 2007; O'Connell et al., 2011b; Showalter et al., 2016; Yoder et al., 2014) and non-invasive techniques (Tsantrizos et al., 2005) of strain measurement. These similarities show that the two techniques can be used to measure internal disc strains however, this is predominantly in compression. Axial strain was only reported by those studies using a non-invasive technique (O'Connell et al., 2007; Showalter et al., 2016; Yoder et al., 2014), and the magnitudes were similar in both the anterior and posterior regions under compression. O'Connell et al. 2011 measured the effect of degeneration on internal disc strains and found that degenerated tissue exhibited larger compressive axial and tensile radial strains. Maximum shear strains were only reported by Costi et al., and O'Connell et al., reported just shear strain (Costi et al., 2007; O'Connell et al., 2007; O'Connell et al., 2011b). However, O'Connell et al. 2011, did a comparison of maximum shear strain (~9%) under compression calculated from the non-invasive technique and compared it to Cost et al., (5 – 14%), finding similar magnitudes. Comparing strains in other directions and combined loading may become difficult as different rotations or moments would be applied between studies.

### 2.10.3 Conclusion

In conclusion, there are two methods used to measured internal disc strains, which include marker or wire grid insertion with stereoradiographs, or non-invasively using digital image correlation and MRI. Studies present either radial, axial, circumferential, or shear strain, under various loading regimes, resulting in difficulties comparing strain magnitudes (**Table 2-2**). Radial and axial strains are commonly reported, however, only some studies report circumferential strains as 3D internal strains were challenging to measure. Although shear strains are important indicators of injury, they are rarely reported. All these differences coupled with only a few studies (two research groups) quantifying internal disc strains results in a poor understanding of internal disc deformation. In addition, due to limitations of the strain measurement techniques, internal discs strains have not been quantified under complex loading or used to understand injury initiation and propagation. Based on this review, to apply combined loads associated with disc injury, a material testing device is needed, which cannot be coupled with an MRI to measure non-invasive strain. Therefore, the marker or wire grid technique with stereoradiographs would need to be utilised.

## Chapter 3      New findings confirm regional internal disc strain changes during simulation of repetitive lifting motions<sup>2</sup>

In the previous chapter (**Chapter 2**), it was determined that for a better understanding of LDH as a result of repetitive lifting, it was important to measure internal disc strains during physiological loading. These strains can give insights into the deformation throughout loading as well as the initiation and propagation of disc injuries. Therefore, this chapter measures internal disc strains during simulated safe repetitive lifting. Two strain measurement techniques were identified previously, however, only one was viable with the multi-axial physiological loading utilised in this chapter, which utilised inserting a wire grid into the disc with radiostereometric analysis. Within this chapter, this technique was also further validated.

---

<sup>2</sup> The information presented in this chapter has been submitted to *Annals of Biomedical Engineering* on October 24 2018 and has been reviewed. Minor revisions were made to provide additional information for consistency throughout this thesis.

Amin, D.B., Moawad, C.M., Costi, J.J., 2018 Manuscript Under Review. New findings confirm regional internal disc strain changes during simulation of repetitive lifting motions. *Annals of Biomedical Engineering*.

### 3.1 Abstract

To understand the mechanisms of disc injuries that result from repetitive loading, it is important to measure disc deformations and use MRI to quantify disc damage. The aim of this study was to measure internal disc strains during simulated repetitive lifting and their relation to disc injury. Eight cadaveric lumbar segments underwent a pre-test MRI and 20000 cycles of loading under combined compression (1.0 MPa), hyperflexion, and right axial rotation (2°), which simulated bending and twisting while lifting a 20kg box for one year. The additional eight segments had a grid of tantalum wires inserted and used stereoradiography to calculate MSS at increasing cycles. Post-test MRI revealed that 73% of specimens were injured after repetitive loading (annular protrusion, endplate failure, or LDH). MSS at cycle 20000 was significantly larger than all earlier cycles ( $p < 0.003$ ). MSS in the anterior, left posterolateral, and left lateral regions was significantly greater than the nucleus region ( $p < 0.006$ ). Large strains, annular protrusion and herniation in the posterolateral regions were found in this study, which is consistent with clinical observations. *In vitro* strains can be used to develop more-robust computational models for the understanding of specimen-specific effects of repetitive lifting on disc tissue.

### 3.2 Introduction

LDH is commonly associated with work-related injuries that involve low back stressing through repetitive lifting or movement seen in individuals aged 25-55 years (Jordan et al., 2011). Epidemiological and *in vitro* studies have shown that LDH can occur during compression combined with flexion, axial rotation and/or lateral bending, resulting in posterior-lateral or posterior herniation (Adams and Hutton, 1985; Gordon et al., 1991; Kelsey, 1975; Kelsey et al., 1984a; Kelsey et al., 1984b). Furthermore, studies have looked at propagation of the injury, where nuclear extrusion or protrusion occurred via endplate junction failure (Rajasekaran et al., 2013; Wade et al., 2014) or annular tears (Gordon et al., 1991). However, successfully reproducing LDH during repetitive loading has proven challenging, which limits a full understanding of the injury.

Few *in vitro* studies have examined herniation under repetitive loading in human spine segments, where a combination of bending and compression resulted in nuclear extrusion (herniation) or annular protrusion. Adams et al. applied cyclic compression to physiologically flexed human spine segments and found no herniation (Adams and Hutton, 1985). However, they found that increasing the flexion angle to just beyond the physiological limit resulted in herniation in 24% of specimens (Adams and Hutton, 1985). Gordon et al. employed a fixed flexion and axial rotation angle while applying cyclic

compression in displacement control at 1.5 Hz on human lumbar spine segments, resulting in herniation in 29% of specimens (Gordon et al., 1991). However, 71% of specimens failed via annular protrusion, where the nucleus was contained and did not extrude (Gordon et al., 1991). Callaghan et al. applied cyclic flexion-extension to porcine discs in load and position control at three different constant compressive preloads, finding that repetitive flexion-extension resulted in cumulative damage with herniation occurring at higher compressive preloads (Callaghan and McGill, 2001). Herniation occurred in 50% of the specimens under torque control and 70% of the specimens in position control (Callaghan and McGill, 2001). While these studies were able to reproduce herniation, the loading methods differed, and further investigation of load application is required. Furthermore, only one loading direction was applied cyclically while the others were held at a constant displacement or rotation, and specimens were not hydrated, nor at body temperature, which may limit their physiological relevance.

In addition, studies have tracked nucleus migration during repetitive loading, to demonstrate qualitatively how herniation propagates (Adams and Hutton, 1985; Callaghan and McGill, 2001). However, to further understand the mechanism of disc injury and its initiation resulting from repetitive loading, it is important to measure internal disc strains with disc failure assessment. Experimental internal disc strains have only been measured after a single loading cycle (Costi et al., 2007; O'Connell et al., 2007; O'Connell et al., 2011b; Showalter et al., 2016) and not used to study injury initiation and propagation. Studies have used both invasive (Krag et al., 1987; Seroussi et al., 1989; Tsantrizos et al., 2005) and non-invasive (O'Connell et al., 2011b; Showalter et al., 2016; Yoder et al., 2014) techniques to measure strains, each with their benefits and limitations. Non-invasive measurements restrict the type of loading that can be applied, while invasive measurements can disrupt the disc tissue, however, they can be used in combination with complex loading. Shirazi-Adl et al. in a finite element (FE) study, first presented internal disc strains from various complex loading cases, as reported clinically (Shirazi-Adl, 1989). They found that maximum fibre strains in the innermost posterolateral annulus layers during flexion and compressive loading increased with the addition of axial rotation and lateral bending. However, to further validate these FE results, *in vitro* internal disc strains need to be measured during repetitive complex loading in human lumbar segments.

Therefore, the primary aim of this study was to measure internal disc strains and to track their regional changes during simulation of repetitive lifting motions. A secondary aim was to identify the disc injuries that arose from repetitive lifting from MR images. Since

strains were measured using an intradiscal wire grid technique (Costi et al., 2007), a subsequent aim was to validate the technique. It was hypothesised that strains will increase during the simulation of repetitive lifting, with the largest magnitudes occurring in the posterolateral and posterior regions.

### 3.3 Materials and Methods

#### 3.3.1 Specimens and Preparation

This study was approved by the Southern Adelaide Clinical Human Research Ethics Committee in March 2015. Sixteen cadaver lumbar functional spinal units (FSUs), including posterior elements, were dissected from eight freshly frozen spines (6 male and 2 female, mean (SD) age: 53 (13) years, range: 31-69 years, levels: L1-2 x 3, L2-3 x 4, L3-4 x 1, L4-5 x 7). Spines were stored at -20°C and then thawed at room temperature for pre-test MRI. Mid-sagittal images of whole spines for assessment of Pfirrmann grade were obtained from a 3T MR scanner (Siemens Skyra) using a T2 weighted sequence (TR: 3000 ms TE: 79 ms thickness: 4 mm). Spines were then dissected of all non-ligamentous tissue, keeping both the anterior and posterior longitudinal ligaments and facet joint capsules intact. The superior and inferior vertebral surfaces were then cut parallel to the mid-transverse plane of the disc where the FSU was composed of a full superior and inferior vertebra, and re-frozen until the day of testing. Specimens were then thawed overnight at 4 °C while wrapped in cotton-lined sheets, followed by a minimum of three hours at room temperature unwrapped.

Each FSU was randomly assigned to a control or experimental group, where only the experimental group had a wire grid inserted for strain measurement (**Figure 3-1**). Four tantalum beads (1.5 mm diameter) were placed on the periphery (anterior, posterior, right and left lateral) and centre, of each superior and inferior endplate of experimental FSUs using cyanoacrylate. For the central bead, a hand drill with a 2 mm drill bit was used to manually drill a hole down the centre of the superior and inferior vertebra until resistance was felt, indicating that the endplate was reached.

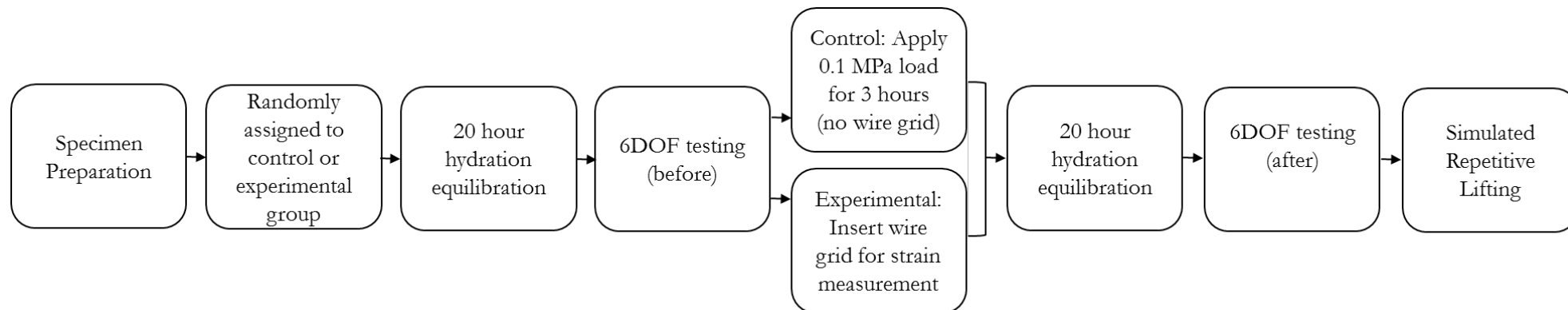
Each vertebral body was secured with three nylon screws and embedded in radiolucent nylon cups using polymethyl methacrylate (PMMA). An alignment device was used to ensure that the superior and inferior surfaces of each cup were parallel to each other and parallel to the mid-transverse plane of the disc. Axial and lateral radiographs were taken to measure the instantaneous axis of rotation of the disc (Pearcy and Tibrewal, 1984) relative to the cups, which was used as the centre of rotation for all testing. A waterproof sleeve was then placed over the specimen to contain 200 mL of protease inhibitors,

antibacterial, and antifungal agents (Amphotericin B – 2 mL (10 mL/L), Benzamidine – 32 mg (1 mM), EDTA – 4 mL (1 mM), Iodoacetamide – 4 mL (1 mM), Gentamicin – 10 mg (10 µg/mL), Pepstatin A – 3 mL (0.3 µM), Deionised water – 168 mL, and phosphate buffered saline 10x – 18 mL (0.15M)) to keep the disc hydrated, while reducing putrefaction and tissue autolysis. The prepared specimen was then installed into a custom-developed six degree of freedom (6DOF) hexapod robot (Amin et al., 2016b; Ding et al., 2014; Lawless et al., 2014) for testing and warmed to 37 °C to mimic *in vivo* conditions (**Figure 3-2**)

### 3.3.2 Mechanical Testing

#### 3.3.2.1 6DOF

Testing was conducted in a 6DOF hexapod robot using a combined position-load control strategy, where the primary axis was driven in position control while the compressive axis was held at a constant preload and the other four axes were unconstrained with a force/moment target of zero (Lawless et al., 2014). Each FSU was subjected to a 20-hour axial compressive preload equivalent to a nucleus pressure of 0.1 MPa, which allows the disc to reach steady-state hydration and represents the unloaded lumbar disc during sleeping (Edwards et al., 2001; Johannessen et al., 2004; O'Connell et al., 2011a; Wilke et al., 1999). The relationship between the applied external FSU compressive stress and nucleus pressure is linear, having a slope of approximately 1.5 (Edwards et al., 2001), which was used to calculate the required external compressive force from radiographs of the unloaded disc area (Nachemson and Morris, 1964).



a.

b.

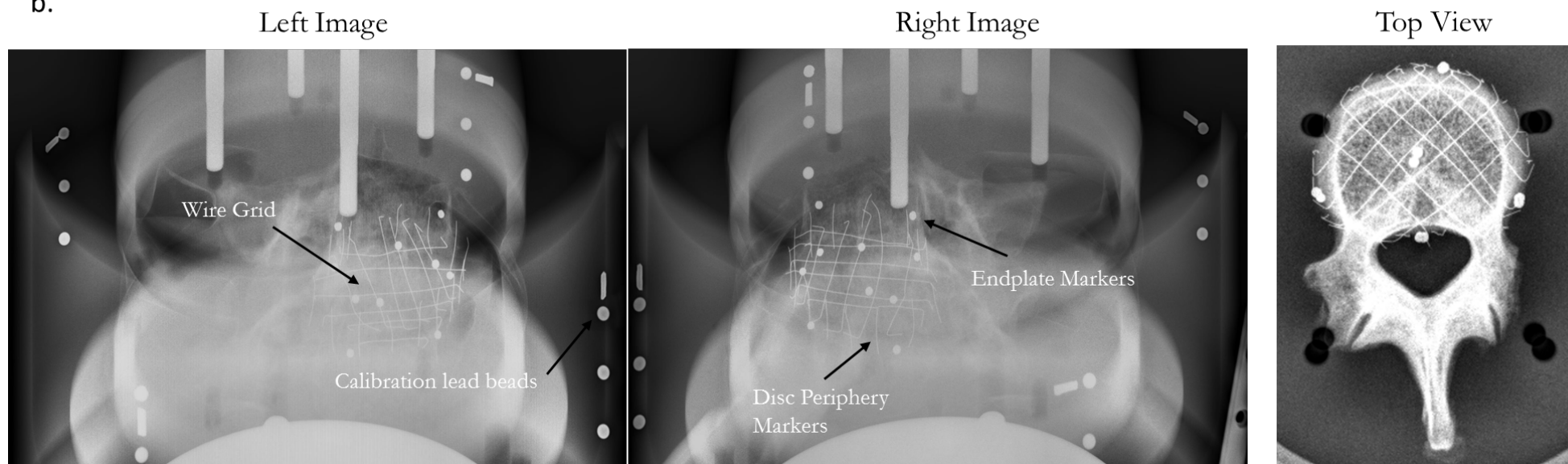


**Figure 3-1** a. An overview of the testing sequence. b. Left and right stereoradiographs showing the wire grid, calibration beads, disc periphery and endplate markers in addition to a top view showing the wire grid and endplate markers

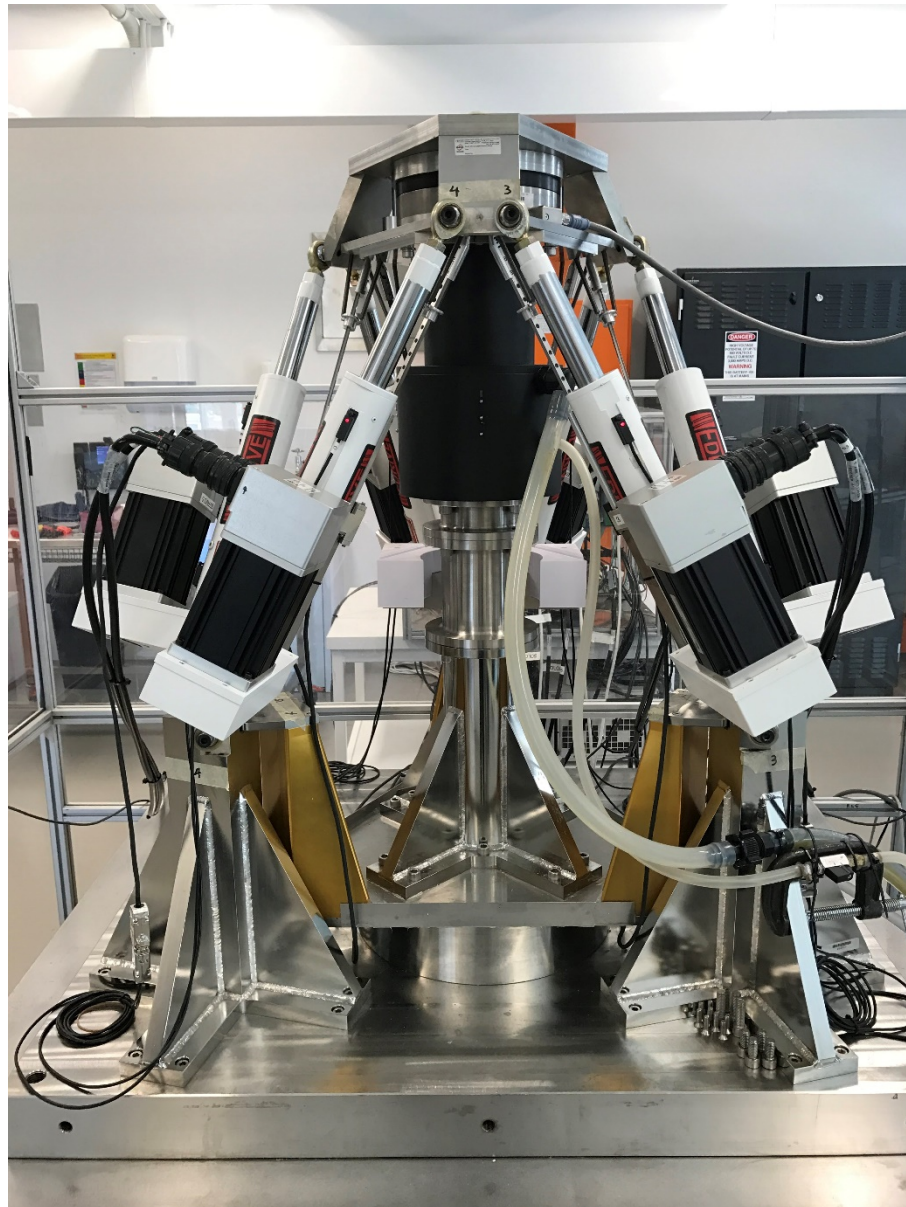


**Figure 3-2** This photo shows the testing setup used in this research. The specimen is inside the calibration cage which is coupled to the hexapod robot

After hydration equilibration, the FSU underwent dynamic haversine displacements or rotations in each DOF under a 0.5 MPa follower preload. The sequence of loading directions was chosen to minimise the biphasic effect (Costi et al., 2008), with shear and axial rotation tests conducted first, followed by bending and axial compression tests. Displacement amplitudes for each DOF were:  $\pm 0.6$  mm for all shear tests (anterior/posterior/lateral shear);  $\pm 2^\circ$  for axial rotation;  $\pm 3^\circ$  for lateral bending;  $5^\circ$  for flexion, and  $2^\circ$  for extension (Costi et al., 2008; Lu et al., 2005; Percy and Tibrewal, 1984; Stokes and Frymoyer, 1987). For the axial compression test, loading was between 0.5 MPa and 1.1 MPa.

For each DOF, five haversine cycles at 1 Hz, 0.1 Hz, and 0.01 Hz were applied, followed by a ten-minute creep recovery period under a compressive load equivalent to a nucleus

pressure of 0.1 MPa (Amin et al., 2016a). Two cycles at 0.001 Hz were then applied followed by another recovery period. The FSU then underwent stress relaxation in each respective DOF (0.6 mm for shears and compression; 2° for flexion, extension, and axial rotation; 3° for lateral bending) for five minutes, and creep (300 N for shears; 10 Nm for flexion, extension, axial rotation and lateral bending; 1.1 MPa for compression) for five minutes, with a creep recovery period of 10 minutes in between. A final ten minutes recovery period at 0.1 MPa was conducted. This sequence of testing was then repeated for each DOF. The total duration for equilibration and testing was approximately 33 hours for each specimen. For this study, data from only the 0.1 Hz dynamic tests were analysed for each DOF since only the 6DOF testing was conducted at 0.1 Hz after wire grid insertion (**Figure 3-1**).

After the initial 6 DOF testing, the control specimens were kept at a preload of 0.1 MPa for three hours to keep the same exposure time as the experimental group between testing (**Figure 3-1**). For the experimental group, the sleeve and superior nylon cup were removed from the specimen. Two perpendicular rows of 0.25 mm diameter tantalum wires (5 mm spacing) were inserted into the mid-transverse plane of the disc using an 18G needle and aligned at  $\pm 45^\circ$  to the mid-sagittal plane (Costi et al., 2007). The periphery of the disc was then marked using approximately 20 equally spaced tantalum wires of length 5 mm, which were fixed to the disc using a small amount of superglue (**Figure 3-1b**).

The superior vertebral body was then re-potted, with axial and lateral radiographs taken to confirm the position of the wires, endplate and disc periphery markers (**Figure 3-1**). The waterproof sleeve, PBS and chemicals were added as previously described. The prepared FSU was then bolted into a calibration cage with twelve 2 mm diameter lead beads that defined a Cartesian coordinate system (Costi et al., 2007). This cage was then coupled to the hexapod robot in a temperature-controlled environment (37 °C).

Each specimen (control and experimental) underwent another 20 hours of hydration equilibration at 0.1 MPa, after which a pair of stereoradiographs were taken to define the reference state of the FSU. The FSU was in an upright position under 0.1 MPa load for the reference state stereoradiographs (Philips DigitalDiagnost). After, hydration equilibrium, a sequence of 6DOF testing was conducted on both control and experimental groups to assess the mechanical properties of the disc after wire grid insertion. Each FSU was subjected to 6DOF testing at 0.1 Hz (haversine) for five loading cycles under a physiological compressive preload (0.5 MPa) in all directions. Once the 6DOF tests were completed, the FSU was subjected to simulated repetitive lifting (3.3.2.2).

### 3.3.2.2 Simulated repetitive lifting

Repetitive compression (1.0 MPa) + hyperflexion + right axial rotation (2°) at 1 Hz was applied to all specimens (control and experimental) for 20000 cycles (one year of lifting assuming 80 lifts per 8 hour working day) or until failure. A compressive force equivalent to the nucleus pressure of 1.0 MPa was applied, where 1.0 MPa represents the nucleus pressure when standing and holding a 20kg box close to the body (Wilke et al., 1999). The degree of hyperflexion applied was based on Adams et al. where L1-2 underwent 13° of flexion and L2-3, L3-4 and L4-5 underwent 15° of flexion (see Appendix E, (Adams and Hutton, 1985). Failure was defined as the loss of disc height by 5 mm relative to the initial height prior to cycle 1. During the repetitive loading, stereoradiographs were taken after application of cycles 1, 500, 1000, 5000, 10000, 15000, and 20000 at the peak of the applied cycle. The stereoradiograph pair were taken by positioning the x-ray tube at 60° to the mid-sagittal plane and 56° to the transverse plane (**Figure 3-1**, (Costi et al., 2007). Due to space limitations in the hexapod robot, digital detectors were mounted behind the specimen such that they were vertical and not perpendicular to the x-ray tube. The mean (95% CI) RMS error of the wire grid intersections between positioning the detector vertically and positioning it perpendicular to the x-ray tube was 0.076 mm (0.0002 mm, see Appendix A), therefore, the error due to having the detector positioned vertical was negligible. After each set of stereoradiographs were taken, the disc was preloaded to 0.1 MPa for five minutes to allow for a creep recovery period before starting the next batch of repetitive cycles.

After completion of testing, each specimen (control and experimental) underwent post-test MRI scans to assess tissue damage. Sagittal images of each FSU were taken from a 3T MR scanner using a T2 (TR: 3760 ms TE: 98.0 thickness: 4 mm) and T1 (TR: 750 ms TE: 13 ms thickness: 4 mm) weighted sequence. Axial images were also taken using both T2 (TR: 2200 ms TE: 81 ms thickness: 2 mm) and T1 (TR: 2900 TE: 14 thickness: 2 mm) weighted sequences. The MR sequence for these images was different to the pre-test since they were optimised for scanning isolated FSUs instead of whole lumbar spines.

### 3.3.3 Data and Statistical Analysis

Each stereoradiograph pair were manually digitised using custom-written software to identify the calibration, endplate and disc periphery markers, and midpoints of each wire. The method described by Costi et al. was used to calculate the 3D coordinates of endplate and disc periphery markers, and the intersections of the wire grid (Costi et al., 2007), however, twelve to fifteen points were chosen to define each wire instead of nine (Costi et al., 2007). The worst-case mean (95% CI) RMS error of marker coordinates, after repeating

the digitising five times was 0.060 mm (0.018mm) with an intraclass correlation coefficient of 0.891. Displacement vectors of each disc nodal coordinate (**Figure 3-3**) were calculated relative to the reference state, from which the 3D strain tensor was calculated (Costi et al., 2007). MSS were calculated from the 3-D strain tensor and expressed as % (Costi et al., 2007). For regional assessment of MSS, the grid was divided into nine regions: anterior, left/right anterolateral, left/right lateral, posterior, left/right posterolateral, and nucleus (**Figure 3-3**). A repeated measures ANOVA was performed on MSS having a within-subjects factor of cycle number and a between-subjects factor of disc region ( $p < 0.05$ ). Post-hoc multiple comparisons using a Bonferroni correction on alpha were performed when significant main effects were present.

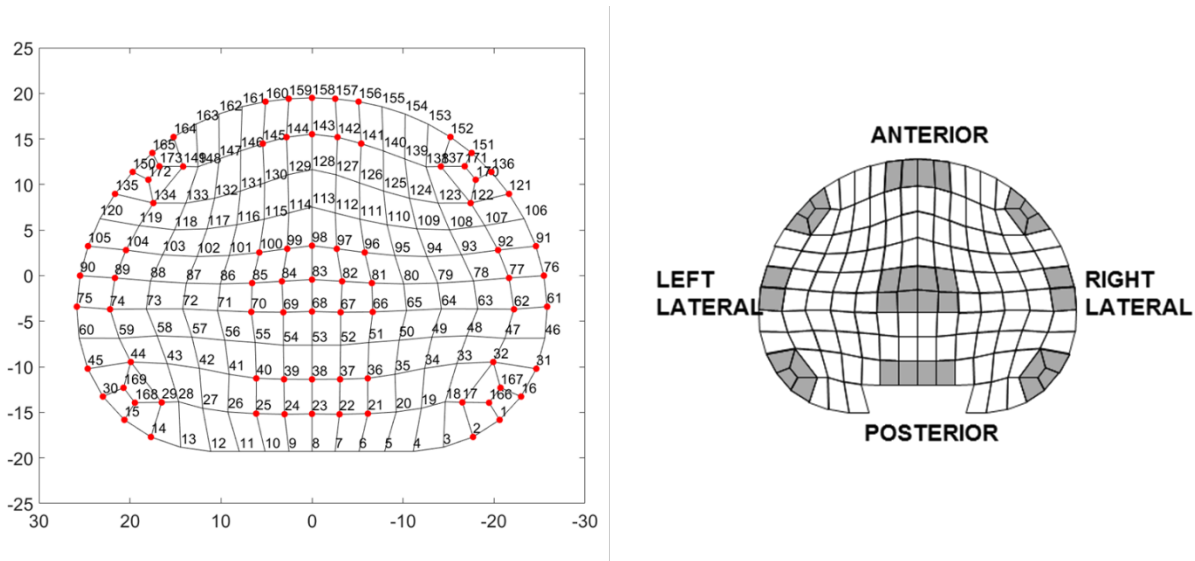


**Figure 3-3** Left Image: Nodal coordinates of the disc grid used to interpolate displacements and calculated strains (173 nodes). Right image: nine regions were defined: anterior, left/right anterolateral, left/right lateral, left/right posterolateral, posterior, and nucleus. The nine regions are highlighted in the grey and by the red dots on the left image

### 3.3.3.1 Validation of Wire Grid Technique

To validate the use of the wire grid technique, the 6DOF properties of the FSU were compared before and after insertion of the grid. For the 6DOF properties, stiffness over a specific range (Amin et al., 2016b) and phase angle (energy absorption) over all five cycles were calculated in each DOF for all specimens. To assess if the mechanical properties of the FSU were affected after wire grid insertion, separate repeated measures ANOVA were performed for each DOF on the outcome measures of stiffness and phase angle, having a within-subjects factor of intervention (before and after wire grid insertion), and a between-subjects factor of group (control vs. experimental). Post-hoc multiple comparisons using a Bonferroni correction on alpha were performed where significant differences were accepted when  $p < 0.05$ .

### 3.4 Results

Assessment of degenerative grade from three raters using the Pfirrmann method revealed grades I (N=2), II (N=12), and III (N=2), **Table 3-1**). There was high inter-observer reliability on the grade of disc degeneration for each specimen, with an alpha value of 0.823. One specimen was excluded after four wires were ejected from the specimen during testing.

No significant difference was found for applied cycles between control and experimental groups ( $p=0.581$ , **Table 3-1**), with one specimen from each group failing at 500 cycles due to a failure of the superior endplate of the L5 vertebra. No significant overall interaction effects between intervention (before and after wire grid insertion) and group (control and experimental) were found for stiffness and phase angle in all DOFs ( $p>0.074$ , see **Appendix B**), indicating that there were no differences in 6DOF mechanical properties before and after wire grid insertion. After fatigue testing, similar failure modes were seen between the two groups, where 38% of specimens failed via herniation or annular protrusion in the control group and 50% in the experimental group (**Table 3-1, Figure 3-4**). In addition, there were 14% endplate failures in the control group and 25% in the experimental group (**Table 3-1**).

Tissue displacement vectors calculated from the experimental group confirm the bending and rotation applied to the disc (**Figure 3-5**), with anterior displacements negative, indicating tissue is in compression in compression and posterior displacements positive, indicating tissue is in tension. In addition, the displacement vectors in the right anterior (central region) of the disc revealed migration of the tissue towards the posterior region (**Figure 3-5**). Within the anterior region of the outer annulus, there were adjacent rows of tissue that displaced in opposite (anterior vs posterior) directions, which may indicate a region at risk of potential delamination.

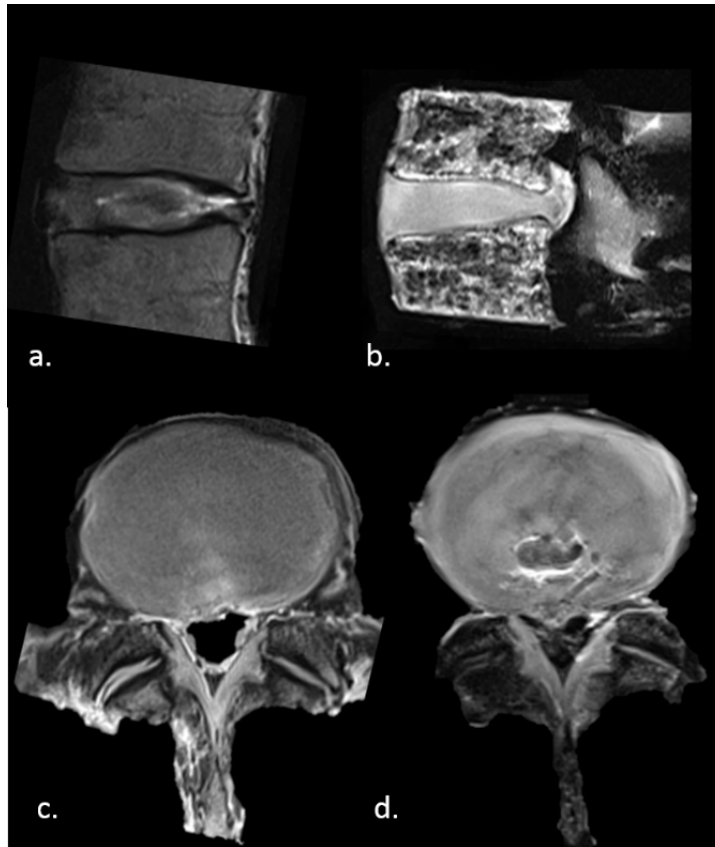


**Figure 3-4** T1 MRI images of FSUs pre- and post-repetitive lifting. a. Pre-test sagittal (TR: 750 ms TE: 13 ms thickness: 4 mm) b. Post-test sagittal (TR: 750 ms TE: 13 ms thickness: 4 mm) c. Pre-test axial (TR: 2900 TE: 14 ms thickness: 2 mm) d. Post-test axial (TR: 2900 TE: 14 ms thickness: 2 mm). Images (ab) and (cd) are two different specimens. Herniation is evident in (b) and nucleus disruption and posterior annular tears are evident in (d)

**Table 3-1** Specimen characteristics, including degenerative (Pfirrmann) grade, initial disc height, applied cycles, disc height loss, and failure mode. Initial disc height was calculated from the unloaded FSU using lateral x-ray image

<b>Specimen</b>	<b>Group</b>	<b>Pfirrmann Grade</b>	<b>Initial Disc Height (mm)</b>	<b>Applied Cycles</b>	<b>Disc height loss (mm)</b>	<b>Failure Mode</b>
1	Control	2	9.0	20000	-1.82	No Injury
2	Control	2	12.3	20000	-4.00	Annular protrusion
3	Control	2	10.3	500	-5.10	Superior Endplate Failure of L5
4	Control	2	9.3	20000	-3.17	No Injury
5	Control	3	10.3	20000	-3.48	No Injury
6	Control	3	9.7	20000	-2.73	LDH
7	Control	3	10.0	20000	-4.57	LDH
8	Experimental	3	13.3	500	-5.15	Superior Endplate Failure of L5
9	Experimental	2	11.3	20000	-3.69	Annular protrusion
10	Experimental	2	11.30	20000	-1.33	Annular protrusion
11	Experimental	2	9.70	20000	-1.02	No Injury
12	Experimental	2	12.3	20000	-3.09	Annular protrusion
13	Experimental	2	9.3	5000	-5.00	Superior Endplate Failure of L2
14	Experimental	3	8.0	20000	-3.73	Superior Endplate Failure of L2 and Annular protrusion
15	Experimental	3	10.0	20000	-3.91	LDH

**Figure 3-5** Internal disc average displacements in the axial and lateral view at each cycle interval (averaged across all seven specimens, lateral view: positive x is anterior). Magnification: 2x

There was a significant overall within-subjects effect between cycles for MSS ( $p < 0.001$ , **Figure 3-6** and **Figure 3-7**, see **Appendix C** for principal strains). *Post-hoc* pairwise comparisons revealed that MSS at cycle 20,000 was significantly greater than all other cycles ( $p < 0.003$ , Figure 4). MSS at cycle 1 and cycle 500 were significantly lower than all other cycles ( $p < 0.004$ ). MSS at cycle 15,000 was significantly lower than cycle 10,000 by 3% and cycle 20,000 by 7% ( $p < 0.018$ , Figure 4). The mean (95% CI) MSS for the whole disc at cycle 1 was 51% (2%) and was 59% (3%) at cycle 20000.

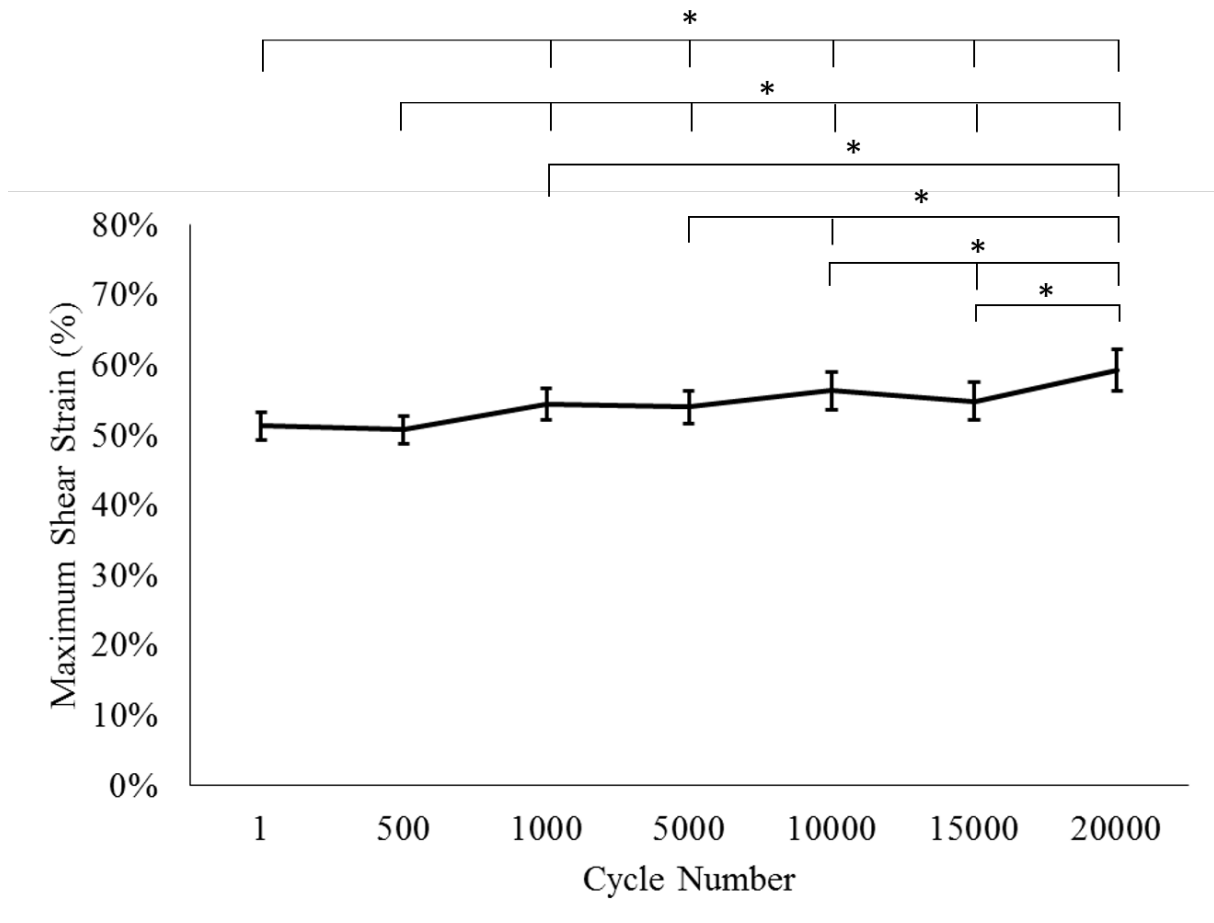


**Figure 3-6** Mean (95% CI) MSS as a function of cycle number (averaged across seven specimens and all regions combined). \* indicates a significant difference in respect to the cycle on the left of the bar (i.e. for the top horizontal bar, a significant difference in respect to cycle 1)

**Figure 3-7** Contour plots showing MSS (%) at each of the different cycle time points (averaged across seven specimens, see **Appendix D** for individual specimen MSS contour plots)

A significant between-subjects effect for region was found for MSS ( $p < 0.001$ , **Figure 3-7** and **Figure 3-8**). *Post-hoc* pairwise comparisons found that MSS in the anterior, left posterolateral, and left lateral regions were significantly greater than the nucleus region ( $p < 0.006$ ). The MSS in the anterior and left posterolateral regions were significantly larger than the left anterolateral and right lateral regions ( $p < 0.022$ ). The anterior region MSS was also significantly greater than the posterior, right anterolateral, and posterior regions ( $p < 0.001$ ). The anterior region had the largest mean (95% CI) MSS of 76% (6%) and the nucleus region had the lowest MSS at 42% (5%). The left posterolateral and left lateral were the other regions with high strains, 64 % (7%) and 60 % (8%), respectively. Trends show that four regions (Ant, LPostLat, RPostLat, and LLat) had MSS greater than 50%.

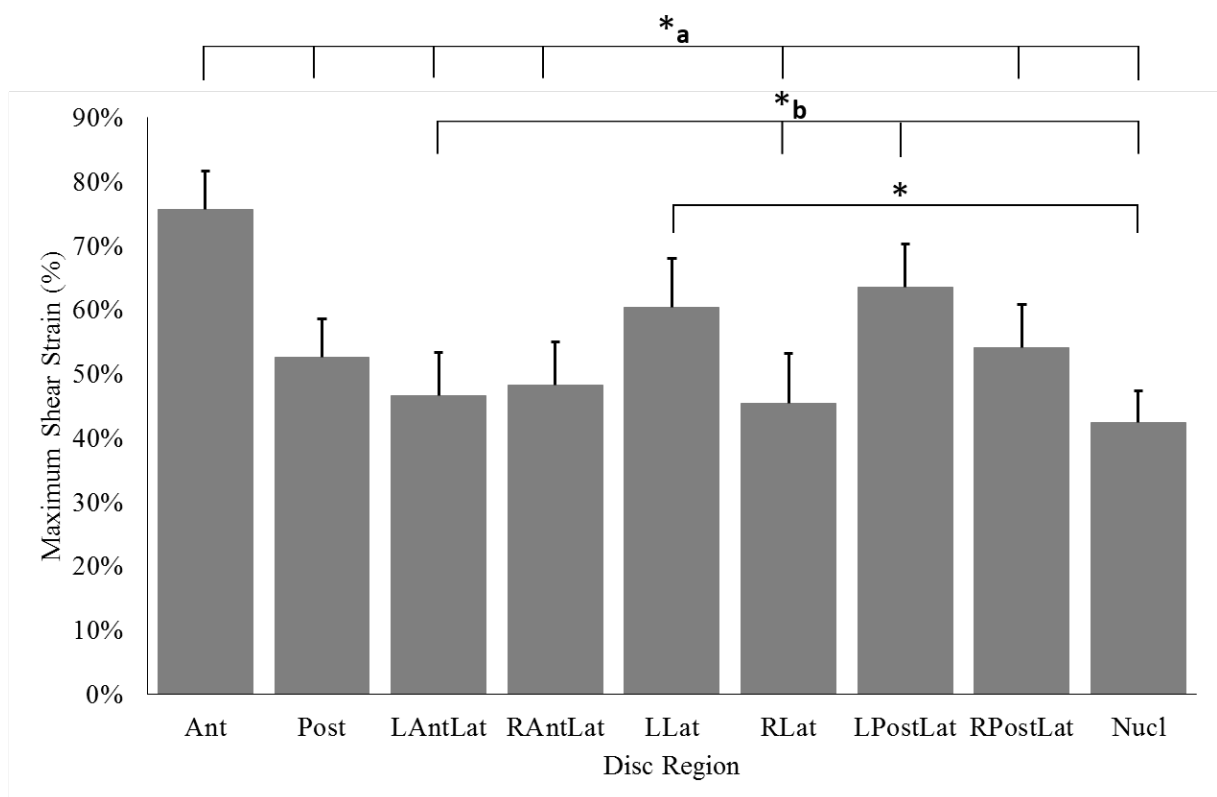


**Figure 3-8** Mean (95% CI) MSS as a function of disc region (average across seven specimens and all cycles combined). Ant: anterior, LAntLat: left anterior lateral, LLat: left lateral, LPostLat: left posterolateral, RAntLat: right anterior lateral, RLat: right lateral, RPostLat: right posterolateral, Post: posterior, and Nucl: nucleus. \*a: significant difference compared in relation to the anterior region. \*b: significance difference compared to the left posterolateral region

There was a significant interaction effect between cycle number and region ( $p < 0.001$ , **Figure 3-9**). Post hoc comparisons revealed that there were no significant differences in MSS between cycles in the left anterolateral, right lateral, and nucleus regions ( $p > 0.070$ ). Within the anterior region, MSS at cycle 20,000 was significantly greater than cycle 500, 10,000, and 15,000 ( $p < 0.033$ ). MSS at cycle 15,000 was significantly lower than at cycle 15,000 for the following regions as well: left posterolateral ( $p < 0.001$ ), right posterolateral

( $p < 0.001$ ), and right anterolateral ( $p = 0.006$ ). At cycle 500, MSS was significantly lower than cycle 1 in the left and right posterolateral regions ( $p < 0.002$ ).

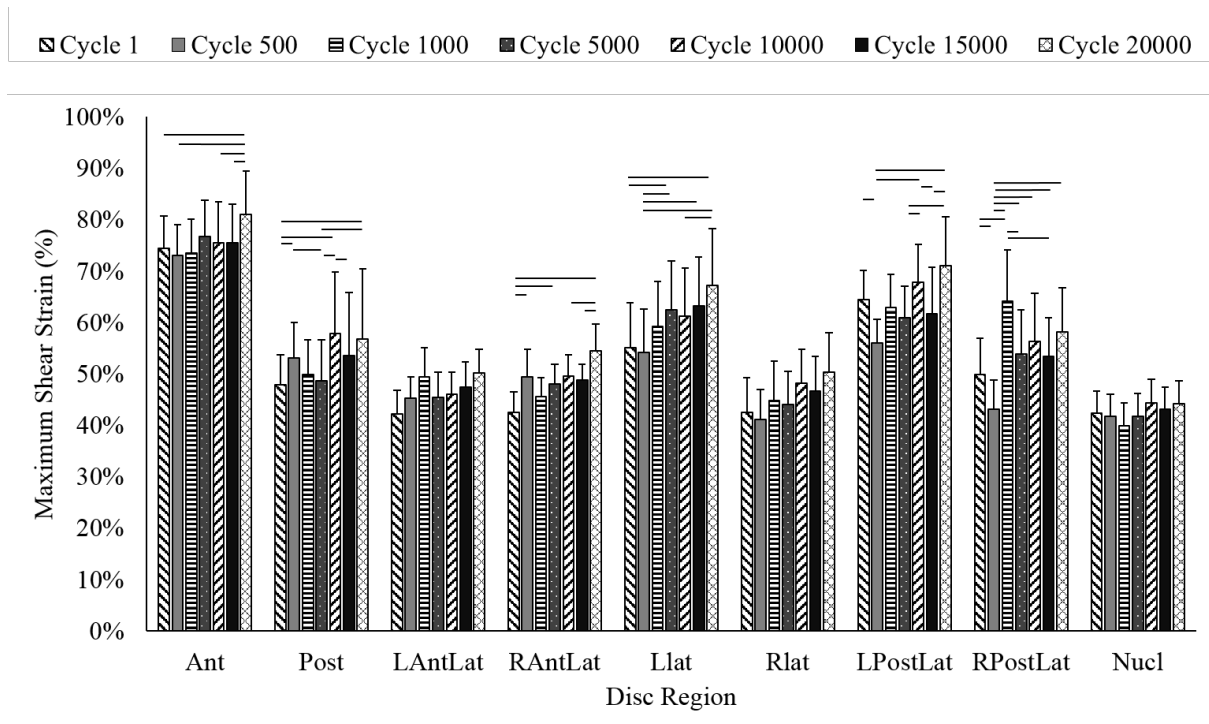


**Figure 3-9** Mean (95% CI) MSS as a function of disc region and cycle number (averaged across all seven specimens). Bars represent significant interactions within each region and cycle number ( $p < 0.05$ )

### 3.5 Discussion

This study sought to quantify the disc tissue behaviour during repetitive loading by measuring internal disc strains. MSS was reported in this study since shear loading plays an important role in the creation of disc injuries such as delamination, which is a precursor to LDH (Tavakoli et al., 2018) and disc degeneration (Fazzalari et al., 2001). A combination of flexion, right axial rotation, and 1.0 MPa of physiological compression was used to simulate repetitive lifting, which led to the largest shear strain in the anterior, left posterolateral and left lateral regions. Interestingly, the strains did not consistently increase in all regions as cycle number increased, however, the largest MSS were found after cycle 20000 and the lowest shear strain was found after cycles 1 and 500. The applied combined loading lead to LDH in three specimens, and annular protrusion in five specimens, which is a precursor to herniation.

The technique for measuring internal disc strains was invasive, where tantalum wires were inserted into the disc to form a grid (Tsantrizos et al., 2005). While metallic markers have been used in the past to measure 2D and 3D internal disc strains (Costi et al., 2007; Krag et al., 1987; Seroussi et al., 1989; Tsantrizos et al., 2005), it has been previously documented that needle puncture can alter disc mechanics *in vivo* (Carragee et al., 2009;

Korecki et al., 2008). Therefore, further validation of this technique was performed in this study by measuring the mechanical properties of the disc before and after wire grid insertion. However, no consistent significant differences in mechanical properties were found in any direction before and after wire grid insertion, indicating the wire grid likely had minimal effect on the outcomes of this research. Furthermore, the change in disc height after hydration under 0.1 MPa compressive load between the control and experimental group (wires inserted) was not significant, implying that the wire grid did not depressurise the disc.

It is important to acknowledge the absence of biology as cadaveric human tissue was used for this study. However, the focus of this study was to measure the internal disc strains and as blood supply to the disc is minimal (Maroudas et al., 1975), adaptive remodelling would not be as quick as bone or muscle (Maroudas et al., 1975), therefore repetitive loading would result in cumulative mechanically-induced damage that outpaces the disc's ability to repair. In addition, the initial baseline level of prior repetitive loading activity on each donor's lumbar spine was unknown, which would indeed be impossible to know. It is, therefore, possible that differences in strains and failure modes between specimens may, in some part, be caused by variations in donor activity levels, i.e. the levels of fatigue that each spine had experienced. Another limitation is the long duration of testing with cadaveric tissue, however, anti-fungal, anti-bacterial, and protease inhibitors were used to eliminate putrefaction. There was no evidence of tissue putrefaction in any specimen and disc mechanical integrity was maintained since the mechanical properties after 3 days did not significantly change. The use of hydration and these agents, together with testing at body temperature, strengthens this study since testing was performed in a more-physiological environment. Furthermore, it is important to note that only five minute recovery periods were used after each cycle time point, whereas in real life, there would be more time for the disc tissue to recover between lifting periods.

Even though cycle number significantly affected MSS overall, there wasn't a consistent increase in strain from cycle 1 to cycle 20000 (**Figure 3-6**, see **Appendix E** for moment and force data). There was a significant decrease in MSS from cycle 10000 (56%) to cycle 15000 (55%) followed by an increase in strain at cycle 20000 (59%), which could be an indication of potential progression of tissue damage. Interestingly, within the strain contour plots, at cycle 10000, there are higher strains in the left lateral and posterolateral regions as shown by the increase in brighter colours. These higher strains may indicate the initiation of tissue damage and subsequent annular protrusion or herniation. During repetitive loading, there was a mean (95%CI) loss of disc height of 3.4 (0.6) mm due to

compressive creep, which may stiffen the disc and resist large increases in tissue deformations. Therefore, this creep effect is likely the reason why there were gradual changes in strain with cycle number.

MSS was hypothesised to be the largest in the posterolateral region, which is a common site of herniation and a region that is subjected to high strains when axial rotation is applied (Costi et al., 2007), however, found the largest strains were found in the anterior region. According to Costi et al., the largest MSS during flexion were found in the anterior and right anterolateral regions. The majority of the specimens in the present study were subjected to 15° of flexion (hyperflexion), which could attribute to the 76 % MSS in the anterior region seen in the present study. Intuitively, large shear strains of 64% and 60% were measured in the opposite side, left posterolateral and left lateral, respectively, to the direction of right axial rotation that was applied to the specimens, which is consistent with findings in the literature (Schmidt et al., 2007a). The high shear strains seen in the left posterolateral region are consistent with Schmidt et al., who also found MSS to be the highest in the left posterolateral region under a combination of flexion and right axial rotation (Schmidt et al., 2007b). Strains as high as 47% were seen for Grade 1 discs (mildly degenerated), which are smaller than the present study strains, however, this was with only 500 N of compression (Schmidt et al., 2007b), compared to a mean (95% CI) of 946 (46) N in the present study. In addition, the mean (95% CI) flexion bending moment was 51.2 Nm (14.7 Nm) at cycle 1. The combination of this flexion moment with the compressive force (-1364 N (355 N)), may lead to the large magnitudes of shear strain found in this study. Interestingly, smaller strains were seen in the posterior region, implying that there is a stiffer tissue structure in shear within that region. This also indicates that the combination of compression, flexion and axial rotation has more of an impact on the posterolateral regions (Veres et al., 2010), and may explain the reason for why posterolateral annular protrusion and herniation were observed.

Only 20% of the specimens failed via LDH in this study, which was consistent with other studies (Adams and Hutton, 1985; Gordon et al., 1991). However, the loading applied between those studies and the present study was different. This study was able to apply more physiological loading by applying cyclic flexion and rotation with a constant compressive preload, hydration and temperature control. Therefore, it was hypothesised that LDH would be more prevalent in this cohort of specimens. As testing was conducted at a frequency of 1Hz, the control system, which was operating in load control in real-time for all other axes, was unable to allow for the migration of the centre of rotation (Lawless et al., 2014), which is likely occurring *in vivo*. This load control challenge would likely have

implications on the consistency in reproducing LDH in cadaveric specimens. However, since eight specimens either had no injury or annular protrusion, it may be possible that a greater number of applied loading cycles could have also resulted in a larger percentage of LDH.

### 3.6 Conclusion

This study, for the first time, measured internal disc strains during simulated repetitive lifting, which has previously been associated with LDH. Repetitive combined flexion, right axial rotation, and compression resulted in large MSS in the anterior (76%), left posterolateral (64%) and left lateral (60%) regions. The large shear strains in the posterolateral region further support current clinical evidence regarding LDH occurring more frequently within that region. Normal to mildly degenerated discs are resilient to large changes in tissue deformation since only an 8% increase in shear strain was found between cycle 1 and 20000. It is important for future research to develop an understanding of the threshold of strain within each region that causes disc injury. These strains can be used to develop and further validate robust finite element models to help understand the mechanisms of LDH and other disc injuries.



## Chapter 4 Lumbar Intervertebral Disc Multiaxial Mechanics are Altered after Simulated Repetitive Lifting Movements<sup>3</sup>

The previous chapter (**Chapter 3**) measured the internal disc strains during simulated repetitive lifting, which can be characterised as tissue level mechanics. However, the FSU (organ level) mechanics may be altered after simulated repetitive lifting as well. Knowing which directions are affected by repetitive lifting may help determine which muscles need to be strengthened to stabilise the changes in 6DOF mechanics. It is important to measure both tissue and organ level mechanics to develop a multiscale understanding of the effect of repetitive lifting. Therefore, this chapter explores changes in 6DOF mechanics after simulated safe repetitive lifting and in relation to the resulting failure modes.

---

<sup>3</sup> The information in this chapter has been submitted to Journal of Biomechanics on November 26, 2018 and is currently under review.

Amin, D.B., Moawad, C.M., Costi, J.J., 2018 Manuscript Under Review. Lumbar intervertebral disc multiaxial mechanics are altered after simulated repetitive lifting movements. Journal of Biomechanics.

## 4.1 Abstract

No studies have quantified the changes in six degree of freedom (6DOF) functional spinal unit (FSU) stability after disc injury due to repetitive lifting. Therefore, the aim of this study was to determine the effect of simulated repetitive lifting and the resulting failure modes on 6DOF FSU stiffness and phase angle. Fifteen FSUs underwent  $\pm$ 6DOF tests at 0.1 Hz for five cycles followed by simulated repetitive lifting, and repeated 6DOF testing. Combined compression (1.0 MPa), flexion (13-15°) and right axial rotation (2°) was applied for 20,000 cycles or until failure to simulate repetitive lifting. Significant decreases in stiffness were seen in compression, flexion, and lateral shear with an increase in extension ( $p < 0.047$ ). For phase angle, significant increases were found in compression, left axial rotation, and posterior shear with a decrease in extension ( $p < 0.049$ ). There was no effect of failure mode on mechanical properties ( $p > 0.054$ ). The changes in mechanical properties could be caused by a combination of deformation in anterior annulus due to the applied flexion, tissue damage, reduced disc height, and a migrating centre of rotation. Further investigation is needed to understand the changes in mechanical properties associated with LDH and protrusion.

## 4.2 Introduction

Repetitive lifting is commonly undertaken by manual labourer workers, with consequences of LDH or protrusion that leads to sciatica (Heneweer et al., 2011; Jordan et al., 2011; Lavender et al., 1999; Marras et al., 1993). Epidemiological and *in vitro* studies have shown that combinations of bending and twisting during repetitive lifting can lead to those disc injuries and low back pain (Adams and Hutton, 1985; Kelsey et al., 1984b; Marras et al., 2001; Wilke et al., 2016). Furthermore, kinematic studies have investigated the effects of repetitive lifting on muscles and whole-body mechanics to develop safe lifting practices (Dolan and Adams, 1998; Mehta et al., 2014). These studies have found muscle fatigue occurred during repetitive lifting (Dempsey, 1998; Dolan and Adams, 1998; Mehta et al., 2014), leading to a significant increase in lumbar flexion angle (4.7°), and a 36% increase in bending moment acting on the lumbar spine (Dolan and Adams, 1998). However, there's little understanding of the effect that repetitive lifting has on the intervertebral disc, which is important to measure as the disc is a site of injury.

*In vitro* studies have examined how repetitive loading affects disc injury to understand the propagation of LDH (Adams and Hutton, 1985; Berger-Roscher et al., 2017; Callaghan and McGill, 2001; Drake et al., 2005; Gordon et al., 1991). These *in vitro* studies measured mechanical properties of the disc during repetitive loading in the direction of load

application. Gordon et al. 1991 found that compressive stiffness decreased by approximately 40% and energy loss increased after repetitive combined flexion, rotation, and compression on human lumbar functional spinal units (FSUs). It is therefore likely that the 6DOF mechanical behaviour of the FSU is affected by repetitive lifting, which may result in destabilisation. However, no studies have quantified the effect of repetitive lifting and resulting failure modes on 6DOF FSU stability to understand disc mechanics.

Therefore, the aim of this study was to determine the effect of simulated repetitive lifting movements on 6DOF stiffness and energy absorption of normal to mildly degenerated human lumbar spinal segments. A secondary aim was to examine the effect of failure mode on 6DOF mechanical properties. It was hypothesised that repetitive lifting would decrease the stiffness and increase the energy absorption of the FSU in all loading directions due to cumulative tissue damage to the disc, facet capsule, and ligaments.

## 4.3 Methods

### 4.3.1 Specimens

This study was approved by the Human Research Ethics Committee (OFR 18.14). Eight fresh-frozen spines (mean (SD) age 53 (14) years) were stored at  $-20^{\circ}\text{C}$  and then thawed at room temperature before undergoing a pre-test MRI for Pfirrmann degenerative grade assessment (Pfirrmann et al., 2001). These spines and specimens are the same as the ones used in Chapter 3. Spines were then dissected of all non-ligamentous tissue, keeping both the anterior and posterior longitudinal ligaments (ALL and PLL, respectively) and facet joint capsules intact. Fifteen cadaveric lumbar FSUs, including posterior elements, were dissected (L1-2 x 3, L2-3 x 4, L3-4 x 1, L4-5 x 7). The superior and inferior vertebral surfaces of the FSU were then cut parallel to the mid-transverse plane of the disc using a bandsaw, where the FSU was composed of a full superior and inferior vertebra. Specimens were re-frozen until the day prior to testing, thawed overnight in the refrigerator, followed by a minimum of three hours at room temperature.

### 4.3.2 Specimen Preparation

Each vertebral body was embedded in a cup using polymethyl methacrylate (PMMA) and three fixation screws. An alignment device was used to ensure that the superior and inferior surfaces of each cup were parallel to each other and parallel to the mid-transverse plane of the disc. Axial, anterior-posterior (AP) and lateral (LAT) radiographs were taken of all specimens to determine the instantaneous axis of rotation of the disc relative to the cups, which was used as the centre of rotation for all testing (Percy and Bogduk, 1988). An encapsulating sleeve was then placed over the specimen, which contained 200 mL of a

mixture of protease inhibitors, antibacterial, and antifungal agents (Amphotericin B – 2 mL (10 mL/L), Benzamidine – 32 mg (1 mM), EDTA – 4 mL (1 mM), Iodoacetamide – 4 mL (1 mM), Gentamicin – 10 mg (10 µg/mL), Pepstatin A – 3 mL (0.3 µM), deionised water – 168 mL, and phosphate buffered saline – 18 mL (0.15 M)) to reduce putrefaction and tissue autolysis. The potted specimen with the mixture was then immersed into a 37°C water bath to mimic *in vivo* conditions and then installed into a custom-developed six degree of freedom (6DOF) hexapod robot for testing (Ding et al., 2014; Lawless et al., 2014). Each FSU was randomly assigned to one of two groups (control (n = 7) or experimental (n = 8)), where control FSUs underwent repetitive loading without strain measurement and experimental FSUs underwent testing with strain measurement (Amin et al., 2018 Manuscript Under Review-b; Costi et al., 2007).

#### 4.3.3 Mechanical Testing

Before testing, each FSU was hydrated for 20 hours with an axial compressive preload applied that was equivalent to a nucleus pressure of 0.1 MPa to represent the unloaded lumbar disc during sleeping (Wilke et al., 1999). The relationship between the applied external FSU compressive stress and nucleus pressure is linear, with nucleus pressure being greater by a factor of approximately 1.5 (Edwards et al., 2001). This factor was used to calculate the required external compressive force based on the unloaded disc area, to generate the equivalent nucleus pressure. The unloaded disc area was estimated based on the formula  $0.84 \times AP \times LAT$  (Nachemson and Morris, 1964), where AP and LAT were the largest anteroposterior and lateral dimensions of the inferior and superior vertebrae, averaged over three measurements from the AP and LAT x-rays. Disc area measurements were taken before potting the FSU.

Each FSU was then subjected to 6DOF testing at 0.1 Hz (haversine) for five loading cycles under a physiological compressive preload (0.5 MPa), and hydration (protease-inhibitors, phosphate-buffered saline bath) and temperature (37°C) conditions in a hexapod robot. The primary testing axis was driven in position control while off-axis coupling forces and moments were simultaneously minimised to zero in load control. The sequence of loading directions was chosen to minimise the biphasic effect (Amin et al., 2016a; Amin et al., 2016b; Costi et al., 2008), with shear and axial rotation tests conducted first, followed by bending and axial compression tests. Non-destructive applied  $\pm 6$ DOF amplitudes were 0.6 mm in shear, 2° axial rotation, 3° lateral bending, 5° flexion, 2° extension and 1.1 MPa compression (Costi et al., 2008; Lu et al., 2005; Percy and Tibrewal, 1984; Stokes and Frymoyer, 1987). Between each DOF, a ten-minute creep recovery period under a compressive load equivalent to a nucleus pressure of 0.1 MPa was applied.

After 6DOF testing, simulated repetitive lifting of a 20 kg box while bending and twisting was applied for 20,000 cycles to simulate one year of manual handling. This lifting was replicated in the hexapod robot by applying repetitive flexion (13-15°, (Adams and Hutton, 1985; Pearcy and Tibrewal, 1984), and right axial rotation (2°) under a constant compressive preload of 1.0 MPa for 20,000 cycles or until failure (Amin et al., 2018 Manuscript Under Review-b; Wilke et al., 1999). Failure was defined by a decrease in FSU height by 5 mm, and the test was aborted before 20,000 cycles. After completion of repetitive loading, each FSU then underwent a repeat of the 6DOF mechanical testing, followed by a post-test MRI to assess failure mode after 20,000 cycles.

#### 4.3.4 Data and Statistical Analysis

Data from the final cycle of each 6DOF test was analysed in MATLAB (2017b, The Mathworks Inc.). Stiffness for each DOF was calculated using linear regression to determine the slope (MATLAB: POLYFIT.m having an order of 1) over a specific range of the loading portion of the load-displacement curve. The ranges for stiffness calculations for each DOF were: 0.4–0.58 mm for all shear tests, 3.45°–4.75° for flexion and lateral bending, 0.85°–1.25° for extension, 1.5°–1.8° for axial rotation, and 0.77–1 MPa for axial compression (Amin et al., 2016b). Phase angle (a measure of energy absorption/damping) for each DOF was calculated between the input displacements and measured forces for all cycles using the cross-spectral density estimate function (MATLAB: CSD.m).

Statistical analyses were performed using SPSS v25 (IBM, Illinois, USA). Shapiro-Wilk and Levene's tests were performed to assess the normality and homogeneity of variance of the dependent variables (stiffness, and phase angle), respectively. If the data was not normal and homogenous, statistically significant outliers were removed and/or data were log-transformed. Unpaired t-tests were used to assess the effect of group (control vs. experimental) on stiffness and phase angle for each DOF and paired t-tests for FSU symmetry (left vs. right) in lateral shear, lateral bending, and axial rotation. Separate repeated measures ANOVA were performed for each DOF on each of the outcome measures of stiffness and phase angle, having a within-subjects factor of time (before and after repetitive lifting). To assess the effect of failure mode on mechanical properties, a one-way ANOVA was performed for each DOF on stiffness and phase angle after repetitive lifting with a fixed factor of failure mode. Post-hoc multiple comparisons using a Bonferroni correction on alpha were performed where significant differences were found ( $p < 0.05$ ).

## 4.4 Results

Three specimens were excluded from the analysis as they failed prior to completion of 20,000 cycles. Pfirrmann grade assessment of pre-test MRI on the remaining 12 specimens revealed that 58% were grade 2 and 42% were grade 3 (**Table 4-1**). Twenty-five percent of specimens failed via LDH, 42% had a disc protrusion and 33% had no injury after 20,000 cycles (**Table 4-1**). Disc protrusion was defined as posterior migration of the nucleus, however, the nucleus was still contained the within annulus. LDH was defined as extrusion of nuclear material outside of the annulus. For both stiffness and phase angle, there were no significant differences between the control and experimental groups in all 6DOF directions at both time points (before and after repetitive loading,  $p>0.068$ ). Therefore, the data was pooled for analysis.

**Table 4-1** Characteristics for those specimens that were successfully tested to 20,000 loading cycles, which include Pfirrmann grade, lumbar level, change in FSU height, and failure mode

Specimen	Group	Pfirrmann Grade	Lumbar level	Change in FSU height over 20,000 cycles (mm)	Failure Mode (Assessed from post-test MRI)
1	Control	2	L1-2	-1.82	No Injury
2	Control	2	L2-3	-4.00	Disc Protrusion
4	Control	2	L2-3	-3.17	No Injury
5	Control	3	L4-5	-3.48	No Injury
6	Control	3	L3-4	-2.73	LDH
7	Control	3	L4-5	-4.57	LDH
9	Experimental	2	L4-5	-3.69	Disc Protrusion
10	Experimental	2	L4-5	-1.33	Disc Protrusion
11	Experimental	2	L2-3	-1.02	No Injury
12	Experimental	2	L4-5	-3.09	Disc Protrusion
14	Experimental	3	L1-2	-3.73	Superior Endplate Failure of L2 and Disc Protrusion
15	Experimental	3	L4-5	-3.91	LDH

Paired t-tests to analyse symmetry found no significant differences between left and right lateral bending for stiffness and phase angle ( $p>0.180$ ), which were pooled (pooled lateral bending). However, significant differences were found for both stiffness and phase angle between left and right axial rotation ( $p<0.049$ ) as well as lateral shear ( $p<0.015$ ), therefore this data was not pooled. Similar load versus displacement behaviour was exhibited before and after repetitive lifting for lateral bending, anterior and posterior shear (**Figure 4-1**

and **Figure 4-2**). Differences in the mechanical response were observed in flexion and extension, where moments were considerably different between before and after repetitive lifting (**Figure 4-2**).

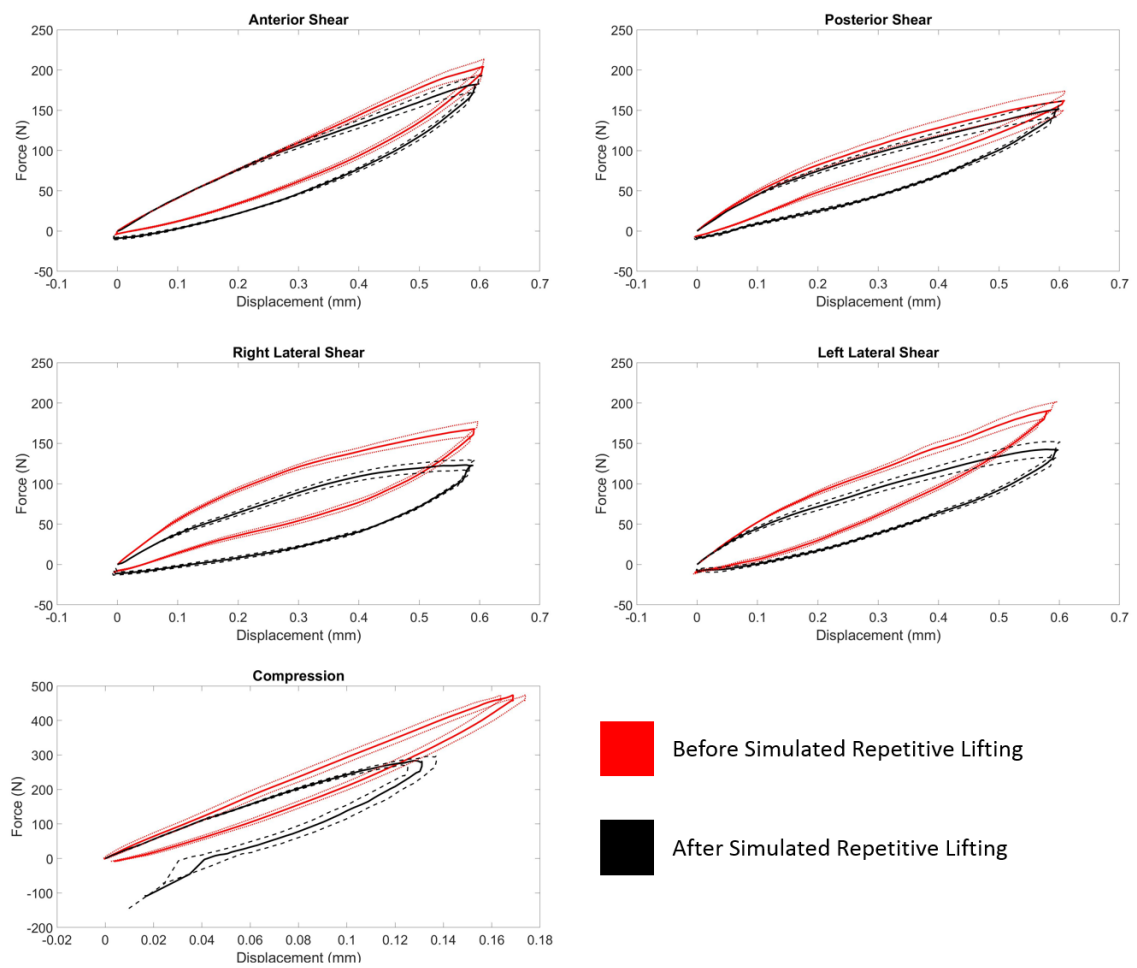


**Figure 4-1** Average load vs. displacement curves for shear and compression DOF, before and after simulated repetitive lifting (averaged over 14 specimens). Dotted lines represent 95% CI

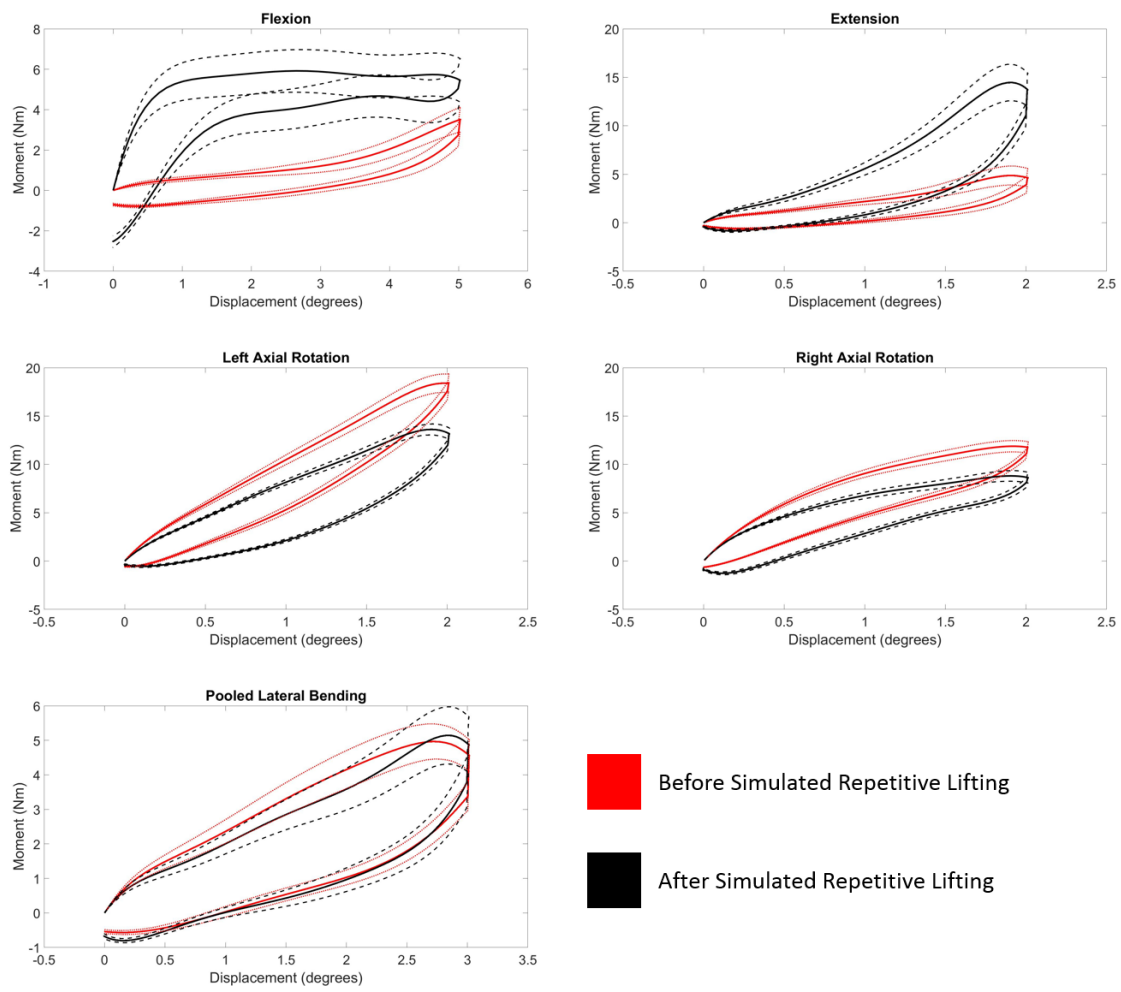


**Figure 4-2** Average load vs. displacement curves for all bending 6DOF directions before and after simulated repetitive lifting (averaged over 14 specimens). Dotted lines represent 95 % CI

#### 4.4.1 Stiffness

Significant decreases in stiffness were found in compression ( $p = 0.046$ , **Figure 4-3**), flexion ( $p = 0.0014$ , **Figure 4-4**), and right and left lateral shear ( $p < 0.016$ , **Figure 4-5**). A significant increase in stiffness was seen for extension ( $p = 0.013$ , **Figure 4-4**). No significant differences were observed in left and right axial rotation, pooled lateral bending, anterior and posterior shear ( $p > 0.071$ ). No significant effect of failure mode on stiffness in any direction was observed ( $p > 0.104$ , **Figure 4-6**).

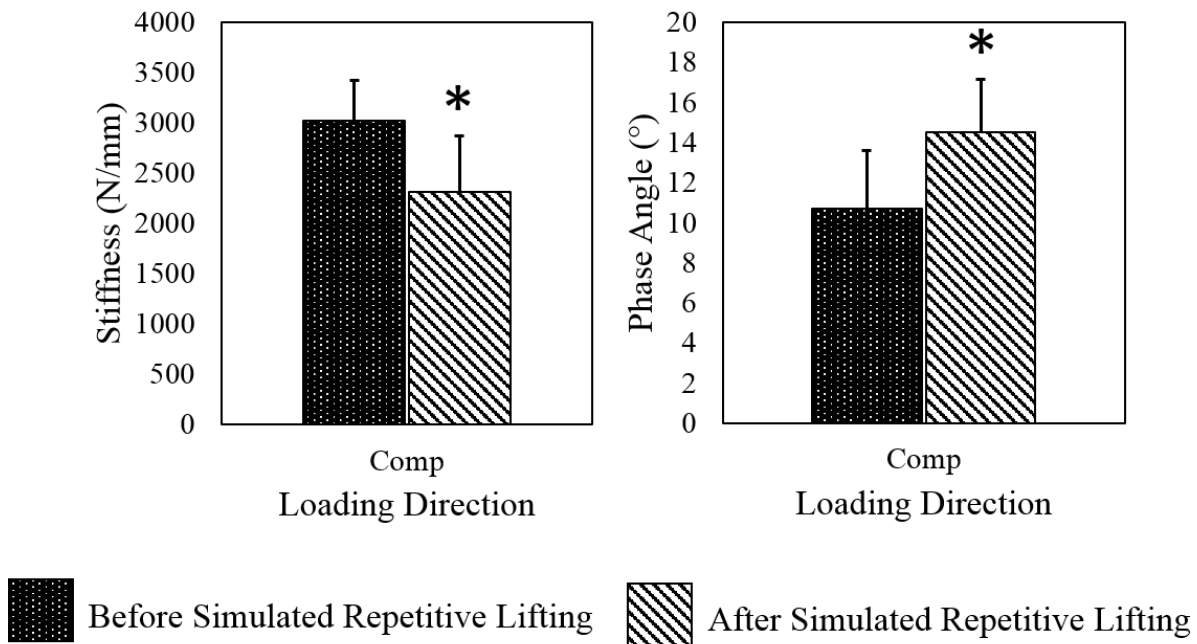


**Figure 4-3** Mean (95% CI) stiffness and phase angle before and after repetitive loading (averaged over 14 specimens) in compression (C). \* denotes significance ( $p < 0.05$ )

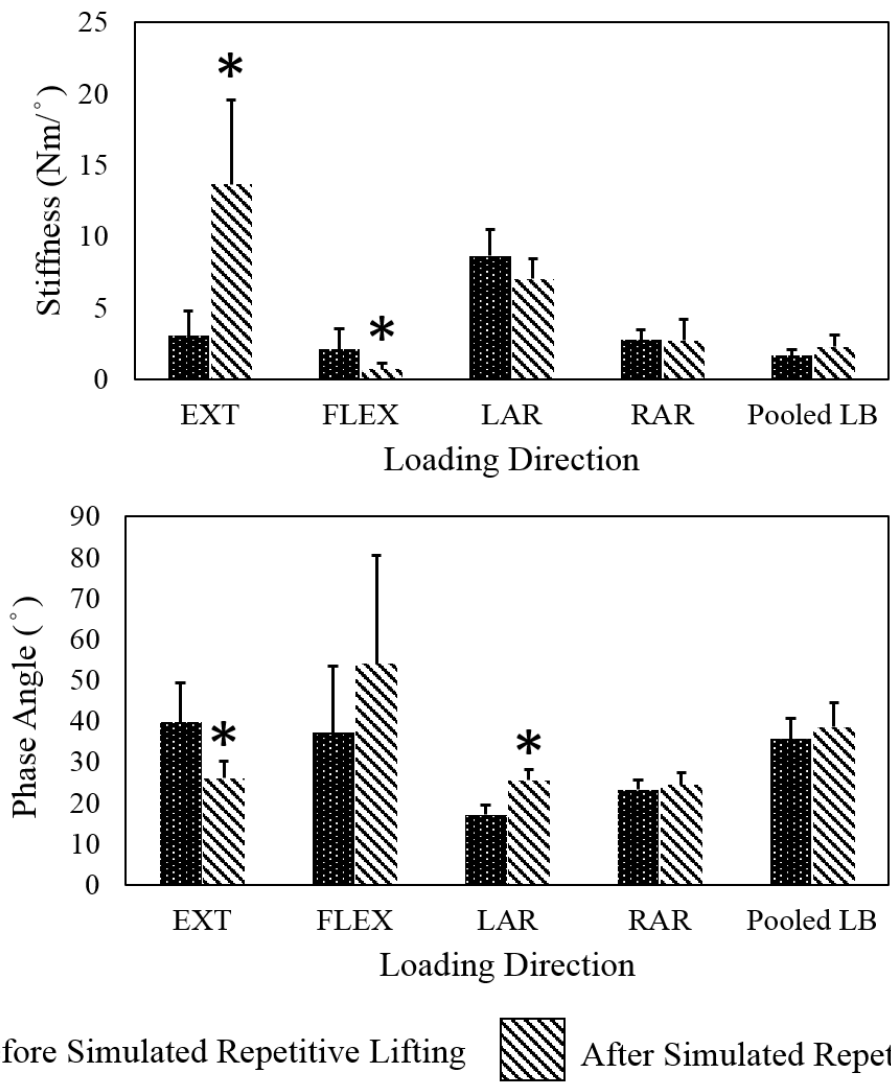


**Figure 4-4** Mean (95% CI) stiffness and phase angle before and after repetitive loading (averaged over 14 specimens) in bending directions: extension (EXT), flexion (FLEX), left and right axial rotation (LAR, RAR, respectively) and lateral bending (LB). \* denotes significance (p<0.05)

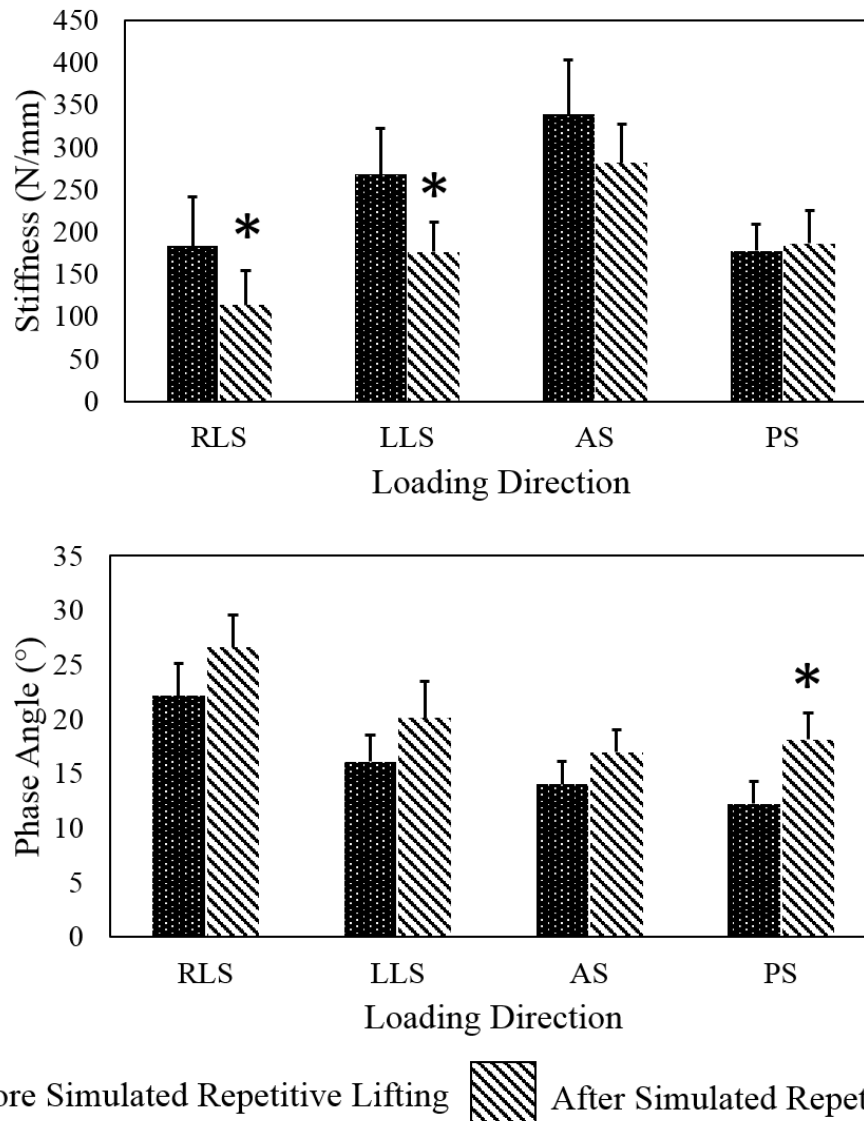


**Figure 4-5** Mean (95% CI) stiffness and phase angle before and after repetitive loading (averaged over 14 specimens) in shear directions: right and left lateral shear (RLS, LLS, respectively), anterior shear (AS), and posterior shear (PS). \* denotes significance ( $p < 0.05$ )

#### 4.4.2 Phase Angle

Significant increases in phase angle were found in compression ( $p = 0.048$ , **Figure 4-3**), left axial rotation ( $p < 0.001$ , **Figure 4-4**), and posterior shear ( $p = 0.010$ , **Figure 4-5** and **Figure 4-4**). A significant decrease in phase angle was found in extension ( $p = 0.022$ , **Figure 4-4**). No significant differences were observed in flexion, right axial rotation, pooled lateral bending, anterior shear, right and left lateral shear ( $p > 0.052$ ). Trends of increasing phase angle after repetitive loading occurred in all directions except extension. In addition, no significant effect of failure mode on phase angle was observed in any direction ( $p > 0.054$ , **Figure 4-7**).

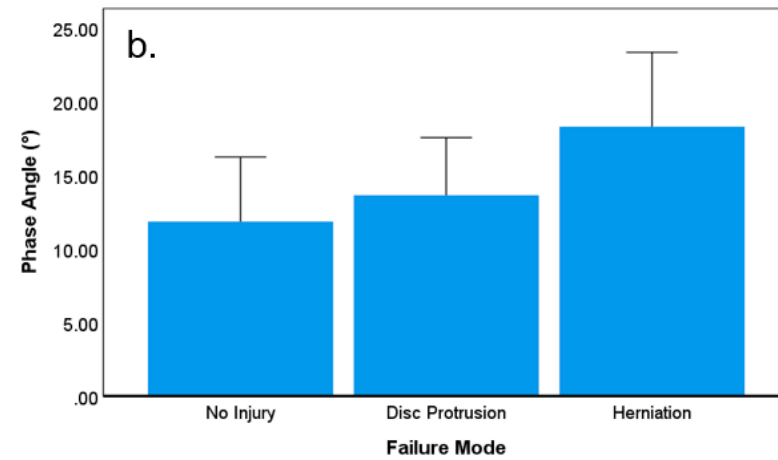
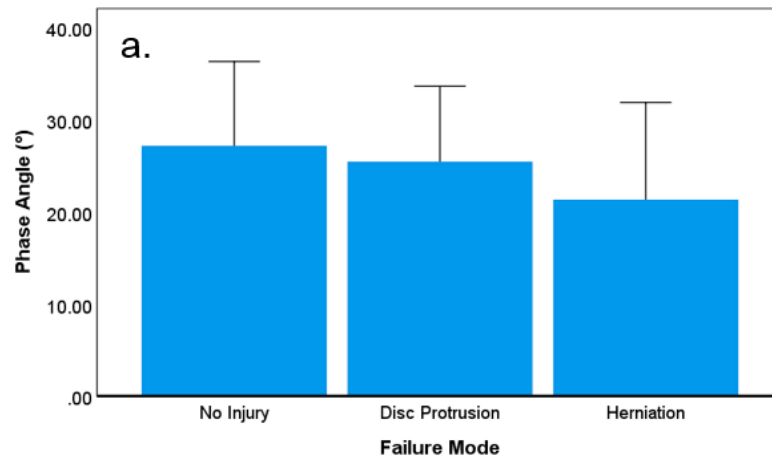


**Figure 4-6** Effect of failure mode on stiffness (Mean, 95%CI,  $p > 0.104$ , averaged over 14 specimens) for extension (a.) and flexion (b.)

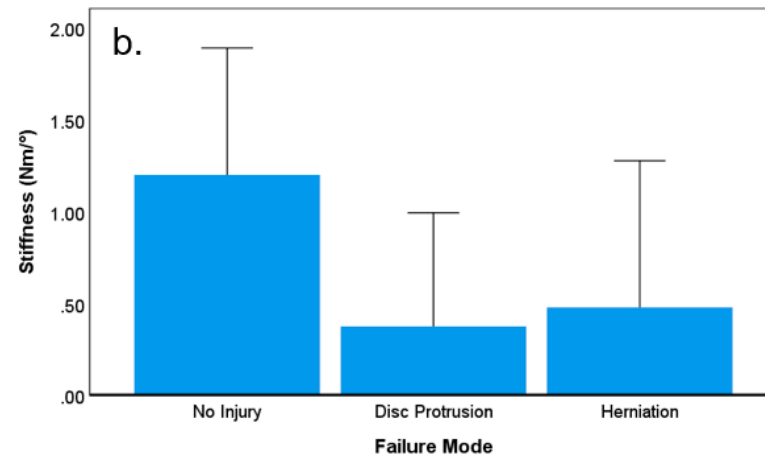
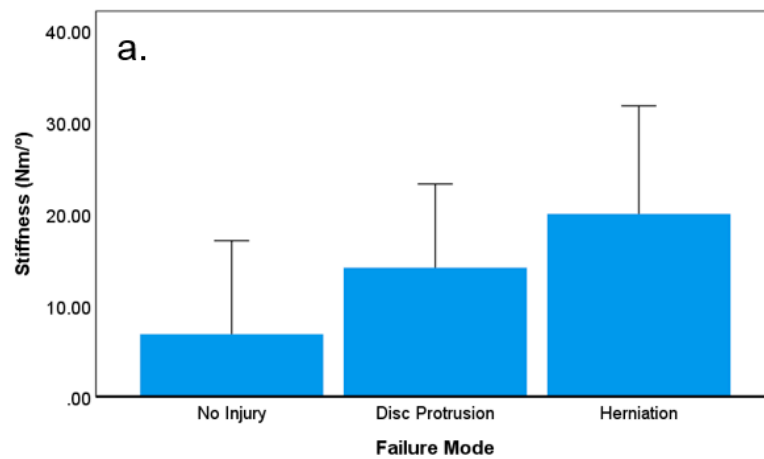


**Figure 4-7** Effect of failure mode on phase angle (Mean, 95%CI,  $p > 0.054$ , averaged over 14 specimens) for extension (a.) and compression (b.)

## 4.5 Discussion

For the first time, this study has quantified the change in FSU mechanics in all 6DOF loading directions after simulated repetitive lifting. Stiffness decreased in compression, flexion, and lateral shear and phase angle increased for compression, left axial rotation, and posterior shear. However, for extension, the stiffness increased and the phase angle decreased, a trend opposite to the other directions. The changes in mechanical properties between before and after simulated repetitive lifting could be a result of multiple factors, which include increased laxity in the facet joint capsule and ligaments, disc tissue and vertebral body damage, reduced disc height, loss of water within the tissue, and a migrating centre of rotation.

The present study found asymmetry between left and right lateral shear as well as axial rotation, which is a potential limitation. This asymmetry could be a result of the control method used in the study where after each test, the compressive load was returned to the baseline 0.1 MPa, while simultaneously minimising off-axis shear forces and moments. This load minimisation strategy allowed for the specimen centre of rotation (CoR) to migrate as required. Therefore, the starting position was not the same for each DOF, likely resulting in left/right asymmetry (**Figure 4-1**). In addition, this asymmetry could be a result of an incorrect CoR, however, the CoR in the present study was based on *in vivo* data (Pearcy and Bogduk, 1988). It is important to note that bending stiffness is not linear and does not always increase with increased rotation angle. In this study, the bending stiffness was measured over a specific range, therefore, the results may be different if another range was used to measure the stiffness.

Repetitive loading did affect mechanical properties however, there were no differences when assessing the effect of failure mode. The no differences could be due to the low sample size within each group resulting in large variations. According to the power analysis, on average, between 25 and 30 specimens in each group would be required to detect the present differences between groups as significant (**Table 4-2**). Trends of decreasing stiffness as the severity of disc injury increased from no injury to disc protrusion to herniation was seen in flexion, axial rotation, and lateral shear, while increasing stiffness was seen in extension (**Figure 4-6**). For energy absorption, trends of increasing phase angle with increasing severity of disc injury were seen in compression, and axial rotation, while decreasing phase angle was seen in extension (**Figure 4-7**). These trends suggest that further investigation may reveal differences in mechanical properties for specific failure modes.

**Table 4-2** Required sample size for each failure mode to detect significance for stiffness and phase angle in all loading directions

<b>Loading Direction</b>	<b>Mechanical Parameter</b>	<b>Sample Size per failure mode</b>
Right Lateral Shear	Stiffness	13
	Phase Angle	43
Left Lateral Shear	Stiffness	8
	Phase Angle	29
Anterior Shear	Stiffness	37
	Phase Angle	12
Posterior Shear	Stiffness	299
	Phase Angle	19
Compression	Stiffness	91
	Phase Angle	9
Extension	Stiffness	12
	Phase Angle	43
Flexion	Stiffness	10
	Phase Angle	18
Left Axial Rotation	Stiffness	35
	Phase Angle	6
Right Axial Rotation	Stiffness	28
	Phase Angle	18
Pooled Lateral Bending	Stiffness	21
	Phase Angle	16

In compression, intuitively, as disc height decreases, there would be an increase in stiffness. However, there was a significant decrease in stiffness after repetitive loading. This could be attributed to the combination of reduced disc height, and depressurisation of the nucleus leading to more load sharing in the annulus and facet joints after repetitive lifting (Adams and Hutton, 1985; Gordon et al., 1991). In addition, more energy was absorbed in compression after repetitive lifting, indicating that there may be tissue damage present (Cannella et al., 2008). A previous study found that compressive stiffness decreased by about 40% from initial stiffness and energy loss increased as time (number of cycles) increased, agreeing with the results from the present study (Gordon et al., 1991). However, the calculations for stiffness and energy loss from this previous study were not documented and should be interpreted with caution (Gordon et al., 1991).

Changes in stiffness were found in flexion and extension, which increased in extension and decreased in flexion. The decrease in flexion stiffness could be related to the deformation in the anterior annulus and intervertebral ligament laxity secondary to disc height loss. Upon removing the specimen from the hexapod, it was evident that the final neutral position of the FSU was in flexion accompanied with laxity in the facet joint

capsule, which was not the case before repetitive loading. This final neutral position in flexion indicates that the anterior annulus underwent non-recoverable deformation, which required an extension moment to keep the specimens upright (**Figure 4-2**), resulting in an increased extension stiffness.

Increased stiffness in extension could also be a result of the reduced disc height after repetitive loading (**Table 4-1**), where the facets were more engaged, as well as changes to the CoR due to posterior migration of the nucleus. Another possible explanation could be that the posterior/posterolateral tissue of the disc underwent stiffening due to the development of disc protrusion during local compaction and buckling of the annulus, which is related to the migration of nuclear material. The decreased phase angle after repetitive loading in extension was expected since there was a corresponding increase in stiffness. Kinematic studies found an increased range of flexion in the lumbar spine during repetitive lifting (Dolan and Adams, 1998; Mehta et al., 2014), which is consistent with the decreased stiffness found in the present study. In addition, studies have found an increased flexion bending moment acting on the lumbar spine (Dolan and Adams, 1998; Lavender et al., 1999). In relation to this study, an increase in extension moment was found instead of the flexion moment, however, it is important to note that muscle actions were not replicated during testing.

There were no significant changes in stiffness or phase angle in right axial rotation, which may be a result of the asymmetry mentioned previously. However, there was an increase in phase angle in left axial rotation, which is the contralateral direction to the applied repetitive loading. Changes in mechanical properties were observed in the same loading directions that were applied during repetitive lifting (i.e. flexion, compression, and axial rotation), however, changes in other loading directions, such as in shear, were also found. It is important to understand the effects of repetitive loading on shear since shear plays an important role in disc injury (Fazzalari et al., 2001; Iatridis et al., 1999; Tavakoli et al., 2018) and low back pain (Marras et al., 2001). Significant decreases in stiffness were found for both left and right lateral shear, while anterior and posterior shear were not significant. The two major ligaments (ALL and PLL) and facet joints protect the spine anteriorly and posteriorly, leaving the lateral regions more vulnerable. This decrease in lateral shear could be a result of tissue damage (i.e. annulus buckling) and increased facet joint laxity after repetitive loading. Increases in energy absorption were found in the FSU when tested in posterior shear, which could be a result of changing the centre of rotation due to nucleus migration during repetitive lifting.

## 4.6 Conclusion

In conclusion, this study has found that after repetitive lifting, the mechanical properties in compression and flexion changed since these were in the same direction of loading. However, by measuring the mechanical properties in other directions, it was found that repetitive lifting also affected extension, left axial rotation (contralateral to the applied rotation), and lateral shear directions. Knowing which directions are affected by repetitive lifting may help determine which muscles need to be strengthened to counteract the changes in stiffness and phase angle seen in the FSU. Furthermore, this study highlights the importance of future work focusing on the understanding the relationship between whole-body kinematics and mechanics of the FSU as this is the primary initiating site of injury.

## Chapter 5      Effect of unsafe repetitive lifting on disc mechanics: an internal disc threshold and multiaxial mechanical properties<sup>4</sup>

In the previous chapters (**Chapter 3** and **Chapter 4**), internal disc strains and 6DOF mechanics were measured under simulated *safe* repetitive lifting (1.0 MPa compression + bending + rotation). The second largest magnitude of shear strains was found in the posterolateral regions, which is the where the site of injury occurs in LDH and disc protrusion. Changes in 6DOF disc mechanics were observed in directions other than those applied during the repetitive lifting (flexion, rotation, compression). More specifically, the lateral shear and extension mechanical properties were altered, implying structural changes were associated with the applied loading regime. However, the question then remains, how do these internal disc strains and changes in 6DOF mechanics under *safe* lifting compare to *unsafe* lifting (1.7 MPa compression + bending + rotation)? Therefore, this chapter focuses on understanding the effects of simulated *unsafe* repetitive lifting on internal disc strains and 6DOF mechanics.

---

<sup>4</sup> The information in this chapter has been submitted to Journal of Biomechanics on December 11, 2018.

Amin, D.B., Moawad, C. M., Costi, J.J., 2018 Manuscript Submitted. Effect of unsafe repetitive lifting on disc mechanics: an internal disc threshold and multiaxial mechanical properties. European Spine Journal.

## 5.1 Abstract

Studies have shown there is a greater risk of LDH with unsafe lifting, which involves lifting while twisting with straight knees. Therefore, the aim of this study was to determine the effect of simulated repetitive unsafe lifting and the resulting failure modes on MSS, 6DOF disc stiffness, and phase angle. Fifteen functional spinal units (FSUs) underwent a sequence of  $\pm$ 6DOF tests at 0.1 Hz for 5 cycles before and after simulated repetitive unsafe lifting. Repetitive unsafe lifting was simulated by applying combined compression (1.7 MPa), flexion ( $13^\circ$ ) and right axial rotation ( $2^\circ$ ) for 20,000 cycles or until failure. MSS were measured in eight specimens by using a wire grid and radiostereometric analysis. MSS was larger at failure in all regions ( $p < 0.010$ ), except the posterior and posterolateral ( $p > 0.081$ ). Disc protrusion and endplate failure groups had larger MSS than the no injury group ( $p < 0.040$ ), revealing a strain threshold of injury of 50%. Significant decreases in stiffness were found in compression, flexion, right axial rotation, and lateral shear, with an increase in extension ( $p < 0.001$ ). For phase angle, significant increases were found in all directions except lateral bending and flexion, and a decrease in extension ( $p = 0.010$ ). Changes in disc mechanics were observed in directions other than those applied in repetitive lifting, highlighting the importance of measuring the 6DOF response. A threshold of shear strain was determined, which if exceeded, may lead to tissue damage associated with gross disc injuries.

## 5.2 Introduction

Epidemiological studies have identified the risk factors for LDH in relation to manual handling lifting activities (Kelsey, 1975; Kelsey et al., 1984b; Mundt et al., 1993). These studies have found that there is a greater risk of LDH when lifting more than 11.3 kg while twisting the body with straight knees (Kelsey et al., 1984b). In addition, *in vivo* disc nucleus pressure measured while lifting a 20 kg box with straight knees was 2.3 MPa in comparison to 1.7 MPa with flexed knees (Wilke et al., 1999). Similar increases in nucleus pressure were observed when holding a 20 kg box close to the body (1.0 MPa), versus at arm's length (1.8 MPa, (Wilke et al., 1999). Taken together, unsafe lifting can be classified as lifting while bending and twisting, without flexing the knees, or by holding the object at arm's length.

*In vitro* studies on human lumbar spine segments have applied bending and/or twisting with compression to produce LDH, understand injury mechanisms, and measure mechanical properties (e.g. stiffness, (Adams and Hutton, 1985; Gordon et al., 1991). However, no studies have measured internal disc strains during repetitive loading that have mimicked unsafe

lifting combinations. Furthermore, disc mechanics (i.e. stiffness and phase angle) in all 6DOF directions have not been measured before and after simulated repetitive unsafe lifting. The measurement of internal strains and disc mechanics can provide a quantitative understanding of the effects of repetitive unsafe lifting and identify the strain/stiffness thresholds that indicate damage progression to LDH.

Previous work (**Chapter 3** and **Chapter 4**) measured internal disc MSS during simulated repetitive safe lifting (Amin et al., 2018 Manuscript Under Review-b). The largest MSS occurred in the anterior, left lateral, and left/right posterolateral regions with an 8% increase in strain from cycle 1 to cycle 20,000. 6DOF properties were also measured before and after simulated safe repetitive lifting, where stiffness during extension increased and decreased in compression, flexion, and lateral shear (Amin et al., 2018 Manuscript Under Review-a). Repetitive lifting also affected phase angle (energy absorption), where it increased in compression, left axial rotation, and posterior shear, and decreased in extension (Amin et al., 2018 Manuscript Under Review-a). However, no previous study, to the author's knowledge, has measured internal disc strains or 6DOF mechanical properties during unsafe repetitive lifting to understand the mechanical effects on the disc.

Therefore, the primary aim of this study was to measure the regional internal disc strain under simulated unsafe repetitive lifting and the resulting failure modes. A secondary aim was to determine the effect of unsafe lifting and failure mode on the 6DOF mechanical properties of the disc.

## 5.3 Methods

### 5.3.1 Specimens and Preparation

This study was approved by the Southern Adelaide Clinical Human Research Ethics Committee (OFR 18.14) and detailed methods are outlined in the previous chapters (**Chapter 3** and **Chapter 4**, (Amin et al., 2018 Manuscript Under Review-b). Nine cadaver lumbar spines (male (n=8), female (n=1)) were stored at -20°C and then thawed to room temperature for pre-test MRI (3T Siemens Skyra, (Amin et al., 2018 Manuscript Under Review-b) for assessment of Pfirrmann grade (Pfirrmann et al., 2001). Spines were then dissected of all non-ligamentous tissue, keeping both the anterior and posterior longitudinal ligaments and facet joint capsules intact. The superior and inferior vertebral surfaces were then cut parallel to the mid-transverse plane of the disc to form a functional spinal unit (FSU). Fifteen FSUs were used (mean (SD) age: 53 (9.6) years, range: 32-64 years, levels: L1-2 x 3, L2-3 x 5, L3-4

x 3, L4-5 x 4). Specimens were then thawed overnight at 4°C, followed by a minimum of three hours at room temperature. Each FSU was randomly assigned to a control (n = 7) or experimental group (n = 8), where only the experimental group had a wire grid inserted for strain measurement.

Each vertebral body was embedded in radiolucent nylon cups using polymethyl methacrylate. Axial and lateral radiographs were taken to measure the instantaneous axis of rotation of the disc relative to the cups, which was used as the centre of rotation for all testing. A waterproof sleeve was then placed over the specimen to contain 200 mL of protease inhibitors, antibacterial, antifungal agents and phosphate buffered saline to keep the disc hydrated while reducing putrefaction and tissue autolysis. The prepared specimen was then installed into a custom-developed 6DOF hexapod robot (Amin et al., 2016b; Ding et al., 2014; Lawless et al., 2014) for testing and warmed to 37°C to mimic *in vivo* conditions.

### 5.3.2 Mechanical Testing

#### 5.3.2.1 6DOF Testing

Each FSU was subjected to a 20-hour axial compressive preload equivalent to a nucleus pressure of 0.1 MPa to mimic the unloaded lumbar disc pressure during sleeping and allow the disc to reach steady-state hydration (**Figure 5-1**, (Edwards et al., 2001; Wilke et al., 1999). After hydration equilibration, the FSU underwent dynamic haversine displacements/rotations in each DOF under a 0.5 MPa (equivalent nucleus pressure) follower preload. The sequence of loading directions was chosen to minimise the biphasic effect (Costi et al., 2008), with shear and axial rotation tests conducted first, followed by bending and axial compression tests. Displacement amplitudes for each DOF were:  $\pm 0.6$  mm for all shear tests (anterior/posterior/lateral shear);  $\pm 2^\circ$  for axial rotation;  $\pm 3^\circ$  for lateral bending;  $5^\circ$  for flexion, and  $2^\circ$  for extension (Costi et al., 2008; Lu et al., 2005; Pearcy and Tibrewal, 1984; Stokes and Frymoyer, 1987). For the axial compression test, loading was from 0.5 MPa to 1.1 MPa. For each DOF, five cycles at 0.1 Hz were applied, followed by a ten minute creep recovery period under a compressive load equivalent to a nucleus pressure of 0.1 MPa (Amin et al., 2018 Manuscript Under Review-b; Amin et al., 2016b).

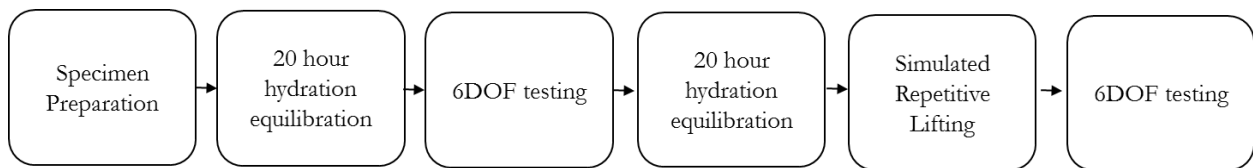


**Figure 5-1** An overview of the testing sequence (adapted from (Amin et al., 2018 Manuscript Under Review-b). The disc underwent fluid re-equilibration before the first set of 6DOF testing and before the simulated repetitive lifting. The two sets of 6DOF testing were used to characterise viscoelastic behaviour of the disc before and after repetitive lifting, respectively

### 5.3.2.2 Simulated Repetitive Lifting

After 6DOF testing, each specimen (control and experimental) underwent another 20 hours of hydration equilibration at 0.1 MPa, after which a pair of stereoradiographs (Philips DigitalDiagnost) were taken to define the reference state of FSU (Amin et al., 2018 Manuscript Under Review-b). The FSU was in an upright position under 0.1 MPa load for the reference state stereoradiograph. Repetitive compression (1.7 MPa) + flexion (13°) + right axial rotation (2°) was applied to all specimens (control and experimental) at 1 Hz for 20,000 cycles or until failure. A compressive force equivalent to the nucleus pressure of 1.7 MPa was applied, where 1.7 MPa represented the nucleus pressure measured when standing and holding a 20kg box away from the body (i.e. *unsafe lifting*, (Wilke et al., 1999). This compressive load was larger than the load applied under *safe lifting* (1.0 MPa), which represented holding a 20kg box close to the body. Failure was defined when a loss of FSU height by 5 mm relative to the initial height prior to cycle 1 was detected, after which the test was aborted. The experimental groups underwent strain measurement using a wire grid inserted into the disc and radiostereometric analysis (Amin et al., 2018 Manuscript Under Review-b; Costi et al., 2007; Tsantrizos et al., 2005). During the simulated repetitive lifting, stereoradiographs were taken after application of cycles 1, 500, 1000, 5000, 10000, 15000, and 20000 at the peak of the applied cycle. Each FSU then underwent another sweep of 6DOF testing (as previously described) to characterise mechanical properties of the disc after simulated unsafe repetitive lifting (**Figure 5-1**).

After completion of testing, each specimen (control and experimental) underwent post-test MRI scans (see **Chapter 3** for MRI parameters) to assess tissue damage.

### 5.3.3 Data and Statistical Analysis

Displacement vectors of each disc nodal coordinate were calculated relative to the reference state, from which the 3D strain tensor was calculated (Amin et al., 2018 Manuscript Under Review-b; Costi et al., 2007). MSS was then calculated from the 3D strain tensor and

expressed as % (Amin et al., 2018 Manuscript Under Review-b; Costi et al., 2007). For regional assessment of MSS, the grid was divided into nine regions: anterior, left/right anterolateral, left/right lateral, posterior, left/right posterolateral, and nucleus (Amin et al., 2018 Manuscript Under Review-b; Costi et al., 2007). For specimens that failed prior to 20,000 cycles, the shear strain at the cycle of failure was defined as failure MSS. If the specimen reached 20,000 cycles, then the strain at that point was used as failure MSS.

Data from the final cycle of each test were processed and analysed in MATLAB (2017b, The Mathworks Inc.). Stiffness for each DOF was calculated using linear regression to determine the slope (MATLAB: POLYFIT.m having an order of 1) over a specific range of the loading portion of the load-displacement curve. The ranges for stiffness calculations for each DOF were: 0.4–0.58 mm for all shear tests, 3.45°–4.75° for flexion and lateral bending, 0.85°–1.25° for extension, 1.5°–1.8° for axial rotation, and 0.77–1 MPa for axial compression (Amin et al., 2016b). Phase angle (energy absorption) for each DOF were calculated between the input displacements and measured forces for all cycles using the cross-spectral density estimate function (MATLAB: CSD.m).

Shapiro-Wilk and Levene's tests were performed to assess the normality and homogeneity of variance of the dependent variables (MSS, stiffness, and phase angle), respectively. If the tests were violated, statistically significant outliers were removed and/or data were log-transformed to meet these criteria. A repeated measures ANOVA was performed on MSS having a within-subjects factor of cycle number (cycle 1 or failure (20,000 or prior)) and a between-subjects factor of disc region ( $p < 0.05$ ). To assess the effect of failure mode on failure MSS, a univariate ANOVA was performed having fixed factors of disc region and failure mode ( $p < 0.05$ ). For the comparison of mechanical properties before and after repetitive lifting, a repeated measures ANOVA was performed on stiffness and phase angle for each DOF having a within-subjects factor of time (before and after repetitive lifting) and a between-subjects factor of group (control vs experimental,  $p < 0.05$ ). Paired t-tests were used to assess the effect of FSU symmetry (left vs. right) in lateral shear, lateral bending, and axial rotation. To assess the effect of failure mode on mechanical properties, a one-way ANOVA was performed for each DOF on stiffness and phase angle after repetitive lifting with a fixed factor of failure mode. Post-hoc multiple comparisons using a Bonferroni correction on alpha were performed where significant differences were found ( $p < 0.05$ ).

## 5.4 Results

### 5.4.1 Maximum shear strain at cycle 1 and last loading cycle (failure)

As the majority of the specimens failed prior to 20,000 cycles, the strains at cycle 1 and 20,000 (or at failure) were compared (**Figure 5-2**). There was a significant overall interaction effect between cycle number and region for MSS ( $p < 0.001$ ). Post-hoc pairwise comparisons revealed that significantly larger MSS were found at failure compared to cycle 1 in all regions ( $p < 0.010$ ) except posterior, left and right posterolateral ( $p > 0.081$ , **Figure 5-3**).

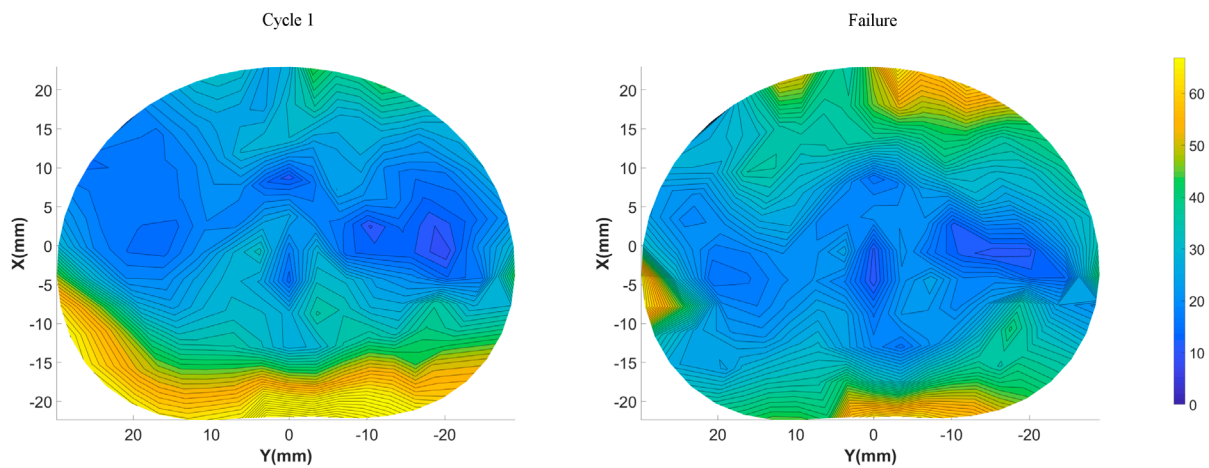


**Figure 5-2** Contour plots showing MSS (%) at cycle 1 and failure averaged over all specimens ( $n = 8$ )

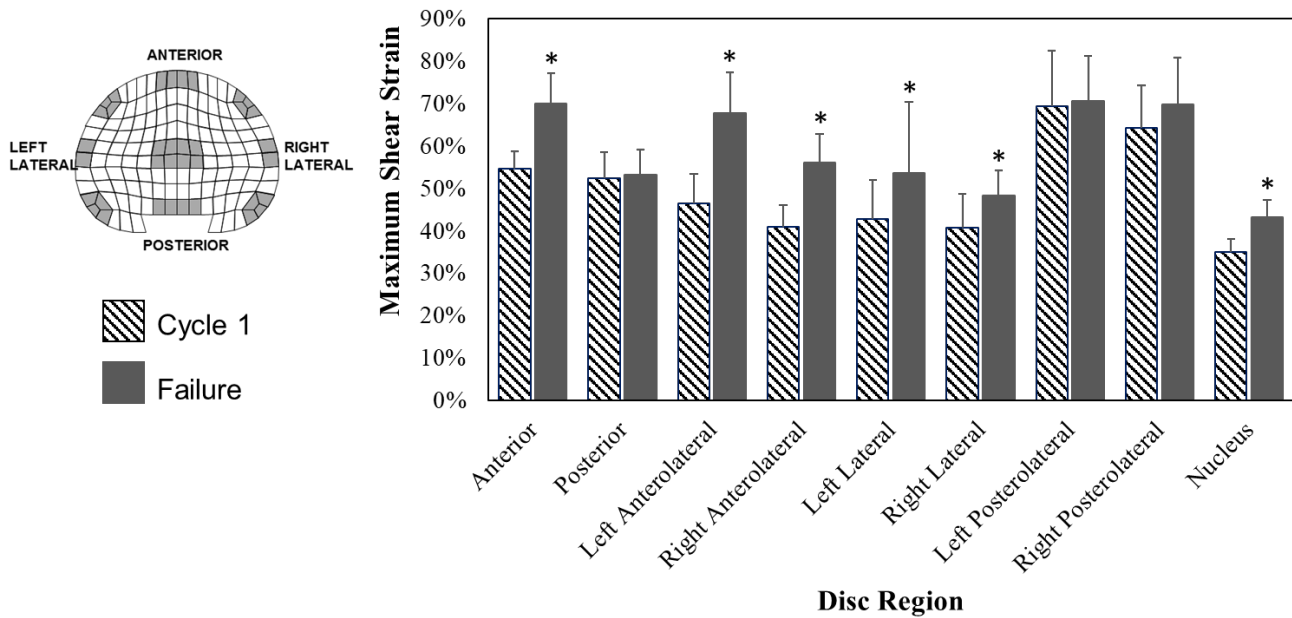


**Figure 5-3** Mean (95% CI) MSS as a function of disc region for cycle 1 and at failure. The image of the disc identifies the nine regions (shaded). \* denotes regions having significant differences in MSS between cycle 1 and failure

#### 5.4.2 Failure Mode

After simulated repetitive lifting, the failure modes were defined as no injury, endplate failure, or disc protrusion (**Table 5-1**). Twelve of the fifteen specimens (80%) failed prior to 20,000 cycles with injuries that included disc protrusion and endplate failure. Two specimens in the experimental group lasted the entire 20,000 cycles with no injury. In contrast to Chapter 3, unsafe repetitive lifting led to no LDH and safe repetitive lifting led to three LDH. Three-dimensional displacement vectors revealed that tissue migration was different between each failure mode (**Figure 5-4**). Within the disc protrusion group, displacements are showing tissue migration towards the right posterolateral region. For the endplate failure group, displacements are showing tissue migration towards the site of injury, which is near the centre of the disc. The majority of specimens failed by endplate failure at the superior endplate (inferior vertebra), comprising 70% in the control group and 50% in the experimental group. The number of cycles to failure and mean disc height loss between the control and experimental groups were not statistically significant ( $p = 0.260$ ,  $p = 0.603$ , respectively, **Table 5-1**).

**Table 5-1** Mean cycles to failure, disc height loss, and breakdown of the failure mode of specimens for control and experimental groups

Group	Mean Cycles to Failure (95%CI)	Mean Disc Height Loss (95% CI)	No Injury	Disc Protrusion	Endplate Failure
Control	5450 (5411)	5.1 (0.78) mm	n = 0	n = 2	n = 5
Experimental	6664 (4722)	5.0 (0.53) mm	n = 2	n = 2	n = 4

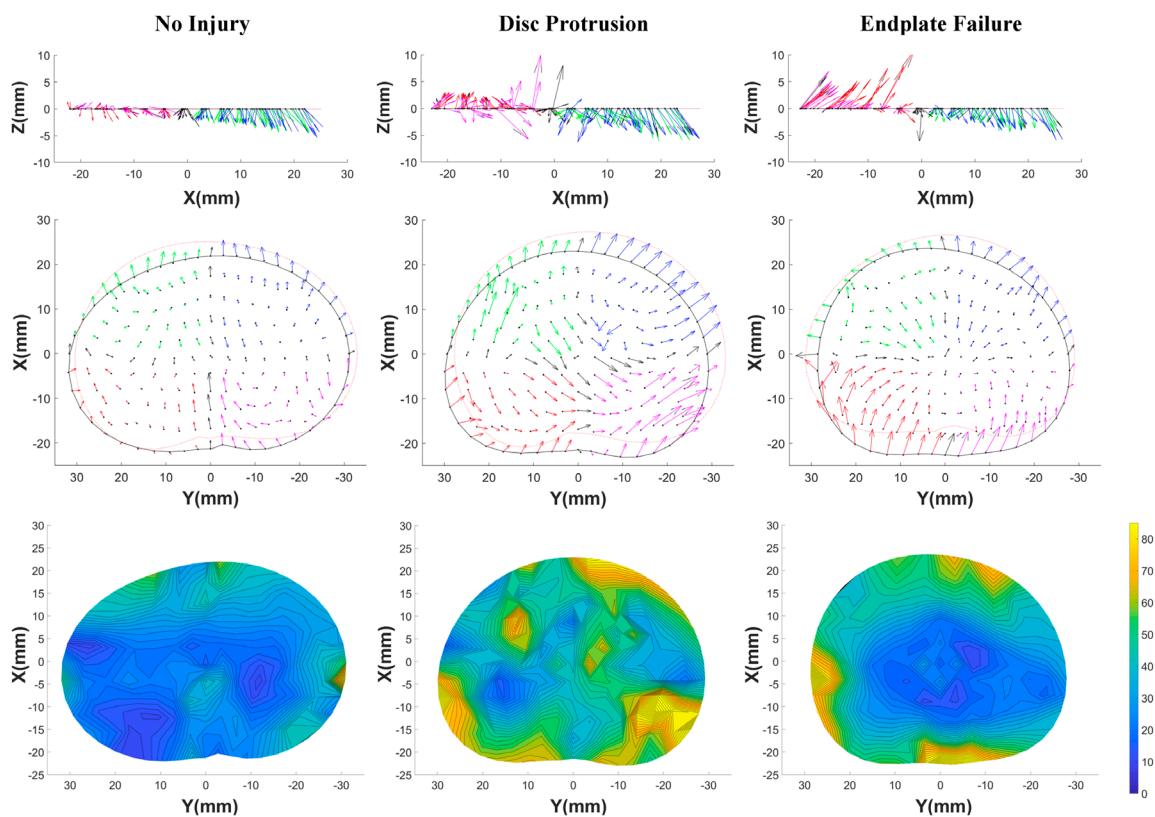


**Figure 5-4** Internal average tissue displacement vectors (top row: lateral view, middle row: axial view) and average MSS (bottom row: axial view) for the three different failure modes (no injury, disc protrusion, and endplate failure). Displacements are relative to the reference state of the FSU. The red dotted line indicates the disc periphery at the last cycle, compared to the reference state (black solid line,). Vectors are colour coded by disc quadrant, green: left anterolateral, blue: right anterolateral, red: left posterolateral and magenta: right posterolateral. Vectors and red dotted disc periphery are scaled by a magnification of 2x

### 5.4.3 Failure strain by failure mode

A significant interaction effect between failure mode and disc region was found for failure MSS ( $p < 0.001$ ). Post-hoc pairwise comparisons revealed significant differences between the no injury and endplate failure modes for failure MSS in all regions ( $p < 0.024$ , **Figure 5-5**) except for right anterolateral, right lateral, and nucleus regions ( $p > 0.157$ ). Significant differences between the no injury and disc protrusion groups for failure MSS were found in the anterior, right anterolateral, left/right posterolateral, and nucleus regions ( $p < 0.040$ , **Figure 5-4**). Comparing the endplate failure and disc protrusion groups at failure MSS, significant differences were observed in the left lateral, and left/right posterolateral regions ( $p < 0.011$ , **Figure 5-5**).

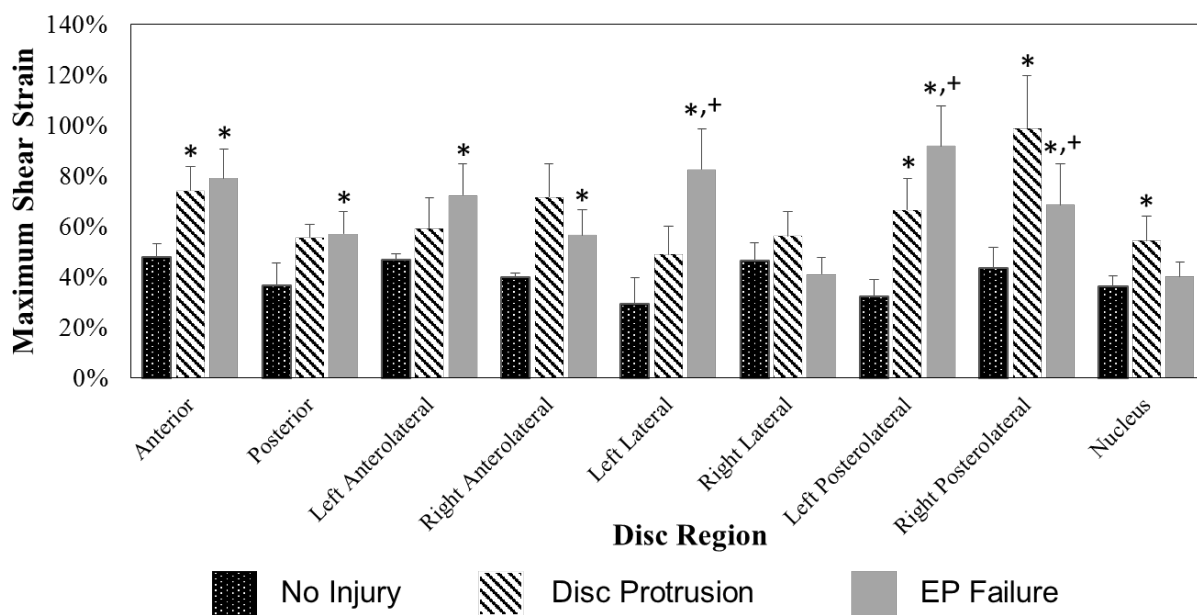


**Figure 5-5** Mean (95% CI) MSS as a function of disc region broken down by failure mode: no injury, disc protrusion, and endplate failure. \* denotes significant difference compared to no injury. + denotes significant difference compared to a disc protrusion

### 5.4.4 6DOF before and after simulated repetitive lifting

#### 5.4.4.1 Control vs Experimental Groups

There were no overall interaction effects between time point (before and after repetitive lifting) and group (control and experimental) for both stiffness ( $p > 0.070$ ) and phase angle ( $p > 0.076$ ) for all DOFs. Therefore, data from both groups were pooled for this analysis ( $n = 15$ ).

#### 5.4.4.2 Symmetry

Tests of symmetry found no significant differences between right and left lateral bending for both stiffness ( $p > 0.128$ ) and phase angle ( $p > 0.391$ ) at both time points. For left and right lateral shear, no statistical differences were seen for stiffness ( $p > 0.607$ ), however,

there were significant differences for phase angle ( $p < 0.034$ ) at both time points. For right and left axial rotation, statistically significant differences were observed for both stiffness ( $p < 0.001$ ) and phase angle ( $p < 0.007$ ) at both time points. Therefore, results from left and right lateral bending were pooled for both stiffness and phase angle analyses ( $n = 30$ ). Left and right lateral shear results were only pooled for stiffness ( $n = 30$ ).

#### 5.4.4.3 Stiffness

Significant decreases in stiffness between before and after simulated repetitive lifting were observed for pooled lateral shear, flexion, right axial rotation and compression ( $p < 0.042$ , **Figure 5-6** and **Figure 5-7**), with significant increases in extension ( $p < 0.001$ , **Figure 5-6**, see **Appendix F**). No significant effect of failure mode on stiffness in any direction was observed ( $p > 0.053$ ).

#### 5.4.4.4 Phase angle

For phase angle, significant increases comparing before to after simulated repetitive lifting were observed for right/left lateral shear, anterior shear, posterior shear, left/right axial rotation, and compression ( $p < 0.032$ , **Figure 5-6** and **Figure 5-7**). Significant decreases in phase angle from before to after simulated repetitive lifting were found in extension ( $p = 0.010$ , **Figure 5-6**, see **Appendix F**). A significant effect of failure mode on phase angle was observed for compression ( $p = 0.035$ ). Post-hoc comparisons revealed a significant difference between the no injury and endplate failure groups ( $p = 0.035$ ), with the endplate failure group having a 25% greater phase angle than the no injury group.

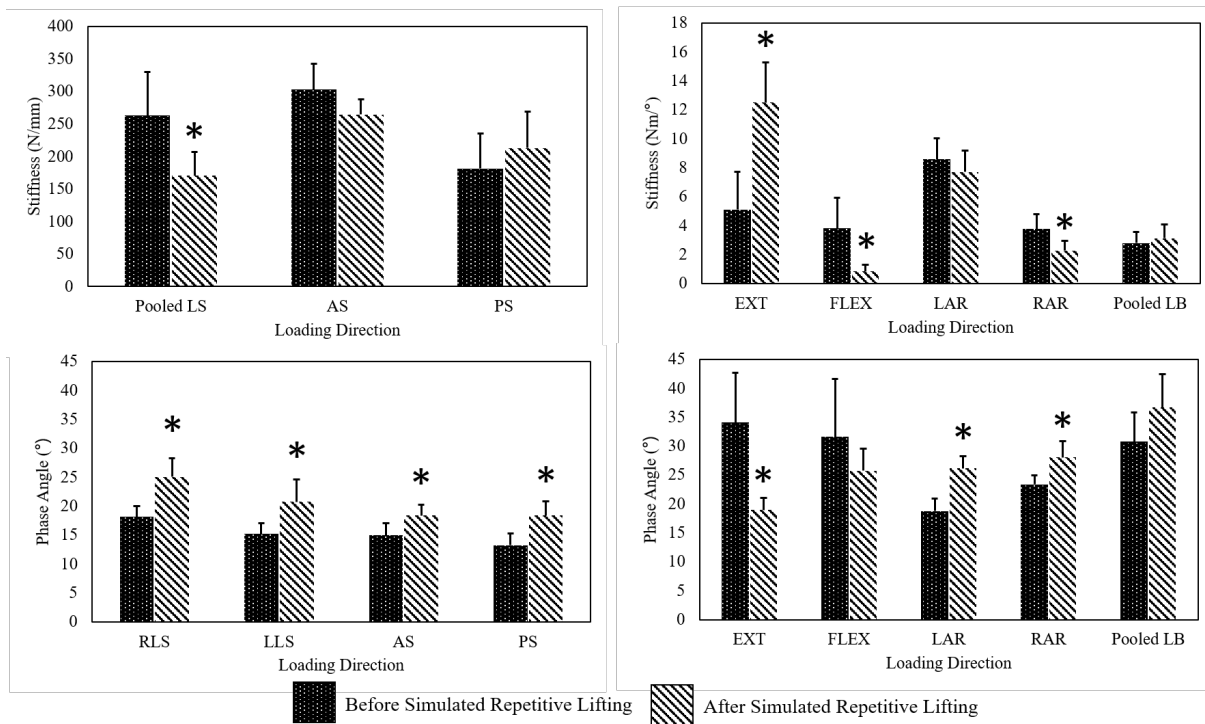


**Figure 5-6** Mean (95% CI) stiffness and phase angle before and after simulated repetitive lifting in shear and bending directions: pooled lateral shear (Pooled LS), right/left lateral shear (RLS, LLS), anterior shear (AS), posterior shear (PS), extension (EXT), flexion (FLEX), left/right axial rotation (LAR, RAR) and pooled lateral bending (Pooled LB). \* denotes significance between before and after simulated repetitive lifting ( $p < 0.05$ )

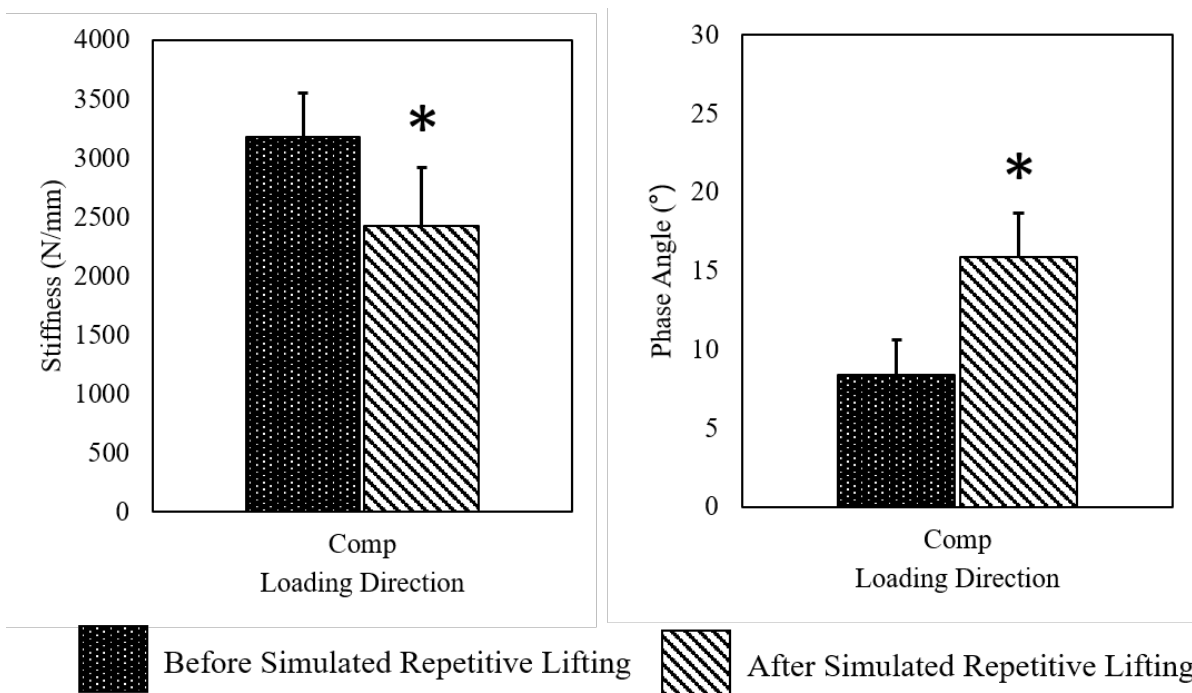


**Figure 5-7** Mean (95% CI) stiffness and phase angle before and after simulated repetitive lifting in compression (Comp). \* denotes significance between before and after simulated repetitive lifting ( $p < 0.05$ )

## 5.5 Discussion

This study demonstrated that MSS and disc viscoelastic behaviour were affected by simulated unsafe repetitive lifting. Unsafe lifting resulted in 60% of the specimens failing via endplate failure, where the endplate failure group had largest MSS in the left lateral and left posterolateral regions in comparison to the no injury and disc protrusion groups. Failure MSS was larger than cycle 1 in all regions except the posterior, left and right posterolateral regions. For disc mechanics after repetitive lifting, increased stiffness was seen in extension, while decreased stiffness was observed in pooled lateral shear, flexion, right axial rotation, and compression. Increased energy absorption was found in all directions except extension. Failure mode affected the compressive phase angle, where the endplate failure group had the largest phase angle.

The internal disc strains were measured using an invasive technique that required the insertion of tantalum wires into the disc. Therefore, a control group was used to confirm that the wire grid did not alter the responses to the applied loading. Mean cycles to failure were not significantly different between the two groups, indicating the wire grid did not affect failure. In addition, 6DOF mechanical properties measured before and after wire grid insertion revealed no significant differences for any DOF (see Appendix B, (Amin et al., 2018 Manuscript Under Review-b)), indicating that disc mechanics were not affected. During simulated repetitive loading, substantial recovery periods were not used, therefore the results of this study would mimic the worst-case scenario of tissue damage accumulation in the absence of biological repair and fluid re-equilibration. In addition, there was asymmetry in lateral shear and axial rotation, which may be a result of the hexapod robot 6DOF control system limitation for allowing migration of the centre of rotation during testing at 1 Hz. To the authors' knowledge, there is no 6DOF testing control system that is able to adapt in real-time to minimise off-axis loads and moments at frequencies of above 0.3 Hz without introducing significant tracking errors (Lawless et al., 2014).

Shear is known to cause failure of the annulus (Michalek et al., 2009), which is linked to disc injuries like herniation, therefore, the present study measured tissue level shear strains. However, only a few studies have measured internal disc shear strains under different loading regimes, resulting in an unclear understanding of disc failure criteria. The shear strains found in the present research are comparable to magnitudes found in a finite element study on the effects of complex loading and risk of LDH (Schmidt et al., 2007b). Comparing the present failure strains to those calculated in the previous study (**Chapter 3**) under simulated safe repetitive lifting, the present MSS were significantly

lower in the anterior and nucleus regions only (Amin et al., 2018 Manuscript Under Review-b), see **Appendix G**). This difference in magnitudes could be attributed to the larger compressive preload (1.7 MPa) used in simulating unsafe lifting in comparison to safe lifting (1.0 MPa), resulting in a stiffening effect within the tissue. However, both lifting groups generated the largest magnitude of MSS in the anterior, lateral, and posterolateral regions, suggesting that those regions were the most vulnerable under the applied flexion and right axial rotation motions that are commonly undertaken during lifting.

Unsafe lifting resulted in twelve specimens failing prior to 20,000 cycles, however, no LDH was observed. Endplate failure in nine specimens was likely a result of the large magnitude of compression applied, causing an overload injury that is associated with heavy lifting. The remaining three specimens also had a 5 mm reduction in FSU height, however, these discs resulted in a protrusion. Assessment of bone mineral density (BMD) showed no significant differences in BMD between the three failure modes ( $p > 0.197$ ). The large shear strains found in the anterior, posterior, and posterolateral regions after endplate failure confirm its effect on the disc. There were three LDH under safe repetitive lifting (Chapter 3) in comparison to none under unsafe lifting. This difference could be attributed to the increased compression under unsafe repetitive lifting, resulting in more endplate failures than LDH.

By investigating the effect of failure mode on MSS, it was apparent that there was a threshold of strain that was associated with disc injury (**Figure 5-5**). Failure MSS of the disc protrusion and endplate failure groups after repetitive lifting was larger than 48% in all regions, whereas the no injury group strain was lower than this threshold. This magnitude is specific to the loading applied in the present study. In comparison to the safe lifting group from the previous research (**Chapter 3**, (Amin et al., 2018 Manuscript Under Review-a), the shear strain threshold was similar at 50% based on one specimen with no injury. Within both studies, there was a small sample size for the no injury group and this should be recognised as a limitation. However, taken together, a general MSS threshold of 50% can be proposed as the failure criteria for tissue damage associated with bending and twisting while lifting. This information may be valuable in establishing the safe levels of MSS within the disc tissue and potentially the failure criteria at which LDH or disc injury may occur. With the ever-increasing focus on specimen-specific responses and treatments, it is important to consider specimen-specific strains with regards to the strain threshold. Variation was found between specimens in the MSS contour plots within each failure mode. However, for each specimen, the regions of MSS greater than 50% were

associated with visible tissue damage from the post-test MRI and macroscopic assessment (see Appendix I, (Amin et al., 2018 Manuscript Under Review-c)). This correspondence between shear strain and tissue damage further supports the proposed shear strain threshold.

Decreases in stiffness were found in the directions of applied repetitive lifting (compression, flexion, right axial rotation), which was expected as tissue was consistently being deformed in those directions. However, stiffness changes were also found in other directions of loading (lateral shear and extension). The decrease in lateral shear stiffness indicates there may be lateral annulus disruption. Shear strain in the lateral regions increased significantly after simulated repetitive lifting (**Figure 5-4**), indicating that there may be tissue damage. In extension, there was an increase in stiffness, which was also found in the previous study (**Chapter 4**) looking at changes in 6DOF mechanics after simulated safe lifting (Amin et al., 2018 Manuscript Under Review-a). This increase may be a result of the deformed anterior annulus due to the applied repetitive flexion, which is also confirmed by the large shear strains seen in the anterior region (**Figure 5-4**). Another possible explanation could be tissue damage, as an increase in extension stiffness is associated with disc lesions, such as annular tears (radial and concentric) and rim lesions (Thompson et al., 2000). No effect of failure mode on stiffness was observed, however, there was a marginal significance for extension ( $p=0.054$ ). With an increased sample size, this effect may be significant and lead to an understanding of the mechanics associated with disc protrusion and endplate failure.

Corresponding differences were seen in phase angle with increases found in compression, right and left axial rotation, anterior shear, posterior shear and lateral shear and a decrease in extension (**Figure 5-6** and **Figure 5-7**). The increase in phase angle further supports the presence of tissue damage and possible damage to the facet joints, likely due to asymmetric loading. Furthermore, the compressive phase angle of the endplate failure group was 25% greater than the no injury group, which may be a result of the failed endplate and decompression of the nucleus (**Figure 5-4** - vector plot for endplate failure).

In comparison to the mechanical properties measured after repetitive safe lifting, similar changes were observed to those found in the present study (Amin et al., 2018 Manuscript Under Review-a). Statistical tests showed that there were no differences between stiffness and phase angle measured after simulated safe and unsafe repetitive lifting in all directions ( $p > 0.103$ , see **Appendix G**). These mechanical properties were measured independent of the applied simulated repetitive lifting and used the same 6DOF test protocols, which may explain the lack of no differences between the two studies, and

indicating that the changes in properties before and after simulated repetitive lifting were a result of tissue damage. In addition, since the 6DOF properties were measured at the FSU (organ) scale, it would be difficult to detect the subtle differences between the simulated safe and unsafe lifting.

## 5.6 Conclusion

In conclusion, it was found that simulated unsafe lifting led to large MSS in the posterolateral and anterior regions, with the posterolateral region being of more concern as this region is commonly the site of injury. MSS for disc protrusion and endplate failure specimens were larger than no injury specimens, suggesting the existence of a damage MSS threshold (failure criteria) of 50%. Above this threshold, the risk of tissue damage associated with disc injuries such as disc protrusion and endplate failure increases. As variation in MSS between specimens at failure was observed, finite element models validated using this experimental data can lead to further exploration of the specimen-specific response. Disc mechanics were altered after simulated unsafe repetitive lifting in all 6DOF directions, highlighting the importance of measuring the 6DOF response after disc injury. However, these changes were no different than those found during safe lifting, suggesting that measuring the 6DOF mechanics alone is not sufficient to detect tissue level and regional disc damage. As more tissue engineering therapies and disc implants are being designed, both internal disc strain thresholds and multiaxial disc mechanics should be considered.

## Chapter 6 Understanding the Impact of Repetitive Lifting Towards Lumbar Disc Herniation: A Clinically Relevant Biomechanical Cadaveric Study<sup>5</sup>

The previous chapters (**Chapter 3**, **Chapter 4**, and **Chapter 5**) measured the effect of simulated safe (1.0 MPa + bending + rotation) and unsafe (1.7 MPa + bending + rotation) repetitive lifting on disc mechanics which included internal disc strains. The largest magnitudes of shear strains were found in the anterior, posterolateral, and lateral regions. These strains were also stratified by failure mode to determine the differences and a strain threshold. However, the associations between regional strain and disc damage as assessed via MRI and macroscopic images have not been explored. This chapter uses the results of the previous chapters (Chapter 3 and Chapter 5) to examine the correlations between the strain measured at failure and disc damage to understand the structure-function-injury relationship.

---

<sup>5</sup> This information presented in this chapter has been submitted to Spine on October 31, 2018 and is under review.

Amin, D.B., Tavakoli, J., Freeman, B.J.C., Costi, J.J., 2018 Manuscript Under Review. Understanding the impact of repetitive lifting towards lumbar disc herniation: a clinically relevant biomechanics cadaveric study. Spine.

## 6.1 Abstract

Repetitive lifting has been shown to lead to LDH. *In vitro* studies have developed a qualitative understanding of the effect of repetitive loading on LDH. However, no studies have measured internal disc strains and subsequently correlated these with disc damage. Thirty human cadaver lumbar functional spinal units were subjected to an equivalent of one year of simulated repetitive lifting under safe (1.0 MPa) and unsafe (1.7 MPa) levels of compression, in combination with flexion (13-15°), and right axial rotation (2°) for 20,000 cycles or until failure. Safe or unsafe lifting was applied as a compressive load to mimic holding a 20 kg weight either close to, or at arm's length, from the body, respectively. MSS were measured, and disc damage scores were determined in nine regions from axial post-test MRI and macroscopic images. Twenty percent of specimens in the safe lifting group failed before 20,000 cycles, compared to 80% in the unsafe group. Significant positive correlations were found between MRI and macroscopic damage scores in all regions ( $r_s > 0.385$ ,  $p < 0.049$ ). A significant positive correlation was observed in the left lateral region for MSS vs. macroscopic damage score ( $r_s = 0.486$ ,  $p < 0.037$ ) and MSS vs. failure mode ( $r_s = 0.724$ ,  $p = 0.018$ ). Pfirrmann Grade 3 discs were strongly associated with subsequent LDH ( $p = 0.003$ ). Increased shear strains were observed in the contralateral side to the applied rotation as disc injury progressed from protrusion to LDH. This study demonstrated that unsafe lifting leads to greater risk of injury compared to safe lifting, and LDH and disc protrusion were more common in the posterior/posterolateral regions.

## 6.2 Introduction

Repetitive lifting can lead to low back pain (Heneweer et al., 2011), or sciatica as a result of disc protrusion or LDH (Jordan et al., 2011; Kelsey, 1975; Kelsey et al., 1984a; Kelsey et al., 1984b). Manual handling guidelines recommend safe lifting limits of 25 kg for men and 16 kg for women when loads are held close to the body (Cooper, 2018). The recommended maximum weight is *reduced* to 5 kg for loads being held at arm's length (Cooper, 2018). Unsafe lifting practice occurs when these limits have been exceeded. Furthermore, epidemiological studies have shown an increased risk of LDH when lifting more than 11 kg while twisting and not having the knees flexed (Kelsey et al., 1984b). Kinematic studies have found that repetitive lifting leads to muscle fatigue and increased flexion in the spine (Dolan and Adams, 1998; Mehta et al., 2014). However, it is important to understand the effects of repetitive lifting at the disc level as that is the site of injury.

*In vitro* studies have attempted to reproduce LDH under repetitive combined compression, flexion and/or rotation loading using human tissue and mechanical testing devices (Adams

and Hutton, 1985; Gordon et al., 1991). These studies developed a qualitative understanding of LDH through the use of injectable dyes and imaging, which demonstrated the migration of the nucleus, together with a macroscopic evaluation of the disc to identify damage (Adams and Hutton, 1985; Gordon et al., 1991). However, a quantitative measurement of internal disc tissue mechanical behaviour is lacking. Disc pressure measurements can provide information on internal tissue ‘stress profiles’, in particular for the nucleus (McMillan et al., 1996), and internal disc strains have been measured using various techniques (Costi et al., 2007; O’Connell et al., 2007; Seroussi et al., 1989; Showalter et al., 2016; Tsantrizos et al., 2005). The measurement of internal strains can provide insight into the effect of repetitive lifting on tissue damage and identify the strain thresholds that indicate damage progression towards disc protrusion and LDH. Furthermore, internal disc strains in addition to magnetic resonance imaging (MRI) and macroscopic assessment of the intervertebral disc can lead to a more thorough understanding of clinically relevant disc injuries after repetitive lifting.

Therefore, there were two aims of this study: **1.)** To examine whether unsafe simulated repetitive lifting places the disc at greater risk of injury compared to safe lifting. **2.)** To explore correlations between tissue damage (MRI and macroscopic), internal disc strains, and failure mode; as well as between failure mode, Pfirrmann grade and disc level after simulated repetitive lifting.

## 6.3 Materials and Methods

### 6.3.1 Specimens and preparation

This study was approved by the Human Research Ethics Committee (OFR 18.14). Eighteen fresh frozen cadaver lumbar spines were thawed at room temperature for pre-test MRI (3T MR scanner (Siemens Skyra) using a T2 weighted sequence (TR: 3000 ms TE: 79 ms thickness: 4 mm), and Pfirrmann grade (Pfirrmann et al., 2001) was assessed by three independent observers (interclass correlation coefficient: 0.823). Thirty functional spinal units (FSUs), with posterior elements and ligaments intact, were dissected parallel to the mid-transverse plane of the disc (**Table 6-1**).

The vertebral bodies were then embedded in parallel cups using polymethyl methacrylate. The instantaneous axis of rotation was measured for each FSU (Pearcy and Bogduk, 1988), and used for all testing. The FSU was then installed into a custom-developed six degree of freedom (6DOF) hexapod robot for testing (Ding et al., 2014) in phosphate buffered saline at 37°C (Amin et al., 2016b). Each FSU was randomly assigned to either a control or experimental group for repetitive loading (**Figure 6-1**).

### 6.3.2 Simulated repetitive lifting and internal disc strain

Before testing, each FSU underwent a 20-hour compressive preload equivalent to an *in vivo* nucleus pressure of 0.1 MPa (Wilke et al., 2001) to hydrate and establish the unloaded neutral position. Repetitive bending and twisting was applied for 20,000 cycles (Adams and Hutton, 1983, 1985) to mimic one year's worth of lifting a 20 kg box. Fifteen specimens underwent repetitive hyperflexion (13-15°),(Adams and Hutton, 1985; Pearcy et al., 1984; Stokes and Frymoyer, 1987) and right axial rotation (2°),(Pearcy and Tibrewal, 1984) with a compressive preload of 1.0 MPa (nucleus pressure), based on *in vivo* measurements while holding a 20 kg box close to the body(Wilke et al., 2001), and was defined as safe lifting. The unsafe lifting group underwent repetitive flexion (13°) and right axial rotation (2°) with a compressive preload of 1.7 MPa (holding a 20 kg box at arm's length(Wilke et al., 2001), Figure 1). Testing was aborted if the FSU height was reduced by 5 mm (failure). The experimental groups underwent strain measurement using a wire grid inserted into the disc and radiostereometric analysis (Costi et al., 2007; Tsantrizos et al., 2005). MSS relative to the neutral position was calculated in the nine regions after 1 and 20,000 cycles, or after failure. The nine regions were: anterior, left/right anterolateral, left/right lateral, posterior, left/right posterolateral, and nucleus (Costi et al., 2007).

**Table 6-1** Specimen demographics, Pfirrmann grade, applied cycles and failure mode. Data is sorted by lifting regime, failure mode and cycles. The specimens that underwent strain measurement are identified in the MSS column

<b>Lifting Regime</b>	<b>Failure Mode</b>	<b>MSS</b>	<b>Level</b>	<b>Age</b>	<b>Gender</b>	<b>BMI</b>	<b>Pfirrmann Grade</b>	<b>Cycles</b>
Safe	No Injury	No	L1-2	65	Male	30	2	20,000
Safe	No Injury	No	L2-3	50	Female	30	2	20,000
Safe	No Injury	No	L4-5	34	Male	22	3	20,000
Safe	No Injury	Yes	L2-3	34	Male	22	2	20,000
Safe	Endplate Failure	No	L2-3	31	Male	43	2	500
Safe	Endplate Failure	Yes	L4-5	60	Male	21	3	500
Safe	Endplate Failure	Yes	L1-2	69	Female	22	2	5,000
Safe	Disc Protrusion	No	L2-3	60	Male	21	2	20,000
Safe	Disc Protrusion	Yes	L4-5	65	Male	30	2	20,000
Safe	Disc Protrusion	Yes	L1-2	55	Male	17	3	20,000
Safe	Disc Protrusion	Yes	L4-5	50	Female	30	2	20,000
Safe	Disc Protrusion	Yes	L4-5	31	Male	43	2	20,000
Safe	LDH	No	L3-4	69	Female	22	3	20,000
Safe	LDH	No	L4-5	55	Male	17	3	20,000
Safe	LDH	Yes	L4-5	61	Male	28	3	20,000
				<b>Mean</b>	<b>53</b>	<b>27</b>		
				<b>SD</b>	<b>14</b>	<b>8</b>		
Unsafe	No Injury	Yes	L4-5	32	Male	29	1	20,000
Unsafe	No Injury	Yes	L2-3	32	Male	29	1	20,000
Unsafe	Endplate Failure	No	L4-5	54	Male	25	2	500
Unsafe	Endplate Failure	No	L1-2	64	Male	17	2	500
Unsafe	Endplate Failure	No	L4-5	58	Male	20	3	500
Unsafe	Endplate Failure	Yes	L2-3	53	Male	28	2	500
Unsafe	Endplate Failure	Yes	L2-3	58	Male	20	3	500
Unsafe	Endplate Failure	Yes	L3-4	64	Male	17	2	500
Unsafe	Endplate Failure	No	L2-3	58	Male	38	2	1,000
Unsafe	Endplate Failure	No	L3-4	59	Male	29	2	5,000
Unsafe	Endplate Failure	No	L1-2	59	Male	29	2	5,000
Unsafe	Endplate Failure	Yes	L1-2	49	Female	42	2	5,000
Unsafe	Disc Protrusion	Yes	L2-3	54	Male	25	2	10,000
Unsafe	Disc Protrusion	Yes	L3-4	49	Female	42	2	10,000
Unsafe	Disc Protrusion	No	L4-5	51	Male	15	2	20,000
				<b>Mean</b>	<b>53</b>	<b>27</b>		
				<b>SD</b>	<b>10</b>	<b>9</b>		

**Note:** All endplate failures occurred at the superior endplate of the inferior vertebra of the FSU; Strain measurement column: No = Control and Yes = Experimental (**Figure 6-1**).

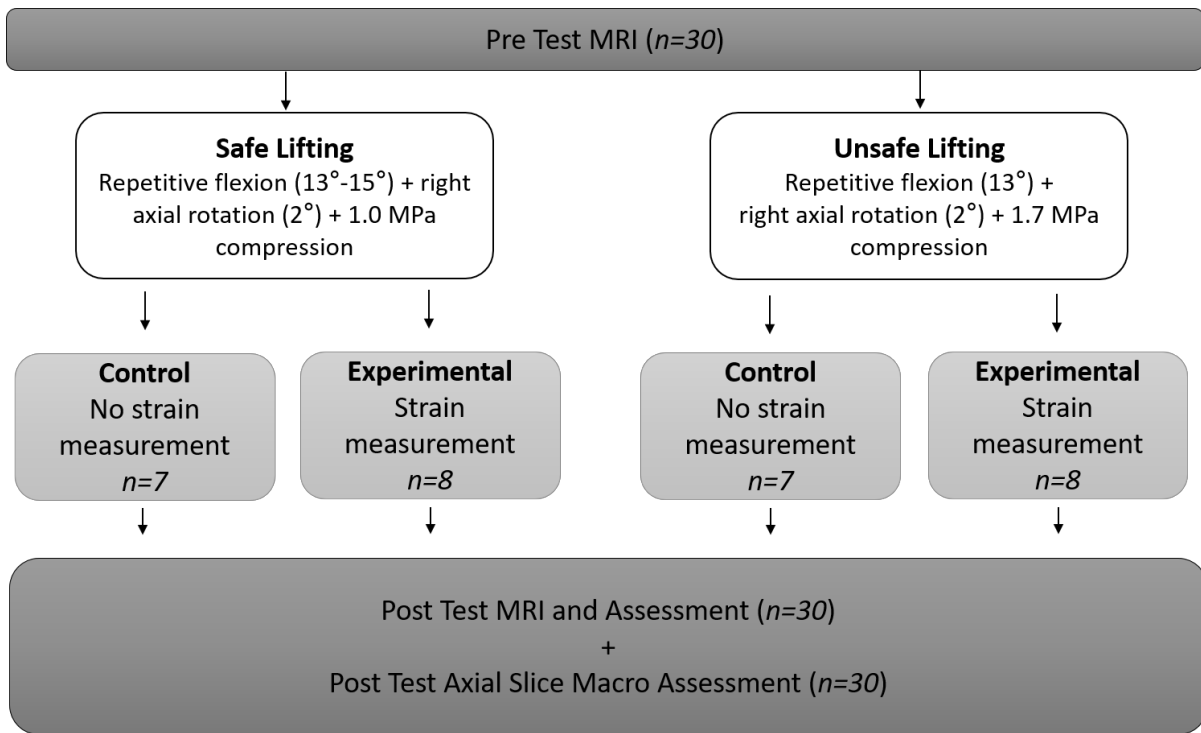


**Figure 6-1** Schematic of the testing procedure

### 6.3.3 Damage assessment

For post-test MRI, wire grids were removed from experimental specimens and sagittal images of each FSU were taken from a 3T MR scanner using a T2 weighted sequence (TR: 3760 ms, TE: 98.0, thickness: 4 mm) and T1 (TR: 750 ms, TE: 13 ms, thickness: 4 mm). Axial images were also taken using both T2 (TR: 2200 ms, TE: 81 ms, thickness: 2 mm) and T1 (TR: 2900, TE: 14, thickness: 2 mm) weighted sequences. Failure mode was assessed by a clinician from a series of sagittal and axial images.

From each T1 image, the mid-transverse slice was assessed for damage in nine regions by three independent observers, who were blinded to each specimen. Damage was assigned a score of 0-4, where 0 indicated no damage, 1 the presence of annular tears or delamination, 2 the presence of buckling annulus and migrating nucleus, 3 disc protrusion and 4 indicated disc herniation (see **Appendix H**). Each observer repeated their assessment three times for assessment of intra- and inter-rater repeatability.

After MRI, each FSU was fixed in formaldehyde, then sliced through the mid-transverse plane and photographed. Each photograph was then scored for damage in each of the nine regions and repeated three times.

### 6.3.4 Data and statistical analysis

MSS (%) was calculated from the 3-D strain tensor (mid-transverse disc plane) in each of the nine regions (Costi et al., 2007). A one-way between-subjects ANOVA was conducted

to compare the effect of loading regime on MSS in all nine regions ( $p < 0.05$  significant). Repeatability between- and within-raters for MRI and macroscopic damage scores was assessed using intra-class correlation coefficient. Correlations between MSS, MRI damage score, macroscopic damage score, and with failure mode were assessed using a Spearman's correlation ( $p < 0.05$  significant). A chi-square test of independence was performed to examine the relation between grade and failure mode as well as level and failure mode.

## 6.4 Results

### 6.4.1 Safe versus unsafe lifting

Three of fifteen specimens (20%) from the safe lifting group failed prior to the 20,000 cycles, compared to twelve of fifteen (80%) from the unsafe lifting group (**Table 6-1**). After repetitive lifting, the failure modes were defined as no injury, endplate failure, disc protrusion or LDH (**Figure 6-2**, **Table 6-1**). All endplate failures occurred at the superior endplate (inferior vertebra), and were 3x more prevalent in the unsafe, compared to the safe lifting group. There were a similar number of disc protrusions in each lifting group, however, early failure by disc protrusion by 10,000 cycles (i.e. loss of FSU height  $> 5$  mm) occurred twice as fast in the unsafe group. Significant differences in MSS were only seen in the anterior and nucleus regions between the two lifting groups ( $p < 0.001$ , **Figure 6-3**), allowing for MSS to be pooled in all other regions for correlation analyses.

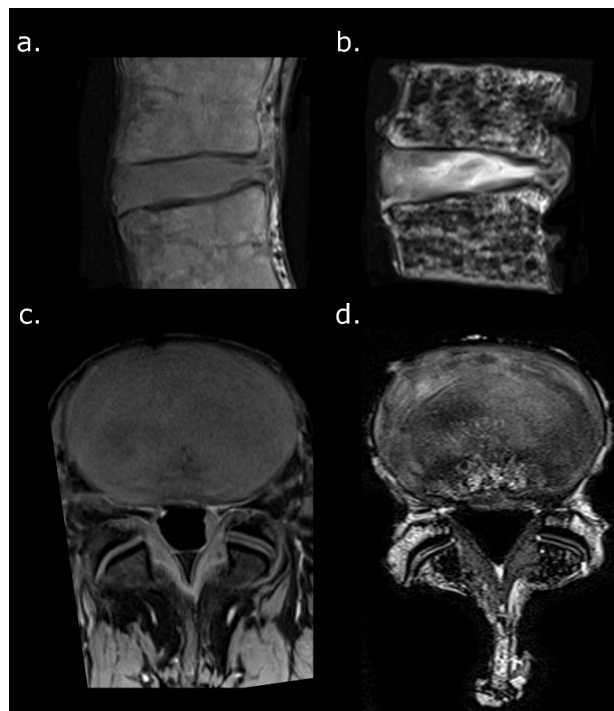


**Figure 6-2** Pre-test MRI (a) mid-sagittal T1 (c) mid-axial T2. Post-test MRI (b) mid-sagittal T1 (d) mid-axial T2, demonstrating an LDH in the same specimen

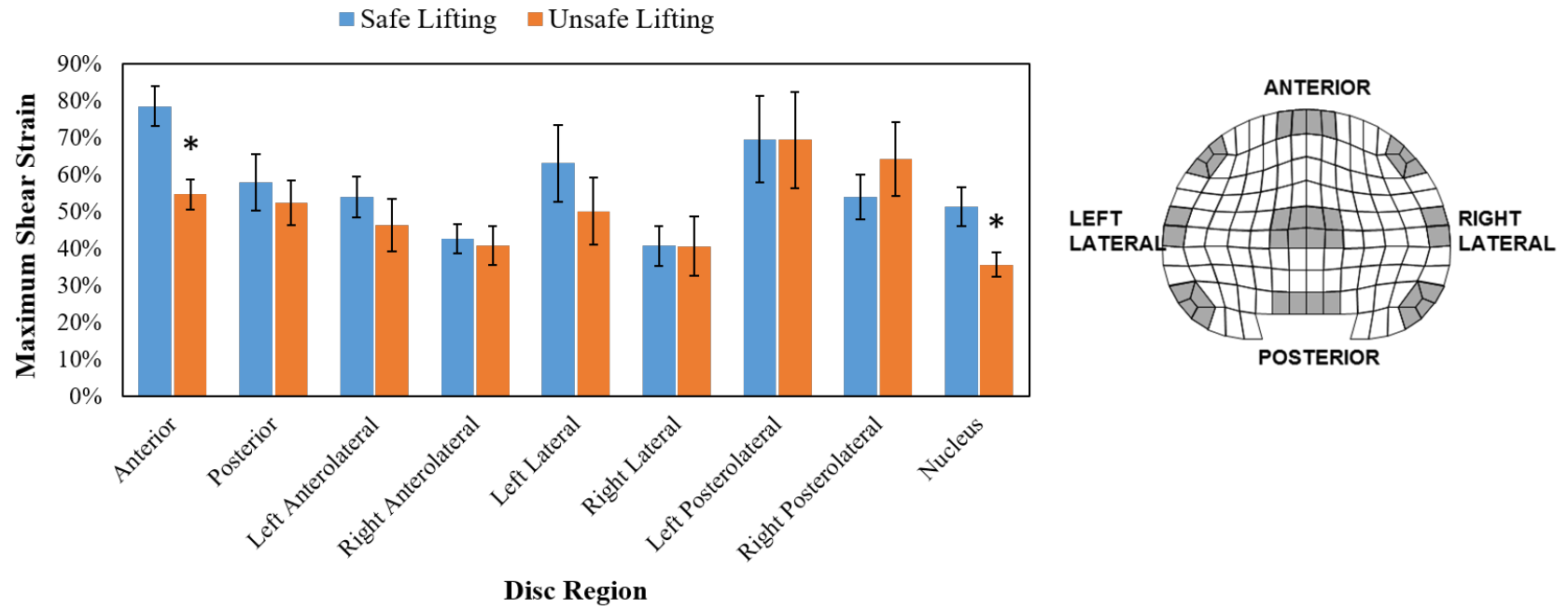


**Figure 6-3** MSS for the safe and unsafe lifting groups. Right image identifies each of the nine regions. \* denotes significant differences between each group ( $p < 0.05$ )

#### 6.4.2 MRI and macroscopic damage score

Repeatability coefficients were 0.930 (intra-rater) and 0.873 (inter-rater) for MRI damage score, and 0.804 (intra-rater) and 0.782 (inter-rater) for macroscopic damage. With all regions combined, significant positive correlations were observed between MRI and macroscopic damage scores ( $r_s = 0.651$ ,  $p < 0.001$ , **Figure 6-4** and **Figure 6-5**). Significant positive correlations between MRI and macroscopic damage scores were observed in each of the nine regions ( $r_s > 0.385$ ,  $p < 0.049$ ).

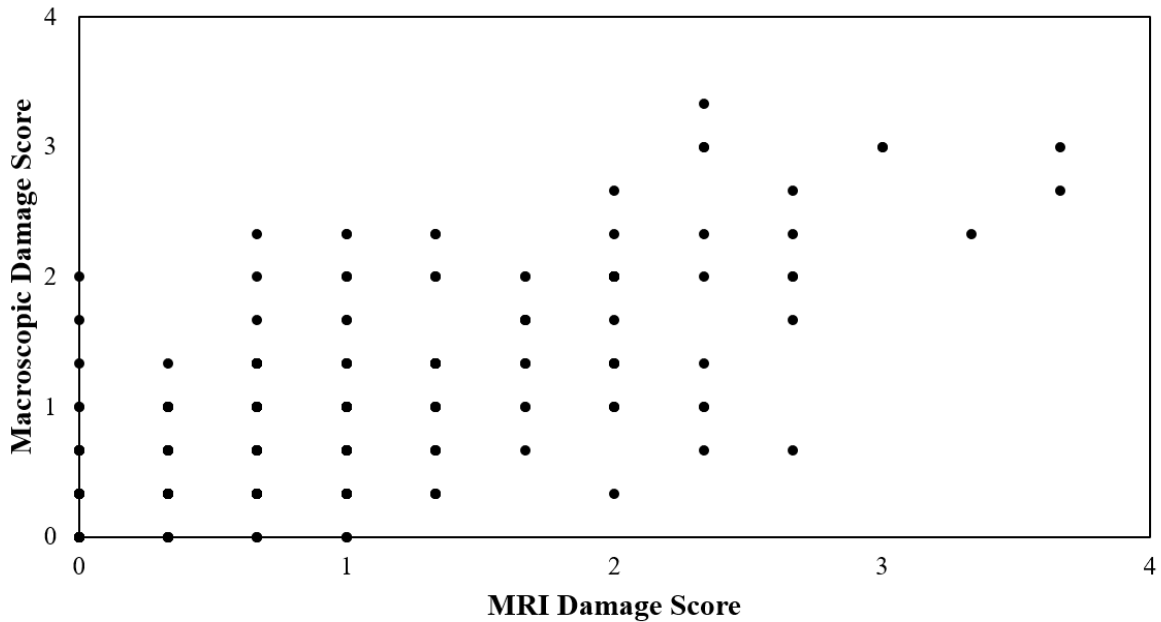


**Figure 6-4** Correlation between MRI damage score and macroscopic damage score for all regions combined ( $r_s = 0.651$ ,  $p < 0.001$ ), where the scores were averaged over all three raters (inter-observer). Scores from all 30 specimens and 9 disc regions are represented here (270 data points, some data points are overlapping). The scoring scale was 0 = no damage; 1 = annular tears/delamination; 2 = migrating nucleus; 3 = disc protrusion; 4 = disc herniation

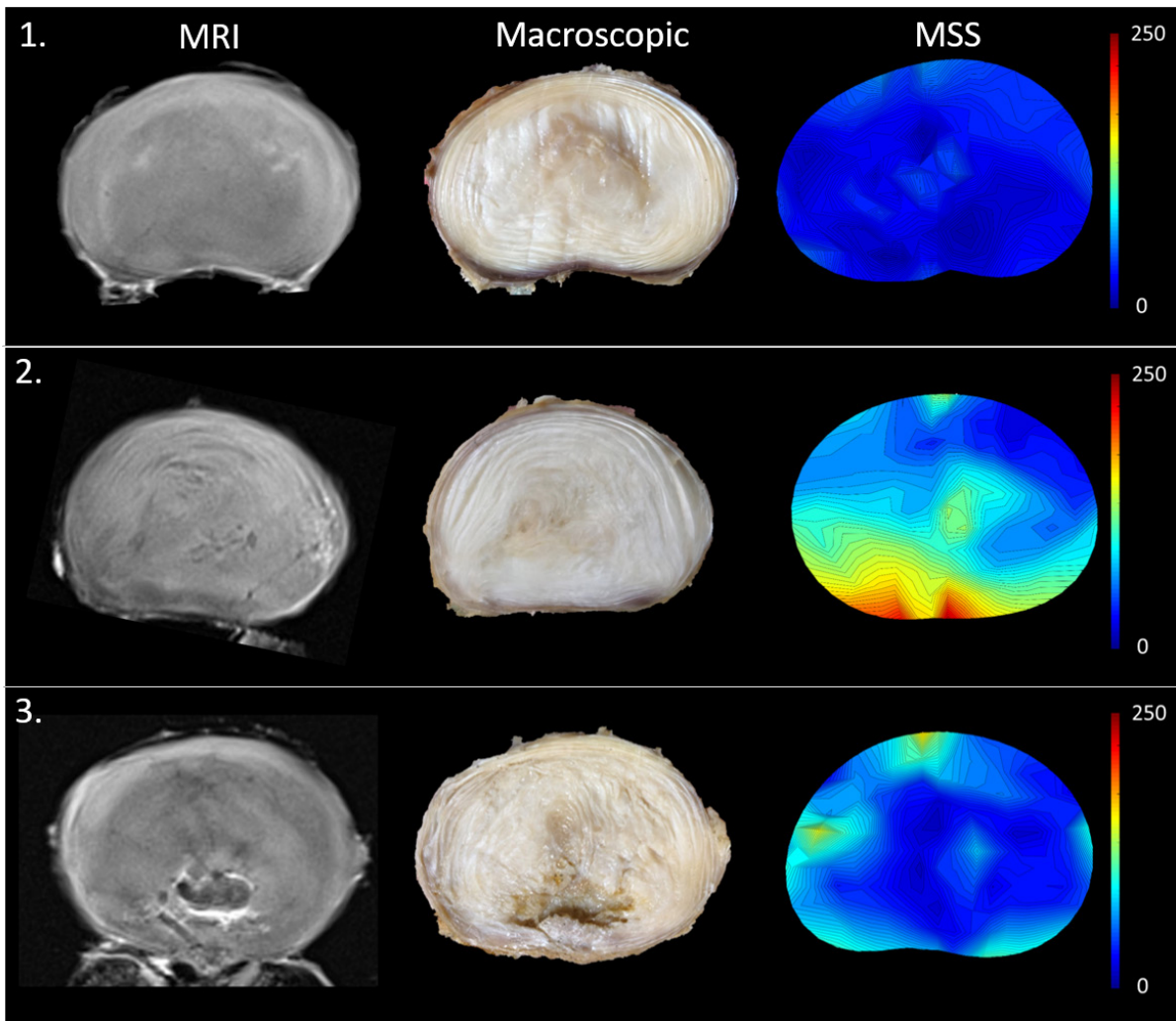


**Figure 6-5.** Left to right images: MRI axial slice, macroscopic axial slice, and the MSS map after repetitive loading for example specimens with (1) No injury, (2) Nucleus migration (left and right posterolateral) and (3) A posterior central LDH (see **Appendix I**)

### 6.4.3 MRI damage score and MSS

MRI damage score and MSS were not significantly correlated in any of the regions ( $p > 0.120$ , **Figure 6-6**).

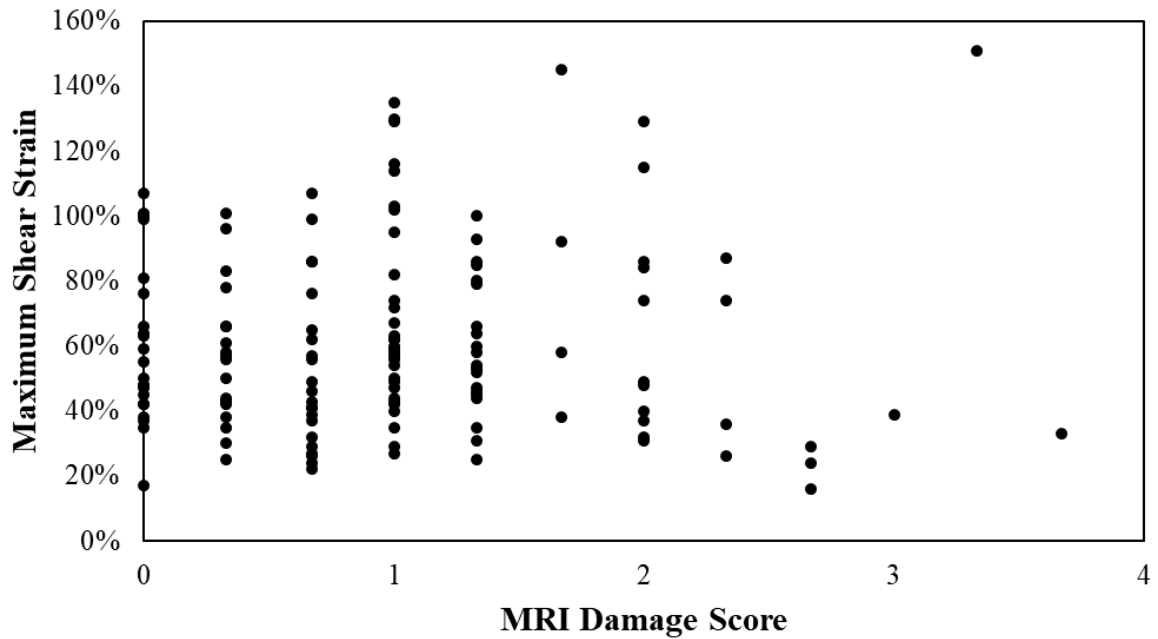


**Figure 6-6** Correlation between MRI damage score and MSS for all regions combined ( $p > 0.120$ ), where the scores were averaged over all three raters (inter-observer). Scores from 16 specimens and 9 disc regions are represented here (144 data points, some data points are overlapping). The scoring scale was 0 = no damage; 1 = annular tears/delamination; 2 = migrating nucleus; 3 = disc protrusion; 4 = disc herniation

### 6.4.4 Macroscopic damage score and MSS

Macroscopic damage and MSS were not significantly correlated in almost all regions ( $p > 0.083$ ), apart for the significant positive association in the left lateral region only ( $r_s = 0.486$ ,  $p < 0.037$ , **Figure 6-5** and **Figure 6-7**).

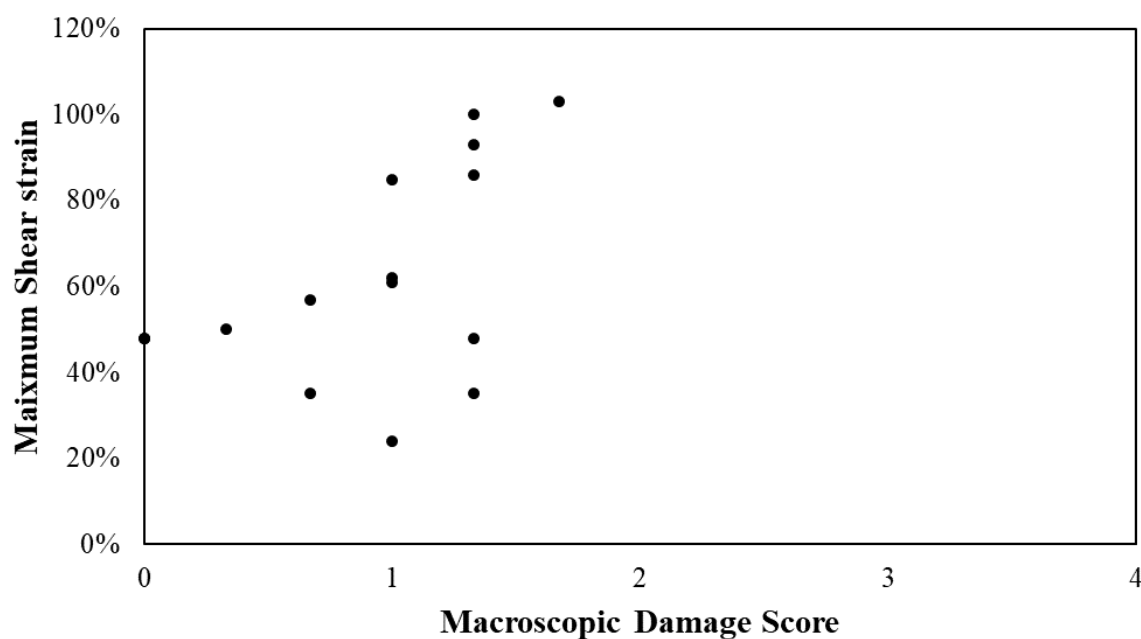


**Figure 6-7** Macroscopic damage score vs MSS for the left lateral region ( $r_s = 0.486$ ,  $p < 0.037$ ,  $n=16$ , only experimental group). The macroscopic damage score was averaged between the three observers

#### 6.4.5 Failure mode and MSS

Failure mode was divided into two subsets: herniation pathway and endplate failure. Herniation pathway included specimens that had no injury, disc protrusion and herniation. The endplate failure group included specimens that had no injury and endplate failure. The no injury specimens were the same for both pathways. Positive correlations between failure mode (herniation pathway) and MSS were found only in the left lateral region ( $r_s = 0.724$ ,  $p = 0.018$ , **Figure 6-8**), with no significant correlations between MSS and the endplate failure mode ( $p > 0.161$ ).

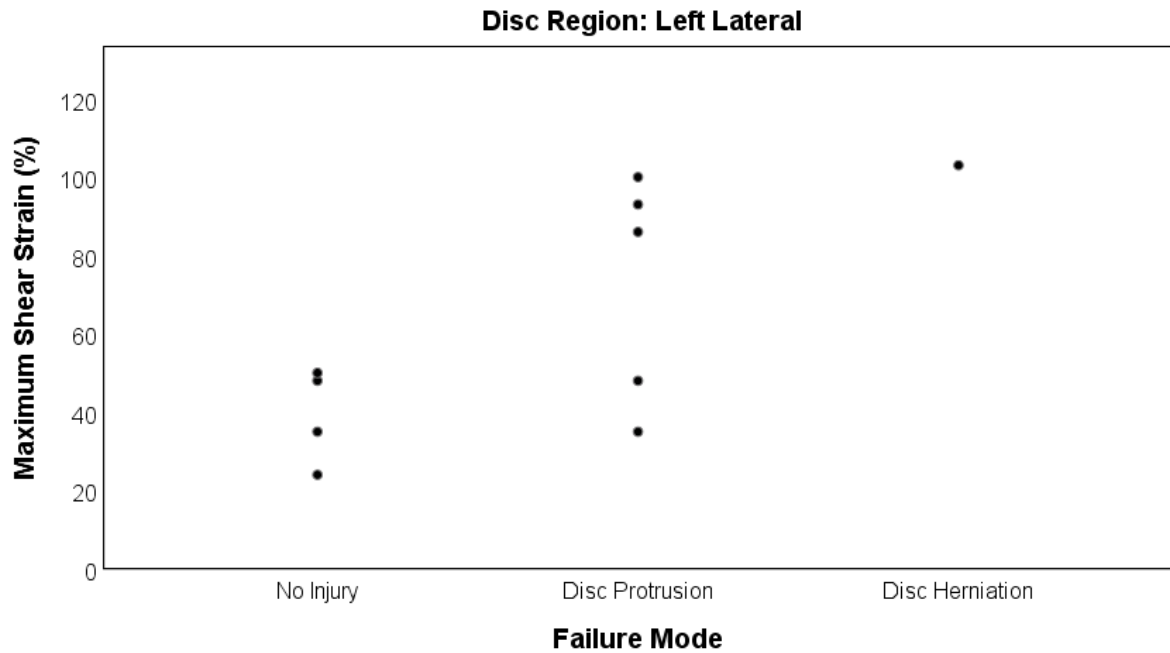


**Figure 6-8** Failure mode vs MSS for left lateral ( $r_s = 0.724$ ,  $p = 0.018$ ,  $n=16$ , experimental group, some data points are overlapping)

#### 6.4.6 Failure mode and MRI damage score

Significant positive correlations between failure mode (herniation pathway) and MRI damage were observed in the posterior ( $r_s = 0.703$ ) and left posterolateral ( $r_s = 0.522$ ) regions ( $p < 0.037$ , **Figure 6-9**). For the anterior and nucleus regions, failure mode (herniation pathway) and MRI damage score were significantly correlated for the safe lifting group only ( $r_s > 0.751$ ,  $p < 0.009$ ). Significant correlations between failure mode (endplate failure) and MRI damage were seen in the nucleus region for the unsafe lifting group ( $r_s = 0.671$ ,  $p = 0.034$ ).

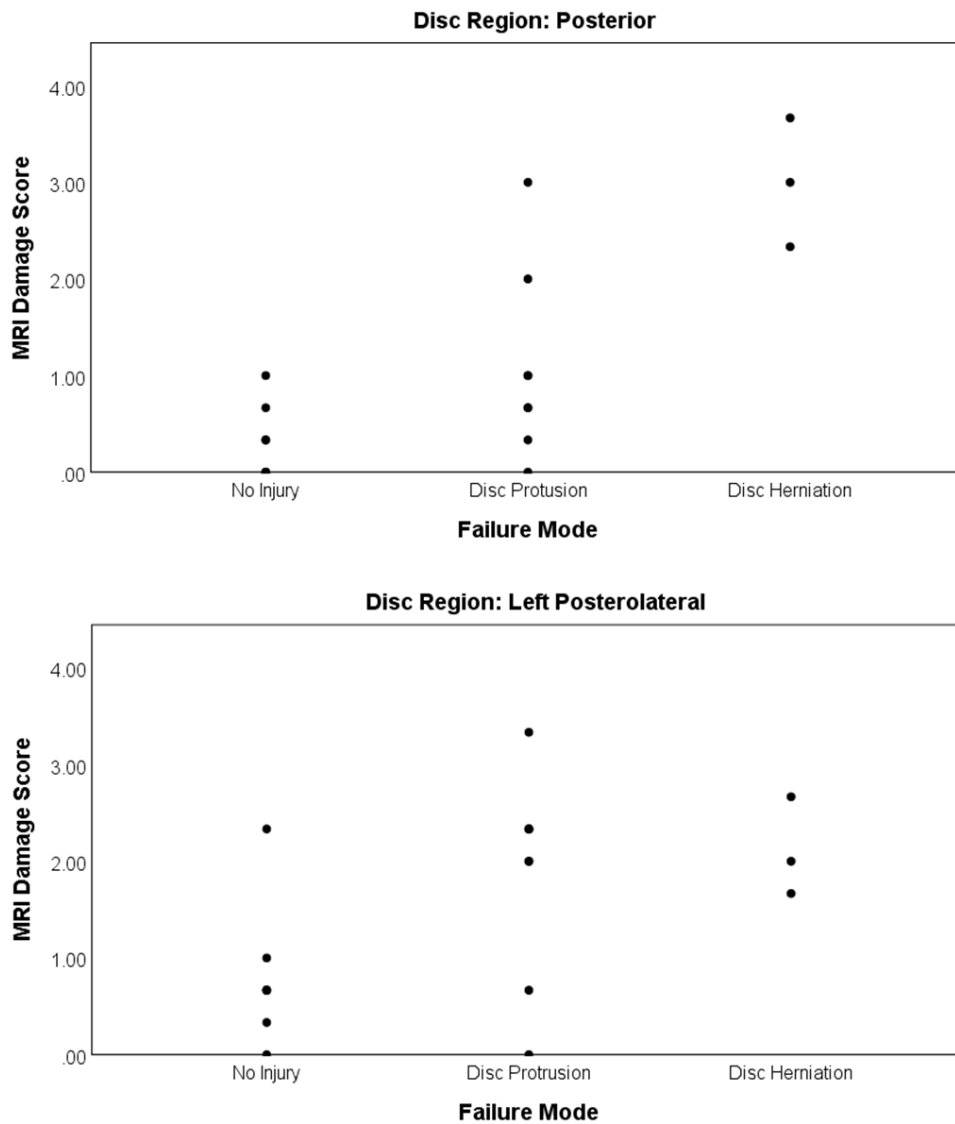


**Figure 6-9** Failure mode (herniation pathway) vs MRI damage score for the posterior and left posterolateral regions ( $p < 0.037$ ,  $n=30$ , both control and experimental groups, some data points are overlapping)

#### 6.4.7 Failure mode and macroscopic damage score

Positive correlations between failure mode (herniation pathway) and macroscopic damage were significant for the posterior ( $r_s = 0.496$ ), left and right posterolateral ( $r_s > 0.756$ ), right lateral ( $r_s = 0.545$ ) and left anterolateral ( $r_s = 0.786$ ) regions ( $p < 0.031$ , **Figure 6-10**). For the nucleus and anterior regions, significant positive correlations were found in both safe and unsafe lifting groups ( $r_s > 0.658$ ,  $p < 0.032$ ). Significant positive correlations were observed between failure mode (endplate failure) and macroscopic damage in the nucleus and anterior regions for the safe lifting group ( $r_s = 0.687$ ,  $p < 0.029$ ).

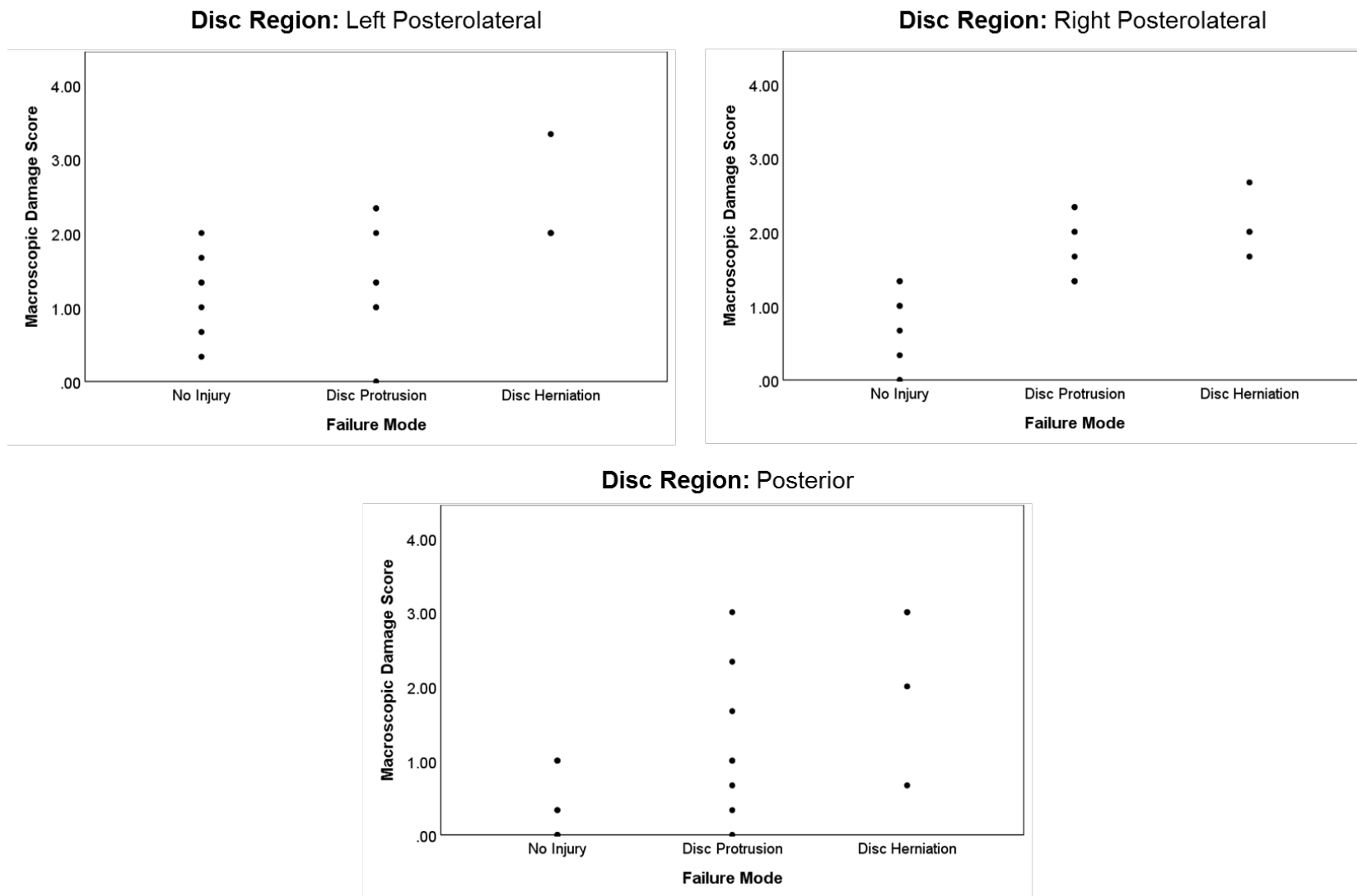


**Figure 6-10** Failure mode vs macroscopic grading for left and right posterolateral, and posterior regions ( $p < 0.031$ ,  $n = 30$ , both control and experimental groups, some data points are overlapping)

#### 6.4.8 Failure mode, Pfirrmann grade and disc level

There were significant interactions between failure mode and Pfirrmann grade ( $p = 0.003$ , **Figure 6-11**), where LDH only occurred in Pfirrmann grade 3 discs. There was no significant interaction between failure mode and disc level ( $p = 0.104$ ). However, LDH only occurred at the L3-4 and L4-5 levels.

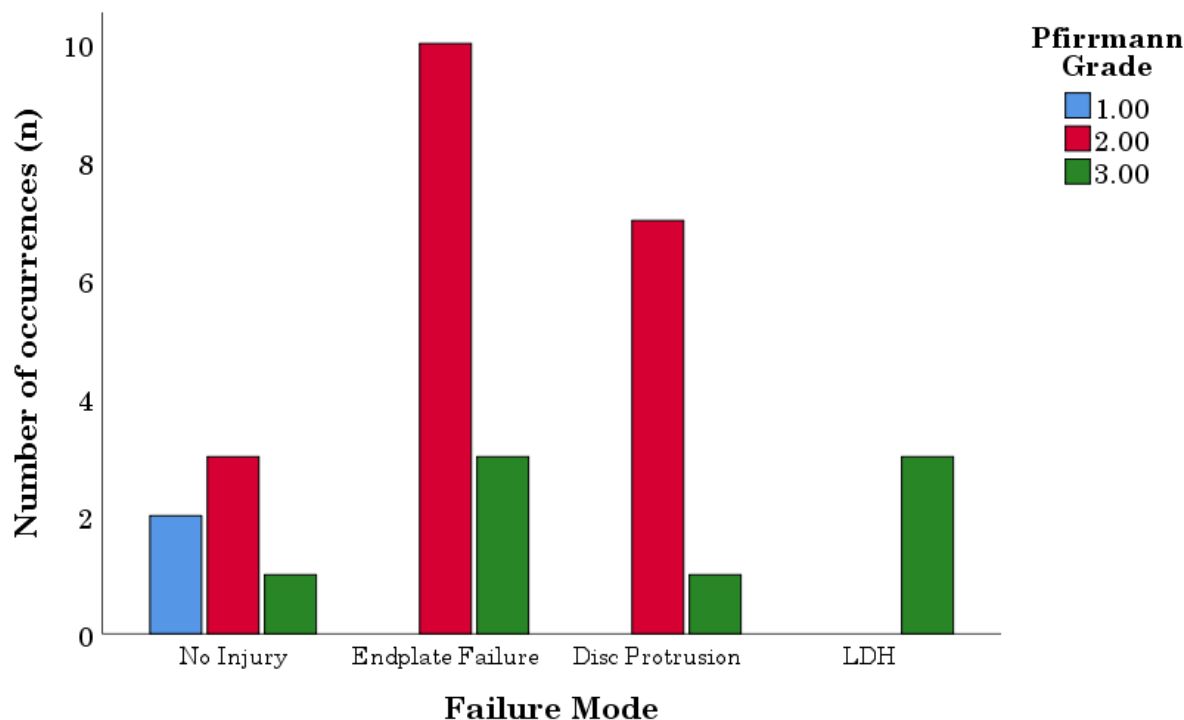


**Figure 6-11** Failure mode vs Pfirrmann grade

## 6.5 Discussion

This study investigated, for the first time, the effect of safe and unsafe repetitive lifting on disc injury by examining the correlations between MSS, tissue damage (MRI and macroscopic), and failure mode. Early failure of specimens prior to 20,000 cycles proved that unsafe lifting leads to a greater risk of injury. High damage scores for disc protrusion and LDH were observed in the posterior and posterolateral regions. In addition, there was increasing MSS with increasing severity of disc injury in the left lateral region. Furthermore, it was found that there was a relationship between LDH and Pfirrmann grade, where only grade 3 discs herniated. This finding verifies predictions based on finite element (FE) modeling (Schmidt et al., 2007b) and is consistent with current clinical anecdotal knowledge.

The present study developed a scoring system to assess damage in each disc, which was then compared to the MSS in the same plane. While this scoring system has not been

previously validated, the average scores from three independent observers resulted in significant positive correlations between MRI and macroscopic damage scores. In addition, for MSS measurement, an invasive wire grid was used, however, a control group with no grid was included in this study where MRI versus macroscopic damage scores had the same correlations in both control and experimental groups. Stiffness measured in all 6DOF directions was not statistically different before and after wire grid insertion, indicating that mechanical properties of the disc were not altered.

Unsafe lifting resulted in early specimen failure, however, the MSS between the two lifting groups were only different in the anterior and nucleus regions, with smaller strains in the unsafe lifting group. Smaller strains were likely the result of increased compression, which caused a stiffening effect within the disc tissue. This increased compression during unsafe lifting resulted in more endplate failures than LDH. It is important to note that *in vitro* internal disc strains during *repetitive loading* have not previously been measured. However, strains calculated from an FE model from one loading cycle (Schmidt et al., 2007b) in the posterolateral region, were smaller (47%, (Schmidt et al., 2007b) than the present study (70%). This difference is likely attributed to the twofold larger compressive load applied in the present study.

Predicting MSS from MRI damage scores was not possible since there were no correlations between the two. Furthermore, no strong correlations were seen between MSS and macroscopic damage score in any region except left lateral, where strain increased with damage score. It may be expected that strains would increase with severity of damage, however, voids/tears in the disc tissue, together with the migration of the nucleus and compaction of the annulus (e.g. annulus buckling into the 'bell' shape), would likely result in regional stiffening of the annulus with smaller associated strains. LDH has been linked to annular clefts (Moore et al., 1996) that leave voids within the disc tissue, as were found in the current study (**Figure 6-5**). Therefore, the relationship between MSS, damage score (MRI and macroscopic), and/or failure mode is likely to be multifactorial and nonlinear. Right axial rotation was applied within the present study, however, damage-strain relationships were seen in the left lateral (contralateral) region, which confirms the findings from previous studies (Schmidt et al., 2007b; Veres et al., 2010).

The site of herniation and protrusion mainly occurred in the posterolateral regions, which is consistent with current clinical knowledge and commonly associated with this combination of loading (Fazey et al., 2006; Veres et al., 2010), **Table 6-1**). For the majority of specimens within the disc protrusion group, the region of protrusion was where the highest damage score was found, and the largest MSS (**Table 6-2**, see **Appendix I**).

Damage scores and macroscopic images showed that delamination, annulus buckling, and nuclear migration were present in the *no injury* and *disc protrusion* groups, with radial tears only found in one specimen. Classical stages of gradual disc prolapse determined by Adams et al. were also seen in this study with apparent distortion of lamellae in the disc protrusion and LDH groups (Adams and Hutton, 1985). Regionally, the lower damage scores related to delamination were seen in the anterior, left and right anterolateral regions. Gross damage associated with LDH occurred in the posterior and posterolateral regions and not the anterior regions (Adams and Hutton, 1985; Gordon et al., 1991; Veres et al., 2010). Looking at the disc damage score overall (independent of the region), higher damage scores were associated with LDH in comparison to other failure modes (**Figure 6-12**).

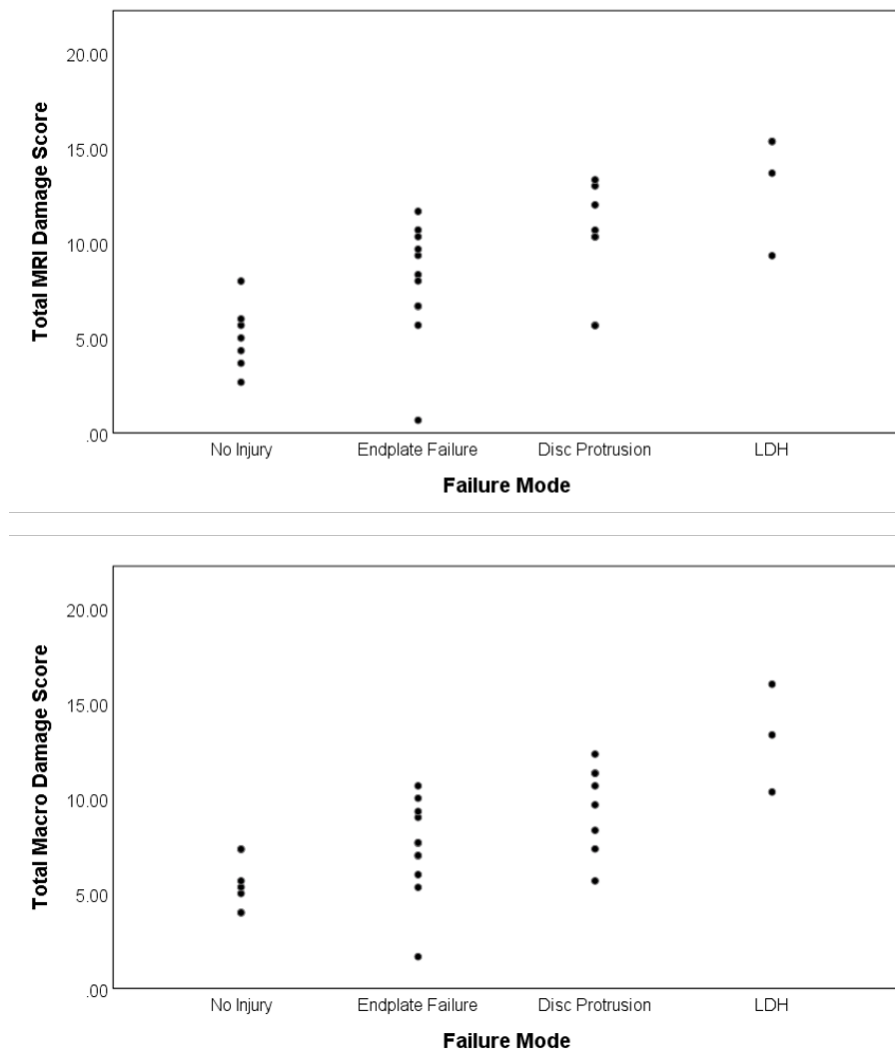


**Figure 6-12.** Failure mode vs. total MRI damage score (left) and failure mode vs macroscopic damage score (right). Total damage scores are independent of region (i.e. all scores within 9 regions for each specimen were added together). Significant positive correlations were seen for both comparisons (Failure mode vs MRI:  $r_s = 0.618$ , Failure mode vs Macro:  $r_s = 0.675$ ,  $p < 0.001$ ,  $n = 30$ )

**Table 6-2** Specimen-specific results for specimens that failed by LDH or disc protrusion and their relationships to the injury site, regions of highest MRI and macroscopic damage, and regions of largest and smallest MSS. Specimens 1-3 failed by LDH, and specimens 4-11 failed by disc protrusion

Specimen Number	Lifting	MSS Measurement	Site of herniation or protrusion	Region of highest Damage Score MRI	Region of Highest Damage Score Macro	Region of Largest MSS	Region of Smallest MSS
1	safe	Yes	Post	Post	Post	LLat	Post
2	safe	No	LPostLat	LPostLat	LPostLat	-	-
3	safe	No	RPostLat	RPostLat	RPostLat	-	-
4	unsafe	Yes	RPostLat	RPostLat	RPostLat, Nucl	RPostLat	Nucl
5	unsafe	No	LPostLat, RPostLat	LPostLat	LPostLat, RPostLat	-	-
6	unsafe	Yes	RPostLat	Post	Nucl	LLat	Post
7	unsafe	Yes	Post	Post	Post	LPostLat	Nucl
8	safe	No	LPostLat	LPostLat	LPostLat	-	-
9	safe	Yes	RPostLat	RPostLat	RPostLat	RPostLat	LAntLat
10	safe	Yes	LPostLat	LPostLat	LPostLat	LPostLat	RLat
11	safe	Yes	Post	LPostLat	Post	Ant	RPostLat

Notes: LPostLat = left posterolateral, RPostLat = right posterolateral, Nucl = nucleus, Post = posterior, Ant = anterior, LAntLat = left anterolateral, LLat = left lateral, RLat = right lateral. MSS measurement column: No = Control and Yes = Experimental (**Figure 6-1**).

The only correlation between failure mode (herniation pathway) and MSS was found in the left lateral region, where MSS increased with injury severity. This observation suggests the existence of an MSS threshold (approximately 50%, **Figure 6-7**), which may increase the risk of disc protrusion and LDH if exceeded. The correlation between MSS and failure mode in the lateral region implies that it may be the weakest within the disc. The anterior and posterior regions are protected by the anterior and posterior longitudinal ligaments, leaving the lateral and posterolateral regions exposed. Research using ovine discs have identified new mechanisms of herniation where nucleus material migrated laterally and then tracked to the posterolateral region (van Heeswijk et al., 2017). No nucleus material was identified in the lateral region in this study, however buckling of the annulus and delamination were frequently observed. Taken together, these findings provide further evidence in support of the current mechanistic understanding of the relationship between lateral region damage and LDH. The lateral region may be one of the first sites to experience disc damage during repetitive compression, flexion, and axial rotation loading.

## 6.6 Conclusion

In summary, it has been shown, for the first time that MSS increased with progression of disc injury towards herniation in the left lateral (contralateral) region under a combination of repetitive compression, flexion and right axial rotation. This finding provides evidence that the lateral region is more vulnerable than previously understood. In addition, the magnitudes of MSS reported in this study suggests there may be a shear strain threshold, which if exceeded, may result in LDH. Correlations between MSS and tissue damage were identified, which has further verified current clinical knowledge, where damage associated with disc protrusion and LDH was predominantly located in the posterior and posterolateral regions. This study further demonstrated that unsafe lifting places the FSU at greatest risk of injury. All LDH occurred in Pfirrmann Grade 3 discs, confirming that mildly degenerated discs are more likely to herniate. This work provides an opportunity to examine how disc shear strain and damage are associated with various unsafe lifting techniques.

## Chapter 7      Conclusions and Future Recommendations

The overall aims of this research were to investigate the effects of simulated repetitive lifting on disc tissue by measuring internal disc strains and 6DOF mechanics. More specifically, the aims were:

1. To measure and compare the change in internal 3D disc strains during simulated safe and unsafe repetitive lifting in lumbar spinal segments
2. To measure and compare the effect of simulated safe and unsafe repetitive lifting on 6DOF mechanical properties (stiffness, and phase angle)
3. To examine the correlations between tissue damage assessed via imaging, internal disc strains, and failure mode after simulated repetitive lifting.

### 7.1 Principle Findings

#### 7.1.1 Internal disc strains are the largest in the anterior and posterolateral regions under both safe and unsafe simulated repetitive lifting

As shear is an important component of disc injury, MSS was measured in this research. For both safe and unsafe repetitive lifting, there were large shear strains in the lateral, posterolateral and anterior regions with the posterolateral region being of more concern since this region is commonly the site of injury. In addition, the contralateral side to the applied loading saw the largest shear strains. Comparable shear strains were found in all regions between safe and unsafe lifting, however, smaller shear strains were found under unsafe repetitive lifting in the anterior and nucleus regions. This finding suggests that when subjected to larger compressive loads, the disc tissue becomes stiffer. The normal to mildly degenerated tissue used in this research demonstrated the resiliency in the disc, where large changes in shear strain were not observed over time. Shear strains for disc protrusion and endplate failure specimens were larger than no injury specimens, suggesting the existence of a damage threshold (failure criteria) of 50% MSS. Above this threshold, the risk of tissue damage associated with disc injuries, such as disc protrusion and endplate failure, increases. This research showed that unsafe lifting leads to a greater risk of injury as a result of specimens failed earlier than those under safe lifting. Clinically, this suggests that unsafe lifting postures and techniques should be avoided.

#### 7.1.2 6DOF mechanics are altered after simulated repetitive lifting

After simulated repetitive lifting, the mechanical properties in compression, flexion, and axial rotation changed since these were in the same direction of combined loading. However, by measuring the mechanical properties in other directions, it was found that

repetitive lifting also affected extension, left axial rotation (contralateral to the applied rotation), and lateral shear directions. The effect of failure mode on mechanical properties was minor and differences were only associated between endplate failure and compressive mechanics. Measuring 6DOF mechanics alone was not sufficient to detect tissue level disc damage since no difference in mechanical properties were observed between safe and unsafe repetitive lifting. Furthermore, the lack of differences suggests that measuring disc tissue strains provide a greater sensitivity to detecting tissue damage. Knowing which directions are affected by repetitive lifting may help determine which muscles need to be strengthened to counteract the changes in stiffness and phase angle seen in the FSU.

### 7.1.3 Large shear strains correlated with tissue damage

The loading applied in this study lead to annulus buckling, nuclear migration, and delamination as seen from the MRI and macroscopic assessments. In addition, it was shown that failure of the endplate can lead to associated disc tissue damage. For a majority of the specimens, regions of large shear strains were associated with tissue damage as assessed via MRI and macroscopic assessment. It was observed that MSS increased with tissue damage and progression of disc injury towards herniation in the left lateral (contralateral) region under a combination of repetitive compression, flexion and right axial rotation. This finding provided evidence that the lateral region was more vulnerable than previously understood. Correlations between MSS and tissue damage further verified current clinical knowledge, where damage associated with disc protrusion and LDH was predominantly located in the posterior and posterolateral regions. All LDH occurred in Pfirrmann Grade 3 discs, confirming that mildly degenerated discs were more likely to herniate. This work provided an opportunity to examine how disc shear strain and damage were associated with various lifting techniques.

### 7.1.4 Mechanistic understanding of disc herniation

Taken together, this research leads to a mechanistic theory that is similar to that proposed by Adams et al., 1985. LDH is more likely to occur in the lower lumbar discs with mildly degenerated tissue. Discs under repetitive loading will likely initiate LDH with inward buckling of the lamellae in the lateral region (contralateral side to applied rotation), causing nuclear migration towards the posterior and posterolateral regions as well as delamination in adjacent regions (**Figure 7-1**). This inward buckling and delamination was found in the macroscopic assessment after loading and was associated with on the largest magnitudes of shear strain observed in the lateral region. With continued repetitive loading, migration of the nucleus leads to compaction of the posterior and posterolateral lamellae, which generates counteracting radial stresses against the nucleus (**Figure 7-1**).

LDH is more likely to occur in the posterolateral region since the posterior longitudinal ligament protects the posterior lamellae. At this stage, the compaction would lead to a decrease in strain, which was also found in this research. After a number of cycles or a sudden episode after repetitive loading, progressive damage to the annulus will lead to extrusion of the nucleus via radial and/or circumferential tears within the posterolateral annulus.

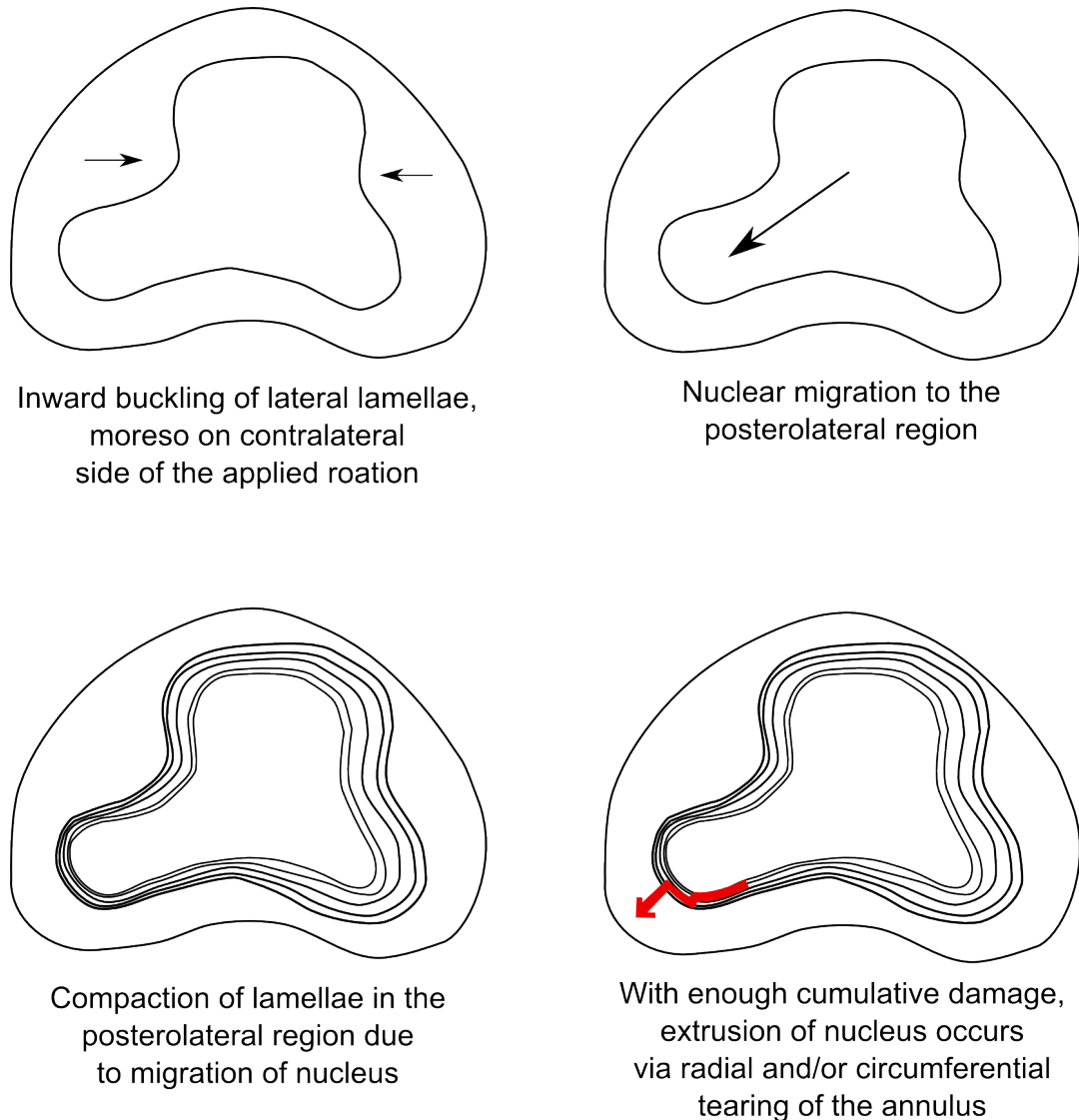


**Figure 7-1** Drawing of mechanistic theory of LDH developed from this research

## 7.2 Significance

The research presented in this thesis has advanced current knowledge of possible mechanisms for LDH and supplied vital information regarding disc mechanics that are important for finite element models, and the development of future disc implants. Disc deformations and 6DOF mechanics associated with repetitive safe and unsafe lifting that lead to LDH have been measured. The internal disc strains can be used to develop and

validate robust finite element models to help further understand the mechanisms of disc herniation and other disc injuries under various combinations of loads. Furthermore, validation of finite element models using this experimental data can lead to an exploration of the specimen-specific response which is becoming increasingly important as the variation between humans is vast. As more tissue engineering therapies and disc implants are being designed, both internal disc strain thresholds and multiaxial disc mechanics need to be considered.

### 7.3 Future Recommendations

Based on the findings presented in this thesis, the future recommendations are as follows:

Combinations of flexion, axial rotation, and compression, which mimic bending and twisting motions were explored in this research, however, there are other motions that can lead to repetitive loading injuries. For example, studying the effects of combined flexion, lateral bending, and compression, which has been shown by Costi et al., 2007 to place the disc at a greater risk of injury. In addition, the effect of various unsafe lifting techniques on disc injury needs to be studied to develop better guidelines for safe work organisations.

Mechanistically, measuring inner and outer annulus strains would improve current understanding of disc injury. There may be differences between these two regions of the annulus that are critical in injury initiation or propagation, which were not discovered before. In addition, analysing the tissue microstructurally after repetitive loading in both the sagittal and axial planes can give better insight into the migration of the nucleus as well as the failure of the annulus. A multiscale approach is required as strain thresholds at the micro level would be different to those found at the macro level, which provides information regarding the structures that influence disc injury under repetitive loading.

Strains in this thesis increased by 8% over the 20,000 cycles and the strain profiles were similar throughout the loading, which may be a result of the hybrid loading control used to simulate repetitive lifting. The primary axes of flexion and axial rotation were driven in position control with a compressive load held constant. The failure patterns found in this research may be different to those found under load (moment) control, where the rotation would increase throughout loading. Using moment control may better mimic the human condition *in vivo*. Furthermore, this research highlights the importance of future work focusing on understanding the relationship between whole-body kinematics and mechanics of the disc since the disc (including the endplate) is the primary initiating site of injury. Applying the forces/moments measured at L4-5 during repetitive lifting on an

L4-5 FSU would provide an understanding of how the *in vivo* response affects disc tissue. This would increase our knowledge of the effects of repetitive lifting on disc injury.

Currently *in vitro* studies subject FSUs to either sudden overload or repetitive loading. The injury mechanism may be a combination of repetitive lifting, which leads to cumulative damage, and a final sudden overload episode, which causes the injury. This overload may just be one awkward or incorrect lift that results in LDH. The effect of repetitive loading followed by sudden overload on disc tissue needs to be explored.

#### 7.4 Concluding Statement

The findings of this study contribute to the mechanistic understanding of LDH under repetitive loading. Internal disc strains were measured for the first time under combined flexion, axial rotation, and compressive loading, which simulated safe and unsafe repetitive lifting by bending and twisting. Largest magnitudes of shear strains were found in the lateral, posterolateral and anterior regions, which correlated with regions of tissue damage. Unsafe lifting led to a greater risk of disc injury, further supporting advice to avoid unsafe lifting practices. A threshold of MSS was determined to be 50%, above which, would result in tissue damage associated with gross disc injuries such as disc protrusion and endplate failure. In addition, disc mechanics showed that it's important to measure mechanical properties in all 6DOF directions. These multiaxial mechanics and internal disc strains should be considered during development of new disc implants and therapies. Based on the findings from this research, future work is required to understand failure criteria and tissue deformation under other combinations of risky motions. In addition, this experimental data can be used to validate finite element models and predict the specimen-specific response to repetitive loading.



## Chapter 8      References

- (AIHW), A.I.o.H.a.W., 2009. Health expenditure for arthritis and musculoskeletal conditions, 2004-05, in: 10, A.s.n. (Ed.), Cat. no. PHE 115, Canberra.
- Adams, M.A., 2002. *The Biomechanics of Back Pain*. Churchill Livingstone.
- Adams, M.A., Dolan, P., 2012. Intervertebral disc degeneration: Evidence for two distinct phenotypes. *Journal of anatomy* 221, 497-506.
- Adams, M.A., Freeman, B.J., Morrison, H.P., Nelson, I.W., Dolan, P., 2000. Mechanical initiation of intervertebral disc degeneration. *Spine* 25, 1625-1636.
- Adams, M.A., Hutton, W.C., 1981. The relevance of torsion to the mechanical derangement of the lumbar spine. *Spine* 6, 241-248.
- Adams, M.A., Hutton, W.C., 1982. Prolapsed intervertebral disc. A hyperflexion injury 1981 Volvo Award in Basic Science. *Spine* 7, 184-191.
- Adams, M.A., Hutton, W.C., 1983. The effect of fatigue on the lumbar intervertebral disc. *The Journal of bone and joint surgery. British volume* 65, 199-203.
- Adams, M.A., Hutton, W.C., 1985. Gradual disc prolapse. *Spine* 10, 524-531.
- Adams, M.A., McNally, D.S., Dolan, P., 1996. 'Stress' distributions inside intervertebral discs. The effects of age and degeneration. *The Journal of bone and joint surgery. British volume* 78, 965-972.
- Adams, P., Eyre, D.R., Muir, H., 1977. Biochemical aspects of development and ageing of human lumbar intervertebral discs. *Rheumatology* 16, 22-29.
- Administration, O.S.a.H., *Ergonomics eTool: Materials Handling: Heavy Lifting*, in: Besser, B. (Ed.). *Occupational Safety and Health Administration*.
- AIHW, A.I.o.H.a.W., 2009: Cat. no. PHE 115. Health expenditure for arthritis and musculoskeletal conditions, 2004-05, Canberra.
- AIHW, A.I.o.H.a.W., 2015. *Back Pain and Problems*, Arthritis series no. 21, Canberra.
- Al-Rawahi, M., Luo, J., Pollintine, P., Dolan, P., Adams, M.A., 2011. Mechanical function of vertebral body osteophytes, as revealed by experiments on cadaveric spines. *Spine* 36, 770-777.
- Alkalay, R.N., Burstein, D., Westin, C.F., Meier, D., Hackney, D.B., 2015. MR diffusion is sensitive to mechanical loading in human intervertebral disks ex vivo. *Journal of magnetic resonance imaging : JMRI* 41, 654-664.
- Amin, D.B., Lawless, I.M., Sommerfeld, D., Stanley, R.M., Ding, B., Costi, J.J., 2016a. The effect of six degree of freedom loading sequence on the in-vitro compressive properties of human lumbar spine segments. *Journal of biomechanics* 49, 3407-3414.

Amin, D.B., Moawad, C.M., Costi, J.J., 2018 Manuscript Under Review-a. Lumbar Intervertebral Disc Multiaxial Mechanics are Altered after Simulated Repetitive Lifting Movements. *Journal of biomechanics*.

Amin, D.B., Moawad, C.M., Costi, J.J., 2018 Manuscript Under Review-b. New findings confirm regional internal disc strain changes during simulation of repetitive lifting motions. *Annals of biomedical engineering*.

Amin, D.B., Sommerfeld, D., Lawless, I.M., Stanley, R.M., Ding, B., Costi, J.J., 2016b. Effect of degeneration on the six degree of freedom mechanical properties of human lumbar spine segments. *Journal of orthopaedic research : official publication of the Orthopaedic Research Society*.

Amin, D.B., Tavakoli, J., Freeman, B.J., Costi, J.J., 2018 Manuscript Under Review-c. Understanding the Impact of Repetitive Lifting Towards Lumbar Disc Herniation: A Clinically Relevant Biomechanical Cadaveric Study Spine.

Andersson, G., Örtengren, R., Nachemson, A., 1976. Quantitative Studies of Back Loads in Lifting. *Spine* 1, 178-185.

Andersson, G.B., 1981. Epidemiologic aspects on low-back pain in industry. *Spine* 6, 53-60.

Awad, J.N., Moskovich, R., 2006. Lumbar disc herniations: surgical versus nonsurgical treatment. *Clinical orthopaedics and related research* 443, 183-197.

Beckstein, J.C., Sen, S., Schaer, T.P., Vresilovic, E.J., Elliott, D.M., 2008. Comparison of animal discs used in disc research to human lumbar disc: axial compression mechanics and glycosaminoglycan content. *Spine* 33, E166-173.

Benneker, L.M., Heini, P.F., Alini, M., Anderson, S.E., Ito, K., 2005. 2004 Young Investigator Award Winner: vertebral endplate marrow contact channel occlusions and intervertebral disc degeneration. *Spine* 30, 167-173.

Berger-Roscher, N., Casaroli, G., Rasche, V., Villa, T., Galbusera, F., Wilke, H.J., 2017. Influence of Complex Loading Conditions on Intervertebral Disc Failure. *Spine* 42, E78-e85.

Bonato, P., Ebenbichler, G.R., Roy, S.H., Lehr, S., Posch, M., Kollmitzer, J., Della Croce, U., 2003. Muscle fatigue and fatigue-related biomechanical changes during a cyclic lifting task. *Spine* 28, 1810-1820.

Brinckmann, P., Biggemann, M., Hilweg, D., 1988. Fatigue fracture of human lumbar vertebrae. *Clinical Biomechanics* 3, S1-S23.

Buckwalter, J.A., 1995. Spine update: Aging and degeneration of the human intervertebral disc. *Spine* 20, 1307-1314.

- Callaghan, J.P., McGill, S.M., 2001. Intervertebral disc herniation: studies on a porcine model exposed to highly repetitive flexion/extension motion with compressive force. *Clinical biomechanics* (Bristol, Avon) 16, 28-37.
- Cannella, M., Arthur, A., Allen, S., Keane, M., Joshi, A., Vresilovic, E., Marcolongo, M., 2008. The role of the nucleus pulposus in neutral zone human lumbar intervertebral disc mechanics. *Journal of biomechanics* 41, 2104-2111.
- Carragee, E.J., Don, A.S., Hurwitz, E.L., Cuellar, J.M., Carrino, J.A., Herzog, R., 2009. 2009 ISSLS Prize Winner: Does discography cause accelerated progression of degeneration changes in the lumbar disc: a ten-year matched cohort study. *Spine* 34, 2338-2345.
- Cassidy, J.J., Hiltner, A., Baer, E., 1989. Hierarchical Structure of the Intervertebral Disc. *Connective Tissue Research* 23, 75-88.
- Chan, D.D., Neu, C.P., 2014. Intervertebral disc internal deformation measured by displacements under applied loading with MRI at 3T. *Magnetic resonance in medicine* 71, 1231-1237.
- Chang, T.-S., Chang, J.-H., Cheng, C.-W., 2011. A Pure Moment Based Tester for Spinal Biomechanics.
- Cooper, S., 2018. Safe Work Australia, Lifting, pushing and pulling (manual handling).
- Costi, J.J., Stokes, I.A., Gardner-Morse, M., Laible, J.P., Scoffone, H.M., Iatridis, J.C., 2007. Direct measurement of intervertebral disc maximum shear strain in six degrees of freedom: motions that place disc tissue at risk of injury. *Journal of biomechanics* 40, 2457-2466.
- Costi, J.J., Stokes, I.A., Gardner-Morse, M.G., Iatridis, J.C., 2008. Frequency-dependent behavior of the intervertebral disc in response to each of six degree of freedom dynamic loading: solid phase and fluid phase contributions. *Spine* 33, 1731-1738.
- Cribb, G.L., Jaffray, D.C., Cassar-Pullicino, V.N., 2007. Observations on the natural history of massive lumbar disc herniation. *The Journal of bone and joint surgery. British volume* 89, 782-784.
- Davis, M.A., Onega, T., Weeks, W.B., Lurie, J.D., 2012. Where the United States spends its spine dollars: expenditures on different ambulatory services for the management of back and neck conditions. *Spine* 37, 1693-1701.
- Dempsey, P.G., 1998. A critical review of biomechanical, epidemiological, physiological and psychophysical criteria for designing manual materials handling tasks. *Ergonomics* 41, 73-88.
- Development, A.C.f.C., 2014. The International Statistical Classification of Diseases and Related Health Problems, 10th Revision, in: Database, A.N.H.M. (Ed.).

Dickson, I.R., Happey, F., Pearson, C.H., Naylor, A., Turner, R.L., 1967. Variations in the Protein Components of Human Intervertebral Disk with Age. *Nature* 215, 52.

Ding, B., Cazzolato, B.S., Stanley, R.M., Grainger, S., Costi, J.J., 2014. Stiffness Analysis and Control of a Stewart Platform-Based Manipulator With Decoupled Sensor–Actuator Locations for Ultrahigh Accuracy Positioning Under Large External Loads. *Journal of Dynamic Systems, Measurement, and Control* 136, 061008.

Dolan, P., Adams, M.A., 1998. Repetitive lifting tasks fatigue the back muscles and increase the bending moment acting on the lumbar spine. *Journal of biomechanics* 31, 713-721.

Drake, J.D., Aultman, C.D., McGill, S.M., Callaghan, J.P., 2005. The influence of static axial torque in combined loading on intervertebral joint failure mechanics using a porcine model. *Clinical biomechanics (Bristol, Avon)* 20, 1038-1045.

Edwards, W.T., Ordway, N.R., Zheng, Y., McCullen, G., Han, Z., Yuan, H.A., 2001. Peak stresses observed in the posterior lateral annulus. *Spine* 26, 1753-1759.

Eyre, D.R., 1988. *Collagens of the Disc the Biology of the Intervertebral Disc* 171-188.

Farfan, H.F., Cossette, J.W., Robertson, G.H., Wells, R.V., Kraus, H., 1970. The effects of torsion on the lumbar intervertebral joints: the role of torsion in the production of disc degeneration. *The Journal of bone and joint surgery. American volume* 52, 468-497.

Fazey, P.J., Song, S., Monsas, S., Johansson, L., Haukalid, T., Price, R.I., Singer, K.P., 2006. An MRI investigation of intervertebral disc deformation in response to torsion. *Clinical biomechanics (Bristol, Avon)* 21, 538-542.

Fazzalari, N.L., Costi, J.J., Hearn, T.C., Fraser, R.D., Vernon-Roberts, B., Hutchinson, J., Manthey, B.A., Parkinson, I.H., Sinclair, C., 2001. Mechanical and pathologic consequences of induced concentric annular tears in an ovine model. *Spine* 26, 2575-2581.

Fujiwara, A., An, H.S., Lim, T.H., Haughton, V.M., 2001. Morphologic changes in the lumbar intervertebral foramen due to flexion-extension, lateral bending, and axial rotation: an in vitro anatomic and biomechanical study. *Spine* 26, 876-882.

Galante, J.O., 1967. Tensile properties of the human lumbar annulus fibrosus. *Acta Orthop Scand, Suppl* 100:101-191.

Galbusera, F., van Rijsbergen, M., Ito, K., Huyghe, J.M., Brayda-Bruno, M., Wilke, H.J., 2014. Ageing and degenerative changes of the intervertebral disc and their impact on spinal flexibility. *European spine journal : official publication of the European Spine Society, the European Spinal Deformity Society, and the European Section of the Cervical Spine Research Society* 23 Suppl 3, S324-332.

- Goertzen, D.J., Lane, C., Oxland, T.R., 2004. Neutral zone and range of motion in the spine are greater with stepwise loading than with a continuous loading protocol. An in vitro porcine investigation. *Journal of biomechanics* 37, 257-261.
- Gordon, S.J., Yang, K.H., Mayer, P.J., Mace, A.H., Jr., Kish, V.L., Radin, E.L., 1991. Mechanism of disc rupture. A preliminary report. *Spine* 16, 450-456.
- Hamanishi, C., Kawabata, T., Yosii, T., Tanaka, S., 1994. Schmorl's nodes on magnetic resonance imaging: Their incidence and clinical relevance. *Spine* 19, 450-453.
- Hashizume, H., 1980. Three-dimensional architecture and development of lumbar intervertebral discs. *Acta Medica Okayama* 34, 301-314.
- Heneweer, H., Staes, F., Aufdemkampe, G., van Rijn, M., Vanhees, L., 2011. Physical activity and low back pain: a systematic review of recent literature. *European spine journal : official publication of the European Spine Society, the European Spinal Deformity Society, and the European Section of the Cervical Spine Research Society* 20, 826-845.
- Iatridis, J.C., Kumar, S., Foster, R.J., Weidenbaum, M., Mow, V.C., 1999. Shear mechanical properties of human lumbar annulus fibrosus. *Journal of orthopaedic research : official publication of the Orthopaedic Research Society* 17, 732-737.
- Iatridis, J.C., Weidenbaum, M., Setton, L.A., Mow, C.V., 1996. Is the nucleus pulposus a solid or a fluid? Mechanical behaviors of the nucleus pulposus of the human intervertebral disc. *Spine* 21, 1174-1184.
- Inoue, H., 1981. Three-dimensional architecture of lumbar intervertebral discs. *Spine* 6, 139-146.
- Inoue, H., Takeda, T., 1975. Three-Dimensional Observation of Collagen Framework of Lumbar Intervertebral Discs. *Acta Orthopaedica Scandinavica* 46, 949-956.
- Johannessen, W., Vresilovic, E.J., Wright, A.C., Elliott, D.M., 2004. Intervertebral disc mechanics are restored following cyclic loading and unloaded recovery. *Annals of biomedical engineering* 32, 70-76.
- Jordan, J.L., Konstantinou, K., O'Dowd, J., 2011. Herniated lumbar disc. *BMJ Clin Evid* 2011.
- Kasra, M., Shirazi-Adl, A., Drouin, G., 1992. Dynamics of human lumbar intervertebral joints. Experimental and finite-element investigations. *Spine* 17, 93-102.
- Kelsey, J.L., 1975. An epidemiological study of the relationship between occupations and acute herniated lumbar intervertebral discs. *International journal of epidemiology* 4, 197-205.
- Kelsey, J.L., Githens, P.B., O'Conner, T., Weil, U., Calogero, J.A., Holford, T.R., White, A.A., 3rd, Walter, S.D., Ostfeld, A.M., Southwick, W.O., 1984a. Acute prolapsed lumbar

intervertebral disc. An epidemiologic study with special reference to driving automobiles and cigarette smoking. *Spine* 9, 608-613.

Kelsey, J.L., Githens, P.B., White, A.A., 3rd, Holford, T.R., Walter, S.D., O'Connor, T., Ostfeld, A.M., Weil, U., Southwick, W.O., Calogero, J.A., 1984b. An epidemiologic study of lifting and twisting on the job and risk for acute prolapsed lumbar intervertebral disc. *Journal of orthopaedic research : official publication of the Orthopaedic Research Society* 2, 61-66.

Kelsey, J.L., Greenberg, R.A., Hardy, R.J., Johnson, M.F., 1975. Pregnancy and the syndrome of herniated lumbar intervertebral disc; an epidemiological study. *The Yale journal of biology and medicine* 48, 361-368.

Keyes, D.C., Compere, E.L., 1932. The normal and pathological physiology of the nucleus pulposus of the intervertebral disc. *J Bone Joint Surg* 14, 897-938.

Kim, J., Yang, S.J., Kim, H., Kim, Y., Park, J.B., Dubose, C., Lim, T.H., 2012. Effect of shear force on intervertebral disc (IVD) degeneration: an in vivo rat study. *Annals of biomedical engineering* 40, 1996-2004.

Kirkaldy-Willis, W.H., Farfan, H.F., 1982. Instability of the lumbar spine. *Clinical orthopaedics and related research*, 110-123.

Koebbe, C.J., Maroon, J.C., Abl, A., El-Kadi, H., Bost, J., 2002. Lumbar microdiscectomy: a historical perspective and current technical considerations. *Neurosurgical focus* 13, E3.

Koeller, W., Meier, W., Hartmann, F., 1984. Biomechanical properties of human intervertebral discs subjected to axial dynamic compression. A comparison of lumbar and thoracic discs. *Spine* 9, 725-733.

Korecki, C.L., MacLean, J.J., Iatridis, J.C., 2008. Dynamic compression effects on intervertebral disc mechanics and biology. *Spine* 33, 1403-1409.

Krag, M.H., Seroussi, R.E., Wilder, D.G., Pope, M.H., 1987. Internal displacement distribution from in vitro loading of human thoracic and lumbar spinal motion segments: experimental results and theoretical predictions. *Spine* 12, 1001-1007.

Krismer, M., Haid, C., Behensky, H., Kapfinger, P., Landauer, F., Rachbauer, F., 2000. Motion in lumbar functional spine units during side bending and axial rotation moments depending on the degree of degeneration. *Spine* 25, 2020-2027.

Lama, P., Le Maitre, C.L., Dolan, P., Tarlton, J.F., Harding, I.J., Adams, M.A., 2013. Do intervertebral discs degenerate before they herniate, or after? *The bone & joint journal* 95-b, 1127-1133.

Lavender, S.A., Li, Y.C., Andersson, G.B., Natarajan, R.N., 1999. The effects of lifting speed on the peak external forward bending, lateral bending, and twisting spine moments. *Ergonomics* 42, 111-125.

- Lawless, I.M., Ding, B., Cazzolato, B.S., Costi, J.J., 2014. Adaptive velocity-based six degree of freedom load control for real-time unconstrained biomechanical testing. *Journal of biomechanics* 47, 3241-3247.
- Lipson, S.J., Muir, H., 1980. Vertebral osteophyte formation in experimental disc degeneration. Morphologic and proteoglycan changes over time. *Arthritis and rheumatism* 23, 319-324.
- Lu, W.W., Luk, K.D., Holmes, A.D., Cheung, K.M., Leong, J.C., 2005. Pure shear properties of lumbar spinal joints and the effect of tissue sectioning on load sharing. *Spine* 30, E204-209.
- Lysack, J.T., Dickey, J.P., Dumas, G.A., Yen, D., 2000. A continuous pure moment loading apparatus for biomechanical testing of multi-segment spine specimens. *Journal of biomechanics* 33, 765-770.
- Marchand, F., Ahmed, A.M., 1990. Investigation of the laminate structure of lumbar disc annulus fibrosus. *Spine* 15, 402-410.
- Maroudas, A., Stockwell, R.A., Nachemson, A., Urban, J., 1975. Factors involved in the nutrition of the human lumbar intervertebral disc: cellularity and diffusion of glucose in vitro. *Journal of anatomy* 120, 113-130.
- Marras, W.S., Davis, K.G., Ferguson, S.A., Lucas, B.R., Gupta, P., 2001. Spine loading characteristics of patients with low back pain compared with asymptomatic individuals. *Spine* 26, 2566-2574.
- Marras, W.S., Lavender, S.A., Leurgans, S.E., Rajulu, S.L., Allread, W.G., Fathallah, F.A., Ferguson, S.A., 1993. The role of dynamic three-dimensional trunk motion in occupationally-related low back disorders. The effects of workplace factors, trunk position, and trunk motion characteristics on risk of injury. *Spine* 18, 617-628.
- Marras, W.S., Parakkat, J., Chany, A.M., Yang, G., Burr, D., Lavender, S.A., 2006. Spine loading as a function of lift frequency, exposure duration, and work experience. *Clinical biomechanics (Bristol, Avon)* 21, 345-352.
- McMillan, D.W., McNally, D.S., Garbutt, G., Adams, M.A., 1996. Stress distributions inside intervertebral discs: the validity of experimental 'stress profilometry'. *Proceedings of the Institution of Mechanical Engineers. Part H, Journal of engineering in medicine* 210, 81-87.
- McNally, D.S., Adams, M.A., 1992. Internal intervertebral disc mechanics as revealed by stress profilometry. *Spine* 17, 66-73.
- Mehta, J.P., Lavender, S.A., Jagacinski, R.J., 2014. Physiological and biomechanical responses to a prolonged repetitive asymmetric lifting activity. *Ergonomics* 57, 575-588.

- Michalek, A.J., Buckley, M.R., Bonassar, L.J., Cohen, I., Iatridis, J.C., 2009. Measurement of local strains in intervertebral disc anulus fibrosus tissue under dynamic shear: contributions of matrix fiber orientation and elastin content. *Journal of biomechanics* 42, 2279-2285.
- Mikawa, Y., Hamagami, H., Shikata, J., Yamamuro, T., 1986. Elastin in the human intervertebral disk - A histological and biochemical study comparing it with elastin in the human yellow ligament. *Archives of Orthopaedic and Traumatic Surgery* 105, 343-349.
- Moore, R.J., Vernon-Roberts, B., Fraser, R.D., Osti, O.L., Schembri, M., 1996. The origin and fate of herniated lumbar intervertebral disc tissue. *Spine* 21, 2149-2155.
- Morgan, F.P., King, T., 1957. Primary instability of lumbar vertebrae as a common cause of low back pain. *The Journal of bone and joint surgery. British volume* 39-b, 6-22.
- Mundt, D.J., Kelsey, J.L., Golden, A.L., Pastides, H., Berg, A.T., Sklar, J., Hosea, T., Panjabi, M.M., 1993. An epidemiologic study of non-occupational lifting as a risk factor for herniated lumbar intervertebral disc. The Northeast Collaborative Group on Low Back Pain. *Spine* 18, 595-602.
- Nachemson, A., Morris, J.M., 1964. In vivo measurements of intradiscal pressure. Discometry, a method for the determination of pressure in the lower lumbar discs. *The Journal of bone and joint surgery. American volume* 46, 1077-1092.
- Natarajan, R.N., Lavender, S.A., An, H.A., Andersson, G.B., 2008. Biomechanical response of a lumbar intervertebral disc to manual lifting activities: a poroelastic finite element model study. *Spine* 33, 1958-1965.
- Newell, N., Little, J.P., Christou, A., Adams, M.A., Adam, C.J., Masouros, S.D., 2017. Biomechanics of the human intervertebral disc: A review of testing techniques and results. *Journal of the mechanical behavior of biomedical materials* 69, 420-434.
- Newman, P.H., 1952. Sprung back. *The Journal of bone and joint surgery. British volume* 34-b, 30-37.
- O'Connell, G.D., Jacobs, N.T., Sen, S., Vresilovic, E.J., Elliott, D.M., 2011a. Axial creep loading and unloaded recovery of the human intervertebral disc and the effect of degeneration. *Journal of the mechanical behavior of biomedical materials* 4, 933-942.
- O'Connell, G.D., Johannessen, W., Vresilovic, E.J., Elliott, D.M., 2007. Human internal disc strains in axial compression measured noninvasively using magnetic resonance imaging. *Spine* 32, 2860-2868.
- O'Connell, G.D., Leach, J.K., Klineberg, E.O., 2015. Tissue Engineering a Biological Repair Strategy for Lumbar Disc Herniation. *BioResearch open access* 4, 431-445.

O'Connell, G.D., Vresilovic, E.J., Elliott, D.M., 2011b. Human intervertebral disc internal strain in compression: The effect of disc region, loading position, and degeneration. *Journal of Orthopaedic Research* 29, 547-555.

Osti, O.L., Vernon-Roberts, B., Moore, R., Fraser, R.D., 1992. Annular tears and disc degeneration in the lumbar spine. A post-mortem study of 135 discs. *The Journal of bone and joint surgery. British volume* 74, 678-682.

Panjabi, M.M., Brand, R.A., Jr., White, A.A., 3rd, 1976. Mechanical properties of the human thoracic spine as shown by three-dimensional load-displacement curves. *The Journal of bone and joint surgery. American volume* 58, 642-652.

Panjabi, M.M., Krag, M.H., Goel, V.K., 1981. A technique for measurement and description of three-dimensional six degree-of-freedom motion of a body joint with an application to the human spine. *Journal of biomechanics* 14, 447-460.

Patwardhan, A.G., Havey, R.M., Meade, K.P., Lee, B., Dunlap, B., 1999. A follower load increases the load-carrying capacity of the lumbar spine in compression. *Spine* 24, 1003-1009.

Pearcy, M., Portek, I., Shepherd, J., 1984. Three-dimensional x-ray analysis of normal movement in the lumbar spine. *Spine* 9, 294-297.

Pearcy, M.J., Bogduk, N., 1988. Instantaneous axes of rotation of the lumbar intervertebral joints. *Spine* 13, 1033-1041.

Pearcy, M.J., Tibrewal, S.B., 1984. Axial rotation and lateral bending in the normal lumbar spine measured by three-dimensional radiography. *Spine* 9, 582-587.

Pfarrmann, C.W., Metzendorf, A., Zanetti, M., Hodler, J., Boos, N., 2001. Magnetic resonance classification of lumbar intervertebral disc degeneration. *Spine* 26, 1873-1878.

Przybyla, A., Pollintine, P., Bedzinski, R., Adams, M.A., 2006. Outer annulus tears have less effect than endplate fracture on stress distributions inside intervertebral discs: relevance to disc degeneration. *Clinical biomechanics (Bristol, Avon)* 21, 1013-1019.

Rajasekaran, S., Bajaj, N., Tubaki, V., Kanna, R.M., Shetty, A.P., 2013. ISSLS Prize winner: The anatomy of failure in lumbar disc herniation: an in vivo, multimodal, prospective study of 181 subjects. *Spine* 38, 1491-1500.

Rajasekaran, S., Vidyadhara, S., Subbiah, M., Kamath, V., Karunanithi, R., Shetty, A.P., Venkateswaran, K., Babu, M., Meenakshi, J., 2010. ISSLS prize winner: a study of effects of in vivo mechanical forces on human lumbar discs with scoliotic disc as a biological model: results from serial postcontrast diffusion studies, histopathology and biochemical analysis of twenty-one human lumbar scoliotic discs. *Spine* 35, 1930-1943.

Rissanen, P.M., 1960. The surgical anatomy and pathology of the supraspinous and interspinous ligaments of the lumbar spine with special reference to ligament ruptures. *Acta orthopaedica Scandinavica. Supplementum* 46, 1-100.

Rodrigues, S.A., Wade, K.R., Thambyah, A., Broom, N.D., 2012. Micromechanics of annulus-end plate integration in the intervertebral disc. *Spine Journal* 12, 143-150.

Schmidt, H., Kettler, A., Heuer, F., Simon, U., Claes, L., Wilke, H.J., 2007a. Intradiscal pressure, shear strain, and fiber strain in the intervertebral disc under combined loading. *Spine* 32, 748-755.

Schmidt, H., Kettler, A., Rohlmann, A., Claes, L., Wilke, H.J., 2007b. The risk of disc prolapses with complex loading in different degrees of disc degeneration - a finite element analysis. *Clinical biomechanics (Bristol, Avon)* 22, 988-998.

Schollum, M.L., Wade, K.R., Shan, Z., Robertson, P.A., Thambyah, A., Broom, N.D., 2018. The Influence of Concordant Complex Posture and Loading Rate on Motion Segment Failure: A Mechanical and Microstructural Investigation. *Spine* 43, E1116-e1126.

Seidler, A., Bolm-Audorff, U., Siol, T., Henkel, N., Fuchs, C., Schug, H., Leheta, F., Marquardt, G., Schmitt, E., Ulrich, P.T., Beck, W., Missalla, A., Elsner, G., 2003. Occupational risk factors for symptomatic lumbar disc herniation; a case-control study. *Occupational and environmental medicine* 60, 821-830.

Seroussi, R.E., Krag, M.H., Muller, D.L., Pope, M.H., 1989. Internal deformations of intact and denucleated human lumbar discs subjected to compression, flexion, and extension loads. *Journal of orthopaedic research : official publication of the Orthopaedic Research Society* 7, 122-131.

Shah, J.S., Hampson, W.G., Jayson, M.I., 1978. The distribution of surface strain in the cadaveric lumbar spine. *The Journal of bone and joint surgery. British volume* 60-b, 246-251.

Shan, Z., Wade, K.R., Schollum, M.L., Robertson, P.A., Thambyah, A., Broom, N.D., 2017. A more realistic disc herniation model incorporating compression, flexion and facet-constrained shear: a mechanical and microstructural analysis. Part II: high rate or 'surprise' loading. *European spine journal : official publication of the European Spine Society, the European Spinal Deformity Society, and the European Section of the Cervical Spine Research Society* 26, 2629-2641.

Shirazi-Adl, A., 1989. Strain in fibers of a lumbar disc: Analysis of the role of lifting in producing disc prolapse. *Spine* 14, 96-103.

Shiri, R., Lallukka, T., Karppinen, J., Viikari-Juntura, E., 2014. Obesity as a risk factor for sciatica: a meta-analysis. *American journal of epidemiology* 179, 929-937.

Showalter, B.L., DeLucca, J.F., Peloquin, J.M., Cortes, D.H., Yoder, J.H., Jacobs, N.T., Wright, A.C., Gee, J.C., Vresilovic, E.J., Elliott, D.M., 2016. Novel human intervertebral disc strain template to quantify regional three-dimensional strains in a population and compare to internal strains predicted by a finite element model. *Journal of orthopaedic research : official publication of the Orthopaedic Research Society* 34, 1264-1273.

Showalter, B.L., Malhotra, N.R., Vresilovic, E.J., Elliott, D.M., 2014. Nucleotomy reduces the effects of cyclic compressive loading with unloaded recovery on human intervertebral discs. *Journal of biomechanics* 47, 2633-2640.

Siddiq, M., Rahim, M.A., Khan, M., Shikder, A., 2019. Lumbar Ligament Sprain-degeneration and Prolapsed Lumbar Intervertebral Disc: A Frequent Missed Combination. *Cureus* 11.

Stokes, I.A., Frymoyer, J.W., 1987. Segmental motion and instability. *Spine* 12, 688-691.

Stokes, I.A., Gardner-Morse, M., Churchill, D., Laible, J.P., 2002. Measurement of a spinal motion segment stiffness matrix. *Journal of biomechanics* 35, 517-521.

Tanaka, N., An, H.S., Lim, T.H., Fujiwara, A., Jeon, C.H., Haughton, V.M., 2001. The relationship between disc degeneration and flexibility of the lumbar spine. *The spine journal : official journal of the North American Spine Society* 1, 47-56.

Tavakoli, J., Amin, D.B., Freeman, B.J.C., Costi, J.J., 2018. The Biomechanics of the Inter-Lamellar Matrix and the Lamellae During Progression to Lumbar Disc Herniation: Which is the Weakest Structure? *Annals of biomedical engineering* 46, 1280-1291.

Thompson, R.E., Barker, T.M., Pearcy, M.J., 2003. Defining the Neutral Zone of sheep intervertebral joints during dynamic motions: an in vitro study. *Clinical biomechanics (Bristol, Avon)* 18, 89-98.

Thompson, R.E., Pearcy, M.J., Downing, K.J., Manthey, B.A., Parkinson, I.H., Fazzalari, N.L., 2000. Disc lesions and the mechanics of the intervertebral joint complex. *Spine* 25, 3026-3035.

Tsantrizos, A., Ito, K., Aebi, M., Steffen, T., 2005. Internal strains in healthy and degenerated lumbar intervertebral discs. *Spine* 30, 2129-2137.

van Heeswijk, V.M., Thambyah, A., Robertson, P.A., Broom, N.D., 2017. Posterolateral Disc Prolapse in Flexion Initiated by Lateral Inner Annular Failure: An Investigation of the Herniation Pathway. *Spine* 42, 1604-1613.

Veres, S.P., Robertson, P.A., Broom, N.D., 2010. The influence of torsion on disc herniation when combined with flexion. *European spine journal : official publication of the European Spine Society, the European Spinal Deformity Society, and the European Section of the Cervical Spine Research Society* 19, 1468-1478.

- Vernon-Roberts, B., Fazzalari, N.L., Manthey, B.A., 1997. Pathogenesis of tears of the annulus investigated by multiple-level transaxial analysis of the T12-L1 disc. *Spine* 22, 2641-2646.
- Vernon-Roberts, B., Moore, R.J., Fraser, R.D., 2007. The natural history of age-related disc degeneration: the pathology and sequelae of tears. *Spine* 32, 2797-2804.
- Videman, T., Nurminen, M., Troup, J.D., 1990. 1990 Volvo Award in clinical sciences. Lumbar spinal pathology in cadaveric material in relation to history of back pain, occupation, and physical loading. *Spine* 15, 728-740.
- Virgin, W.J., 1951. Experimental investigations into the physical properties of the intervertebral disc. *The Journal of bone and joint surgery. British volume* 33-b, 607-611.
- Wade, K.R., Robertson, P.A., Thambyah, A., Broom, N.D., 2014. How healthy discs herniate: a biomechanical and microstructural study investigating the combined effects of compression rate and flexion. *Spine* 39, 1018-1028.
- Wade, K.R., Robertson, P.A., Thambyah, A., Broom, N.D., 2015. Surprise loading in flexion increases the risk of disc herniation due to annulus-endplate junction failure: A mechanical and microstructural investigation. *Spine* 40, 891-901.
- Wade, K.R., Schollum, M.L., Robertson, P.A., Thambyah, A., Broom, N.D., 2017. A more realistic disc herniation model incorporating compression, flexion and facet-constrained shear: a mechanical and microstructural analysis. Part I: Low rate loading. *European spine journal : official publication of the European Spine Society, the European Spinal Deformity Society, and the European Section of the Cervical Spine Research Society* 26, 2616-2628.
- Wang, Y., Videman, T., Battie, M.C., 2012. ISSLS prize winner: Lumbar vertebral endplate lesions: associations with disc degeneration and back pain history. *Spine* 37, 1490-1496.
- Weber, H., 1994. The natural history of disc herniation and the influence of intervention. *Spine* 19, 2234-2238; discussion 2233.
- Wilder, D.G., Pope, M.H., Frymoyer, J.W., 1988. The biomechanics of lumbar disc herniation and the effect of overload and instability. *Journal of spinal disorders* 1, 16-32.
- Wilke, H., Neef, P., Hinz, B., Seidel, H., Claes, L., 2001. Intradiscal pressure together with anthropometric data--a data set for the validation of models. *Clinical biomechanics (Bristol, Avon)* 16 Suppl 1, S111-126.
- Wilke, H.J., Claes, L., Schmitt, H., Wolf, S., 1994. A universal spine tester for in vitro experiments with muscle force simulation. *European spine journal : official publication of the European Spine Society, the European Spinal Deformity Society, and the European Section of the Cervical Spine Research Society* 3, 91-97.

Wilke, H.J., Kienle, A., Maile, S., Rasche, V., Berger-Roscher, N., 2016. A new dynamic six degrees of freedom disc-loading simulator allows to provoke disc damage and herniation. *European spine journal : official publication of the European Spine Society, the European Spinal Deformity Society, and the European Section of the Cervical Spine Research Society*.

Wilke, H.J., Neef, P., Caimi, M., Hoogland, T., Claes, L.E., 1999. New in vivo measurements of pressures in the intervertebral disc in daily life. *Spine* 24, 755-762.

Yoder, J.H., Peloquin, J.M., Song, G., Tustison, N.J., Moon, S.M., Wright, A.C., Vresilovic, E.J., Gee, J.C., Elliott, D.M., 2014. Internal three-dimensional strains in human intervertebral discs under axial compression quantified noninvasively by magnetic resonance imaging and image registration. *Journal of biomechanical engineering* 136.

Yu, J., Fairbank, J.C.T., Roberts, S., Urban, J.P.G., 2005. The elastic fiber network of the annulus fibrosus of the normal and scoliotic human intervertebral disc. *Spine* 30, 1815-1820.

Zirbel, S.A., Stolworthy, D.K., Howell, L.L., Bowden, A.E., 2013. Intervertebral disc degeneration alters lumbar spine segmental stiffness in all modes of loading under a compressive follower load. *The spine journal : official journal of the North American Spine Society* 13, 1134-1147.



# Appendices

## Appendix A

### A.1 Error between detector positions

#### A.1.1 Methods

For strain measurement, a wire grid technique was used where x-rays from the left and right side of the specimen (within the hexapod) were taken. The x-ray head was at  $56^\circ$  from vertical, therefore, the x-ray detector would be at  $56^\circ$  from horizontal. However, due to space restrictions in the materials testing device (hexapod), the detector could only sit upright. To determine the error between the two positions of the detector, benchtop validation experiments were completed.

The entire setup within the hexapod (**Chapter 3**) was replicated on a bench top (**Figure A-1**). A mock-up specimen with a wire grid, disc periphery markers, and endplate markers (**Figure A-2**) was placed within the calibration cage with twelve calibration beads that determined the x-, y- and z-axes. The wire grid was at approximately the same z-position as it would be within a human FSU. Once the setup was finished and using the same protocol as described in **Chapter 3**, two x-ray images (left and right) of the mock-up specimen were taken with the detector at  $56^\circ$  and two x-ray images were taken with the detector upright (**Figure A-1**, **Figure A-3** and **Figure A-4**).

The x, y, and z coordinates of the wire grid intersection points, disc periphery markers, and endplate markers were calculated from digitising the x-ray images when the detector was at  $56^\circ$ , and from digitizing the images when the detector was upright. The x-rays were digitised five times for assessment of repeatability using intraclass correlation coefficient (see Chapter 3 for repeatability coefficient) and the RMS error was calculated between the two positions of the detector (**Table A-1 – Table A-3**). The digitised coordinates of intersections, disc periphery and endplate makers from the detector at  $56^\circ$  and upright are plotted on the figures below (**Figure A-5**, **Figure A-6** and **Figure A-7**). The RMS error reported in **Chapter 3** is the largest error of the x-, y- and z- coordinates found within the five repeats.

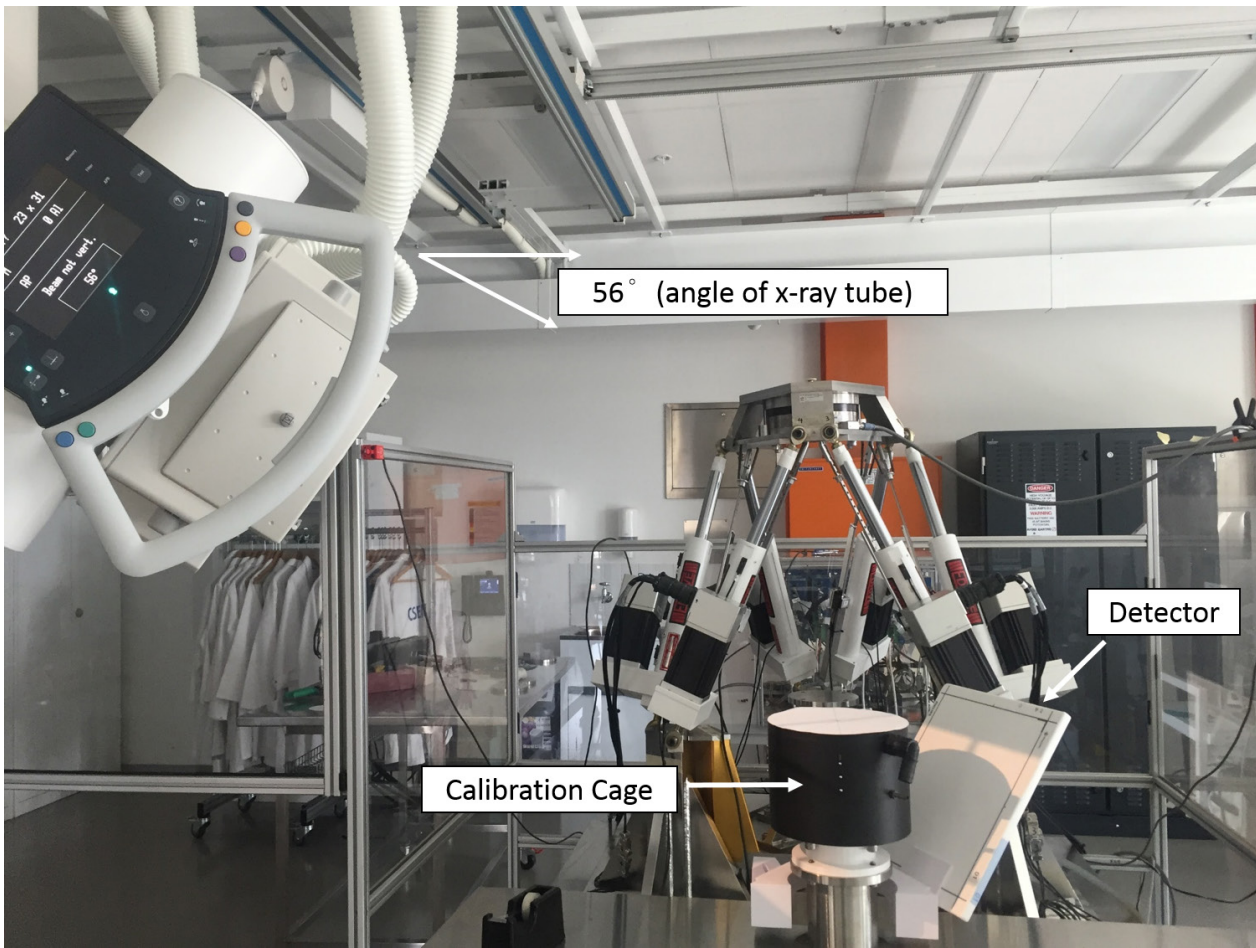


**Figure A-1** Image of the setup for determining the error between positioning the detector at  $56^\circ$  and upright. In this figure, the detector is placed at  $56^\circ$ . After taking the images, the detector was positioned upright (vertical against the calibration cage)

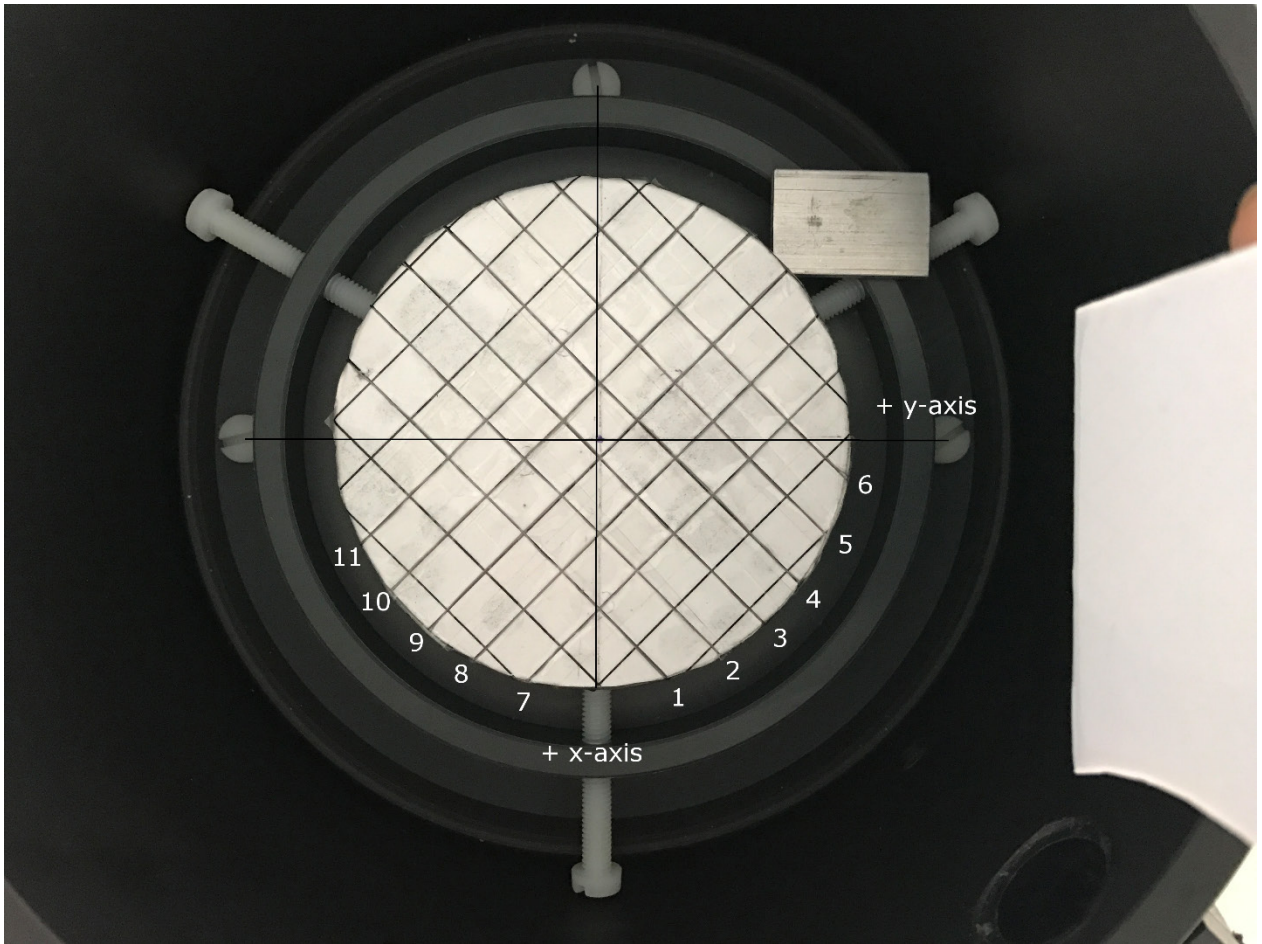


**Figure A-2** Axial image of the mock-up specimen with wire grid (5 by 6). The wires are represented by numbers, which were used to identify the intersections (i.e. 1 x 7 is the intersection of wires 1 and 7). The mock-up specimen is positioned inside the calibration cage in this photo

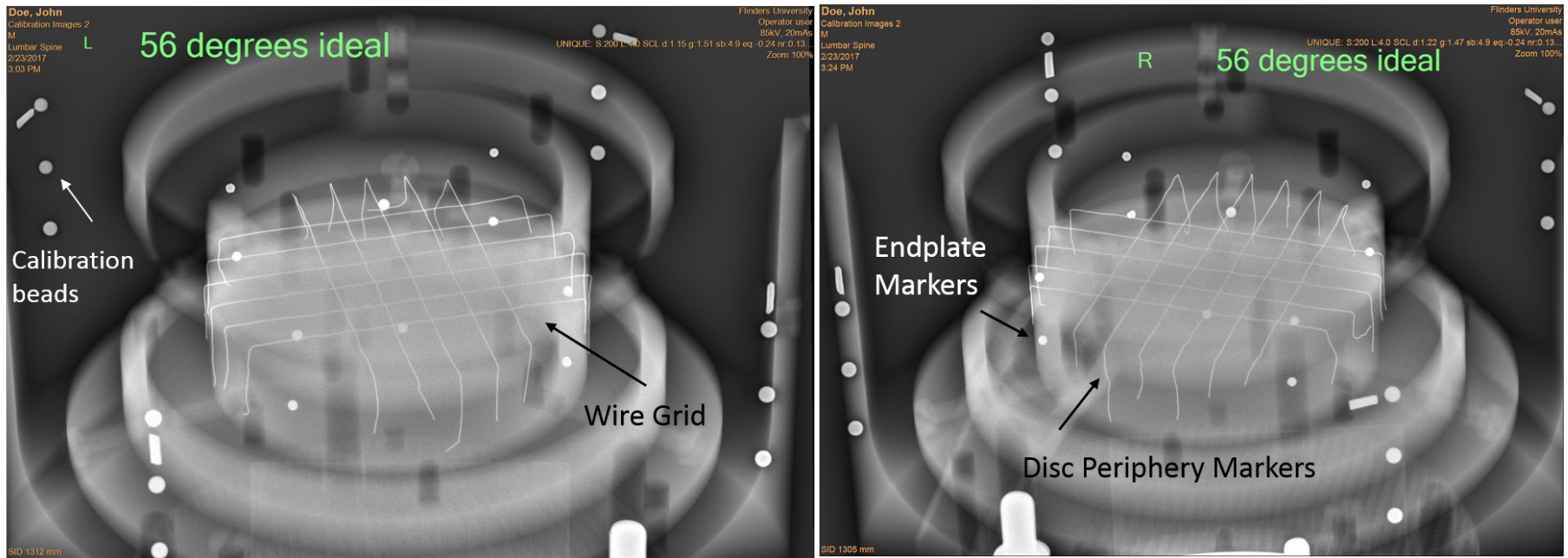


**Figure A-3** Left (left image) and right (right image) x-ray images when detector was positioned at 56 degrees. The calibration beads, wire grid, disc periphery, and endplate markers are annotated on the figure

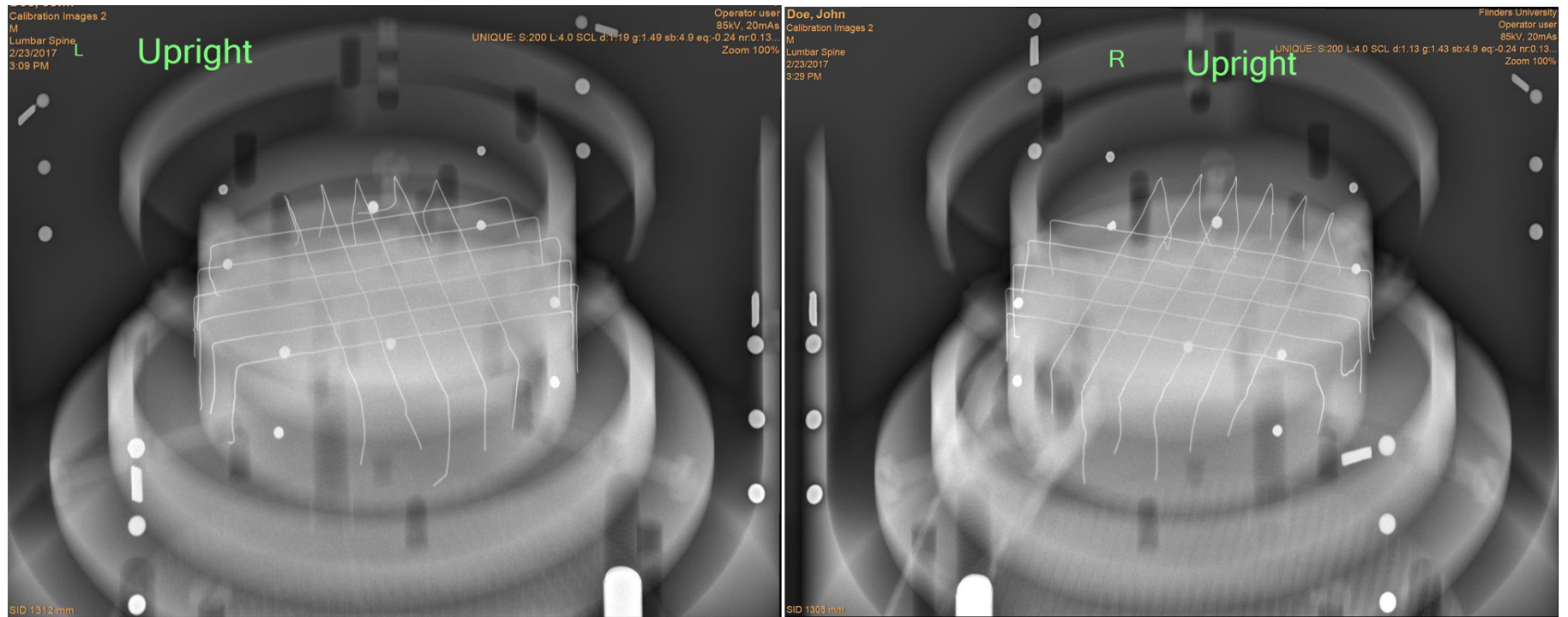


**Figure A-4** Left (left image) and right (right image) x-ray images when detector was positioned upright. A visual understanding of the different markers is outlined in **Figure A-3**

## A.1.2 Results

### A.1.2.1 Wire Grid Intersections

**Table A-1** Mean (95% CI) x-, y- and z-coordinate values of the intersections calculated from the five repeats of the digitised x-rays where the detector was positioned at 56° and upright. Wire grid intersections are based on **Figure A-2**, where 1 x 7 represents the intersection of wires 1 and 7

Wire Grid Intersections	x coordinate				y coordinate				z coordinate			
	56° Detector		Upright Detector		56° Detector		Upright Detector		56° Detector		Upright Detector	
	mean	95% CI	mean	95% CI	mean	95% CI	mean	95% CI	mean	95% CI	mean	95% CI
1 x 7	33.38	0.08	33.3	0.05	0.9	0.06	0.97	0.1	1.08	0.05	1.13	0.1
1 x 8	26.38	0.04	26.29	0.06	-5.96	0.06	-6.05	0.03	1.18	0.05	1.14	0.01
1 x 9	19.22	0.05	19.25	0.15	-13.12	0.05	-13.13	0.15	1.16	0.03	1.21	0.02
1 x 10	12.53	0.07	12.54	0.1	-19.78	0.06	-19.81	0.07	1.21	0.04	1.19	0.08
1 x 11	5.71	0.1	5.71	0.05	-26.48	0.04	-26.5	0.07	1.22	0.03	1.18	0.06
2 x 7	26.13	0.06	26.11	0.05	7.8	0.09	7.76	0.04	1.12	0.05	1.11	0.04
2 x 8	19.39	0.03	19.36	0.02	0.88	0.05	0.9	0.05	1.18	0.01	1.13	0.02
2 x 9	12.3	0.05	12.35	0.06	-6.22	0.06	-6.16	0.06	1.23	0.02	1.17	0.06
2 x 10	5.84	0.07	5.89	0.01	-13.08	0.04	-13.13	0.02	1.25	0.03	1.22	0.01
2 x 11	-1.17	0.06	-1.18	0.06	-20.02	0.03	-20.07	0.02	1.23	0.03	1.15	0.06

Wire Grid Intersections	x coordinate				y coordinate				z coordinate			
	56° Detector		Upright Detector		56° Detector		Upright Detector		56° Detector		Upright Detector	
	mean	95% CI	mean	95% CI	mean	95% CI	mean	95% CI	mean	95% CI	mean	95% CI
3 x 7	19.41	0.07	19.4	0.12	14.58	0.07	14.52	0.05	1.24	0.03	1.16	0.02
3 x 8	12.49	0.08	12.52	0.02	7.53	0.04	7.56	0.12	1.14	0.02	1.1	0.03
3 x 9	5.23	0.05	5.31	0.09	0.98	0.06	0.97	0.01	1.21	0.04	1.2	0.05
3 x 10	-1.35	0.08	-1.31	0.06	-5.56	0.12	-5.62	0.11	1.19	0.03	1.11	0.05
3 x 11	-8.43	0.05	-8.39	0.03	-12.91	0.01	-12.88	0.05	1.24	0.05	1.19	0.01
4 x 7	12.2	0.05	12.04	0.06	22.14	0.07	22.2	0.08	1.09	0.05	1.11	0.01
4 x 8	5.21	0.06	5.21	0.09	15.06	0.03	15.01	0.01	1.18	0.06	1.1	0.07
4 x 9	-1.81	0.06	-1.84	0.02	7.86	0.02	7.85	0.01	1.15	0.03	1.14	0.03
4 x 10	-8.02	0.05	-8.08	0.14	0.8	0.02	0.73	0.08	1.21	0.04	1.13	0.1
4 x 11	-15.26	0.08	-15.23	0.15	-6.03	0.01	-5.98	0.15	1.21	0.05	1.23	0.06
5 x 7	5.76	0.04	5.78	0.05	28.6	0.04	28.53	0.13	1.18	0.04	1.08	0.01
5 x 8	-1.28	0.05	-1.25	0.22	21.94	0.05	21.9	0.12	1.3	0.06	1.24	0.03
5 x 9	-8.56	0.04	-8.57	0.01	14.62	0.07	14.55	0.07	1.23	0.05	1.22	0.03
5 x 10	-15.61	0.06	-15.66	0.06	7.99	0.03	8.01	0.03	1.19	0.03	1.2	0.05

Wire Grid Intersections	x coordinate				y coordinate				z coordinate			
	56° Detector		Upright Detector		56° Detector		Upright Detector		56° Detector		Upright Detector	
	mean	95% CI	mean	95% CI	mean	95% CI	mean	95% CI	mean	95% CI	mean	95% CI
5 x 11	-22.28	0.03	-22.27	0.01	0.99	0.03	1.04	0.06	1.35	0.02	1.28	0.03
6 x 7	-1.42	0.01	-1.52	0.03	35.49	0.03	35.49	0.07	1.18	0.02	1.11	0.06
6 x 8	-8.28	0.07	-8.29	0.08	28.86	0.04	28.87	0.11	1.2	0.03	1.12	0.01
6 x 9	-15.61	0.06	-15.67	0.03	21.66	0.05	21.71	0.01	1.21	0.05	1.13	0.01
6 x 10	-22.08	0.06	-22.12	0.05	14.54	0.02	14.58	0.06	1.28	0.02	1.22	0.02
6 x 11	-29.01	0.05	-28.98	0.07	8.23	0.04	8.22	0.07	1.3	0.04	1.25	0.02
1 x 7	33.38	0.08	33.3	0.05	0.9	0.06	0.97	0.1	1.08	0.05	1.13	0.1
1 x 8	26.38	0.04	26.29	0.06	-5.96	0.06	-6.05	0.03	1.18	0.05	1.14	0.01

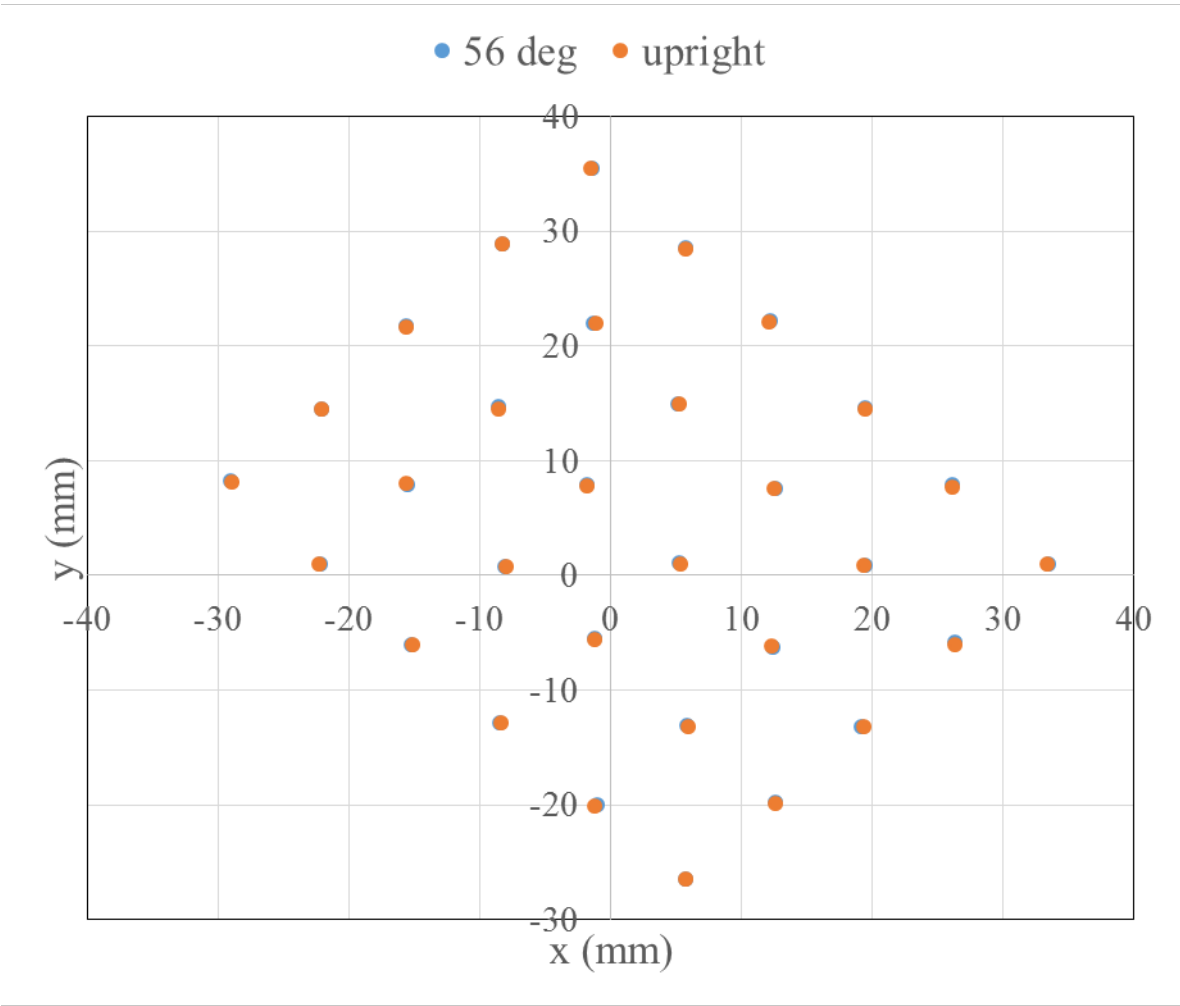


**Figure A-5** Digitised coordinates (x and y) of the wire grid intersections calculated from the detector positioned at 56° and upright

### A.1.2.2 Disc Periphery Markers

**Table A-2** The mean (95% CI) x-, y- and z-coordinate values for the disc periphery makers calculated from five repeats of the digitised x-rays where the detector was positioned at 56° and upright

Disc Periphery Marker	x coordinate				y coordinate				z coordinate			
	56° Detector		Upright Detector		56° Detector		Upright Detector		56° Detector		Upright Detector	
	mean	95% CI	mean	95% CI	mean	95% CI	mean	95% CI	mean	95% CI	mean	95% CI
1	21.40	0.05	21.25	0.71	-42.20	0.14	-42.46	2.62	0.93	0.15	1.34	1.35
2	30.08	0.06	30.12	0.06	-37.10	0.15	-37.60	1.50	0.95	0.12	0.67	0.74
3	37.31	0.11	37.40	0.01	-30.00	0.09	-29.91	0.09	0.74	0.10	0.86	0.07
4	42.71	0.20	42.83	0.07	-21.85	0.23	-22.04	0.37	0.79	0.31	0.57	0.34
5	46.49	0.11	46.50	0.05	-11.94	0.14	-11.73	0.27	1.42	0.13	1.41	0.08
6	46.22	0.09	46.28	0.08	13.44	0.11	13.43	0.20	0.69	0.15	0.59	0.03
7	42.06	0.08	41.96	0.07	23.67	0.21	23.44	0.15	0.77	0.26	0.81	0.08
8	35.86	0.05	35.87	0.01	31.39	0.05	31.30	0.04	0.75	0.10	0.76	0.07
9	28.67	0.31	28.22	0.44	38.50	0.44	37.79	0.33	0.12	0.53	0.98	0.48
10	19.72	0.09	19.36	0.59	42.96	0.14	42.57	0.37	0.80	0.15	1.30	0.79
11	8.63	0.14	8.59	0.25	46.76	0.05	46.40	0.33	0.87	0.08	1.24	0.69
12	-10.91	0.03	-11.06	0.01	44.88	0.09	45.00	0.21	0.65	0.13	0.51	0.07
13	-20.95	0.06	-20.90	0.00	40.83	0.12	40.74	0.14	0.69	0.12	0.76	0.13
14	-28.90	0.03	-28.95	0.09	35.05	0.08	35.32	0.20	0.70	0.14	0.68	0.03
15	-35.47	0.04	-35.37	0.07	28.73	0.16	28.61	0.13	0.63	0.14	0.67	0.09
16	-40.81	0.09	-40.74	0.07	19.29	0.11	19.25	0.01	0.82	0.08	0.97	0.09
17	-44.64	0.07	-44.64	0.07	-8.12	0.05	-8.15	0.15	0.60	0.11	0.49	0.05
18	-41.60	0.09	-41.67	0.00	-17.84	0.10	-18.00	0.19	0.78	0.09	0.59	0.07
19	-36.09	0.11	-36.11	0.01	-27.39	0.08	-27.44	0.00	0.79	0.10	0.78	0.00
20	-29.39	0.08	-29.39	0.06	-35.08	0.10	-35.18	0.21	0.76	0.05	0.72	0.00
21	-21.74	0.08	-21.82	0.14	-40.80	0.09	-40.88	0.09	0.76	0.06	0.61	0.03
22	-11.80	0.06	-11.77	0.08	-44.89	0.05	-44.89	0.02	0.67	0.10	0.74	0.10

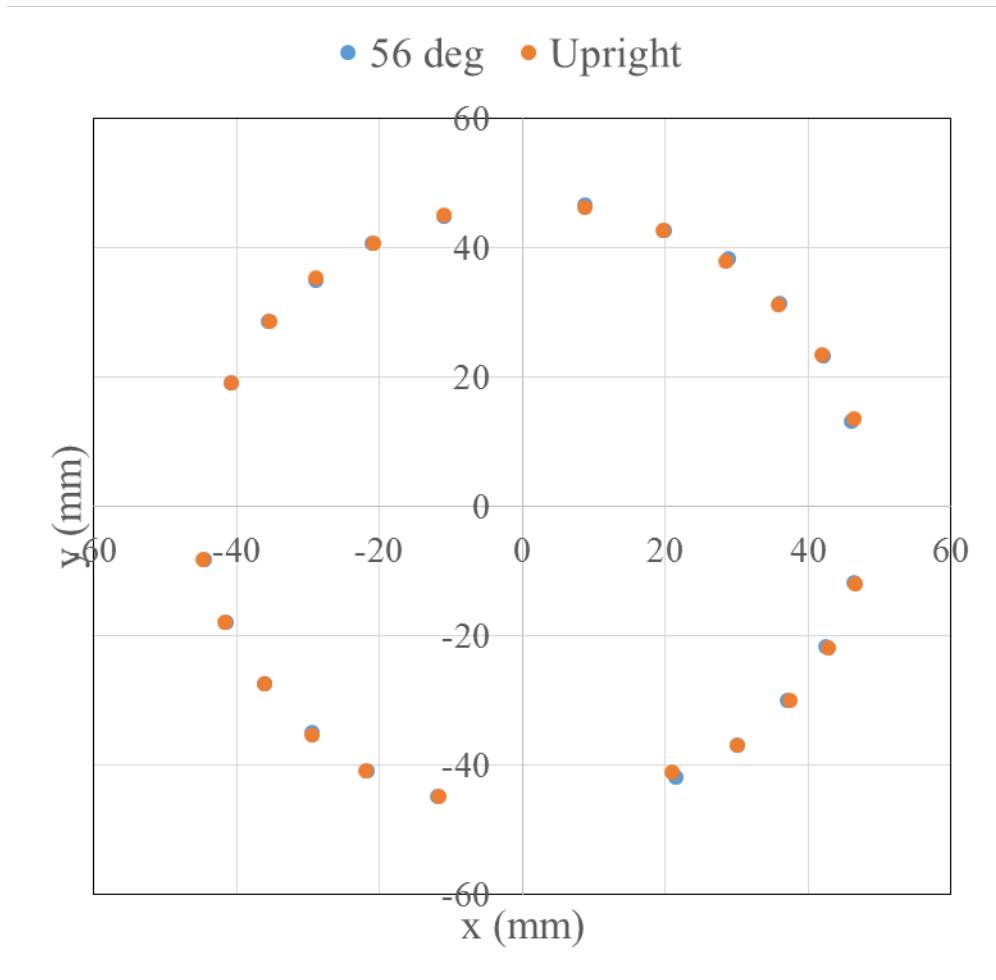


**Figure A-6** Digitised coordinates (x and y) of the disc periphery markers calculated from the detector positioned at 56° and upright

### A.1.2.3 Endplate Markers

**Table A-3** Mean (95% CI) x-, y- and z-coordinate values for the endplate makers calculated from five repeats of the digitised x-rays where the detector was positioned at 56° and upright

Endplate Marker	x coordinate				y coordinate				z coordinate			
	56° Detector		Upright Detector		56° Detector		Upright Detector		56° Detector		Upright Detector	
	mean	95% CI	mean	95% CI	mean	95% CI	mean	95% CI	mean	95% CI	mean	95% CI
1	-46.56	0.00	-46.49	0.01	0.19	0.00	0.13	0.01	10.58	0.00	10.54	0.01
2	-37.90	16.42	-46.46	0.09	1.99	1.10	1.68	0.06	-4.21	10.15	-9.51	0.03
3	-12.81	16.38	2.61	0.00	3.64	1.04	-46.38	0.02	11.31	10.13	9.55	0.13
4	2.57	0.03	-4.41	0.01	-46.36	0.03	4.12	0.01	9.58	0.01	16.35	0.01
5	1.47	0.00	1.51	0.01	-47.71	0.02	-47.57	0.00	-9.41	0.03	-9.46	0.03
6	0.64	0.03	0.71	0.06	47.98	0.03	47.96	0.12	-9.40	0.01	-9.47	0.07
7	2.37	0.00	2.41	0.06	1.00	0.03	0.94	0.13	-14.25	0.03	-14.30	0.04
8	49.56	0.46	49.22	0.15	0.14	0.46	0.39	0.10	10.84	0.80	11.06	0.04
9	49.28	0.09	0.20	0.01	-0.13	0.10	49.39	0.01	-8.05	0.07	9.32	0.00
10	0.12	0.15	49.23	0.24	49.38	0.07	-0.21	0.19	9.69	0.70	-8.10	0.21

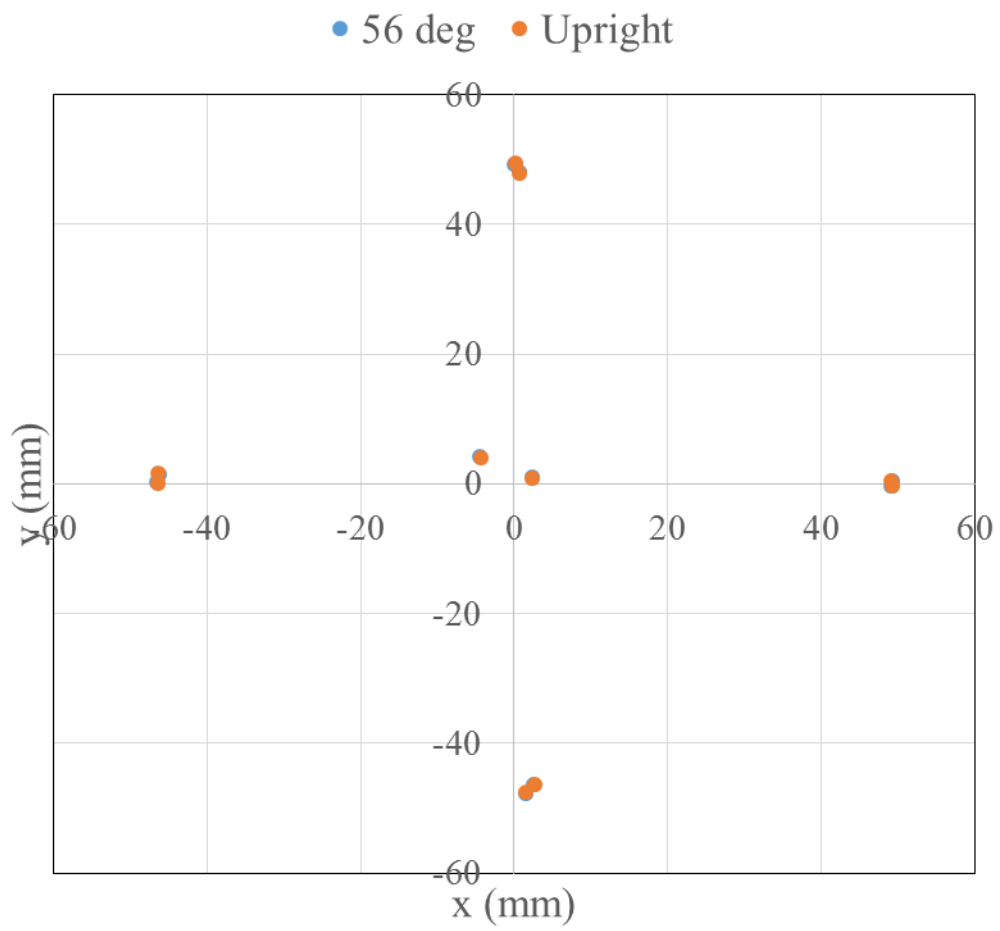


**Figure A-7** Digitised coordinates (x and y) of the endplate markers calculated from the detector positioned at 56° and upright



## Appendix B

### B.1 Validation of the strain measurement technique

This appendix presents 6DOF mechanical properties before and after wire grid insertion for both simulated safe and unsafe repetitive lifting groups. The control group did not undergo wire grid insertion however, mechanical properties were measured at the same time points as the experimental group (see **Figure 3-1**).

**Table B-1** The p-values showing the interactions between group (control and experimental) and intervention (before and after wire grid insertion) for each loading direction. There were no significant differences before and after wire gird insertion in any direction for both stiffness and phase angle

<b>Loading Direction</b>	<b>Mechanical Parameter</b>	<b>Safe lifting (p-value)</b>	<b>Unsafe lifting (p-value)</b>
Right Lateral	Stiffness	0.968	0.945
Shear	Phase Angle	0.646	0.348
Left Lateral	Stiffness	0.39	0.819
Shear	Phase Angle	0.095	0.441
Anterior Shear	Stiffness	0.971	0.898
	Phase Angle	0.319	0.666
Posterior Shear	Stiffness	0.76	0.577
	Phase Angle	0.944	0.973
Compression	Stiffness	0.169	0.307
	Phase Angle	0.569	0.419
Extension	Stiffness	0.545	0.9
	Phase Angle	0.075	0.473
Flexion	Stiffness	0.729	0.374
	Phase Angle	0.756	0.399
Left Axial	Stiffness	0.491	0.517
Rotation	Phase Angle	0.565	0.892
Right Axial	Stiffness	0.869	0.144
Rotation	Phase Angle	0.609	0.506
Right Lateral	Stiffness	0.741	0.427
Bending	Phase Angle	0.823	0.274
Left Lateral	Stiffness	0.414	0.067
Bending	Phase Angle	0.1	0.22

## B.2 Simulated Safe Lifting

### B.2.1 Stiffness

#### B.2.1.1 Shears and Compression

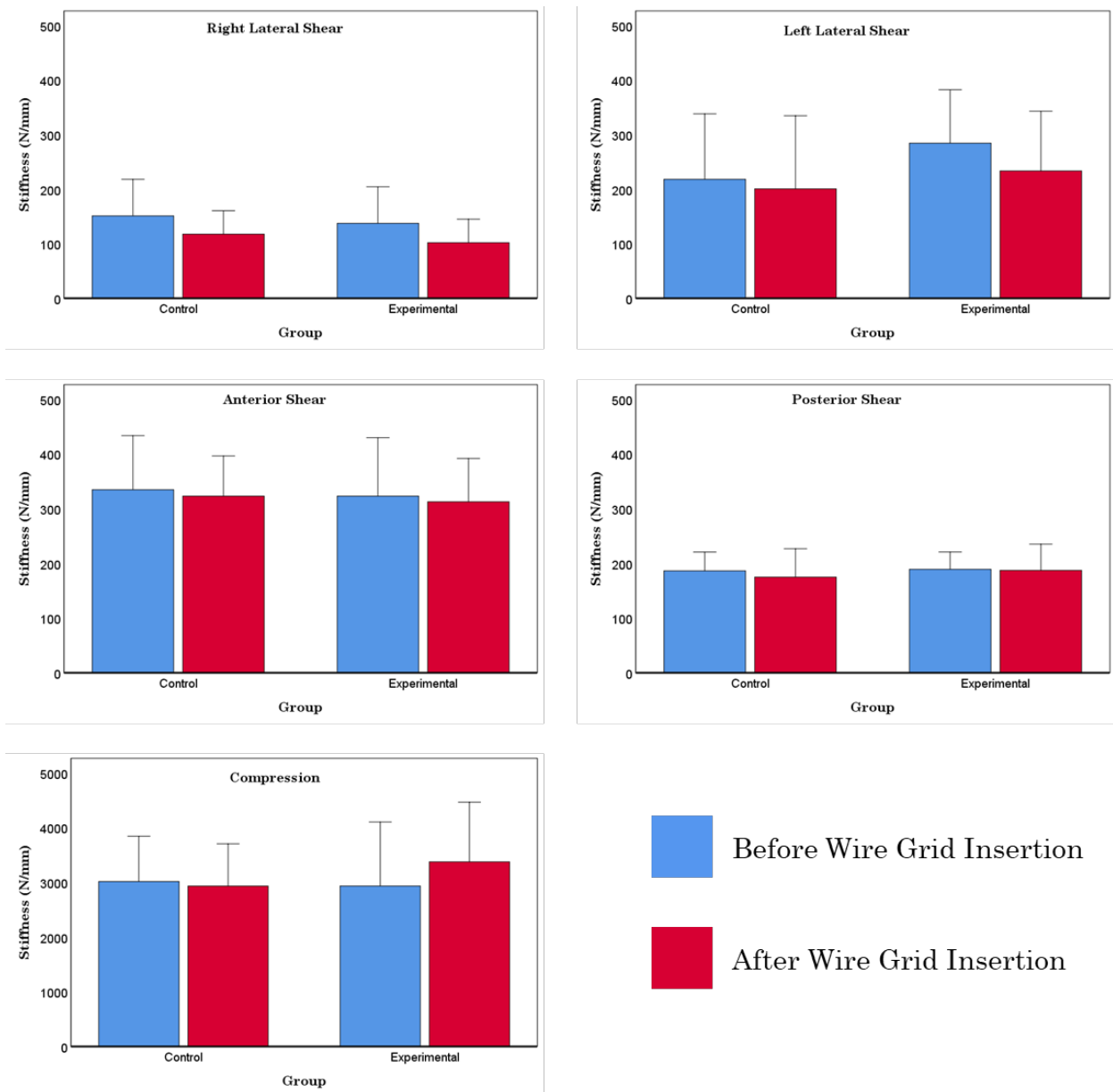


**Figure B-1** Mean (95% CI) stiffness before and after wire grid insertion of specimens in the simulated safe repetitive lifting group for shear and compression directions. The control group did not undergo wire grid insertion, however, mechanical properties were measured at the same time points as the experimental group. \* denotes significance ( $p < 0.05$ ). Top left: right lateral shear, top right: left lateral shear, middle row left: anterior shear, middle row right: posterior shear, bottom left: compression

### B.2.1.2 Bending and Rotation

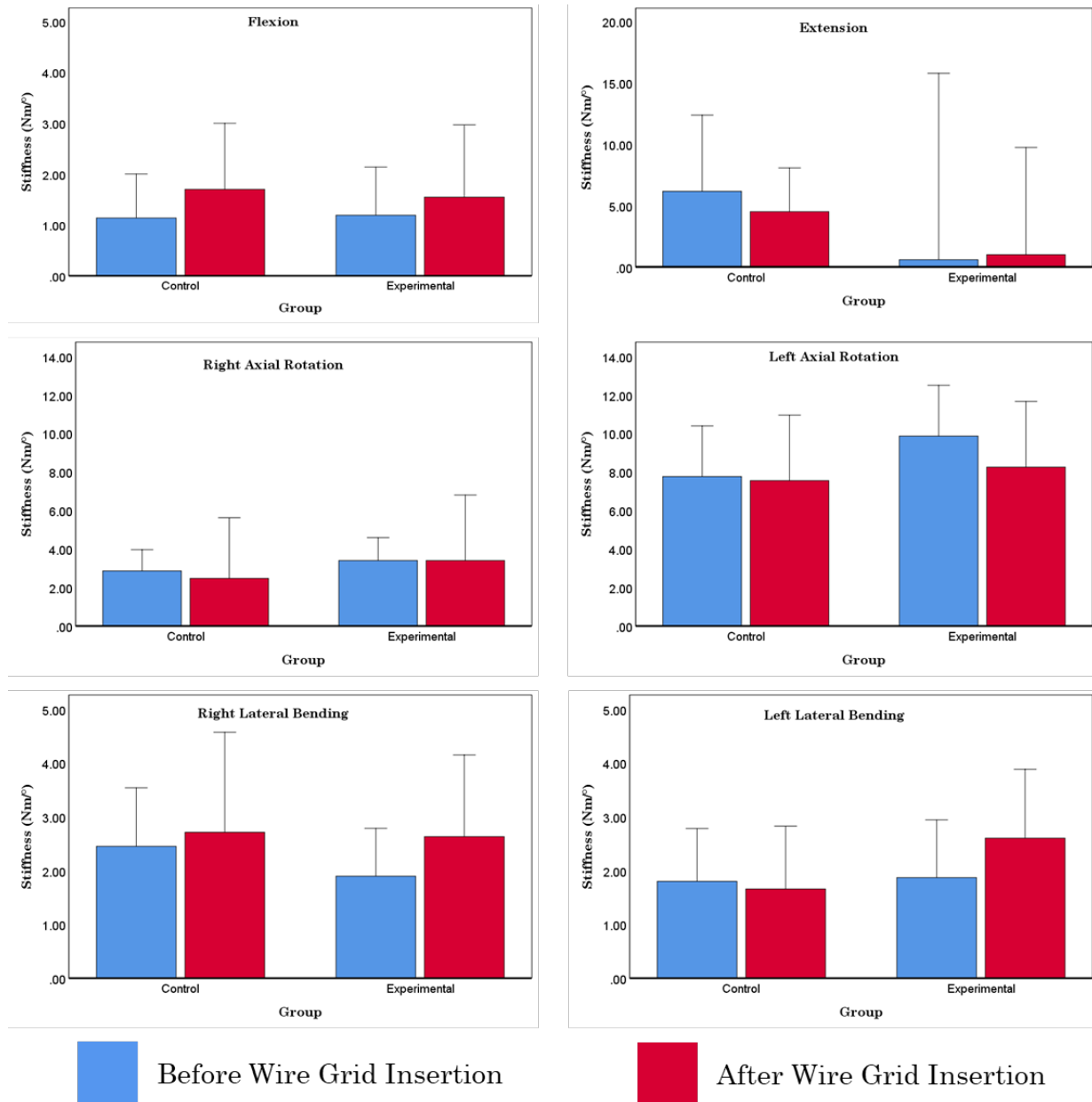


**Figure B-2** Mean (95% CI) stiffness before and after wire grid insertion of the specimen in the simulated safe repetitive lifting group for bending and rotation directions. The control group did not undergo wire grid insertion, however, mechanical properties were measured at the same time points as the experimental group. \* denotes significance ( $p < 0.05$ ). Top left: flexion, top right: extension, middle row left: right axial rotation, middle row right: left axial rotation, bottom left: right lateral bending, bottom right: left lateral bending

## B.2.2 Phase Angle

### B.2.2.1 Shears and Compression

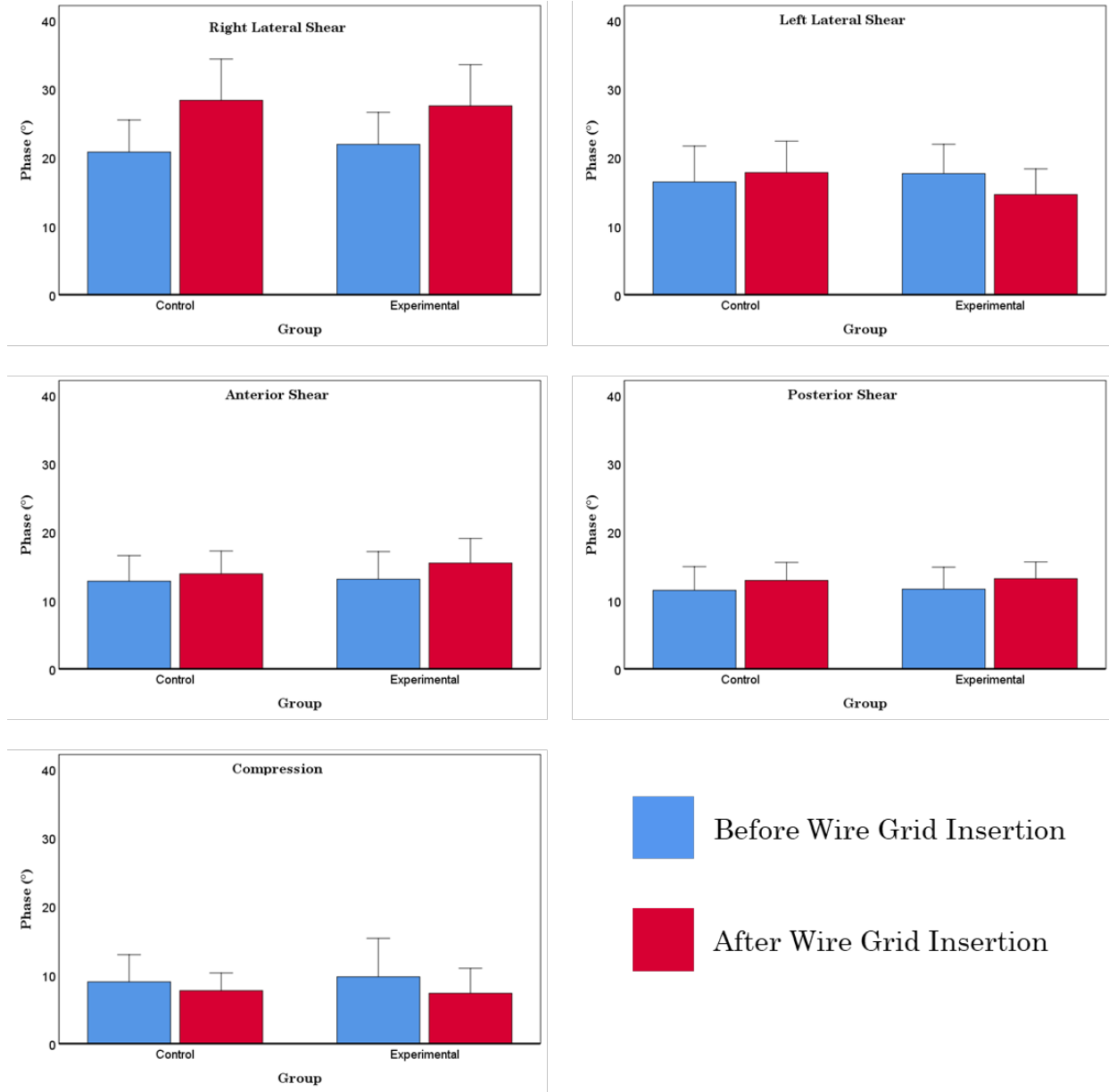


**Figure B-3** Mean (95% CI) phase angle before and after wire grid insertion of the specimen in the simulated safe repetitive lifting group for shear and compression directions. The control group did not undergo wire grid insertion, however, mechanical properties were measured at the same time points as the experimental group. \* denotes significance ( $p < 0.05$ ). Top left: right lateral shear, top right: left lateral shear, middle row left: anterior shear, middle row right: posterior shear, bottom left: compression

### B.2.2.2 Bending and Rotation

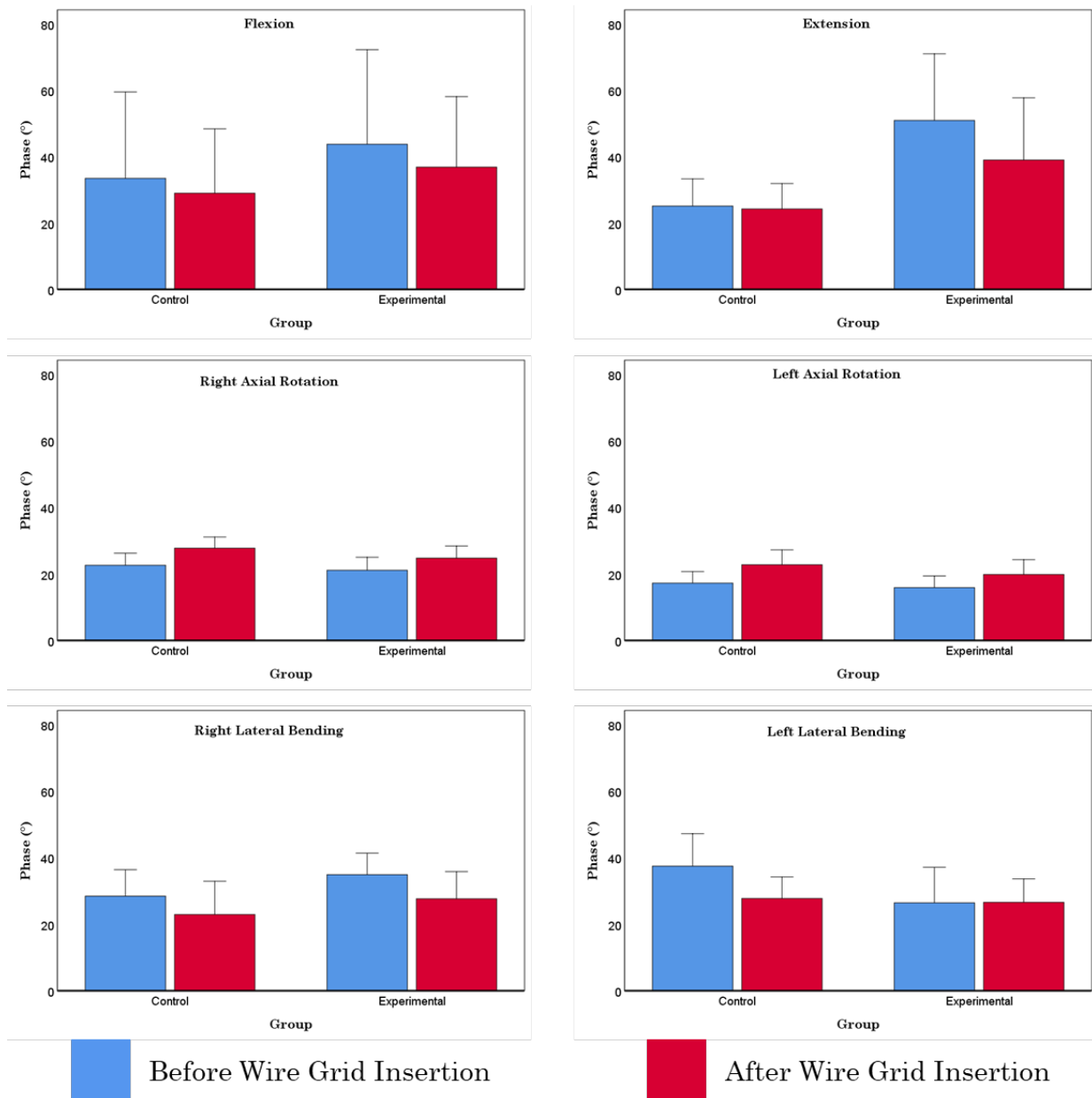


**Figure B-4** Mean (95% CI) phase angle before and after wire grid insertion of the specimen in the simulated safe repetitive lifting group for bending and rotation directions. The control group did not undergo wire grid insertion, however, mechanical properties were measured at the same time points as the experimental group. \* denotes significance ( $p < 0.05$ ). Top left: flexion, top right: extension, middle row left: right axial rotation, middle row right: left axial rotation, bottom left: right lateral bending, bottom right: left lateral bending

## B.3 Simulated Unsafe Lifting

### B.3.1 Stiffness

#### B.3.1.1 Shears and Compression

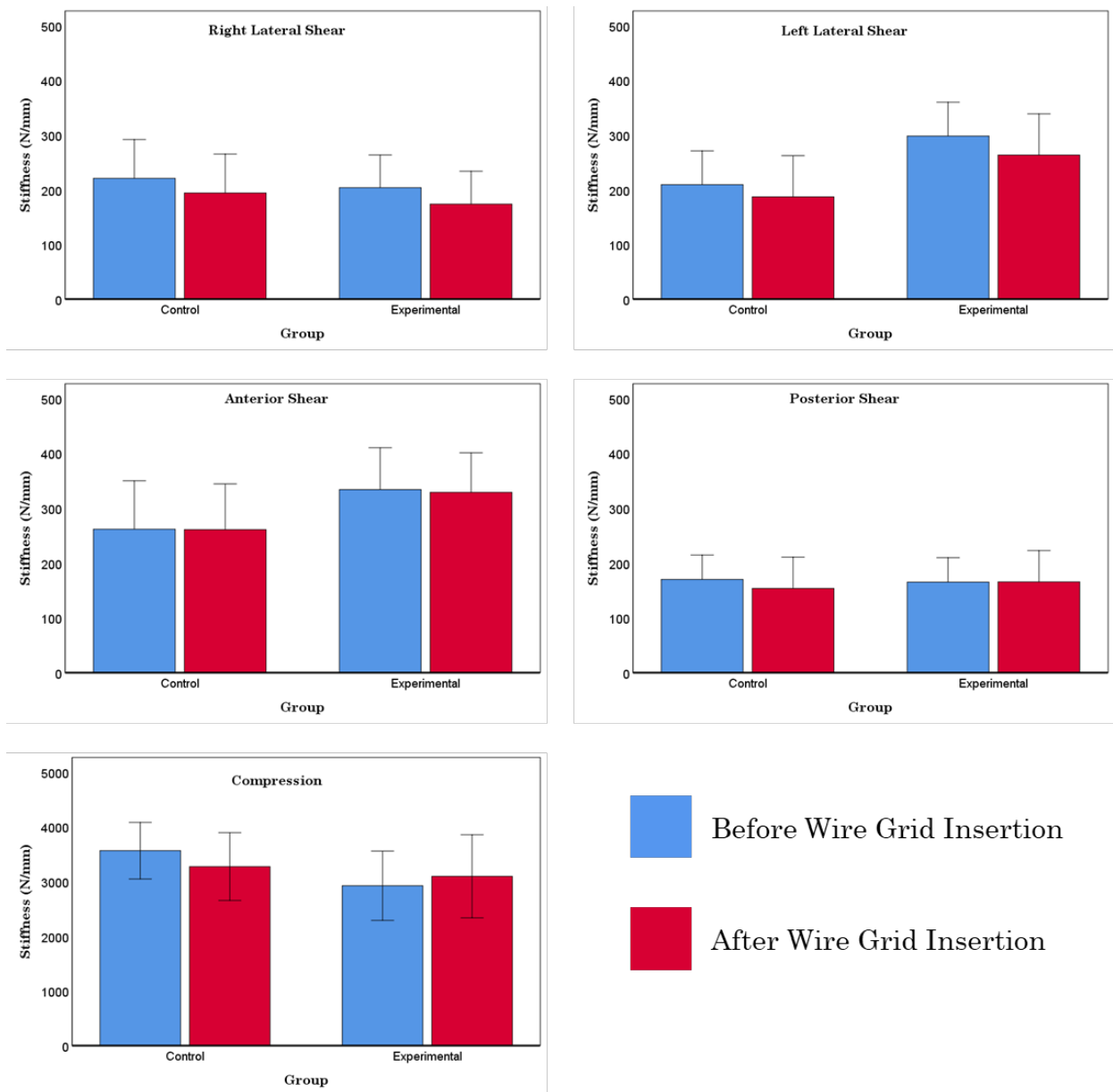


**Figure B-5** Mean (95% CI) stiffness before and after wire grid insertion of the specimen in the simulated unsafe repetitive lifting group for shear and compression directions. The control group did not undergo wire grid insertion, however, mechanical properties were measured at the same time points as the experimental group. \* denotes significance ( $p < 0.05$ ). Top left: right lateral shear, top right: left lateral shear, middle row left: anterior shear, middle row right: posterior shear, bottom left: compression

### B.3.1.2 Bending and Rotation

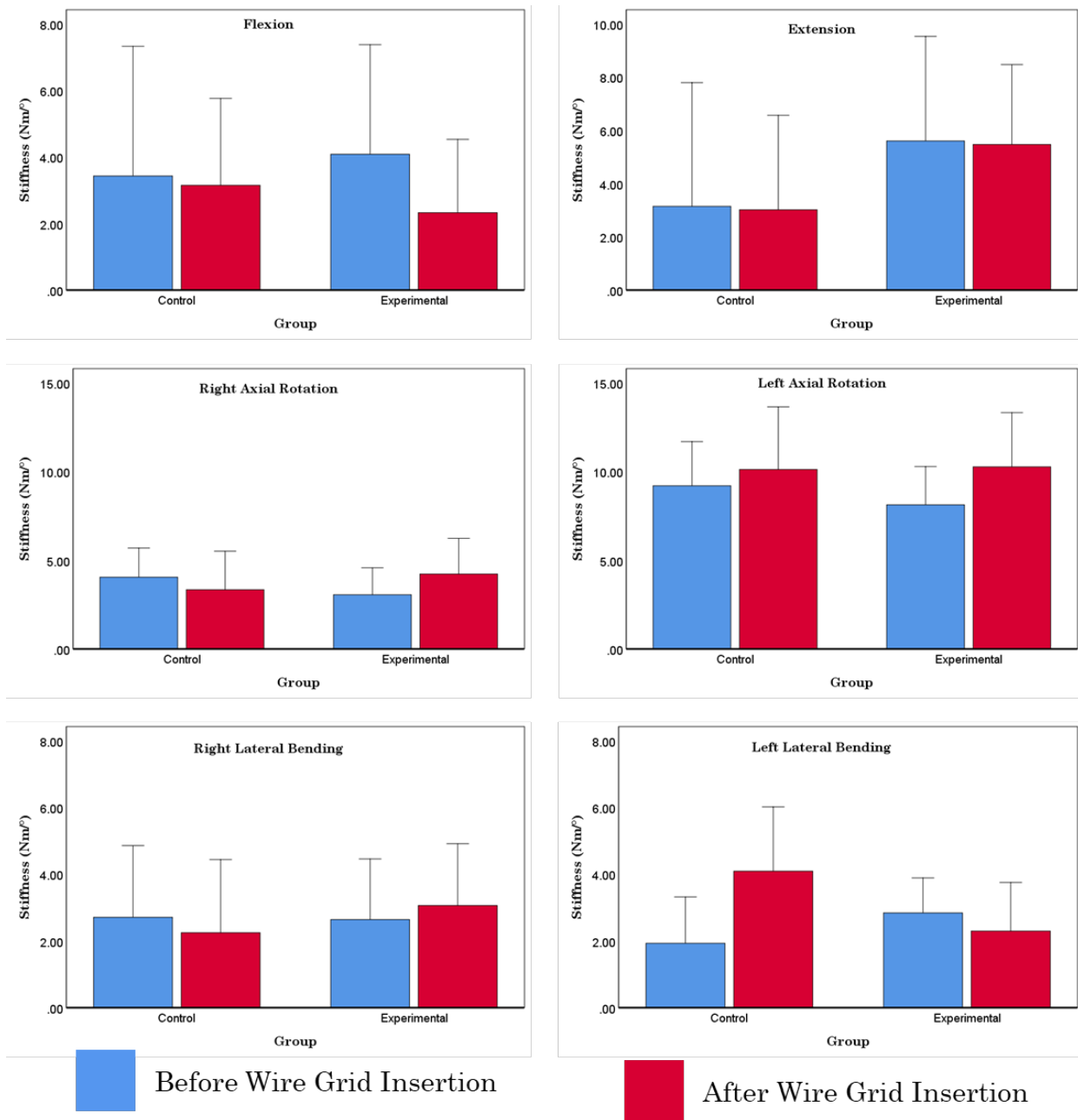


**Figure B-6** Mean (95% CI) stiffness before and after wire grid insertion of the specimen in the simulated unsafe repetitive lifting group for bending and rotation directions. The control group did not undergo wire grid insertion, however, mechanical properties were measured at the same time points as the experimental group. \* denotes significance ( $p < 0.05$ ). Top left: flexion, top right: extension, middle row left: right axial rotation, middle row right: left axial rotation, bottom left: right lateral bending, bottom right: left lateral bending

## B.3.2 Phase Angle

### B.3.2.1 Shears and Compression

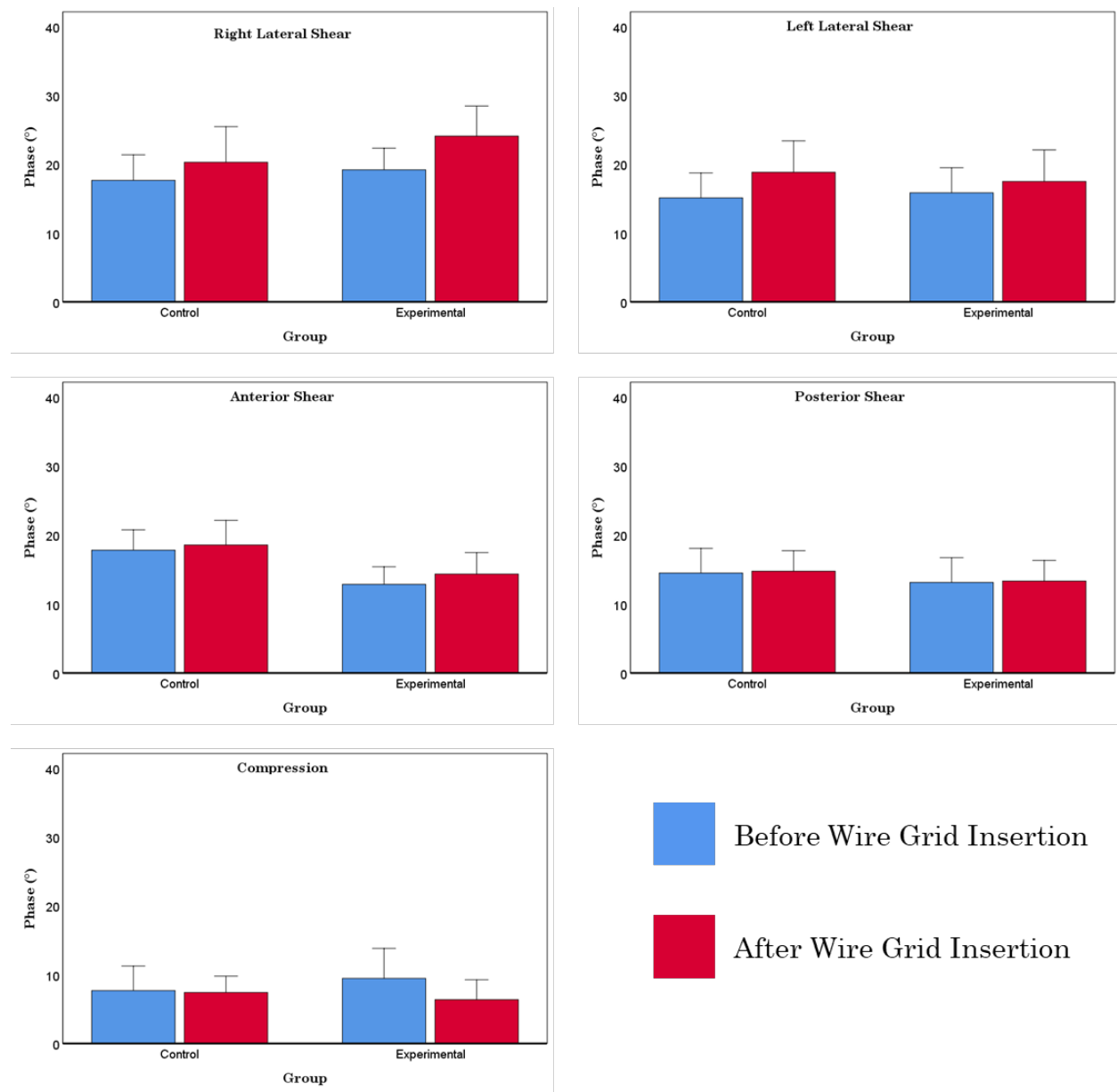


**Figure B-7** Mean (95% CI) phase angle before and after wire grid insertion of the specimen in the simulated unsafe repetitive lifting group for shear and compression directions. The control group did not undergo wire grid insertion, however, mechanical properties were measured at the same time points as the experimental group. \* denotes significance ( $p < 0.05$ ). Top left: right lateral shear, top right: left lateral shear, middle row left: anterior shear, middle row right: posterior shear, bottom left: compression

### B.3.2.2 Bending and Rotation

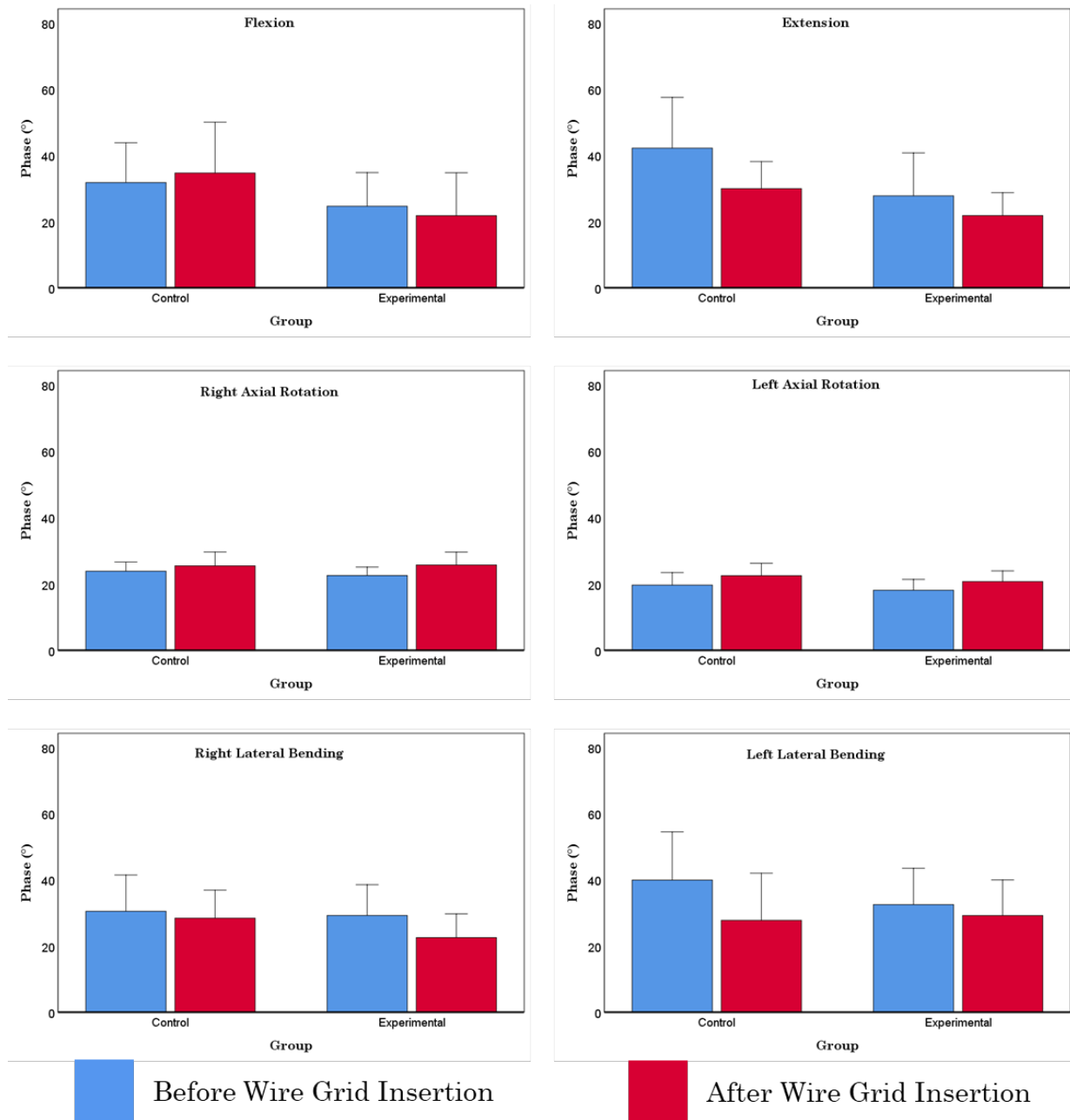


**Figure B-8** Mean (95% CI) phase angle before and after wire grid insertion of the specimen in the simulated unsafe repetitive lifting group for bending and rotation directions. The control group did not undergo wire grid insertion, however, mechanical properties were measured at the same time points as the experimental group. \* denotes significance ( $p < 0.05$ ). Top left: flexion, top right: extension, middle row left: right axial rotation, middle row right: left axial rotation, bottom left: right lateral bending, bottom right: left lateral bending

## Appendix C

### C.1 Principal Strains

This appendix presents mean (95% CI) 3D principal strains at each node (1 – 173) for both simulated safe and unsafe lifting. For safe lifting, average principal strains at each node are presented for the seven cycle time points (cycles 1, 500, 1000, 5000, 10000, 15000, 20000). For unsafe lifting, average principal strains at each node are present for cycle 1 and failure. Figures of the 3D principal strains are also presented to show directions of the strain components. The principal strains presented in this appendix are calculated from all specimens without outliers removed.

## C.1.1 Simulated safe repetitive lifting

### C.1.1.1 Cycle 1

**Table C-1** Mean (95% CI) of 3D principal strains at each node (1 – 173) for simulated safe repetitive lifting at cycle 1

Node	P1		P2		P3	
	Mean	95% CI	Mean	95% CI	Mean	95% CI
1	-0.26	0.16	0.06	0.09	0.36	0.12
2	-0.25	0.13	0.04	0.07	0.35	0.14
3	-0.27	0.14	0.02	0.07	0.38	0.16
4	-0.34	0.14	0.05	0.06	0.41	0.16
5	-0.34	0.15	0.07	0.07	0.44	0.18
6	-0.25	0.10	0.05	0.08	0.44	0.20
7	-0.28	0.16	0.05	0.11	0.45	0.22
8	-0.40	0.24	0.05	0.09	0.52	0.24
9	-0.36	0.14	0.12	0.11	0.48	0.23
10	-0.34	0.12	0.04	0.14	0.47	0.26
11	-0.35	0.17	-0.02	0.14	0.50	0.30
12	-0.28	0.15	-0.05	0.14	0.49	0.34
13	-0.27	0.15	-0.04	0.10	0.48	0.37
14	-0.28	0.16	0.00	0.09	0.48	0.38
15	-0.30	0.18	0.02	0.10	0.47	0.38
16	-0.35	0.22	0.02	0.07	0.27	0.10
17	-0.24	0.10	0.02	0.07	0.27	0.12
18	-0.23	0.07	0.01	0.06	0.26	0.14
19	-0.27	0.10	0.01	0.05	0.29	0.14
20	-0.28	0.10	0.02	0.06	0.32	0.16
21	-0.25	0.12	0.03	0.06	0.35	0.17
22	-0.25	0.16	0.03	0.08	0.36	0.19
23	-0.28	0.18	0.01	0.07	0.35	0.21
24	-0.25	0.09	-0.02	0.05	0.34	0.24
25	-0.27	0.07	-0.03	0.09	0.34	0.27
26	-0.27	0.11	-0.06	0.11	0.35	0.28
27	-0.24	0.11	-0.07	0.09	0.35	0.30
28	-0.21	0.11	-0.07	0.06	0.35	0.31
29	-0.22	0.12	-0.05	0.07	0.38	0.33
30	-0.31	0.16	0.01	0.08	0.48	0.37
31	-0.28	0.19	-0.01	0.07	0.19	0.10
32	-0.22	0.13	-0.03	0.05	0.19	0.10
33	-0.16	0.08	-0.02	0.04	0.20	0.11

Node	P1		P2		P3	
	Mean	95% CI	Mean	95% CI	Mean	95% CI
34	-0.21	0.12	-0.01	0.03	0.23	0.12
35	-0.24	0.14	0.03	0.06	0.24	0.14
36	-0.27	0.15	0.06	0.08	0.27	0.15
37	-0.29	0.18	0.02	0.07	0.29	0.17
38	-0.29	0.16	0.00	0.06	0.27	0.19
39	-0.29	0.12	0.01	0.06	0.25	0.22
40	-0.28	0.11	-0.01	0.07	0.26	0.23
41	-0.27	0.07	-0.03	0.07	0.27	0.24
42	-0.23	0.07	-0.04	0.04	0.27	0.26
43	-0.21	0.05	-0.06	0.03	0.29	0.28
44	-0.22	0.08	-0.05	0.06	0.36	0.30
45	-0.26	0.11	-0.02	0.06	0.43	0.36
46	-0.21	0.10	0.01	0.08	0.16	0.07
47	-0.15	0.07	-0.01	0.04	0.18	0.07
48	-0.16	0.09	0.00	0.05	0.18	0.09
49	-0.19	0.13	0.01	0.06	0.18	0.10
50	-0.20	0.14	0.04	0.07	0.20	0.13
51	-0.22	0.13	0.08	0.14	0.25	0.14
52	-0.24	0.09	0.08	0.15	0.27	0.14
53	-0.23	0.05	0.03	0.05	0.26	0.17
54	-0.23	0.08	0.01	0.05	0.26	0.20
55	-0.24	0.09	-0.01	0.06	0.25	0.21
56	-0.22	0.07	-0.01	0.03	0.23	0.22
57	-0.19	0.07	-0.02	0.03	0.23	0.24
58	-0.20	0.06	-0.05	0.04	0.26	0.27
59	-0.20	0.04	-0.04	0.06	0.34	0.30
60	-0.22	0.08	-0.04	0.05	0.40	0.35
61	-0.25	0.05	0.02	0.07	0.27	0.10
62	-0.13	0.06	0.04	0.05	0.21	0.07
63	-0.16	0.08	0.01	0.06	0.16	0.08
64	-0.21	0.14	0.00	0.07	0.15	0.09
65	-0.22	0.15	0.02	0.05	0.19	0.11
66	-0.22	0.10	0.04	0.08	0.24	0.17
67	-0.26	0.09	0.06	0.14	0.31	0.25
68	-0.27	0.16	0.08	0.16	0.38	0.20
69	-0.17	0.08	0.03	0.07	0.27	0.16
70	-0.18	0.08	0.01	0.03	0.23	0.19
71	-0.16	0.05	-0.01	0.04	0.23	0.20
72	-0.15	0.06	-0.03	0.04	0.25	0.23

Node	P1		P2		P3	
	Mean	95% CI	Mean	95% CI	Mean	95% CI
73	-0.17	0.07	-0.05	0.04	0.28	0.25
74	-0.22	0.04	-0.07	0.04	0.31	0.29
75	-0.26	0.04	-0.01	0.09	0.45	0.30
76	-0.22	0.09	-0.04	0.06	0.30	0.08
77	-0.16	0.09	0.03	0.05	0.17	0.07
78	-0.17	0.09	0.02	0.08	0.16	0.06
79	-0.21	0.12	-0.02	0.07	0.15	0.08
80	-0.24	0.12	-0.02	0.05	0.20	0.09
81	-0.27	0.12	-0.03	0.02	0.23	0.15
82	-0.38	0.12	-0.02	0.09	0.31	0.23
83	-0.32	0.09	0.02	0.16	0.24	0.18
84	-0.25	0.12	-0.02	0.11	0.27	0.16
85	-0.19	0.08	0.01	0.04	0.25	0.16
86	-0.15	0.05	0.00	0.05	0.23	0.18
87	-0.14	0.05	-0.03	0.06	0.25	0.21
88	-0.16	0.04	-0.06	0.04	0.31	0.24
89	-0.21	0.05	-0.07	0.06	0.37	0.28
90	-0.27	0.07	-0.06	0.07	0.44	0.25
91	-0.20	0.12	-0.04	0.06	0.24	0.09
92	-0.16	0.10	-0.03	0.08	0.14	0.07
93	-0.16	0.08	-0.03	0.08	0.19	0.08
94	-0.20	0.10	-0.03	0.06	0.19	0.08
95	-0.24	0.12	-0.03	0.04	0.21	0.09
96	-0.29	0.12	-0.07	0.04	0.25	0.15
97	-0.36	0.15	-0.05	0.07	0.20	0.16
98	-0.45	0.21	-0.05	0.14	0.13	0.12
99	-0.33	0.12	-0.06	0.12	0.11	0.13
100	-0.22	0.04	-0.04	0.05	0.15	0.14
101	-0.20	0.05	-0.02	0.06	0.20	0.16
102	-0.17	0.06	-0.02	0.05	0.26	0.19
103	-0.16	0.04	-0.03	0.03	0.32	0.21
104	-0.21	0.05	-0.09	0.06	0.39	0.28
105	-0.33	0.14	-0.12	0.07	0.33	0.26
106	-0.21	0.08	-0.06	0.08	0.15	0.08
107	-0.17	0.09	-0.03	0.06	0.16	0.06
108	-0.17	0.08	-0.02	0.07	0.22	0.10
109	-0.21	0.08	-0.01	0.04	0.25	0.13
110	-0.25	0.09	0.00	0.07	0.25	0.11
111	-0.27	0.10	0.02	0.07	0.27	0.10

Node	P1		P2		P3	
	Mean	95% CI	Mean	95% CI	Mean	95% CI
112	-0.29	0.10	0.01	0.06	0.26	0.08
113	-0.30	0.09	-0.01	0.06	0.16	0.09
114	-0.33	0.10	-0.08	0.05	0.13	0.11
115	-0.26	0.07	-0.09	0.04	0.17	0.14
116	-0.22	0.07	-0.07	0.04	0.23	0.15
117	-0.22	0.08	-0.03	0.05	0.27	0.15
118	-0.21	0.08	-0.01	0.07	0.26	0.15
119	-0.24	0.10	-0.06	0.07	0.20	0.19
120	-0.35	0.14	-0.11	0.09	0.21	0.22
121	-0.23	0.08	-0.06	0.08	0.14	0.07
122	-0.21	0.08	-0.02	0.06	0.15	0.05
123	-0.20	0.08	0.00	0.07	0.27	0.10
124	-0.20	0.08	0.00	0.07	0.32	0.14
125	-0.22	0.07	0.05	0.07	0.35	0.11
126	-0.24	0.07	0.07	0.06	0.38	0.12
127	-0.28	0.08	0.01	0.07	0.35	0.14
128	-0.28	0.07	-0.05	0.09	0.36	0.17
129	-0.26	0.08	-0.03	0.08	0.31	0.16
130	-0.25	0.07	-0.01	0.05	0.28	0.16
131	-0.25	0.06	-0.03	0.06	0.29	0.14
132	-0.26	0.07	-0.02	0.09	0.28	0.13
133	-0.27	0.10	-0.01	0.10	0.22	0.13
134	-0.29	0.12	-0.04	0.11	0.19	0.17
135	-0.32	0.12	-0.10	0.12	0.24	0.18
136	-0.28	0.08	-0.08	0.10	0.16	0.11
137	-0.26	0.09	-0.03	0.07	0.15	0.08
138	-0.24	0.11	0.00	0.06	0.23	0.07
139	-0.24	0.12	0.02	0.06	0.37	0.12
140	-0.26	0.12	0.03	0.07	0.43	0.14
141	-0.32	0.17	0.03	0.08	0.35	0.12
142	-0.34	0.13	0.01	0.12	0.39	0.16
143	-0.30	0.09	0.03	0.09	0.45	0.10
144	-0.28	0.11	0.08	0.10	0.47	0.14
145	-0.28	0.11	0.12	0.10	0.38	0.12
146	-0.29	0.09	0.09	0.09	0.27	0.11
147	-0.29	0.07	0.03	0.12	0.25	0.09
148	-0.30	0.07	0.00	0.14	0.21	0.10
149	-0.32	0.07	-0.02	0.14	0.21	0.13
150	-0.32	0.07	-0.08	0.15	0.26	0.17

Node	P1		P2		P3	
	Mean	95% CI	Mean	95% CI	Mean	95% CI
151	-0.31	0.09	-0.08	0.13	0.16	0.11
152	-0.33	0.09	-0.07	0.11	0.19	0.10
153	-0.35	0.09	-0.05	0.08	0.26	0.10
154	-0.36	0.10	-0.03	0.08	0.34	0.11
155	-0.36	0.15	-0.05	0.11	0.39	0.14
156	-0.40	0.21	-0.03	0.14	0.38	0.12
157	-0.35	0.15	-0.03	0.10	0.47	0.09
158	-0.35	0.14	0.04	0.09	0.59	0.17
159	-0.33	0.18	0.15	0.09	0.63	0.26
160	-0.33	0.17	0.11	0.13	0.46	0.17
161	-0.34	0.15	0.03	0.11	0.30	0.13
162	-0.35	0.11	0.03	0.09	0.26	0.12
163	-0.36	0.09	0.00	0.11	0.24	0.12
164	-0.35	0.08	-0.04	0.13	0.23	0.14
165	-0.32	0.07	-0.07	0.15	0.21	0.18
166	-0.23	0.13	0.04	0.09	0.30	0.11
167	-0.32	0.22	0.01	0.07	0.25	0.10
168	-0.27	0.16	-0.02	0.08	0.42	0.35
169	-0.27	0.13	-0.02	0.07	0.41	0.34
170	-0.27	0.08	-0.06	0.10	0.15	0.09
171	-0.28	0.08	-0.08	0.13	0.14	0.09
172	-0.33	0.11	-0.07	0.14	0.22	0.16
173	-0.31	0.06	-0.05	0.14	0.22	0.16

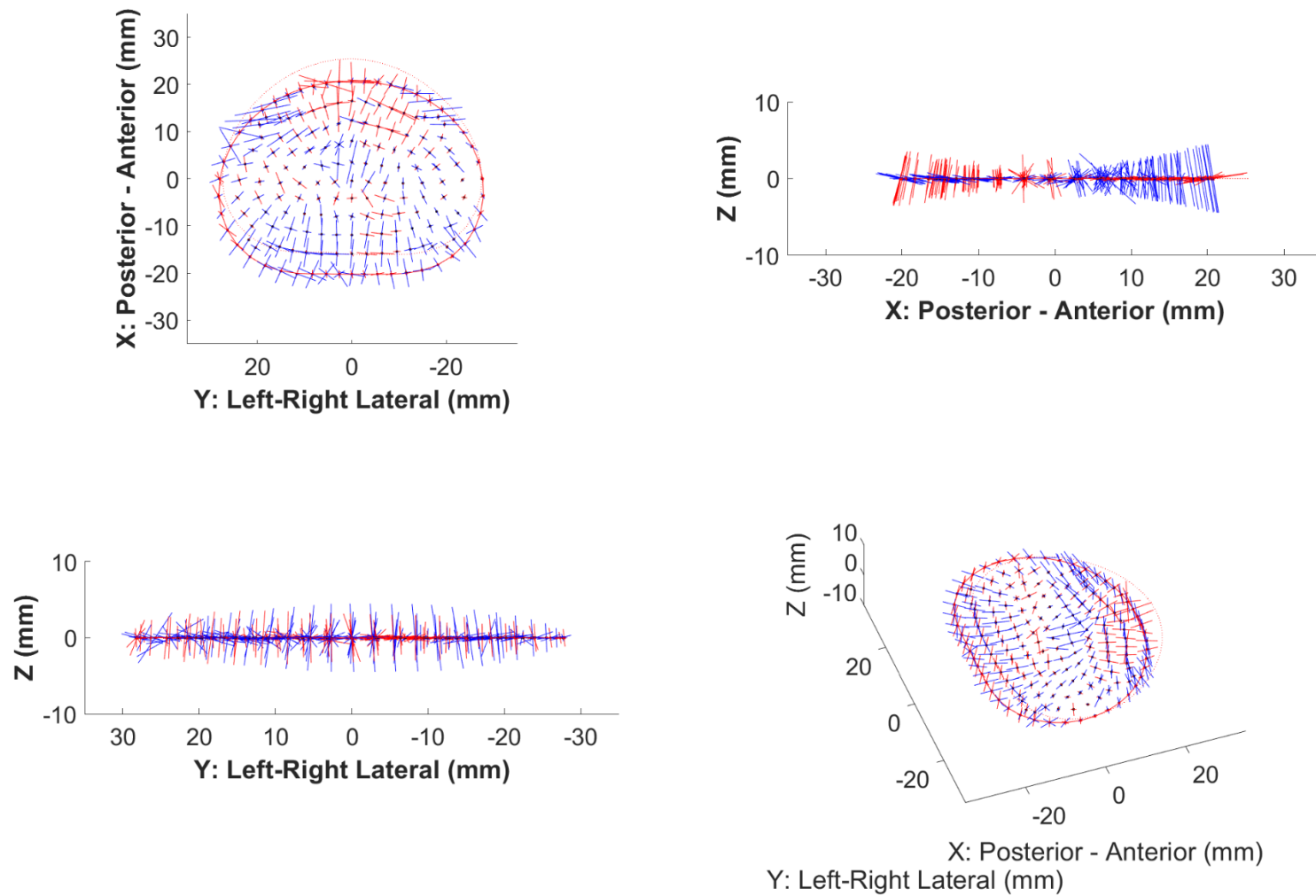


**Figure C-1** Average 3D Principal strains for cycle 1 of the simulated safe repetitive lifting group. The blue vectors represent compressive strain and red vectors represent tensile strain. Four views are presented in this figure. Top Left: Axial View, Top Right: Lateral View, Bottom Left: Posterior View, Bottom Right: Oblique View

C.1.1.2 Cycle 500

**Table C-2** Mean (95% CI) of 3D principal strains at each node (1 – 173) for simulated safe repetitive lifting at cycle 500

Node	P1		P2		P3	
	Mean	95% CI	Mean	95% CI	Mean	95% CI
1	-0.18	0.13	0.12	0.11	0.39	0.13
2	-0.16	0.12	0.09	0.08	0.36	0.13
3	-0.17	0.11	0.08	0.07	0.38	0.13
4	-0.23	0.12	0.12	0.09	0.41	0.14
5	-0.23	0.14	0.14	0.09	0.45	0.14
6	-0.20	0.12	0.12	0.06	0.46	0.17
7	-0.24	0.15	0.03	0.09	0.47	0.18
8	-0.31	0.22	0.04	0.11	0.51	0.21
9	-0.27	0.11	0.19	0.15	0.47	0.19
10	-0.21	0.14	0.10	0.13	0.44	0.21
11	-0.24	0.15	0.04	0.06	0.46	0.25
12	-0.22	0.14	0.03	0.07	0.46	0.28
13	-0.21	0.14	0.02	0.09	0.46	0.30
14	-0.20	0.12	0.03	0.10	0.46	0.31
15	-0.22	0.15	0.03	0.09	0.44	0.31
16	-0.31	0.19	0.07	0.07	0.33	0.13
17	-0.18	0.09	0.05	0.07	0.29	0.10
18	-0.17	0.05	0.03	0.09	0.29	0.11
19	-0.23	0.09	0.05	0.07	0.31	0.12
20	-0.24	0.12	0.06	0.07	0.33	0.13
21	-0.22	0.12	0.06	0.04	0.36	0.15
22	-0.24	0.14	0.03	0.07	0.37	0.16
23	-0.28	0.16	0.02	0.09	0.37	0.18
24	-0.23	0.06	0.01	0.08	0.35	0.20
25	-0.23	0.07	0.01	0.07	0.35	0.23
26	-0.24	0.10	0.01	0.06	0.36	0.24
27	-0.22	0.11	0.00	0.04	0.36	0.25
28	-0.20	0.10	0.00	0.05	0.35	0.26
29	-0.17	0.10	0.01	0.07	0.37	0.27
30	-0.24	0.15	0.03	0.08	0.44	0.31
31	-0.25	0.19	0.04	0.06	0.25	0.11
32	-0.22	0.13	0.00	0.03	0.25	0.10
33	-0.17	0.09	0.00	0.03	0.22	0.08
34	-0.23	0.13	0.01	0.05	0.23	0.10
35	-0.25	0.15	0.02	0.07	0.25	0.11
36	-0.28	0.14	0.04	0.07	0.27	0.12
37	-0.32	0.15	0.03	0.07	0.30	0.13
38	-0.35	0.15	0.03	0.08	0.28	0.15
39	-0.35	0.12	0.03	0.08	0.26	0.18
40	-0.31	0.13	-0.01	0.07	0.27	0.19
41	-0.27	0.11	-0.02	0.05	0.28	0.20
42	-0.23	0.09	-0.02	0.02	0.28	0.21
43	-0.21	0.07	-0.01	0.04	0.28	0.23

Node	P1		P2		P3	
	Mean	95% CI	Mean	95% CI	Mean	95% CI
44	-0.19	0.09	-0.01	0.05	0.34	0.26
45	-0.23	0.14	-0.01	0.05	0.41	0.31
46	-0.19	0.13	0.05	0.07	0.26	0.16
47	-0.15	0.07	0.03	0.04	0.26	0.18
48	-0.19	0.12	0.01	0.04	0.19	0.07
49	-0.22	0.17	0.02	0.05	0.18	0.09
50	-0.24	0.17	0.03	0.07	0.21	0.10
51	-0.24	0.11	0.08	0.13	0.24	0.12
52	-0.26	0.10	0.09	0.13	0.28	0.13
53	-0.28	0.08	0.04	0.03	0.26	0.16
54	-0.28	0.10	0.02	0.05	0.24	0.17
55	-0.28	0.09	0.01	0.06	0.24	0.18
56	-0.22	0.08	0.00	0.04	0.23	0.19
57	-0.18	0.07	-0.01	0.03	0.23	0.20
58	-0.20	0.06	-0.01	0.05	0.26	0.23
59	-0.18	0.04	-0.01	0.05	0.33	0.26
60	-0.20	0.11	-0.01	0.06	0.40	0.30
61	-0.26	0.08	0.06	0.07	0.46	0.54
62	-0.13	0.07	0.05	0.06	0.35	0.35
63	-0.20	0.12	0.03	0.04	0.18	0.08
64	-0.24	0.20	0.01	0.06	0.14	0.08
65	-0.23	0.18	0.00	0.07	0.19	0.10
66	-0.23	0.10	0.04	0.08	0.25	0.16
67	-0.31	0.13	0.08	0.12	0.35	0.29
68	-0.33	0.19	0.09	0.14	0.39	0.23
69	-0.20	0.09	0.01	0.08	0.28	0.15
70	-0.20	0.05	0.03	0.04	0.23	0.17
71	-0.16	0.07	0.00	0.03	0.23	0.17
72	-0.14	0.06	-0.03	0.05	0.23	0.19
73	-0.15	0.08	-0.02	0.04	0.27	0.22
74	-0.22	0.05	-0.04	0.03	0.34	0.25
75	-0.20	0.03	0.00	0.08	0.46	0.28
76	-0.23	0.07	-0.01	0.05	0.44	0.36
77	-0.20	0.11	0.02	0.06	0.23	0.16
78	-0.23	0.21	0.04	0.05	0.13	0.05
79	-0.23	0.19	-0.01	0.05	0.14	0.07
80	-0.23	0.12	-0.03	0.08	0.21	0.08
81	-0.28	0.11	-0.01	0.02	0.27	0.16
82	-0.39	0.12	-0.01	0.08	0.37	0.29
83	-0.32	0.10	0.00	0.15	0.26	0.21
84	-0.27	0.13	0.00	0.12	0.29	0.16
85	-0.19	0.06	0.04	0.05	0.28	0.14
86	-0.16	0.06	0.01	0.03	0.25	0.15
87	-0.13	0.05	-0.03	0.05	0.24	0.17
88	-0.15	0.06	-0.02	0.04	0.31	0.21
89	-0.18	0.05	-0.02	0.05	0.38	0.24
90	-0.24	0.10	-0.03	0.07	0.45	0.24

Node	P1		P2		P3	
	Mean	95% CI	Mean	95% CI	Mean	95% CI
91	-0.20	0.14	-0.02	0.07	0.30	0.07
92	-0.21	0.22	-0.01	0.07	0.17	0.07
93	-0.21	0.16	-0.01	0.04	0.15	0.06
94	-0.21	0.11	-0.04	0.06	0.17	0.08
95	-0.23	0.11	-0.03	0.04	0.23	0.09
96	-0.29	0.13	-0.05	0.04	0.28	0.18
97	-0.35	0.17	-0.05	0.06	0.24	0.20
98	-0.44	0.20	-0.07	0.15	0.16	0.13
99	-0.35	0.11	-0.04	0.13	0.11	0.13
100	-0.24	0.04	-0.01	0.06	0.18	0.13
101	-0.21	0.06	0.00	0.04	0.22	0.13
102	-0.17	0.07	-0.03	0.04	0.26	0.16
103	-0.15	0.07	-0.01	0.03	0.31	0.19
104	-0.20	0.05	-0.04	0.05	0.39	0.25
105	-0.29	0.13	-0.09	0.08	0.33	0.26
106	-0.22	0.15	-0.03	0.08	0.23	0.10
107	-0.20	0.12	-0.01	0.07	0.20	0.06
108	-0.17	0.07	-0.02	0.05	0.17	0.08
109	-0.21	0.06	-0.02	0.04	0.21	0.12
110	-0.25	0.09	-0.01	0.07	0.23	0.13
111	-0.27	0.10	0.02	0.08	0.28	0.12
112	-0.30	0.11	0.00	0.05	0.26	0.09
113	-0.33	0.12	-0.04	0.06	0.16	0.08
114	-0.37	0.12	-0.09	0.06	0.12	0.10
115	-0.28	0.07	-0.10	0.06	0.17	0.13
116	-0.22	0.06	-0.06	0.05	0.21	0.14
117	-0.21	0.08	-0.03	0.06	0.24	0.15
118	-0.22	0.10	-0.01	0.06	0.26	0.15
119	-0.24	0.12	-0.03	0.07	0.22	0.18
120	-0.30	0.13	-0.07	0.09	0.19	0.23
121	-0.21	0.09	-0.04	0.06	0.24	0.15
122	-0.20	0.06	-0.02	0.06	0.22	0.07
123	-0.21	0.05	0.01	0.07	0.21	0.10
124	-0.21	0.07	-0.02	0.07	0.25	0.13
125	-0.23	0.06	0.04	0.07	0.30	0.11
126	-0.25	0.06	0.06	0.07	0.36	0.12
127	-0.30	0.09	0.01	0.08	0.33	0.13
128	-0.31	0.09	-0.05	0.09	0.34	0.14
129	-0.30	0.12	-0.01	0.05	0.26	0.15
130	-0.27	0.11	-0.03	0.04	0.24	0.14
131	-0.24	0.08	-0.05	0.07	0.25	0.14
132	-0.22	0.07	-0.04	0.08	0.26	0.13
133	-0.25	0.09	0.00	0.10	0.24	0.13
134	-0.28	0.12	0.00	0.10	0.24	0.15
135	-0.29	0.12	-0.08	0.13	0.25	0.18
136	-0.25	0.10	-0.06	0.07	0.32	0.17
137	-0.27	0.09	-0.03	0.07	0.24	0.09

Node	P1		P2		P3	
	Mean	95% CI	Mean	95% CI	Mean	95% CI
138	-0.25	0.09	0.00	0.06	0.26	0.11
139	-0.25	0.10	0.02	0.07	0.35	0.15
140	-0.27	0.11	0.04	0.08	0.38	0.16
141	-0.34	0.16	0.01	0.10	0.30	0.09
142	-0.37	0.16	-0.02	0.12	0.36	0.12
143	-0.32	0.10	0.01	0.10	0.43	0.10
144	-0.30	0.08	0.12	0.08	0.48	0.12
145	-0.28	0.11	0.13	0.09	0.40	0.10
146	-0.28	0.11	0.08	0.11	0.28	0.12
147	-0.29	0.09	0.04	0.12	0.26	0.10
148	-0.28	0.08	0.01	0.14	0.24	0.10
149	-0.30	0.09	0.01	0.14	0.24	0.11
150	-0.30	0.10	-0.04	0.14	0.28	0.15
151	-0.29	0.12	-0.06	0.08	0.30	0.12
152	-0.33	0.13	-0.01	0.05	0.27	0.09
153	-0.35	0.11	0.04	0.12	0.29	0.10
154	-0.36	0.12	0.03	0.15	0.36	0.16
155	-0.36	0.15	-0.04	0.13	0.39	0.17
156	-0.41	0.21	-0.07	0.14	0.31	0.12
157	-0.37	0.18	-0.09	0.11	0.42	0.11
158	-0.39	0.09	0.07	0.06	0.58	0.16
159	-0.37	0.12	0.19	0.08	0.63	0.25
160	-0.33	0.18	0.12	0.11	0.49	0.14
161	-0.34	0.15	0.08	0.09	0.37	0.11
162	-0.36	0.12	0.04	0.12	0.33	0.11
163	-0.36	0.11	0.00	0.12	0.27	0.12
164	-0.34	0.10	-0.02	0.13	0.24	0.14
165	-0.31	0.10	-0.03	0.13	0.24	0.14
166	-0.18	0.11	0.09	0.08	0.32	0.11
167	-0.30	0.20	0.05	0.07	0.32	0.13
168	-0.20	0.13	0.02	0.08	0.39	0.29
169	-0.23	0.13	0.00	0.07	0.38	0.29
170	-0.24	0.08	-0.07	0.08	0.28	0.13
171	-0.28	0.11	-0.05	0.07	0.27	0.11
172	-0.31	0.11	-0.02	0.13	0.25	0.14
173	-0.30	0.09	-0.01	0.13	0.25	0.13

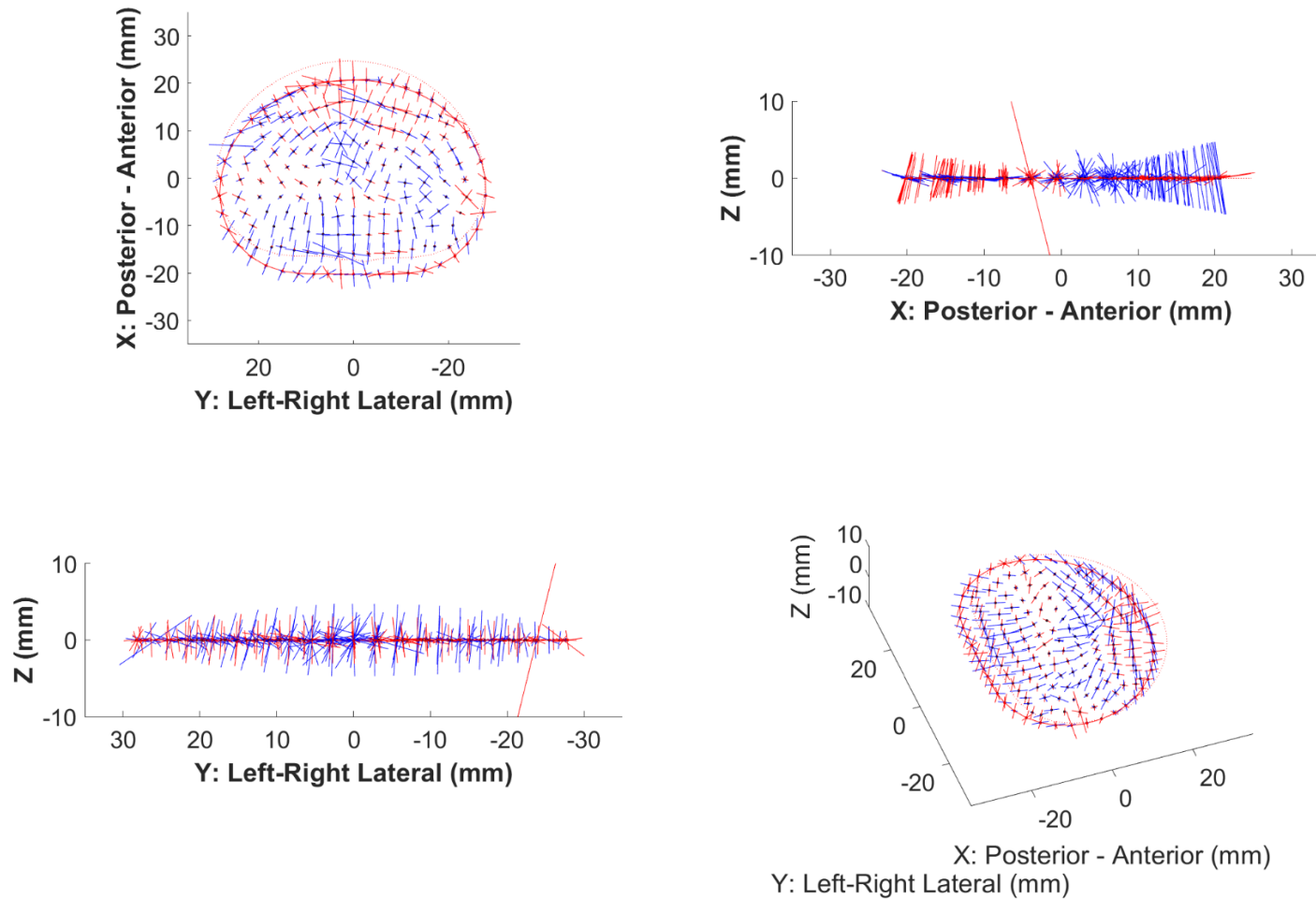


**Figure C-2** Average 3D Principal strains for cycle 500 of the simulated safe repetitive lifting group. The blue vectors represent compressive strain and red vectors represent tensile strain. Four views are presented in this figure. Top Left: Axial View, Top Right: Lateral View, Bottom Left: Posterior View, Bottom Right: Oblique View

C.1.1.3 Cycle 1000

**Table C-3** Mean (95% CI) of 3D principal strains at each node (1 – 173) for simulated safe repetitive lifting at cycle 1000

Node	P1		P2		P3	
	Mean	95% CI	Mean	95% CI	Mean	95% CI
1	-0.38	0.23	0.11	0.12	0.37	0.12
2	-0.31	0.20	0.09	0.10	0.36	0.12
3	-0.30	0.20	0.05	0.07	0.37	0.13
4	-0.39	0.23	0.03	0.11	0.39	0.13
5	-0.42	0.28	0.07	0.10	0.42	0.13
6	-0.35	0.24	0.10	0.07	0.46	0.15
7	-0.34	0.22	0.12	0.08	0.58	0.23
8	-0.36	0.22	0.10	0.12	0.65	0.25
9	-0.25	0.13	0.19	0.13	0.46	0.17
10	-0.23	0.17	0.05	0.18	0.45	0.18
11	-0.31	0.16	-0.02	0.14	0.51	0.21
12	-0.30	0.15	-0.05	0.13	0.49	0.25
13	-0.31	0.14	-0.04	0.11	0.46	0.29
14	-0.31	0.14	-0.01	0.11	0.46	0.30
15	-0.30	0.19	0.01	0.11	0.46	0.30
16	-0.49	0.28	0.03	0.10	0.27	0.11
17	-0.30	0.15	0.06	0.08	0.28	0.09
18	-0.25	0.12	0.04	0.07	0.27	0.09
19	-0.28	0.12	0.03	0.06	0.29	0.10
20	-0.29	0.14	0.04	0.06	0.31	0.11
21	-0.26	0.16	0.08	0.06	0.34	0.12
22	-0.25	0.17	0.10	0.09	0.39	0.14
23	-0.23	0.17	0.07	0.12	0.35	0.16
24	-0.20	0.05	0.02	0.07	0.33	0.20
25	-0.24	0.08	-0.02	0.10	0.36	0.20
26	-0.28	0.11	-0.06	0.10	0.38	0.21
27	-0.28	0.10	-0.07	0.09	0.37	0.22
28	-0.25	0.09	-0.07	0.07	0.36	0.25
29	-0.23	0.11	-0.05	0.09	0.38	0.26
30	-0.27	0.21	0.00	0.08	0.48	0.29
31	-0.35	0.24	0.02	0.14	0.20	0.13
32	-0.27	0.16	-0.01	0.09	0.18	0.09
33	-0.16	0.09	0.01	0.06	0.22	0.08
34	-0.16	0.09	0.00	0.05	0.23	0.08
35	-0.19	0.09	0.03	0.07	0.24	0.10
36	-0.23	0.13	0.05	0.07	0.28	0.11
37	-0.26	0.16	0.04	0.07	0.32	0.12
38	-0.25	0.17	0.01	0.07	0.28	0.15
39	-0.29	0.14	0.00	0.07	0.25	0.18
40	-0.30	0.13	-0.03	0.08	0.26	0.18
41	-0.28	0.10	-0.06	0.06	0.28	0.19
42	-0.24	0.09	-0.06	0.03	0.29	0.20
43	-0.22	0.06	-0.04	0.04	0.31	0.23

Node	P1		P2		P3	
	Mean	95% CI	Mean	95% CI	Mean	95% CI
44	-0.19	0.10	-0.02	0.06	0.38	0.25
45	-0.23	0.17	-0.02	0.05	0.45	0.30
46	-0.28	0.21	0.04	0.08	0.23	0.14
47	-0.21	0.13	0.01	0.08	0.17	0.08
48	-0.14	0.08	0.02	0.06	0.19	0.09
49	-0.12	0.08	0.02	0.05	0.19	0.09
50	-0.13	0.08	0.03	0.08	0.19	0.10
51	-0.18	0.09	0.06	0.14	0.27	0.14
52	-0.21	0.11	0.05	0.14	0.27	0.14
53	-0.23	0.07	0.02	0.04	0.22	0.14
54	-0.24	0.11	0.00	0.05	0.23	0.19
55	-0.28	0.10	-0.01	0.07	0.23	0.19
56	-0.23	0.07	-0.01	0.05	0.22	0.19
57	-0.20	0.07	-0.01	0.02	0.25	0.20
58	-0.19	0.06	0.00	0.02	0.29	0.22
59	-0.17	0.05	0.01	0.06	0.38	0.25
60	-0.22	0.12	-0.02	0.06	0.46	0.31
61	-0.38	0.21	0.00	0.06	0.30	0.11
62	-0.18	0.13	0.02	0.08	0.21	0.06
63	-0.13	0.06	0.02	0.05	0.15	0.08
64	-0.13	0.07	0.03	0.05	0.14	0.09
65	-0.14	0.08	0.01	0.05	0.19	0.10
66	-0.19	0.08	0.01	0.08	0.24	0.19
67	-0.30	0.14	0.06	0.13	0.25	0.27
68	-0.33	0.19	0.08	0.14	0.31	0.19
69	-0.18	0.09	0.01	0.09	0.26	0.17
70	-0.20	0.06	0.00	0.04	0.21	0.18
71	-0.17	0.06	-0.01	0.04	0.23	0.17
72	-0.15	0.06	0.01	0.03	0.27	0.19
73	-0.14	0.08	0.00	0.04	0.33	0.21
74	-0.21	0.05	-0.05	0.05	0.40	0.24
75	-0.26	0.06	0.00	0.09	0.53	0.28
76	-0.29	0.17	-0.06	0.04	0.29	0.11
77	-0.13	0.05	-0.01	0.05	0.19	0.06
78	-0.12	0.04	0.04	0.04	0.12	0.05
79	-0.14	0.06	0.01	0.04	0.13	0.07
80	-0.17	0.08	0.00	0.05	0.20	0.09
81	-0.24	0.11	-0.03	0.03	0.20	0.14
82	-0.39	0.13	-0.01	0.09	0.25	0.17
83	-0.33	0.12	0.00	0.15	0.22	0.22
84	-0.27	0.14	0.00	0.12	0.27	0.18
85	-0.19	0.07	0.01	0.05	0.25	0.14
86	-0.15	0.05	-0.01	0.03	0.24	0.16
87	-0.13	0.04	-0.02	0.05	0.28	0.18
88	-0.16	0.06	-0.03	0.03	0.35	0.21
89	-0.18	0.05	-0.05	0.08	0.42	0.26
90	-0.25	0.10	-0.04	0.06	0.48	0.25
91	-0.18	0.10	-0.04	0.06	0.29	0.10

Node	P1		P2		P3	
	Mean	95% CI	Mean	95% CI	Mean	95% CI
92	-0.12	0.06	-0.01	0.05	0.16	0.05
93	-0.14	0.05	0.00	0.04	0.13	0.06
94	-0.17	0.08	-0.01	0.05	0.15	0.07
95	-0.22	0.11	-0.03	0.03	0.20	0.07
96	-0.26	0.12	-0.07	0.03	0.20	0.09
97	-0.32	0.16	-0.06	0.05	0.16	0.13
98	-0.41	0.20	-0.04	0.14	0.15	0.14
99	-0.34	0.12	-0.04	0.14	0.10	0.14
100	-0.22	0.03	-0.03	0.07	0.15	0.13
101	-0.19	0.04	-0.02	0.05	0.21	0.15
102	-0.16	0.04	-0.04	0.03	0.27	0.19
103	-0.16	0.04	-0.01	0.02	0.32	0.22
104	-0.21	0.06	-0.05	0.06	0.41	0.27
105	-0.30	0.13	-0.09	0.07	0.35	0.26
106	-0.20	0.07	-0.05	0.08	0.25	0.15
107	-0.16	0.04	-0.01	0.05	0.19	0.04
108	-0.16	0.03	-0.01	0.05	0.15	0.08
109	-0.21	0.06	-0.03	0.04	0.17	0.09
110	-0.25	0.08	-0.05	0.04	0.19	0.08
111	-0.26	0.10	-0.03	0.05	0.23	0.07
112	-0.28	0.10	0.00	0.06	0.23	0.06
113	-0.29	0.08	-0.02	0.06	0.16	0.08
114	-0.32	0.09	-0.07	0.07	0.12	0.11
115	-0.24	0.06	-0.10	0.07	0.16	0.15
116	-0.20	0.04	-0.07	0.05	0.21	0.16
117	-0.19	0.07	-0.05	0.05	0.24	0.17
118	-0.20	0.09	-0.02	0.06	0.26	0.17
119	-0.24	0.11	-0.02	0.07	0.23	0.19
120	-0.32	0.18	-0.07	0.09	0.28	0.22
121	-0.22	0.06	-0.06	0.07	0.21	0.10
122	-0.20	0.03	-0.02	0.06	0.21	0.04
123	-0.19	0.04	0.00	0.07	0.19	0.10
124	-0.19	0.06	-0.04	0.06	0.22	0.12
125	-0.22	0.04	0.00	0.04	0.27	0.11
126	-0.24	0.04	0.03	0.05	0.34	0.13
127	-0.28	0.06	0.00	0.08	0.33	0.13
128	-0.27	0.05	-0.04	0.10	0.34	0.14
129	-0.24	0.07	0.00	0.08	0.28	0.15
130	-0.23	0.07	-0.01	0.04	0.24	0.16
131	-0.22	0.06	-0.04	0.06	0.26	0.15
132	-0.21	0.05	-0.05	0.09	0.28	0.14
133	-0.24	0.09	-0.02	0.10	0.27	0.13
134	-0.27	0.14	-0.01	0.12	0.22	0.17
135	-0.28	0.14	-0.06	0.15	0.22	0.22
136	-0.26	0.05	-0.06	0.08	0.25	0.11
137	-0.23	0.07	-0.01	0.06	0.20	0.07
138	-0.21	0.10	0.01	0.06	0.22	0.08
139	-0.22	0.11	0.01	0.07	0.33	0.14

Node	P1		P2		P3	
	Mean	95% CI	Mean	95% CI	Mean	95% CI
140	-0.26	0.10	0.00	0.06	0.37	0.17
141	-0.33	0.16	-0.02	0.08	0.25	0.09
142	-0.33	0.14	-0.02	0.13	0.37	0.19
143	-0.27	0.10	0.05	0.10	0.43	0.11
144	-0.27	0.09	0.12	0.08	0.49	0.14
145	-0.26	0.10	0.12	0.10	0.41	0.13
146	-0.27	0.08	0.06	0.11	0.32	0.12
147	-0.27	0.06	0.03	0.12	0.33	0.10
148	-0.27	0.06	0.00	0.14	0.34	0.13
149	-0.30	0.10	0.00	0.14	0.32	0.13
150	-0.32	0.16	-0.05	0.15	0.24	0.19
151	-0.28	0.05	-0.04	0.08	0.25	0.10
152	-0.28	0.08	-0.02	0.06	0.26	0.08
153	-0.30	0.10	-0.03	0.09	0.31	0.09
154	-0.32	0.14	-0.01	0.12	0.37	0.12
155	-0.35	0.17	-0.05	0.11	0.34	0.12
156	-0.43	0.22	-0.12	0.15	0.28	0.15
157	-0.37	0.13	-0.12	0.13	0.52	0.17
158	-0.37	0.10	-0.02	0.10	0.65	0.20
159	-0.33	0.15	0.12	0.15	0.67	0.29
160	-0.32	0.17	0.15	0.15	0.49	0.16
161	-0.33	0.13	0.10	0.12	0.36	0.13
162	-0.36	0.09	0.05	0.13	0.39	0.10
163	-0.35	0.08	0.04	0.12	0.37	0.13
164	-0.32	0.10	0.01	0.13	0.34	0.14
165	-0.32	0.13	-0.03	0.14	0.29	0.14
166	-0.34	0.18	0.08	0.10	0.31	0.09
167	-0.45	0.27	0.02	0.08	0.25	0.10
168	-0.27	0.17	-0.02	0.10	0.42	0.29
169	-0.25	0.18	-0.03	0.08	0.42	0.28
170	-0.25	0.03	-0.06	0.09	0.25	0.09
171	-0.25	0.04	-0.03	0.07	0.23	0.09
172	-0.30	0.15	-0.06	0.16	0.22	0.18
173	-0.32	0.14	-0.01	0.14	0.31	0.13

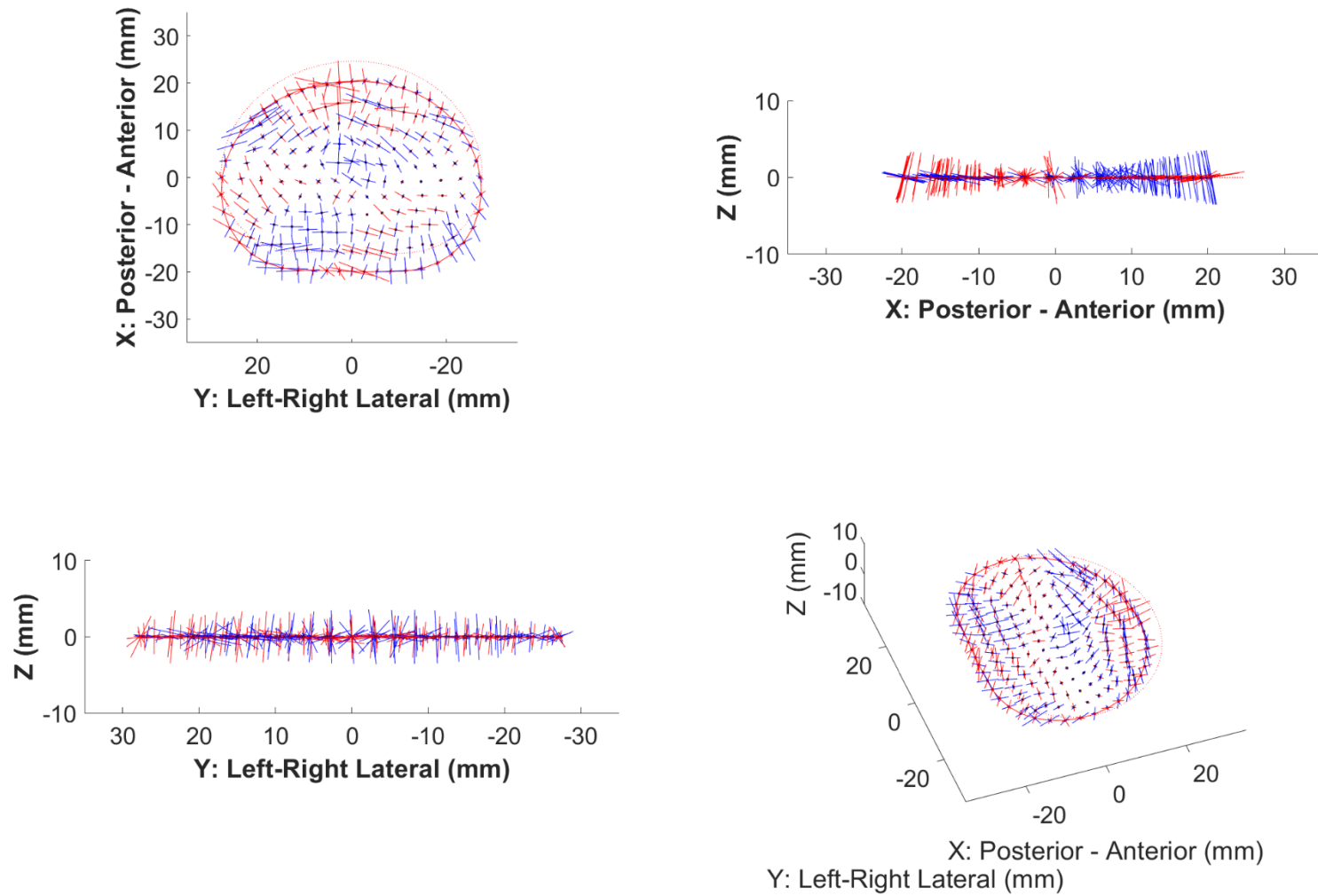


**Figure C-3** Average 3D Principal strains for cycle 1000 of the simulated safe repetitive lifting group. The blue vectors represent compressive strain and red vectors represent tensile strain. Four views are presented in this figure. Top Left: Axial View, Top Right: Lateral View, Bottom Left: Posterior View, Bottom Right: Oblique View

C.1.1.4 Cycle 5000

**Table C-4** Mean (95% CI) of 3D principal strains at each node (1 – 173) for simulated safe repetitive lifting at cycle 5000

Node	P1		P2		P3	
	Mean	95% CI	Mean	95% CI	Mean	95% CI
1	-0.32	0.22	0.06	0.10	0.38	0.17
2	-0.26	0.15	0.05	0.09	0.35	0.15
3	-0.23	0.15	0.03	0.09	0.38	0.16
4	-0.25	0.17	0.04	0.06	0.40	0.16
5	-0.27	0.18	0.09	0.07	0.43	0.16
6	-0.24	0.12	0.11	0.06	0.45	0.20
7	-0.25	0.20	0.10	0.07	0.50	0.22
8	-0.32	0.27	0.11	0.07	0.55	0.23
9	-0.24	0.11	0.16	0.11	0.48	0.23
10	-0.24	0.13	0.08	0.14	0.45	0.27
11	-0.31	0.21	0.00	0.14	0.48	0.32
12	-0.26	0.17	-0.06	0.13	0.51	0.35
13	-0.25	0.15	-0.05	0.10	0.52	0.37
14	-0.24	0.15	-0.01	0.10	0.52	0.38
15	-0.26	0.16	0.01	0.10	0.53	0.38
16	-0.44	0.31	0.02	0.11	0.25	0.13
17	-0.24	0.12	0.03	0.09	0.27	0.13
18	-0.19	0.09	0.02	0.08	0.28	0.13
19	-0.19	0.09	0.01	0.06	0.31	0.13
20	-0.21	0.07	0.05	0.07	0.33	0.13
21	-0.21	0.09	0.08	0.08	0.38	0.15
22	-0.21	0.16	0.06	0.06	0.41	0.18
23	-0.23	0.20	0.05	0.07	0.39	0.20
24	-0.19	0.06	0.01	0.07	0.35	0.24
25	-0.25	0.09	0.00	0.11	0.36	0.27
26	-0.29	0.13	-0.04	0.11	0.37	0.28
27	-0.26	0.11	-0.06	0.09	0.39	0.29
28	-0.23	0.09	-0.05	0.06	0.40	0.31
29	-0.21	0.10	-0.04	0.05	0.43	0.32
30	-0.25	0.15	0.00	0.08	0.54	0.37
31	-0.35	0.28	-0.02	0.11	0.18	0.12
32	-0.24	0.17	-0.03	0.07	0.17	0.11
33	-0.12	0.07	-0.02	0.04	0.23	0.10
34	-0.14	0.07	0.00	0.06	0.25	0.11
35	-0.15	0.08	0.03	0.07	0.26	0.12
36	-0.20	0.13	0.06	0.08	0.32	0.13
37	-0.25	0.18	0.03	0.06	0.36	0.15
38	-0.27	0.18	0.02	0.06	0.31	0.19
39	-0.28	0.14	0.01	0.07	0.27	0.22
40	-0.28	0.13	-0.02	0.08	0.27	0.24
41	-0.28	0.09	-0.04	0.05	0.28	0.24
42	-0.26	0.08	-0.04	0.04	0.30	0.26
43	-0.23	0.05	-0.02	0.05	0.33	0.28

Node	P1		P2		P3	
	Mean	95% CI	Mean	95% CI	Mean	95% CI
44	-0.20	0.06	-0.02	0.07	0.42	0.31
45	-0.26	0.14	-0.02	0.07	0.50	0.37
46	-0.25	0.21	0.03	0.08	0.18	0.08
47	-0.17	0.10	0.01	0.05	0.17	0.08
48	-0.14	0.06	0.00	0.04	0.21	0.09
49	-0.13	0.08	0.01	0.05	0.20	0.10
50	-0.12	0.08	0.02	0.08	0.21	0.12
51	-0.17	0.09	0.08	0.15	0.28	0.16
52	-0.22	0.11	0.08	0.15	0.27	0.18
53	-0.24	0.07	0.03	0.07	0.23	0.18
54	-0.23	0.10	-0.01	0.06	0.26	0.21
55	-0.25	0.10	-0.01	0.06	0.26	0.23
56	-0.22	0.08	-0.01	0.06	0.23	0.23
57	-0.21	0.07	0.00	0.05	0.26	0.24
58	-0.21	0.06	-0.01	0.02	0.32	0.26
59	-0.20	0.04	0.01	0.05	0.42	0.30
60	-0.25	0.09	-0.03	0.06	0.53	0.35
61	-0.29	0.09	0.01	0.07	0.20	0.07
62	-0.15	0.07	0.03	0.06	0.18	0.05
63	-0.15	0.06	0.02	0.05	0.17	0.08
64	-0.16	0.08	0.01	0.05	0.15	0.09
65	-0.15	0.08	-0.01	0.07	0.19	0.12
66	-0.20	0.10	0.03	0.10	0.23	0.22
67	-0.29	0.17	0.06	0.15	0.27	0.28
68	-0.33	0.20	0.08	0.17	0.34	0.19
69	-0.19	0.09	0.03	0.10	0.28	0.19
70	-0.20	0.06	-0.01	0.05	0.25	0.21
71	-0.17	0.06	-0.02	0.04	0.26	0.20
72	-0.16	0.05	0.00	0.03	0.30	0.22
73	-0.15	0.07	0.02	0.04	0.35	0.24
74	-0.24	0.05	-0.04	0.03	0.46	0.27
75	-0.28	0.07	0.01	0.09	0.60	0.31
76	-0.24	0.08	-0.04	0.03	0.26	0.06
77	-0.16	0.07	0.02	0.05	0.16	0.05
78	-0.15	0.04	0.03	0.06	0.13	0.05
79	-0.18	0.06	0.00	0.05	0.13	0.08
80	-0.19	0.07	-0.02	0.05	0.20	0.10
81	-0.25	0.11	-0.04	0.05	0.22	0.15
82	-0.38	0.14	-0.01	0.10	0.28	0.17
83	-0.34	0.13	0.02	0.17	0.23	0.23
84	-0.28	0.14	0.00	0.13	0.27	0.20
85	-0.21	0.07	0.02	0.07	0.25	0.17
86	-0.16	0.07	-0.02	0.04	0.27	0.18
87	-0.14	0.04	-0.03	0.05	0.31	0.20
88	-0.17	0.05	-0.01	0.03	0.38	0.22
89	-0.19	0.05	-0.03	0.07	0.46	0.26
90	-0.28	0.11	0.00	0.07	0.54	0.29
91	-0.19	0.12	-0.02	0.06	0.28	0.08

Node	P1		P2		P3	
	Mean	95% CI	Mean	95% CI	Mean	95% CI
92	-0.14	0.07	0.00	0.05	0.14	0.05
93	-0.16	0.05	0.00	0.05	0.14	0.06
94	-0.19	0.09	-0.01	0.05	0.14	0.07
95	-0.23	0.11	-0.03	0.03	0.19	0.08
96	-0.27	0.11	-0.06	0.03	0.21	0.09
97	-0.33	0.14	-0.04	0.06	0.18	0.13
98	-0.43	0.20	-0.03	0.15	0.15	0.14
99	-0.36	0.12	-0.05	0.15	0.10	0.14
100	-0.23	0.04	-0.04	0.08	0.17	0.15
101	-0.20	0.06	-0.02	0.06	0.24	0.16
102	-0.17	0.07	-0.05	0.05	0.31	0.21
103	-0.15	0.06	-0.04	0.04	0.36	0.24
104	-0.22	0.07	-0.04	0.07	0.44	0.28
105	-0.32	0.14	-0.06	0.06	0.34	0.28
106	-0.21	0.09	-0.04	0.07	0.21	0.09
107	-0.17	0.07	-0.01	0.04	0.19	0.05
108	-0.17	0.06	0.00	0.06	0.16	0.06
109	-0.21	0.07	-0.01	0.04	0.18	0.07
110	-0.25	0.09	-0.03	0.04	0.18	0.08
111	-0.26	0.11	-0.03	0.04	0.24	0.07
112	-0.29	0.10	0.00	0.06	0.24	0.07
113	-0.31	0.08	-0.03	0.06	0.18	0.08
114	-0.35	0.08	-0.07	0.07	0.15	0.10
115	-0.27	0.06	-0.09	0.06	0.19	0.14
116	-0.23	0.09	-0.06	0.05	0.25	0.16
117	-0.22	0.10	-0.05	0.06	0.29	0.17
118	-0.21	0.10	-0.02	0.07	0.29	0.18
119	-0.25	0.13	-0.03	0.07	0.25	0.20
120	-0.34	0.17	-0.05	0.09	0.25	0.24
121	-0.22	0.07	-0.04	0.06	0.20	0.07
122	-0.21	0.05	-0.01	0.05	0.22	0.06
123	-0.20	0.06	0.00	0.07	0.22	0.09
124	-0.21	0.08	-0.03	0.06	0.24	0.09
125	-0.23	0.07	0.02	0.06	0.29	0.09
126	-0.25	0.07	0.02	0.05	0.35	0.12
127	-0.30	0.09	-0.01	0.06	0.32	0.13
128	-0.29	0.07	-0.05	0.09	0.39	0.15
129	-0.26	0.09	0.00	0.06	0.35	0.14
130	-0.24	0.09	0.01	0.04	0.28	0.14
131	-0.25	0.09	-0.02	0.07	0.30	0.14
132	-0.26	0.10	-0.03	0.09	0.31	0.13
133	-0.26	0.12	-0.02	0.11	0.29	0.14
134	-0.29	0.16	-0.02	0.11	0.25	0.18
135	-0.31	0.17	-0.06	0.13	0.26	0.21
136	-0.26	0.07	-0.05	0.07	0.24	0.09
137	-0.25	0.08	-0.03	0.07	0.24	0.07
138	-0.23	0.10	-0.01	0.06	0.26	0.07
139	-0.23	0.13	0.02	0.08	0.36	0.13

Node	P1		P2		P3	
	Mean	95% CI	Mean	95% CI	Mean	95% CI
140	-0.26	0.13	0.03	0.08	0.40	0.16
141	-0.34	0.19	-0.01	0.08	0.30	0.07
142	-0.35	0.16	-0.01	0.14	0.39	0.16
143	-0.29	0.11	0.05	0.09	0.46	0.12
144	-0.28	0.11	0.11	0.09	0.54	0.15
145	-0.27	0.12	0.13	0.11	0.44	0.13
146	-0.28	0.11	0.09	0.11	0.33	0.14
147	-0.30	0.09	0.03	0.14	0.33	0.10
148	-0.31	0.11	0.01	0.14	0.30	0.12
149	-0.31	0.11	0.00	0.14	0.27	0.15
150	-0.31	0.13	-0.06	0.15	0.29	0.17
151	-0.28	0.07	-0.05	0.09	0.26	0.09
152	-0.29	0.11	-0.04	0.04	0.27	0.08
153	-0.31	0.14	-0.03	0.11	0.31	0.07
154	-0.33	0.16	0.00	0.13	0.39	0.13
155	-0.36	0.19	-0.05	0.13	0.42	0.16
156	-0.44	0.24	-0.12	0.16	0.33	0.11
157	-0.38	0.16	-0.06	0.10	0.50	0.15
158	-0.40	0.12	0.07	0.06	0.68	0.21
159	-0.34	0.16	0.13	0.14	0.73	0.30
160	-0.32	0.19	0.13	0.17	0.55	0.16
161	-0.33	0.15	0.11	0.12	0.39	0.14
162	-0.38	0.12	0.05	0.11	0.41	0.12
163	-0.39	0.12	0.03	0.13	0.35	0.16
164	-0.37	0.14	0.00	0.14	0.31	0.17
165	-0.31	0.13	-0.04	0.15	0.27	0.18
166	-0.27	0.17	0.04	0.09	0.30	0.13
167	-0.39	0.30	0.01	0.09	0.24	0.13
168	-0.23	0.14	-0.02	0.07	0.48	0.35
169	-0.24	0.13	-0.03	0.08	0.48	0.34
170	-0.25	0.06	-0.04	0.07	0.23	0.08
171	-0.26	0.07	-0.03	0.07	0.25	0.08
172	-0.32	0.16	-0.04	0.13	0.27	0.16
173	-0.29	0.11	-0.02	0.14	0.28	0.17

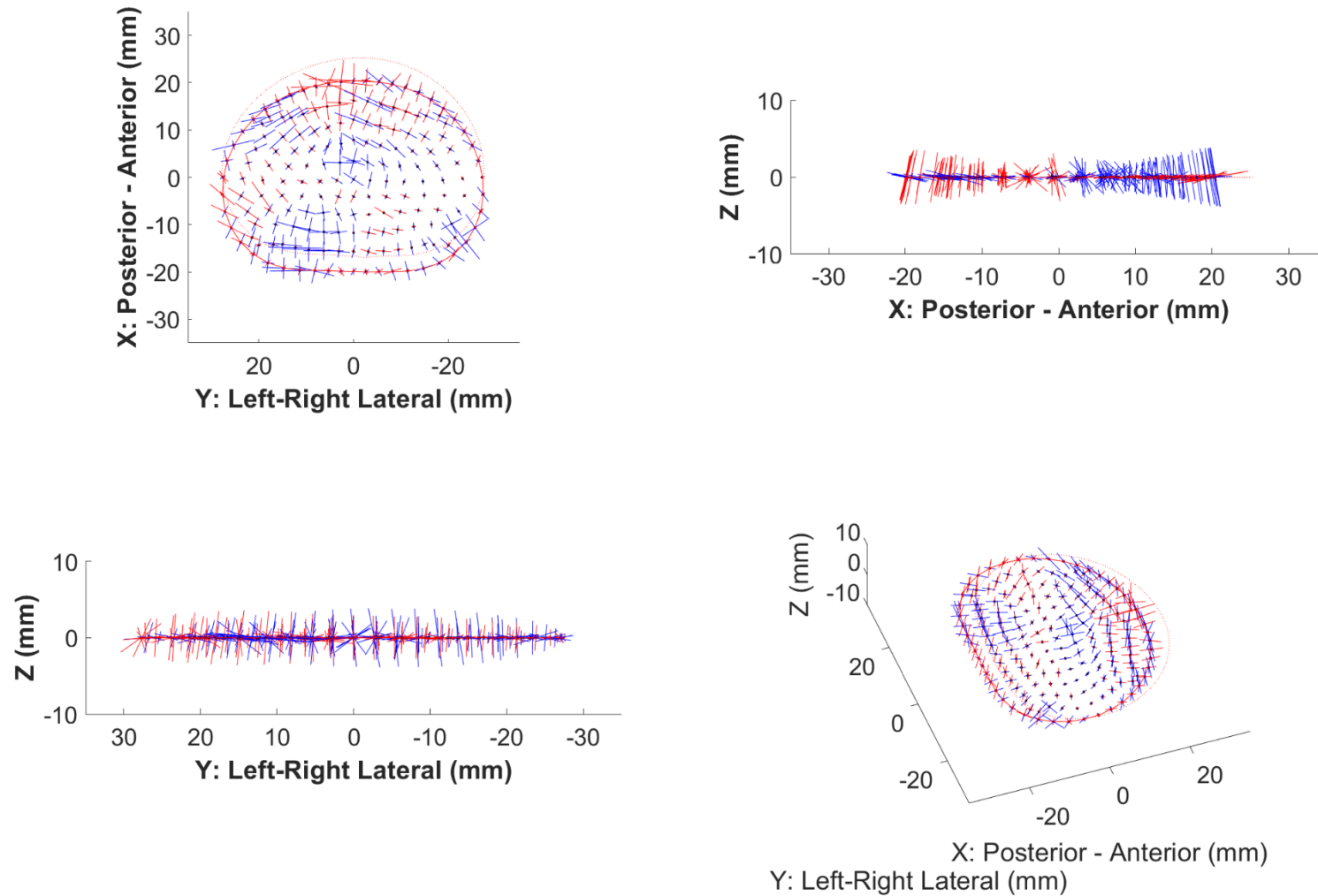


**Figure C-4** Average 3D Principal strains for cycle 5000 of the simulated safe repetitive lifting group. The blue vectors represent compressive strain and red vectors represent tensile strain. Four views are presented in this figure. Top Left: Axial View, Top Right: Lateral View, Bottom Left: Posterior View, Bottom Right: Oblique View

C.1.1.5 Cycle 10000

**Table C-5** Mean (95% CI) of 3D principal strains at each node (1 – 173) for simulated safe repetitive lifting at cycle 10000

Node	P1		P2		P3	
	Mean	95% CI	Mean	95% CI	Mean	95% CI
1	-0.34	0.25	0.01	0.13	0.31	0.22
2	-0.27	0.21	0.03	0.13	0.33	0.23
3	-0.26	0.21	0.06	0.12	0.37	0.23
4	-0.32	0.21	0.11	0.11	0.39	0.22
5	-0.36	0.21	0.14	0.10	0.41	0.22
6	-0.30	0.15	0.14	0.10	0.43	0.23
7	-0.27	0.23	0.15	0.12	0.48	0.25
8	-0.33	0.27	0.14	0.13	0.54	0.24
9	-0.23	0.16	0.20	0.18	0.46	0.24
10	-0.21	0.15	0.12	0.20	0.45	0.27
11	-0.28	0.19	0.01	0.18	0.46	0.27
12	-0.28	0.16	-0.06	0.18	0.45	0.29
13	-0.30	0.16	-0.08	0.13	0.45	0.30
14	-0.31	0.17	-0.05	0.11	0.46	0.30
15	-0.33	0.21	0.00	0.09	0.47	0.29
16	-0.40	0.37	-0.03	0.15	0.25	0.23
17	-0.24	0.16	0.01	0.12	0.26	0.22
18	-0.20	0.13	0.01	0.11	0.27	0.21
19	-0.24	0.11	0.02	0.11	0.30	0.21
20	-0.29	0.07	0.05	0.10	0.32	0.22
21	-0.27	0.13	0.07	0.09	0.38	0.24
22	-0.22	0.21	0.04	0.06	0.44	0.24
23	-0.21	0.23	0.05	0.07	0.39	0.26
24	-0.19	0.05	0.01	0.09	0.35	0.29
25	-0.24	0.08	-0.02	0.11	0.35	0.30
26	-0.27	0.12	-0.08	0.13	0.36	0.27
27	-0.28	0.14	-0.10	0.13	0.36	0.26
28	-0.28	0.13	-0.09	0.10	0.36	0.27
29	-0.26	0.14	-0.06	0.07	0.39	0.27
30	-0.32	0.21	0.02	0.08	0.50	0.27
31	-0.33	0.36	-0.04	0.13	0.20	0.22
32	-0.23	0.21	-0.05	0.09	0.18	0.20
33	-0.13	0.06	-0.03	0.07	0.23	0.18
34	-0.15	0.08	-0.02	0.07	0.24	0.17
35	-0.19	0.13	0.00	0.09	0.25	0.17
36	-0.23	0.20	0.00	0.10	0.33	0.18
37	-0.30	0.27	0.01	0.07	0.39	0.17
38	-0.34	0.26	0.02	0.05	0.31	0.18
39	-0.34	0.20	-0.01	0.06	0.27	0.23
40	-0.32	0.16	-0.05	0.10	0.27	0.23
41	-0.30	0.13	-0.08	0.08	0.28	0.22

42	-0.33	0.16	-0.07	0.03	0.30	0.22
43	-0.28	0.13	-0.03	0.04	0.31	0.24
44	-0.25	0.11	-0.03	0.04	0.40	0.24
45	-0.30	0.22	0.01	0.06	0.51	0.27
46	-0.30	0.24	0.00	0.05	0.23	0.17
47	-0.17	0.10	0.00	0.06	0.18	0.17
48	-0.13	0.06	0.00	0.06	0.22	0.16
49	-0.13	0.08	0.01	0.07	0.22	0.14
50	-0.13	0.10	0.02	0.08	0.23	0.16
51	-0.16	0.13	0.03	0.13	0.34	0.21
52	-0.22	0.16	0.03	0.11	0.31	0.20
53	-0.26	0.11	0.01	0.06	0.23	0.18
54	-0.29	0.16	-0.02	0.08	0.27	0.20
55	-0.30	0.15	-0.04	0.07	0.28	0.22
56	-0.32	0.17	-0.04	0.07	0.25	0.21
57	-0.33	0.23	-0.03	0.05	0.27	0.21
58	-0.23	0.11	0.00	0.03	0.32	0.23
59	-0.20	0.07	-0.01	0.04	0.43	0.24
60	-0.20	0.15	0.00	0.07	0.50	0.28
61	-0.31	0.07	-0.03	0.05	0.29	0.09
62	-0.15	0.07	0.02	0.04	0.23	0.11
63	-0.14	0.08	0.02	0.04	0.20	0.12
64	-0.16	0.10	0.00	0.05	0.19	0.12
65	-0.14	0.10	-0.01	0.06	0.24	0.13
66	-0.16	0.11	0.03	0.09	0.29	0.24
67	-0.19	0.07	0.03	0.12	0.31	0.32
68	-0.25	0.19	0.06	0.13	0.40	0.20
69	-0.18	0.11	0.04	0.09	0.33	0.16
70	-0.22	0.10	-0.04	0.07	0.29	0.19
71	-0.27	0.22	-0.05	0.07	0.28	0.19
72	-0.23	0.16	0.00	0.02	0.32	0.20
73	-0.16	0.11	0.02	0.02	0.43	0.25
74	-0.19	0.07	-0.03	0.03	0.46	0.25
75	-0.20	0.09	0.04	0.10	0.53	0.28
76	-0.28	0.10	0.01	0.10	0.25	0.11
77	-0.18	0.08	0.02	0.06	0.19	0.08
78	-0.14	0.05	0.03	0.07	0.16	0.08
79	-0.17	0.07	0.00	0.04	0.16	0.09
80	-0.19	0.08	-0.02	0.05	0.24	0.10
81	-0.24	0.12	-0.03	0.05	0.23	0.16
82	-0.34	0.15	0.00	0.11	0.29	0.17
83	-0.27	0.11	0.02	0.16	0.30	0.26
84	-0.22	0.15	0.03	0.16	0.33	0.22
85	-0.21	0.12	0.03	0.13	0.29	0.16
86	-0.17	0.12	-0.05	0.08	0.34	0.15
87	-0.15	0.06	-0.02	0.06	0.45	0.26
88	-0.17	0.07	-0.01	0.04	0.53	0.31
89	-0.16	0.05	-0.01	0.07	0.56	0.25

90	-0.21	0.10	0.00	0.13	0.50	0.29
91	-0.23	0.14	-0.01	0.09	0.29	0.08
92	-0.13	0.07	-0.02	0.07	0.16	0.06
93	-0.13	0.07	0.00	0.06	0.15	0.06
94	-0.18	0.10	0.00	0.06	0.17	0.05
95	-0.22	0.13	-0.02	0.05	0.22	0.05
96	-0.27	0.13	-0.06	0.03	0.21	0.07
97	-0.34	0.17	-0.04	0.07	0.16	0.11
98	-0.43	0.24	-0.02	0.16	0.14	0.14
99	-0.33	0.13	-0.03	0.17	0.14	0.16
100	-0.21	0.05	0.00	0.11	0.20	0.15
101	-0.17	0.06	0.00	0.08	0.31	0.16
102	-0.15	0.07	-0.03	0.07	0.48	0.29
103	-0.14	0.06	-0.01	0.05	0.51	0.27
104	-0.19	0.07	-0.02	0.12	0.53	0.28
105	-0.33	0.20	-0.08	0.12	0.35	0.34
106	-0.21	0.09	-0.04	0.09	0.21	0.12
107	-0.14	0.07	-0.03	0.05	0.20	0.05
108	-0.14	0.08	0.01	0.07	0.17	0.06
109	-0.19	0.09	0.00	0.06	0.20	0.03
110	-0.23	0.11	-0.01	0.08	0.20	0.05
111	-0.24	0.13	-0.01	0.07	0.24	0.06
112	-0.25	0.14	0.01	0.07	0.23	0.07
113	-0.29	0.09	0.00	0.08	0.16	0.10
114	-0.34	0.11	-0.06	0.10	0.15	0.12
115	-0.23	0.07	-0.06	0.08	0.21	0.15
116	-0.16	0.08	-0.03	0.06	0.28	0.16
117	-0.17	0.10	-0.01	0.07	0.38	0.20
118	-0.19	0.11	0.01	0.09	0.39	0.19
119	-0.24	0.16	0.01	0.10	0.27	0.24
120	-0.32	0.22	-0.05	0.11	0.23	0.33
121	-0.19	0.08	-0.04	0.07	0.22	0.10
122	-0.17	0.07	0.01	0.07	0.23	0.09
123	-0.16	0.08	0.02	0.08	0.23	0.11
124	-0.16	0.09	-0.01	0.08	0.25	0.10
125	-0.18	0.08	0.04	0.07	0.31	0.09
126	-0.19	0.09	0.04	0.07	0.37	0.14
127	-0.25	0.13	0.00	0.08	0.33	0.15
128	-0.23	0.09	-0.05	0.12	0.37	0.17
129	-0.20	0.10	0.00	0.08	0.32	0.17
130	-0.17	0.10	-0.01	0.06	0.30	0.17
131	-0.17	0.10	0.00	0.08	0.32	0.17
132	-0.17	0.09	0.02	0.11	0.35	0.17
133	-0.20	0.10	0.02	0.14	0.33	0.17
134	-0.27	0.18	0.01	0.15	0.26	0.22
135	-0.29	0.17	-0.05	0.16	0.26	0.29
136	-0.22	0.09	-0.03	0.09	0.27	0.13
137	-0.19	0.10	0.01	0.10	0.26	0.08

138	-0.17	0.13	0.04	0.07	0.28	0.10
139	-0.16	0.15	0.05	0.06	0.39	0.16
140	-0.21	0.12	0.05	0.06	0.42	0.19
141	-0.30	0.22	0.00	0.10	0.29	0.06
142	-0.29	0.19	0.02	0.18	0.39	0.18
143	-0.21	0.11	0.10	0.12	0.47	0.13
144	-0.19	0.12	0.14	0.13	0.52	0.18
145	-0.18	0.14	0.12	0.17	0.45	0.18
146	-0.19	0.12	0.08	0.19	0.36	0.17
147	-0.21	0.10	0.07	0.19	0.34	0.14
148	-0.22	0.09	0.04	0.20	0.32	0.15
149	-0.25	0.09	0.02	0.20	0.29	0.17
150	-0.26	0.11	-0.06	0.20	0.30	0.24
151	-0.23	0.08	-0.02	0.13	0.30	0.10
152	-0.22	0.13	0.03	0.06	0.31	0.07
153	-0.23	0.16	0.11	0.09	0.34	0.08
154	-0.24	0.16	0.11	0.08	0.41	0.17
155	-0.27	0.17	0.00	0.12	0.40	0.19
156	-0.34	0.24	-0.11	0.17	0.31	0.09
157	-0.29	0.10	-0.02	0.14	0.53	0.14
158	-0.30	0.09	0.10	0.13	0.70	0.23
159	-0.24	0.17	0.19	0.15	0.72	0.35
160	-0.21	0.23	0.19	0.16	0.53	0.18
161	-0.23	0.18	0.06	0.19	0.41	0.16
162	-0.28	0.13	0.00	0.22	0.40	0.17
163	-0.28	0.10	0.00	0.21	0.34	0.19
164	-0.27	0.08	-0.02	0.20	0.31	0.21
165	-0.26	0.09	-0.04	0.20	0.30	0.23
166	-0.28	0.19	0.01	0.14	0.26	0.23
167	-0.36	0.37	-0.04	0.11	0.23	0.22
168	-0.30	0.19	-0.03	0.08	0.42	0.28
169	-0.31	0.18	-0.02	0.07	0.44	0.26
170	-0.21	0.07	-0.02	0.10	0.26	0.11
171	-0.21	0.08	0.00	0.10	0.27	0.09
172	-0.29	0.16	-0.03	0.18	0.28	0.22
173	-0.25	0.09	0.00	0.20	0.30	0.20

---

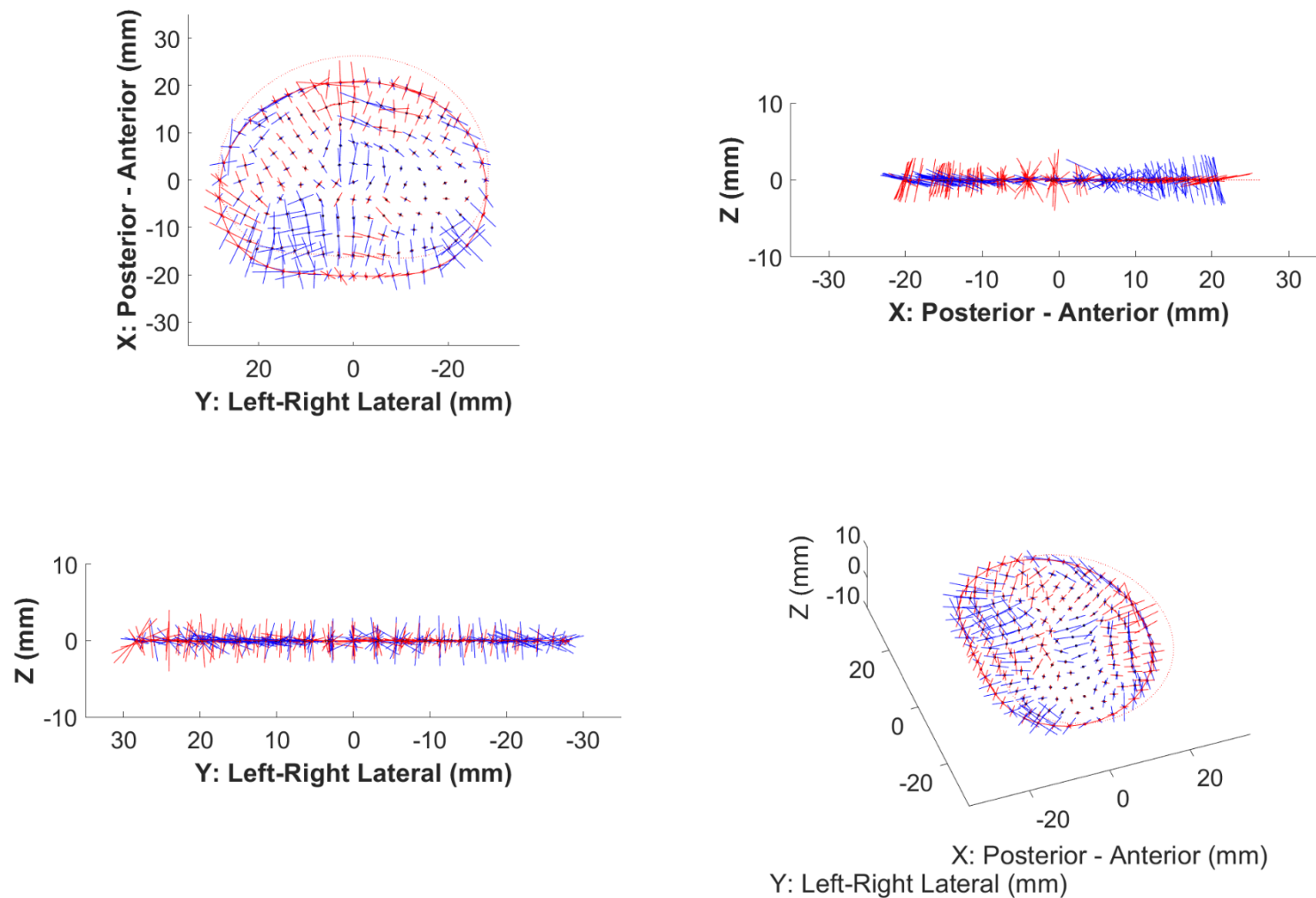


**Figure C-5** Average 3D Principal strains for cycle 10000 of the simulated safe repetitive lifting group. The blue vectors represent compressive strain and red vectors represent tensile strain. Four views are presented in this figure. Top Left: Axial View, Top Right: Lateral View, Bottom Left: Posterior View, Bottom Right: Oblique View

C.1.1.6 Cycle 15000

**Table C-6** Mean (95% CI) of 3D principal strains at each node (1 – 173) for simulated safe repetitive lifting at cycle 15000

Node	P1		P2		P3	
	Mean	95% CI	Mean	95% CI	Mean	95% CI
1	-0.26	0.19	0.02	0.12	0.40	0.20
2	-0.23	0.16	0.03	0.13	0.43	0.23
3	-0.24	0.16	0.05	0.12	0.48	0.23
4	-0.27	0.17	0.09	0.13	0.51	0.23
5	-0.26	0.19	0.14	0.14	0.53	0.25
6	-0.20	0.17	0.19	0.14	0.55	0.28
7	-0.18	0.27	0.15	0.12	0.60	0.30
8	-0.35	0.36	0.15	0.13	0.66	0.31
9	-0.23	0.17	0.23	0.23	0.59	0.31
10	-0.19	0.17	0.11	0.22	0.57	0.40
11	-0.29	0.25	0.01	0.18	0.61	0.45
12	-0.26	0.18	-0.04	0.17	0.61	0.51
13	-0.27	0.15	-0.04	0.12	0.61	0.55
14	-0.28	0.15	0.00	0.10	0.61	0.56
15	-0.29	0.19	0.03	0.10	0.60	0.56
16	-0.32	0.27	0.02	0.12	0.33	0.22
17	-0.21	0.13	0.03	0.11	0.34	0.23
18	-0.20	0.09	0.03	0.09	0.35	0.23
19	-0.22	0.07	0.05	0.09	0.39	0.24
20	-0.23	0.04	0.09	0.09	0.42	0.25
21	-0.22	0.12	0.11	0.10	0.45	0.28
22	-0.20	0.21	0.05	0.06	0.49	0.30
23	-0.23	0.26	0.02	0.06	0.48	0.33
24	-0.17	0.05	-0.01	0.08	0.45	0.38
25	-0.22	0.08	0.00	0.12	0.45	0.41
26	-0.27	0.14	-0.05	0.12	0.48	0.41
27	-0.25	0.12	-0.06	0.11	0.49	0.43
28	-0.24	0.09	-0.05	0.08	0.48	0.45
29	-0.22	0.12	-0.03	0.07	0.51	0.48
30	-0.28	0.19	0.02	0.09	0.63	0.53
31	-0.26	0.25	0.04	0.08	0.26	0.22
32	-0.20	0.18	-0.01	0.07	0.25	0.20
33	-0.13	0.05	0.00	0.05	0.29	0.18
34	-0.16	0.08	0.01	0.06	0.30	0.20
35	-0.18	0.13	0.03	0.08	0.31	0.22
36	-0.24	0.20	0.05	0.10	0.35	0.24
37	-0.31	0.27	0.01	0.08	0.37	0.25
38	-0.32	0.26	-0.01	0.07	0.35	0.29
39	-0.31	0.19	-0.03	0.06	0.36	0.32
40	-0.30	0.15	-0.03	0.08	0.37	0.34
41	-0.28	0.12	-0.05	0.05	0.38	0.34
42	-0.25	0.08	-0.04	0.04	0.40	0.36
43	-0.21	0.04	-0.03	0.04	0.42	0.39

Node	P1		P2		P3	
	Mean	95% CI	Mean	95% CI	Mean	95% CI
44	-0.19	0.09	-0.04	0.06	0.49	0.43
45	-0.25	0.16	0.00	0.08	0.60	0.50
46	-0.22	0.13	0.03	0.08	0.25	0.17
47	-0.14	0.07	0.02	0.06	0.22	0.17
48	-0.12	0.04	0.02	0.07	0.25	0.16
49	-0.14	0.07	0.03	0.09	0.25	0.17
50	-0.15	0.11	0.05	0.10	0.25	0.20
51	-0.18	0.14	0.10	0.19	0.30	0.23
52	-0.23	0.15	0.09	0.20	0.30	0.24
53	-0.25	0.11	0.02	0.09	0.28	0.26
54	-0.26	0.15	-0.02	0.07	0.33	0.28
55	-0.28	0.14	-0.03	0.07	0.34	0.30
56	-0.25	0.10	-0.02	0.07	0.33	0.30
57	-0.21	0.09	-0.01	0.06	0.35	0.32
58	-0.17	0.07	0.00	0.02	0.39	0.36
59	-0.17	0.08	-0.02	0.06	0.49	0.40
60	-0.20	0.10	0.00	0.09	0.56	0.48
61	-0.28	0.08	0.00	0.07	0.27	0.12
62	-0.14	0.06	0.05	0.06	0.22	0.11
63	-0.14	0.05	0.02	0.05	0.21	0.13
64	-0.15	0.07	0.02	0.08	0.20	0.15
65	-0.16	0.09	0.01	0.09	0.24	0.18
66	-0.16	0.11	0.07	0.12	0.29	0.26
67	-0.17	0.08	0.07	0.19	0.33	0.33
68	-0.23	0.18	0.12	0.22	0.40	0.20
69	-0.16	0.10	0.06	0.10	0.36	0.21
70	-0.19	0.08	-0.01	0.07	0.32	0.27
71	-0.20	0.07	-0.04	0.06	0.34	0.26
72	-0.17	0.07	0.01	0.03	0.36	0.29
73	-0.15	0.09	0.03	0.03	0.43	0.31
74	-0.20	0.07	-0.04	0.06	0.52	0.35
75	-0.24	0.08	0.00	0.11	0.60	0.40
76	-0.28	0.09	-0.01	0.07	0.28	0.08
77	-0.17	0.07	0.02	0.05	0.22	0.07
78	-0.13	0.05	0.03	0.06	0.18	0.09
79	-0.17	0.07	0.00	0.07	0.17	0.12
80	-0.21	0.08	-0.01	0.06	0.25	0.13
81	-0.25	0.13	-0.01	0.05	0.25	0.19
82	-0.31	0.15	0.00	0.12	0.30	0.21
83	-0.25	0.09	0.05	0.22	0.29	0.26
84	-0.20	0.14	0.06	0.18	0.35	0.23
85	-0.19	0.08	0.06	0.12	0.31	0.20
86	-0.15	0.08	-0.03	0.06	0.33	0.22
87	-0.14	0.05	-0.01	0.05	0.38	0.24
88	-0.17	0.06	-0.01	0.05	0.48	0.26
89	-0.18	0.06	-0.02	0.12	0.56	0.32
90	-0.25	0.13	0.00	0.15	0.54	0.36
91	-0.23	0.14	0.00	0.08	0.30	0.08

Node	P1		P2		P3	
	Mean	95% CI	Mean	95% CI	Mean	95% CI
92	-0.13	0.07	-0.02	0.06	0.19	0.06
93	-0.13	0.09	-0.01	0.07	0.18	0.06
94	-0.18	0.11	0.00	0.06	0.18	0.08
95	-0.23	0.13	-0.02	0.05	0.22	0.08
96	-0.29	0.13	-0.06	0.02	0.23	0.11
97	-0.34	0.15	-0.04	0.07	0.16	0.15
98	-0.42	0.24	-0.01	0.18	0.15	0.18
99	-0.32	0.12	-0.02	0.18	0.15	0.18
100	-0.21	0.07	0.00	0.11	0.21	0.19
101	-0.18	0.08	0.02	0.06	0.28	0.19
102	-0.15	0.08	-0.02	0.05	0.39	0.21
103	-0.14	0.07	-0.01	0.06	0.44	0.26
104	-0.21	0.06	-0.03	0.15	0.51	0.36
105	-0.34	0.19	-0.06	0.14	0.40	0.36
106	-0.22	0.08	-0.04	0.08	0.22	0.14
107	-0.14	0.07	-0.02	0.06	0.21	0.05
108	-0.13	0.09	0.00	0.07	0.19	0.05
109	-0.19	0.09	0.01	0.07	0.21	0.04
110	-0.23	0.12	-0.01	0.07	0.21	0.07
111	-0.24	0.13	-0.02	0.06	0.25	0.07
112	-0.25	0.13	0.00	0.07	0.22	0.08
113	-0.28	0.09	0.00	0.08	0.15	0.10
114	-0.33	0.10	-0.05	0.10	0.14	0.13
115	-0.23	0.07	-0.06	0.09	0.20	0.15
116	-0.18	0.09	-0.03	0.07	0.29	0.16
117	-0.18	0.11	-0.01	0.07	0.34	0.17
118	-0.19	0.13	0.01	0.09	0.34	0.19
119	-0.23	0.17	0.00	0.11	0.27	0.25
120	-0.32	0.23	-0.06	0.13	0.28	0.30
121	-0.22	0.09	-0.04	0.07	0.21	0.08
122	-0.17	0.08	0.00	0.07	0.22	0.06
123	-0.16	0.09	0.02	0.08	0.24	0.11
124	-0.17	0.09	-0.01	0.09	0.27	0.10
125	-0.19	0.09	0.04	0.07	0.32	0.09
126	-0.19	0.09	0.03	0.07	0.37	0.15
127	-0.24	0.14	-0.01	0.09	0.32	0.16
128	-0.22	0.10	-0.05	0.12	0.36	0.16
129	-0.20	0.10	0.01	0.08	0.29	0.16
130	-0.19	0.09	0.00	0.07	0.28	0.15
131	-0.19	0.08	0.01	0.10	0.31	0.15
132	-0.18	0.09	0.03	0.12	0.33	0.14
133	-0.22	0.12	0.02	0.15	0.31	0.15
134	-0.26	0.21	0.00	0.15	0.24	0.22
135	-0.28	0.19	-0.06	0.16	0.25	0.27
136	-0.25	0.09	-0.05	0.09	0.26	0.12
137	-0.21	0.09	-0.02	0.08	0.24	0.06
138	-0.18	0.11	0.01	0.06	0.27	0.08
139	-0.18	0.13	0.03	0.06	0.38	0.15

Node	P1		P2		P3	
	Mean	95% CI	Mean	95% CI	Mean	95% CI
140	-0.21	0.12	0.03	0.06	0.42	0.18
141	-0.29	0.24	-0.03	0.07	0.30	0.06
142	-0.29	0.21	0.01	0.15	0.39	0.17
143	-0.21	0.11	0.09	0.07	0.45	0.13
144	-0.21	0.11	0.12	0.08	0.49	0.16
145	-0.19	0.13	0.11	0.13	0.42	0.16
146	-0.21	0.11	0.07	0.17	0.35	0.15
147	-0.22	0.09	0.08	0.16	0.34	0.12
148	-0.23	0.09	0.05	0.19	0.32	0.12
149	-0.27	0.12	0.01	0.19	0.28	0.14
150	-0.26	0.13	-0.06	0.20	0.26	0.23
151	-0.25	0.08	-0.05	0.11	0.28	0.11
152	-0.25	0.09	-0.02	0.04	0.30	0.08
153	-0.25	0.12	0.04	0.10	0.33	0.08
154	-0.26	0.13	0.07	0.09	0.38	0.14
155	-0.29	0.15	-0.03	0.11	0.38	0.13
156	-0.36	0.23	-0.12	0.14	0.32	0.07
157	-0.30	0.09	-0.05	0.09	0.53	0.13
158	-0.32	0.08	0.04	0.10	0.65	0.21
159	-0.26	0.15	0.12	0.14	0.67	0.32
160	-0.24	0.18	0.15	0.14	0.51	0.17
161	-0.24	0.17	0.03	0.14	0.43	0.14
162	-0.30	0.14	0.03	0.16	0.41	0.14
163	-0.31	0.12	0.02	0.15	0.33	0.17
164	-0.29	0.10	-0.03	0.16	0.29	0.18
165	-0.27	0.11	-0.07	0.19	0.27	0.20
166	-0.23	0.15	0.02	0.13	0.34	0.22
167	-0.29	0.28	0.00	0.10	0.31	0.21
168	-0.26	0.18	-0.01	0.08	0.54	0.51
169	-0.26	0.16	-0.02	0.09	0.55	0.49
170	-0.23	0.09	-0.03	0.09	0.24	0.10
171	-0.23	0.08	-0.03	0.09	0.25	0.09
172	-0.29	0.18	-0.04	0.19	0.24	0.21
173	-0.27	0.12	-0.02	0.19	0.29	0.17

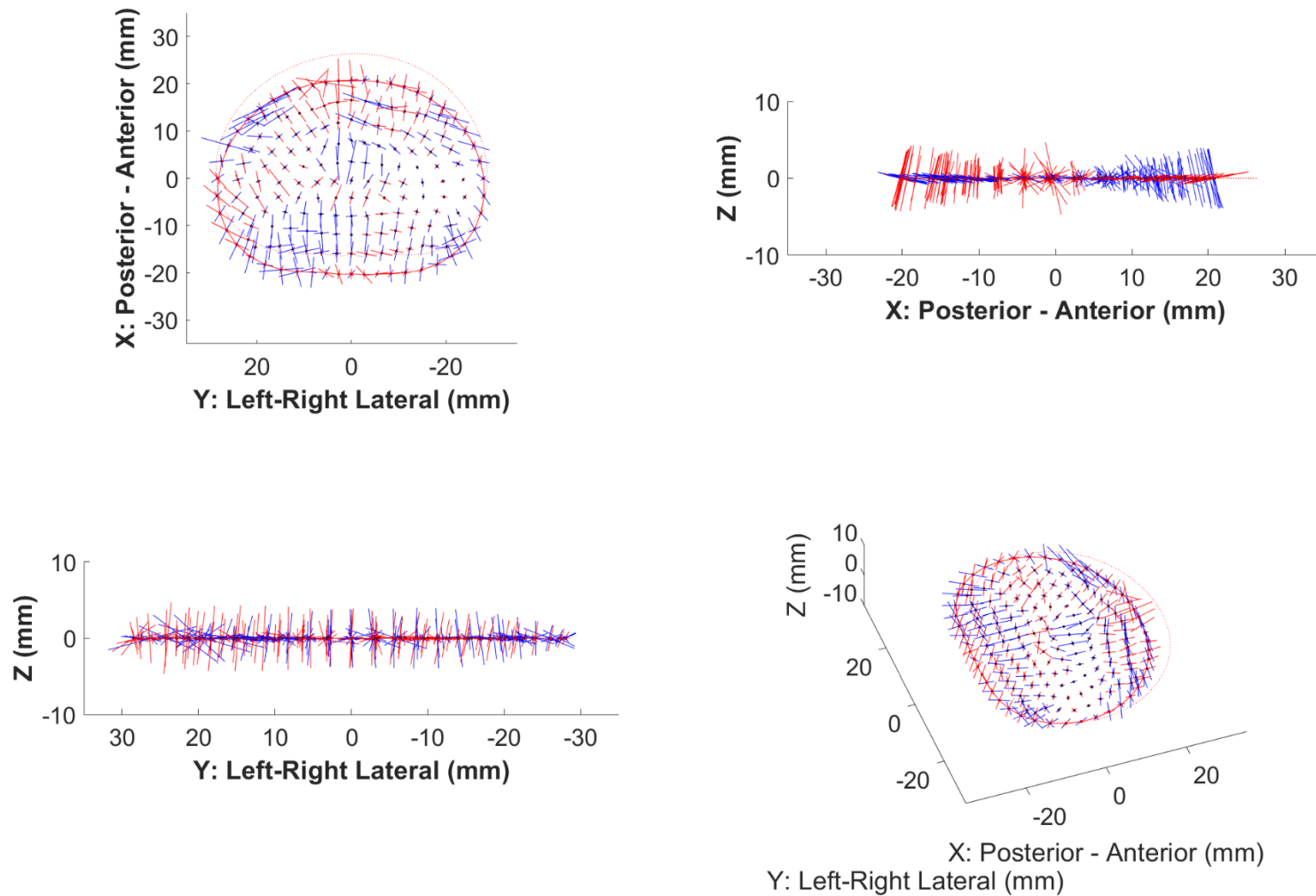


**Figure C-6** Average 3D Principal strains for cycle 15000 of the simulated safe repetitive lifting group. The blue vectors represent compressive strain and red vectors represent tensile strain. Four views are presented in this figure. Top Left: Axial View, Top Right: Lateral View, Bottom Left: Posterior View, Bottom Right: Oblique View

C.1.1.7 Cycle 20000

**Table C-7** Mean (95% CI) of 3D principal strains at each node (1 – 173) for simulated safe repetitive lifting at cycle 20000

Node	P1		P2		P3	
	Mean	95% CI	Mean	95% CI	Mean	95% CI
1	-0.29	0.21	0.04	0.12	0.47	0.26
2	-0.23	0.17	0.05	0.11	0.49	0.30
3	-0.22	0.17	0.05	0.12	0.53	0.30
4	-0.25	0.18	0.09	0.13	0.56	0.30
5	-0.27	0.20	0.12	0.11	0.58	0.31
6	-0.23	0.16	0.15	0.09	0.61	0.33
7	-0.19	0.24	0.14	0.13	0.65	0.35
8	-0.32	0.32	0.15	0.15	0.72	0.33
9	-0.29	0.22	0.20	0.22	0.64	0.35
10	-0.26	0.13	0.08	0.22	0.59	0.44
11	-0.29	0.20	-0.03	0.21	0.61	0.46
12	-0.24	0.17	-0.09	0.19	0.61	0.49
13	-0.25	0.15	-0.08	0.12	0.62	0.49
14	-0.28	0.16	-0.02	0.07	0.62	0.48
15	-0.33	0.23	0.01	0.08	0.60	0.45
16	-0.35	0.33	0.01	0.14	0.41	0.29
17	-0.21	0.14	0.03	0.10	0.40	0.30
18	-0.18	0.10	0.03	0.08	0.41	0.30
19	-0.21	0.09	0.04	0.09	0.44	0.30
20	-0.24	0.07	0.08	0.10	0.45	0.31
21	-0.23	0.14	0.09	0.09	0.51	0.33
22	-0.20	0.21	0.04	0.05	0.55	0.35
23	-0.22	0.23	0.03	0.06	0.51	0.38
24	-0.21	0.07	0.00	0.09	0.48	0.42
25	-0.23	0.09	-0.03	0.13	0.46	0.43
26	-0.26	0.14	-0.08	0.12	0.49	0.41
27	-0.23	0.12	-0.09	0.11	0.50	0.40
28	-0.22	0.10	-0.07	0.09	0.49	0.39
29	-0.22	0.12	-0.04	0.07	0.52	0.40
30	-0.36	0.26	0.00	0.10	0.59	0.40
31	-0.29	0.31	0.02	0.12	0.34	0.27
32	-0.21	0.19	-0.01	0.08	0.32	0.26
33	-0.12	0.07	-0.01	0.04	0.36	0.24
34	-0.13	0.09	-0.01	0.06	0.36	0.26
35	-0.16	0.11	0.02	0.10	0.36	0.27
36	-0.23	0.20	0.03	0.11	0.41	0.28
37	-0.31	0.28	0.00	0.08	0.43	0.29
38	-0.33	0.26	-0.01	0.06	0.39	0.32
39	-0.33	0.19	-0.02	0.07	0.38	0.35
40	-0.32	0.15	-0.03	0.08	0.37	0.36
41	-0.29	0.12	-0.05	0.06	0.39	0.34
42	-0.27	0.08	-0.05	0.05	0.42	0.32
43	-0.22	0.05	-0.03	0.07	0.44	0.32

Node	P1		P2		P3	
	Mean	95% CI	Mean	95% CI	Mean	95% CI
44	-0.23	0.10	-0.05	0.08	0.46	0.34
45	-0.32	0.27	-0.03	0.08	0.53	0.38
46	-0.26	0.21	0.04	0.10	0.33	0.21
47	-0.15	0.10	0.02	0.06	0.31	0.21
48	-0.11	0.06	0.01	0.06	0.33	0.21
49	-0.12	0.09	0.01	0.08	0.30	0.23
50	-0.11	0.11	0.03	0.12	0.28	0.25
51	-0.16	0.13	0.10	0.22	0.34	0.25
52	-0.23	0.16	0.08	0.20	0.37	0.26
53	-0.26	0.12	0.01	0.08	0.33	0.28
54	-0.27	0.14	-0.02	0.08	0.34	0.31
55	-0.30	0.13	-0.02	0.07	0.33	0.33
56	-0.28	0.09	-0.02	0.06	0.34	0.29
57	-0.24	0.09	-0.02	0.05	0.38	0.27
58	-0.20	0.05	-0.01	0.05	0.39	0.28
59	-0.21	0.10	-0.06	0.05	0.43	0.30
60	-0.29	0.19	0.00	0.09	0.48	0.36
61	-0.30	0.08	0.03	0.10	0.35	0.15
62	-0.14	0.07	0.07	0.07	0.30	0.16
63	-0.13	0.07	0.02	0.04	0.28	0.18
64	-0.16	0.08	0.01	0.07	0.24	0.21
65	-0.15	0.11	0.01	0.11	0.26	0.22
66	-0.16	0.11	0.08	0.16	0.31	0.26
67	-0.16	0.07	0.09	0.22	0.37	0.32
68	-0.24	0.16	0.13	0.22	0.42	0.22
69	-0.17	0.10	0.04	0.11	0.35	0.24
70	-0.22	0.08	-0.03	0.08	0.31	0.28
71	-0.21	0.07	-0.05	0.07	0.33	0.25
72	-0.18	0.07	0.00	0.04	0.36	0.23
73	-0.17	0.07	0.03	0.04	0.37	0.24
74	-0.23	0.09	-0.08	0.04	0.41	0.26
75	-0.29	0.11	-0.02	0.13	0.52	0.24
76	-0.27	0.09	0.00	0.07	0.36	0.09
77	-0.16	0.09	0.04	0.05	0.26	0.13
78	-0.14	0.06	0.03	0.07	0.24	0.14
79	-0.17	0.06	-0.01	0.06	0.21	0.17
80	-0.21	0.08	-0.02	0.07	0.27	0.16
81	-0.24	0.14	-0.02	0.05	0.28	0.20
82	-0.32	0.17	0.00	0.15	0.30	0.23
83	-0.26	0.09	0.06	0.22	0.28	0.28
84	-0.21	0.14	0.05	0.18	0.39	0.24
85	-0.20	0.10	0.05	0.14	0.30	0.20
86	-0.17	0.09	-0.04	0.08	0.32	0.20
87	-0.15	0.07	-0.01	0.04	0.36	0.19
88	-0.16	0.05	0.01	0.07	0.40	0.24
89	-0.21	0.02	0.01	0.07	0.49	0.25
90	-0.28	0.11	-0.03	0.16	0.48	0.21
91	-0.20	0.17	0.01	0.10	0.39	0.04

Node	P1		P2		P3	
	Mean	95% CI	Mean	95% CI	Mean	95% CI
92	-0.13	0.08	0.01	0.08	0.24	0.10
93	-0.13	0.09	-0.01	0.07	0.22	0.11
94	-0.18	0.11	-0.01	0.06	0.22	0.12
95	-0.24	0.13	-0.02	0.05	0.25	0.11
96	-0.30	0.13	-0.06	0.03	0.23	0.14
97	-0.36	0.15	-0.06	0.08	0.15	0.18
98	-0.43	0.24	-0.03	0.19	0.12	0.20
99	-0.32	0.11	-0.03	0.19	0.15	0.19
100	-0.22	0.07	0.01	0.10	0.22	0.17
101	-0.20	0.08	0.01	0.08	0.28	0.15
102	-0.18	0.09	-0.04	0.05	0.38	0.15
103	-0.16	0.08	0.01	0.02	0.41	0.20
104	-0.20	0.07	0.00	0.12	0.49	0.30
105	-0.34	0.19	-0.08	0.13	0.35	0.24
106	-0.18	0.14	-0.01	0.10	0.31	0.13
107	-0.13	0.09	0.01	0.10	0.27	0.08
108	-0.14	0.09	0.02	0.08	0.24	0.08
109	-0.20	0.09	0.01	0.07	0.25	0.07
110	-0.24	0.12	-0.01	0.07	0.23	0.08
111	-0.25	0.13	-0.03	0.04	0.25	0.09
112	-0.26	0.12	-0.01	0.07	0.21	0.11
113	-0.29	0.08	-0.02	0.10	0.13	0.12
114	-0.34	0.10	-0.07	0.11	0.13	0.14
115	-0.25	0.07	-0.08	0.10	0.20	0.14
116	-0.20	0.09	-0.04	0.08	0.28	0.14
117	-0.21	0.11	-0.03	0.08	0.33	0.13
118	-0.22	0.14	0.00	0.08	0.33	0.10
119	-0.25	0.18	0.02	0.07	0.24	0.15
120	-0.33	0.20	-0.06	0.12	0.22	0.17
121	-0.17	0.12	0.00	0.09	0.28	0.12
122	-0.16	0.09	0.04	0.10	0.27	0.11
123	-0.17	0.09	0.05	0.11	0.27	0.12
124	-0.17	0.10	-0.01	0.08	0.30	0.11
125	-0.19	0.09	0.04	0.07	0.35	0.08
126	-0.19	0.11	0.03	0.07	0.38	0.14
127	-0.25	0.14	-0.02	0.09	0.33	0.16
128	-0.22	0.09	-0.06	0.13	0.35	0.16
129	-0.21	0.11	0.00	0.06	0.28	0.14
130	-0.21	0.10	-0.03	0.07	0.28	0.13
131	-0.21	0.09	-0.03	0.09	0.31	0.13
132	-0.21	0.09	-0.01	0.12	0.32	0.12
133	-0.24	0.13	0.00	0.14	0.29	0.09
134	-0.29	0.19	0.00	0.14	0.22	0.13
135	-0.30	0.17	-0.05	0.15	0.20	0.16
136	-0.21	0.12	-0.02	0.11	0.33	0.13
137	-0.20	0.11	0.02	0.12	0.29	0.08
138	-0.18	0.13	0.05	0.09	0.30	0.09
139	-0.19	0.13	0.05	0.08	0.41	0.15

Node	P1		P2		P3	
	Mean	95% CI	Mean	95% CI	Mean	95% CI
140	-0.23	0.12	0.05	0.07	0.45	0.17
141	-0.30	0.24	-0.02	0.10	0.32	0.07
142	-0.30	0.21	-0.01	0.16	0.43	0.17
143	-0.22	0.12	0.09	0.07	0.48	0.15
144	-0.23	0.11	0.13	0.07	0.53	0.19
145	-0.22	0.12	0.10	0.10	0.46	0.18
146	-0.23	0.11	0.04	0.13	0.37	0.16
147	-0.24	0.10	0.03	0.11	0.34	0.12
148	-0.25	0.09	0.01	0.14	0.30	0.10
149	-0.28	0.10	-0.02	0.16	0.28	0.10
150	-0.28	0.11	-0.07	0.16	0.24	0.15
151	-0.22	0.12	-0.02	0.15	0.34	0.10
152	-0.22	0.16	0.04	0.09	0.34	0.08
153	-0.24	0.16	0.12	0.10	0.38	0.09
154	-0.26	0.16	0.14	0.10	0.42	0.15
155	-0.31	0.14	0.02	0.11	0.39	0.14
156	-0.39	0.21	-0.09	0.19	0.32	0.12
157	-0.32	0.09	-0.04	0.10	0.56	0.13
158	-0.33	0.09	0.10	0.16	0.70	0.21
159	-0.28	0.14	0.19	0.18	0.73	0.35
160	-0.27	0.17	0.17	0.10	0.56	0.20
161	-0.27	0.17	0.03	0.09	0.41	0.14
162	-0.31	0.13	0.00	0.12	0.36	0.13
163	-0.31	0.11	-0.02	0.12	0.31	0.14
164	-0.31	0.10	-0.05	0.12	0.29	0.14
165	-0.30	0.10	-0.07	0.14	0.26	0.14
166	-0.24	0.16	0.03	0.13	0.42	0.29
167	-0.32	0.34	0.00	0.10	0.38	0.28
168	-0.28	0.19	-0.02	0.08	0.56	0.40
169	-0.32	0.20	-0.03	0.10	0.54	0.38
170	-0.20	0.11	-0.01	0.12	0.30	0.12
171	-0.21	0.11	0.00	0.12	0.31	0.09
172	-0.32	0.16	-0.05	0.16	0.22	0.12
173	-0.29	0.10	-0.04	0.16	0.28	0.10

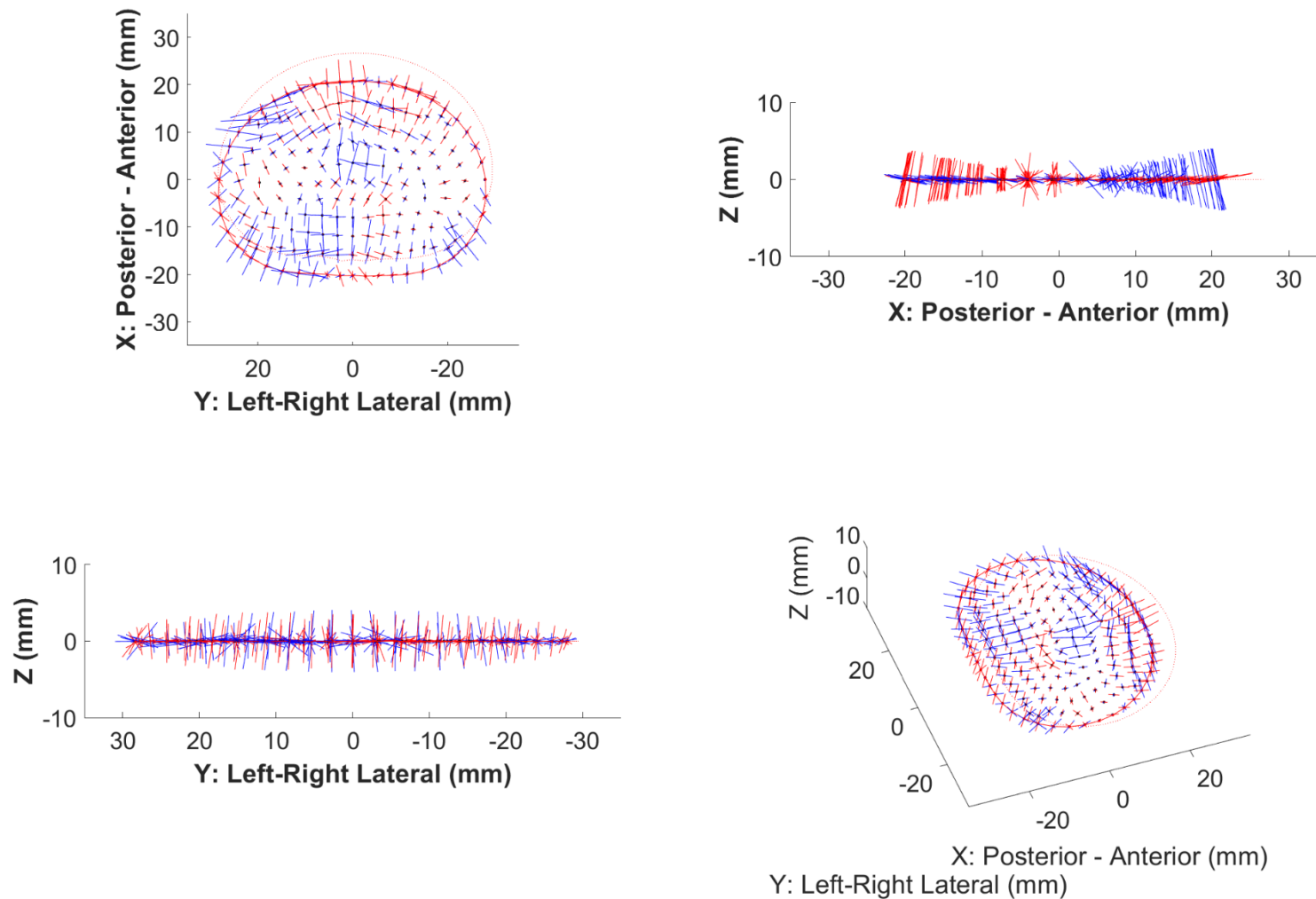


**Figure C-7** Average 3D Principal strains for cycle 20000 of the simulated safe repetitive lifting group. The blue vectors represent compressive strain and red vectors represent tensile strain. Four views are presented in this figure. Top Left: Axial View, Top Right: Lateral View, Bottom Left: Posterior View, Bottom Right: Oblique View

## C.1.2 Simulated unsafe repetitive lifting

### C.1.2.1 Cycle 1

**Table C-8** Mean (95% CI) of 3D principal strains at each node (1 – 173) for simulated unsafe repetitive lifting at cycle 1

Node	P1		P2		P3	
	Mean	95% CI	Mean	95% CI	Mean	95% CI
1	-0.45	0.24	0.06	0.11	0.34	0.07
2	-0.40	0.17	-0.04	0.13	0.38	0.09
3	-0.41	0.16	-0.06	0.11	0.42	0.08
4	-0.44	0.19	-0.03	0.07	0.43	0.07
5	-0.48	0.21	0.06	0.11	0.48	0.09
6	-0.54	0.28	0.11	0.11	0.58	0.28
7	-0.59	0.42	0.14	0.08	0.57	0.22
8	-0.75	0.47	0.20	0.06	0.54	0.17
9	-0.70	0.35	0.20	0.13	0.49	0.18
10	-0.42	0.16	0.20	0.10	0.46	0.13
11	-0.39	0.16	0.15	0.09	0.46	0.11
12	-0.36	0.17	0.10	0.08	0.45	0.11
13	-0.33	0.17	0.08	0.14	0.45	0.11
14	-0.34	0.18	0.07	0.15	0.48	0.16
15	-0.36	0.20	0.08	0.11	0.50	0.24
16	-0.49	0.31	0.11	0.08	0.33	0.08
17	-0.33	0.16	-0.03	0.07	0.31	0.09
18	-0.25	0.10	-0.02	0.06	0.37	0.17
19	-0.28	0.08	0.04	0.06	0.36	0.11
20	-0.32	0.09	0.10	0.08	0.36	0.07
21	-0.33	0.13	0.14	0.10	0.35	0.08
22	-0.35	0.20	0.14	0.10	0.37	0.08
23	-0.38	0.21	0.14	0.09	0.37	0.10
24	-0.36	0.22	0.09	0.10	0.36	0.13
25	-0.31	0.16	0.09	0.10	0.35	0.11
26	-0.27	0.13	0.08	0.06	0.35	0.09
27	-0.23	0.13	0.06	0.07	0.34	0.10
28	-0.22	0.13	0.06	0.12	0.34	0.10
29	-0.26	0.14	0.08	0.14	0.37	0.13
30	-0.39	0.24	0.08	0.09	0.47	0.29
31	-0.40	0.23	0.07	0.08	0.29	0.08
32	-0.39	0.28	0.05	0.06	0.23	0.08

Node	P1		P2		P3	
	Mean	95% CI	Mean	95% CI	Mean	95% CI
33	-0.24	0.18	0.04	0.05	0.29	0.14
34	-0.13	0.06	0.03	0.06	0.38	0.29
35	-0.19	0.07	0.07	0.05	0.28	0.08
36	-0.21	0.08	0.09	0.08	0.28	0.09
37	-0.17	0.09	0.09	0.08	0.33	0.12
38	-0.15	0.13	0.07	0.06	0.34	0.14
39	-0.18	0.10	0.05	0.08	0.32	0.13
40	-0.22	0.08	0.07	0.07	0.30	0.10
41	-0.20	0.07	0.09	0.05	0.29	0.09
42	-0.14	0.08	0.05	0.04	0.28	0.10
43	-0.17	0.12	0.04	0.08	0.29	0.10
44	-0.32	0.21	0.03	0.06	0.34	0.16
45	-0.48	0.35	0.03	0.07	0.44	0.26
46	-0.26	0.10	0.07	0.06	0.28	0.11
47	-0.26	0.16	0.05	0.03	0.20	0.07
48	-0.27	0.34	0.09	0.04	0.19	0.08
49	-0.15	0.12	0.07	0.06	0.23	0.11
50	-0.15	0.07	0.05	0.04	0.28	0.18
51	-0.20	0.09	0.02	0.05	0.21	0.09
52	-0.21	0.18	0.02	0.08	0.22	0.09
53	-0.18	0.18	0.05	0.07	0.28	0.10
54	-0.19	0.12	0.04	0.06	0.26	0.10
55	-0.19	0.08	0.04	0.05	0.24	0.09
56	-0.16	0.07	0.05	0.05	0.24	0.09
57	-0.11	0.07	0.04	0.03	0.26	0.09
58	-0.12	0.09	0.03	0.05	0.27	0.10
59	-0.34	0.25	0.02	0.05	0.32	0.11
60	-0.56	0.42	0.06	0.05	0.37	0.17
61	-0.30	0.24	0.07	0.05	0.36	0.17
62	-0.14	0.09	0.08	0.04	0.22	0.10
63	-0.09	0.04	0.06	0.06	0.20	0.11
64	-0.15	0.15	0.04	0.06	0.17	0.09
65	-0.16	0.09	0.04	0.04	0.18	0.08
66	-0.21	0.09	0.03	0.05	0.19	0.09
67	-0.23	0.16	0.04	0.06	0.20	0.08
68	-0.18	0.23	0.06	0.05	0.34	0.08
69	-0.21	0.17	0.03	0.08	0.21	0.07

Node	P1		P2		P3	
	Mean	95% CI	Mean	95% CI	Mean	95% CI
70	-0.17	0.09	-0.02	0.04	0.19	0.09
71	-0.14	0.06	0.02	0.04	0.21	0.08
72	-0.10	0.04	0.04	0.04	0.23	0.09
73	-0.12	0.06	0.03	0.02	0.29	0.10
74	-0.25	0.19	0.03	0.05	0.34	0.12
75	-0.42	0.31	0.06	0.08	0.37	0.21
76	-0.21	0.11	0.04	0.05	0.28	0.11
77	-0.04	0.05	0.04	0.05	0.27	0.11
78	-0.04	0.03	0.04	0.05	0.19	0.10
79	-0.09	0.08	0.04	0.04	0.17	0.07
80	-0.11	0.07	0.05	0.05	0.15	0.07
81	-0.17	0.06	0.03	0.05	0.22	0.08
82	-0.22	0.09	0.00	0.05	0.28	0.12
83	-0.19	0.07	0.00	0.05	0.27	0.11
84	-0.26	0.07	0.02	0.05	0.22	0.07
85	-0.21	0.06	-0.02	0.05	0.17	0.07
86	-0.13	0.04	0.02	0.05	0.20	0.09
87	-0.09	0.03	0.03	0.04	0.22	0.09
88	-0.09	0.03	0.00	0.02	0.26	0.09
89	-0.20	0.06	0.04	0.06	0.31	0.12
90	-0.28	0.13	0.04	0.07	0.32	0.14
91	-0.13	0.06	0.03	0.07	0.23	0.06
92	-0.06	0.05	0.05	0.06	0.22	0.09
93	-0.06	0.07	0.04	0.04	0.16	0.07
94	-0.07	0.04	0.04	0.03	0.19	0.08
95	-0.09	0.05	0.04	0.03	0.24	0.17
96	-0.18	0.15	0.02	0.04	0.19	0.06
97	-0.27	0.15	0.00	0.03	0.24	0.12
98	-0.31	0.09	-0.04	0.04	0.15	0.07
99	-0.22	0.08	-0.06	0.03	0.17	0.06
100	-0.14	0.04	-0.01	0.04	0.17	0.05
101	-0.12	0.03	0.02	0.04	0.22	0.08
102	-0.09	0.03	0.04	0.05	0.22	0.07
103	-0.09	0.05	0.02	0.05	0.21	0.07
104	-0.14	0.06	0.01	0.06	0.26	0.07
105	-0.24	0.08	-0.02	0.05	0.31	0.11
106	-0.14	0.05	0.02	0.06	0.24	0.10
107	-0.09	0.05	0.06	0.06	0.17	0.05

Node	P1		P2		P3	
	Mean	95% CI	Mean	95% CI	Mean	95% CI
108	-0.10	0.06	0.03	0.05	0.16	0.05
109	-0.08	0.05	0.04	0.04	0.26	0.18
110	-0.11	0.05	0.04	0.04	0.27	0.15
111	-0.23	0.22	0.04	0.04	0.19	0.04
112	-0.23	0.16	0.03	0.04	0.15	0.03
113	-0.16	0.05	-0.02	0.06	0.17	0.08
114	-0.14	0.05	0.02	0.05	0.18	0.08
115	-0.12	0.04	0.03	0.03	0.23	0.06
116	-0.11	0.04	0.03	0.05	0.24	0.06
117	-0.09	0.04	0.04	0.05	0.21	0.06
118	-0.09	0.06	0.03	0.05	0.19	0.07
119	-0.13	0.06	0.03	0.09	0.22	0.11
120	-0.18	0.07	-0.02	0.08	0.22	0.08
121	-0.15	0.08	0.03	0.07	0.23	0.14
122	-0.13	0.08	0.04	0.06	0.16	0.05
123	-0.13	0.07	0.03	0.05	0.14	0.05
124	-0.13	0.06	0.05	0.05	0.17	0.05
125	-0.15	0.07	0.05	0.05	0.25	0.12
126	-0.13	0.06	0.05	0.05	0.22	0.08
127	-0.13	0.07	0.05	0.06	0.20	0.07
128	-0.13	0.06	0.05	0.06	0.25	0.10
129	-0.12	0.06	0.04	0.07	0.27	0.11
130	-0.11	0.06	0.05	0.06	0.27	0.08
131	-0.10	0.06	0.06	0.06	0.23	0.06
132	-0.09	0.06	0.05	0.07	0.22	0.08
133	-0.10	0.06	0.03	0.07	0.21	0.11
134	-0.14	0.07	0.03	0.08	0.21	0.09
135	-0.24	0.11	-0.01	0.08	0.22	0.10
136	-0.16	0.09	0.02	0.08	0.23	0.16
137	-0.18	0.08	-0.01	0.06	0.19	0.08
138	-0.16	0.08	0.01	0.07	0.19	0.04
139	-0.15	0.09	0.02	0.06	0.22	0.04
140	-0.15	0.09	0.04	0.05	0.20	0.04
141	-0.15	0.10	0.02	0.06	0.23	0.05
142	-0.18	0.11	-0.01	0.07	0.27	0.06
143	-0.20	0.09	-0.03	0.07	0.23	0.09
144	-0.19	0.09	0.02	0.05	0.17	0.06

Node	P1		P2		P3	
	Mean	95% CI	Mean	95% CI	Mean	95% CI
145	-0.17	0.09	0.00	0.06	0.25	0.05
146	-0.15	0.08	0.01	0.06	0.26	0.06
147	-0.14	0.08	0.01	0.07	0.25	0.09
148	-0.12	0.10	-0.01	0.08	0.24	0.09
149	-0.16	0.11	-0.02	0.09	0.19	0.07
150	-0.42	0.42	-0.02	0.07	0.20	0.06
151	-0.18	0.09	-0.01	0.06	0.22	0.13
152	-0.20	0.09	-0.05	0.09	0.22	0.10
153	-0.22	0.10	-0.02	0.07	0.25	0.10
154	-0.22	0.10	0.02	0.07	0.31	0.11
155	-0.23	0.10	0.04	0.08	0.32	0.08
156	-0.25	0.11	0.01	0.05	0.31	0.08
157	-0.29	0.14	-0.06	0.13	0.40	0.17
158	-0.38	0.14	-0.06	0.08	0.26	0.19
159	-0.37	0.10	-0.06	0.12	0.23	0.14
160	-0.31	0.07	-0.05	0.09	0.25	0.11
161	-0.27	0.09	-0.05	0.06	0.26	0.10
162	-0.23	0.11	-0.06	0.08	0.28	0.09
163	-0.20	0.13	-0.04	0.10	0.26	0.11
164	-0.21	0.14	-0.02	0.10	0.21	0.09
165	-0.29	0.23	-0.03	0.07	0.16	0.10
166	-0.41	0.25	0.04	0.06	0.30	0.08
167	-0.46	0.28	0.10	0.07	0.30	0.07
168	-0.31	0.17	0.08	0.12	0.43	0.19
169	-0.34	0.22	0.08	0.09	0.42	0.22
170	-0.16	0.09	0.02	0.07	0.22	0.15
171	-0.17	0.08	-0.01	0.06	0.20	0.12
172	-0.28	0.22	-0.02	0.08	0.19	0.06
173	-0.26	0.20	-0.03	0.09	0.17	0.10

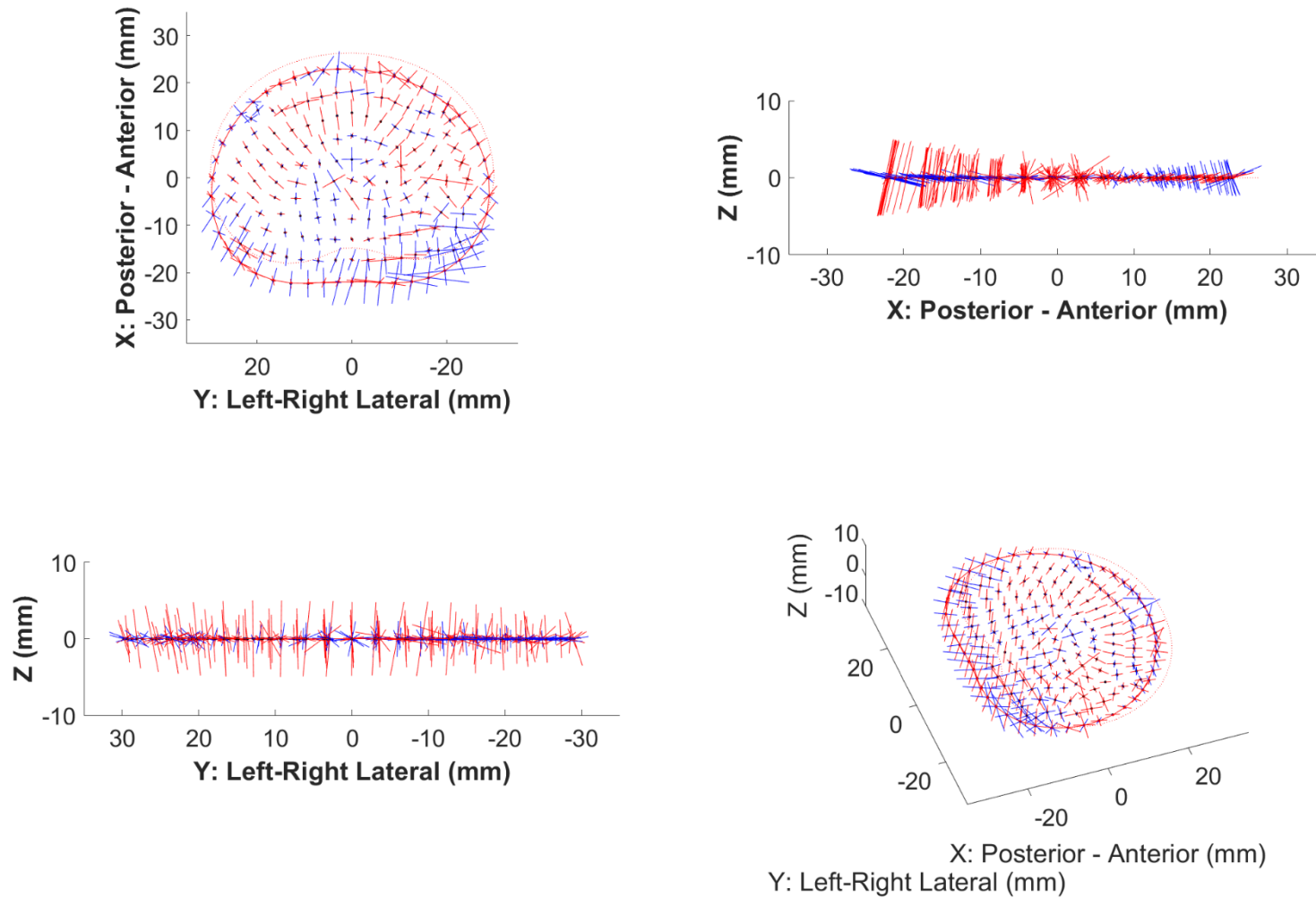


**Figure C-8** Average 3D Principal strains for cycle 1 of the simulated unsafe repetitive lifting group. The blue vectors represent compressive strain and red vectors represent tensile strain. Four views are presented in this figure. Top Left: Axial View, Top Right: Lateral View, Bottom Left: Posterior View, Bottom Right: Oblique View

C.1.2.2 Failure

**Table C-9** Mean (95% CI) of 3D principal strains at each node (1 – 173) for simulated unsafe repetitive lifting at failure

Node	P1		P2		P3	
	Mean	95% CI	Mean	95% CI	Mean	95% CI
1	-0.48	0.26	0.05	0.08	0.30	0.10
2	-0.42	0.20	0.06	0.07	0.31	0.11
3	-0.39	0.20	0.05	0.06	0.32	0.13
4	-0.41	0.19	0.05	0.05	0.34	0.11
5	-0.44	0.19	0.06	0.09	0.38	0.12
6	-0.54	0.24	0.06	0.11	0.44	0.18
7	-0.57	0.44	0.05	0.08	0.45	0.09
8	-0.65	0.48	0.09	0.09	0.45	0.18
9	-0.55	0.33	0.08	0.11	0.40	0.13
10	-0.32	0.15	0.10	0.09	0.34	0.12
11	-0.30	0.20	0.07	0.07	0.34	0.08
12	-0.27	0.18	0.05	0.07	0.35	0.07
13	-0.25	0.17	0.07	0.08	0.33	0.07
14	-0.26	0.15	0.09	0.11	0.37	0.10
15	-0.28	0.13	0.10	0.11	0.45	0.19
16	-0.53	0.34	0.04	0.09	0.30	0.09
17	-0.35	0.20	0.03	0.06	0.31	0.11
18	-0.25	0.13	0.05	0.06	0.33	0.18
19	-0.27	0.10	0.06	0.07	0.30	0.14
20	-0.30	0.09	0.06	0.07	0.29	0.10
21	-0.32	0.11	0.04	0.07	0.33	0.10
22	-0.31	0.16	0.04	0.07	0.34	0.06
23	-0.35	0.16	0.04	0.09	0.32	0.11
24	-0.40	0.26	0.03	0.07	0.30	0.10
25	-0.30	0.12	0.02	0.07	0.26	0.10
26	-0.25	0.15	0.04	0.06	0.26	0.07
27	-0.22	0.13	0.06	0.08	0.25	0.06
28	-0.19	0.12	0.06	0.08	0.27	0.05
29	-0.20	0.11	0.09	0.10	0.32	0.08
30	-0.32	0.15	0.12	0.07	0.51	0.29
31	-0.38	0.24	0.01	0.11	0.26	0.12
32	-0.40	0.26	0.04	0.09	0.23	0.10
33	-0.25	0.16	0.05	0.08	0.29	0.18
34	-0.15	0.07	0.06	0.10	0.32	0.29
35	-0.19	0.07	0.05	0.08	0.21	0.08
36	-0.21	0.08	0.01	0.07	0.25	0.11
37	-0.18	0.07	0.02	0.06	0.28	0.16
38	-0.21	0.10	0.02	0.06	0.30	0.14
39	-0.28	0.08	0.01	0.09	0.25	0.09
40	-0.29	0.05	0.01	0.07	0.22	0.11
41	-0.28	0.06	0.03	0.07	0.22	0.10
42	-0.22	0.09	0.03	0.07	0.22	0.10

Node	P1		P2		P3	
	Mean	95% CI	Mean	95% CI	Mean	95% CI
43	-0.20	0.13	0.04	0.06	0.22	0.09
44	-0.26	0.13	0.01	0.09	0.33	0.07
45	-0.44	0.28	0.03	0.10	0.53	0.25
46	-0.22	0.12	0.05	0.11	0.26	0.11
47	-0.23	0.13	0.01	0.08	0.22	0.08
48	-0.28	0.31	0.02	0.10	0.23	0.11
49	-0.19	0.12	0.01	0.09	0.22	0.14
50	-0.20	0.08	0.02	0.11	0.22	0.16
51	-0.24	0.11	-0.04	0.06	0.17	0.08
52	-0.23	0.16	-0.04	0.10	0.17	0.09
53	-0.24	0.17	0.02	0.11	0.21	0.09
54	-0.26	0.11	0.00	0.08	0.16	0.10
55	-0.27	0.07	-0.02	0.07	0.17	0.11
56	-0.25	0.05	-0.01	0.08	0.18	0.12
57	-0.21	0.09	0.03	0.08	0.19	0.13
58	-0.23	0.17	0.03	0.05	0.22	0.12
59	-0.53	0.40	0.02	0.06	0.28	0.07
60	-0.79	0.58	0.06	0.04	0.34	0.13
61	-0.30	0.18	0.07	0.10	0.33	0.10
62	-0.15	0.10	0.04	0.06	0.24	0.07
63	-0.13	0.07	0.02	0.08	0.24	0.10
64	-0.20	0.15	-0.05	0.09	0.18	0.10
65	-0.23	0.11	-0.04	0.09	0.13	0.08
66	-0.30	0.14	-0.03	0.11	0.14	0.07
67	-0.28	0.17	0.01	0.08	0.16	0.09
68	-0.25	0.22	0.02	0.10	0.27	0.14
69	-0.26	0.17	-0.04	0.11	0.17	0.08
70	-0.21	0.11	-0.08	0.07	0.15	0.10
71	-0.19	0.06	-0.02	0.06	0.16	0.13
72	-0.17	0.07	0.03	0.11	0.18	0.10
73	-0.18	0.07	-0.01	0.07	0.33	0.12
74	-0.34	0.15	-0.03	0.07	0.42	0.19
75	-0.67	0.40	0.00	0.10	0.43	0.26
76	-0.25	0.09	0.06	0.08	0.31	0.10
77	-0.13	0.10	0.09	0.06	0.29	0.10
78	-0.13	0.09	0.05	0.08	0.23	0.10
79	-0.17	0.10	-0.01	0.09	0.15	0.09
80	-0.22	0.11	-0.05	0.09	0.11	0.10
81	-0.32	0.10	-0.01	0.09	0.13	0.11
82	-0.28	0.10	-0.01	0.08	0.28	0.25
83	-0.22	0.11	-0.03	0.10	0.22	0.19
84	-0.34	0.18	-0.04	0.11	0.15	0.06
85	-0.24	0.07	-0.06	0.09	0.13	0.08
86	-0.19	0.07	-0.03	0.07	0.17	0.12
87	-0.17	0.08	0.00	0.08	0.19	0.10
88	-0.13	0.07	-0.02	0.07	0.32	0.12
89	-0.18	0.10	-0.04	0.10	0.46	0.30

Node	P1		P2		P3	
	Mean	95% CI	Mean	95% CI	Mean	95% CI
90	-0.31	0.13	0.01	0.08	0.45	0.35
91	-0.21	0.10	0.06	0.06	0.31	0.09
92	-0.15	0.11	0.08	0.06	0.27	0.07
93	-0.15	0.11	0.06	0.08	0.21	0.09
94	-0.16	0.11	0.01	0.09	0.19	0.14
95	-0.21	0.10	-0.03	0.10	0.19	0.18
96	-0.32	0.17	-0.05	0.07	0.14	0.10
97	-0.38	0.15	-0.05	0.07	0.21	0.16
98	-0.35	0.15	-0.08	0.10	0.15	0.06
99	-0.27	0.12	-0.09	0.08	0.12	0.06
100	-0.23	0.10	-0.04	0.08	0.14	0.06
101	-0.20	0.10	-0.03	0.09	0.21	0.11
102	-0.18	0.09	-0.01	0.07	0.23	0.10
103	-0.15	0.08	0.01	0.05	0.28	0.12
104	-0.14	0.08	0.02	0.05	0.34	0.13
105	-0.25	0.11	0.00	0.08	0.43	0.28
106	-0.20	0.14	0.05	0.06	0.29	0.10
107	-0.15	0.13	0.07	0.07	0.25	0.07
108	-0.16	0.12	0.05	0.07	0.24	0.08
109	-0.18	0.12	0.03	0.09	0.30	0.24
110	-0.21	0.12	0.00	0.06	0.23	0.16
111	-0.33	0.22	-0.02	0.06	0.16	0.05
112	-0.32	0.18	-0.05	0.07	0.15	0.02
113	-0.23	0.14	-0.04	0.06	0.11	0.08
114	-0.20	0.13	-0.03	0.06	0.15	0.07
115	-0.19	0.12	0.00	0.06	0.21	0.07
116	-0.20	0.12	-0.01	0.08	0.24	0.10
117	-0.21	0.14	-0.01	0.08	0.25	0.11
118	-0.19	0.09	0.03	0.07	0.28	0.17
119	-0.19	0.08	0.09	0.07	0.29	0.15
120	-0.26	0.11	0.00	0.08	0.34	0.15
121	-0.19	0.17	0.05	0.05	0.29	0.08
122	-0.17	0.15	0.06	0.04	0.26	0.06
123	-0.18	0.14	0.05	0.06	0.26	0.05
124	-0.19	0.14	0.05	0.06	0.25	0.06
125	-0.23	0.14	0.06	0.05	0.31	0.14
126	-0.21	0.15	0.04	0.05	0.28	0.11
127	-0.19	0.16	0.03	0.07	0.24	0.05
128	-0.20	0.15	0.01	0.07	0.26	0.07
129	-0.20	0.14	0.01	0.06	0.26	0.08
130	-0.17	0.15	0.03	0.04	0.27	0.07
131	-0.19	0.15	0.03	0.05	0.26	0.07
132	-0.26	0.22	0.00	0.08	0.26	0.08
133	-0.25	0.16	0.02	0.08	0.25	0.10
134	-0.27	0.12	0.08	0.07	0.28	0.12
135	-0.33	0.13	-0.01	0.11	0.40	0.25
136	-0.22	0.19	0.05	0.05	0.29	0.09

Node	P1		P2		P3	
	Mean	95% CI	Mean	95% CI	Mean	95% CI
137	-0.22	0.18	0.03	0.06	0.27	0.06
138	-0.23	0.16	0.04	0.06	0.28	0.09
139	-0.24	0.16	0.05	0.03	0.34	0.11
140	-0.20	0.17	0.07	0.03	0.32	0.09
141	-0.19	0.19	0.05	0.05	0.33	0.12
142	-0.22	0.18	0.02	0.07	0.40	0.11
143	-0.24	0.17	0.01	0.05	0.33	0.09
144	-0.26	0.16	0.03	0.05	0.27	0.07
145	-0.23	0.16	0.02	0.06	0.32	0.08
146	-0.21	0.16	0.05	0.05	0.35	0.08
147	-0.21	0.15	-0.01	0.08	0.33	0.08
148	-0.29	0.22	-0.04	0.11	0.30	0.08
149	-0.33	0.21	-0.02	0.11	0.25	0.09
150	-0.51	0.40	0.00	0.14	0.32	0.11
151	-0.28	0.21	0.03	0.06	0.30	0.08
152	-0.30	0.20	-0.01	0.12	0.33	0.10
153	-0.28	0.20	0.01	0.09	0.37	0.13
154	-0.26	0.21	0.07	0.04	0.44	0.19
155	-0.26	0.21	0.11	0.09	0.43	0.18
156	-0.28	0.20	0.10	0.07	0.43	0.14
157	-0.32	0.18	0.01	0.08	0.57	0.18
158	-0.39	0.18	-0.03	0.05	0.44	0.18
159	-0.35	0.17	-0.03	0.06	0.30	0.17
160	-0.35	0.17	0.00	0.06	0.33	0.14
161	-0.33	0.17	0.01	0.05	0.43	0.13
162	-0.28	0.18	0.02	0.07	0.45	0.06
163	-0.26	0.19	-0.01	0.06	0.40	0.13
164	-0.30	0.20	-0.04	0.12	0.30	0.17
165	-0.42	0.28	-0.03	0.16	0.21	0.17
166	-0.44	0.27	0.05	0.07	0.31	0.08
167	-0.50	0.30	0.05	0.09	0.26	0.09
168	-0.23	0.11	0.12	0.10	0.38	0.12
169	-0.27	0.15	0.09	0.09	0.48	0.25
170	-0.22	0.18	0.06	0.05	0.28	0.07
171	-0.23	0.18	0.05	0.04	0.29	0.08
172	-0.39	0.21	-0.01	0.15	0.25	0.08
173	-0.43	0.31	-0.01	0.12	0.21	0.14

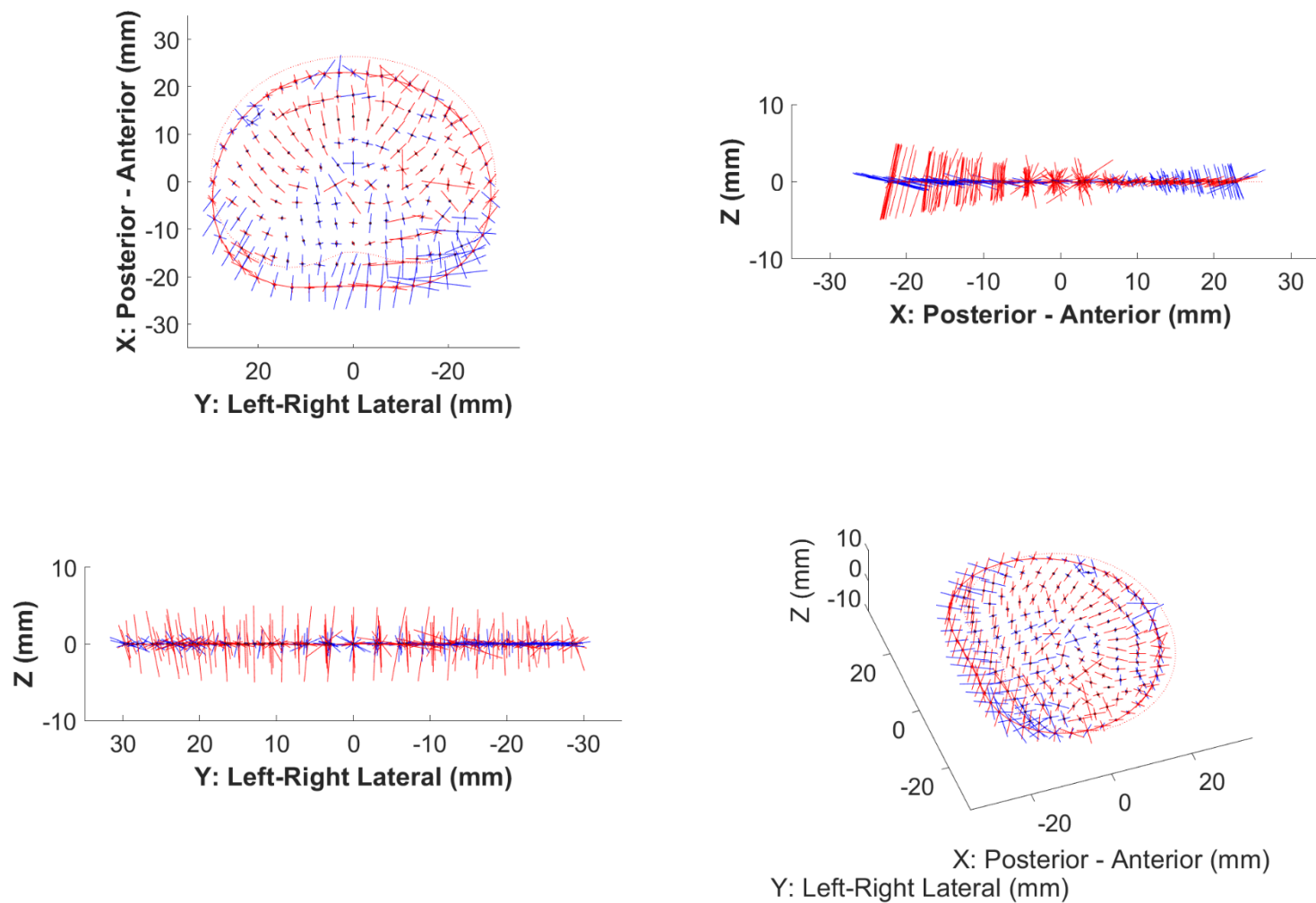


**Figure C-9** Average 3D Principal strains for failure of the simulated unsafe repetitive lifting group. The blue vectors represent compressive strain and red vectors represent tensile strain. Four views are presented in this figure. Top Left: Axial View, Top Right: Lateral View, Bottom Left: Posterior View, Bottom Right: Oblique View

# Appendix D

## D.1 Maximum shear strain plots for individual specimens for both simulated repetitive lifting groups

### D.1.1 Simulated safe repetitive lifting

**Table D-1** Specimen characteristics (failure mode, level, grade, and applied cycles) for the simulated safe repetitive lifting cohort that underwent strain measurement. This table provides a cross-reference for the images presented in this section (D.1.1)

Specimen Number	Failure Mode	Level	Pfarrmann Grade	Applied Cycles
1	Endplate Failure	L4-5	3	500
2	Disc Protrusion	L4-5	2	20,000
3	Disc Protrusion	L4-5	2	20,000
4	No Injury	L2-3	2	20,000
5	Disc Protrusion	L4-5	2	20,000
6	Endplate Failure	L1-2	2	5,000
7	Disc Protrusion	L1-2	3	20,000
8	LDH	L4-5	3	20,000

#### D.1.1.1 Specimen 1

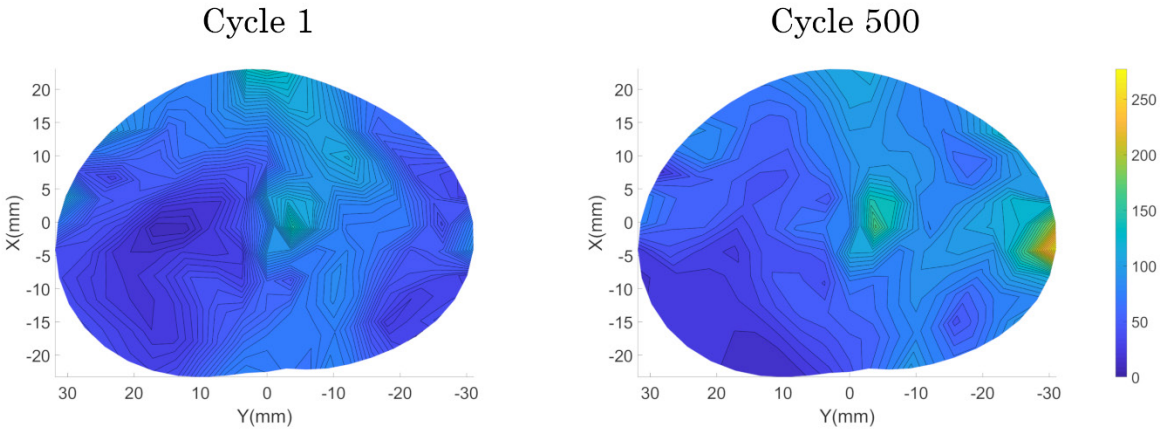


**Figure D-1** Contour plots showing MSS (%) at each of the cycle time points until failure for specimen 1

D.1.1.2 Specimen 2

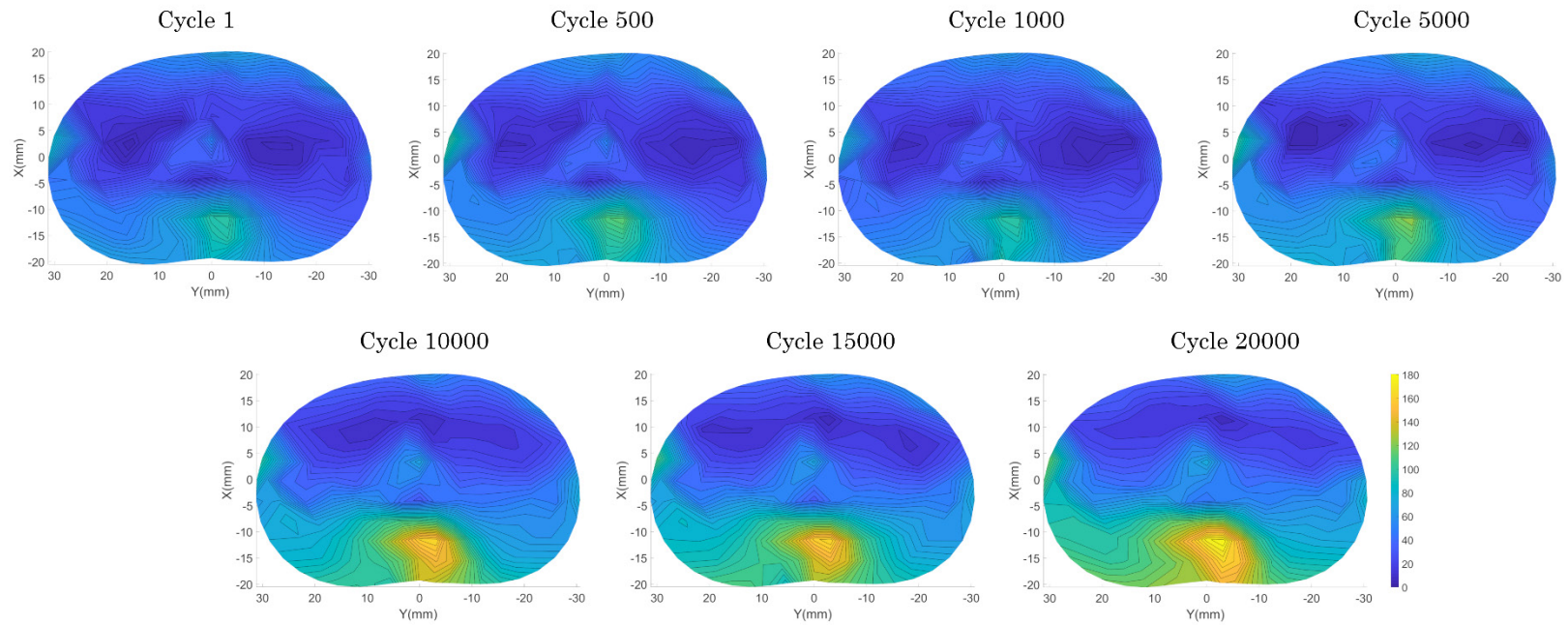


**Figure D-2** Contour plots showing MSS (%) at each of the cycle time points until failure for specimen 2

### D.1.1.3 Specimen 3

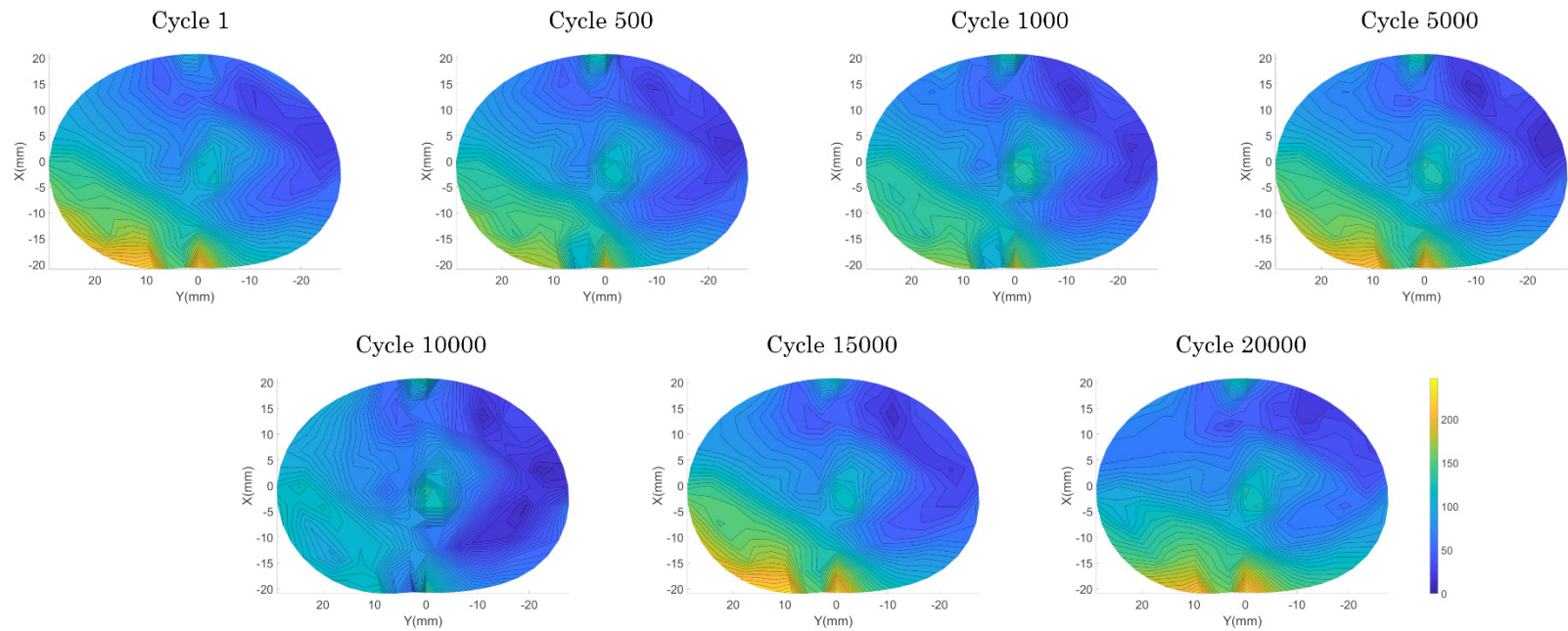


**Figure D-3** Contour plots showing MSS (%) at each of the cycle time points until failure for specimen 3

#### D.1.1.4 Specimen 4

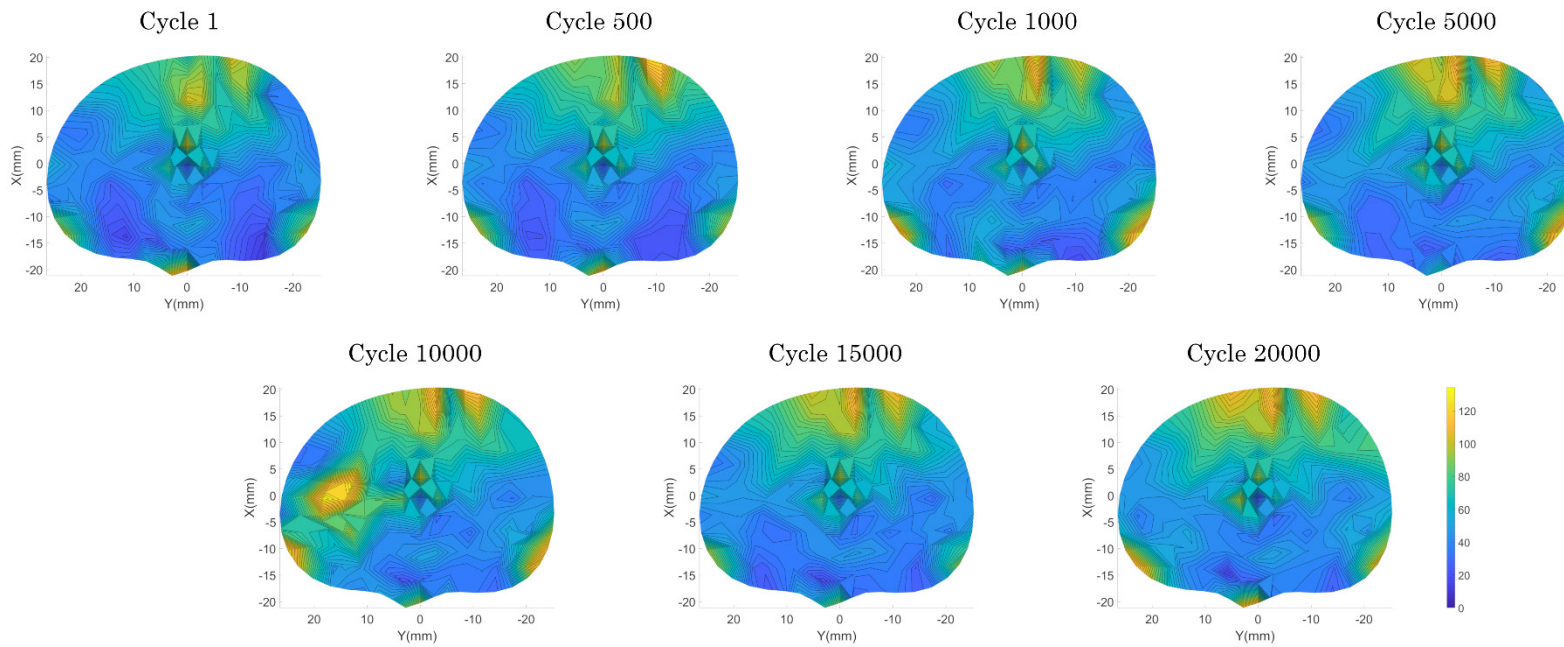


**Figure D-4** Contour plots showing MSS (%) at each of the cycle time points until failure for specimen 4

### D.1.1.5 Specimen 5

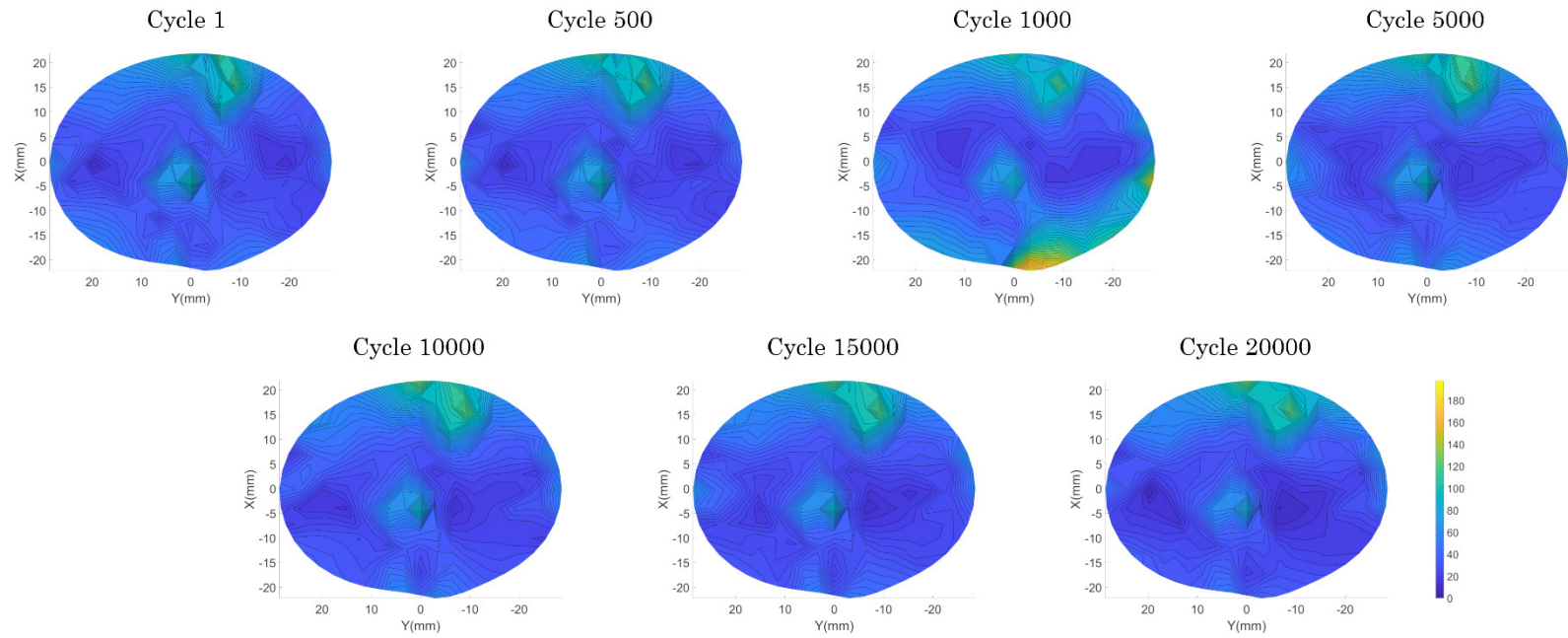


**Figure D-5** Contour plots showing MSS (%) at each of the cycle time points until failure for specimen 5

D.1.1.6 Specimen 6

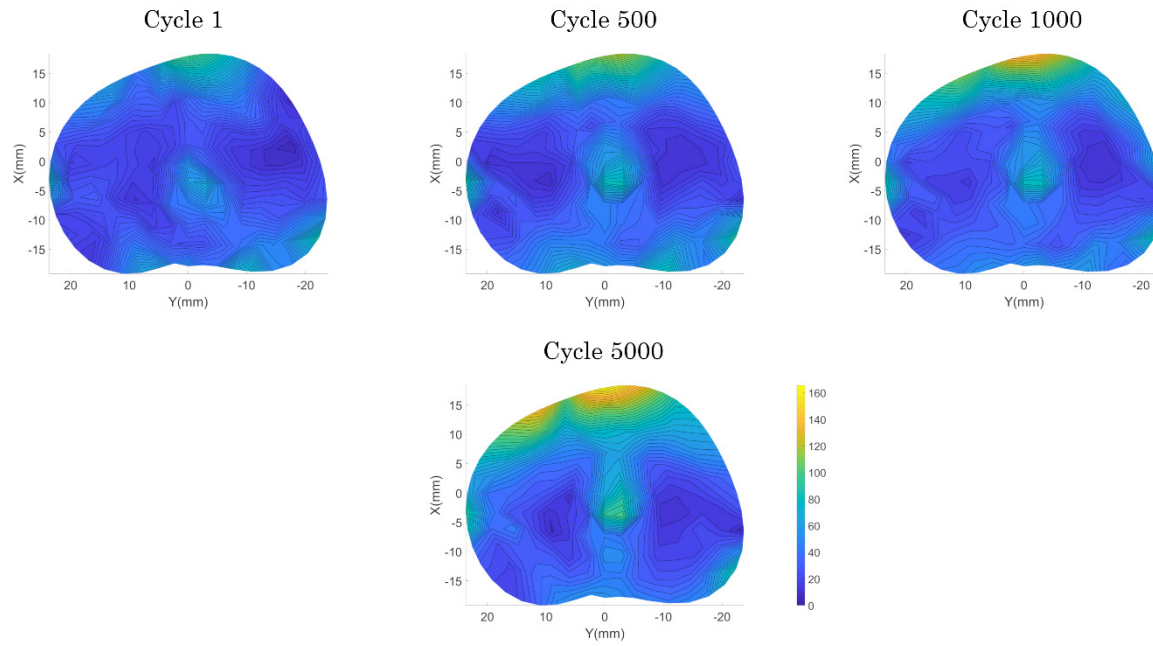


**Figure D-6** Contour plots showing MSS (%) at each of the cycle time points until failure for specimen 6

D.1.1.7 Specimen 7

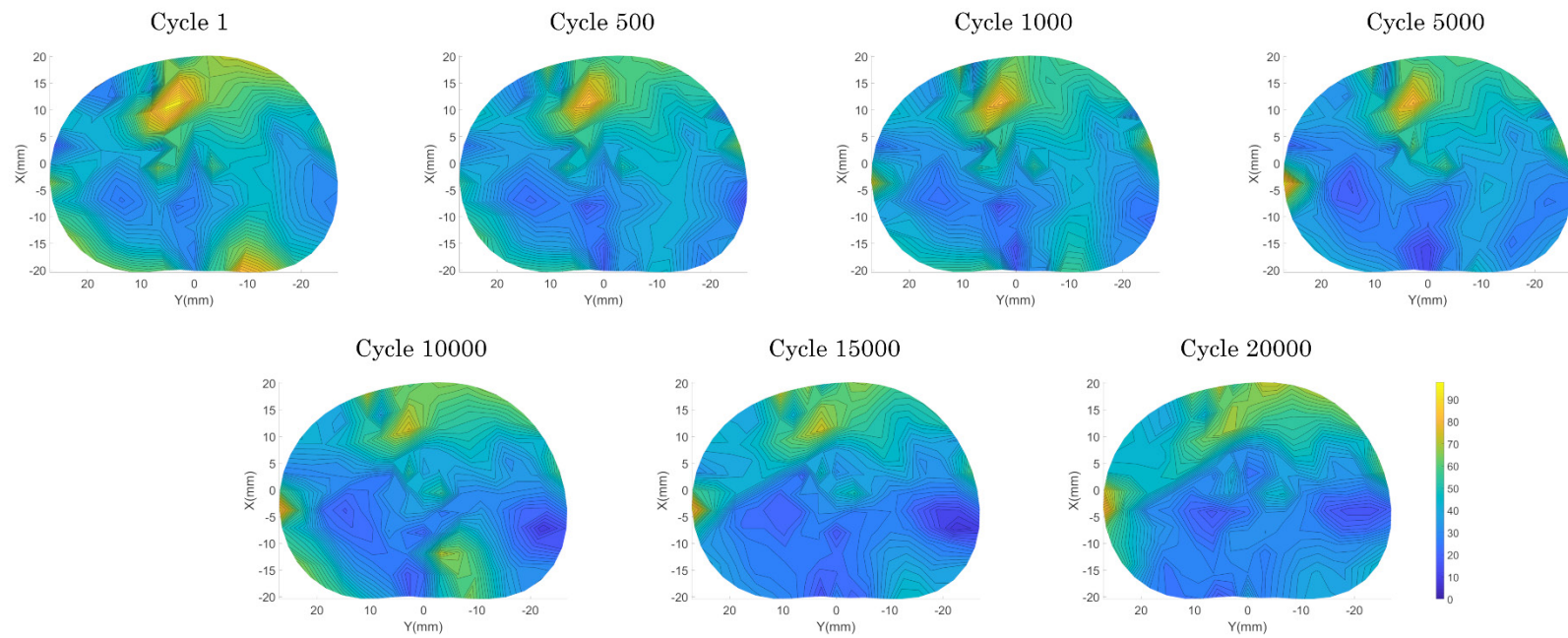
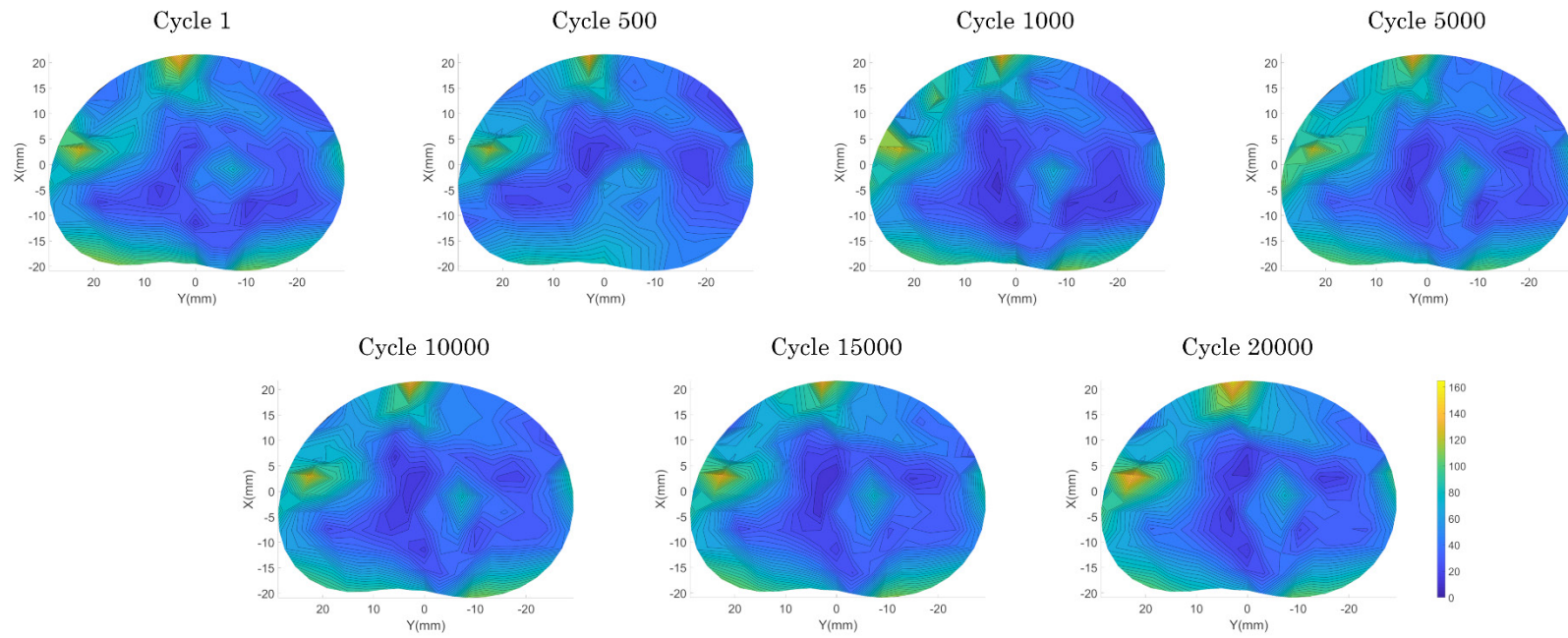


Figure D-7 Contour plots showing MSS (%) at each of the cycle time points until failure for specimen 7

### D.1.1.8 Specimen 8



**Figure D-8** Contour plots showing MSS (%) at each of the cycle time points until failure for specimen 8

## D.1.2 Simulated unsafe repetitive lifting

**Table D-2** Specimen characteristics (failure mode, level, grade, and applied cycles) for the simulated unsafe repetitive lifting cohort that underwent strain measurement. This table provides a cross-reference for the images presented in this section (D.1.2)

Specimen Number	Failure Mode	Level	Pfirmann Grade	Applied Cycles
1	Disc Protrusion	L3-4	2	10,000
2	Endplate Failure	L2-3	2	500
3	Endplate Failure	L1-2	2	5,000
4	No Injury	L4-5	1	20,000
5	Disc Protrusion	L2-3	2	10,000
6	No Injury	L2-3	1	20,000
7	Endplate Failure	L2-3	3	500

### D.1.2.1 Specimen 1

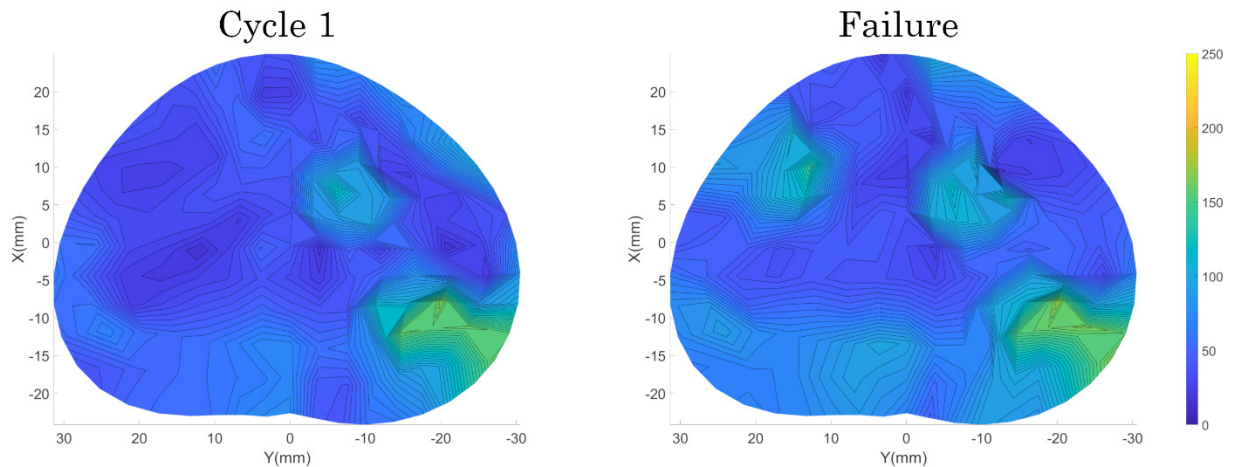


**Figure D-9** Contour plots showing MSS (%) at cycle 1 and failure for specimen 1

D.1.2.2 Specimen 2

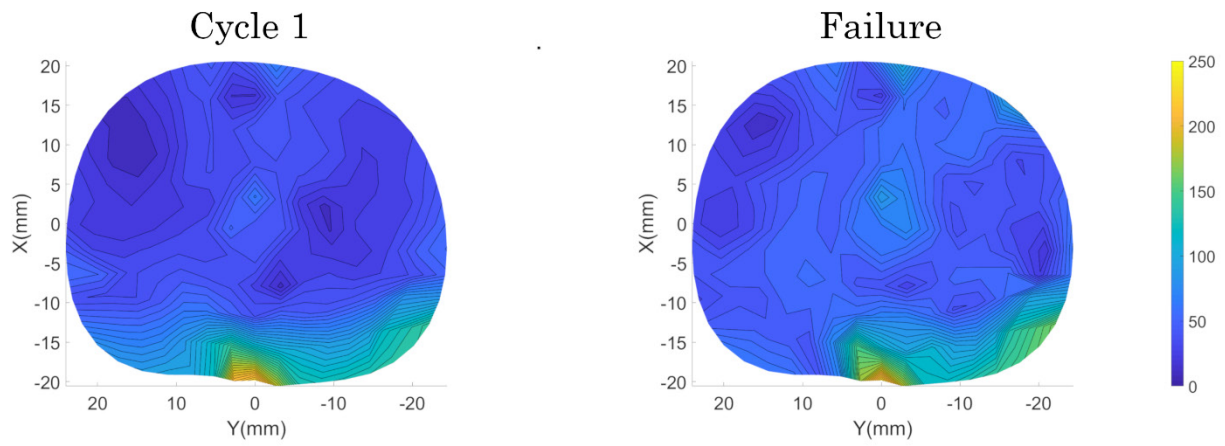


**Figure D-10** Contour plots showing MSS (%) at cycle 1 and failure for specimen 2

D.1.2.3 Specimen 3

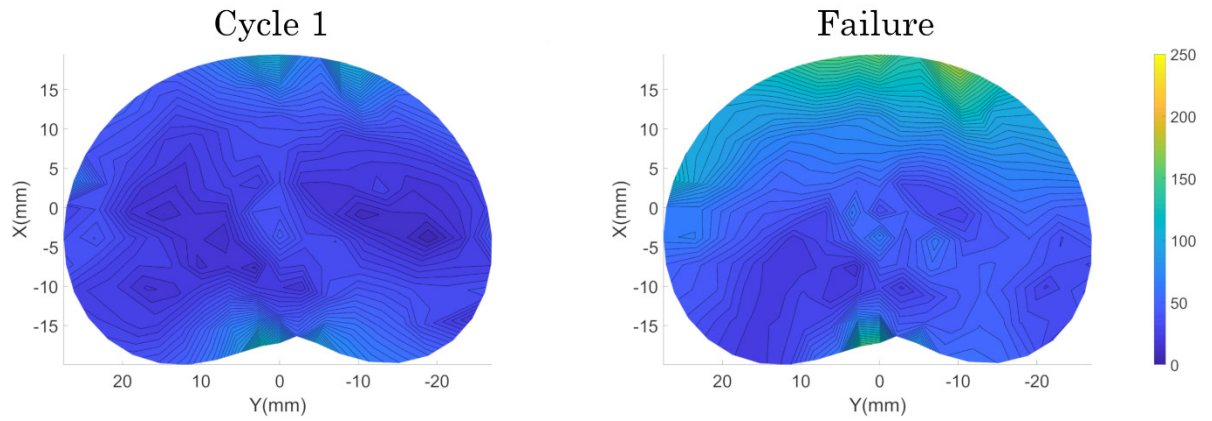


**Figure D-11** Contour plots showing MSS (%) at cycle 1 and failure for specimen 3

D.1.2.4 Specimen 4

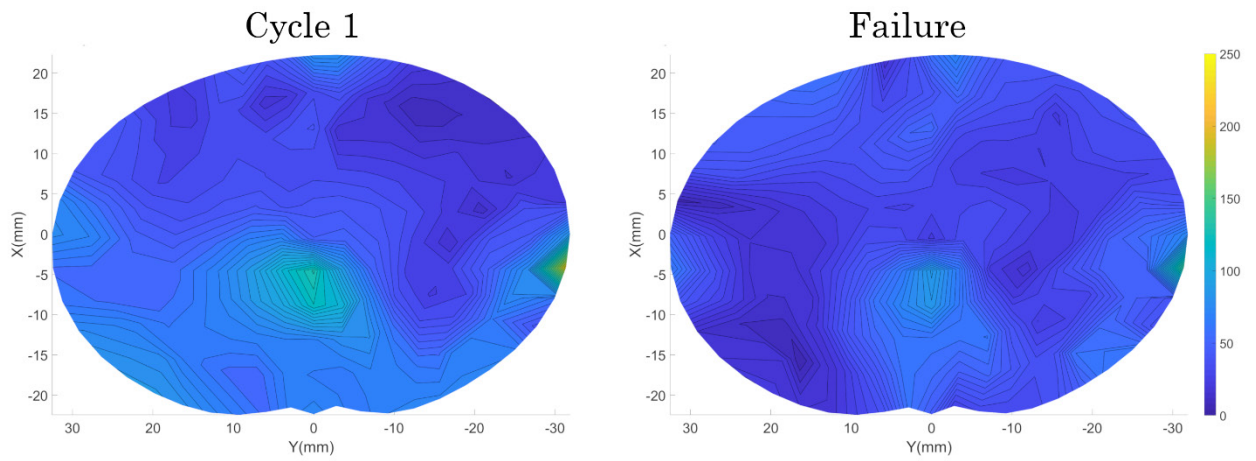


**Figure D-12** Contour plots showing MSS (%) at cycle 1 and failure for specimen 4

D.1.2.5 Specimen 5

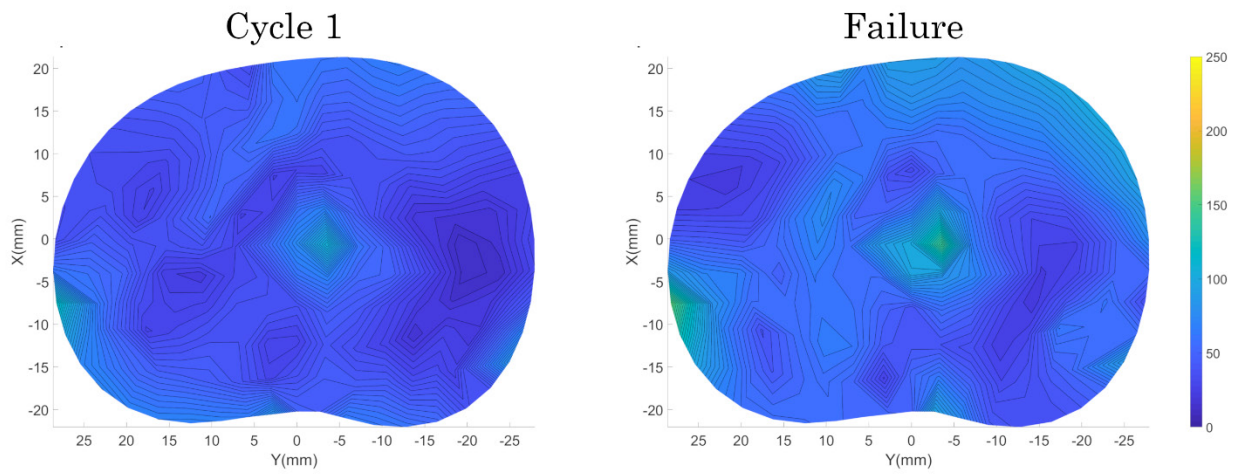


Figure D-13 Contour plots showing MSS (%) at cycle 1 and failure for specimen 5

D.1.2.6 Specimen 6

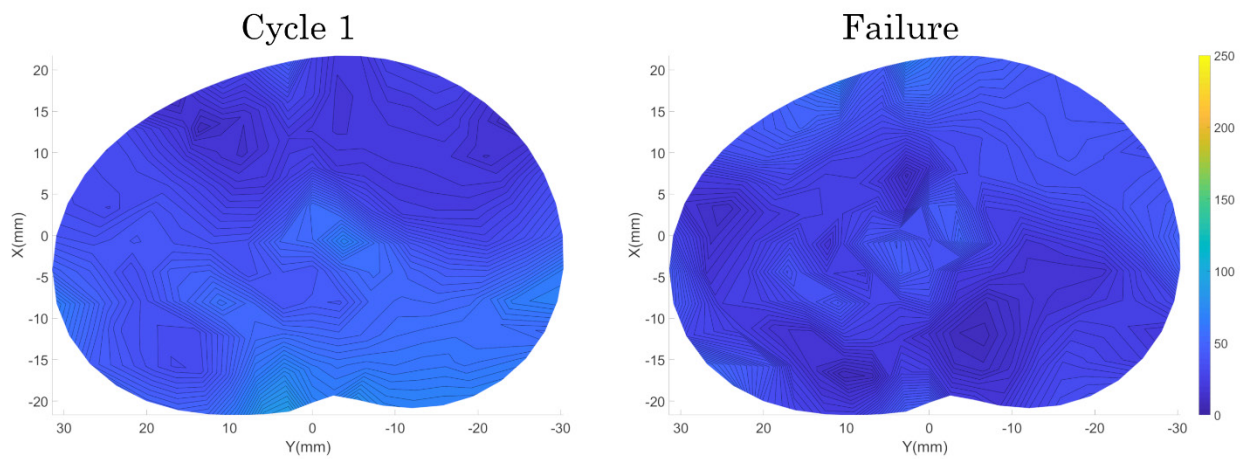
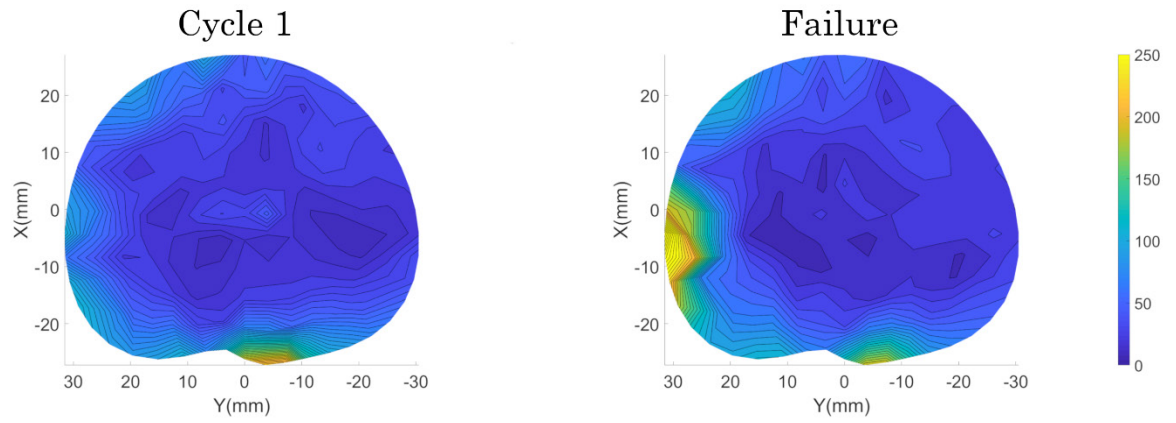


Figure D-14 Contour plots showing MSS (%) at cycle 1 and failure for specimen 6

D.1.2.7 Specimen 7



**Figure D-15** Contour plots showing MSS (%) at cycle 1 and failure for specimen 7



## Appendix E

### E.1 Multiaxial mechanics under simulated repetitive lifting

This appendix presents the average bending moment (flexion), rotational moment (right axial rotation), and compressive force at cycle 1 and the last applied cycle for both simulated safe and unsafe repetitive lifting. It also presents the average disc height loss and initial height for both lifting groups.

### E.1.1 Simulated safe repetitive lifting

**Table E-1** Mean (95% CI) flexion moment (-Mx), right axial rotation moment (-Mz), and compressive force (-Fz) at cycle 1 and the final applied cycle under simulated safe repetitive lifting for the control group, experimental group, and both groups combined. The mean (95% CI) disc height loss over the applied cycles is also presented.

Cycle	Group	Mx (Nm)		Mz (Nm)		Fz (N)		Disc Height Loss (mm)	
		mean	95% CI	mean	95% CI	mean	95% CI	mean	95% CI
Cycle 1	Control	-55.7	15.9	-10.8	4.80	-1246	529	-	-
	Experimental	-49.0	24.6	-10.5	6.26	-1468	501	-	-
	Combined	-52.1	14.7	-10.6	3.9	-1364	355	-	-
Final Applied Cycle	Control	-3.03	1.17	-6.43	1.44	-1661	374	-3.54	0.72
	Experimental	-0.43	3.94	-6.84	1.43	-1375	303	-3.35	1.03
	Combined	-1.64	2.21	-6.65	1.43	-1508	303	-3.44	0.65

**Table E-2** Mean (95% CI) initial disc height (mm) calculated from a lateral x-ray of FSU for the specimens in the safe repetitive lifting group. The initial disc height is presented for the control group, experimental group, and both groups combined.

Group	Mean (mm)	95%CI
Control	10.13	0.80
Experimental	10.65	1.19
Combined	10.41	0.72

### E.1.2 Simulated unsafe repetitive lifting

**Table E-3** Mean (95% CI) flexion moment (-Mx), right axial rotation moment (-Mz), and compressive force (-Fz) at cycle 1 and the final applied cycle under simulated unsafe repetitive lifting for the control group, experimental group, and both groups combined. The mean (95% CI) disc height loss over the applied cycles is also presented.

Cycle	Group	Mx (Nm)		Mz (Nm)		Fz (N)		Disc Height Loss (mm)	
		mean	95% CI	mean	95% CI	mean	95% CI	mean	95% CI
Cycle 1	Control	-35.3	19.2	-11.1	4.60	-2432	1058		
	Experimental	-62.6	21.6	-19.5	9.12	-2224	461		
	Combined	-50.9	16.1	-15.9	5.8	-2313	503		
Final Applied Cycle	Control	-5.41	3.78	-8.35	2.52	-2313	1006	-5.11	0.78
	Experimental	-9.65	3.00	-10.86	3.23	-2742	523	-5.03	0.53
	Combined	-7.83	2.53	-9.78	3.23	-2558	523	-5.07	0.43

**Table E-4** Mean (95% CI) initial disc height (mm) calculated from a lateral x-ray of FSU for the specimens in the unsafe repetitive lifting group. The initial disc height is presented for the control group, experimental group, and both groups combined.

Group	Mean (mm)	95%CI
Control	11.15	1.64
Experimental	10.97	0.96
Combined	11.05	0.85



# Appendix F

## F.1 6DOF load-unload curves before and after simulated unsafe repetitive lifting

This appendix presents the load-unload curves in all 6DOF directions before and after simulated **unsafe** repetitive lifting.

### F.1.1 Shears and Compression

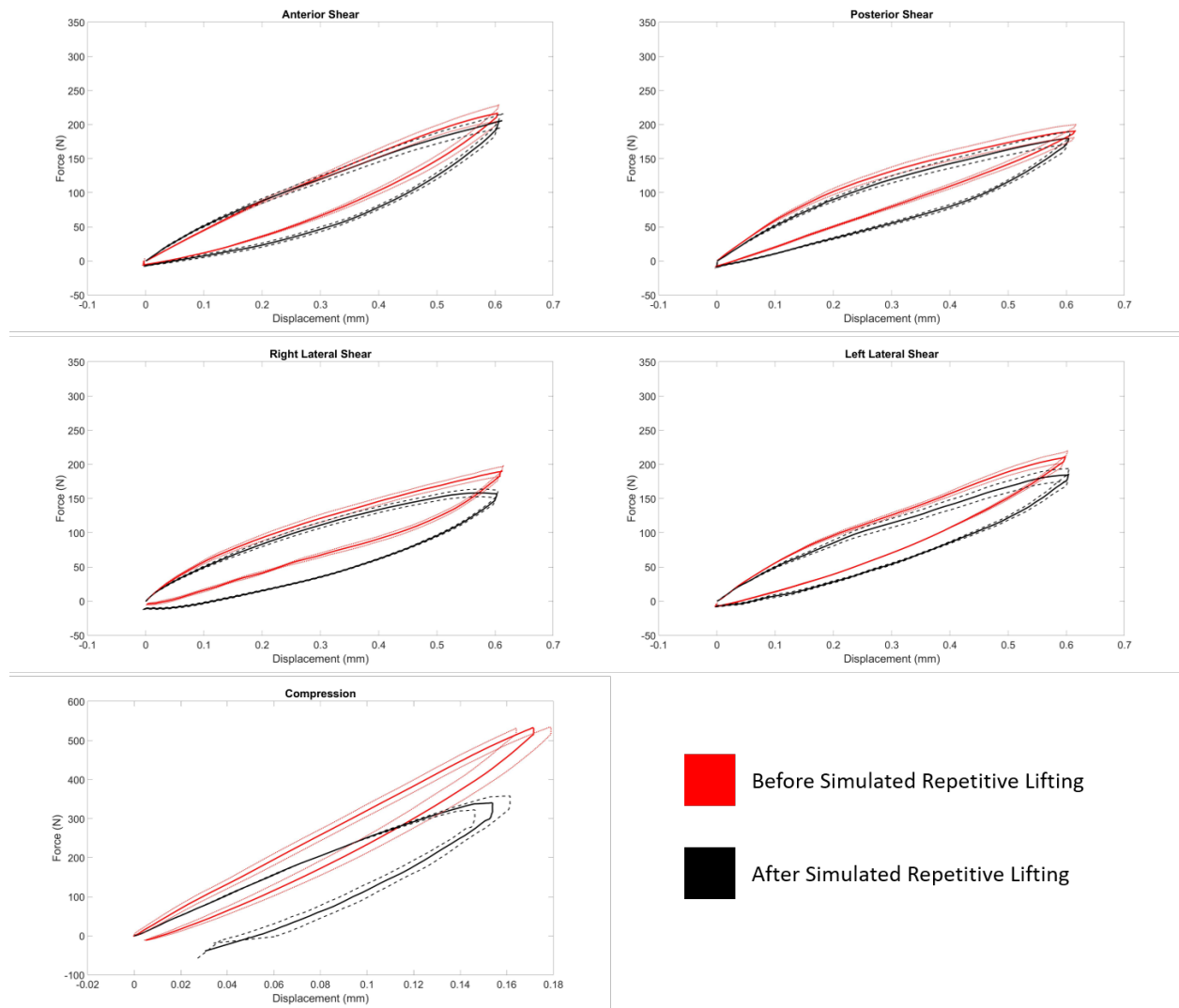


**Figure F-1** Average load vs. displacement curves for shear and compression DOFs, before and after simulated unsafe repetitive lifting. Dotted lines represent 95% CI.

## F.1.2 Bending and Rotation

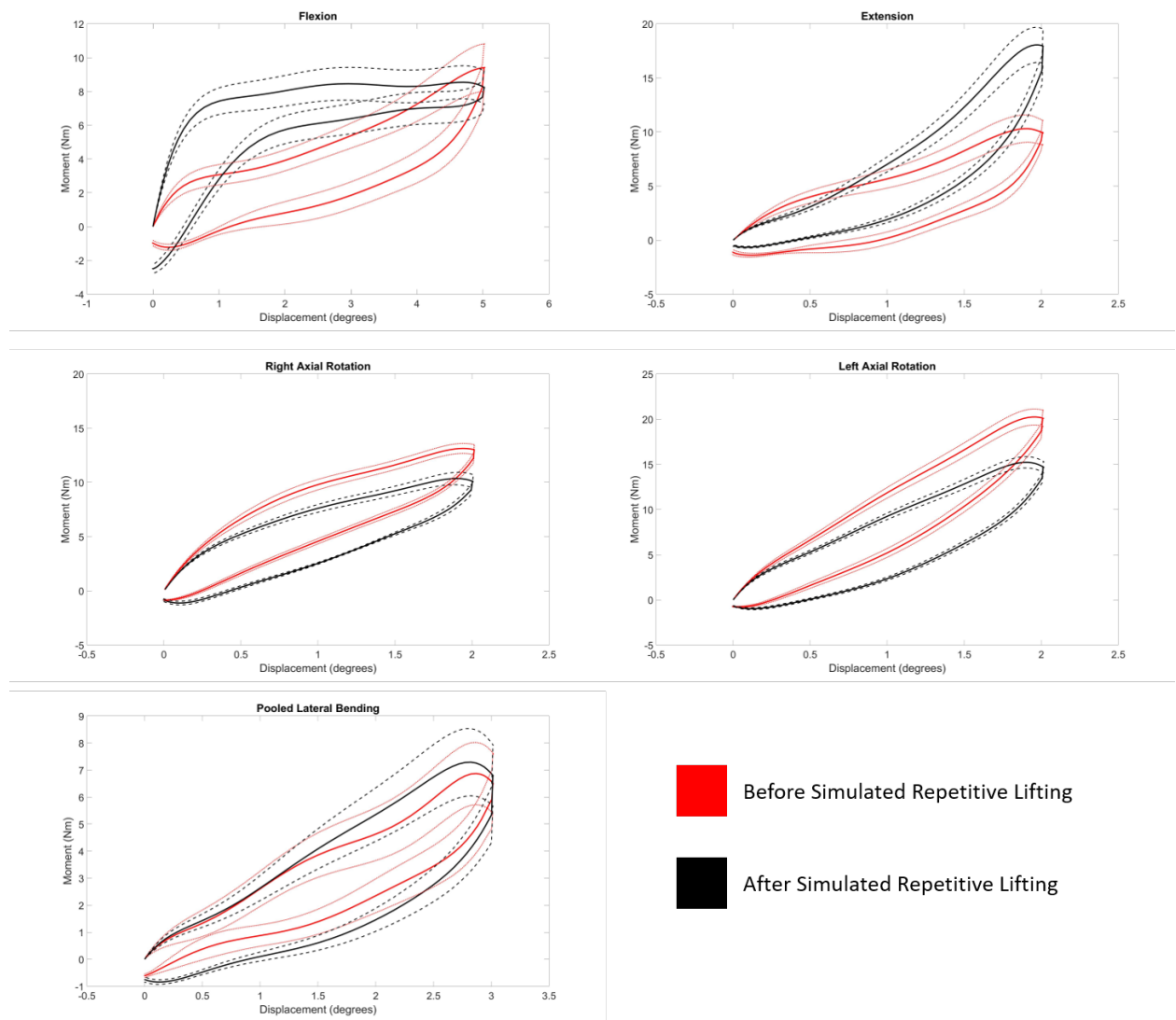


**Figure F-2** Average load vs. displacement curves for all bending 6DOF directions before and after simulated unsafe repetitive lifting. Dotted lines represent 95 % CI.

## Appendix G

### G.1 Comparison of safe and unsafe repetitive lifting

This appendix presents the statistical comparisons between simulated safe and unsafe repetitive lifting for both failure strain and 6DOF mechanics. The failure strain is defined as the MSS at the last applied cycle.

#### G.1.1 Methods: Statistical Analysis

For the comparison of lifting groups, a univariate ANOVA was performed separately on failure MSS, stiffness percent differences, and phase angle percent differences with fixed factors of lifting group and failure mode ( $p < 0.05$ ). For the failure MSS, another fixed factor of the region was added. Percent differences were calculated as follows:  $100 * (\text{after loading} - \text{before loading}) / \text{before loading}$ . These differences were then compared between the two loading modalities.

#### G.1.2 Results

##### G.1.2.1 Failure strain

Comparing failure MSS between safe and unsafe lifting, significant interaction effects between lifting group and region were found ( $p = 0.030$ ). Post-hoc pairwise comparisons revealed significantly lower failure MSS for the unsafe lifting group in the anterior and nucleus regions ( $p < 0.010$ , **Figure G-1**). Significant interaction effects were observed between the lifting group and failure mode ( $p < 0.001$ ). However, for this analysis the only failure modes compared between the two lifting groups was endplate failure and disc protrusion, as there were low specimen numbers (0 or 1) for the no injury and herniation groups. Post-hoc analysis revealed significant differences between the two lifting groups for the endplate failure mode, where significantly lower MSS was observed in the safe lifting group compared to the unsafe ( $p = 0.011$ , **Figure G-2**).

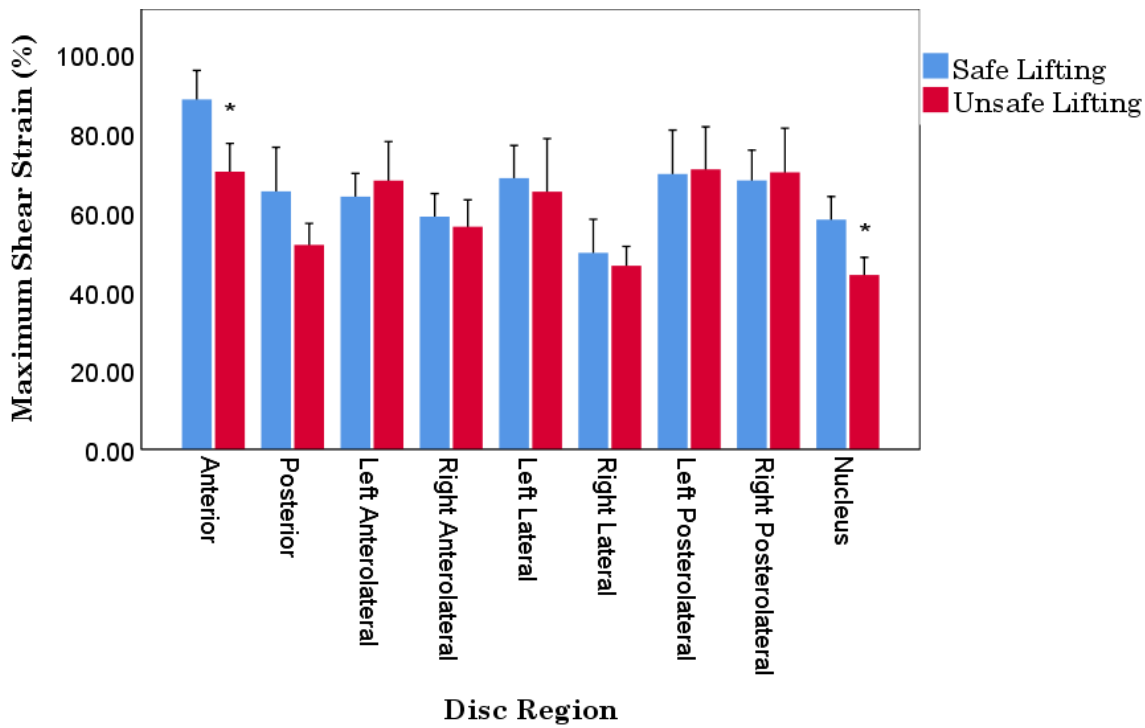


**Figure G-1** Mean (95% CI) failure MSS as a function of disc region for safe and unsafe repetitive lifting. \* denotes significance with respect to safe lifting.

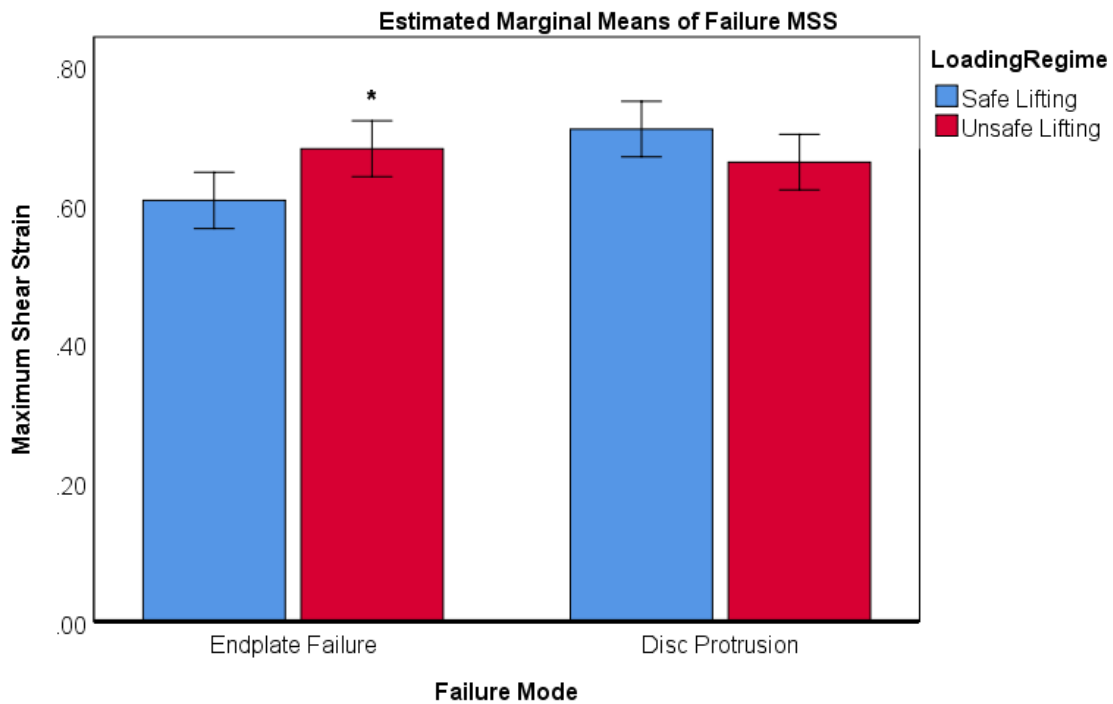


**Figure G-2** Mean (95% CI) failure MSS as a function of failure mode for safe and unsafe repetitive lifting. \* denotes significance with respect to safe lifting

### G.1.2.2 6DOF mechanics

To compare lifting groups, percent differences between time points (before and after repetitive loading) were calculated for both safe and unsafe lifting groups and both mechanical properties (stiffness and phase angle). No significant differences between lifting groups in any of the DOFs were observed for stiffness ( $p > 0.185$ , **Figure G-3**, **Figure G-4**) and phase angle ( $p > 0.103$ , **Figure G-5**, **Figure G-6**). In addition, no significant interaction effects between lifting groups and failure mode in any of the DOFs were found for stiffness ( $p > 0.103$ ) and phase angle ( $p > 0.179$ ).

#### Stiffness

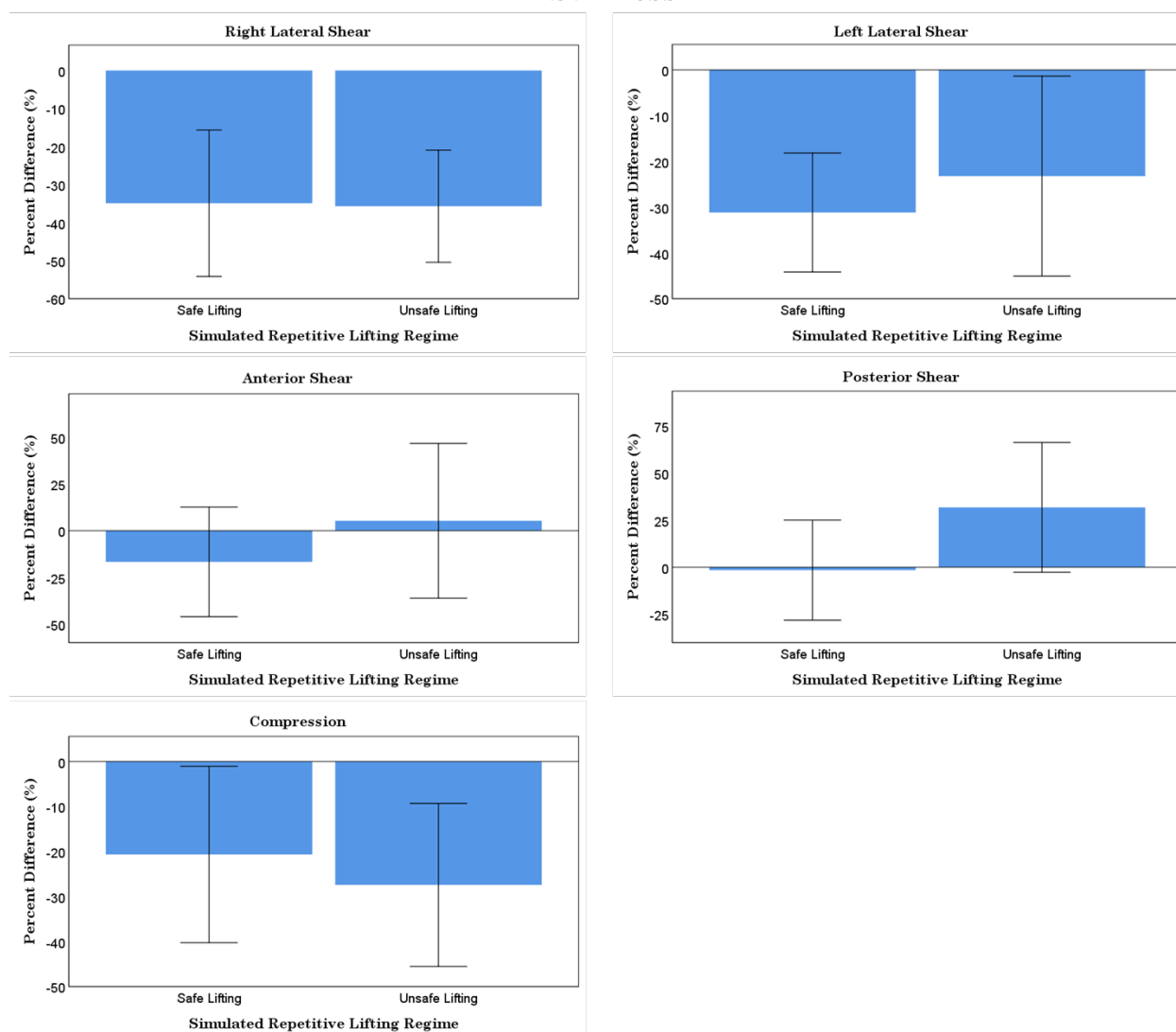


**Figure G-3** Mean (95% CI) stiffness for shear and compression directions comparing simulated safe versus unsafe repetitive lifting. \* denotes significance ( $p < 0.05$ ).

## Stiffness

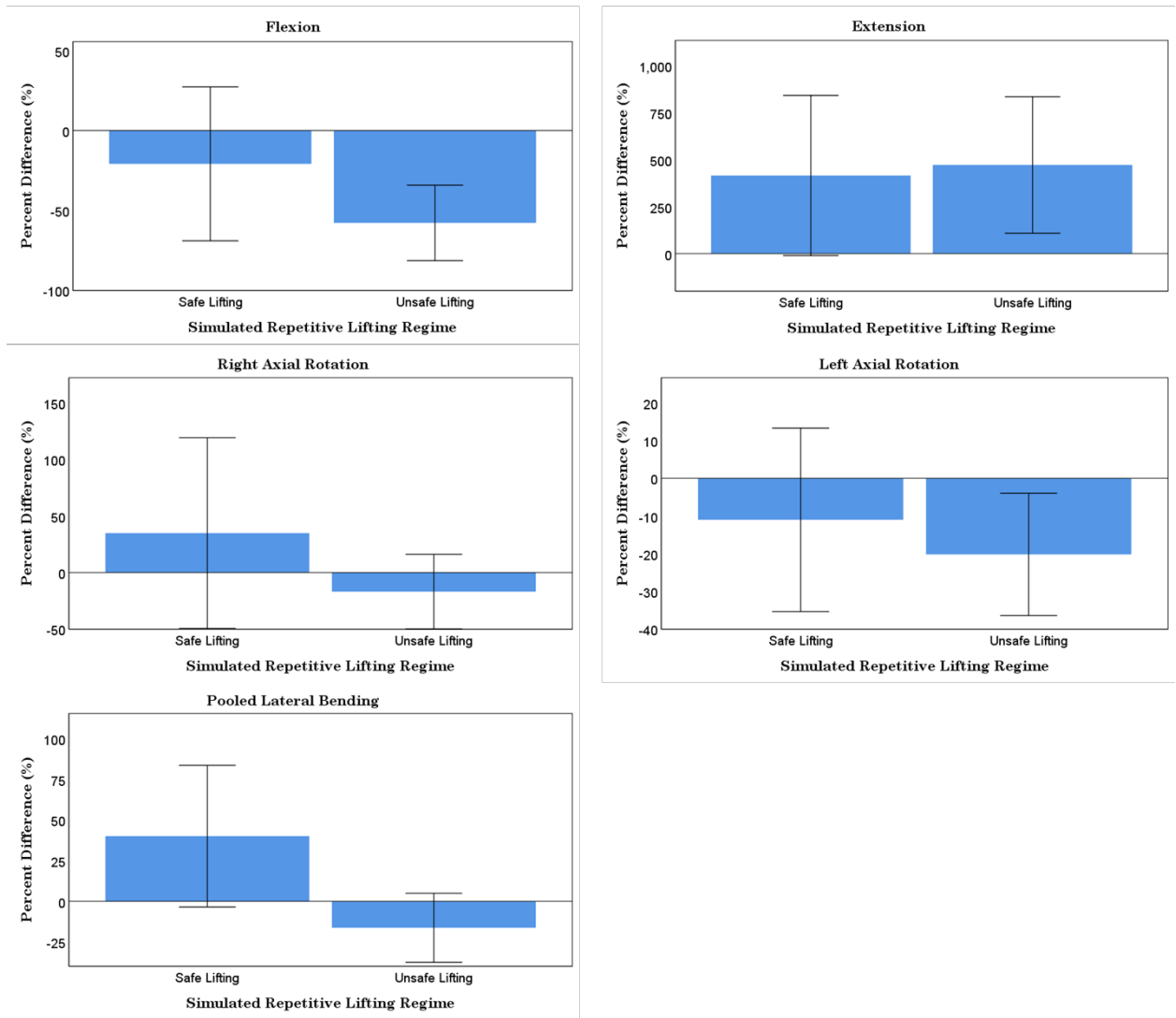


**Figure G-4** Mean (95% CI) stiffness for bending and rotation directions comparing simulated safe versus unsafe repetitive lifting. \* denotes significance (p<0.05).

## Phase Angle

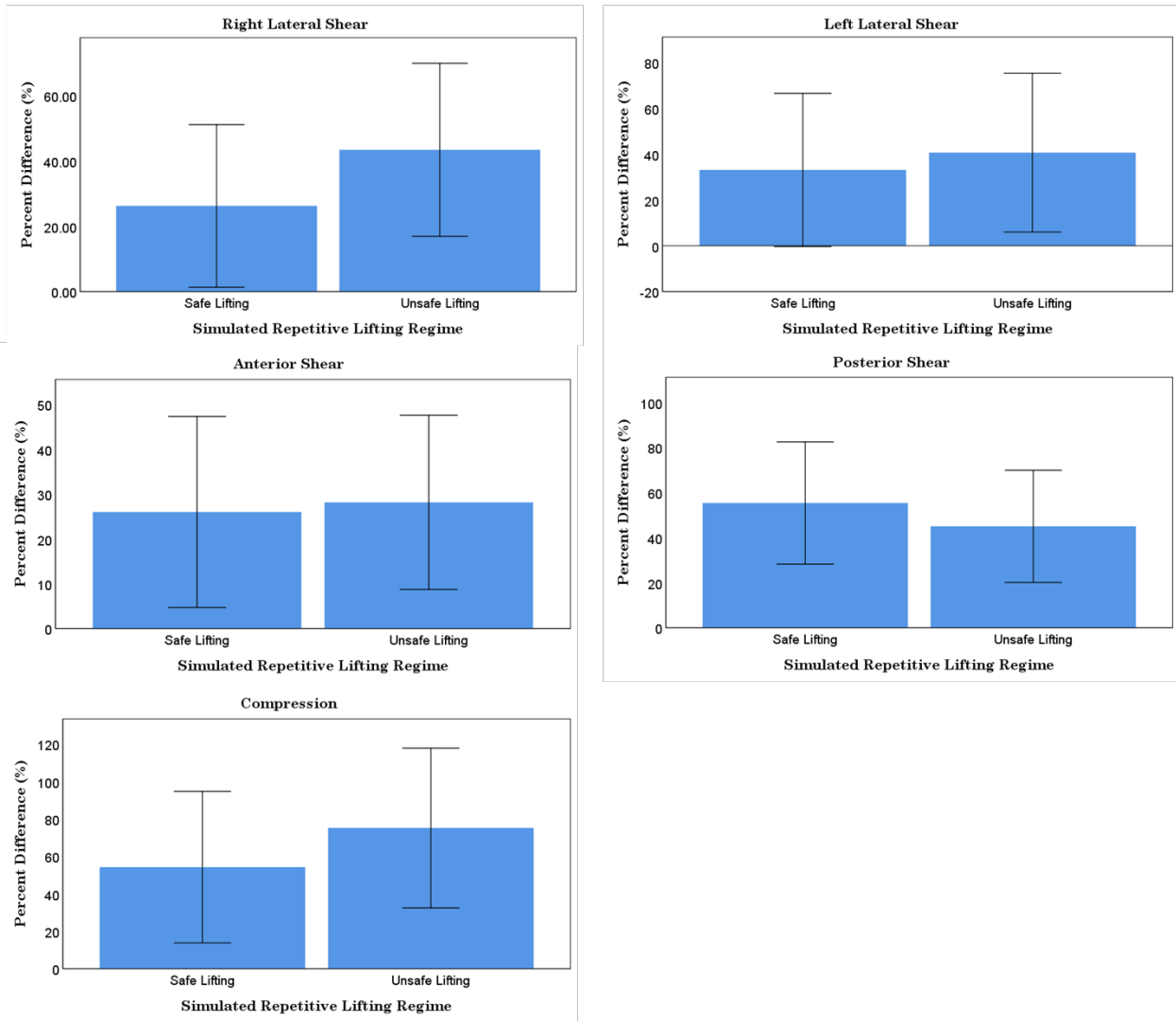


**Figure G-5** Mean (95% CI) phase angle for shear and compression directions comparing simulated safe versus unsafe repetitive lifting. \* denotes significance ( $p < 0.05$ ).

## Phase Angle

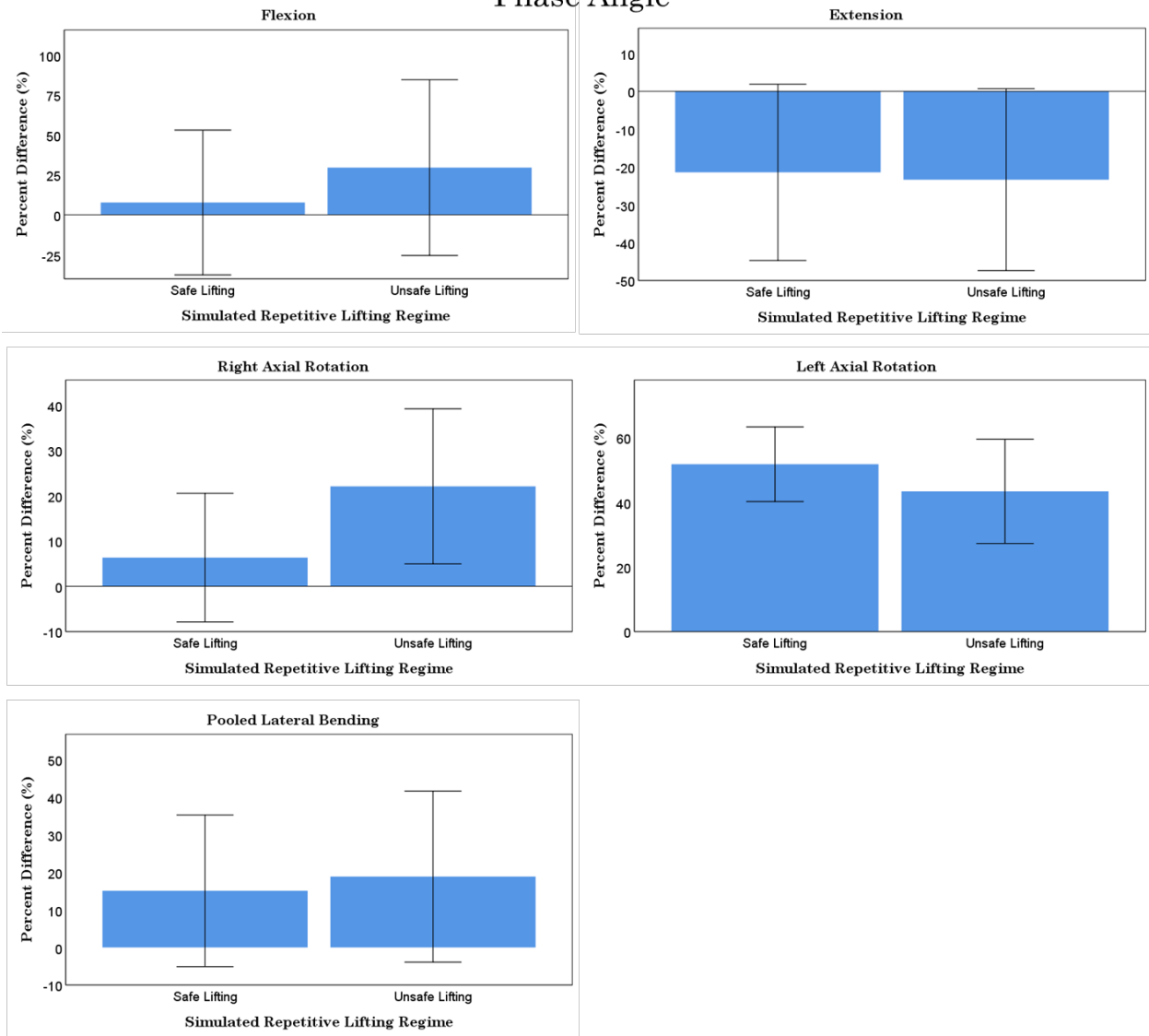


**Figure G-6** Mean (95% CI) phase angle for shear and compression directions comparing simulated safe versus unsafe repetitive lifting. \* denotes significance ( $p < 0.05$ ).

# Appendix H

## H.1 Damage score

This appendix presents the images that were used to formulate the damage score in each region of the disc for each specimen. Three independent reviewers scored the axial MR and macroscopic images of all specimens. Each reviewer then repeated the scoring three times to assess the repeatability (inter-correlation coefficient, see **Chapter 6**) of the scoring system. All images were blinded to each of the reviewers. Scoring system was as follows:

- 0 – no tissue damage
- 1 – delamination and/or annular tears
- 2 – nucleus migration and/or annulus buckling
- 3 – disc protrusion (disc bulge)
- 4 – disc herniation

Table H-1 outlines the details of each specimen for the association of the MRI and macroscopic images presented below. The specimen number presented in this table corresponds to the specimen number presented before each MR and macroscopic image.

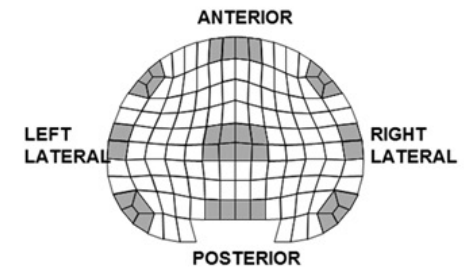
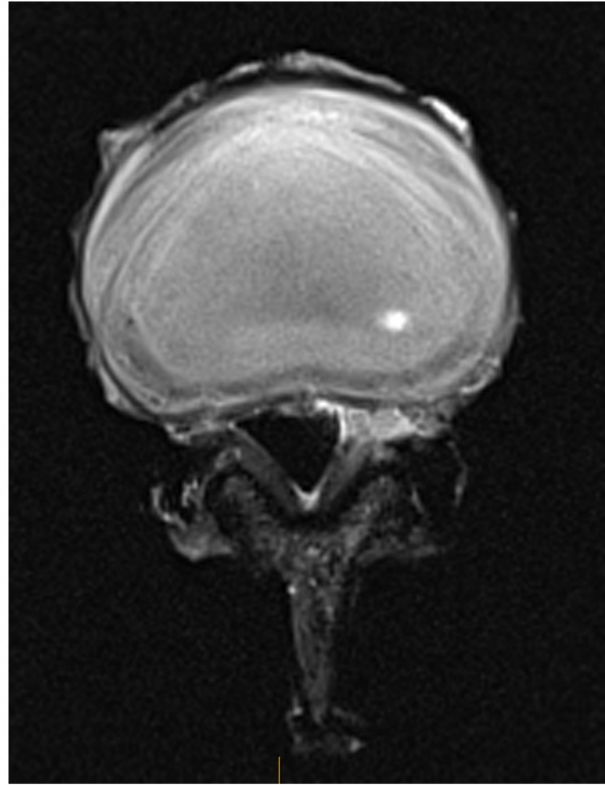
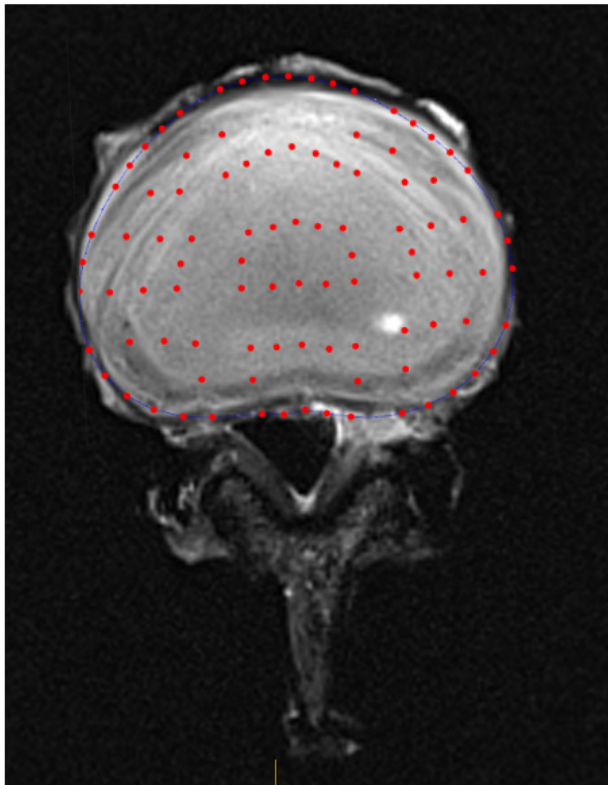
Table H-1 Specimen characteristics, which include lifting regime, failure mode, MSS measurement, level, Pfirrmann grade, and applied cycles. This table provides a cross-reference for the images presented in this appendix

Specimen Number	Lifting Regime	Failure Mode	MSS Measurement	Level	Pfirrmann Grade	Applied Cycles
1	Unsafe	Disc Protrusion	Yes	L3-4	2	10,000
2	Unsafe	Endplate Failure	Yes	L2-3	2	500
3	Unsafe	Endplate Failure	Yes	L1-2	2	5,000
4	Unsafe	No Injury	Yes	L4-5	1	20,000
5	Unsafe	Disc Protrusion	Yes	L2-3	2	10,000
6	Unsafe	Endplate Failure	Yes	L3-4	2	500
7	Unsafe	No Injury	Yes	L2-3	1	20,000
8	Unsafe	Endplate Failure	Yes	L2-3	3	500
9	Safe	Endplate Failure	Yes	L4-5	3	500
10	Safe	Disc Protrusion	Yes	L4-5	2	20,000
11	Safe	Disc Protrusion	Yes	L4-5	2	20,000
12	Safe	No Injury	Yes	L2-3	2	20,000
13	Safe	Disc Protrusion	Yes	L4-5	2	20,000
14	Safe	Endplate Failure	Yes	L1-2	2	5,000
15	Safe	Disc Protrusion	Yes	L1-2	3	20,000
16	Safe	LDH	Yes	L4-5	3	20,000
17	Unsafe	Endplate Failure	No	L3-4	2	5,000
18	Unsafe	Endplate Failure	No	L2-3	2	1,000
19	Unsafe	Disc Protrusion	No	L4-5	2	20,000
20	Unsafe	Endplate Failure	No	L4-5	2	500
21	Unsafe	Endplate Failure	No	L1-2	2	5,000
22	Unsafe	Endplate Failure	No	L1-2	2	500
23	Unsafe	Endplate Failure	No	L4-5	3	500
24	Safe	No Injury	No	L1-2	2	20,000
25	Safe	Disc Protrusion	No	L2-3	2	20,000
26	Safe	Endplate Failure	No	L2-3	2	500
27	Safe	No Injury	No	L2-3	2	20,000
28	Safe	No Injury	No	L4-5	3	20,000
29	Safe	LDH	No	L3-4	3	20,000
30	Safe	LDH	No	L4-5	3	20,000

### H.1.1 MR images

Slides with MR images from both simulated safe and unsafe repetitive lifting, which were given to each reviewer are presented below. The left and right images are identical, however, the left image has the superimposed disc regions for regional grading.

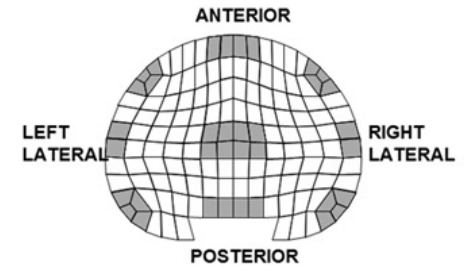
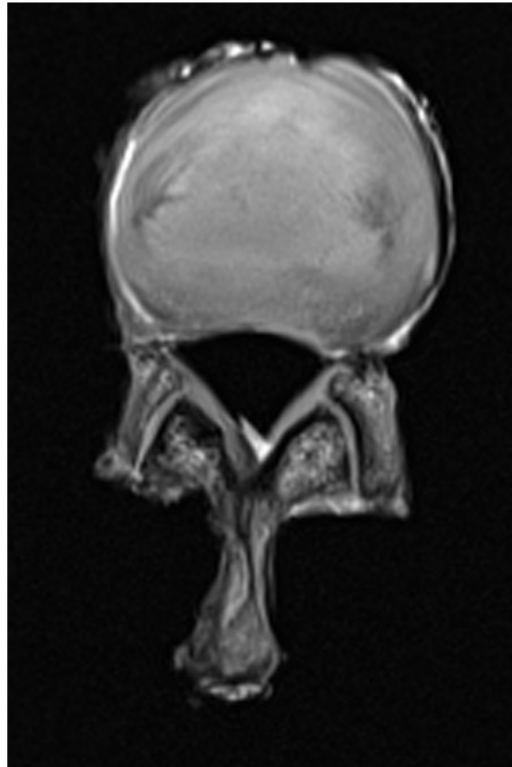
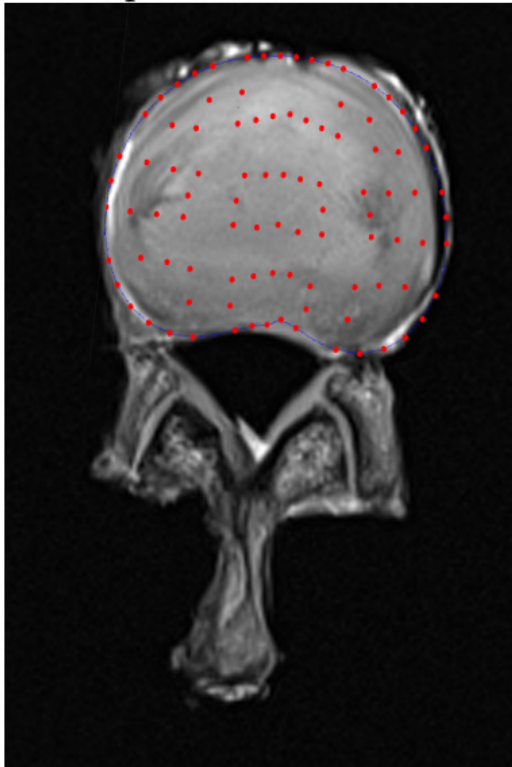
#### Specimen 1



#### SCALE

- 0 – No evidence of damage
- 1 – Delamination or Tears
- 2 – Nucleus Migration and/or  
Annulus Buckling
- 3 – Disc Bulge
- 4 – Disc Herniation

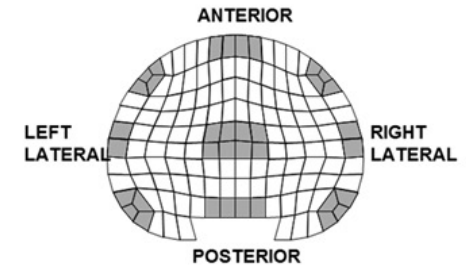
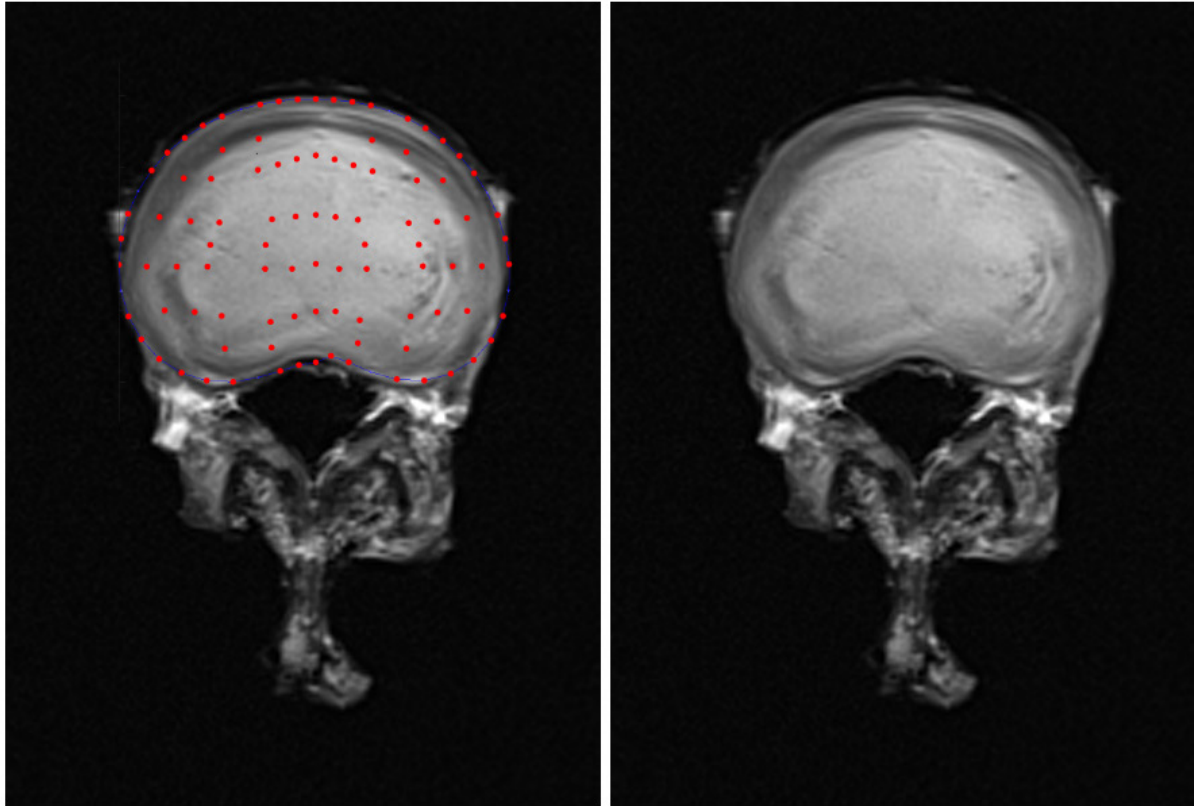
Specimen 2



**SCALE**

- 0 – No evidence of damage
- 1 – Delamination or Tears
- 2 – Nucleus Migration and/or  
Annulus Buckling
- 3 – Disc Bulge
- 4 – Disc Herniation

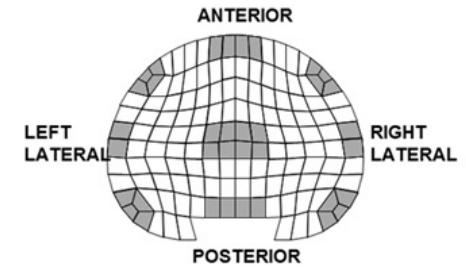
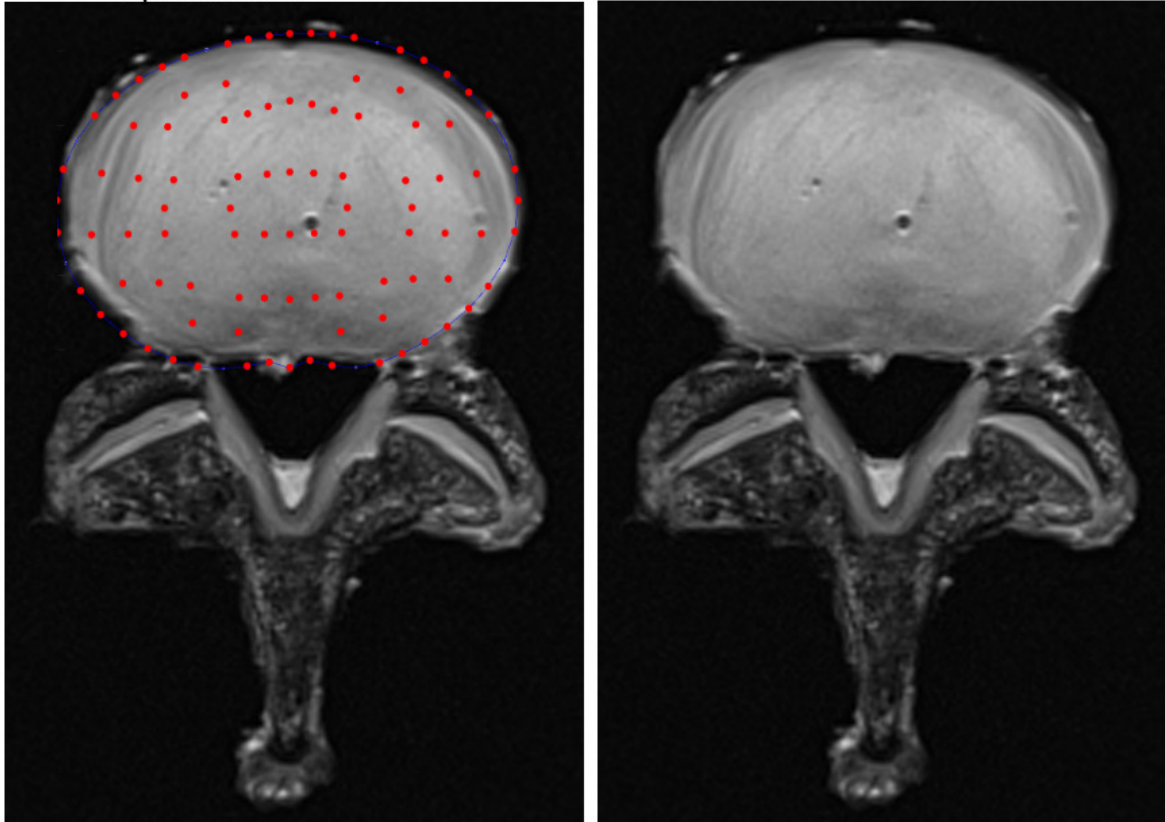
Specimen 3



**SCALE**

- 0 – No evidence of damage
- 1 – Delamination or Tears
- 2 – Nucleus Migration and/or  
Annulus Buckling
- 3 – Disc Bulge
- 4 – Disc Herniation

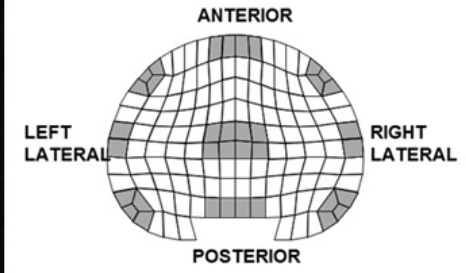
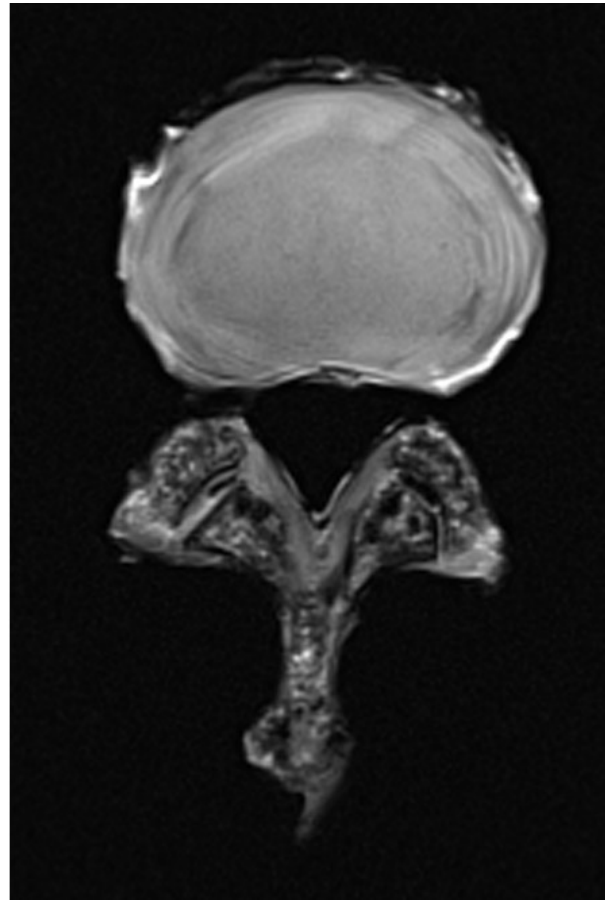
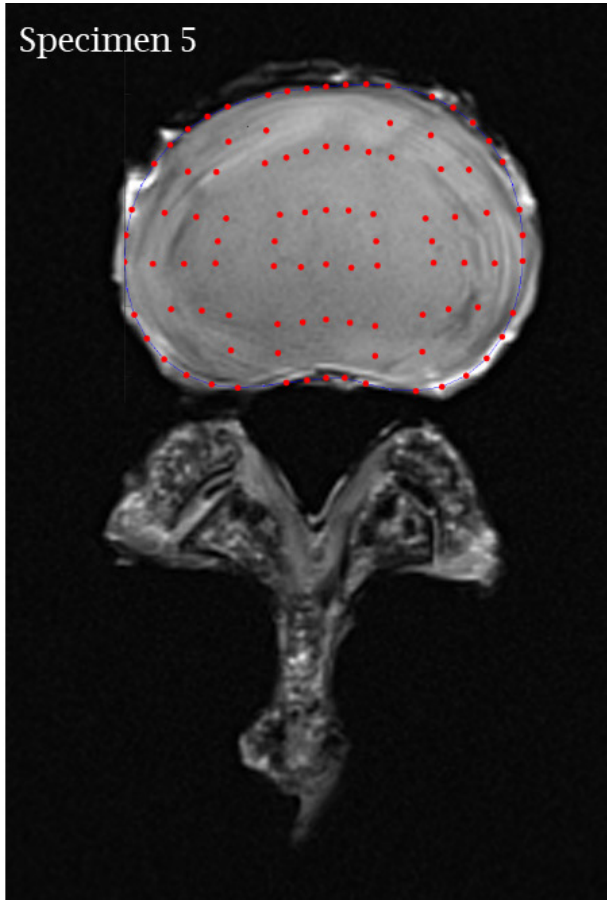
Specimen 4



**SCALE**

- 0 – No evidence of damage
- 1 – Delamination or Tears
- 2 – Nucleus Migration and/or  
Annulus Buckling
- 3 – Disc Bulge
- 4 – Disc Herniation

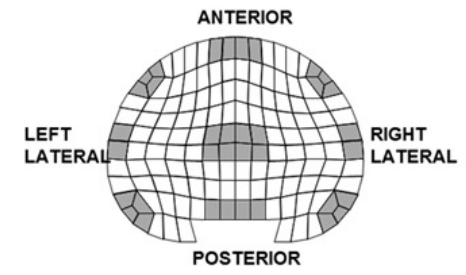
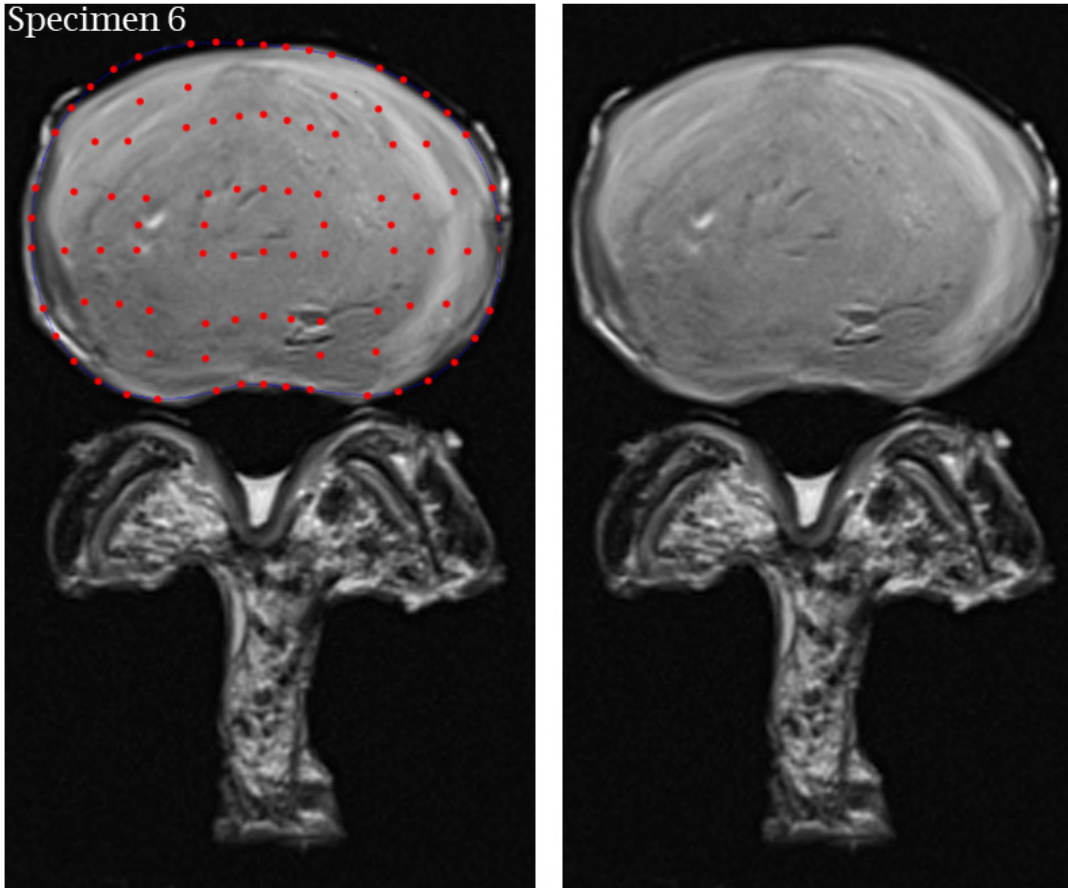
Specimen 5



**SCALE**

- 0 – No evidence of damage
- 1 – Delamination or Tears
- 2 – Nucleus Migration and/or Annulus Buckling
- 3 – Disc Bulge
- 4 – Disc Herniation

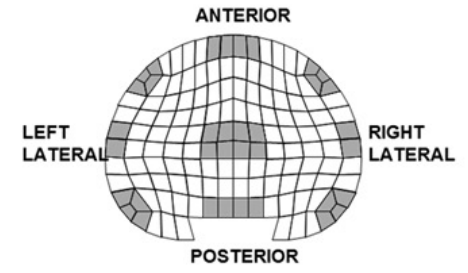
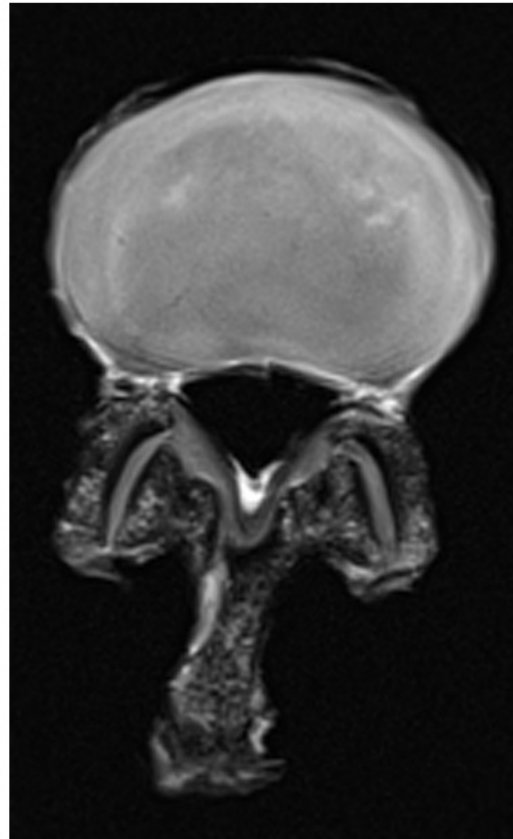
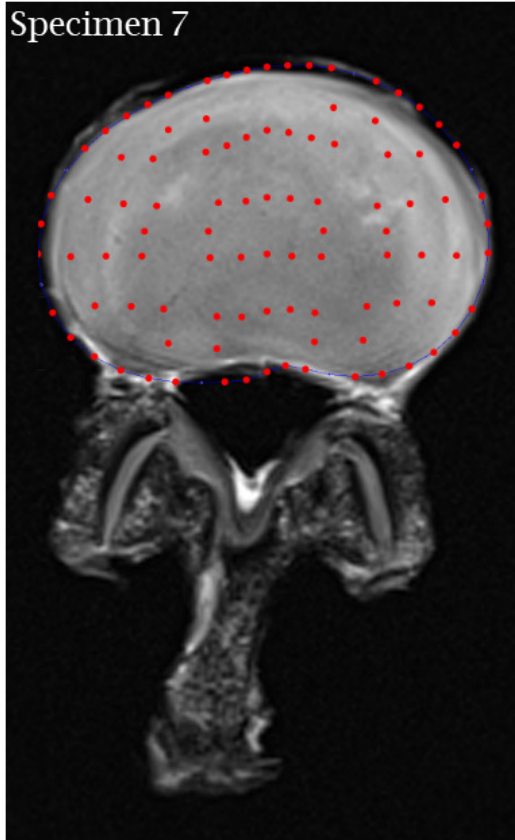
Specimen 6



**SCALE**

- 0 – No evidence of damage
- 1 – Delamination or Tears
- 2 – Nucleus Migration and/or Annulus Buckling
- 3 – Disc Bulge
- 4 – Disc Herniation

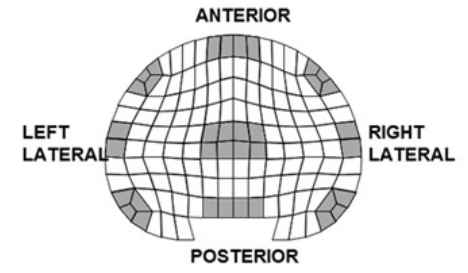
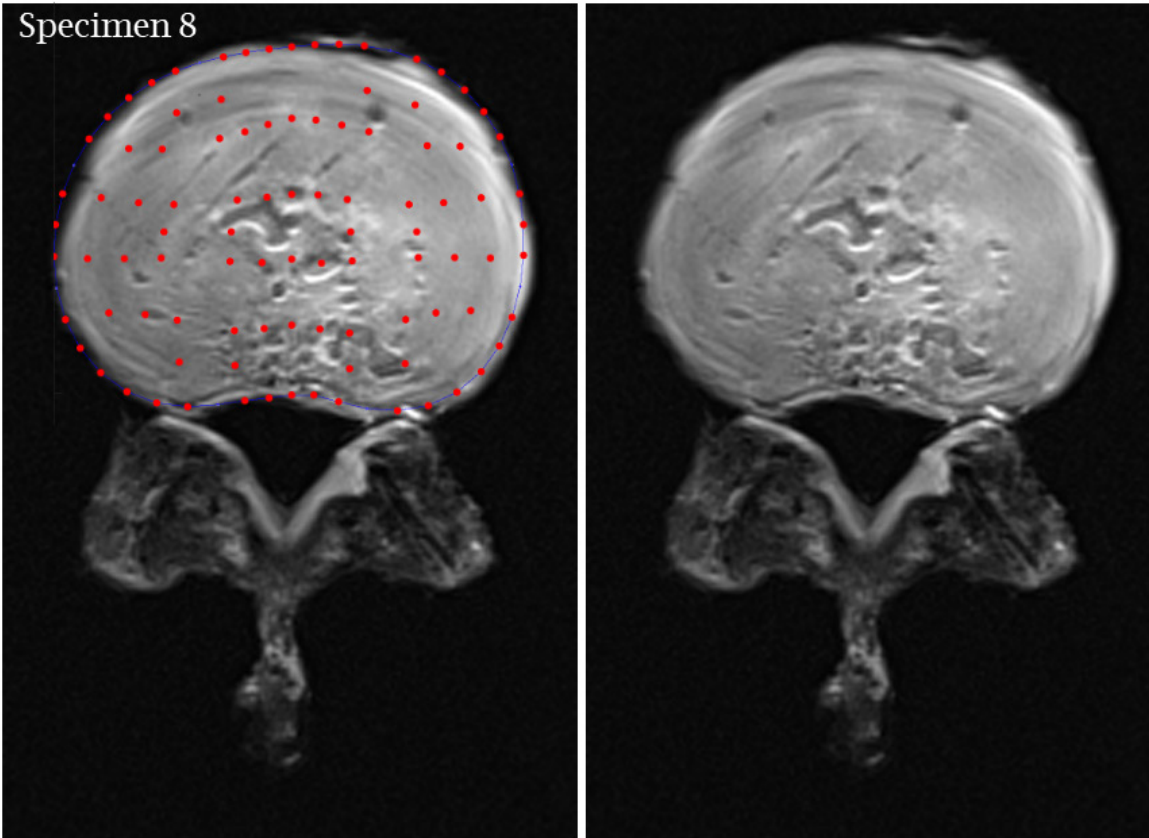
Specimen 7



**SCALE**

- 0 – No evidence of damage
- 1 – Delamination or Tears
- 2 – Nucleus Migration and/or Annulus Buckling
- 3 – Disc Bulge
- 4 – Disc Herniation

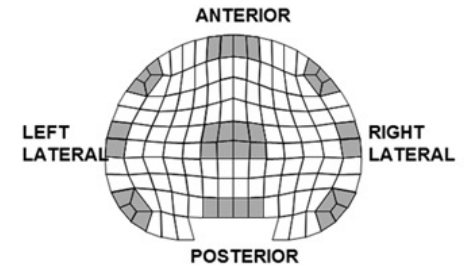
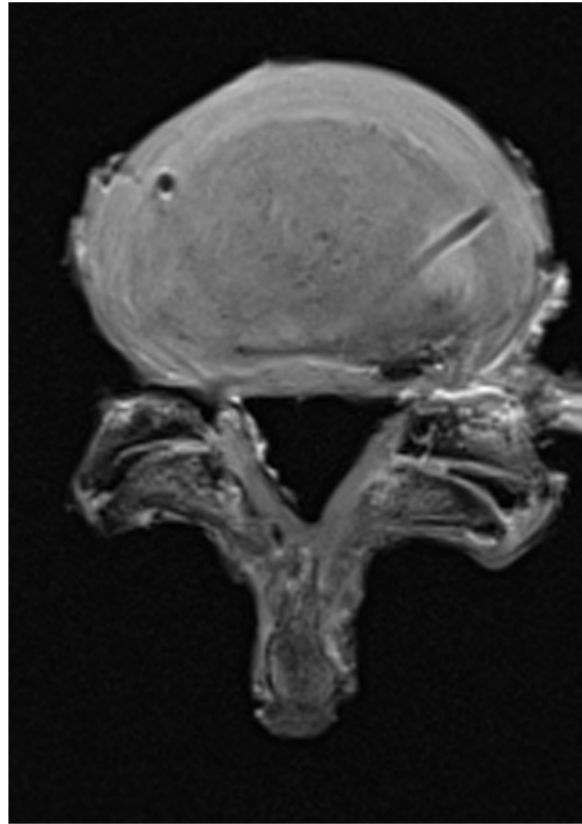
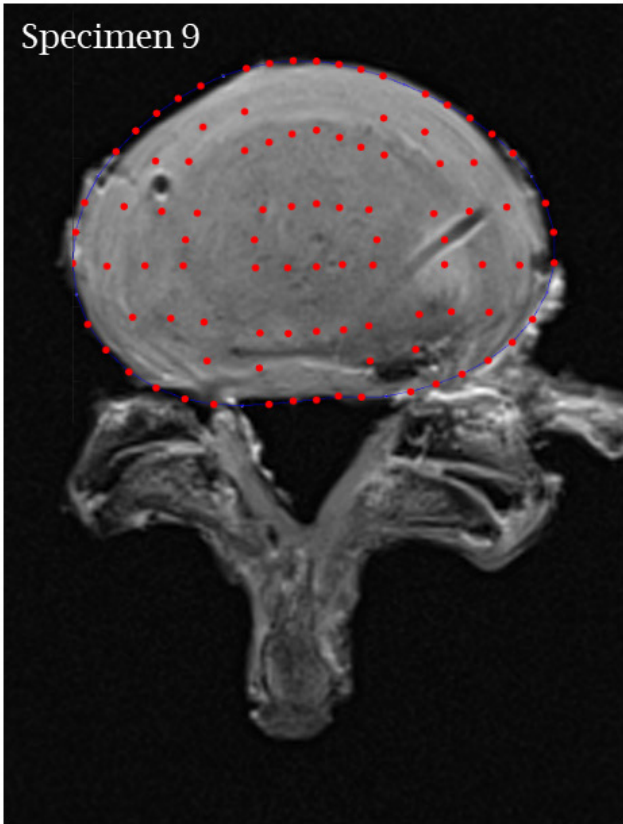
Specimen 8



**SCALE**

- 0 – No evidence of damage
- 1 – Delamination or Tears
- 2 – Nucleus Migration and/or  
Annulus Buckling
- 3 – Disc Bulge
- 4 – Disc Herniation

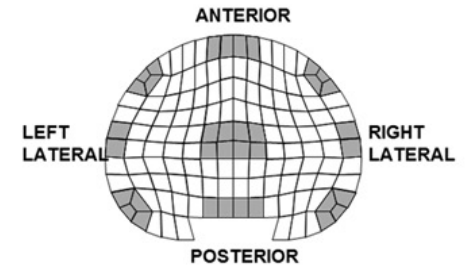
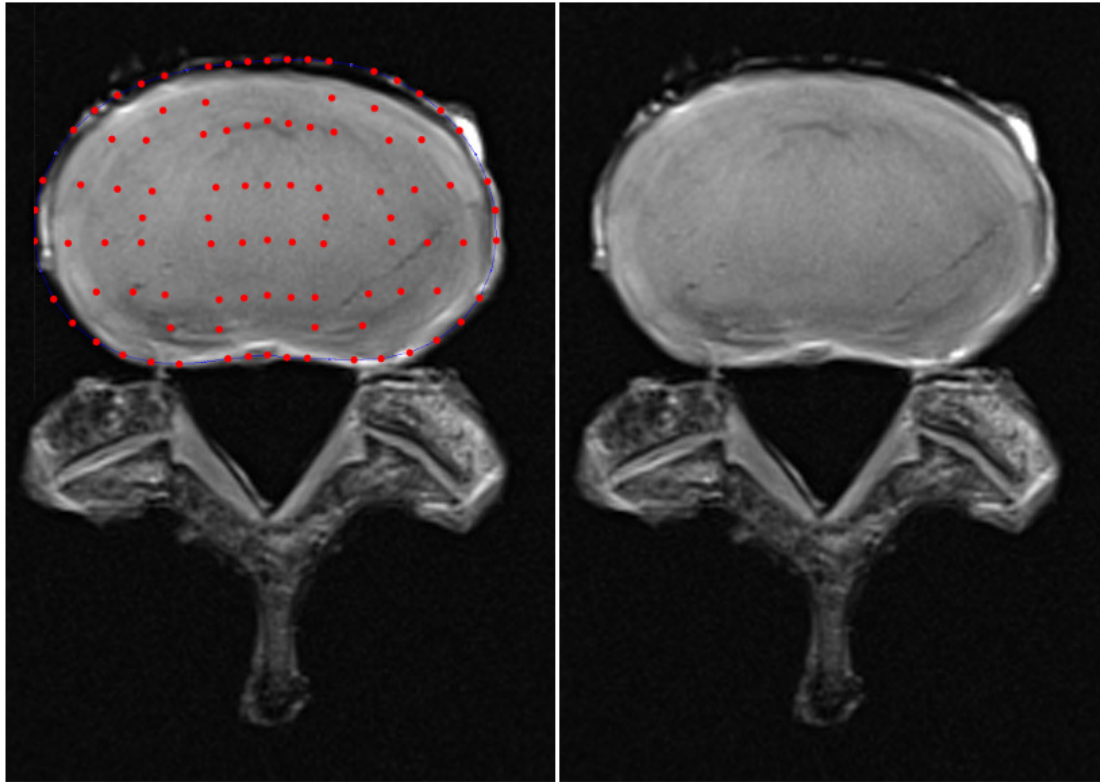
Specimen 9



**SCALE**

- 0 – No evidence of damage
- 1 – Delamination or Tears
- 2 – Nucleus Migration and/or Annulus Buckling
- 3 – Disc Bulge
- 4 – Disc Herniation

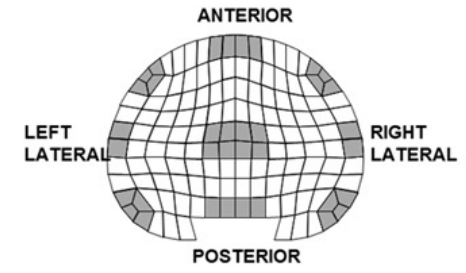
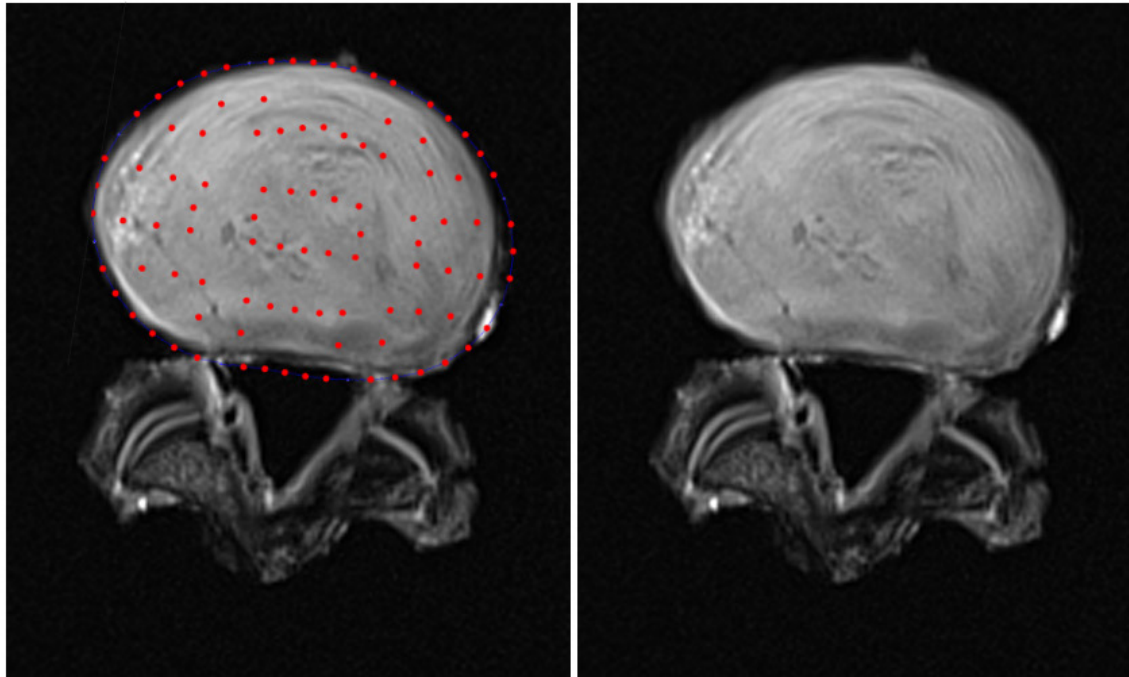
# Specimen 10



### SCALE

- 0 – No evidence of damage
- 1 – Delamination or Tears
- 2 – Nucleus Migration and/or Annulus Buckling
- 3 – Disc Bulge
- 4 – Disc Herniation

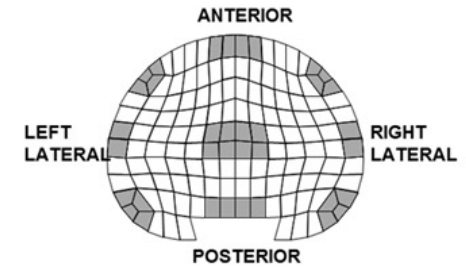
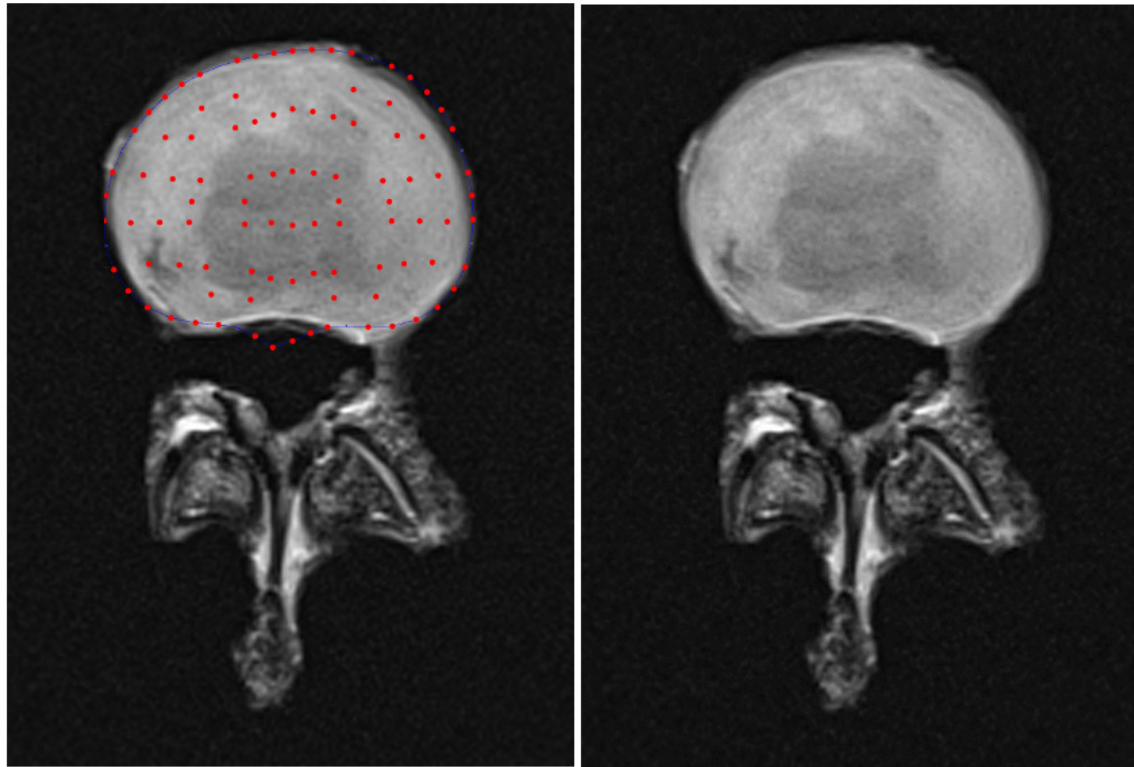
# Specimen 11



## SCALE

- 0 – No evidence of damage
- 1 – Delamination or Tears
- 2 – Nucleus Migration and/or Annulus Buckling
- 3 – Disc Bulge
- 4 – Disc Herniation

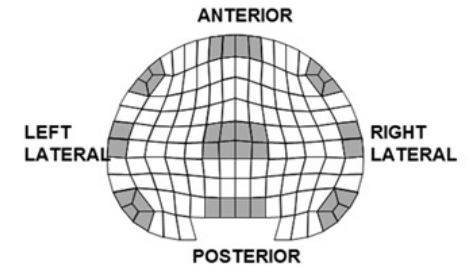
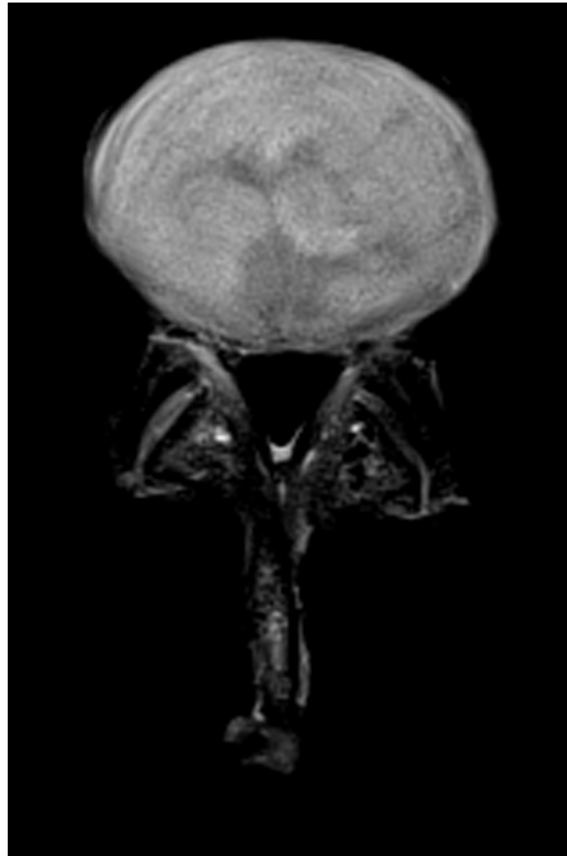
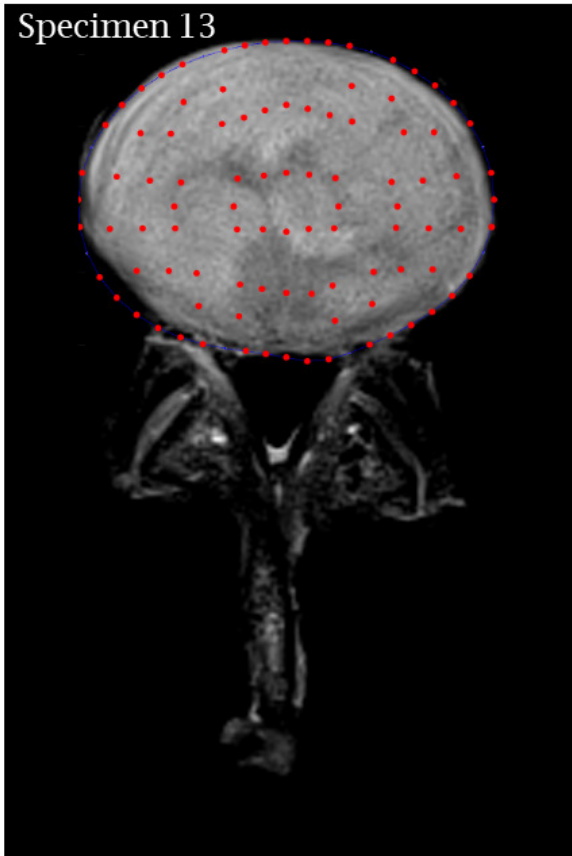
# Specimen 12



### SCALE

- 0 – No evidence of damage
- 1 – Delamination or Tears
- 2 – Nucleus Migration and/or Annulus Buckling
- 3 – Disc Bulge
- 4 – Disc Herniation

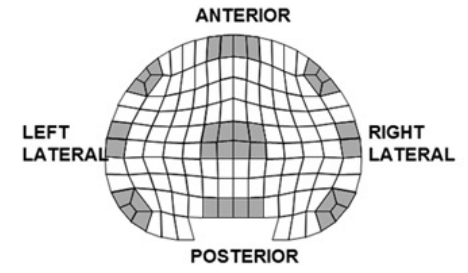
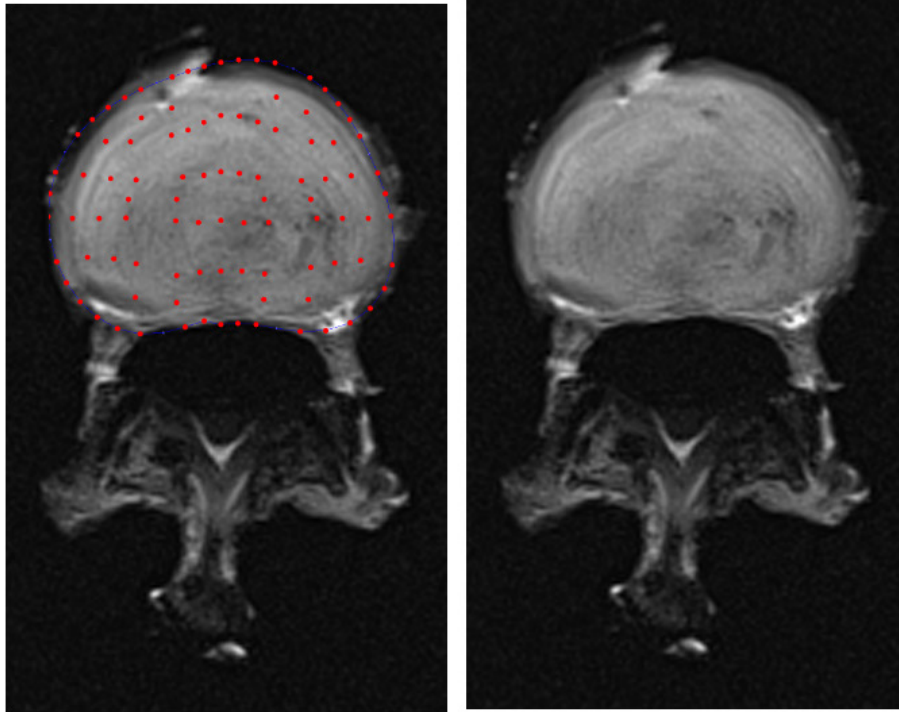
Specimen 13



**SCALE**

- 0 – No evidence of damage
- 1 – Delamination or Tears
- 2 – Nucleus Migration and/or Annulus Buckling
- 3 – Disc Bulge
- 4 – Disc Herniation

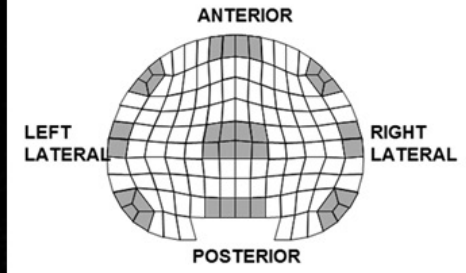
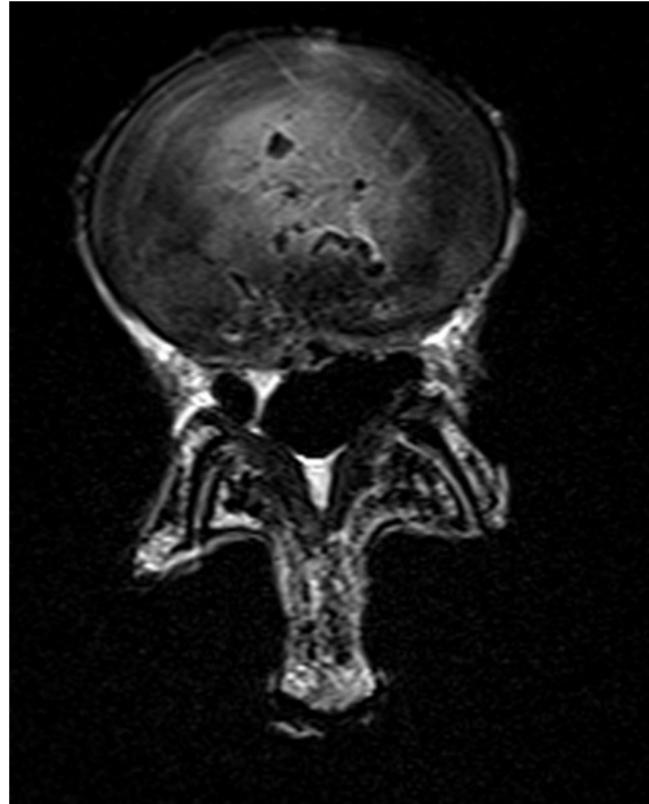
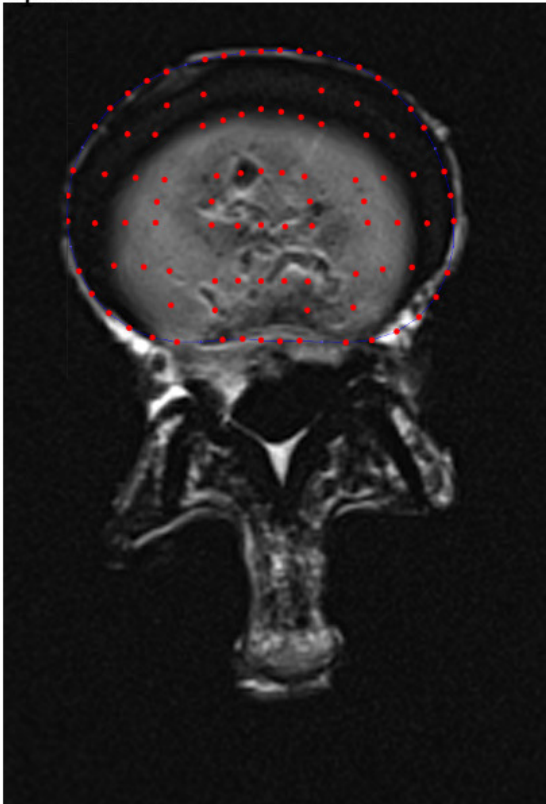
# Specimen 14



### SCALE

- 0 – No evidence of damage
- 1 – Delamination or Tears
- 2 – Nucleus Migration and/or Annulus Buckling
- 3 – Disc Bulge
- 4 – Disc Herniation

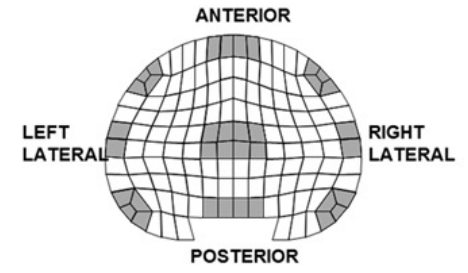
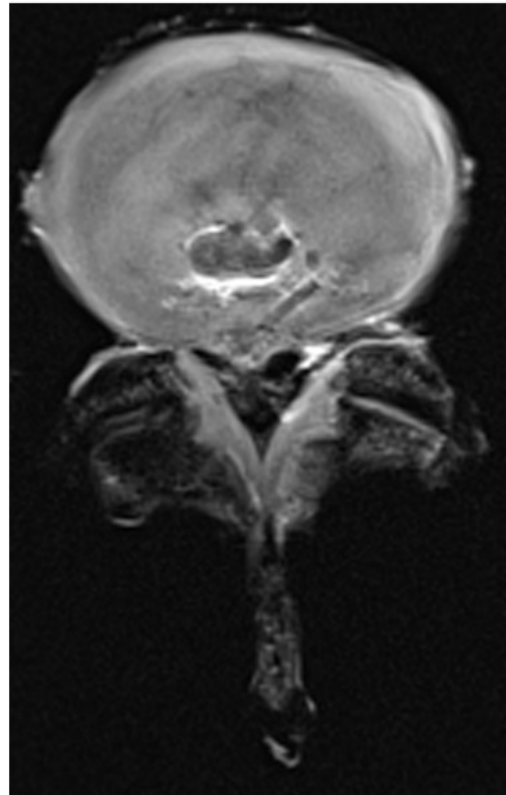
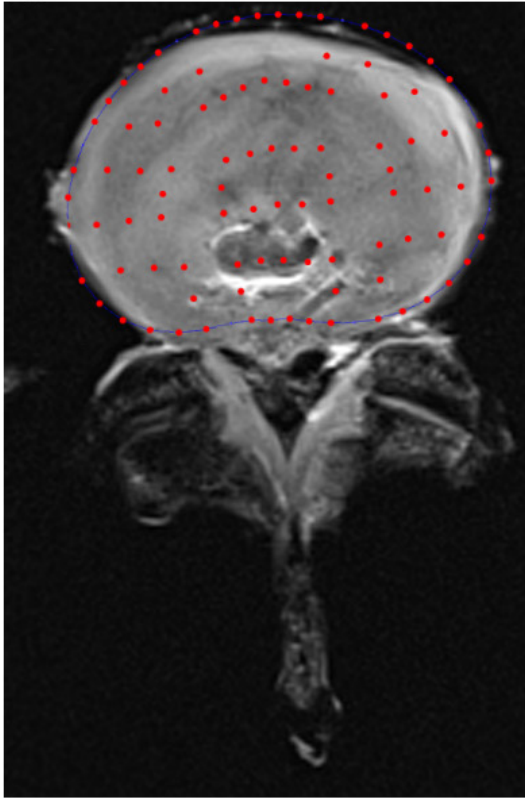
Specimen 15



**SCALE**

- 0 – No evidence of damage
- 1 – Delamination or Tears
- 2 – Nucleus Migration and/or  
Annulus Buckling
- 3 – Disc Bulge
- 4 – Disc Herniation

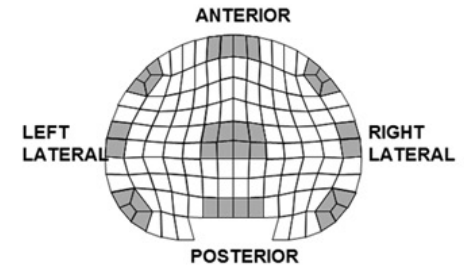
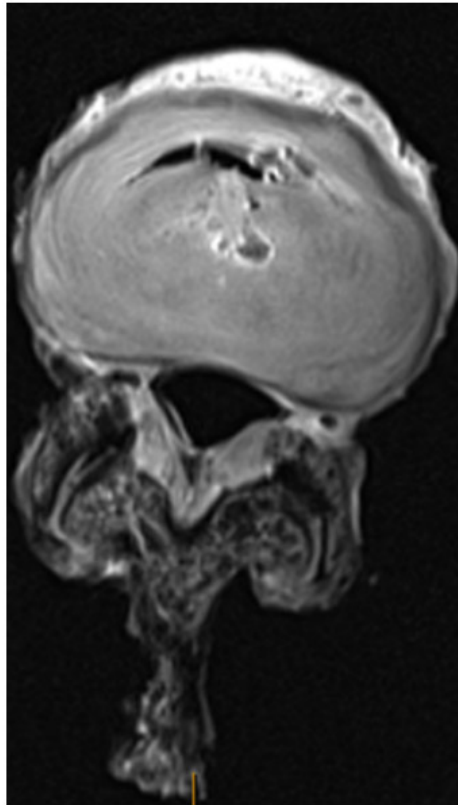
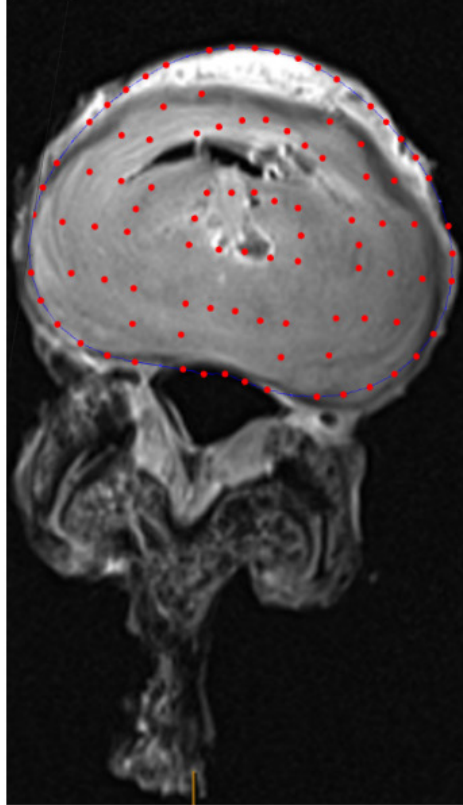
Specimen 16



**SCALE**

- 0 – No evidence of damage
- 1 – Delamination or Tears
- 2 – Nucleus Migration and/or  
Annulus Buckling
- 3 – Disc Bulge
- 4 – Disc Herniation

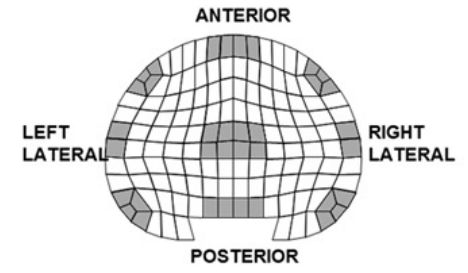
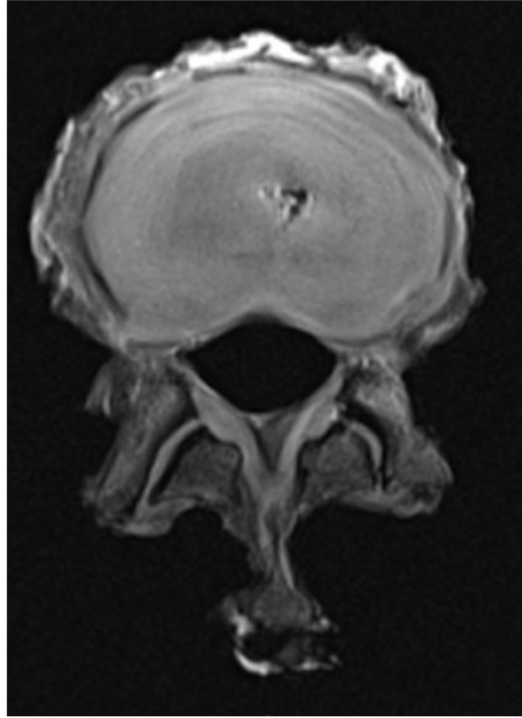
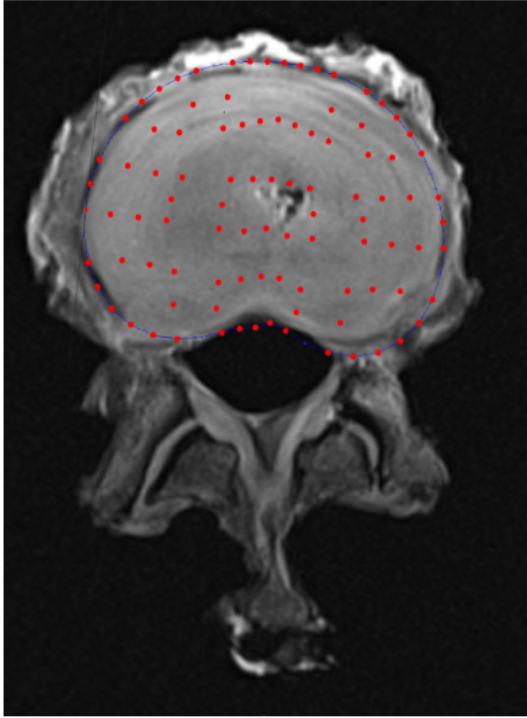
Specimen 17



**SCALE**

- 0 – No evidence of damage
- 1 – Delamination or Tears
- 2 – Nucleus Migration and/or Annulus Buckling
- 3 – Disc Bulge
- 4 – Disc Herniation

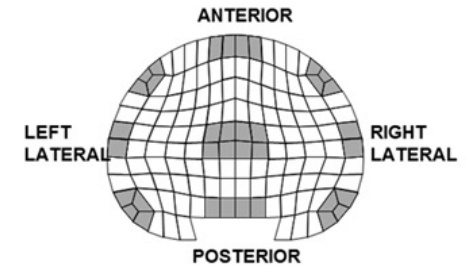
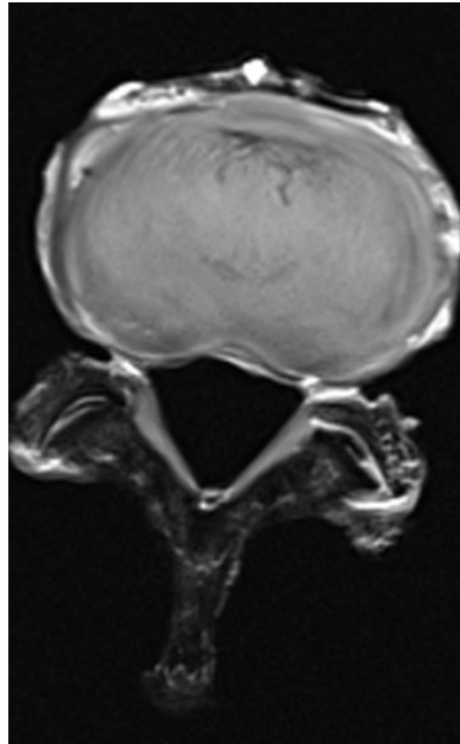
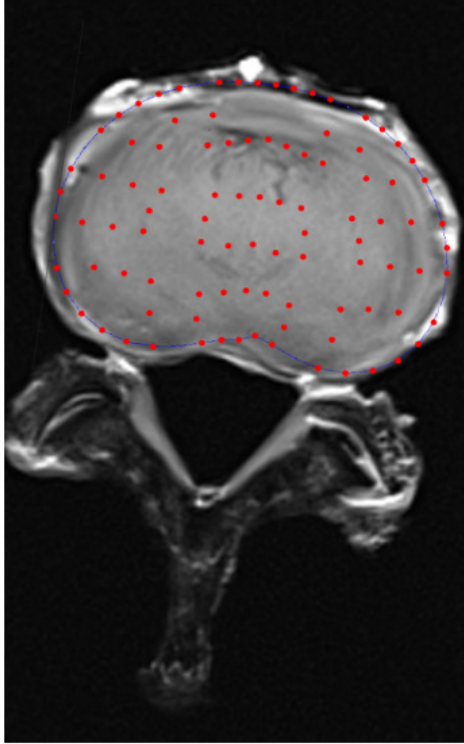
Specimen 18



SCALE

- 0 – No evidence of damage
- 1 – Delamination or Tears
- 2 – Nucleus Migration and/or Annulus Buckling
- 3 – Disc Bulge
- 4 – Disc Herniation

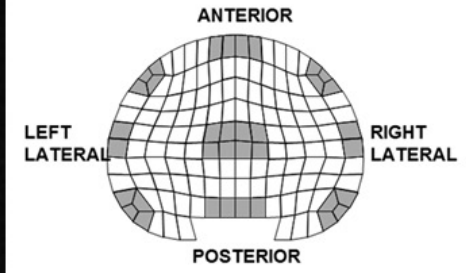
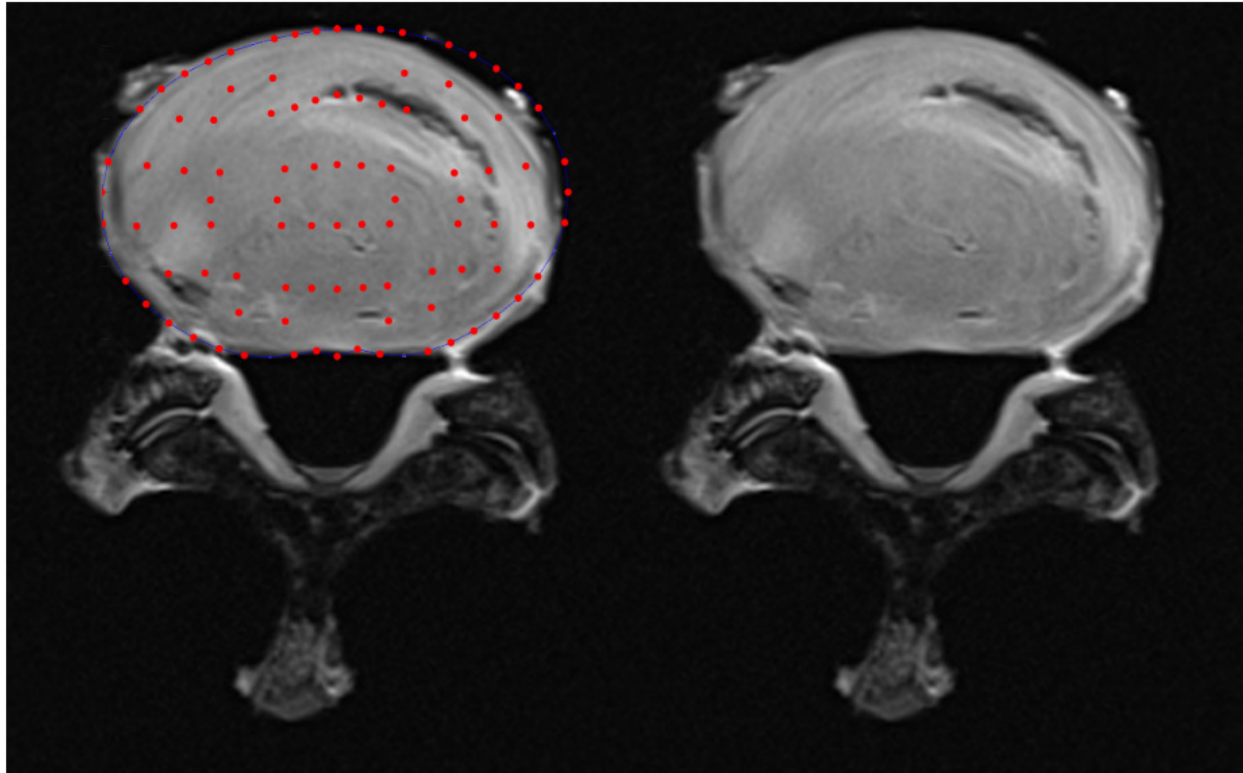
Specimen 19



SCALE

- 0 – No evidence of damage
- 1 – Delamination or Tears
- 2 – Nucleus Migration and/or  
Annulus Buckling
- 3 – Disc Bulge
- 4 – Disc Herniation

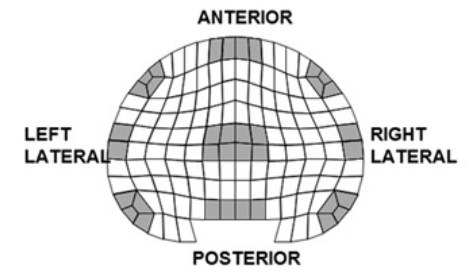
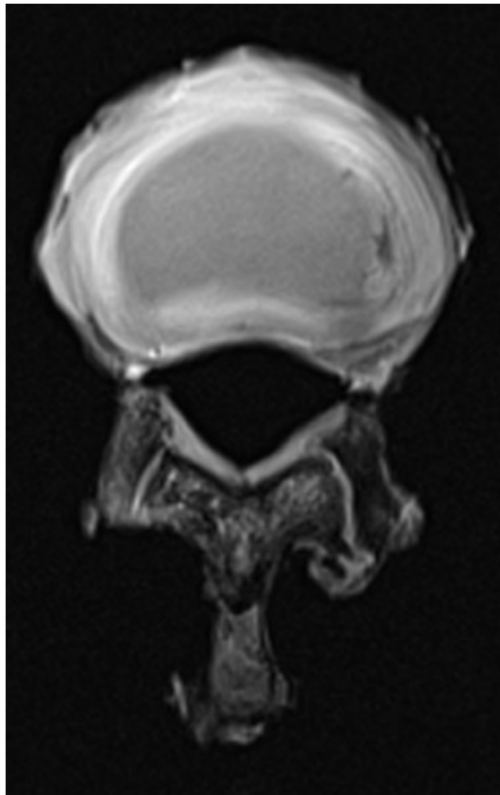
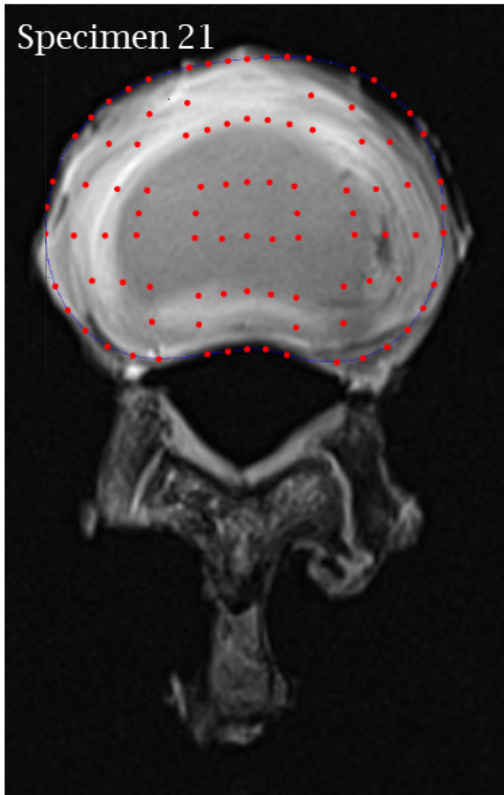
Specimen 20



**SCALE**

- 0 – No evidence of damage
- 1 – Delamination or Tears
- 2 – Nucleus Migration and/or  
Annulus Buckling
- 3 – Disc Bulge
- 4 – Disc Herniation

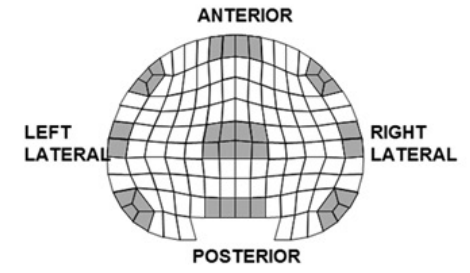
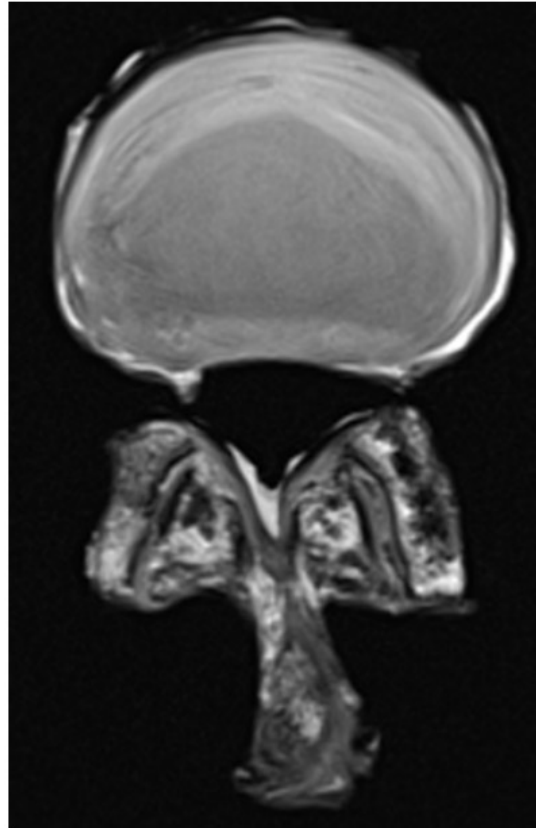
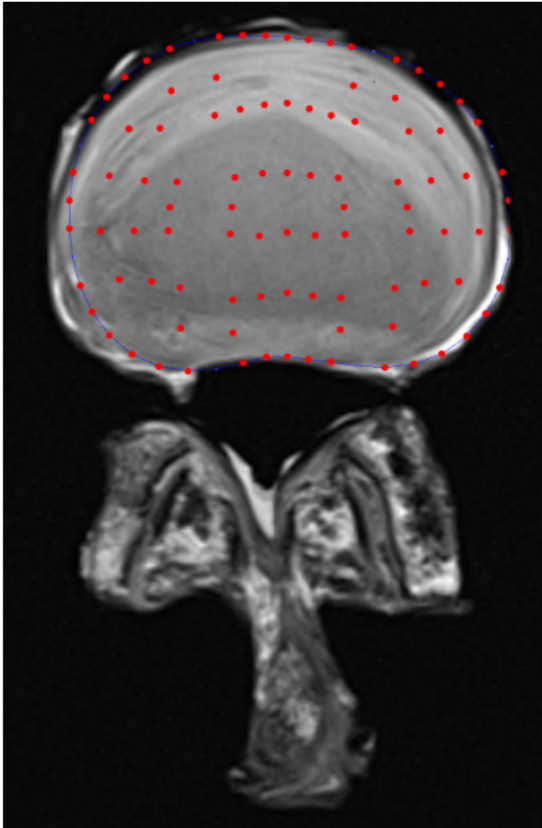
Specimen 21



**SCALE**

- 0 – No evidence of damage
- 1 – Delamination or Tears
- 2 – Nucleus Migration and/or  
Annulus Buckling
- 3 – Disc Bulge
- 4 – Disc Herniation

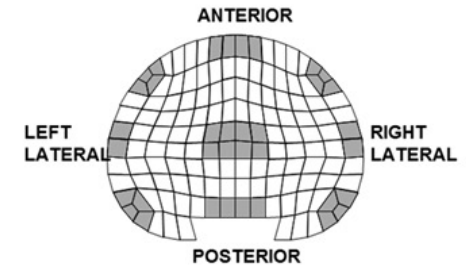
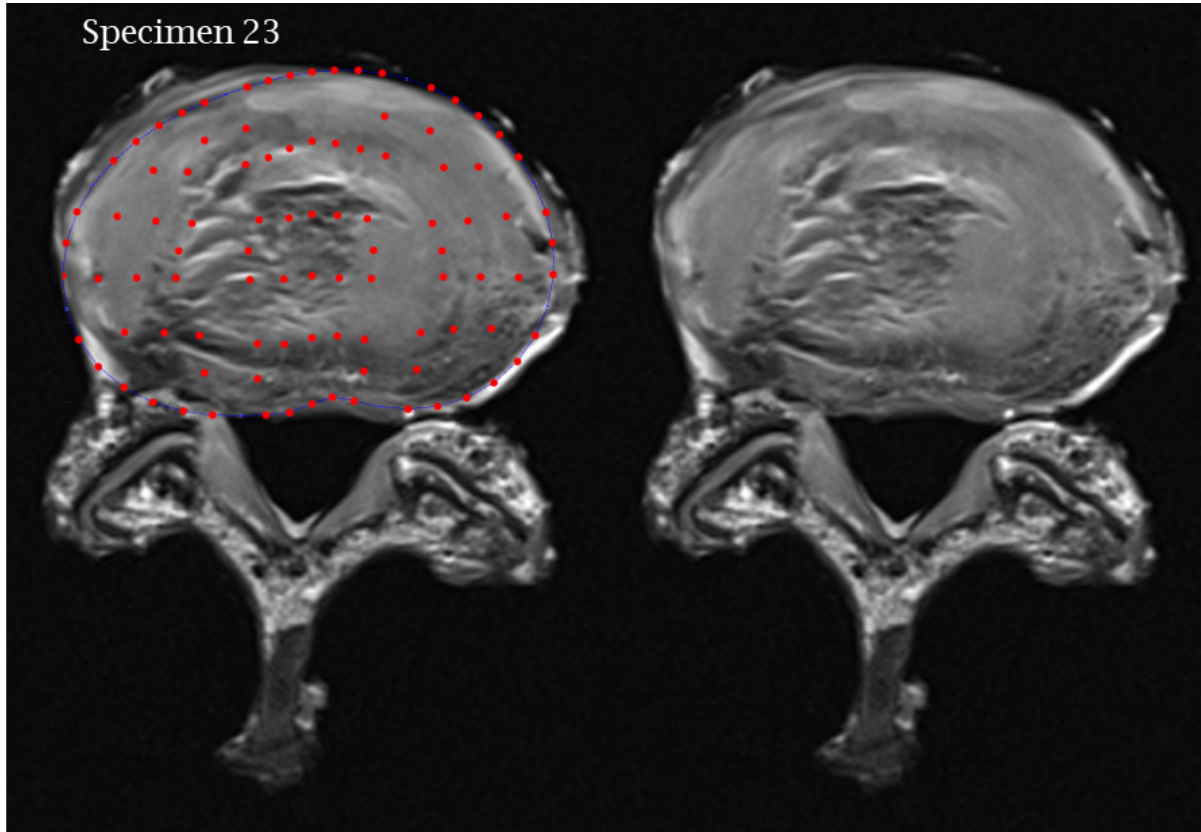
Specimen 22



**SCALE**

- 0 – No evidence of damage
- 1 – Delamination or Tears
- 2 – Nucleus Migration and/or Annulus Buckling
- 3 – Disc Bulge
- 4 – Disc Herniation

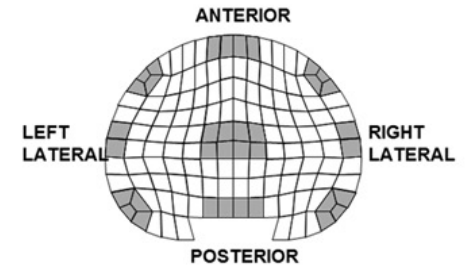
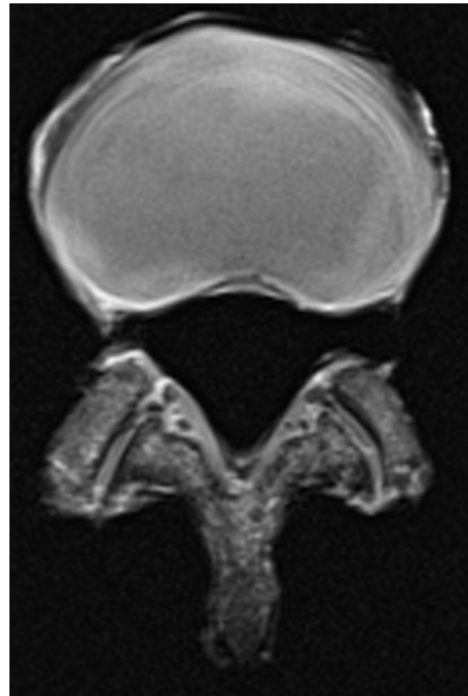
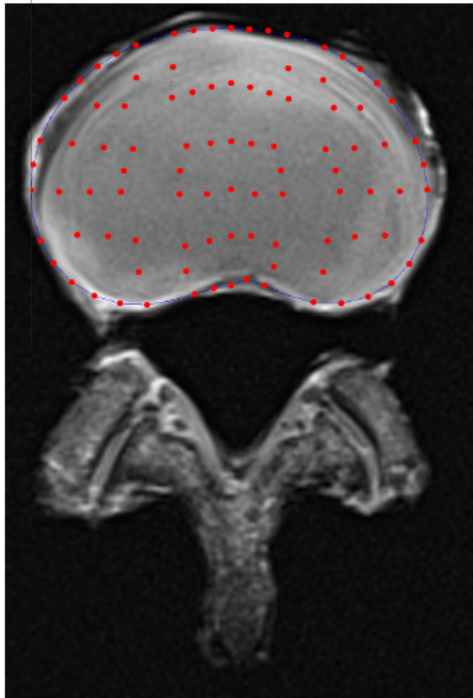
Specimen 23



**SCALE**

- 0 – No evidence of damage
- 1 – Delamination or Tears
- 2 – Nucleus Migration and/or  
Annulus Buckling
- 3 – Disc Bulge
- 4 – Disc Herniation

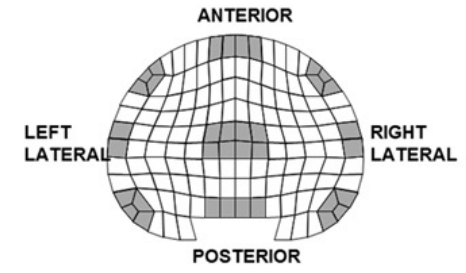
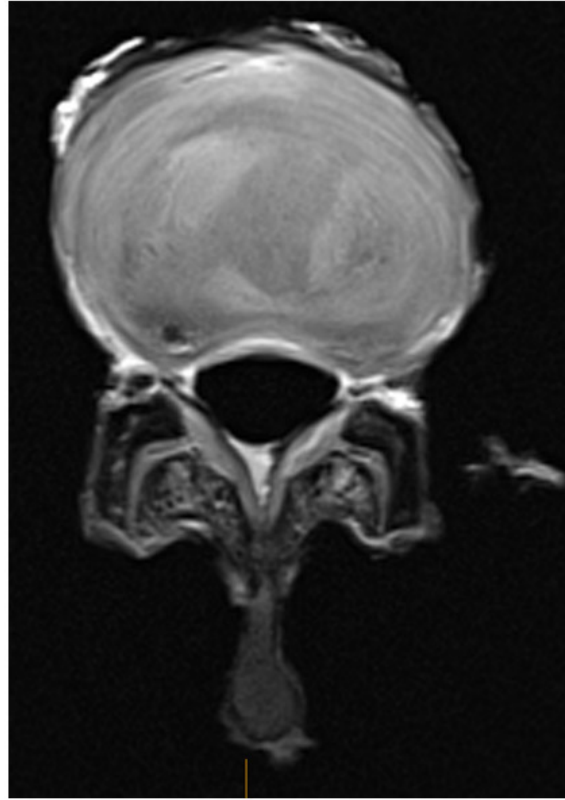
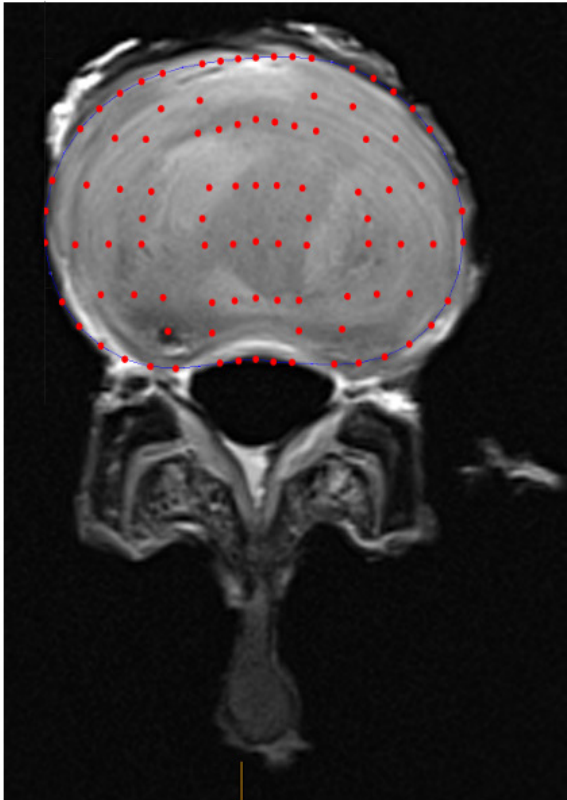
Specimen 24



**SCALE**

- 0 – No evidence of damage
- 1 – Delamination or Tears
- 2 – Nucleus Migration and/or  
Annulus Buckling
- 3 – Disc Bulge
- 4 – Disc Herniation

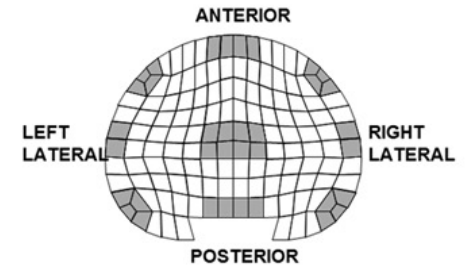
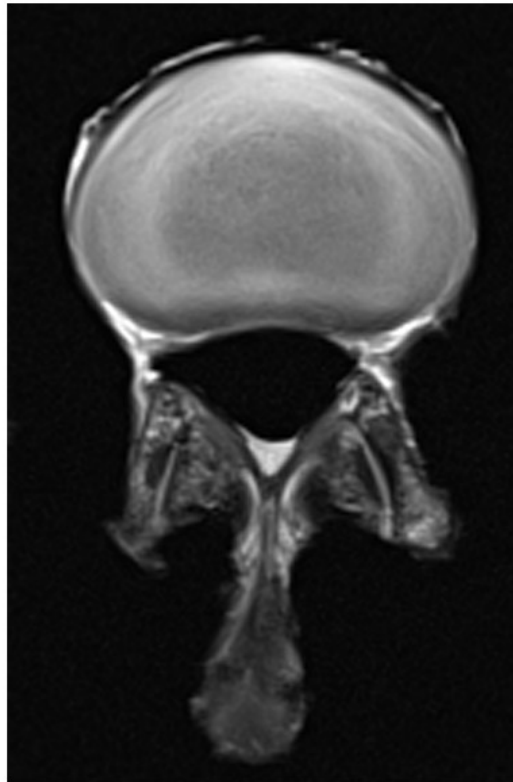
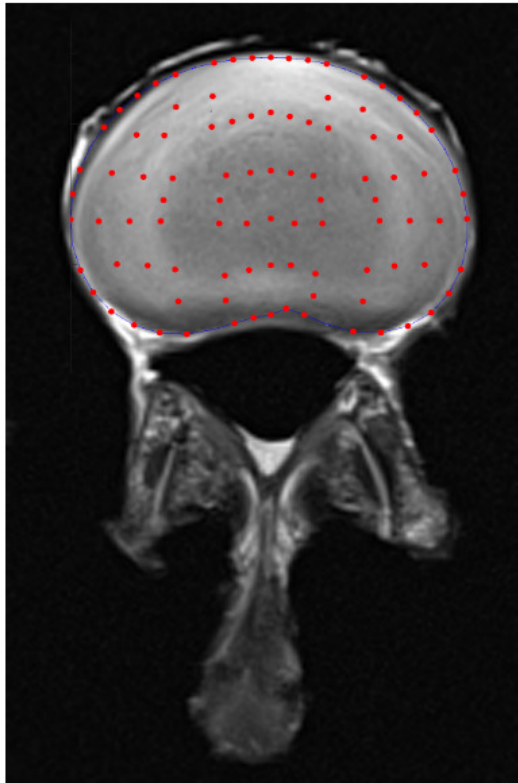
Specimen 25



**SCALE**

- 0 – No evidence of damage
- 1 – Delamination or Tears
- 2 – Nucleus Migration and/or  
Annulus Buckling
- 3 – Disc Bulge
- 4 – Disc Herniation

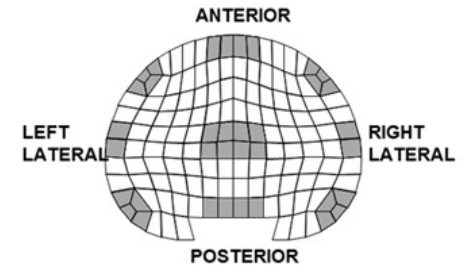
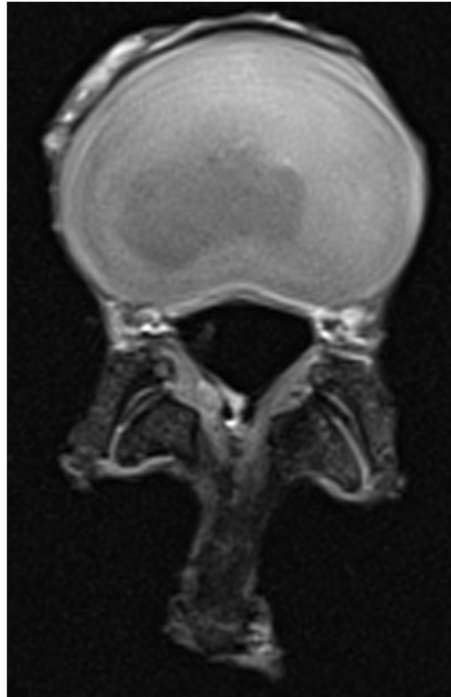
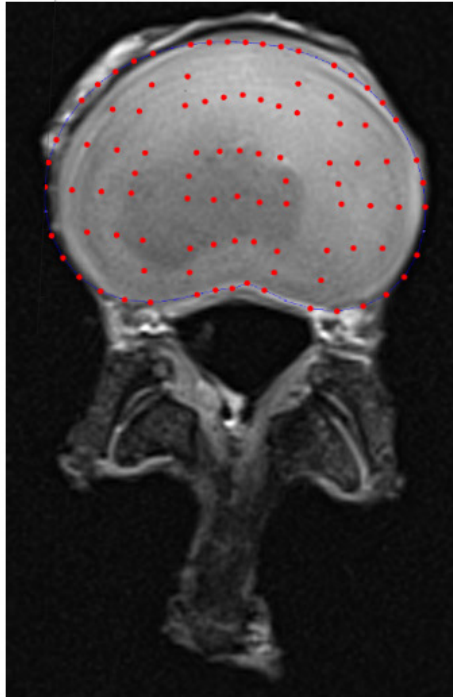
Specimen 26



**SCALE**

- 0 – No evidence of damage
- 1 – Delamination or Tears
- 2 – Nucleus Migration and/or Annulus Buckling
- 3 – Disc Bulge
- 4 – Disc Herniation

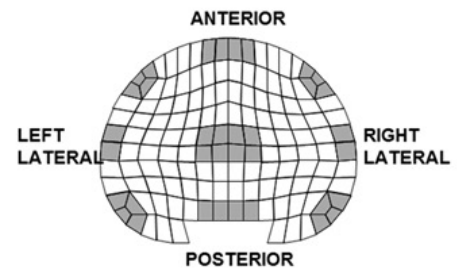
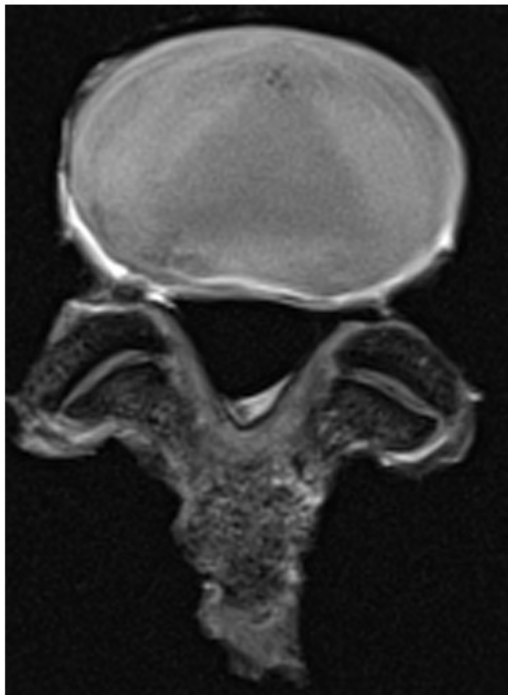
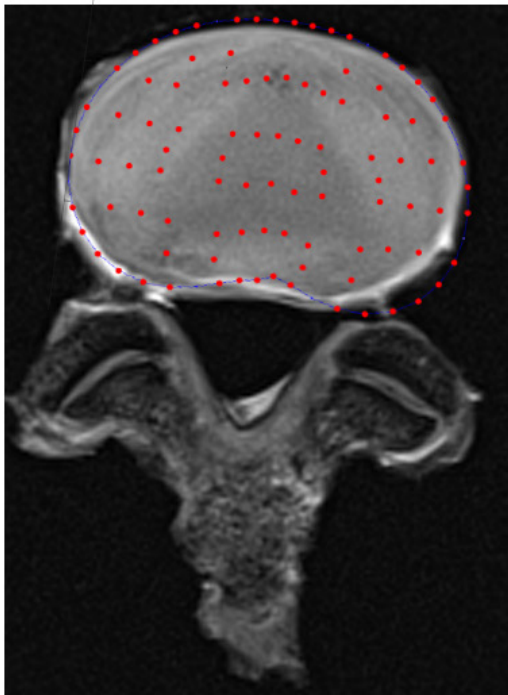
Specimen 27



SCALE

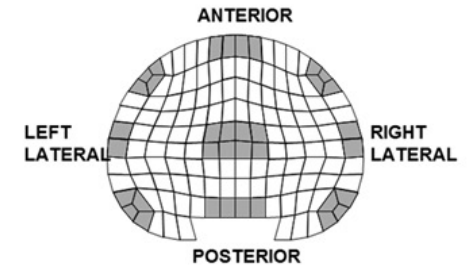
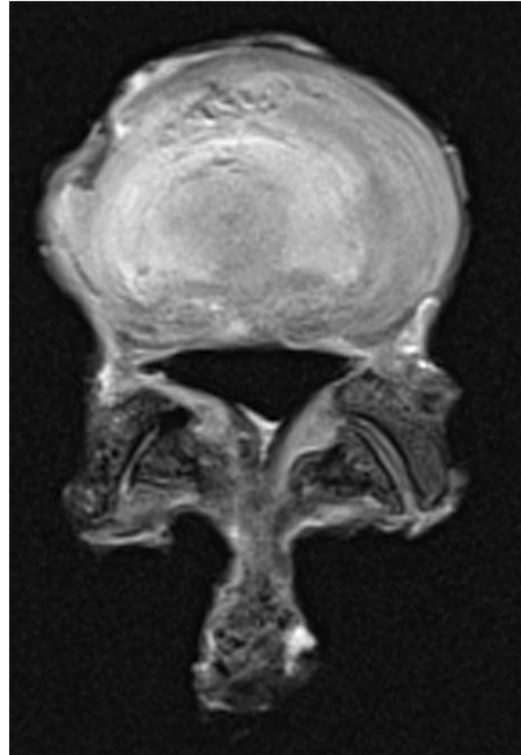
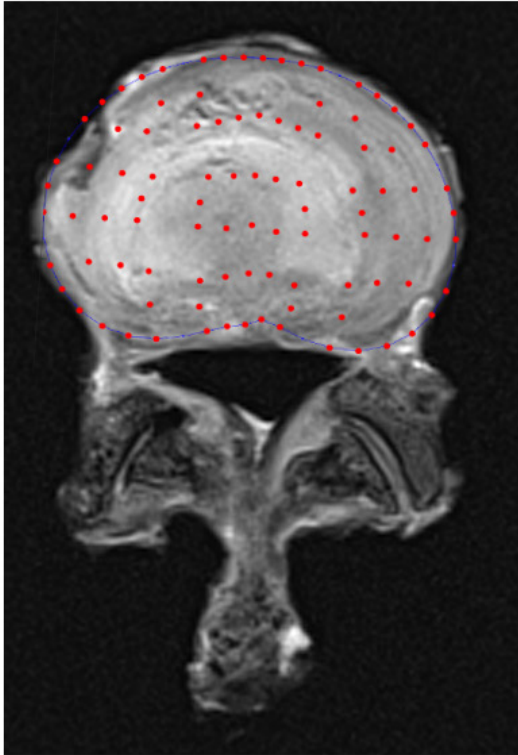
- 0 – No evidence of damage
- 1 – Delamination or Tears
- 2 – Nucleus Migration and/or  
Annulus Buckling
- 3 – Disc Bulge
- 4 – Disc Herniation

Specimen 28



1. Nuclear Prolapse
2. Outward Transverse Annulus Buckling
3. Adjacent Lamella Delamination
4. Circumferential Tears
5. Radial Tears

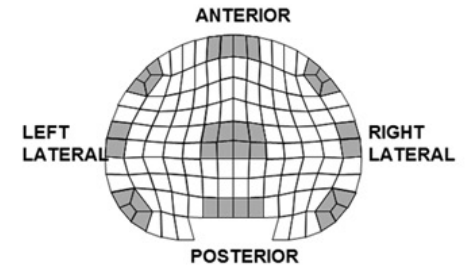
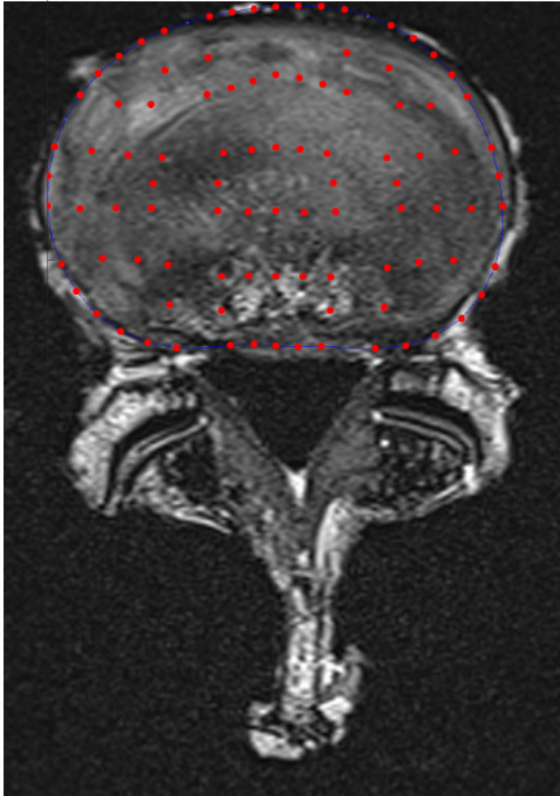
Specimen 29



**SCALE**

- 0 – No evidence of damage
- 1 – Delamination or Tears
- 2 – Nucleus Migration and/or Annulus Buckling
- 3 – Disc Bulge
- 4 – Disc Herniation

Specimen 30



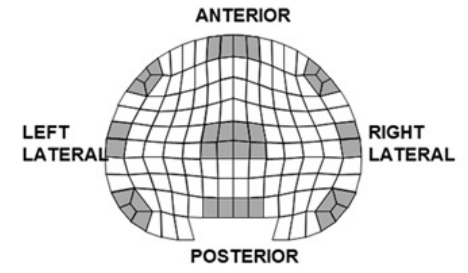
**SCALE**

- 0 – No evidence of damage
- 1 – Delamination or Tears
- 2 – Nucleus Migration and/or Annulus Buckling
- 3 – Disc Bulge
- 4 – Disc Herniation

## H.1.2 Macroscopic Images

Slides with macroscopic images from both simulated safe and unsafe repetitive lifting that were given to each reviewer are presented below. The left and right images are identical, however, the right image has the superimposed disc regions for regional grading.

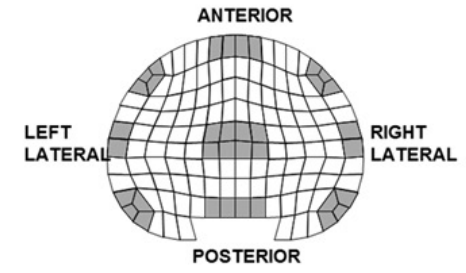
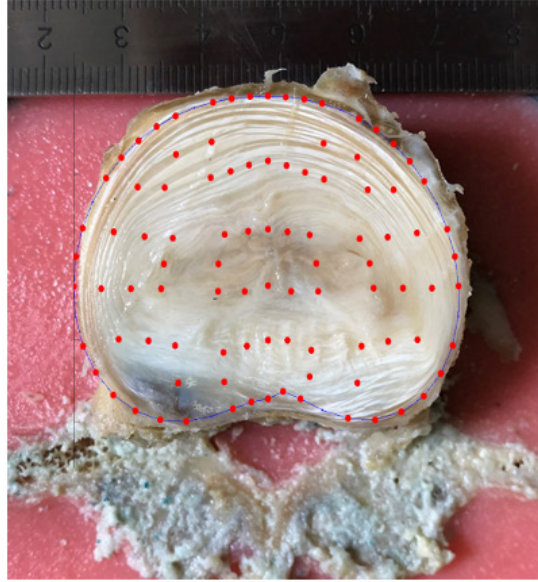
Specimen 1



**SCALE**

- 0 – No evidence of damage
- 1 – Delamination or Tears
- 2 – Nucleus Migration and/or  
Annulus Buckling
- 3 – Disc Bulge
- 4 – Disc Herniation

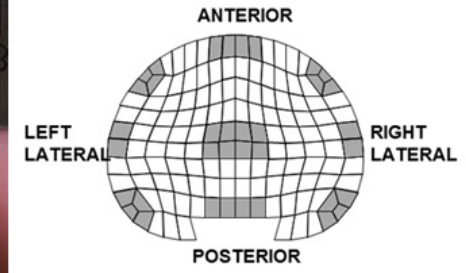
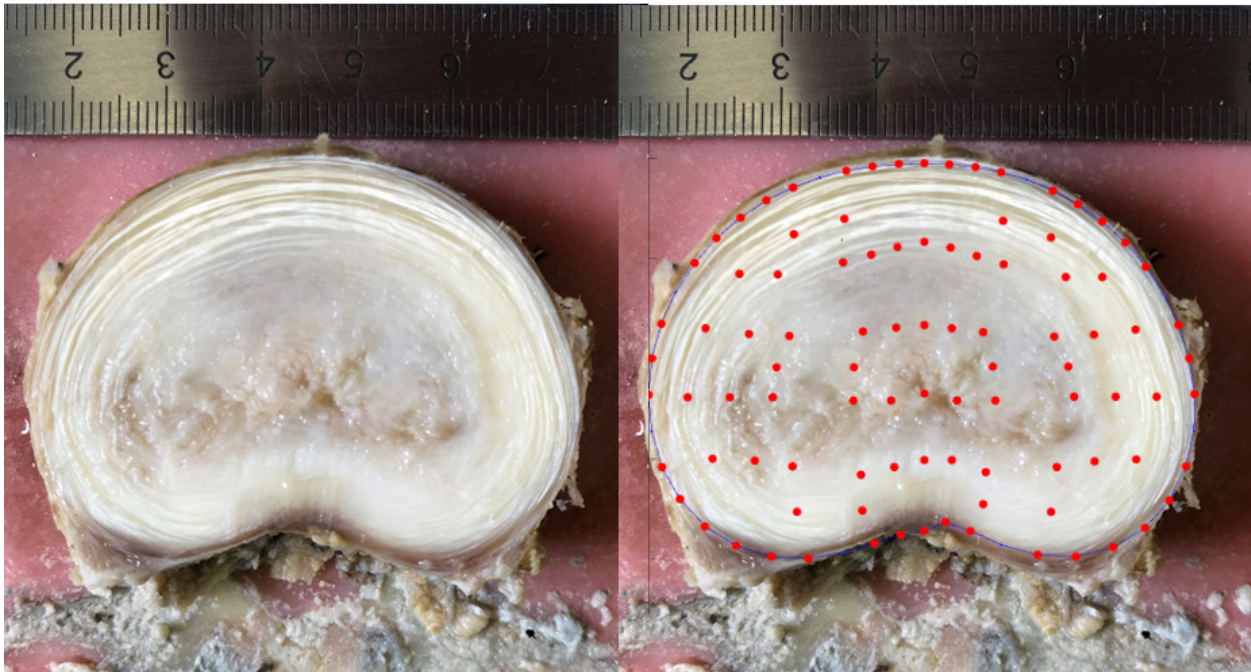
## Specimen 2



### SCALE

- 0 – No evidence of damage
- 1 – Delamination or Tears
- 2 – Nucleus Migration and/or  
Annulus Buckling
- 3 – Disc Bulge
- 4 – Disc Herniation

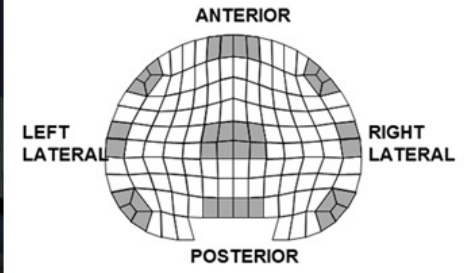
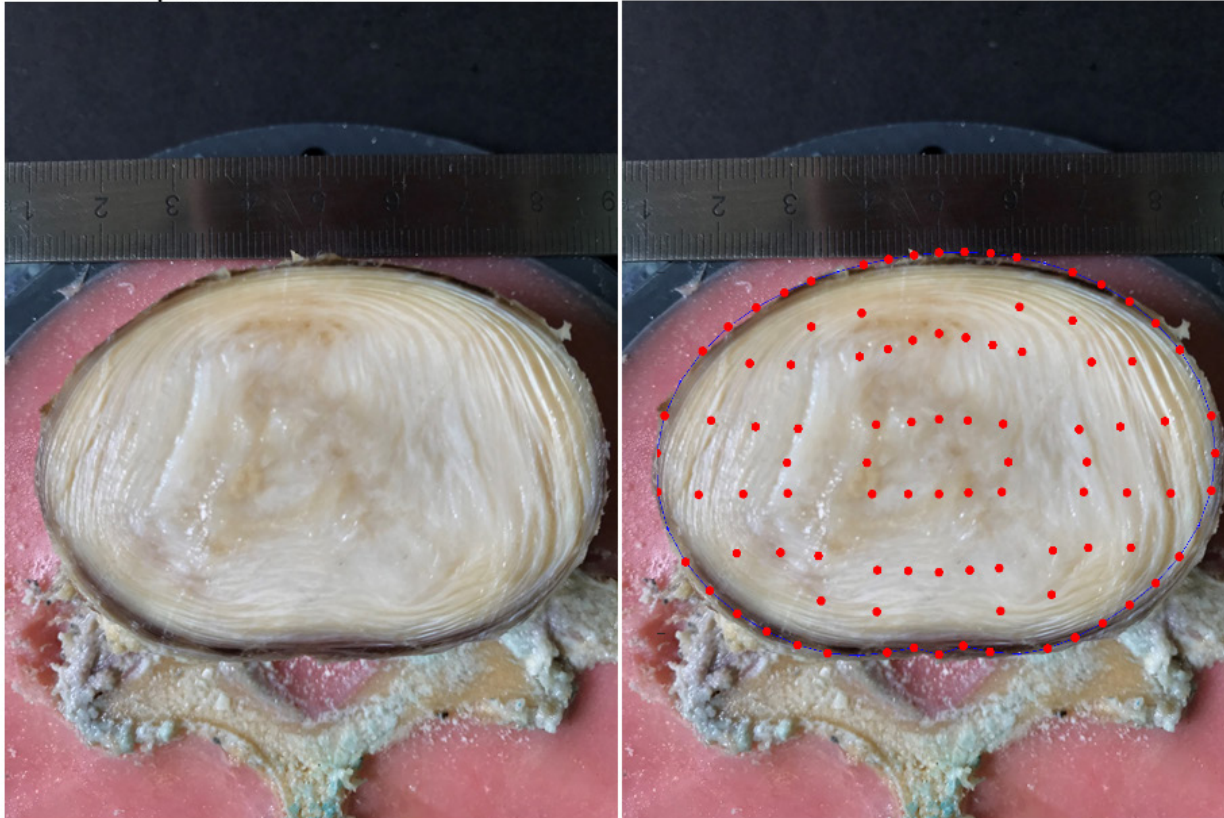
### Specimen 3



#### SCALE

- 0 – No evidence of damage
- 1 – Delamination or Tears
- 2 – Nucleus Migration and/or Annulus Buckling
- 3 – Disc Bulge
- 4 – Disc Herniation

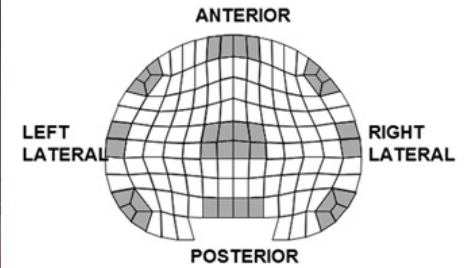
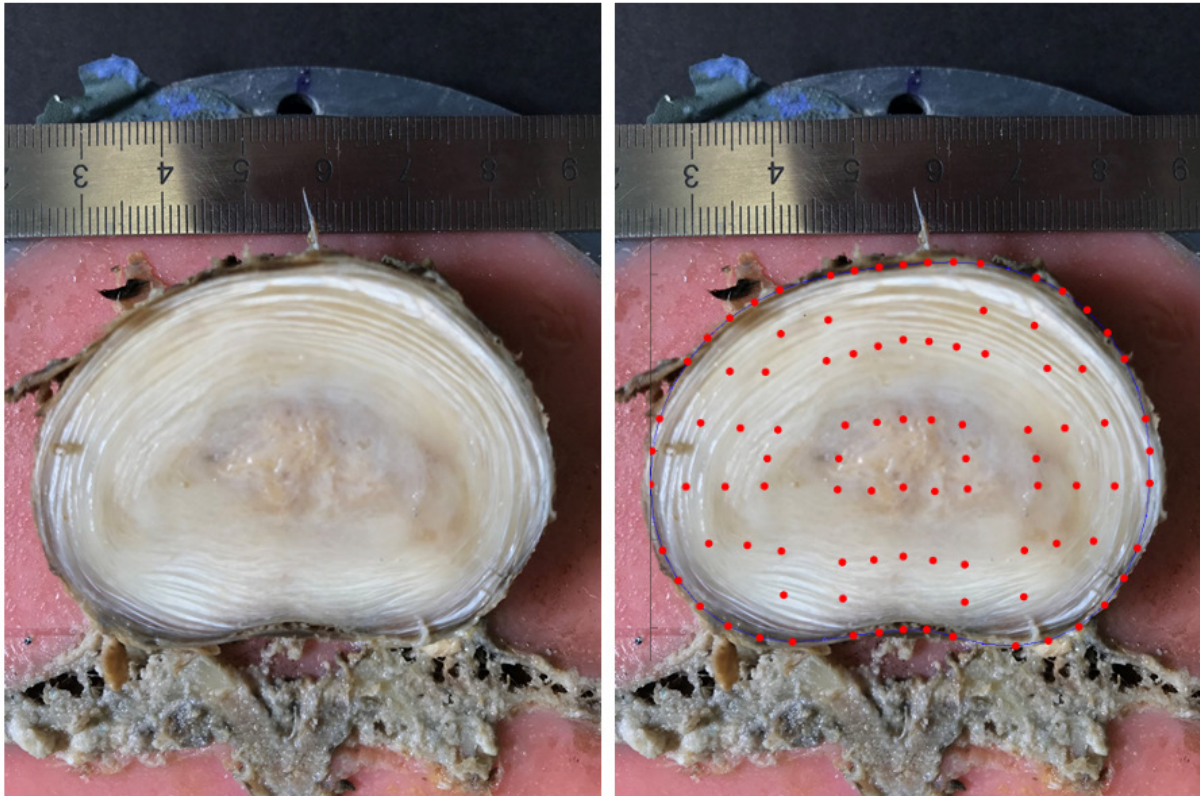
Specimen 4



**SCALE**

- 0 – No evidence of damage
- 1 – Delamination or Tears
- 2 – Nucleus Migration and/or Annulus Buckling
- 3 – Disc Bulge
- 4 – Disc Herniation

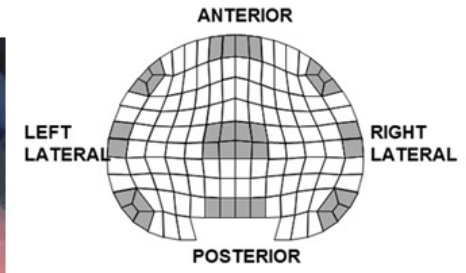
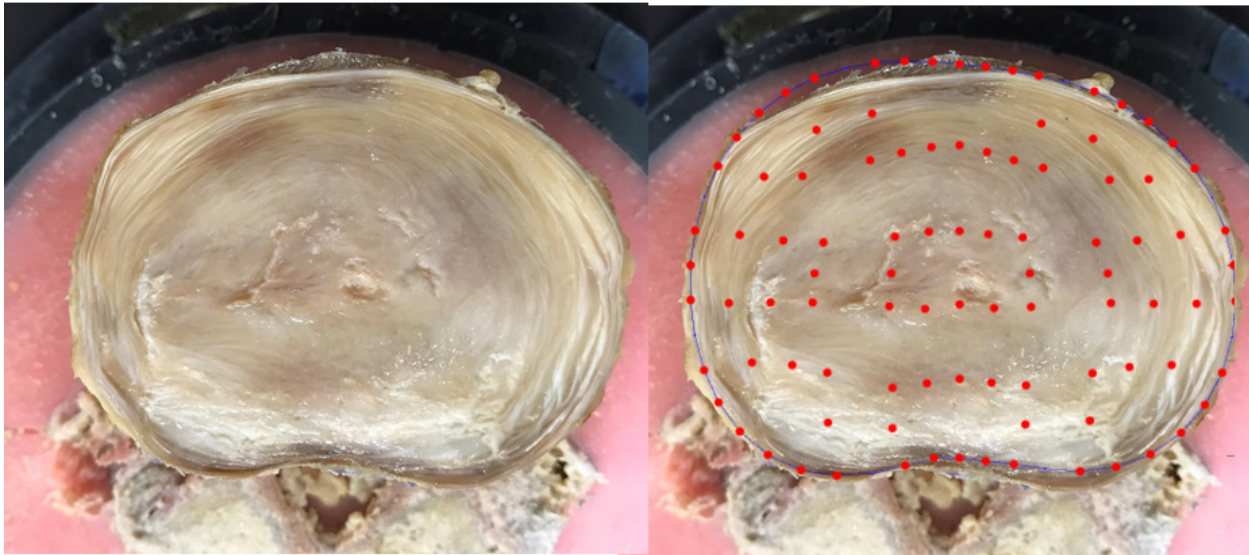
Specimen 5



SCALE

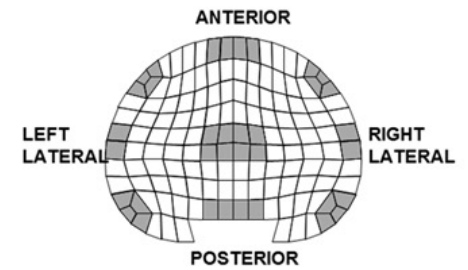
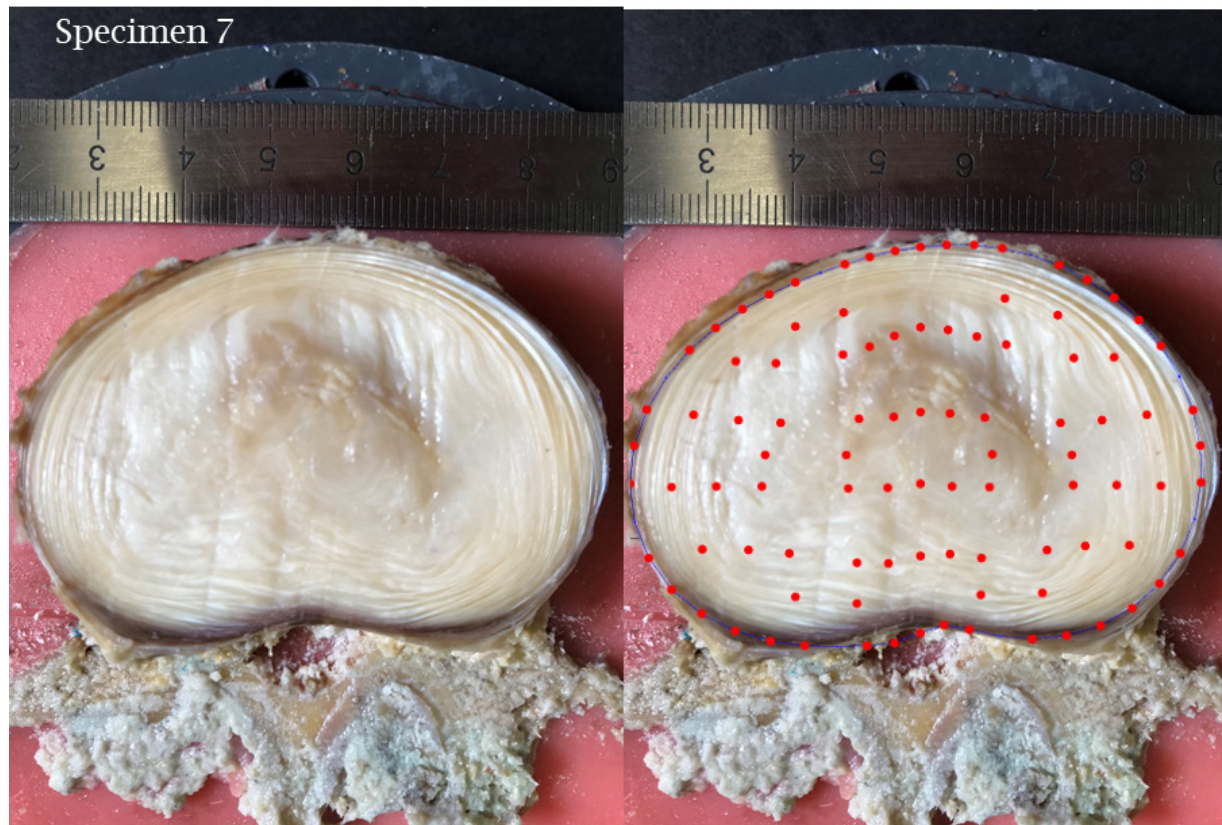
- 0 – No evidence of damage
- 1 – Delamination or Tears
- 2 – Nucleus Migration and/or Annulus Buckling
- 3 – Disc Bulge
- 4 – Disc Herniation

## Specimen 6



### SCALE

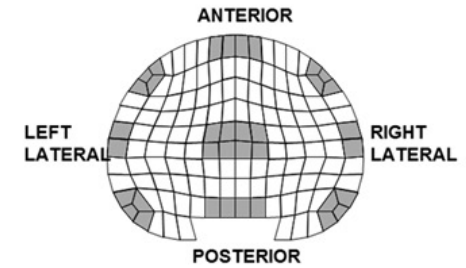
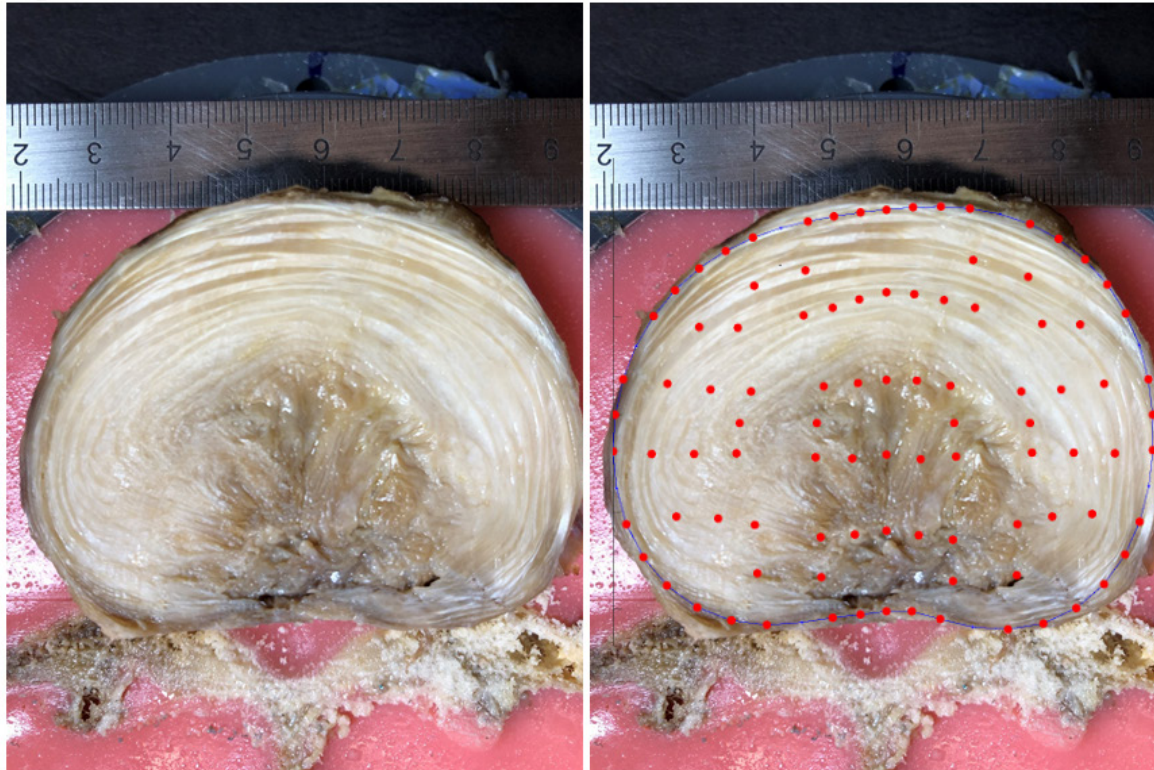
- 0 – No evidence of damage
- 1 – Delamination or Tears
- 2 – Nucleus Migration and/or  
Annulus Buckling
- 3 – Disc Bulge
- 4 – Disc Herniation



**SCALE**

- 0 – No evidence of damage
- 1 – Delamination or Tears
- 2 – Nucleus Migration and/or  
Annulus Buckling
- 3 – Disc Bulge
- 4 – Disc Herniation

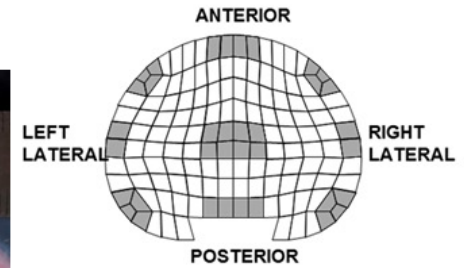
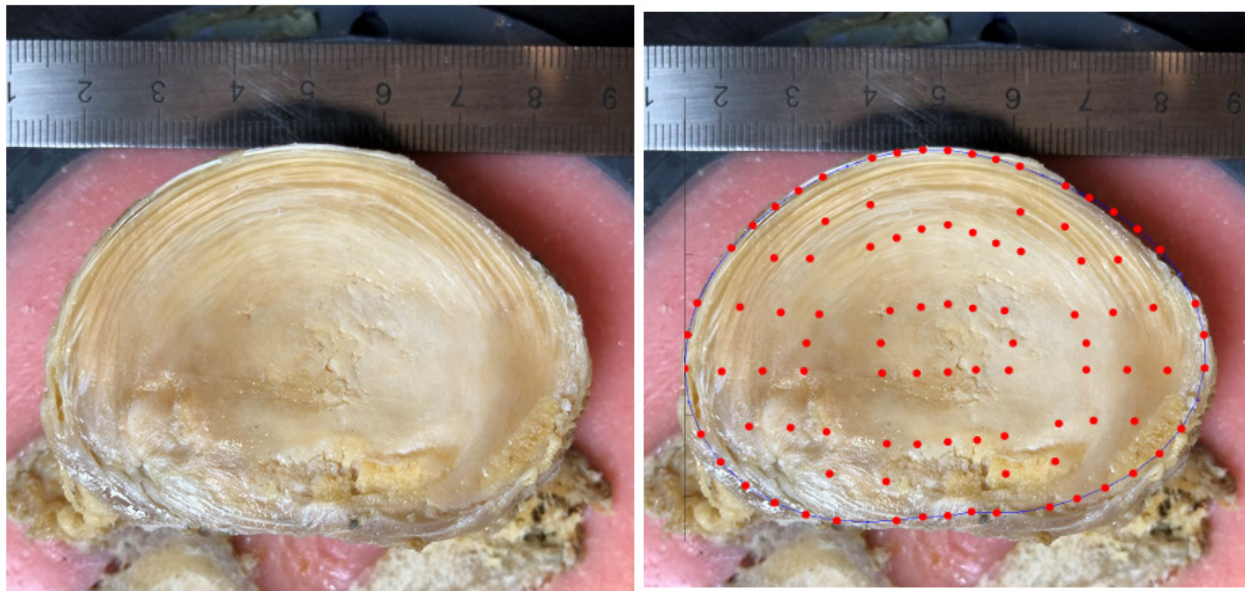
Specimen 8



**SCALE**

- 0 – No evidence of damage
- 1 – Delamination or Tears
- 2 – Nucleus Migration and/or Annulus Buckling
- 3 – Disc Bulge
- 4 – Disc Herniation

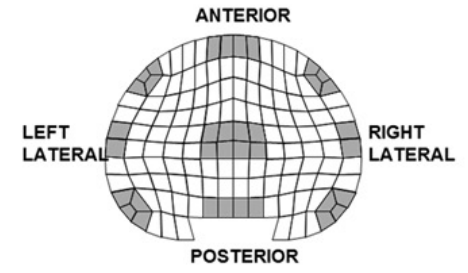
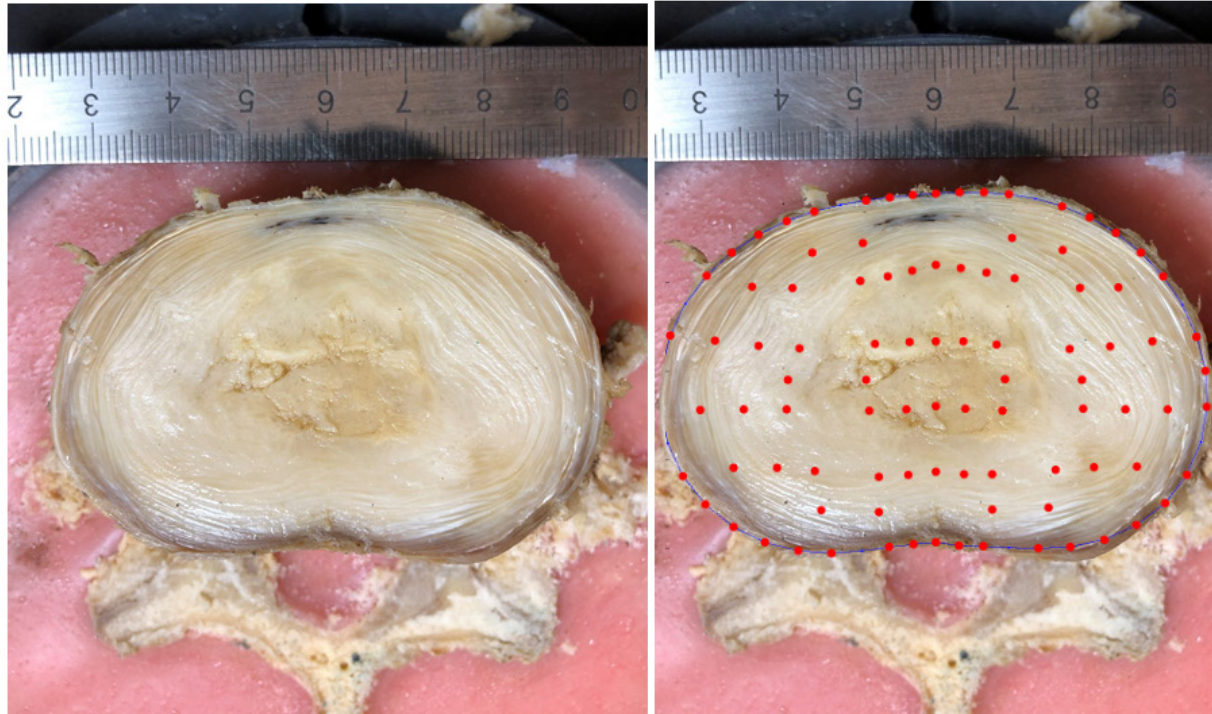
# Specimen 9



### SCALE

- 0 – No evidence of damage
- 1 – Delamination or Tears
- 2 – Nucleus Migration and/or Annulus Buckling
- 3 – Disc Bulge
- 4 – Disc Herniation

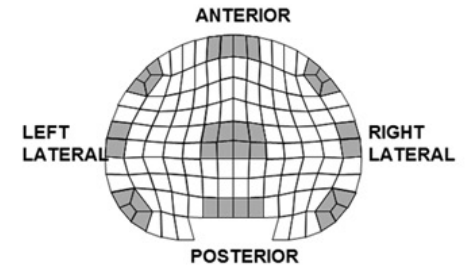
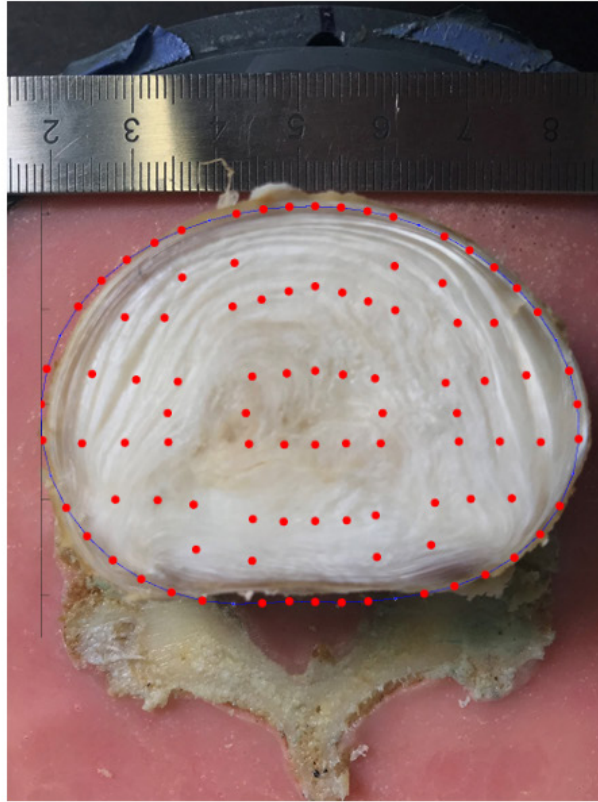
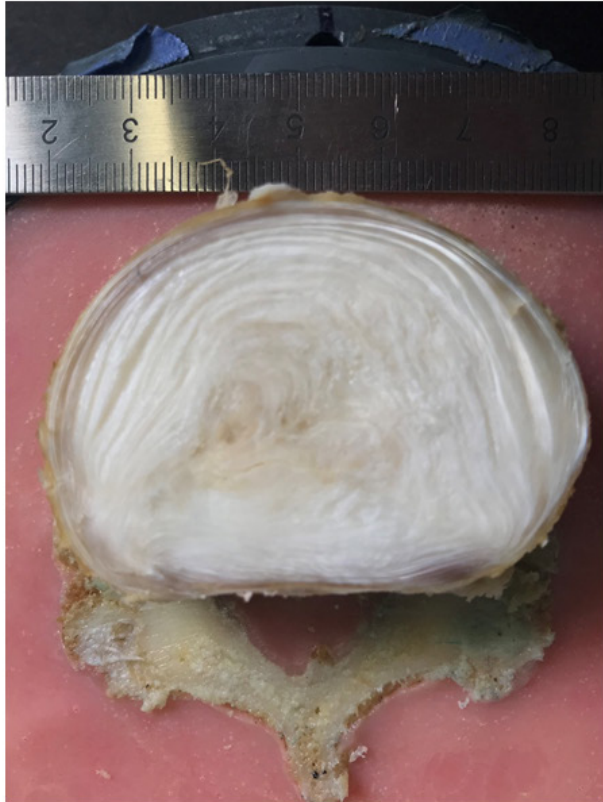
# Specimen 10



### SCALE

- 0 – No evidence of damage
- 1 – Delamination or Tears
- 2 – Nucleus Migration and/or Annulus Buckling
- 3 – Disc Bulge
- 4 – Disc Herniation

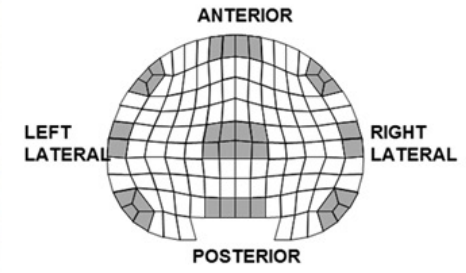
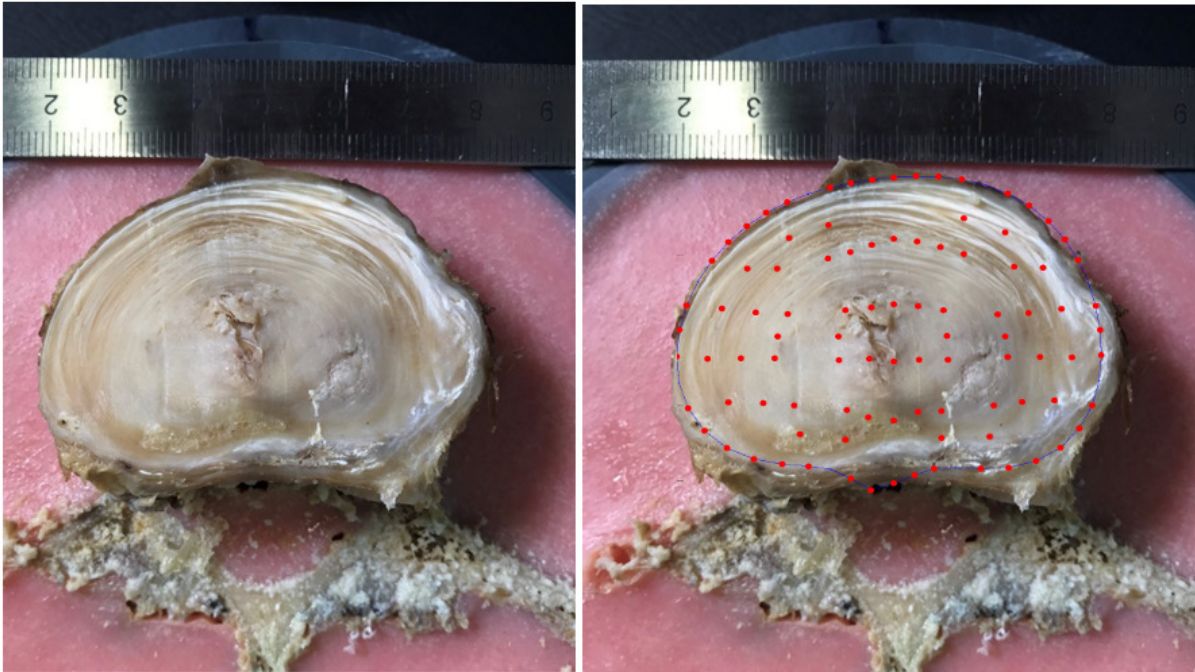
# Specimen 11



### SCALE

- 0 – No evidence of damage
- 1 – Delamination or Tears
- 2 – Nucleus Migration and/or Annulus Buckling
- 3 – Disc Bulge
- 4 – Disc Herniation

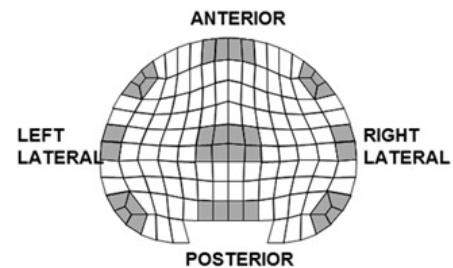
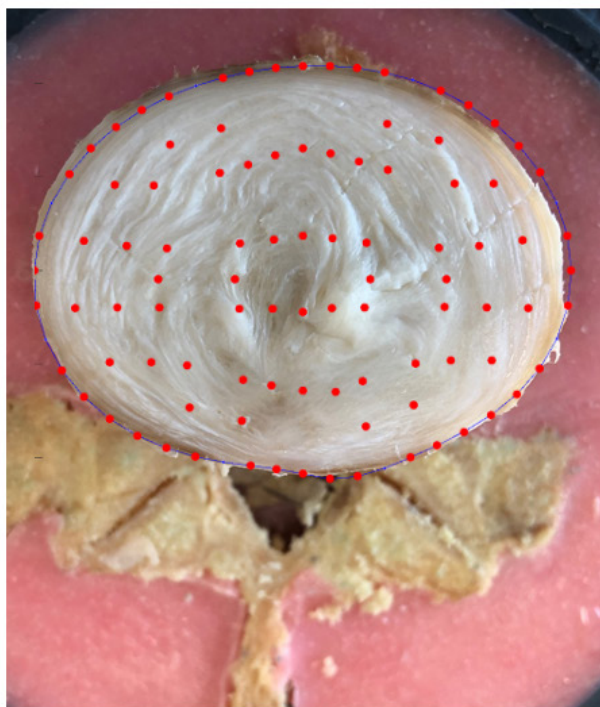
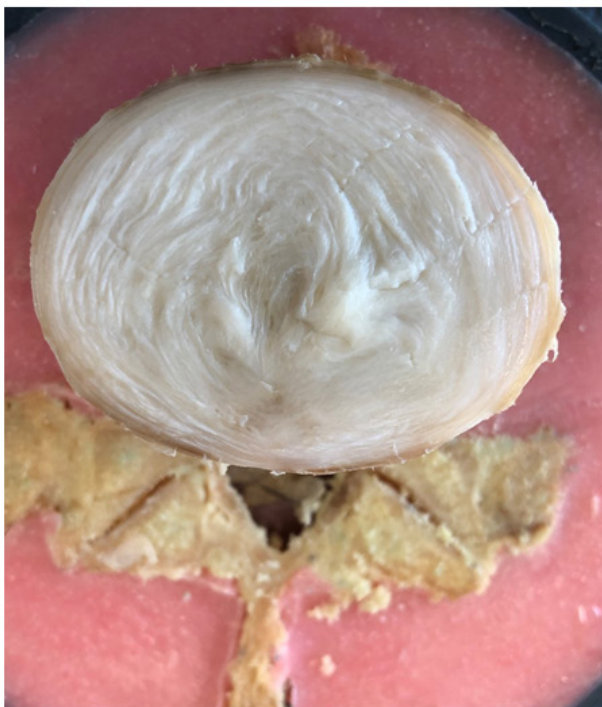
## Specimen 12



### SCALE

- 0 – No evidence of damage
- 1 – Delamination or Tears
- 2 – Nucleus Migration and/or  
Annulus Buckling
- 3 – Disc Bulge
- 4 – Disc Herniation

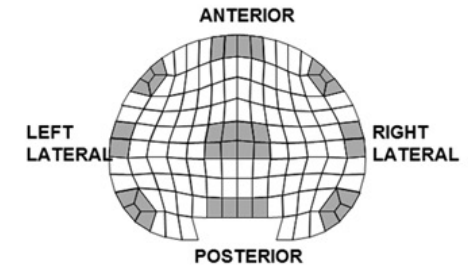
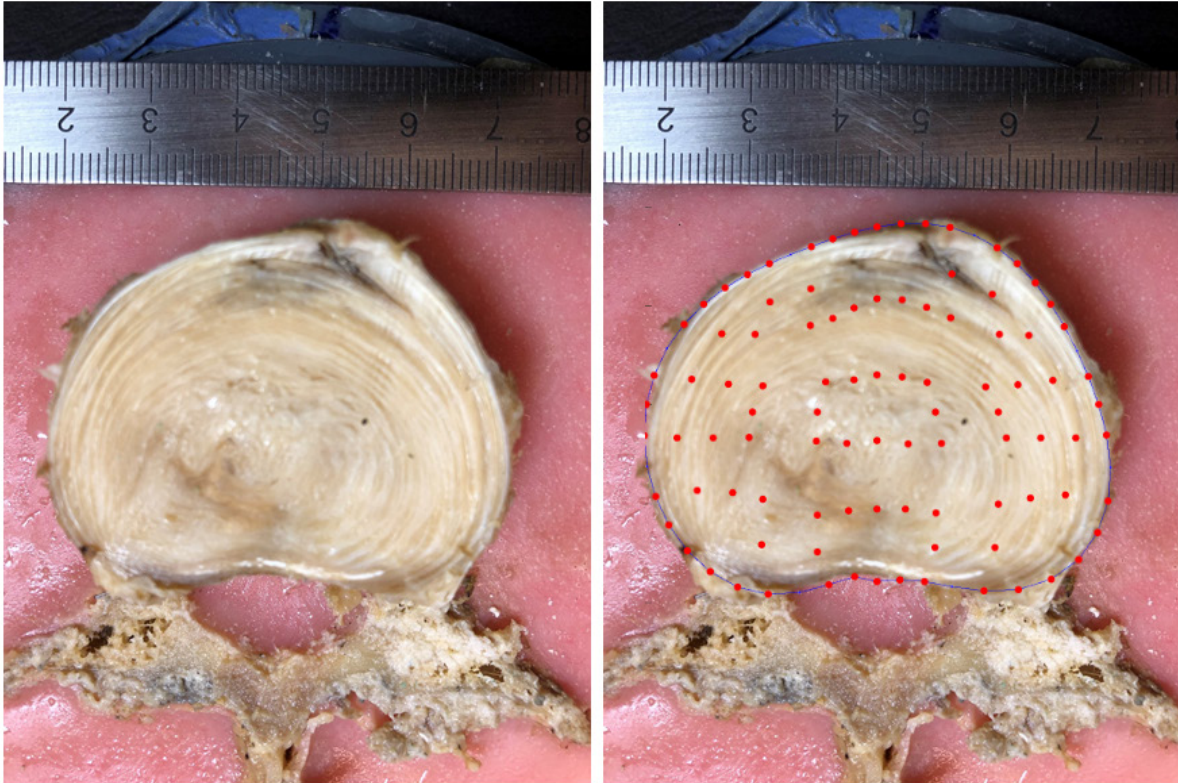
Specimen 13



SCALE

- 0 – No evidence of damage
- 1 – Delamination or Tears
- 2 – Nucleus Migration and/or Annulus Buckling
- 3 – Disc Bulge
- 4 – Disc Herniation

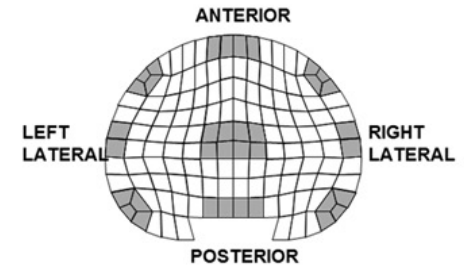
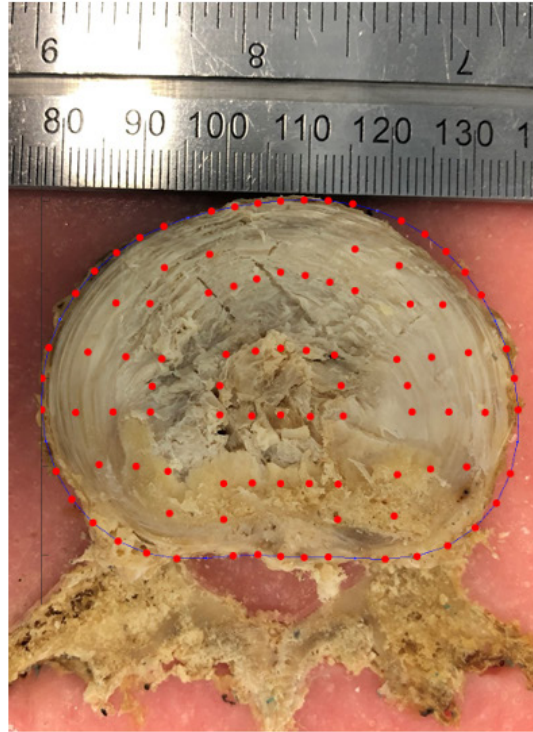
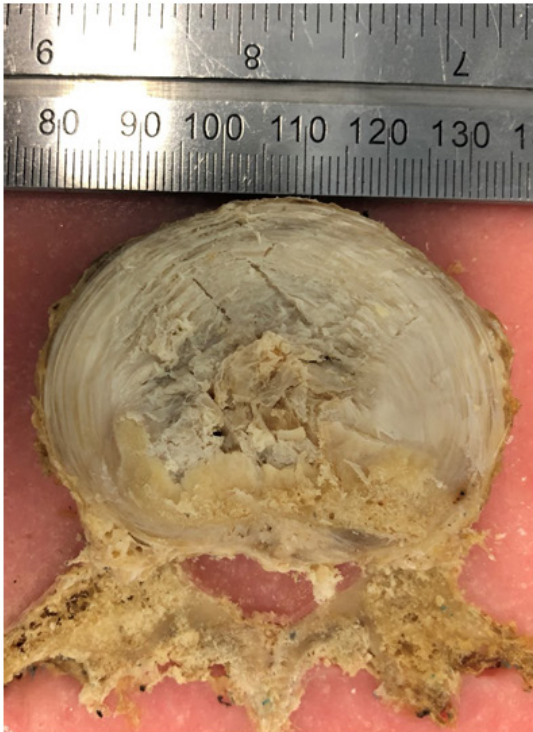
## Specimen 14



### SCALE

- 0 – No evidence of damage
- 1 – Delamination or Tears
- 2 – Nucleus Migration and/or Annulus Buckling
- 3 – Disc Bulge
- 4 – Disc Herniation

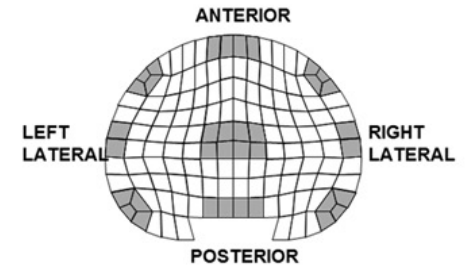
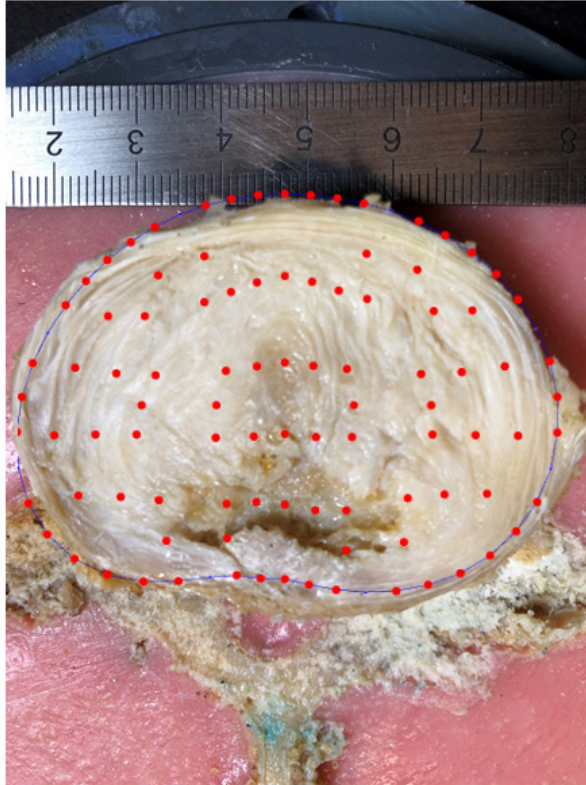
Specimen 15



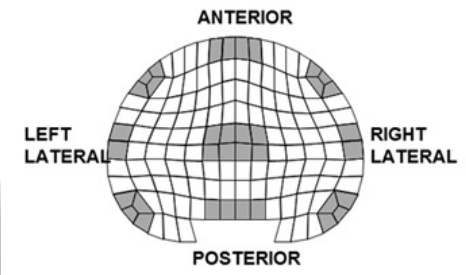
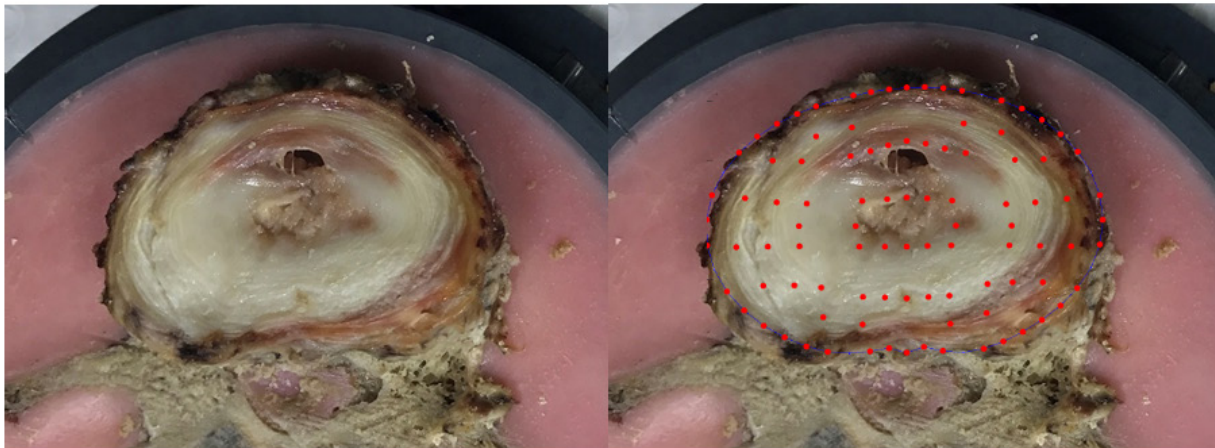
**SCALE**

- 0 – No evidence of damage
- 1 – Delamination or Tears
- 2 – Nucleus Migration and/or Annulus Buckling
- 3 – Disc Bulge
- 4 – Disc Herniation

Specimen 16



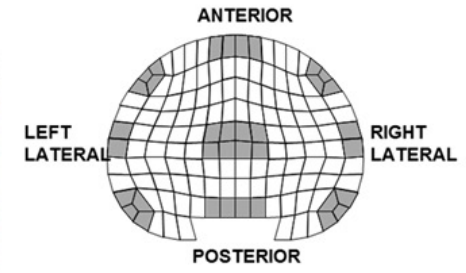
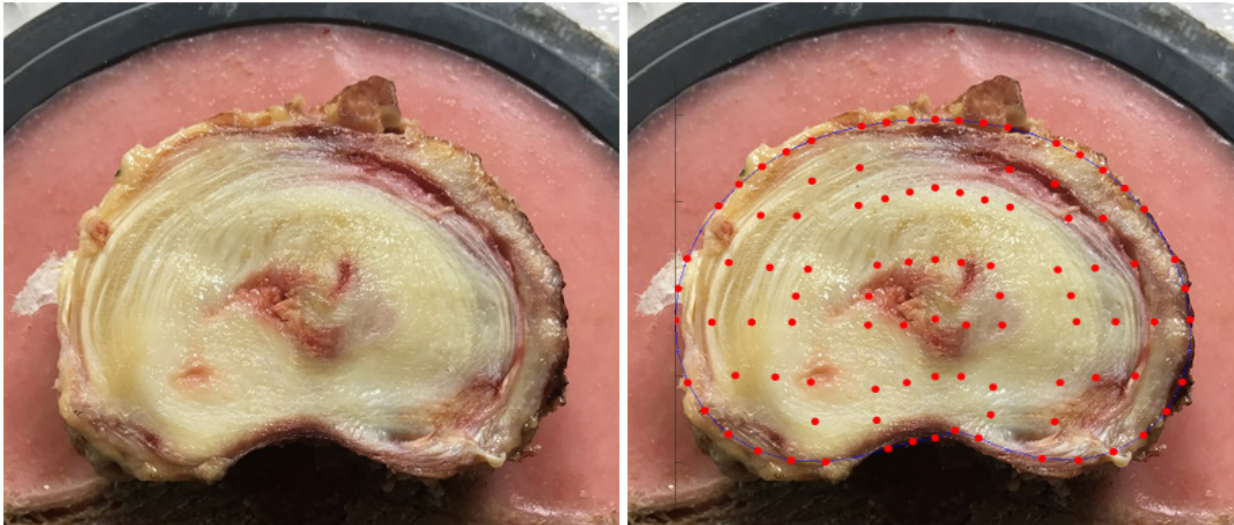
## Specimen 17



### SCALE

- 0 – No evidence of damage
- 1 – Delamination or Tears
- 2 – Nucleus Migration and/or  
Annulus Buckling
- 3 – Disc Bulge
- 4 – Disc Herniation

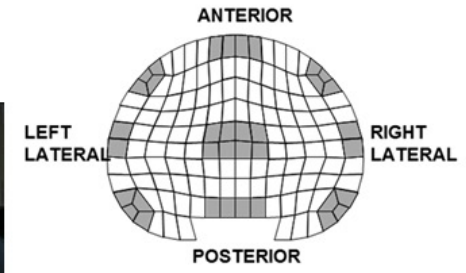
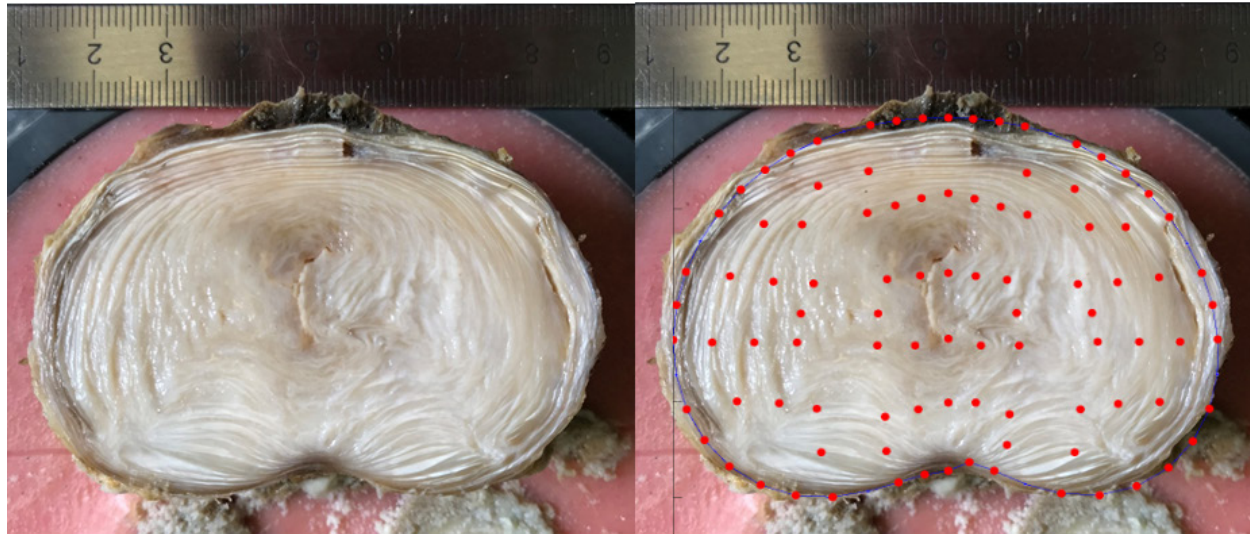
## Specimen 18



### SCALE

- 0 – No evidence of damage
- 1 – Delamination or Tears
- 2 – Nucleus Migration and/or  
Annulus Buckling
- 3 – Disc Bulge
- 4 – Disc Herniation

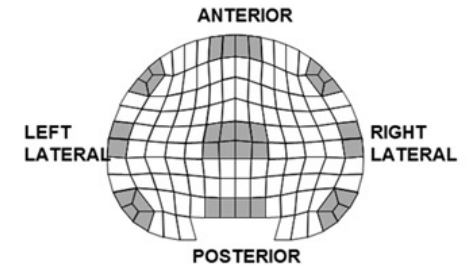
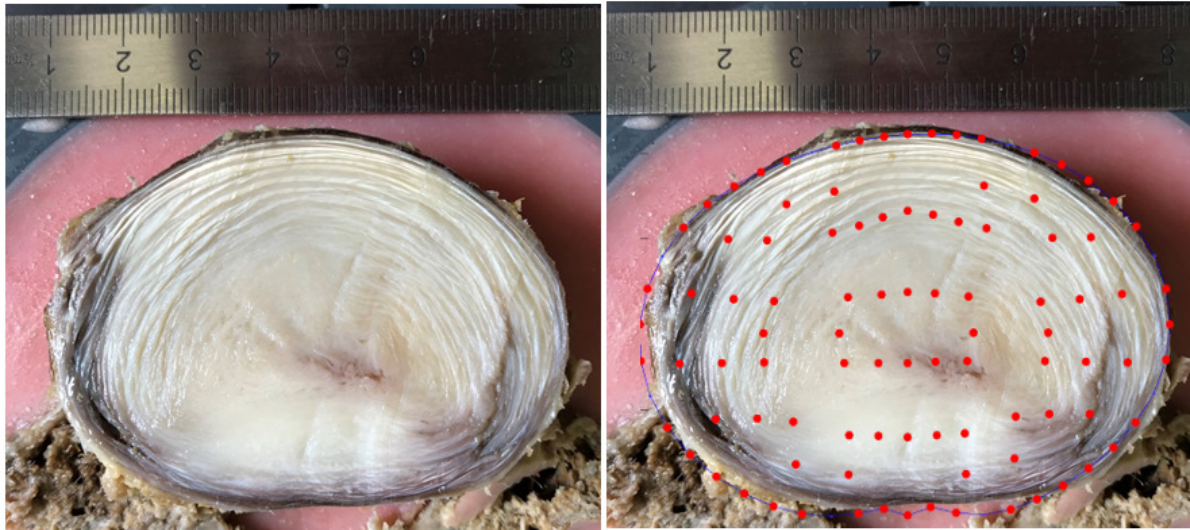
# Specimen 19



## SCALE

- 0 – No evidence of damage
- 1 – Delamination or Tears
- 2 – Nucleus Migration and/or Annulus Buckling
- 3 – Disc Bulge
- 4 – Disc Herniation

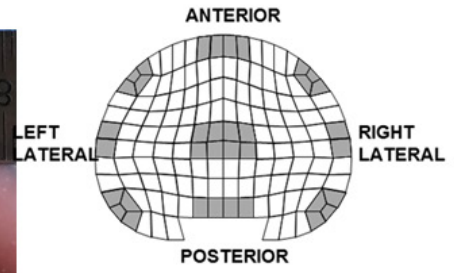
## Specimen 20



### SCALE

- 0 – No evidence of damage
- 1 – Delamination or Tears
- 2 – Nucleus Migration and/or Annulus Buckling
- 3 – Disc Bulge
- 4 – Disc Herniation

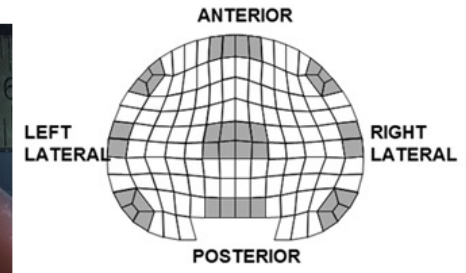
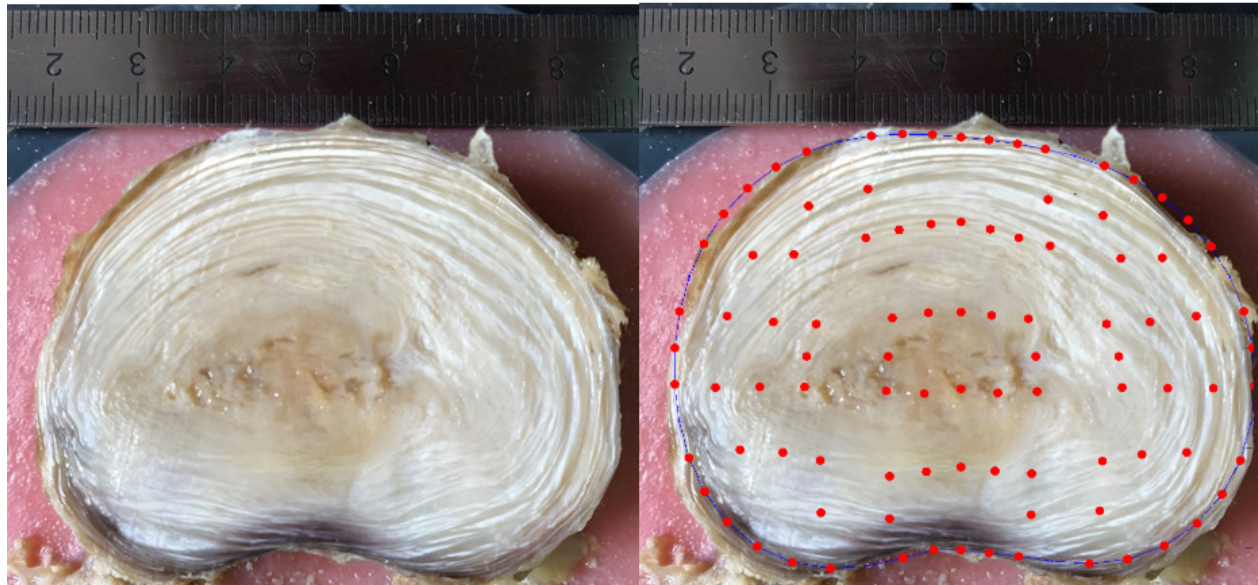
Specimen 21



SCALE

- 0 – No evidence of damage
- 1 – Delamination or Tears
- 2 – Nucleus Migration and/or Annulus Buckling
- 3 – Disc Bulge
- 4 – Disc Herniation

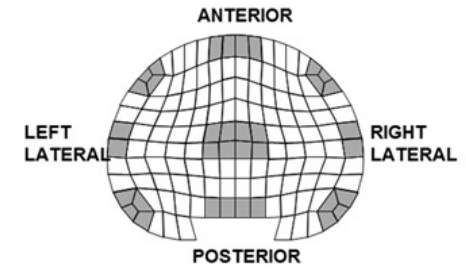
Specimen 22



SCALE

- 0 – No evidence of damage
- 1 – Delamination or Tears
- 2 – Nucleus Migration and/or Annulus Buckling
- 3 – Disc Bulge
- 4 – Disc Herniation

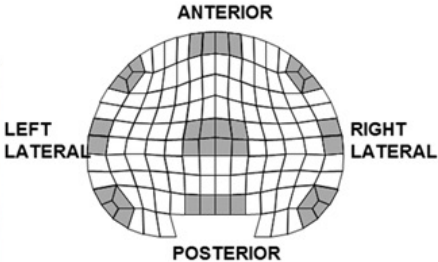
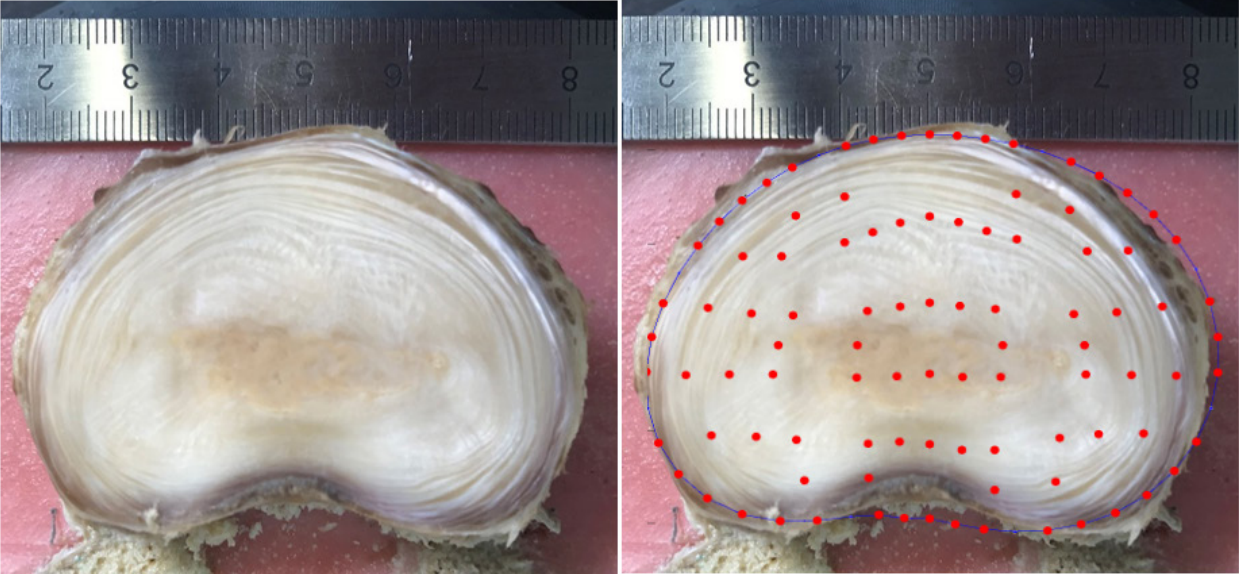
Specimen 23



SCALE

- 0 – No evidence of damage
- 1 – Delamination or Tears
- 2 – Nucleus Migration and/or Annulus Buckling
- 3 – Disc Bulge
- 4 – Disc Herniation

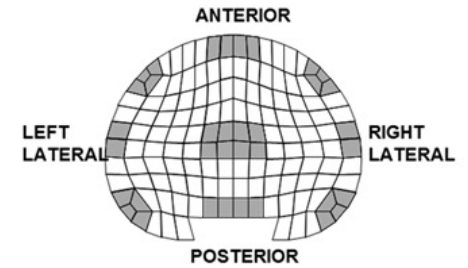
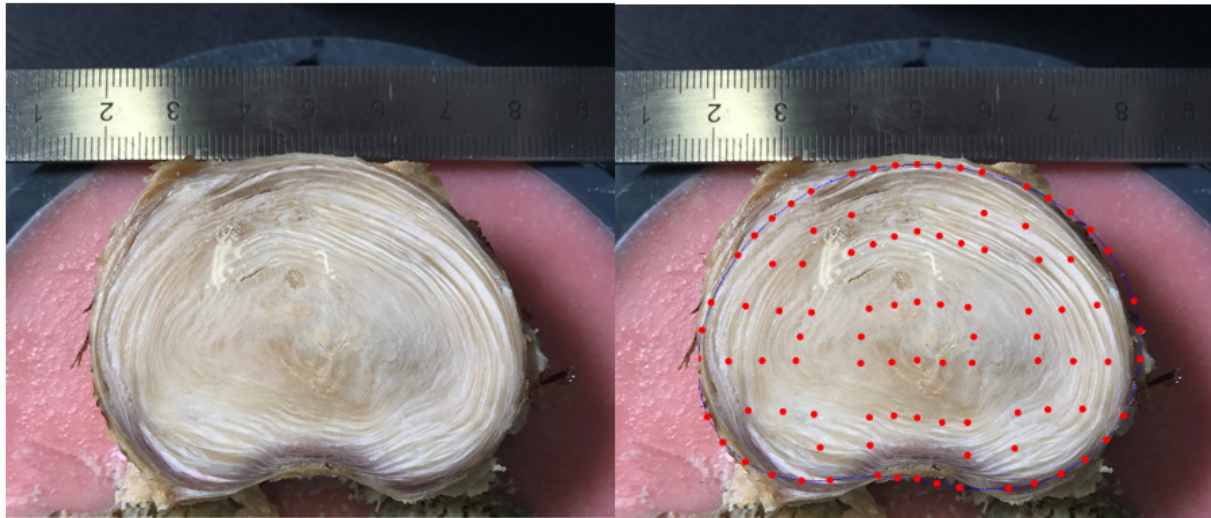
Specimen 24



SCALE

- 0 – No evidence of damage
- 1 – Delamination or Tears
- 2 – Nucleus Migration and/or Annulus Buckling
- 3 – Disc Bulge
- 4 – Disc Herniation

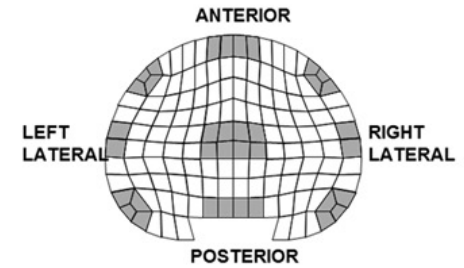
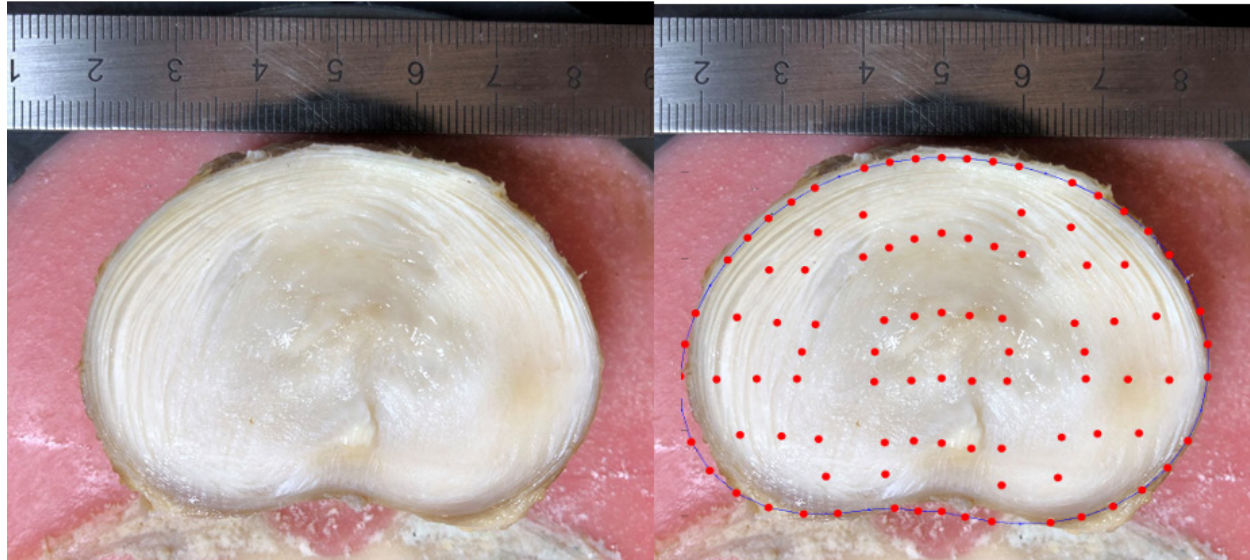
# Specimen 25



### SCALE

- 0 – No evidence of damage
- 1 – Delamination or Tears
- 2 – Nucleus Migration and/or Annulus Buckling
- 3 – Disc Bulge
- 4 – Disc Herniation

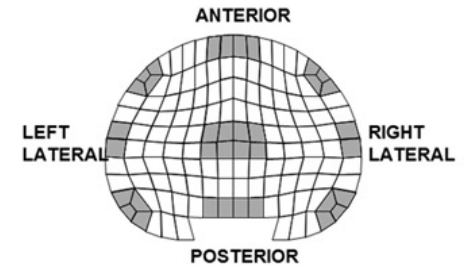
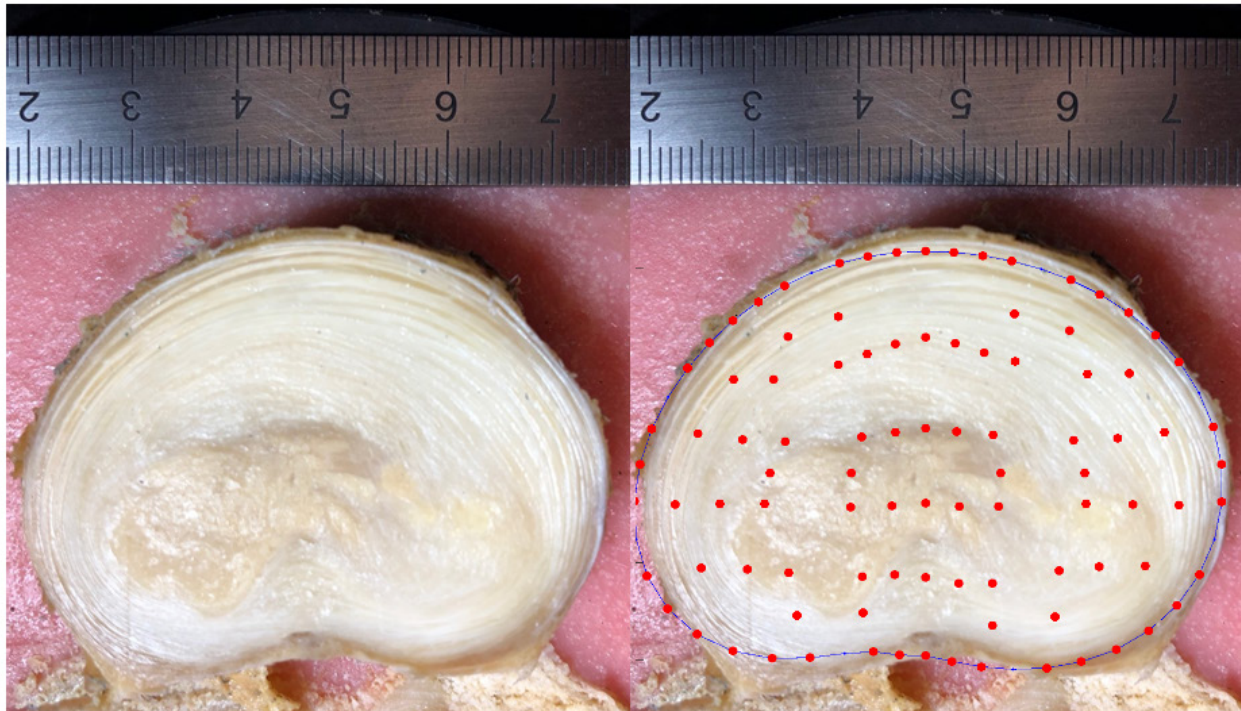
# Specimen 26



### SCALE

- 0 – No evidence of damage
- 1 – Delamination or Tears
- 2 – Nucleus Migration and/or Annulus Buckling
- 3 – Disc Bulge
- 4 – Disc Herniation

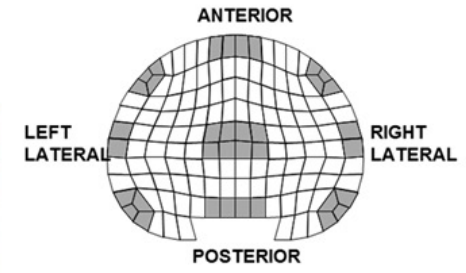
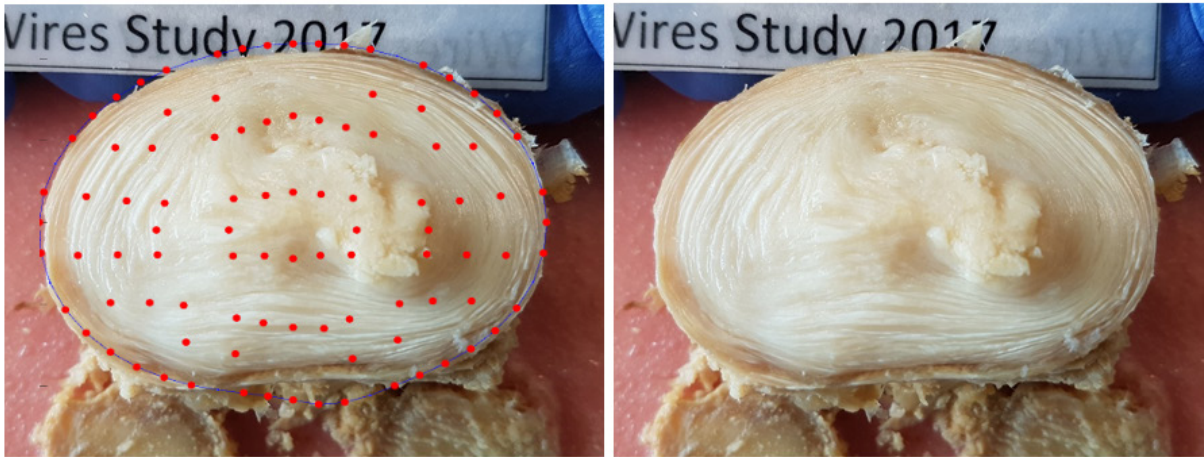
Specimen 27



**SCALE**

- 0 – No evidence of damage
- 1 – Delamination or Tears
- 2 – Nucleus Migration and/or Annulus Buckling
- 3 – Disc Bulge
- 4 – Disc Herniation

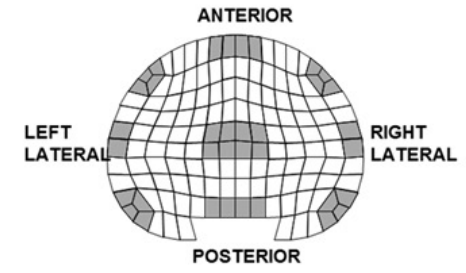
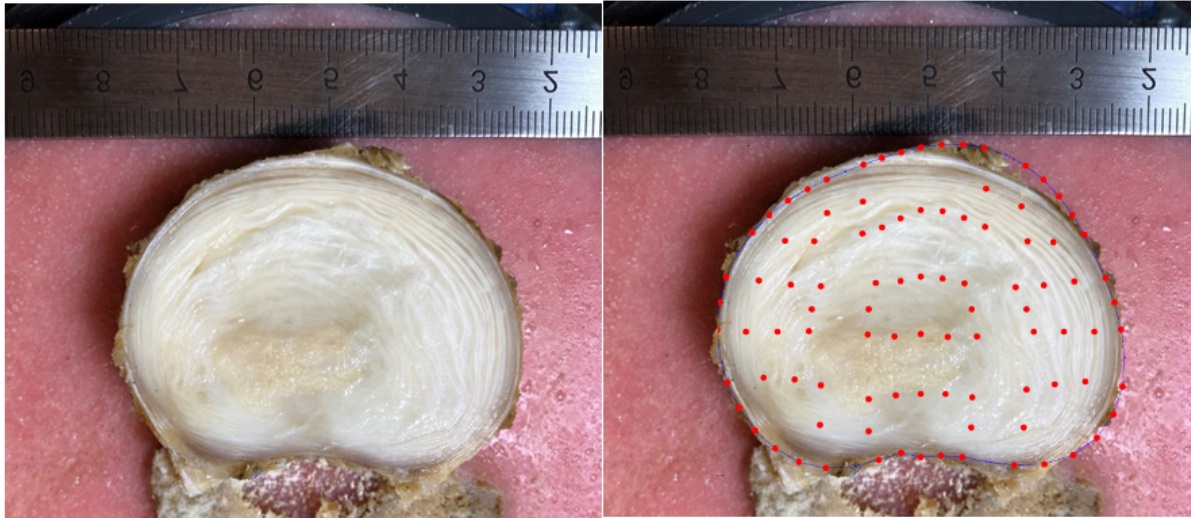
Specimen 28



**SCALE**

- 0 – No evidence of damage
- 1 – Delamination or Tears
- 2 – Nucleus Migration and/or Annulus Buckling
- 3 – Disc Bulge
- 4 – Disc Herniation

Specimen 29



**SCALE**

- 0 – No evidence of damage
- 1 – Delamination or Tears
- 2 – Nucleus Migration and/or Annulus Buckling
- 3 – Disc Bulge
- 4 – Disc Herniation

# Appendix I

## I.1 Corresponding MR images, macroscopic images, and strain maps

This appendix presents the MR image, the macroscopic image, and the strain map for the specimens in the experimental group in both simulated safe and unsafe repetitive lifting. Comparing the images (MR and macroscopic) and the strain map shows associations between shear strain and tissue damage.

### I.1.1 Simulated safe repetitive lifting

**Table I-1** Specimen characteristics (failure mode, level, grade, and applied cycles) for the simulated safe repetitive lifting cohort that underwent strain measurement. This table provides a cross-reference for the images presented in this section (I.1.1)

<b>Specimen Number</b>	<b>Failure Mode</b>	<b>Level</b>	<b>Pfarrmann Grade</b>	<b>Applied Cycles</b>
1	Endplate Failure	L4-5	3	500
2	Disc Protrusion	L4-5	2	20,000
3	Disc Protrusion	L4-5	2	20,000
4	No Injury	L2-3	2	20,000
5	Disc Protrusion	L4-5	2	20,000
6	Endplate Failure	L1-2	2	5,000
7	Disc Protrusion	L1-2	3	20,000
8	LDH	L4-5	3	20,000

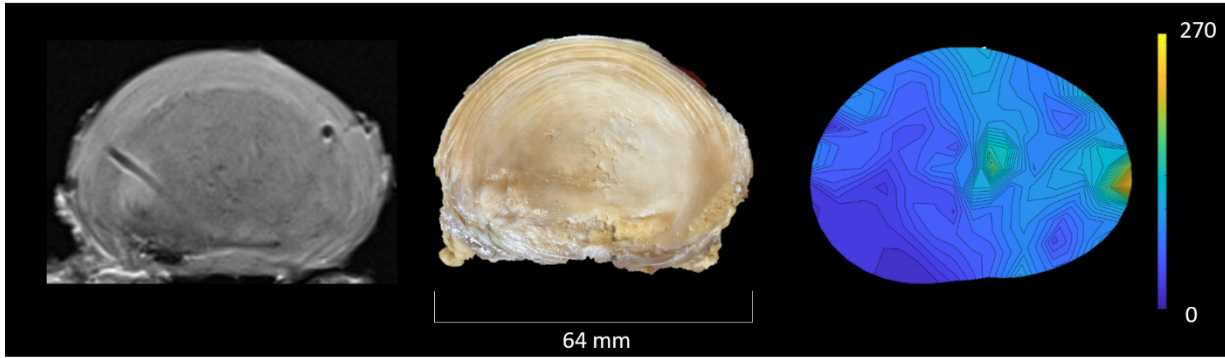


**Figure I-1** Left to right images: MRI axial slice, macroscopic axial slice, and the MSS map after simulated safe repetitive lifting for specimen 1



**Figure I-2** Left to right images: MRI axial slice, macroscopic axial slice, and the MSS map after simulated safe repetitive lifting for specimen 2



**Figure I-3** Left to right images: MRI axial slice, macroscopic axial slice, and the MSS map after simulated safe repetitive lifting for specimen 3



**Figure I-4** Left to right images: MRI axial slice, macroscopic axial slice, and the MSS map after simulated safe repetitive lifting for specimen 4



**Figure I-5** Left to right images: MRI axial slice, macroscopic axial slice, and the MSS map after simulated safe repetitive lifting for specimen 5



**Figure I-6** Left to right images: MRI axial slice, macroscopic axial slice, and the MSS map after simulated safe repetitive lifting for specimen 6



**Figure I-7** Left to right images: MRI axial slice, macroscopic axial slice, and the MSS map after simulated safe repetitive lifting for specimen 7



**Figure I-8** Left to right images: MRI axial slice, macroscopic axial slice, and the MSS map after simulated safe repetitive lifting for specimen 8

### I.1.2 Simulated unsafe repetitive lifting

**Table I-2** Specimen characteristics (failure mode, level, grade, and applied cycles) for the simulated unsafe repetitive lifting cohort that underwent strain measurement. This table provides a cross-reference for the images presented in this section (I.1.2)

Specimen Number	Failure Mode	Level	Pfirschmann Grade	Applied Cycles
1	Disc Protrusion	L3-4	2	10,000
2	Endplate Failure	L2-3	2	500
3	Endplate Failure	L1-2	2	5,000
4	No Injury	L4-5	1	20,000
5	Disc Protrusion	L2-3	2	10,000
6	No Injury	L2-3	1	20,000
7	Endplate Failure	L2-3	3	500

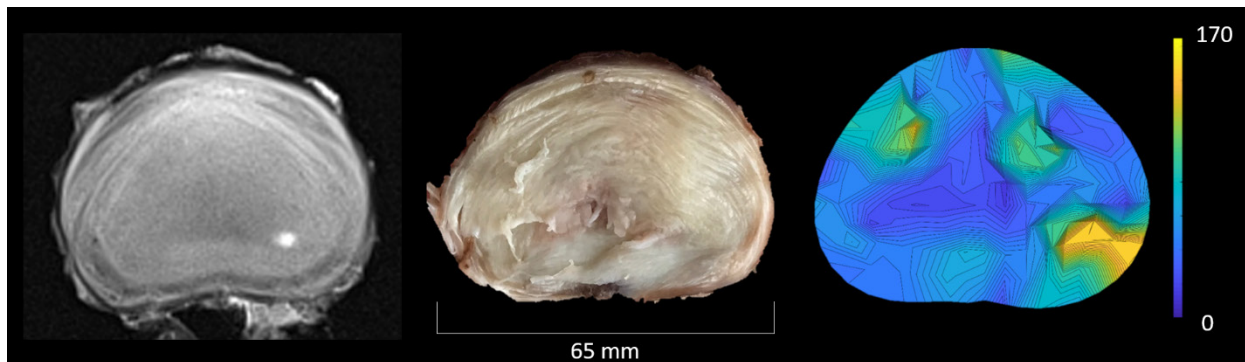


**Figure I-9** Left to right images: MRI axial slice, macroscopic axial slice, and the MSS map after simulated unsafe repetitive lifting for specimen 1



**Figure I-10** Left to right images: MRI axial slice, macroscopic axial slice, and the MSS map after simulated safe repetitive lifting for specimen 2



**Figure I-11** Left to right images: MRI axial slice, macroscopic axial slice, and the MSS map after simulated safe repetitive lifting for specimen 3



**Figure I-12** Left to right images: MRI axial slice, macroscopic axial slice, and the MSS map after simulated safe repetitive lifting for specimen 4



**Figure I-13** Left to right images: MRI axial slice, macroscopic axial slice, and the MSS map after simulated safe repetitive lifting for specimen 5

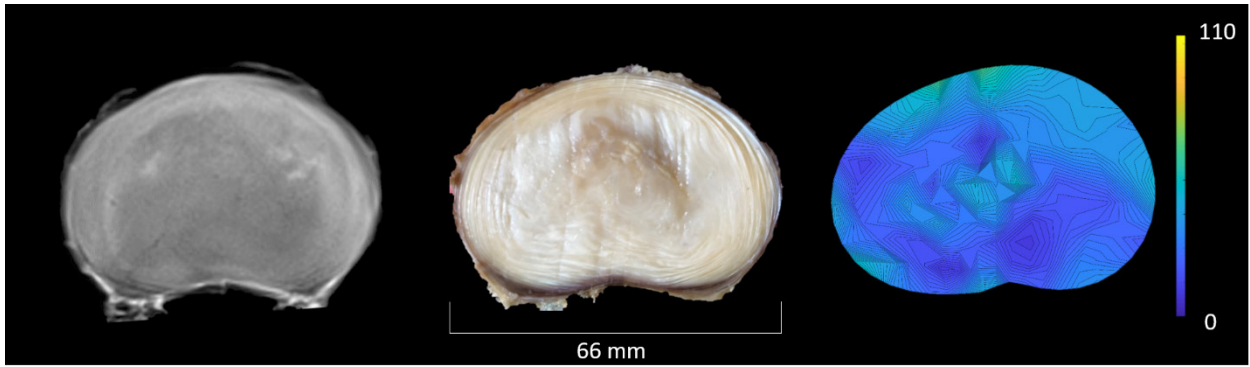


**Figure I-14** Left to right images: MRI axial slice, macroscopic axial slice, and the MSS map after simulated safe repetitive lifting for specimen 6



**Figure I-15** Left to right images: MRI axial slice, macroscopic axial slice, and the MSS map after simulated safe repetitive lifting for specimen 7